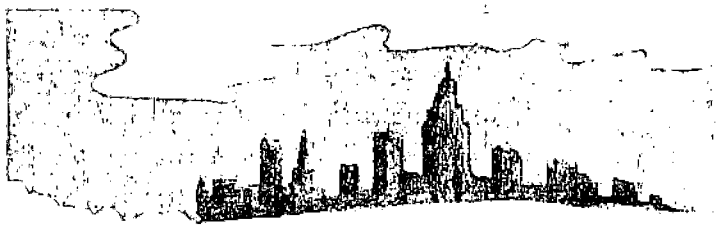

Mining Earth's Heat: Hot Dry Rock Geothermal Energy

Ronald G. Cummings, Glenn E. Morris, Jefferson W. Tester, and Robert L. Bivins

The energy contained in rock within the earth's crust represents a nearly unlimited energy source. Its inherent inaccessibility has limited its use to only a few sites in the world. At those sites, geothermal power plants utilize drilled wells to bring natural underground hot water and/or steam to the surface; the hot geothermal fluid either flows under artesian pressure or is pumped to a power plant, which may use the fluid to produce electricity, process heat, or both. Often reinjection wells are used to return the cooled fluid to the formation.

These natural hydrothermal reservoirs represent only a minute fraction of the total energy in place in the hot rock. Exploitation of the remaining fraction involves the development of methods to extract energy from rock formations where this unique combination of geologic and hydrologic conditions does not exist.

Three major heat sources contribute to the hot dry rock resource:

- ☐ igneous related crustal heat from magma bodies;
- ☐ heat transferred by conduction from the earth's interior;
- ☐ heat generated by radioactive decay of certain

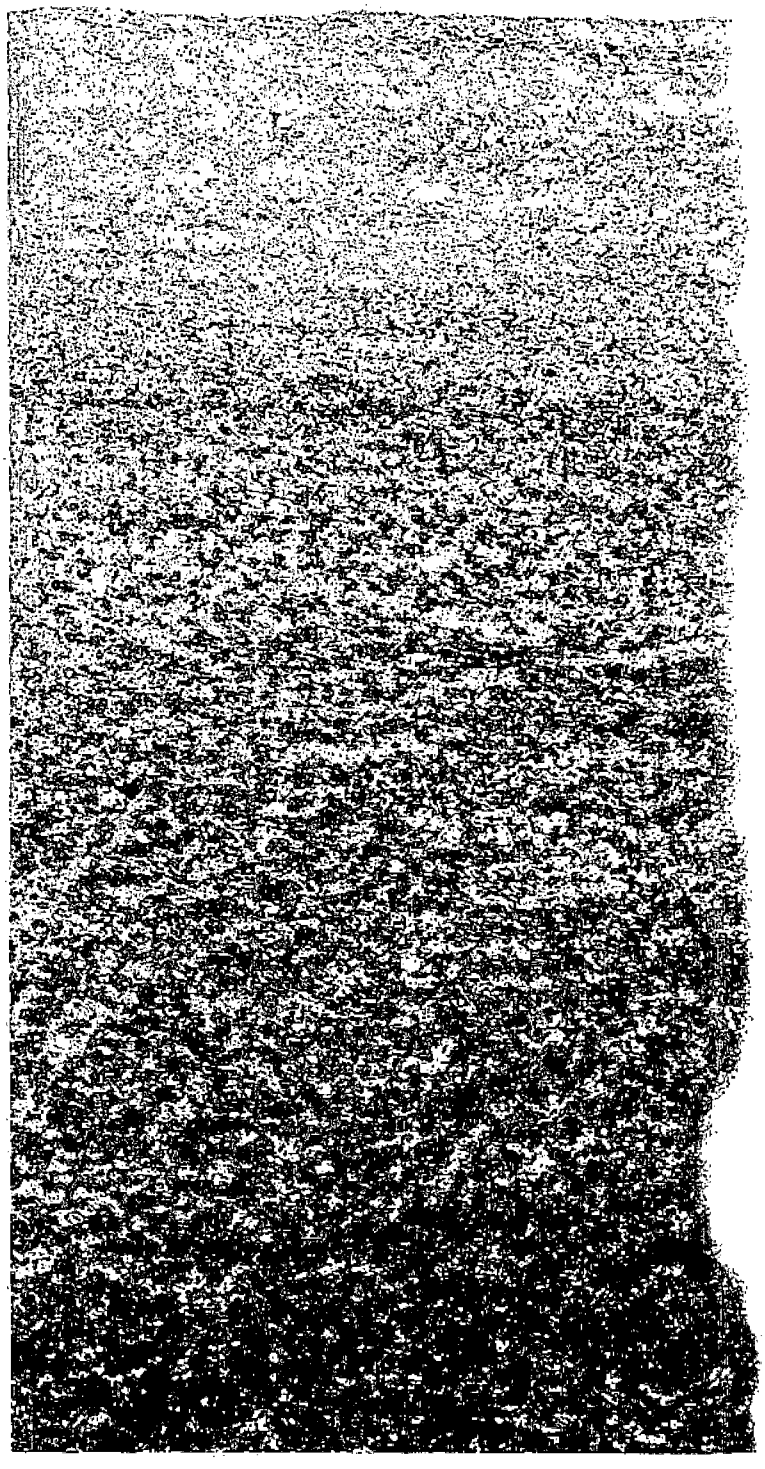

Electricity may be generated by an HDR power plant at costs competitive with existing modes of electrical production in many parts of the United States. The elements of such a plant would be likely to follow the general scheme shown. The single fracture indicated is likely to be workable for a reservoir in rock of low permeability, which would tend to retain most of the injected working fluid.

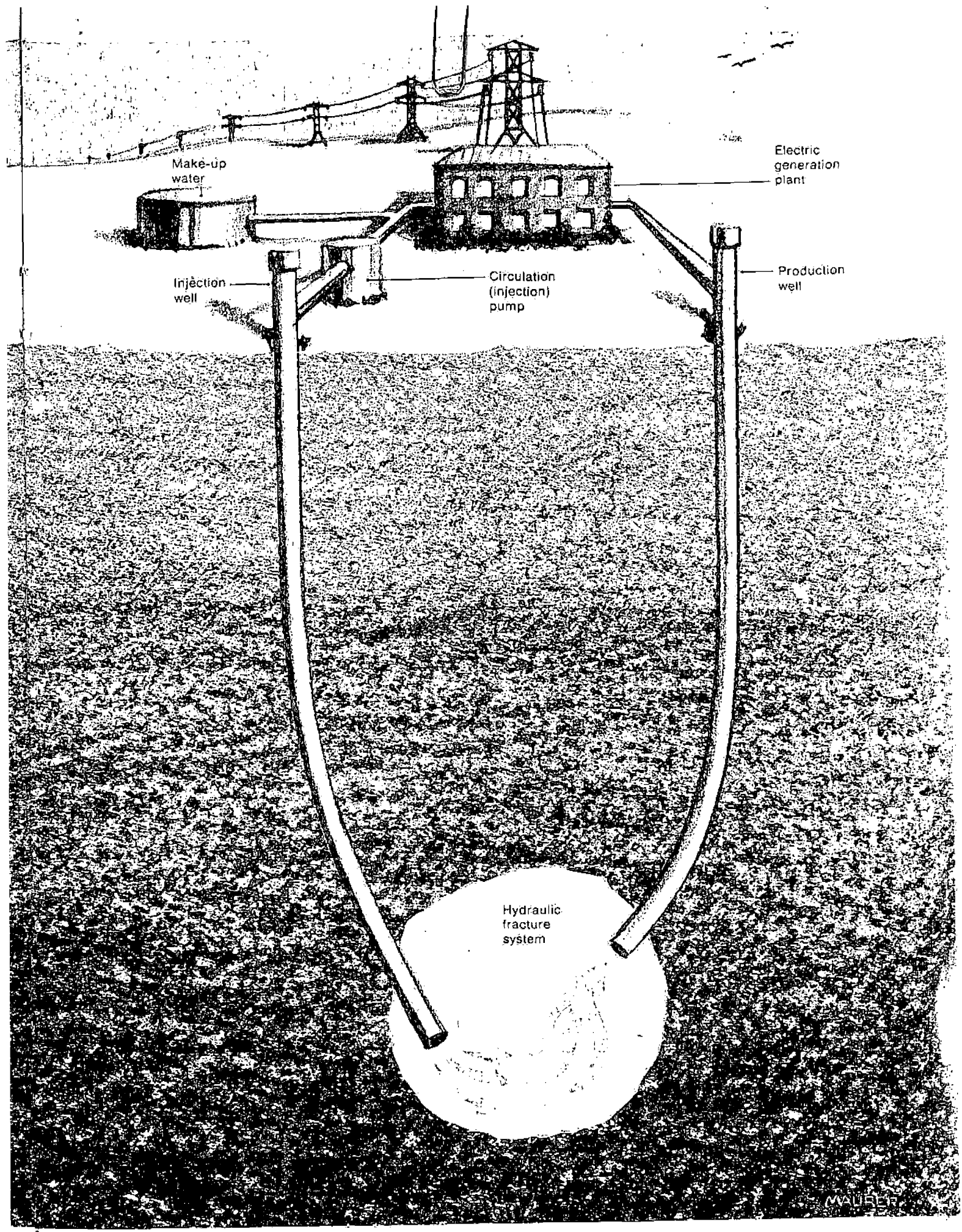
Make-up water
Electric generation plant
Injection well
Circulation (injection) pump
Production well
Hydraulic fracture system

This map of the United States shows the geothermal gradients — rate of increase in temperature with depth — based on data collected by R. M. Potter from American Association of Petroleum Geologists oil and gas well temperature-depth records, and from recent estimates for the Atlantic coastal plain by J. Costain and associates from the Virginia Polytechnic Institute. The large blank areas represent regions for which data are lacking. Note that high gradients are not exclusively located in the western states, nor are they associated with hydrothermal resource areas such as the Geysers region in northern California or the Imperial Valley region of southern California. For example, high geothermal gradients occur on the Atlantic Coast, in Illinois and Indiana, and in South Dakota and Nebraska.

elements contained in the earth's crust.

In some areas of recent volcanic activity, high rates of heat flow may cause visible effects at the surface; for example, erupting geysers and hot springs. In other areas, however, hot rock exists near the surface but there is insufficient water present to produce such phenomena. Thus a potential hot dry rock (HDR) reservoir exists whenever the amount of spontaneously produced geothermal fluid is inadequate for a commercial system. This feature of the HDR resource may provide an advantage in that system temperatures and fluid production rates may be determined by design in contrast to natural hydrothermal reservoirs where these characteristics are determined by prevailing geologic and hydrologic conditions. For example, HDR reservoir temperatures may be selected by drilling to a specified depth determined by the geothermal temperature gradient.

Concepts for creating HDR systems involve drilling holes and connecting them to man-made reservoirs emplaced deep within the crust. In all cases, artificial stimulation is required to create either sufficient permeability or bounded flow paths to allow removal of heat by circulation of a suitable fluid over the surface of the rock.

Many facets related to the technical feasibility of HDR systems have been demonstrated in the first field experiments being conducted by the Los Alamos Scientific Laboratory (L.A.S.L.) at the Fenton Hill site in the Jemez Mountains of New Mexico. At the present time, a hydraulically fractured reservoir in low permeability crystalline basement rock at about 185° C. has been created and flow tested for 75 days at an energy extraction rate of approximately five thermal megawatts (MWt.) Plans are underway to enlarge this to a 50 MWe. capacity with an extended lifetime. The resolution of these technical issues and the inevitable economic trade-offs that exist will determine the fate of HDR as a commercially feasible venture.

Size and Quality of the HDR Resource

Two critical questions confront potential developers of this resource, the responses to which have sig-

nificant impact on the economics of drilling and reservoir development:

☐ How does one precisely define and identify a useful HDR resource?

☐ How are HDR resources distributed throughout the United States?

The HDR resource base is generally defined to include crustal rock that is hotter than 150° C. (though for some applications the minimal usable temperature could be as low as 50° C.), is at depths less than ten kilometers, and can be drilled with presently available equipment. While technically feasible, prevailing economic factors will obviously determine commercially feasible depths. Depending on end use, useful rock temperatures may be as low as 100° C. for space heating purposes. However, temperatures greater than 200° C. are desirable for producing electricity.

The HDR resource base is very large. Using a conservative average geothermal temperature gradient of 22° C. per kilometer (km.) of depth, a staggering 13×10^{21} joules (J.) (13,000,000 quadrillion British thermal units, or *quads*) of total energy are calculated to be contained in crustal rock to a ten km. depth in the United States, including Alaska and Hawaii. In comparison, the present annual U.S. energy consumption is approximately 80 quads. The real question remains as to how much of this resource base can be recovered. If we assume that only about 0.2 per cent is technically recoverable, we find a total that is comparable to the estimated resource base of all the coal remaining in the United States.

The geothermal gradient, which determines the depth of drilling required to reach a specified temperature, is a major factor in the recoverability of geothermal resources. There is an obvious trade-off in HDR systems between the temperature required and the depth of drilling necessary to reach it. The problem is to balance the economics of deeper, hotter, more costly wells versus shallower, cooler, less expensive wells against the value of the final product, electricity and/or heat.

Studies by W. H. Diment and his colleagues at the U.S. Geological Survey (U.S.G.S.) show that rock underlying about five per cent of the total U.S. land

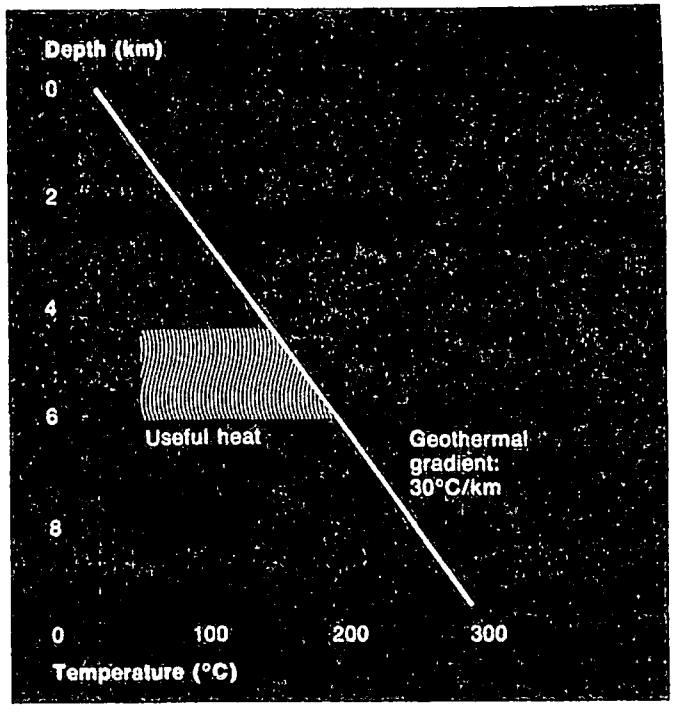

Above: This plot of rock temperature against depth illustrates potentially useful energy contained in an HDR resource. The tinted area denotes the range of heat usable for the commercial generation of electricity in a location with a mean geothermal gradient of 30° C./km. to a minimum useful temperature of 50° C., corresponding to a depth of 4.5 km, is considered. An assumed maximum economic drilling depth of 6 km. then determines the highest reservoir temperature possible, in this case 195° C.

Right: Rock formations with low permeability could produce useful heat by circulating water through "reservoirs" consisting of one or more fractures at appropriate depths.

The first drawing shows a single hydraulic fracture produced by high-pressure fluid injection. After thermal exhaustion of the original fractured zone, a second fracture could be grown from the same borehole. Each fracture would be roughly penny-shaped, 100 m. or more in diameter and a few millimeters wide in cross section.

The second drawing shows the development of the thermal stress cracks that may form during continued operation of an HDR reservoir. Such cracks have the effect of increasing the effective heat transfer surface area available to the circulating fluid.

As suggested by R. M. Potter of L.A.S.L. and C. B. Rayleigh of the U.S.G.S., a possible arrangement of multiple parallel fractures is shown in the third diagram. The fractures would also be grown hydraulically by fluid injection. Perforations in the casing of the lower borehole would be used to regulate the flow of fluid into the fractures.

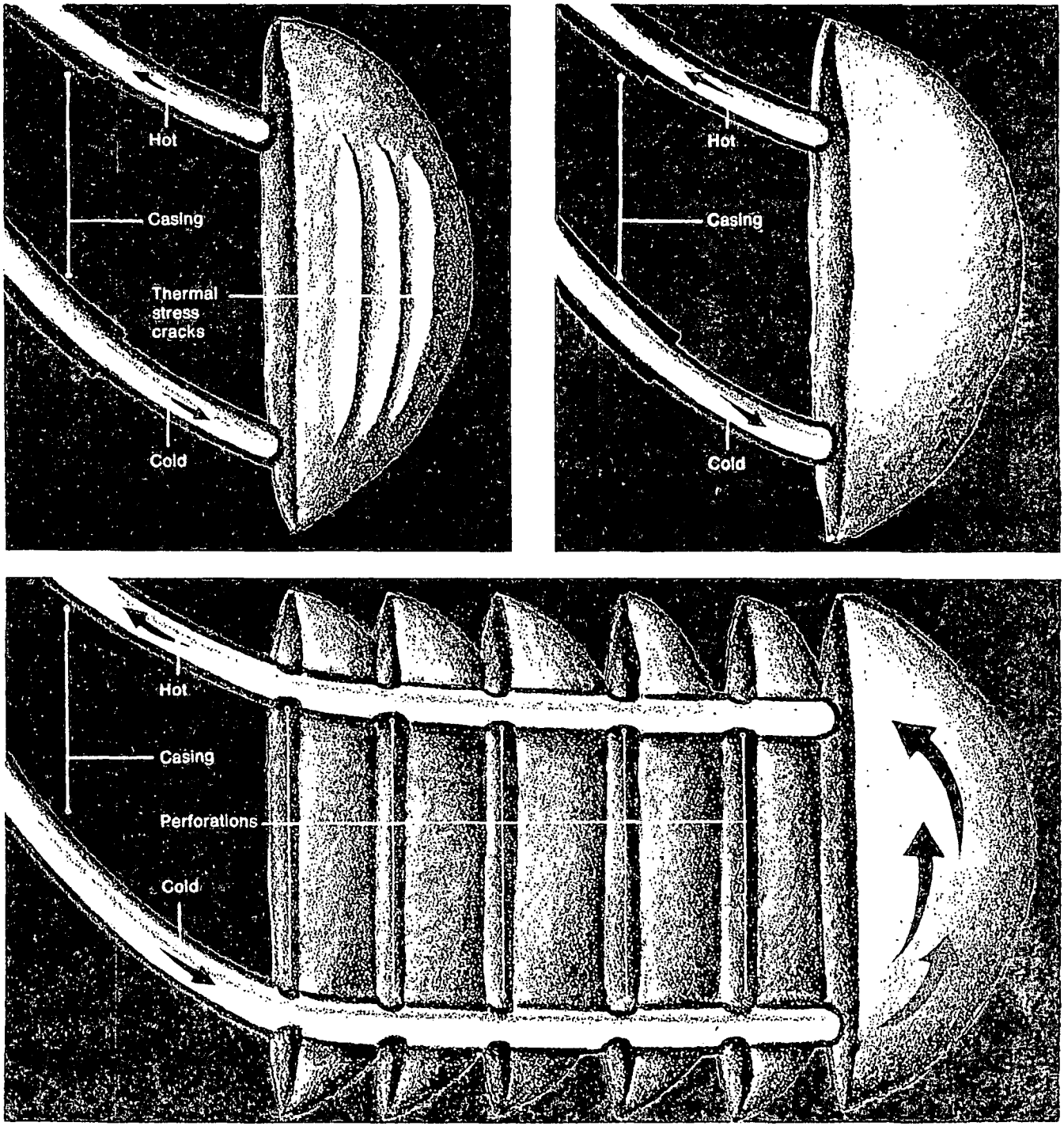
Hot
Casing
Thermal stress cracks
Cold
Hot
Casing
Cold
Hot
Casing
Perforations
Cold

area may have geothermal gradients of 40° C. per km. or more. Conservatively, it can be assumed that over a third of the land area in the United States has above average heat flow with thermal gradients ranging from 30° to 36° C. per km. Igneous rock systems to depths of ten kilometers under the continental United States (not including Alaska and Hawaii) are estimated by R. L. Smith and H. R. Shaw of the U.S.G.S. to contain about 105×11^{21} J. (105,000 quads) and T. R. McGetchin and his associates on the Hot Dry Rock Assessment Panel convened by the U.S. Energy Research and Development Administration estimated that such igneous systems contain 74×10^{21} J. (74,000 quads) of thermal energy at temperatures above 150° C.

Other physical and chemical properties of potential HDR formations are as important to energy extraction feasibility as are the geothermal gradients. Different formation permeabilities, porosities, and chemical reactivities with hot water obviously affect the development of potential HDR reservoirs. These factors are now being incorporated in an extensive evaluation of potential U.S. HDR sites underway at the L.A.S.L. This will be based in part on improvements to the gradient data base provided by the U.S.G.S. resource assessment program.

Extraction of HDR Geothermal Energy

At least two fundamental approaches are now generally accepted for mining HDR geothermal heat. One is appropriate for use in rock formations with low permeability, the other for high permeability rock.

If the permeability of the formation is low, an artificial circulation system can be created by fracturing the rock in the reservoir to provide many flow passages with a large heat-transfer surface area. A fluid — for example, water — is then circulated through the fractured reservoir to recover the energy. Most of the injected fluid is recovered in a second production wellbore simply because of the low natural permeability of the formation. Large fracture surface areas are required because rock conducts heat rather poorly, and it quickly controls

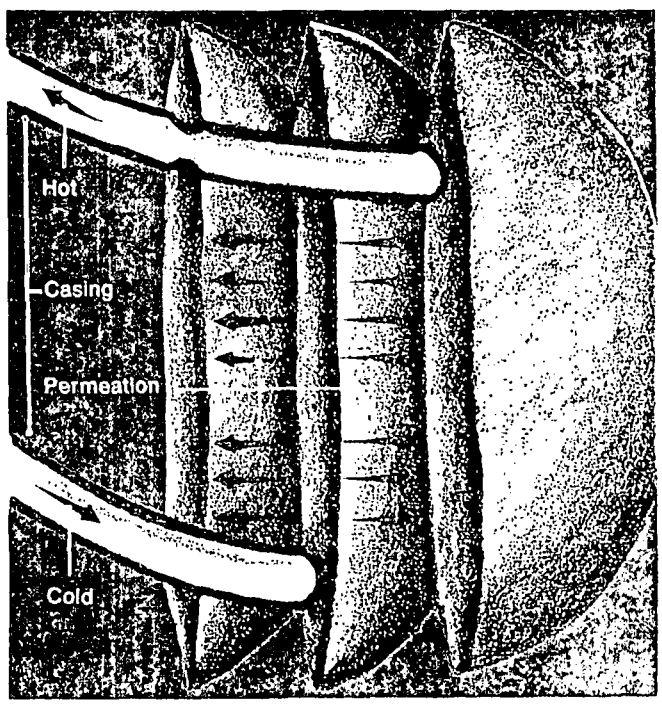

Above: Three parallel fractures could be used to extract energy from rock formations having high permeability. Cold water would be injected into the central fracture under high pressure. The water would then permeate the hot rock, eventually reaching the outer fractures, from which it would exit via the second wellbore. Note how the wellbore casings and perforations force the water to follow the desired path.

Right: These computer simulated flow contours represent the circulation of fluid as heat is transferred to fluid in a single, penny-shaped fracture. The fracture has a radius of 500 m. and a very thin elliptical cross section. The streamlines shown in both diagrams contain approximately 10 per cent of the total 144 kg./sec. flow. An initial mean rock temperature of 250° C. and a geothermal gradient of 50° C./km. were used.

The left diagram indicates the flow of water with buoyancy effects suppressed due to high impedance.

The right diagram shows a similar fracture, but includes buoyancy effects.

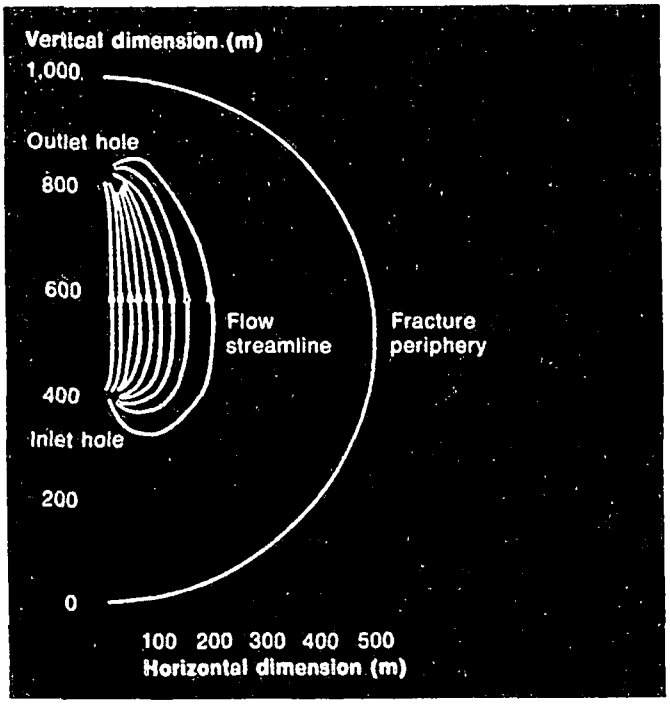

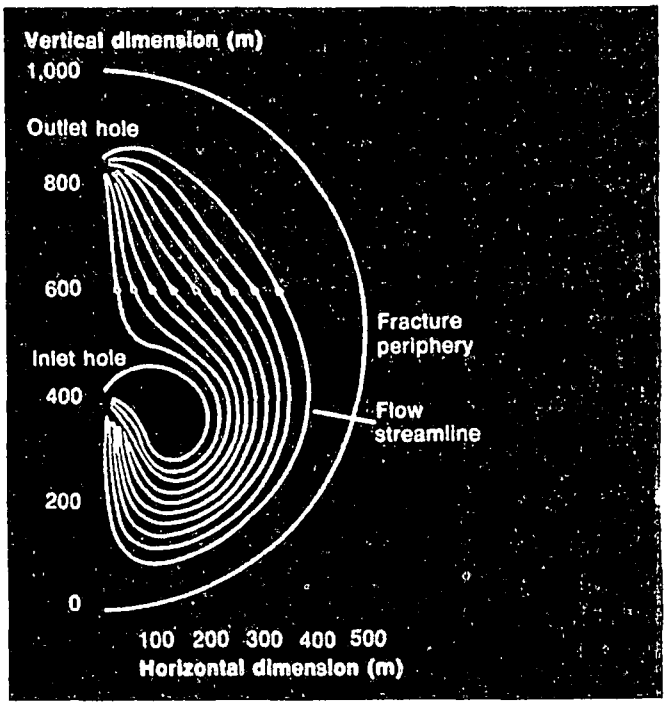

the rate of heat transfer to the fluid contained in the fracture zone.

Such an HDR reservoir will most likely be formed by injecting fluid through a wellbore at pressures sufficient to fracture the rock. Under ideal conditions, the fracture would be vertically oriented, circular in shape, with a maximum radius of typically 100 meters (m.) or more, and a width or opening of only a few millimeters.

Problems of Containment and Recovery

The production wellbore in this downhole circulation system should intersect the fractured region sufficiently above the injection point to maximize the exposure of fluid to the fracture surface by avoiding "short-circuiting" and exploiting buoyancy effects. Heat exchangers at the surface would extract energy from the geothermal fluid, which would then be reinjected to complete a closed cycle. Some water would be lost even in low permeability rock, so that "makeup water" would be added. Because the rock has a low thermal conductivity, fractures separated by greater than 50 m. show only negligible thermal interference over a 20 to 30 year period. Consequently, multiple parallel fracture systems may provide an alternative method of generating large rock surface areas.

In formations with high permeabilities, the problem of fluid circulation may be of only secondary importance to that of containing and recovering the geothermal fluid. Water-drive and flooding methods, long used for the underground recovery of gas and oil, may be applicable to high permeability HDR reservoirs; these methods make use of networks of injection and production wells, arranged to minimize fluid loss to permeable rock surrounding the field. Alternatively, injection and production wells could be located to take advantage of the permeability. For example, three parallel fractures of similar area could be created, of which the central fracture would serve as the fluid injection surface and the two flanking fractures would receive fluid that permeates the rock from the central fracture. If

a uniform flow distribution can be maintained through such a system, the lifetime of the reservoir will be determined by the heat content of the rocks in the fractured region.

Obviously, any HDR reservoir will have a finite rate of temperature decline over time. The thermal drawdown, or cooling rate, for a fractured low permeability HDR reservoir depends on the accessible fracture surface area, mass flow rate of water, distribution of fluid across the fractured surface, and the density, heat capacity, and thermal conductivity of the rock.

Thermal drawdown creates a need to develop strategies for reservoir management to optimize the utilization of the resource. From the standpoint of the power producer, the temperature decline of the output fluid should be minimized while the mass flow rate per pair of wells is maximized over the 20 to 40 year lifetime of an HDR power plant.

This will not be possible in the extreme because of the finite area of the reservoir. In some cases it may be necessary to slow the mass flow rate to reduce the rate of temperature decline. Fortunately, substantial enhancement of reservoir performance may occur spontaneously, because as heat is removed from an HDR reservoir, thermal stresses are likely to cause the rock to crack further. Such cracking would provide additional flow channels for the circulating fluid and would enhance the performance and lifetime of the reservoir. Even without thermal stress cracking, thermal contraction of the rock will increase the width of the fracture opening, allowing buoyancy effects to sweep fluid more uniformly over the fracture surface area.

In the absence of thermal stress cracking enhancement, two remedial stimulation alternatives are possible:

- additional hydraulic fracturing from inclined wellbores by high-pressure fluid injection to produce new surface area in hot sections of the reservoir;
- sidetracking of the original wellbores to a new region and refracturing to produce a new system.

In addition, multiple fractures grown from inclined boreholes may generate sufficient surface area to prolong reservoir lifetime significantly.

Electric Power from HDR Systems

Using a geothermal resource to supply heat to an electric power generating cycle frequently involves a different set of design criteria from conventional fossil fuel fired or nuclear generating cycles. Because conversion efficiencies range from 8 to 20 per cent for geothermal resource temperatures of 100 to 300° C., and because drilling-related costs frequently represent more than 60 per cent of the total capital investment in the power plant, a premium is placed on designing and operating conversion systems near their thermodynamic limiting efficiencies.

Rankine or similar cycles have been used for power production with water as the working fluid, particularly where natural steam is available. For liquid dominated systems, steam vapor can be created by flashing the geothermal fluid at the surface to a lower pressure. Then, the saturated steam phase can be used to drive a turbogenerator unit, with the unflashed liquid fraction either reinjected or discarded. Binary-fluid cycles employing nonaqueous working fluids are alternatives to single and multiple flashing systems currently in use in various parts of the world (for example Cerro Prieto, Mexico, and Wairakei, New Zealand). Binary-fluid cycles involve a primary heat exchange step where heat from the geothermal fluid is transferred to another working fluid, which expands through a turbogenerator and then passes to a condenser/desuperheater for heat rejection to the environment. The cycle is completed by pumping the fluid up to the maximum cycle operating pressure.

Nonaqueous working fluids with large, low-temperature vapor densities would require smaller turbines than the low-pressure steam turbines employed in flashing systems of the same power output. This is particularly true where heat rejection conditions of 30° C. or less exist. Flashing cycles are, of course, simpler because they do not require a primary heat exchanger.

Seven working fluids in addition to water were examined. Refrigerants R-22 ($CHClF_2$), R-600a (isobutane, i-C_4H_{10}), R-32 (CH_2F_2), R-717 (ammonia, NH_3), RC-318 (C_4F_8), R-114 ($C_2Cl_2F_4$) and

Estimating The Energy Worth of an HDR Reservoir

One approach to estimating HDR reservoir performance makes the assumption that a certain fraction η of the recoverable power could be realized by extraction with a uniform flow of working fluid across the face of an ideal plane fracture. By solving a transient problem of one-dimensional heat conduction from the rock into the fracture face — the recoverable power P(t), in joules per second (J./sec.), for uniform flow can be expressed as follows *(see* McFarland and Murphy *and* Wunder and Murphy *in "Further Reading"):*

$$P(t) = \eta \dot{m}_w C_w (T_i - T_{min}) \operatorname{erf}\left(\sqrt{\frac{(\lambda\rho C)_r}{t}}\,\frac{\pi R^2}{\dot{m}_w C_w}\right)$$

where:

$A = \pi R^2$ = area of one face of the fracture (m^2)
C_w = heat capacity of water = 4200 J./kg. K
C_r = heat capacity of granite = 1000 J./kg. K
$\dot{m}_w$ = water mass flow rate through the fracture (kg./sec.)
R = fracture radius (m)
t = time (sec)
T_i = mean initial rock temperature (° C.)
T_{min} = fluid reinjection temperature (° C.)
erf = error function; for example, erf (z) =

$$\text{error function of } z = \frac{2}{\sqrt{\pi}}\int_0^z e^{-x^2}dx$$

λ_r = thermal conductivity of granite = 3.0 W./mK.
ρ_r = rock density ≈ 2,500 kg./m^3

McFarland and Murphy compared P(t) to estimated values that could result from nonuniform flow across the accessible fracture area. Fluid buoyancy and convection effects within an ideal fracture as well as transient conduction of heat through the surrounding rock are treated in a numerical solution of four coupled two-dimensional, nonlinear, partial differential equations describing continuity, fluid momentum, and rock and fluid energy balances. Depending on the location and separation of fluid injection and recovery points within the fracture and the internal fracture permeability (gap width versus radius), the recovered fraction of power η may vary from 0.4 to 0.9 depending on the degree of buoyant circulation through the fracture.

The equation shows that the relative power [P(t)/ P(t=0)] depends directly on the error function of:

$$\left[K\frac{R^2}{\dot{m}_w\sqrt{t}}\right]$$

for constant rock and fluid properties, where

$$K = \pi\sqrt{\frac{(\lambda\rho C)_r}{C_w^2}}$$

Thus, predictions of reservoir lifetime can be made for specified ideal fracture sizes and flow rates.

For cases where large stable fractures cannot be produced, smaller multiple parallel fractures may be used to generate the required surface area to maintain an acceptable reservoir lifetime. Wunder and Murphy and Gringarten, et al. have examined the heat extraction capacity of such multiple fracture systems to determine the effects of variable fracture number and spacing. Because of the low thermal conductivity of granite, the thermal drawdown will resemble that for a single fracture as shown in the graph below if fractures are spaced 50 m. or more apart. Wunder and Murphy also treat an intermediate case with 1 m. spacing between fractures where there is a strong superposition of heat flow between fractures and a very different drawdown behavior. In the extreme case of completely rubblized rock, a square temperature wave would propagate through the reservoir, showing a breakthrough effect similar to that anticipated for water-drive type systems. In this case, the lifetime $\bar{\tau}$ of the reservoir would be given by:

$$\bar{\tau} = \frac{\rho_r C_r A L\left\{(1-\theta) + \dfrac{\rho_w C_w}{\rho_r C_r}\theta\right\}}{\dot{m}_w C_w}$$

where:
L = separation distance between fractures (m)
θ = porosity

In addition, Harlow and Pracht, using a simplified model, showed that substantial enhancement of reservoir performance could be anticipated because of thermal stress cracking, the fracturing of reservoir rock by temperature-induced stresses. Such thermal stress cracking is not well understood even under well-defined laboratory conditions. L.A.S.L. will use its reservoir at the Fenton Hill field test site to identify *in situ* thermal stress effects. Theoretical work on thermal stress cracking, continued over the past years at Northwestern University by S. Nemat-Nasser, L. M. Keer and associates, and at L.A.S.L. by H. D. Murphy, D. W. Brown and others, has produced new ideas. It is hoped that the extraction of heat from fractured HDR reservoirs may introduce secondary thermal cracks, which will be wide enough to permit convective circulation of fluid; this enhanced circulation will greatly increase the heat removal rate, accelerating the propagation of the cracks, and producing an "autocatalytic" effect. Eventually, another set of orthogonal cracks may form along the surface of the first set of deep cracks, enhancing further the performance of the reservoir. Accurate knowledge of *in situ* reservoir heterogeneities and stresses will be required in order to predict the required cooling for crack initiation and the resulting growth rates of this series of thermal cracks. — *R.G.C., G.E.M., J.W.T., and R.L.B.* □

R-115 (C_2ClF_5) were selected because they provided a range of critical temperatures and pressures, and molecular weights. All of these compounds have relatively high vapor densities compared to water at temperatures as low as 20° C.

Detailed calculations of binary-fluid Rankine cycle configurations were performed to examine the effects of cycle operating pressure, heat rejection temperature, temperature differences in the primary heat exchanger and condenser, turbine and pump efficiencies, and fluid temperature. In each case a utilization efficiency η_u was determined which related the actual electrical work produced by the cycle to the maximum work (or availability) possible with specified geothermal source and heat rejection temperatures. Comparisons were also made with single and multistage steam flashing cycles.

For any given working fluid, there is an optimum set of operating conditions yielding a maximum utilization efficiency for particular geothermal fluid and heat rejection temperatures and turbine and pump efficiencies. In screening potential working fluids, some knowledge of the magnitude of the utilization efficiency and how it changes would be useful. Computer optimizations for the seven working fluids studied were conducted for geothermal fluid temperatures ranging from 100 to 300° C. One observes a characteristic maximum efficiency at a particular resource temperature, which is different for each fluid but generally in the range of 60 to 70 per cent assuming an approach (pinch point) temperature difference of 10° C. between the countercurrently flowing geothermal and cycle working fluids in the primary heat exchanger, an 85 per cent dry turbine stage efficiency, and an 80 per cent feed pump efficiency.

Component efficiencies of this magnitude have been achieved in units of 50 megawatts of electrical output (MWe.) or greater capacity. However, binary-fluid turbogenerators have not as yet been placed in commercial geothermal operation with units of greater than about one MWe. capacity even though smaller units have been operated. Power generation from geothermal, solar, as well as waste heat sources using nonaqueous working fluids will continue to evolve in the coming years under private and public support, and it is not anticipated that any serious problems will exist in scaling-up from the existing 60 kWe. to 1 MWe. units currently available.

The selection of optimum plant design conditions becomes more complex as reservoir temperature declines. Performance is severely curtailed when the plant operates below the wellhead or reservoir temperatures for which it was designed.

A geothermal power plant is very sensitive to changes in conditions for heat rejection. H. E. Khalifa of Brown University estimates that the power output from a geothermal plant would vary by ±32 per cent with fluctuations of ±15° C. in ambient temperature. S. L. Milora and J. W. Tester note a similar effect; their calculations show that with a 200° C. liquid resource, a decrease in condensing temperature from 49° to 27° C. increases the potentially available work by as much as 40 per cent. Thus, because of the inherently low efficiency of geothermal cycles operating with wellhead temperatures below 300° C., a premium is placed on optimizing cycle performance by utilizing lower ambient temperatures when and where environmental conditions permit.

To increase efficiency, pressure losses throughout the system must be minimized, as they will affect pumping requirements and therefore costs. These losses are caused by friction in piping, well casing, or within the fracture itself, and by form drag losses at the entrance and exit regions of the fracture in each wellbore. Based on our experience at the L.A.S.L. Fenton Hill test site, the impedance within the fracture system itself and at the entrance and exit regions will probably produce the largest pressure losses. While such fracture system pressure losses are wholly controlled by the complexity of formation characteristics, other losses can be minimized. For example, friction in piping can be reduced by increasing piping diameters. And pressure losses can be partly offset by the net gain in buoyancy between the cold injection and hot recovery wellbores.

As a wellbore is deepened and reservoir temperatures rise, downhole mineral solubility and reaction

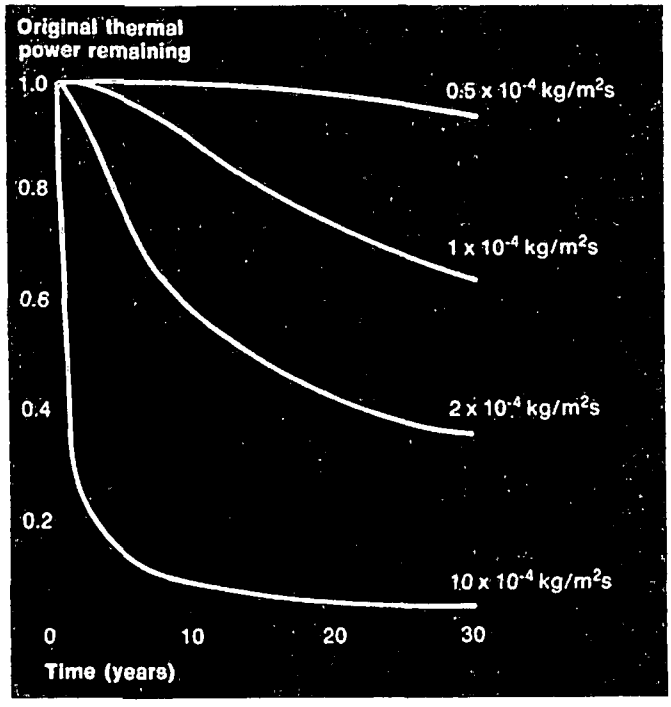

Left: The four curves show different power drawdown (cooling) rates for a hypothetical geothermal reservoir consisting of a single fracture in granite. The greater the ratio of the flow rate divided by the fracture surface area the more rapidly the reservoir cools down. No thermal stress cracking is assumed in the model.

Refrigerants having greater vapor densities than water at low temperatures could be used to power smaller turbines than are required in steam systems, and have comparable or higher overall utilization efficiencies for geothermal fluid temperatures of 100 to 300° C. Seven refrigerants were analyzed to determine operating conditions under which they were thermodynamically most efficient for a specified geothermal temperature. (For details see Milora and Tester, *Geothermal Energy As a Source of Electric Power*, M.I.T. Press, Cambridge, Mass., 1976.)

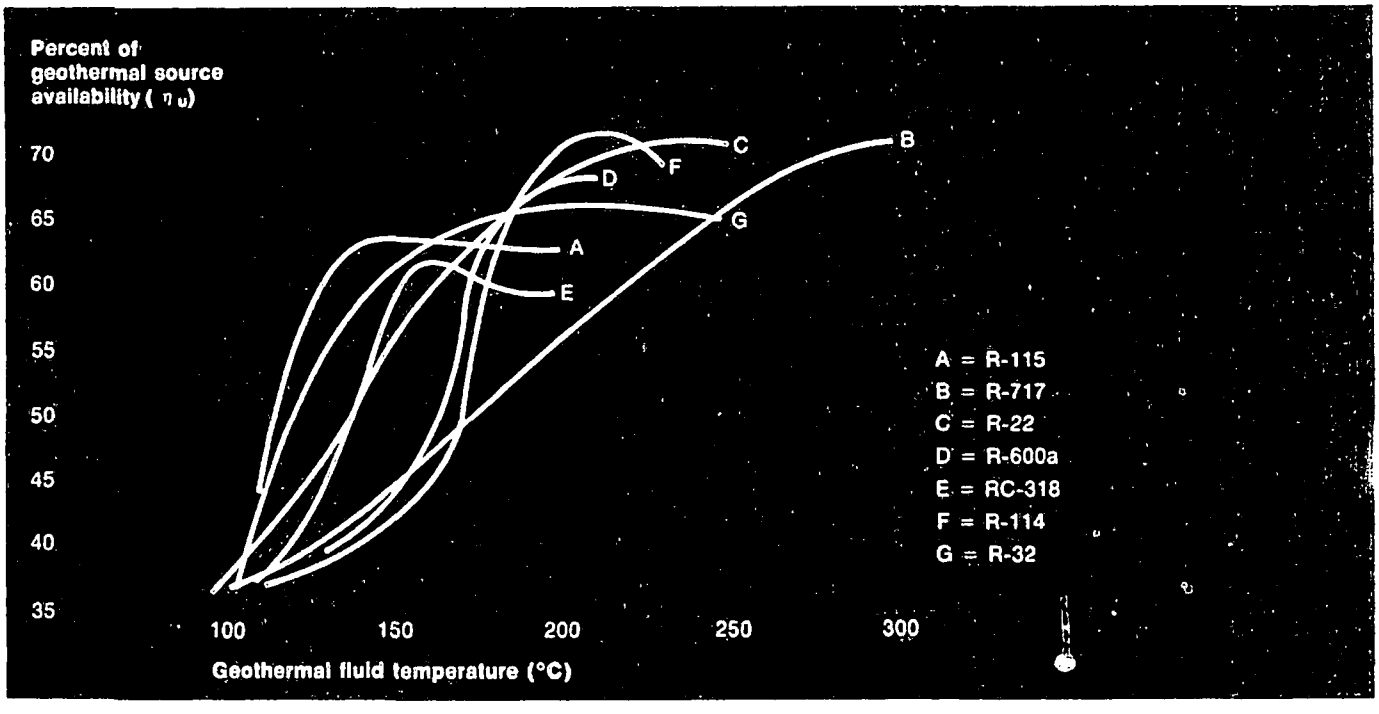

Base Case Conditions
Life of the system = 30 years
Length of time in a decision period = 5 years
Electric plant capacity = 50 MW(e).
Radius per fracture = 300 m.
Maximum well flow rate ($\dot{m}$) = 75 kg./sec.
Fractures per pair of wells = 12
Horizontal fracture spacing = 50 m.
Geothermal gradient = 40° C./km.
Busbar price of electricity = 3 cents/kWh.
Real cost of equity capital = 6% (12% nominal)
Real cost of debt capital = 3% (9% nominal)
Operation and maintenance costs = 0.13 cents/kWh.
Revenue tax = 0.07 cents/kWh. (2.5% of busbar price)
Joint federal and state income tax rate = 51%

These are the base-case parameter values used in the optimization model to evalute hot dry rock (HDR) energy for the production of electricity. The number of fractures were selected to assure that reservoir temperature drawdown does not significantly affect system efficiency; this is equivalent to assuming that sufficient heat transfer area existed to maintain geothermal fluid temperatures within ten per cent of their original design value through the thirty-year lifetime projected for such a plant. Capital costs are referred to as "real" because they are exclusive of the investors' anticipated rate of general price inflation.

rates increase, and the chemical composition of the geothermal fluid may change. Consequently, the potential for corrosion and particularly for silica and carbonate scaling increases. These chemical effects vary with each site and formation so that their economic impact must be evaluated separately for each case.

The Environmental Impact of HDR Operation

The operation of an HDR system should have minimal effect on the environment for several reasons:

☐ The entire fuel cycle is located at the power generating station, in contrast to energy cycles based on oil, gas, coal, and nuclear sources.

☐ Liquid and gaseous effluents should be essentially nonexistent for HDR systems, which are intended to operate in a closed cycle (except for the injection of makeup water).

☐ If water chemistry problems such as corrosion or scaling exist, some treatment may be required and solid effluents (removed deposits) may result. But these should not present a serious environmental impact; for example, a 100 MWe. plant might produce 1 to 10 tons per day of silica or calcium carbonate material.

☐ Although water loss through permeation in the reservoir formation may be a strong economic factor, particularly in arid regions, aquifer contamination is highly unlikely due to the extreme depths of postulated HDR fracture systems — typically 3 to 5 km.

The major environmental concern with HDR systems is seismicity induced by injected fluids. The first extensive test at the L.A.S.L. Fenton Hill test site failed to produce any seismic events (threshold Richter 0.5) that could be detected by surface seismic arrays that surrounded the experiment. The propagation of thermal cracks in rock of this type in a large earth stress field is inherently stable, and we do not anticipate any serious seismic effects to occur. After the system is shut down, the reheating of the cooled section of the reservoir will occur in a quiescent fashion.

Modeling the Economics of HDR Technology

A complete evaluation of producing electricity with HDR technology must include both conventional cost accounting and financial aspects and the unique resource and engineering considerations associated with geothermal systems. *(See "Estimating the Energy Worth of an HDR Reservoir," p. 67.)* We have incorporated these factors — and their effects on capital costs, operating costs, revenues, taxes, and other financial issues — into an intertemporal optimization computer model, which is used to determine the best management strategy for an integrated HDR system of wells, fractures and electric power plant. The model is then used to demonstrate, on the basis of the present value of net benefits (net benefits after taxes and minimal profits) the reservoir design, geothermal well flow rate, and geothermal gradient value that might make HDR-produced

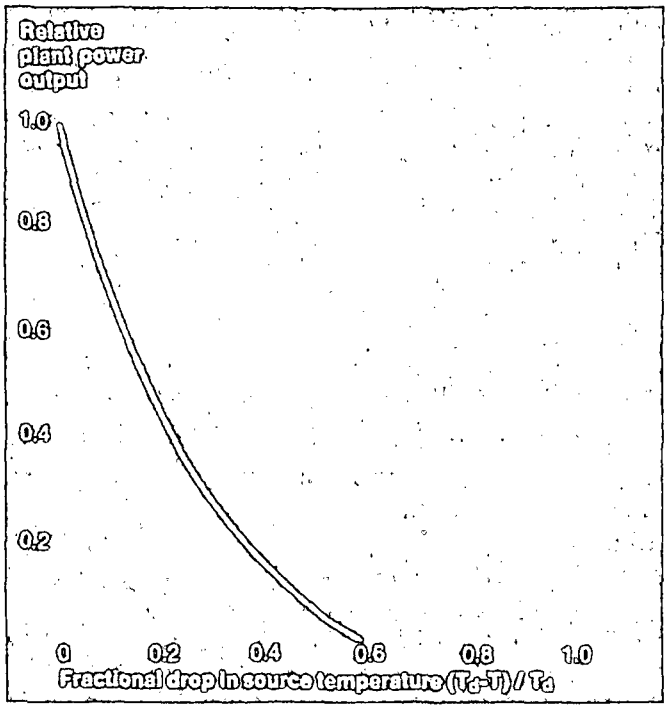

The power output of an HDR geothermal generating plant declines as the reservoir temperature drops below the design temperature. This graph illustrates the decline, plotted against "fractional source temperature drop," which is the difference between design temperature and actual temperature divided by design temperature.

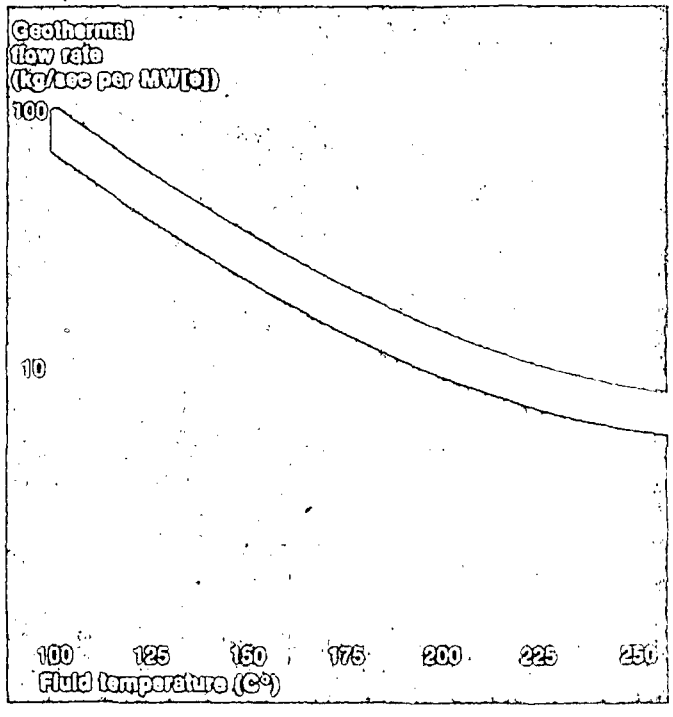

To produce a given amount of electric power, less geothermal fluid is required as the reservoir temperature increases.

electricity commercially competitive in the United States.

Among the variables subject to control in the model are the operating well flow rate, initial drilling depths, and periodic redrilling. Parameters in the model include installed capacity, geothermal gradient, design temperature and design well flow rate for the electric generating plant, and reservoir size (which for the purpose of this paper is varied with the design well flow rate to insure negligible temperature drawdown simultaneously). The effects of design well flow rate and geothermal gradient on costs were examined. Various economic considerations are also specified, for example, a thirty year plant life is assumed and a selling price for electricity at the busbar is set alternatively at three or four cents per kilowatt-hour (kWh.) The table on the opposite page lists the conditions for the base case run of the model.

Given values for geothermal gradient and the price of electricity at the beginning of each decision period (a "decision period" in this case is a five year time interval), the model calculates the present value of net benefits associated with all combinations of operating flow rate and drilling strategies and chooses the combination that maximizes the present values of these net benefits over the life of the system. *(See "Modeling Geothermal Opportunities" on p. 73; a complete specification of this dynamic programming model is given by the authors in an internal L.A.S.L. report, August, 1978.)*

Results from the model indicate, for various

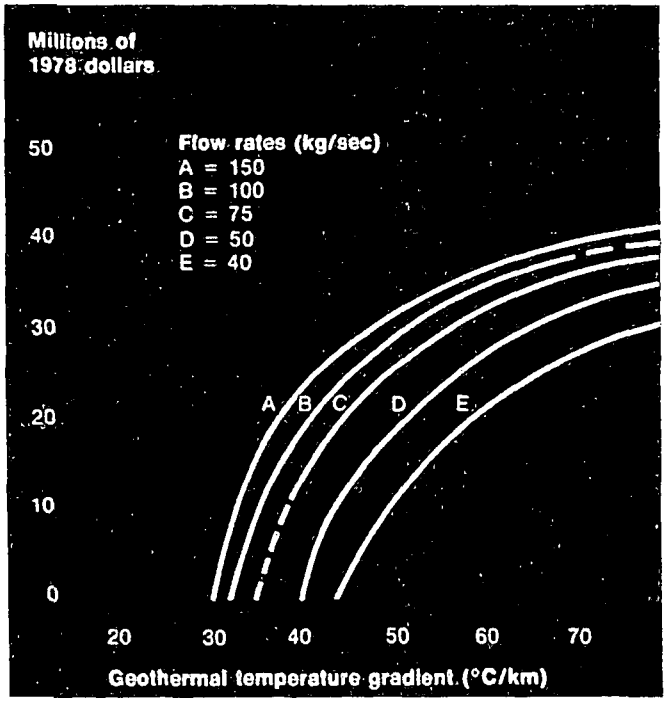

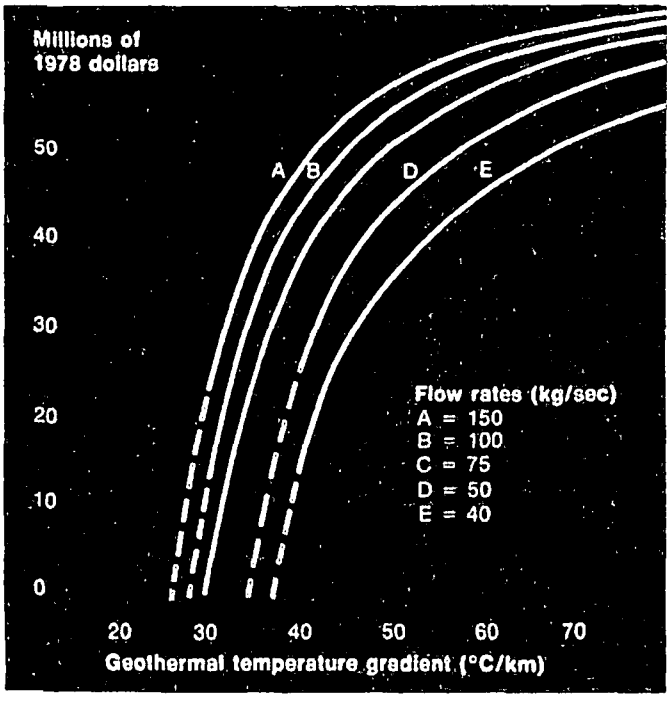

combinations of parameter values, whether the optimally managed HDR plant is commercially attractive or not. For example, with electricity priced at three cents per kWh. at the busbar, a design well flow rate of 40 kilograms per second (kg./sec.), and a geothermal gradient of 40° C. per kilometer (° C./km.), an HDR electric generating facility might lose $9.2 million over its lifetime. But with that same gradient and well flow rates between 50 and 105 kg/sec (all other parameters unchanged) the present value of net benefits from the investment would range from $1 million to $22.8 million. All costs presented are in constant 1978 dollars.

The analysis for reservoirs having negligible temperature drawdown with all other technical issues resolved can be generalized as follows:

☐ In areas with geothermal temperature gradients of 50° C./km. or higher, HDR-produced electricity is commercially feasible *regardless* of the well flow rate (in the range of 40 to 150 kg./sec.) at busbar costs of three cents/kWh.

☐ In areas with a geothermal temperature gradient of 40° C./km., a well flow rate of 40 kg./sec. would require a busbar cost greater than three cents/kWh. for a positive present value of net benefits; however, with flow rates in the range of 50 to 150 kg./sec., HDR-produced electricity would be commercially feasible with busbar costs of three cents/kWh.

☐ In areas with gradients between 20° and 30° C./km., HDR-produced electricity would result in busbar costs that are higher (most likely, *much* higher) than three cents/ kWh. for all well flow rates in the range of 40 to 150 kg./ sec.

☐ In areas with gradients of 40° C./km. or higher, HDR-produced electricity would be commercially competitive at busbar costs of four cents/kWh. for all flow rates.

As the temperature gradient increases, shallower, less expensive wells are required. Consequently, at various design flow rates, the net financial benefits of a typical plant would improve with increasing geothermal gradients. At the top is shown the present value of net benefits of an optimally managed HDR system for a range of geothermal temperature gradients and various design flow rates, assuming a busbar price of three cents; at the bottom is shown the present value of net benefits when the busbar price is four cents/kWh. These figures were generated by an intertemporal computer optimization model developed by the authors.

□ Where gradients of 30° C./km. are available and at flow rates of 75 kg./sec. or more. HDR generation is economically feasible with busbar costs at or above four cents/kWh.

An additional perspective for the relative costs of HDR-produced electricity may be obtained as follows. For a 50 MWe. plant in areas with a 50° C./km. gradient, the present value of total capital costs (wells and power plant) range from $2130/kWe. to $1560/kWe. as the maximum well flow rate varies from 40 kg./sec. to 150 kg./sec. Other economic analyses for hydrothermal systems have shown similar ranges of capital costs for wells and power plants. This compares with plant costs (not including fuel) of $500 to $700/kW. for coal and $1000/ kW. or more for nuclear plants now under construction in the United States. In HDR systems, one then accepts higher initial investment costs in return for lower future fuel costs relative to more conventional technologies.

As an alternative approach to describing feasibility, consider that for a given set of resource and reservoir conditions, including type of formation, geothermal gradient, fracture size, and design flow rate, there exists an optimal management strategy of drilling, redrilling, and plant operation that will result in a minimum "breakeven" price. This breakeven price would generate revenues just sufficient to cover all costs, including taxes and returns to investors and lenders at specified real rates. The graph on p. 74 presents this breakeven price as a function of geothermal gradient and design well flow rate, assuming negligible temperature drawdown. At higher gradients and flow rates, a busbar price of *less than two cents/kWh.* is sufficient to earn the six per cent real rate of return which was specified in the model.

Referring to the lower figure on p. 74, the minimum breakeven price of HDR-produced electricity described above is very sensitive to the assumed real rate of return. As real rates of return for equity and debt increase from the 6 per cent/3 per cent used in the base case rise to 17 per cent/6 per cent, the breakeven price rises from 2 cents/kWh. to around 5.5 cents/kWh.

Finally, it is interesting to note the effect of the

Modeling Geothermal Opportunities

The model employed in this research requires as input basic information about the HDR system under consideration. It then determines the optimal time path of management decisions for this system, where optimal is defined as that management strategy which maximizes Φ, the present value of net benefits where net benefits are defined as net revenues after taxes and minimal profit. This objective is expressed mathematically as:

$$\text{Maximize } \phi = \sum_{n=1}^{N}\left[\sum_{t=1}^{\tau}(R_{n,t})\,(1+r)^{-t}\right].$$

$$-\left\{C_s + \sum_{n=1}^{N} C_d(1+r)^{-\tau(n-1)} + .51\right.$$

$$\left[\sum_{n=1}^{N} C_d(1+r)^{-\tau(n-1)} - \frac{C_d}{(1+r)^{\tau N}}\right]$$

$$\left. - .51\,C_s\left[\frac{(1+i)^{\tau N}}{(1+r)^{\tau N}} - \frac{1}{(1+r)^{\tau N}}\right]\right\} \quad \text{where:}$$

N = the number of decision periods over the assumed life of the HDR system
τ = the number of years in a decision period
r = the opportunity cost of capital (real rate of return)
i = the real debt rate of interest
$R_{n,t}$ = revenues net of revenue tax and operating cost for the t^{th} year of the n^{th} decision period (1978 dollars)
C_s = surface plant costs (1978 dollars) discounted to present value at year 0 (start of plant operation)
C_d = drilling costs (1978 dollars)

This equation is structured so that the system is examined at each decision period. After systematically exploring the ramifications of each management option for every state of the system, the model selects that option which maximizes the objective function. By doing this for all decision periods over the life of the system, it arrives at a determination of the optimal time path of such decisions and, hence, the most economic way of operating.

In this formulation, revenues and costs are discounted to the beginning of electricity production or plant operation ("the present") by an appropriate discount rate and then the difference between revenues and total costs is calculated. The present discounted value of revenues is the double summed term just to the right of the equality in the equation. The present discounted value of costs (in braces) is composed of separate terms for surface costs, drilling costs, income taxes on equity, and income tax *credits* on interest payments to debt holders. As implemented in the model, however, the composition of the terms presented in the equation is more elaborate than this description alone suggests. — *R.G.C., G.E.M., J.W.T., and R.L.B.* □

The busbar price of electricity is critical in determining the profitability of an HDR power plant. Assuming the temperature drawdown of the reservoir is negligible over the lifetime of the plant, the commercial operation would break even financially along the two curves shown in the graph. The higher curve represents a design flow rate of 40 kg./sec.; the lower curve, 150 kg./sec. At higher geothermal gradients, both flow rates could yield profits with a busbar price under three cents/kWh.

Bottom chart:
The sensitivity of busbar price to differing equity rates of return and debt rate of interest under base case conditions is shown. Nominal rates of return and interest were computed by adding the estimated rate of general price inflation to these real value rates.

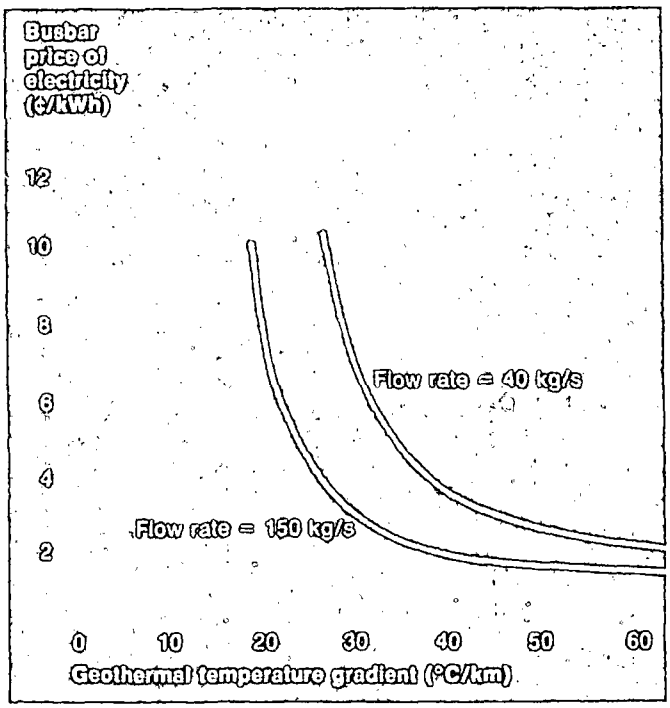

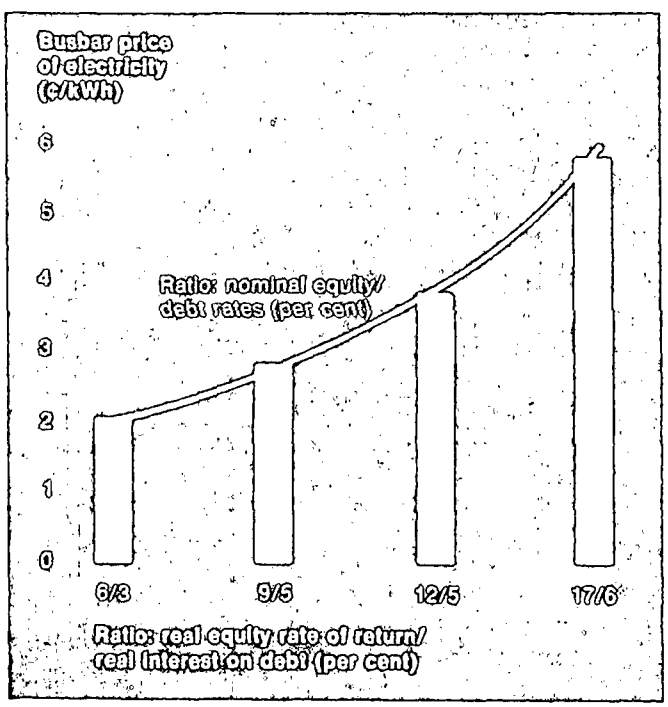

geothermal gradient on the optimal drilling depth and the associated drilling costs. As one would expect, the higher the geothermal gradient, the shallower is the optimal drilling depth. In fact, drilling costs decline more than in proportion to the increase in geothermal gradient. For example, total drilling costs per pair of wells, excluding surface piping and contingency factors, fall from $4.7 million in a 30° C./km. gradient area to $1.1 million in a 60° C./km. gradient area — a doubling of the gradient results in a 76 per cent decline in total drilling costs.

Conclusion: "Guarded Optimism"

As is usual with a technology in a relatively infant stage, definitive statements concerning feasibility must await further development and demonstration. It is encouraging at this point, however, to see that electricity production from HDR resources would seem to be commercially competitive in numerous areas of the United States using economic and reservoir parameter values which, at least at this point, seem "reasonable" to many involved engineers and economists. There are no simple answers and each issue must be treated in detail before the question of commercial feasibility for HDR can be settled.

The analytical results presented in this article are based on a very limiting set of assumptions as to HDR reservoir parameters and designs. Clearly, considerably more experimental and economic research is required before a definitive assessment of the commercial feasibility of HDR-produced electricity can be made. Within this limited context, however, the results provided here suggest grounds for at least guarded optimism as to the possible feasibility of HDR-produced electricity in areas of the United States with temperature gradients in the 40-plus °C./km. range and where "competitive" busbar costs are approximately three cents/kWh. or higher.

Variations in the reservoir design and operating parameter values as well as financial and regulatory criteria used in this paper could markedly influence the potential competitiveness of HDR-produced electricity. As examples, abnormally high plant costs (caused by poor geofluid quality), higher discount (interest) rates, and particularly, increased rates of temperature drawdown or reservoir water losses would decrease the relative attractiveness of HDR-produced electricity. However, advances in drilling technology, lower taxes (via depletion type allowances) and allowing deductions for intangible drilling expenses, investment tax credits, and perhaps system design to accommodate cogeneration or process heat plants might well extend the commercial feasibility of HDR to lower gradient areas.

Certainly another factor that will control the rate of commercial development of HDR, or for that matter all geothermal development, is the current cost and availability of busbar power from more con-

ventional sources such as coal and nuclear fission. In many cases, due partly to environmental and regulatory restrictions, coal-fired and nuclear plant costs have escalated to a point where $500–700/kW. for coal and $1000/kW. or more for nuclear are now commonplace. To these costs add the rapidly rising fuel costs for coal and enriched uranium. A reasonable range for busbar prices for new capacity in 1985–90 might be from 3 to 6 cents/kWh. (in constant 1978 dollars). If busbar costs are at the high end, a considerable incentive for HDR development would exist.

Further Readings

Altseimer, J. H., "Technical and Cost Analysis of Rock-Melting Systems for Producing Geothermal Wells," Los Alamos Scientific Laboratory Report LA-6555-MS, Los Alamos, N.M., November, 1976.

Blair, A. G., et al., "L.A.S.L. Hot Dry Rock Geothermal Project," Los Alamos Scientific Laboratory Report, LA-6525-PR, Los Alamos, N.M., 1976, and LA-7109-PR, "Hot Dry Rock Geothermal Energy Development Project, 1978.

Costain, J. K. L. Grover, III, and A. K. Sinha, "Evaluation and Targeting of Geothermal Energy Reservoirs in the Southeastern United States," Progress Report, Nov. 1, 1976–March 31, 1977, Virginia Polytechnic Institute Report VPI-SU-5103-3, Blacksburg, Va. 1977.

Cummings, R. G., et al., "Electricity from Hot Dry Rock Geothermal Reservoirs: An Economic Analysis," internal report from the Resource Economics Program, U. of New Mexico, Albuquerque, August, 1977.

Diment, W. H., et al., "Temperatures and Heat Contents Based on Conductive Transport of Heat," in "Assessment of Geothermal Resources of the United States–1975," *U.S. Geological Survey Circular 726*, Reston, Va. 1975.

Energy Research and Development Administration Report ERDA-76-1, "National Plan for Energy Research, Development, and Demonstration," U.S. Government Printing Office, Washington, D.C., 1976.

Eskesen, J. H., "Cost and Performance Comparison of Flash Binary and Steam Turbine Cycles for the Imperial Valley," in *Proceedings of 12th Intersociety Energy Conversion Engineering Conference*, Washington, D.C., August, 1978, Vol. 1, p. 842.

Grieder, R., "Economic Considerations of Geothermal Exploration in the Western United States," presented at the Symposium of the Colorado Department of Natural Resources, Denver, Colo., Dec. 1973.

Gringarten, A. C., et al., "Theory of Heat Extraction From fractured Hot Dry Rock," *Journal of Geophysical Research*, Vol. 80 (1975), No. 8, p. 1120.

Hankin, J. W., R. A. Hogue, R. A. V. Cassel, and T. R. Fick, "Effect of Reservoir Temperature Decline on Geothermal Power Plant Design and Economics," in *Proceedings of 12th Intersociety Energy Conversion Engineering Conference*, Washington, D.C., August, 1978, Vol. 1, p. 870.

Harlow, F. H. and W. E. Pracht, "A Theoretical Study of Geothermal Energy Extraction," *Journal of Geophysical Research*, Vol. 77 (1972), No. 35, p. 7038.

Holt, B. and E. L. Ghormley, "Energy Conversion and Economics for Geothermal Power Generation at Heber, California, Valles Caldera, New Mexico, and Raft River, Idaho–Case Studies," Electric Power Research Institute Report EPRI ER-301, Palo Alto, Calif., Nov. 1976.

Khalifa, H. E., "Effect of Seasonal Variations of Ambient Temperatures on the Performance of Low Temperature Power Cycles," Brown University Report COO/4051-10, CATMEC/19, Providence, R.I., June, 1978.

Kruger, P. and C. Otte, *Geothermal Energy*, Stanford, Calif., Stanford University Press.

McFarland, R. D. and H. D. Murphy, "Extracting Energy from Hydraulically-Fractured Geothermal Reservoirs," in *Proceedings of 11th Intersociety Energy Conversion Engineering Conference*, State Line, Nev., 1976.

McGetchin, T. R., *ed.*, "Hot Dry Rock Geothermal Energy: Status of Exploration and Assessment," Report No. 1 of the Hot Dry Rock Assessment Panel, ERDA-77-92, Washington, D.C. (in press).

Milora, S. L. and J. W. Tester, *Geothermal Energy as a Source of Electric Power*, M.I.T. Press, Cambridge, Mass., 1976.

Murphy, H. D., "Thermal Stress Cracking and the Enhancement of Heat Extraction from Fractured Geothermal Reservoirs," Los Alamos Scientific Laboratory Report LA-UR-78-917, April, 1978.

Nemat-Nasser, S., "Minimum Spacing of Thermally Induced Cracks in Brittle Solids," The Technological Institute, Northwestern University, Evanston, Ill. (to be published).

Nemat-Nasser, S., "Thermal Cracks and Their Effects on the Heat Extraction Process," The Technological Institute, Northwestern University, Evanston, Ill. (to be published).

Nemat-Nasser, S., L. M. Keer, and K. S. Parihar, "Unstable Growth of Thermally Induced Interacting Cracks in Brittle Solids," Earthquake Research and Engineering Laboratory Technical Report No. 77-9-2, Northwestern University, Evanston, Ill., Sept., 1977.

Raleigh, C. B., et al., "Multiple Hydraulic Fracturing for the Recovery of Geothermal Energy (abstract)," *E.O.S. Transactions*, American Geophysical Union, Vol. 55, No. 4, p. 4026, 1974.

Ramachandrian, G., et al., "Economic Analysis of Geothermal Energy Development in California," Vol. 1, Stanford Research Institute Report ECU 5013, Menlo Park, Calif., May, 1977.

Rex, R. W., "The U.S. Geothermal Industry in 1978," presented at the Hot Dry Rock Geothermal Information Conference, Santa Fe, N.M., April 19–20, 1978.

Schapiro, A. R. and G. P. Hajela, "Geothermal Power Cycle Analysis," in *Proceedings of 12th Intersociety Energy Conversion Engineering Conference*, Washington, D.C., August, 1978, Vol. 1, p. 857.

Smith, M. C., et al., "Man-Made Geothermal Reservoirs," in *Second United Nations Geothermal Energy Symposium*, San Francisco, Calif., pp. 1981–1787, 1975.

Smith, R. L. and H. R. Shaw, "Igneous-Related Geothermal Systems," in *Assessment of Geothermal Resources of the United States – 1975, U.S. Geological Survey Circular 726*, Reston, Va., 1975.

Starling, K. E., L. W. Fish, K. Z. Iqbal and H. H. West, "The Use of Mixture Working Fluids in Geothermal Power Plants," in *Proceedings of 12th Intersociety Energy Conversion Engineering Conference*, Washington, D.C., August, 1978, Vol. 1, p. 850.

Tester, J. W., *ed.*, "Phase I — Energy Extraction Field Test Results from the Fenton Hill Hot Dry Rock Geothermal System — Segments 1–2," Los Alamos Scientific Laboratory Report (to be published).

Tester, J. W., et al., "Solution Chemistry and Scaling in Hot Dry Rock Geothermal Systems," in *Proceedings of 83rd National Meeting of A.I.Ch.E.*, Houston, Tex., March 21-25, 1977.

Tester, J. W. and M. C. Smith, "Energy Extraction Characteristics of Hot Dry Rock Geothermal Systems," in *Proceedings of 12th Intersociety Energy Conversion and Engineering Conference*, p. 816, August, 1977.

White, D. F. and D. L. Williams, *eds.*, *Assessment of Geothermal Resources of the United States — 1975, U.S. Geological Survey Circular 726*, Reston, Va., 1975.

Wunder, R. and H. D. Murphy, "Thermal Drawdown and Recovery of Singly and Multiply Fractured Hot Dry Rock Reservoirs," Los Alamos Scientific Laboratory Report LA-7219-MS, April, 1978

Ronald G. Cummings is professor of economics at the University of New Mexico, and a visiting staff member to the Los Alamos Scientific Laboratory, where the work reported in this article was done. He was the chairman of the Department of Food and Resource Economics at the University of Rhode Island from 1972–1975 and has held appointments with Resources for the Future, Montana State University and the Kansas Water Board. His degrees (in economics) are from the University of Missouri (B.S., M.A.) and the University of Kansas (Ph.D., 1968). Glenn E. Morris, an economist at Los Alamos Scientific Laboratory since 1975, is currently attached to its Energy Systems and Economic Analysis Group. He holds a B.A. degree (1967) from the University of Connecticut and M.A. (1974) and Ph.D. (1977) degrees from the University of Colorado. Jefferson W. Tester is leader of the Geothermal Technology Group at Los Alamos; he was assistant professor of Chemical Engineering at M.I.T. and Director of the M.I.T. School of Chemical Engineering Practice for several years after receiving his Ph.D. at the Institute in 1971. In addition to his current work in hot dry rock geothermal energy, he has research interests in applied thermodynamics, process design, heat and mass transfer, surface chemistry and physics, and electrochemistry. Robert L. Bivins, a staff member at Los Alamos since 1953, worked in the Theoretical and Computing Divisions before joining the Energy Systems and Economic Analysis Group. He received the B.S. degree from the University of Washington in Seattle in 1952.

The authors acknowledge assistance from R. M. Potter, A. W. Laughlin, and A. C. Eddy in preparing the HDR resource description. R. Hageman and J. McFarland contributed to the computational aspects of the model development, and A. Blair and M. C. Smith reviewed the manuscript. The support of the Division of Geothermal Energy of the U.S. Department of Energy is gratefully acknowledged.

Hot Dry Rock: Widespread But Invisible

Exploration for hot dry rock (HDR) as a potential geothermal resource presents some novel problems and unusual contradictions not to be expected in exploration for other geological resources. This became apparent at a meeting held on June 22, 1976, at Los Alamos Scientific Laboratory (LASL) on the subject of Exploration Methods for Hot Dry Rock. Unlike the case of petroleum or mineral prospecting the search for HDR is not for a region of strong chemical contrasts that are displayed as contrasts of physical properties. Rock suitable for HDR technologies has relatively weak geological manifestations and is almost geophysically invisible on a local scale; it is not so susceptible to direct detection as is, say, a gas reservoir. Thus we must look at related manifestations and for patterns more than for hot dry rock itself.

The indirect nature of exploration for HDR follows directly from the heat extraction technology. In the method of energy extraction being developed at LASL a large crack is created in hot basement rock by hydraulic fracturing at the bottom of a drill hole; a second hole is drilled to intersect the crack (see figure). Water is pumped down one hole, is heated in its passage through the crack, and returns through the second hole to the surface as steam or hot water for power generation, industrial process heat, or a source of domestic heat. Although the crack must be located in nearly impermeable material to prevent loss of water, thermal contraction cracking or other events that enhance the amount of rock surface exposed to fluid are beneficial because they improve heat transfer in the system. At the LASL test site at Fenton Hill in northern New Mexico there has been a successful demonstration of the ability to adapt oil field methods to achieve controlled directional drilling and hydrofracture in hard crystalline rock. Innovative downhole seismic methods have revealed the location and orientation of the crack. Thus a new energy technology has been created.

However, heat extraction, as is true for any geothermal technique, requires a certain set of physical conditions. For electrical power production from HDR the main conditions are temperature in the range of 200°–400°C and a region of very low permeability to fluid flow (10^{-6} darcy or less). The question for exploration is, How and where do we find such a set of physical conditions? The first aspect of this question involves locating a region of thermal concentration, which is a problem common to geothermal exploration in general. Thus characterizing the thermal regime of the Cascade Range would conceivably be beneficial for a variety of geothermal applications. However, the second aspect involves finding volumes of rock within the region where permeability is low. This aspect is somewhat more elusive because an equally hot fractured zone containing steam or water, for which another technology would be appropriate, could be adjacent to an HDR zone. Hence the second aspect of prospecting becomes one of identifying different physical properties at depth. The region of the Valles Caldera in New Mexico affords an example of a geothermal region possessing different geothermal possibilities based upon contrasting physical properties: the porous wet interior of the caldera is being investigated as a steam producer, while the substantially impermeable basement rock at Fenton Hill, just outside the caldera, is the location of the Los Alamos HDR test site.

Geological Methods

On all scales of exploration from local (~1 km) to regional (~100 km), geological observations provide obvious diagnostic features. Virtually all geothermal sites developed so far were selected in regions showing evidence of recent volcanism. But the HDR requirement for low permeability forces attention away from the relatively fractured and open rock in the centers of volcanism to the borders of the region where volcanic heat has penetrated but the rock is less disturbed. Thus volcanism is only an indirect indicator of HDR. In addition to Quaternary volcanism and young calderas, faulted zones, perhaps at the boundaries between geological provinces like the Sierra Nevada and the Basin and Range, were suggested by B. Slemmons (University of Nevada) as other indirect HDR indicators. These zones can be upward conduits for magmas; the relatively large unfractured blocks between fractures,

This meeting report was prepared by F. G. West and T. J. Shankland of the Geological Research Group at the Los Alamos Scientific Laboratory, Los Alamos, New Mexico.

as in the Basin and Range Province, could be large thermal energy reservoirs. On a local scale, hot springs point to heat reservoirs, but the depth to impermeable rock is uncertain.

Heat Flow

Heat flow is of course a highly apparent manifestation of a geothermal source and is applicable on all scales of exploration. But here too the obvious target, namely, the highest heat flow, is not likely to define a region exploitable by HDR technology. D. Blackwell (Southern Methodist University) pointed out that heat flows in excess of 5×10^{-6} cal cm^{-2} s^{-1} (210 mW/m^2) were almost invariably produced by a hydrothermal system. Indeed, heat flow at the LASL test site on the west flank of the Valles Caldera is only 3.7 $\times 10^{-6}$ cal $cm^{-2}s^{-1}$; yet a usable temperature of 200°C has been encountered at 3-km depth. Heat flows in the range 2-4 $\times 10^{-6}$ cal cm^{-2} s^{-1} are more likely to be suitable indicators; these may be found on the flanks of larger anomalies that may be hot wet rock (HWR) geothermal systems.

J. Costain (Virginia Polytechnic Institute and Virginia State University) remarked on two indicators of HDR suitability that apply to eastern North America. One is high heat production, which occurs in the northern Appalachians; with moderate sediment-blanketing a temperature of 200°C can be attained at 6-km depth if the heat production is of the order of 10-20 $\times 10^{-13}$ cal cm^{-3} s^{-1} (4-8 $\times 10^{-6}$ W/m^3). Another indicator is the presence of a low-conductivity sedimentary blanket, which occurs along the Atlantic coastal plain; with little fluid migration to remove heat the basement rock beneath the sediment can become warm even with near-normal heat flow.

Seismic Studies

Seismic methods also are better suited for indirect definition of a thermal regime, because the thermal changes at some boundaries of a suitable HDR region are too gradual to present a sharp interface for reflection or refraction. As an example on a local scale, profiling can locate the boundaries of the interior of a caldera that is too permeable for HDR technology; outside, the caldera is presumably more competent, still hot rock, but how the temperature field decays away with distance from the crater is seismically uncertain. (Here, numerical models of heat intrusion can be especially valuable.) S. Solomon (Massachusetts Institute of Technology) pointed out the seismic indicators of high temperatures on a regional scale, particularly surface wave dispersion and the delayed arrivals of P_n and S_n waves that travel in the upper mantle. K. Aki (Massachusetts Institute of Technology) described the use of three-dimensional block models of crustal and mantle velocities that have been used with inversion theory to obtain evidence for high temperatures and partial melt beneath regions like Yellowstone. From the standpoint of HDR prospecting such methods should be viewed as contributing to a definition of the regional thermal pattern, since they do not directly locate hot dry rock. Finally, the patterns of seismicity in a region must be examined; the relatively high seismicity that maintains an open

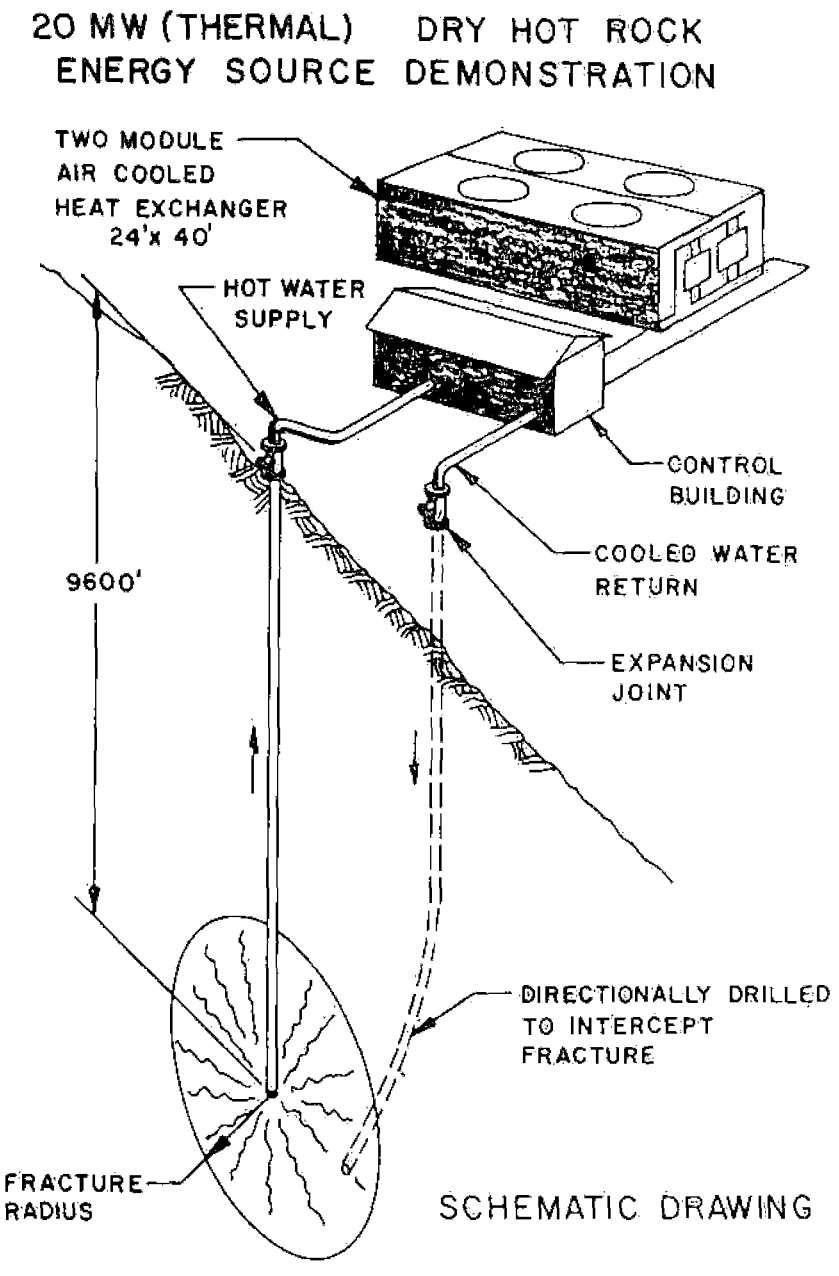

Components for geothermal heat extraction from hot dry rock

crack system in most HWR geothermal systems is undesirable where low natural permeability is a requirement. In conclusion, although seismic techniques do not directly locate high-temperature rock on a local scale, they do help define regions of suitable physical properties, and they can help locate deeper high-contrast magma bodies in the lower crust on a larger scale.

Electromagnetic Methods

As D. Word (Geotronics) emphasized, there is an enormous contrast, up to 6 orders of magnitude, between the electrical conductivities of crustal rocks that are wet or dry and hot or cold; electromagnetic methods can exploit this contrast. A. Duba (Lawrence Livermore Laboratory) mentioned the need for more and better electrical conductivity measurements; for instance, there are no conductivity measurements in water-saturated rocks at temperatures above 65°C. He illustrated the much higher conductivity of molten versus solid basalt but pointed out that much of the conductivity rise occurs about 100°C below the solidus, apparently as a result of disordering of albite, and that some caution must be used in interpreting existing measurements. However, a region of HDR, because of its low total porosity and permeability and its moderate temperature, is likely to be electrically elusive. G. Keller (Colorado School of Mines) observed that a low-conductivity zone of $\sigma \approx 10^{-3}$ S/m beneath a more moist and conductive surface layer will be hard to detect; however, he indicated that higher-power current-generating systems would more successfully induce currents in a deeper, resistive layer and that time-domain electromagnetic sounding (TDEM) is a sensitive diagnostic.

J. Hermance (Lamont-Doherty Geological Observatory and Brown University) spoke about a magma body as a 'first-order geothermal target' for electromagnetic exploration; the high conductivity of a partial melt makes it especially visible to magnetotelluric (MT) and geomagnetic deep sounding (GDS), and there are suitable conductivity models for partial melts to obtain a geotherm from a known conductivity distribution. Again, the evidence is indirect; one looks not for hot dry rock at 3-km depth but for a magma body at 10–30 km. D. Stanley (U.S. Geological Survey) described the use of MT to locate a low-conductivity region (Island Park) by its contrast with Yellowstone and the Raft River high-conductivity zones on either side. Because the region is between two hydrothermal areas, it could satisfy requirements for HDR exploitation and not interfere with the 'plumbing' of Yellowstone Park itself.

Gravity Methods

On a regional scale, of the order of 100 km, indications from gravity measurements may be useful to HDR exploration. C. Aiken (Texas Christian University) computed residual Bouguer anomalies for Arizona using regional trends of topography as the reduction datum in order to eliminate long-wavelength (about 1100 km) correlations of topography with Bouguer anomalies. Negative residual anomalies correlate with magnetic anomalies, P wave delays, and heat flow, all of which relate to probable temperature variations in the crust and upper mantle.

Exploration

Exploration strategies can be sorted out on several different scales, a matter which Solomon and Hermance addressed in detail. The largest or reconnaissance scale for studying temperature distributions would consider dimensions of about 1000 km with the goal of locating broad areas having systematically high temperatures in the crust and upper mantle. At this resolution a great deal is known about North America in a qualitative way, but much more quantitative data are needed. Useful studies at this stage include gravity, heat flow, upper mantle velocities and attenuation, and electrical conductivity.

Many of the same methods are applicable on a regional scale at a resolution of tens to hundreds of kilometers. Geological criteria become especially useful, as do electromagnetic surveys with techniques like MT or TDEM that penetrate sufficiently deep into the crust to identify concentrations of anomalously high crustal temperatures, for example, from an intruded magma body.

At the local scale of site selection, 10 km or less, the goal is selection of possible drilling locations. Sites would be selected within regions on the basis of intensively applied methods already mentioned. On this scale, HDR itself affords few direct manifestations and must be located by indirect indicators: away from active faulting, at the edges of zones of recent intrusion, in localities of moderate but not the highest heat flow, adjacent to crustal conductivity anomalies, and inside seismically stable blocks. In short, it is the pattern of geothermal and geological activity that is the object because HDR itself is hard to perceive.

In a world that must accelerate geothermal development, exploration cannot proceed from large to small scale in a sequential manner; research continues at all scales in any case, but quantitative data are needed at each level if geothermal energy is to be exploited. An ideal goal would be mapping of the depth to the 200°C isotherm. At whatever scale this is done, the results would be of tremendous interest in every part of geophysics, in addition to being essential to all types of geothermal development.

Conclusions

All participants emphasized the importance of using a variety of exploration techniques to assess HDR regions. Further, calibration of such techniques in zones of known geothermal interest is an essential stage. Hot dry rock lies near one end of a range of geothermal possibilities. At one extreme are the vapor-dominated, high-temperature systems, like the Geysers, California, or Wairakei, New Zealand, that are well adapted to existing power technologies. These areas are relatively rare and sometimes found beneath national parks; to halt the action of Old Faithful as a result of thermal extraction as happened to the original Geysir in Iceland would provoke a justifiable public out

cry. At the other extreme is low-grade heat of far wider distribution that is suitable for process heat and domestic heating. Thus should municipal heating networks be developed, then 60°C temperatures would be adequate. Should a technology exist for using 'moist' and permeable regions of lower grade than presently developed hydrothermal systems, then it is important to know where these regions are and how to distinguish them from HDR and HWR.

Accompanying the ranges of technologies is a range of prospecting techniques. Unlike fossil fuel or ore prospecting methods that basically search for chemical concentrations, the goal of geothermal exploration is to characterize the thermal environment by using physical properties to describe variations in the thermal regime. HDR prospecting can be seen as one aspect, required by a particular technology, of mapping of crustal temperature distributions whose description will ultimately benefit all geothermal technologies. Therefore great incentives exist to improve our knowledge of the thermal regimes of the crust and upper mantle.

Acknowledgment

This meeting was supported by the Division of Physical Research of the Energy Research and Development Administration.

Land Subsidence Symposium

The Second International Symposium on Land Subsidence was held in Anaheim, California, December 13–17, 1976. Organized by the AGU within the framework of Unesco's International Hydrological Program, it was sponsored jointly by the International Association of Hydrological Sciences, International Association of Hydrogeologists, International Society for Soil Mechanics and Foundation Engineering, U.S. National Committee for Scientific Hydrology, and Unesco.

Papers presented ranged from mathematical modeling studies through general descriptions of project progress and subsidence case histories to legal and economic aspects of subsidence. The program was very broad in scope, covering theory, investigation, measurement, prediction, and control of subsidence, including land-surface sinking resulting from withdrawal of water, oil, or gas, dewatering of organic deposits, hydrocompaction, extraction of solids by mining, and collapse of limestones.

The symposium was preceded by a 2-day field trip which took participants to points of subsidence, hydrologic, geologic, historical, agricultural, and sociological interest in the Santa Clara and San Joaquin valleys; these areas have the largest magnitude and most widespread man-induced subsidence in the world caused by a great diversity of factors. During the symposium, participants visited the large subsidence area (approximately 10 meters in depth) in Long Beach resulting from pumping of oil, took a boat trip to one of the artificial islands created for the oil wells and the injection wells used to prevent further subsidence, and toured the Los Angeles County Flood Control District's injection well barrier project.

Brief summaries of all technical papers were published in a preprinted program booklet. The full technical papers presented at the symposium will be published as an IAHS proceedings volume. Several additional papers, as well as road log, were published in the preprinted field trip guide. A small supply of both the program booklet and the field trip guide are still available at a cost of $2 and $5, respectively. Orders for either of these publications should be sent directly to the Treasurer, International Association of Hydrological Sciences, 1909 K Street, N.W., Washington, D. C. 20006.

Members of the organizing committee of the Second International Symposium on Land Subsidence. Front row (left to right), R. T. Bean, A. I. Johnson, S. Yamamoto, B. E. Lofgren, and H. L. Koning. Back row, E. G. Figueroa Vega, R. R. Parizek, J. C. Stephens, J. F. Poland, and D. R. Allen.

This report was prepared by A. I. Johnson of the U.S. Geological Survey, Reston, Virginia.

Geothermal Resources Council, TRANSACTIONS, Vol. 3 September 1979

HEAT-FLOW CONTINUATION -- A METHOD TO DELINEATE GEOTHERMAL RESERVOIRS

Charles A. Brott, Teledyne-Geotech, Garland, Texas 75043
David D. Blackwell, Southern Methodist University, Dallas, Texas 75275
Paul Morgan, New Mexico State University, Las Cruces, New Mexico 88003

ABSTRACT

Preliminary work on sourceward continuation of heat-flow data has been initiated with the objective of delineating geothermal reservoirs. A straightforward method of continuation of conductive heat flow in a homogeneous isotropic medium is developed. The method utilizes the surface heat-flow data to estimate a subsurface temperature distribution from which isotherms are constructed. The basis for geothermal reservoir delineation is that the reservoir may be treated as a heat source; thus, subsurface isotherms converge around reservoirs. The spatial limits and behavior of the reservoir can in some cases be defined by the constructed isotherms.

INTRODUCTION

The parameter which is essential for a geothermal resource to exist is heat. Since heat-flow studies directly measure heat, this data set is selected for the delineation of geothermal reservoirs. The basic assumption underlying the delineation is that the heat source producing the heat-flow anomaly in geothermal regions is the reservoir. This assumption implies that heat flows from the reservoir to the surface; thus, isotherms must converge about the reservoir.

If the temperature of a reservoir is uniform, its configuration can be determined precisely by the shape of that isotherm. If the reservoir is related to heat-generation variations, then interpretation of its configuration is more complicated. Isotherms would still converge about the reservoir, and the spatial limits of its boundary could be determined.

A major problem in determining subsurface temperature distribution from heat-flow data is the diffusion of heat flow. Estimation of subsurface temperatures based on simple extrapolation of the surface geothermal gradient is erroneous because of the lateral flow of heat. Continuation is the correct method to calculate subsurface temperatures because it takes into account the spatial spreading of heat.

Continuation methods have been described for gravity and magnetic data by Grant and West (1965, Chapter 8). Although the steady-state heat-flow equation is very similar to the equations for gravity and magnetics, most continuation methods cannot be applied to heat-flow data, because heat-flow data have an additional boundary condition of uniform surface potential (the surface temperature) which does not apply to gravity and magnetic data. Therefore, new techniques have to be developed for the continuation of heat-flow data. In this paper, preliminary work on heat-flow continuation by Brott et al. (1979) is presented. The continuation method is limited to cases where refraction of heat due to thermal conductivity contrast is not present.

CONTINUATION METHOD

The continuation of heat flow is based on a fundamental potential field property: outside of a volume containing sources, the field, once defined, is unique. Even though there is a family of source solutions that will generate the same field, outside the volume of the sources the field is the same. Thus, any source solution satisfying the surface heat-flow field (or geothermal gradient field, if the thermal conductivity is uniform) can be used to define any of the field parameters outside the volume of the source. The source distribution used in this continuation method is a series of line sources or point sources for the two-or three-dimensional cases, respectively. The assumptions used in this method are that (1) the heat-transfer method is conductive; (2) there is a homogeneous isotropic medium with no heat generation between the sources and the surface; and (3) the sources are constant and continuous.

For a homogeneous isotropic medium, the transient heat-conduction equation is:

$$\kappa \nabla^2 T = \frac{\partial T}{\partial t} , \qquad (1)$$

where κ = diffusivity, ∇^2 is the Laplacian differential, T = temperature, and t = time. At steady-state, this equation degenerates into the Laplacian equation:

$$\kappa \nabla^2 T = 0 . \qquad (2)$$

The gradient is the negative partial derivative with respect to the vertical (z):

$$g = \frac{\partial T}{\partial t} . \qquad (3)$$

The solutions for the steady-state and time-dependent temperatures and gradients for the point and

line sources are given in Carslaw and Jaeger (1959, Chapters 10 & 14). These solutions can be written in two terms, a source term and a distance term. The steady-state solutions are shown in Table 1.

TABLE 1. Steady state, $\kappa \nabla^2 = 0$

Temperature (T) = (source term) · (distance term)

Gradient (g) = (source term) · (distance term)

For two-dimensional case (line source):

$$T = (Q/4\pi\kappa) \cdot (-2 \ln (R))$$

$$g = (Q/4\pi\kappa) \cdot (2(z-z')/R^2)$$

For three-dimensional case (point source):

$$T = (Q/4\pi\kappa) \cdot (1/R)$$

$$g = (Q/4\pi\kappa) \cdot ((z-z')/R^3)$$

Individual solutions can be superimposed since they are the solutions of second-order equations. This property allows a complex gradient field to be represented by the sum of the effects of many simple sources. This property can be exploited through the method of images to obtain a constant surface temperature. The use of the line and point sources is illustrated in the following example.

Consider the two-dimensional model at the left side of Figure 1. The gradients are known at points P_1 and P_2. The parameters needed to calculate the gradient distance terms (Z_3 and X_3) are also known. The image sources S_1' and S_2' are the images of the sources S_1 and S_2. An equation can be written for each gradient; thus, the source terms can be evaluated by solution of a series of simultaneous equations. These same sources may also be used to solve for the temperatures at any point. For example, the temperature at point P_3 can be determined, since the vertical distance Z_3 and the horizontal distance X_3 are known (Table 1 and the right side of Figure 1).

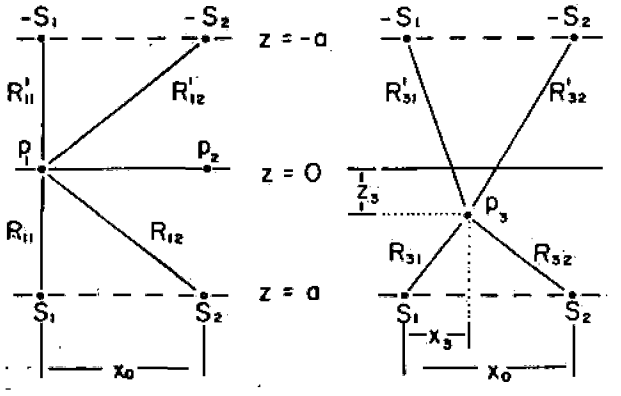

FIGURE 1. Geometry of the continuation method.

Two-Dimensional Fault Model. Figure 2 shows a two-dimensional model of 100°C water circulating along a fault which dips at 45° (represented by the herringbone pattern). The model has a constant background gradient of 54°C/km and a uniform surface temperature of 15°C. The mathematical model was computed by a finite difference technique, and subsurface isotherms (represented by the solid lines) were constructed. The surface geothermal gradient profile is shown above the model.

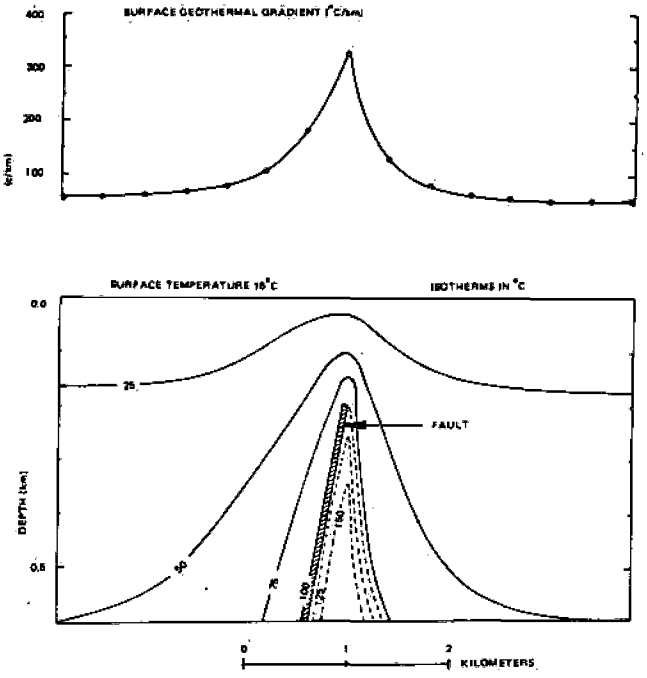

FIGURE 2. Steady-state fault model.

A subsurface temperature distribution was calculated using the two-dimensional (line source) continuation technique and surface gradient, and assuming steady-state. Isotherms were constructed from this temperature distribution. The 25°C, 50°C and 75°C isotherms constructed closely follow the isotherms of the numerical model (Figure 2). The left side of the calculated 100°C isotherm corresponds to the left side of the fault, but the right side (dashed line) diverges from the fault. Isotherms greater than 100°C calculated using the continuation technique occur below the 100°C isotherm (dashed line). By continuation of the temperature field below the top of the circulating 100°C water along the fault (0.2 km), one of the basic continuation premises was violated; thus, the solutions below this depth are not valid.

Continuation of the surface gradient profile of this two-dimensional model demonstrates the possibility of "simple reservoir" delineation in a combined problem of convection and conduction. The circulating 100°C water is transporting heat by convection along the fault, but elsewhere in the model, heat transfer is by conduction. The solution is not unique, because any of the constructed isotherms can be used to define the upper part of a corresponding "simple reservoir." In order to determine which isotherm defines the actual reservoir, knowledge of the temperature or depth of the reservoir is needed. However, the depth to the reservoir can be estimated by applying the half-width rule to the surface gradient profile. Using

this depth (approximately 0.25 km), the temperature of the source would be between 100°C-125°C.

Marysville, Montana. The Marysville geothermal area is characterized by high heat flow (up to 19.5 HFU, top part of Figure 3), a negative gravity anomaly, high electrical resistivity, low seismic ground noise, and nearby microseismic activity (Blackwell and Morgan, 1976). The heat-flow anomaly appears to be bounded to the northeast by the subcrop of a Mesozoic granodiorite body (the Marysville stock shown in Figure 3), and a fault has been located along the south side of this stock. Data from a 2.1 km deep-test well (represented by the derrick in Figure 3) indicate that the anomaly is caused by hydrothermal convection along fracture zones distributed in a Cenozoic granite porphyry. Maximum temperatures of about 98°C were measured in the test well, and the system appears to be a "simple" reservoir with a temperature of approximately 95°C.

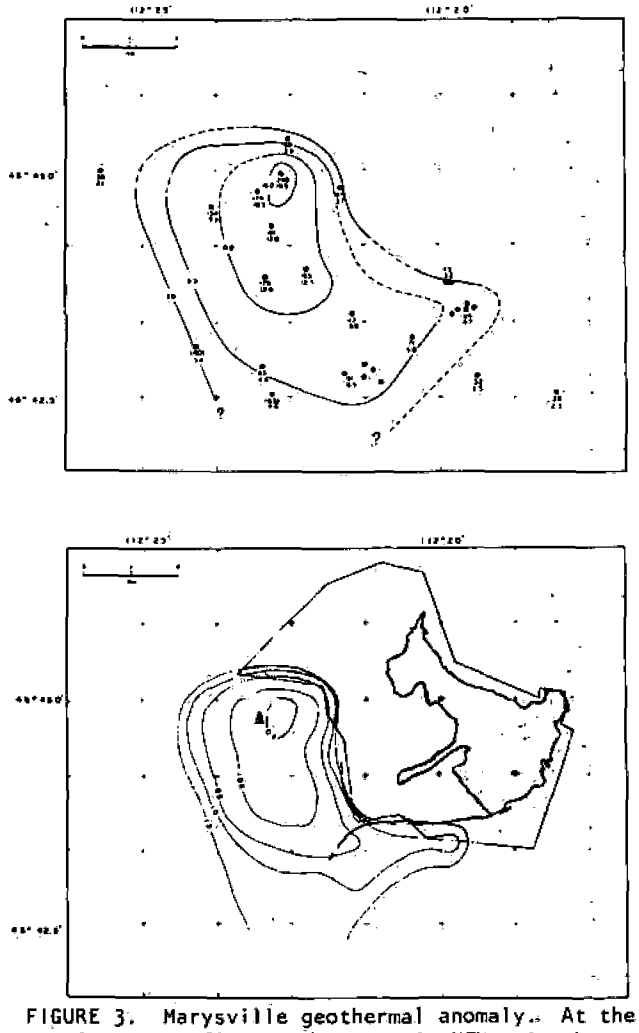

FIGURE 3. Marysville geothermal anomaly. At the top is a heat-flow contour map in HFU. At the bottom is the constructed 95°C isotherm at a depth of 0.4-1.2 km, at intervals of 0.2 km.

The heat-flow data from the Marysville anomaly were continued sourceward, using steady-state point sources. The lower part of Figure 3 shows the contours of the 95°C isotherm between 0.4-1.2 km, at intervals of 0.2 km. The 95°C isotherm is interpreted as defining the geothermal reservoir. Very steep sides for the reservoir are indicated on the north and northeast, with relatively steep sides on the south and southwest, and a complex shape on the south and southeast. The shape of this narrow southeastern salient suggests that its origin may be geothermal fluid moving along a narrow zone, such as a fault. The salient may represent the subsurface extension of the mapped surface fault.

Simple extrapolation of the surface heat-flow data to map the 95°C isotherm results in a set of contours similar to the heat-flow contours. The fine detail of the reservoir is not delineated and no indication of the narrow east-west salient can be obtained by extrapolation of the 3.0 HFU contour. This example clearly illustrates the value of the continuation technique in interpretation of surface heat-flow data.

Mesa, Imperial Valley, California. The Mesa geothermal anomaly is located on the eastern flank of the Salton trough, the sediment-filled structural depression that forms the northern extension of the Gulf of California and the East Pacific Rise. Geophysical and geochemical surveys all outline the anomaly, which covers 40 km, and has a maximum heat flow in excess of 7 HFU (top of Figure 4). Five deep wells have been drilled into the anomaly. Their locations are given in Figure 4 as 31-1, 5-1, 6-1, 8-1, and 6-2. The results of the deep drilling and surface geophysics are summarized by Swanberg (1974).

The geothermal anomaly at Mesa appears to be caused by a complex reservoir, as indicated by temperature-depth data from the deep wells. Three of the wells (6-1, 8-1, and 6-2) become isothermal at temperatures in the range of 175°C-200°C, whereas the other two wells (31-1 and 5-1) become isothermal at around 100°C and 150°C, respectively. Thus the reservoir cannot be assumed to be delineated by a single isothermal surface.

The surface heat-flow contours were used for sourceward continuation. The resulting contours of the 75°C-175°C isotherms at 25°C intervals, at a depth of 0.8 km, are shown at the bottom of Figure 4. The 100°C and greater contours indicate the possibility of two shallow reservoirs probably connected at depth. The contour pattern in the northwest part of the anomaly has a complex shape. The 150°C isotherm is shaped like an X. This shape is suggestive of a fault plexus with the major source of the fluid in the northwest part of T16S, R17E. Faults have been mapped along several of the lobes (Combs and Hadley, 1973). Simple extrapolation of the surface heat-flow data would have revealed none of these complexities, but would simply reflect the surface data. The results of the continuation clearly show the anomaly to be related to the result of fluid flow along narrow zones, with a complex relationship existing between these zones.

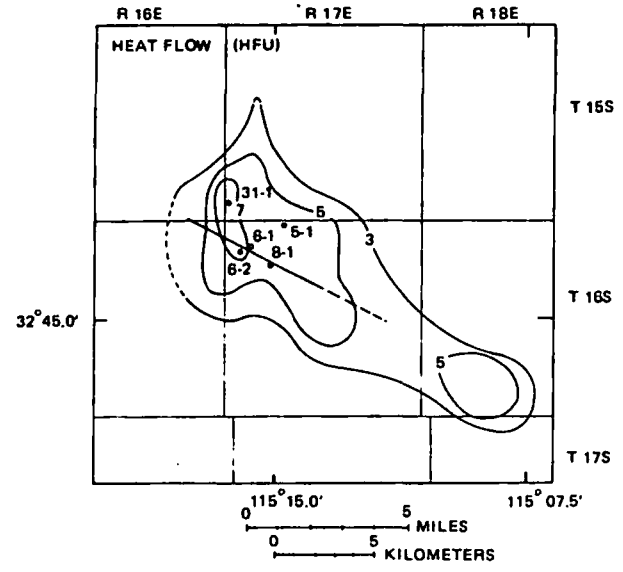

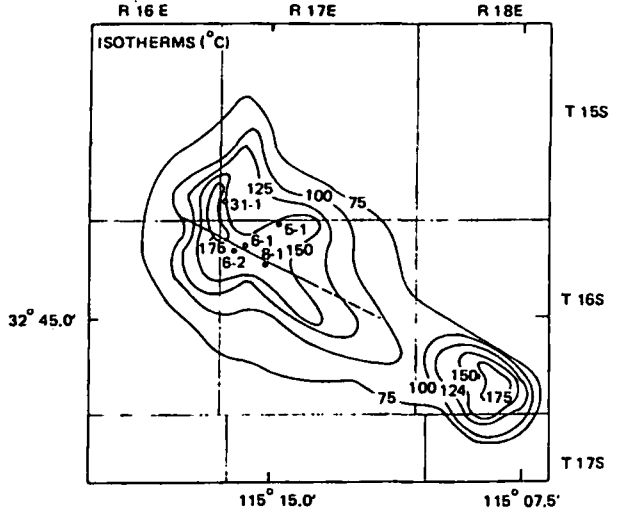

FIGURE 4. Mesa geothermal anomaly. At the top are heat-flow contours (in HFU). At the bottom are isotherms on a plane 0.8 km below the surface.

ACKNOWLEDGEMENTS

The work was supported by National Science Foundation Grant No. HES-74-19550A01 and by U.S. Geological Survey Grant No. 14-08-0001-G-425 to Southern Methodist University.

REFERENCES

Blackwell, D.D., and P. Morgan, 1975, Geological and geophysical exploration of the Marysville geothermal area, Montana, U.S.A., Proc. 2nd U.N. Symp. on Dev. of Geothermal Potential, Washington, D.C., U.S. Govt. Printing Office, p. 895-902.

Brott, C.A., D.D. Blackwell, and P. Morgan, 1979, Heat flow continuation -- a method to construct accurate isotherms in geothermal areas (in preparation).

Carslaw, H.S., and J.C. Jaeger, 1959, Conduction of Heat in Solids, 2nd ed., Oxford, Clarendon Press, 510 p.

Grant, F.S., and G.F. West, 1965, Interpretation Theory in Applied Geophysics, New York, McGraw-Hill Book Co., 584 p.

Swanberg, C.A., 1974, Heat flow and geothermal potential of the East Mesa KGRA, Imperial Valley, California, Proc. Conf. of Res. for Dev. of Geothermal Energy Resources, p. 85-98.

HEAT PUMPS AND GEOTHERMAL

by
Paul J. Lienau
Geo-Heat Utilization Center

Introduction

The basic function of a heat pump is to transfer energy from a low-temperature heat source to a higher temperature medium. This function may be carried out for a range of 50° to 120°F temperatures, although not with the same efficiency. A large heat pump installation for district heating or process heating usually must be specifically adapted to the heat source and the requirements of the heat consumers. Small heat pumps for domestic use are quite standardized, often designed for inexpensive mass production, easy operation, and maintenance.

The heat sources normally used for heat pumps for space heating purposes are the naturally available low-temperature sources, i.e., atmospheric air, various water sources such as rivers, lakes, sea water, ground water within easy reach, soil and solar radiation. The temperatures of these sources fluctuate more or less during the year in accordance with local climatic conditions and with reservoir properties of the source medium. The fluctuations indicate that "solar energy" is the common origin of the sources. Thus, the most obvious drawback of these "solar energy" sources is the mismatch between peak heat demand and decreasing source temperature in the coldest months of the year. Direct solar radiation and air temperature fluctuate most violently and the desirability of these sources is sometimes questionable. It is believed that they will not become realistic possibilities for large heat pumps until the problem of heat storage has been solved effectively.

A natural source of growing interest for heat pumps is geothermal energy. Low temperature geothermal energy (< 212°F) is used for heating purposes by direct heat exchange to the consumers (i.e., via a district heating net). Heat pumps may be employed to extract additional heat by further cooling the geothermal water to temperatures below that of the water returned from the consumers in order to achieve a better utilization of the geothermal resource. Likewise, geothermal temperatures below the heating net supply temperature may be upgraded by the utilization of heat pumps. The main problem with this source is not temperature fluctuation as with the other natural sources, but the difficulty of locating and extracting geothermal water since this may depend on rather expensive deep drilling. Another problem is the development of heat pump evaporators that can withstand the physical and chemical characteristics of geothermal water.

Principles

When the geothermal resource water is below 120°F, most conventional methods of extracting heat from geothermal water become impractical and uneconomical. The 120°F geothermal water still contains a large amount of heat energy and is not the absolute lower limit but is based on typical conditions in which the heating air should be at least 100°F, and a driving force of 20°F is needed to transfer heat across the heat exchanger.

In a residential forced-air heating system, hot air in the temperature range of 100° to 140°F from the heating system is added to the room air to maintain the desired indoor temperature. Absorbing heat from a low-temperature geothermal source of 50° to 120°F and transferring heat to provide 100° to 140°F air temperature might seem impossible when the principle of heat flow from high to low temperature is considered. However, as the name heat pump implies, heat pumps transfer heat or pump heat from a low temperature to a higher temperature medium. The principle is identical to the operation of a refrigerator where heat is removed (pumped) from the colder interior

of the refrigerator and given off to the surrounding room air. A second fluid is used inside the "heat pump machine" called a refrigerant which absorbs heat from geothermal water and transfers this heat to surrounding space. This secondary fluid is the key to the ability of a heat pump to transfer heat from low-temperature sources, and to understand this transfer, some elementary principles of thermodynamics must be considered.

When a refrigerant absorbs heat, it undergoes a change of state from a liquid to a gas at constant temperature, much the same as water changes to steam when heated. The refrigerant will give off heat in the reverse process as it changes from a gas back to a liquid state. If a refrigerant, while in a gaseous state, is brought into a cool surrounding, the refrigerant will condense, giving off heat and raising the temperature of the room.

Pressure is another thermodynamic property important to the operation of the heat pump. A change in pressure of the refrigerant will lower or raise the boiling temperature. Thus, by manipulating the pressure, the refrigerant can be made to either absorb or reflect heat. The refrigerant, under reduced pressure, can absorb heat from a low-temperature source and change to a gas, and at a high pressure, the heat of the refrigerant can be given to a higher temperature substance while changing back to a liquid. Thus, a heat pump refrigerant can absorb heat and become vaporized from a low-temperature geothermal source and transfer this heat to the higher temperature room air by condensing to a liquid.

Figure 2a illustrates schematically a heat pump process and an operational explanation follows:

1) Evaporator. The refrigerant enters the evaporator at low temperature and pressure as a liquid. In the evaporator, low-temperature geothermal water transfers heat to the refrigerant which becomes vaporized. The refrigerant is capable of vaporizing at this low temperature because of its low pressure.

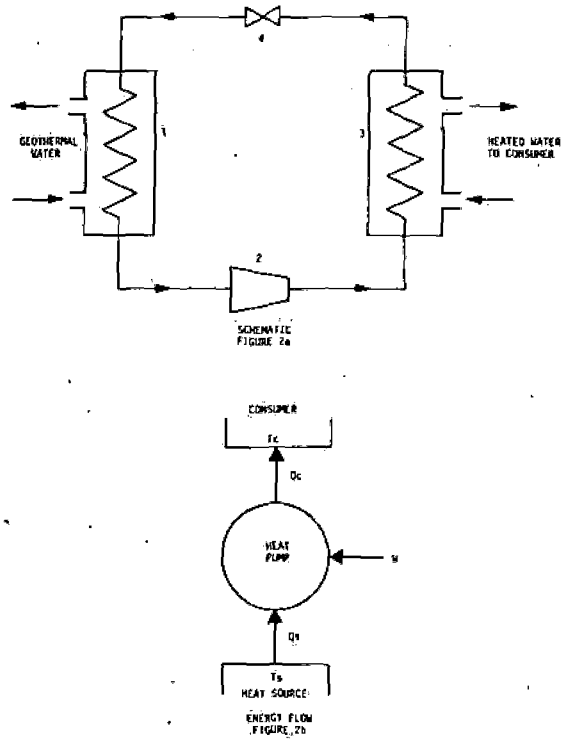

Figure 2. Heat Pump Principle.

2) Compressor. The refrigerant enters the compressor as a gas at low temperature and pressure. Most of the mechanical energy of compression is transferred to the refrigerant, and it leaves the compressor as a gas at high temperature and high pressure.

3) Condenser. The refrigerant enters the condenser as a gas at high temperature and pressure. Heat is given off to the room as the refrigerant condenses to a liquid at high pressure. The refrigerant is capable of condensing at high temperature because of the high pressure.

4) Expansion Valve. The refrigerant enters the expansion valve as a liquid at high pressure and high temperature. As the pressure is reduced, its boiling point decreases and part of the refrigerant is vaporized cooling the remaining liquid. The low temperature-low pressure mixture of gas and liquid enters the evaporator to repeat the cycle.

A requirement for a heat pump is energy (W), usually electrical, to circulate and

compress the refrigerant. But for each unit of electrical energy used, 2, 3, or more equivalent units of heat energy are transferred from the source. By adding the work (W) to a heat pump, the energy Q_S is transferred from the heat source of low temperature T_S to the heat consumer at a higher temperature T_C (Figure 2b). The total energy Q_C delivered to the consumer is

$$Q_C = Q_S + W.$$

The efficiency of the heat pump is the ratio of the energy delivered to the consumer Q_C and the energy supplied to operate the device W, called the coefficient of performance (COP)

$$COP = \frac{\text{energy to consumer } Q_C}{\text{energy to device } W} = \frac{Q_C}{Q_C - Q_S}$$

or

$$Q_C = COP \times W.$$

Thus, with a COP of 3, energy to the consumer Q_C is equal to three times the work energy (electricity) put into the device.

Perhaps at this point, the reader is thoroughly confused on how a heat pump works, so the following excellent hydraulic analogy of COP (Keller, 1977) may be helpful (Figure 3).

Water is collected in a storage tank 60 feet above ground. Piping is connected from this storage tank to a utilization tank at ground level. Another source of water from a tank or well is located 12 feet below ground level and connected such that it can also be pumped into the utilization tank.

Suppose that one gallon of water from the storage tank was released directly into the utilization tank without going through the hydraulic turbine. The work that this gallon of water is capable of doing by dropping 60 feet has been lost, and only one gallon is available at the utilization tank. If another gallon of

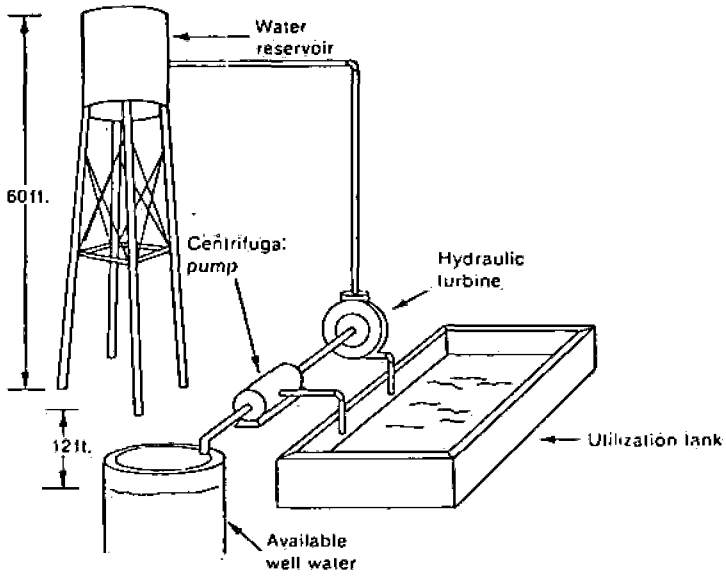

Figure 3. Hydraulic Analogy of COP.

water is released from the storage tank and run through the hydraulic turbine, the centrifugal pump will raise water from the well. If the turbine and centrifugal pump are 100% efficient, one gallon dropped 60 feet will raise five gallons 12 feet, and thus a total of six gallons will now be available in the utilization tank. The analogous COP is 6. Actually, the turbine and pump will not be 100% efficient so something slightly less than five gallons would be transferred.

The value of COP is primarily determined by the temperature ration T_S/T_C. This is most clearly seen with an ideal heat pump operating according to a reversed Carnot cycle. By means of the second law of thermodynamics, it is found that the efficiency COP_{carnot} for such an ideal heat pump forms the upper limit for any heat pump operating between the same temperature T_S and T_C. This upper limit may be expressed:

$$COP_{carnot} = \frac{T_C}{T_C - T_S} = \frac{1}{1 - T_S/T_C}.$$

Thus, the efficiency increases with increasing source temperature level and with

decreasing difference between source and consumer. However, the Carnot process is not realized because of mechanical losses due to friction and heat losses. Figure 4 illustrates a family of curves that enables one to determine the actual COP based upon a given source temperature.

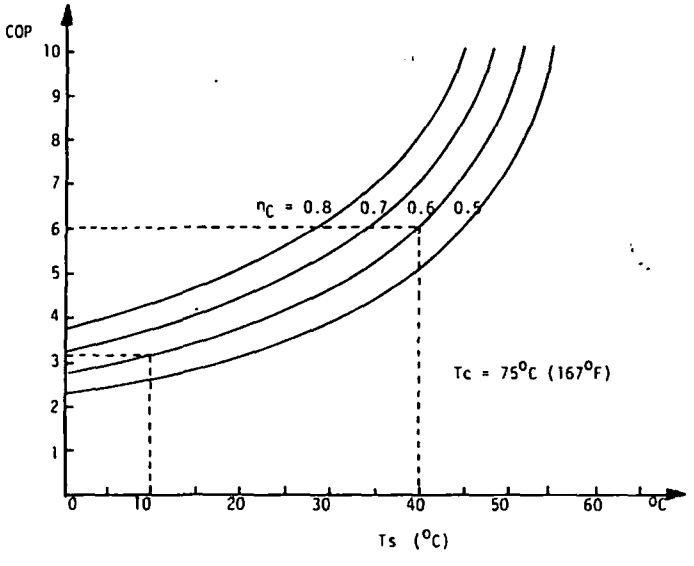

Figure 4. COP vs. Evaporator Temperature T_S.

For large district heating type plants (W > 1 MW) incorporating heat pump values of actual COP (η_C) are 0.6 to 0.7 the ideal. Differences in efficiency are, in part, due to the type of compressor used. Centrifugal compressors are used for the large heat pumps, while reciprocating compressors are usually employed in the smaller residential units. For example, with $\eta_C = 0.6$, $T_C = 75°C$ (167°F) and source temperature $T_S = 10°C$ (50°F ground water for instance), the total heat output will be $Q_C \cong 3.2\ MW_t$ when 1 MW shaft power W is used. If the temperature of the source is $T_S = 40°C$ (104°F, a low temperature geothermal well for instance), the output is raised to $Q_C \cong 6.0\ MW_t$.

Residential Heating

It is estimated that low-temperature shallow geothermal water heat pumps could be used for residential heating and cooling in over 75% of the Continental United States (Gass, 1978). (See Figure 5 on the following page.)

A majority of the 13 million American homes supplied by shallow geothermal water have enough water to meet domestic water and heat pump demands. The 500,000 new homes built annually, which are supplied by domestic wells, could reap significant energy savings (30% to 60%) through the use of ground water heat pumps.

Economic analysis was calculated for a home-heating system in an 1,800-square-foot house in Klamath Falls, Oregon. Costs were calculated for an oil furnace, an electric furnace, a heat pump using existing domestic water, and a heat pump requiring a separate well 300 feet deep and a 100-foot static water level. The economic inflation rate was assumed to be 7%. The inflation rate for electricity was projected to be 8.9% through 1988 and 8.6% thereafter. No. 2 diesel oil was projected to inflate as follows:

Year	Heating Oil
1979-1980	15.4%
1981-1984	7.8%
1985-1989	8.8%
1990-1994	11.3%
1995-2000	11.4%

System costs were as follows:

A	B	C	D	E
Type of System	Capital Investment	20-Year Amortization	First-Year Operating Costs	Total 20-Year Annual Equivalent Costs
Oil Furnace	$2,775	$304	$866	$1,965
Electric Furnace	$1,950	$261	$782	$1,696
Heat Pump Using Domestic Water	$3,640	$487	$261	$967
Heat Pump With Well	$7,760	$905	$261	$1,385

Column A represents the type of system. Column B shows the capital investment required for each system and includes installation costs. Column C amortizes the capital investment at 12% annually over a 20-year period. Column D lists the first-year operating costs. Column E indicates the total 20-year annual equivalent costs and includes capital investment and operating costs inflated at appropriate inflation rates.

Figure 6 on the following page illustrates these costs for the four different heating systems.

The difference in annual equivalent costs between conventional and heat pump systems results because energy, in the form of heat, is being extracted from the ground water at no cost, with the exception of the negligible cost of pumping the ground water at the 10 gpm required by the system. This cost will vary depending on the design of the well and depth to water. For every kilowatt hour of energy

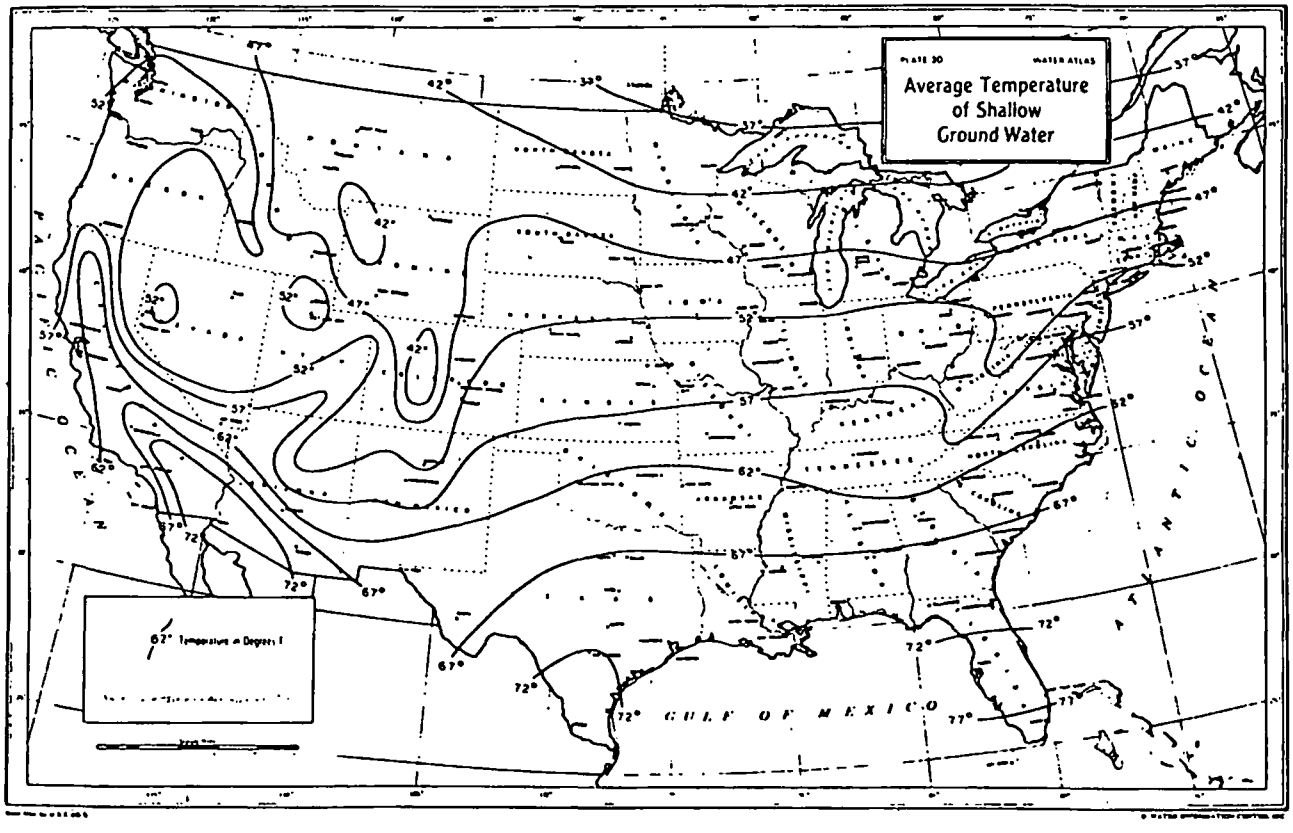

Figure 5. Average Temperature of Shallow Geothermal Water in U.S.

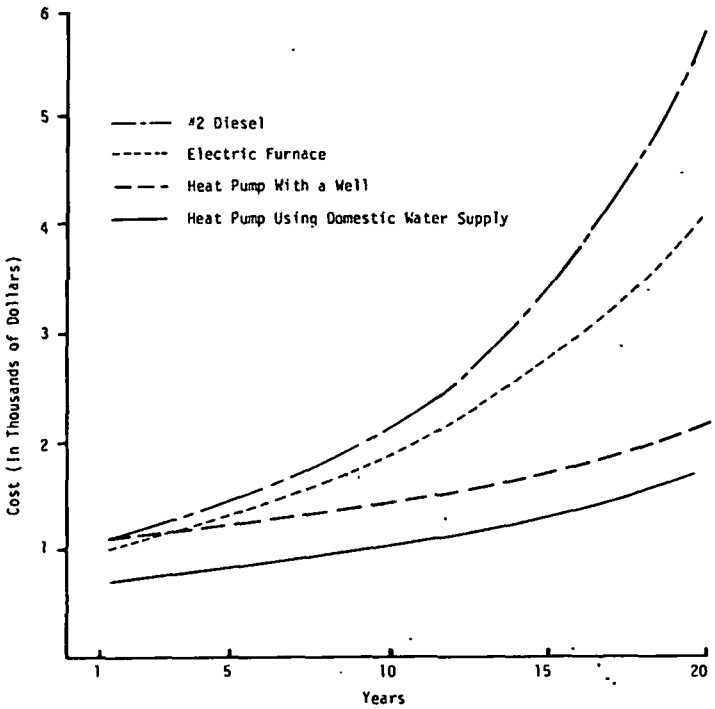

Figure 6. Annual Cost of Heating an 1,800 Ft^2 Home in Klamath Falls, Oregon.

put into the heat pump system, we are deriving 3.0 times the equivalent Btu's per hour. This means the shallow geothermal water source heat pump system described above operates at a coefficient of performance of 3.0.

As fuel costs escalate, the operating energy cost of using a heat pump will increase one-half to one-third that of conventional equipment. This is dependent, of course, upon COP, fuel escalation rates, and types of fuel used.

District and Process Heating

District heating is a method of supplying energy (hot water or steam) to consumers by means of a distribution piping network from a central energy source. A strong incentive to district heating is energy conservation, improved environmental quality and lower energy costs. In Europe, there is a long history of district heating plants. Iceland and Hungary, of course, had extensive plants using geothermal energy a long time before any talk about an energy crisis. In the years after 1974, most countries in Northern Europe have made close examinations of the possibilities and potentials of using geothermal energy as a supplement to imported fuel.

Heat pumps lend themselves well to district heating concepts. As a matter of fact, France had a functional plant in Melun as early as 1971, and today some ten plants are in operation in France. In Denmark and Germany, demonstration projects are being planned as well as Sweden, Holland, Austria, and Switzerland where theories will be put into reality. The Danes are investigating a 10-MW heat pump using 50°F ground water (Petersen, 1978) which is more effective than air. However, the warmer the well water, the more efficient the system will be and the less electrical energy it will consume.

Three schemes, (1) simple exchange, (2) insertion of heat pump, and (3) hybrid, are possible to extract the energy from the geothermal fluid as illustrated in Figure 7 with the following description:

1) A simple heat exchange may be desirable if the resource temperature is greater than 180°F and the cost of developing the resource is relatively low, thus justifying utilization of the resource 30 to 40 percent of the time during heating demand.

2) If the resource temperature is low (50° to 120°F), supply temperatures to the consumer can be boosted with the insertion of a heat pump.

3) A hybrid system may be desirable in the case of a high-cost resource (deep wells) development. The plan would be to construct the plant so the wells could be fully utilized 24 hours per day, thus optimizing the most expensive part of the development, drilling wells. The geothermal heat exchanger represents only 25% of the maximum capacity, however, it will supply over half of the annual heat requirements. When heat requirements increase in the chilly spring and

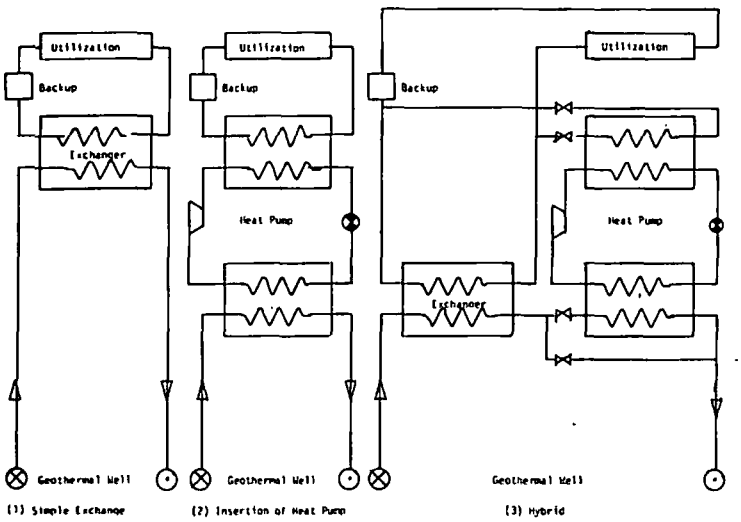

Figure 7. Examples of Heat Extraction Schemes.

autumn months, the heat pump will further cool the geothermal water coming from the heat exchanger. Thus, it will be only necessary to couple in a boiler during the extreme cold winter periods in order to yield the maximum peak load performance.

The economic benefit derived from collectively supplying heat for numerous users can further be increased if the annual use factor is increased; that is by increasing the amount of time the district operates at full capacity. Obviously, heating and cooling using heat pumps is not a continuous operation. The unused portion of time represents a waste of capital equipment.

If a commercial or process use can be found whose peak loads occur at different times than a residential load, a more beneficial use of the district system becomes possible. Most commercial and industrial food processing temperature requirements, however, are between 160° and 300°F. For process use, several heat pump models are capable of delivering up to 230°F when operating on 140°F water source temperature, and several firms are developing models capable of delivering temperatures as high as 350°F.

Conclusions

The effective use of heat pumps makes it possible to extend noticeably the cost-effectiveness of geothermal heating. Heat pumps also make it possible to connect a greater number of homes from a given well. The use of these machines provides an important asset when geothermal water temperature is low. The use of heat pumps should, of course, be adapted to the unique nature of each project. It is important to remember that these systems are sensitive to economic conditions relating to costs of geothermal systems themselves, wells, and backup systems.

References

1. Gass, Tyler E., 1978, "NWWA and the Ground Water Heat Pumps," Water Well Journal.

2. Keller, J. G., 1977, "Heat Pumps Primer for use with Low Temperature Geothermal Sources," EG&G Idaho, Inc., Idaho Falls, ID.

3. Petersen, Benny, 1978, Diesel Heat Pump for District Heating Plants and for the Heating of Large Housing Blocks, Burmeister & Wain AS, Copenhagen, Denmark.

HETEROGENEITY OF THE LIQUID PHASE, AND VAPOR SEPARATION IN LOS AZUFRES (MEXICO) GEOTHERMAL RESERVOIR

*Nieva D., +Quijano L., &Garfias A., *Barragán R.M. and &Laredo F.

*Instituto de Investigaciones Eléctricas, Apdo. Postal 475, Cuernavaca, Morelos 62000, México. +Subgerencia de Estudios and &Coordinadora Ejecutiva de Los Azufres, Gerencia de Proyectos Geotermoeléctricos, Comisión Federal de Electricidad

ABSTRACT

Data of chemical and isotopic composition of fluids from Los Azufres geothermal wells is interpreted in order to characterize the composition of the liquid phase, and to define the relation between this phase and fluids from steam-producing wells.

Chemical and specific enthalpy data show that most wells considered are fed a mixture of steam and liquid. Thus, flashing occurs in the formation. This poses a problem on the interpretation of isotopic data, because the composition of the feeding mixture need not be representative of the composition of the liquid phase in the reservoir. Two extreme alternatives for the interpretation of isotopic data are considered. In the first alternative the composition of the total discharge is considered to be the same as that of the liquid in the reservoir. In the second alternative the feeding fluid is considered to be a mixture of the liquid phase in the reservoir and the calculated fraction of steam. In addition, this steam is assumed to separate from a much larger mass of that liquid phase at the downhole temperature. The contribution of steam is then substracted from the total discharge to yield the composition of the liquid phase. Using data for silica concentration in total discharge and separated water, the chloride concentration in the reservoir liquid is calculated. This result is used to calculate the fraction of steam in the feeding mixture of each well. The isotopic data is then corrected as proposed for the second alternative, to yield the composition of the liquid phase. Comparison of the corrected and uncorrected isotopic valuesshows that the correction has an important effect only when the steam mass fraction in the feeding mixture is large (> 20%). The correction tends to reduce the dispersion of data points in a δ D vs δ^{18}O diagram. Points representing composition of liquid phase show an approximately linear distribution, suggesting a process of mixing of two fluids. Available data appears to rule out the possibility of mixture with local meteoric or shallow ground waters. Some spatial correlations of composition are noted. The composition of fluids produced by two steam wells corresponds to steam separated from a much larger mass of liquid. Temporal variations in the composition of fluid produced by steam well A-6 suggests that this well might be fed with steam from more than one section in the reservoir.

INTRODUCTION

The chemical and isotopic composition of hydrothermal fluids constitute one of the early important sources of information, which could be used to begin the characterization of a geothermal reservoir. It is particularly important to assemble as complete a set of data as possible from the pre- and early exploitation stages, since this would provide valuable information on the natural state of the system. This in turn would make it possible to monitor the changes occurring in the reservoir as exploitation begins and proceeds.

Giggenbach and Quijano (1981) have assembled a set of data of isotopic and chemical composition of fluids from geothermal wells in Los Azufres field, as well as from hydrothermal springs and fumaroles of the area. They have interpreted the evidence in a study of the regional hydro - logy of the Cuitzeo - Los Azufres area. One of the major findings of this study is the clear difference between the isotopic composition of local meteoric and shallow underground waters, and the composition of the geothermal fluids. The authors have concluded that the reservoir fluid consists of paleowaters, and postulate a relation between the Los Azufres aquifer and thermal springs in the Cuitzeo - Araro area, some 30 kilometers north.

The explored area in Los Azufres field covers an extension of about 30 Km^2 (Fig. 1). The field is located in a mountain range, bounded on two sides by valleys. The average altitude of well heads is 2850-2900 meters above sea level; the valleys lie about 300 m to 500 m below. There are two main sections which have been selected for exploitation, based on favorable tempera - ture and permeability conditions. In the north ern section, known as the Maritaro area, one finds only wells that produce a mixture of water and steam. In the southern section, known as the Tejamaniles area, one finds steam-producing wells, interspersed with mixture - producing wells. The present contribution describes the results of a study of the hydrology of the Los Azufres reservoir. The main objective of this investigation has been to determine any possible differences among the liquid phases from the several sections of the field, and to determine the relation between the fluid emanating from steam-producing wells and the liquid phase. We have used a subset of the data included in the work of Giggenbach and Quijano (1981).

OBSERVATIONS

Table 1 shows a set of chemical and isotopic composition data for fluids produced by wells from Los Azufres. The specific enthalpy of

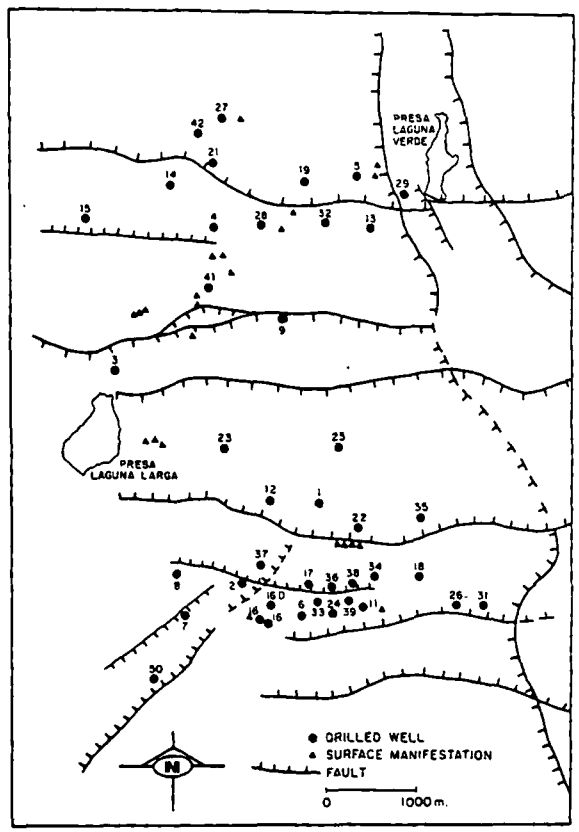

Fig. 1. Map of Los Azufres Geothermal Field.

the total discharge is also shown. Values for the ionic species and silica refer to their concentration in the liquid separated at atmo- spheric pressure. The boiling temperature in Los Azufres area is 92°C. The delta values for deuterium and ^{18}O refer to the composition of the total discharge. These values have been calculated from the composition of the liquid separated at atmospheric pressure, using data given by Truesdell et al (1977) for par- tition coefficients of deuterium and ^{18}O between the vapor and liquid phases.

The Table includes isotopic data for fluids from two steam-producing wells (A-6 and A-17). For some of the mixture-producing wells iso- topic but not chemical data is available. Downhole temperatures obtained with Kuster type equipment are shown in Table 2. Also shown are temperatures calculated by means of a Cationic Composition Geothermometer (Nieva and Nieva, 1982), the Na-K-Ca geothermometer

TABLE 1.- Chemical and isotopic composition data of Los Azufres fluids.

WELL	H J/g	Na^+	K^+ ppm	Cl^-	SiO_2	^{18}O	D	DATE OF SAMPLING
A-1	1750	-	-	-	-	-3.94	-56.6	20/ 3/82
A-2	1400	-	-	-	-	-4.33	-62.6	20/ 3/82
A-4	1460	1804	499	3270		-4.44	-65.2	8/ 5/80
A-5	1885	1876	534	3320	1160	-4.03	-58.8	29/ 4/80
A-5	1671	1638	465	2870	1250	-4.06	-62.4	13/ 1/81
A-6	2660	-	-	-	-	-4.26	-53.4	8/ 5/80
A-6	2756	-	-	-	-	-4.83	-60.6	13/ 1/81
A-6	2673	-	-	-	-	-5.02	-55.7	20/ 3/82
A-7	1360	1496	250	2460	780	-4.23	-65.0	17/ 4/80
A-8	1570	1606	359	2760	1100	-4.67	-65.8	26/ 4/80
A-13	1234	1499	390	2580	1020	-2.76	-60.4	14/ 1/81
A-13	1490	-	-	-	-	-2.57	-57.2	20/ 3/82
A-16D	1230	-	-	-	-	-3.72	-58.9	20/ 3/82
A-17	2673	-	-	-	-	-5.06	-58.8	20/ 3/82
A-19	2452	1689	475	3060	1050	-5.21	-62.4	13/ 1/81

H = specific enthalpy

(Fournier and Truesdell, 1973) and the revised silica geothermometer (Fournier and Potter II, 1982). In all cases there is good agreement among the values calculated with the different geothermometers. The measured values, on the other hand, seem to be consistently below the calculated values. Furthermore, the measured values would appear to be low also from a consideration of the specific enthalpies of total discharge. Given these observations and the general agreement among the geothermometers, only the latter have been considered in selecting a value of downhole temperature for each well. The selected values are shown in Table 2.

TABLE 2.- Measured and calculated downhole temperatures for Los Azufres wells.

WELL	T MEAS. °C	*T CCG °C	°T Na-K-Ca °C	&T SiO_2 °C	DATE OF SAMPLING
A-1	292	304	-	-	
A-2	280	304	290	285	14/ 4/80
A-4	298	308	314	-	8/ 5/80
A-5	270	311	318	308	13/ 1/81
A-7	249	251	254	262	17/ 4/80
A-8	275	282	286	295	26/ 4/80
A-13	265	300	300	287	14/ 1/81
A-13	265	292	297	280	9/ 2/83
A-16D	260	261	265	255	9/ 2/83
A-18	250	284	290	266	2/ 3/82
A-19	271	310	312	290	13/ 1/81

*CCG = Cationic Composition Geothermometer (Nieva and Nieva, 1982).

°Na-K-Ca Geothermometer (Fournier and Truesdell, 1973).

&SiO_2 = Revised and expanded silica (quartz) Geothermometer (Fournier and Potter, 1982).

In most cases listed in Table 1, the specific enthalpy of the total discharge is considerably in excess of the specific enthalpy of liquid water at the downhole temperature. This implies that phase separation occurs in the formation, so that the wellbore is fed a mixture of steam and liquid. This poses a problem on the interpretation of the isotopic composition of total discharge. This problem arises from the fact that, if phase separation occurs in the formation, there is no certainty that the isotopic composition of the total mixture entering the well is representative of the undisturbed liquid phase in the reservoir. The problem is particularly complex because only part of the steam present in the feeding mixture might represent an excess, the rest of it originating from local boiling (see Truesdell et al, these Proceedings, and Nieva et al, 1982, for a discussion of this problem). In view of the unavailability of the necessary information for the estimation of excess steam, it is decided to consider two extreme alternatives and to compare the final conclusions. The first extreme position is to consider the

isotopic composition of the total discharge as identical to that of the liquid phase in the reservoir. The other alternative is to consider as excess all the steam present in the mixture. In this case, it is also to be assumed that the steam has separated from a much larger mass of the reservoir liquid at the downhole temperature. Using partition coefficients for deuterium and ^{18}O, calculated at that temperature, one can correct the isotopic composition of the total discharge in order to obtain the composition of the liquid phase, according to the following expressions:

$$\delta_x^{lp} = (\delta_x^{td} - \Theta) / \Phi \qquad (1)$$

$$\Theta = 1000\ f\ (1 - \alpha)/\alpha \qquad (2)$$

$$\Phi = 1 - f + (f/\alpha) \qquad (3)$$

where f is the fraction of excess steam in the mixture; α is the atomic ratio of ^{18}O over ^{16}O in the steam, divided by the corresponding ratio in the liquid phase, at the downhole temperature. The superscripts lp and td refer to liquid phase and total discharge, respectively. The symbol x stands for ^{18}O or D. In cases where a steam deficit is estimated, the composition of the liquid phase is calculated from:

$$\delta_x^{lp} = (\delta_x^{td} + \Theta) / \Phi \qquad (4)$$

The fraction of steam in the feeding mixture is calculated from the silica concentration in the total discharge and that in the liquid separated at atmospheric pressure. From the latter concentration, and the assumption that the flow inside the borehole occurs adiabatically, one can calculate the downhole temperature (Fournier and Potter II, 1982). In so doing one also obtains the equilibrium concentration of silica in the liquid phase at the calculated downhole temperature. Considering this value and the silica concentration in the total discharge, one obtains the fraction of steam in the feeding mixture by a simple mass balance calculation. Data and results for this calculation are presented in Table 3, for the cases where silica concentrations are available. In all cases except one, the results indicate the presence of a substantial fraction of steam in the feeding mixture; in the case of well A-19 the steam constituted the larger part (80% in weight). For well A-13 a small steam deficit is calculated; given the errors in enthalpy measurements and silica determination, this result probably means that the well was being fed only liquid.

TABLE 3.- Percent steam in feeding mixture calculated from silica concentration. Chloride concentration in the total discharge, and calculated concentration in liquid phase in the reservoir.

WELL	H J/g	T °C (SiO_2)	SiO_2 ppm			% VAPOR
			s.w.	t.d.	eq.	
A-5	1885	308	1250	427	703	39
A-5	1671	300	1160	505	673	25
A-7	1360	262	780	446	519	14
A-8	1570	295	1100	528	653	19
A-13	1234	287	1020	640	623	-3
A-19	2452	290	1050	97	635	85

H = specific enthalpy of total discharge.
s.w. = Water separated at atmospheric pressure.
t.d. = Total discharge.
e.q. = Equilibrium concentration of silica at estimated downhole temperature.

The values of steam fraction calculated above, and the chloride concentration in the separated water, could be used to estimate the chloride concentration in the liquid phase of the reservoir.

Results of these calculations are shown in Table 4. The general agreement between the several calculated values is clear. Two of the six values deviate noticeably from the rest. Since these values correspond to the cases where the steam fraction was largest, and thus are more likely to result from overcorrections, they were not taken into account for the estimation of an average value of chloride concentration in the reservoir. The value obtained is 1650 ppm.

TABLE 4.- Chloride concentration in total discharge and calculated concentration in the liquid phase of the reservoir.

WELL	CHLORIDE (ppm) total discharge	liquid phase in reservoir
A-5	1134	1868
A-5	1250	1667
A-7	1407	1638
A-8	1325	1638
A-13	1619	1575
A-19	284	1856

Inverting the mass balance calculation referred to in the last paragraph, it is possible to calculate the fraction of steam in the feeding mixture from the chloride concentration in the total discharge, and the average concentration in the liquid phase of the reservoir. Table 5 shows the results obtained for samples listed in Table 1. In a few cases of mixture-producing wells where chemical analysis data are not available, the fraction of steam was calculated by means of an enthalpy balance calculation.

TABLE 5.- Percent steam in feeding mixture calculated from chloride concentration in total discharge. Calculated isotopic composition of liquid phase.

WELL	% STEAM	^{18}O	D	DATE OF SAMPLING
A-1	°29	-3.67	-57.5	20/ 3/82
A-2	° 8	-4.25	-62.9	20/ 3/82
A-4	-4	-4.48	-65.1	8/ 5/80
A-5	31	-3.77	-59.6	29/ 4/80
A-5	24	-3.86	-63.7	13/ 1/81
A-7	15	-4.00	-65.5	17/ 4/80
A-8	20	-4.45	-66.5	26/ 4/80
A-13	2	-2.74	-60.4	20/ 3/82
A-13	°10	-2.47	-57.5	20/ 3/82
A-19	83	-4.53	-64.6	13/ 1/81
A-16D	4	-3.66	-59.1	20/ 3/82

°Chloride concentration not available; calculated from specific enthalpy of total discharge.

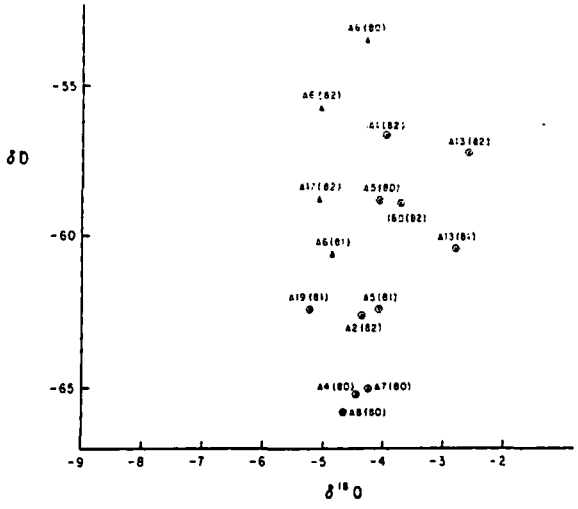

Fig. 2. Isotopic Composition of total discharge from Los Azufres wells. Circles and triangles represent fluids from mixture-producing and steam wells, respectively.

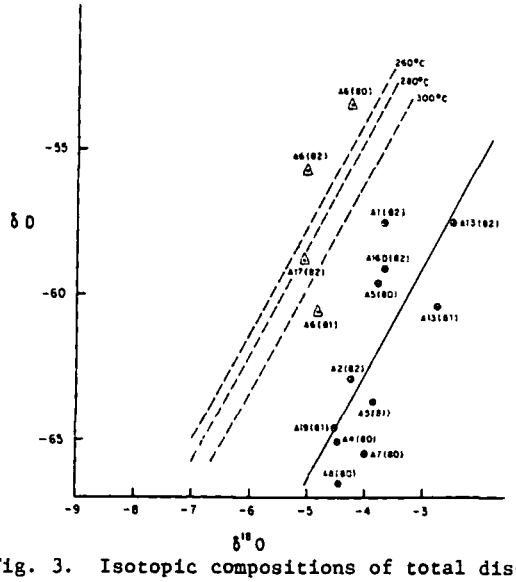

Fig. 3. Isotopic compositions of total discharge after correcting those corresponding to mixture-producing wells, in the manner described in the text. Symbols as for Fig. 2.

DISCUSSION

The uncorrected values of isotopic composition of total discharge are plotted in Fig. 2. It is evident that there is considerable dispersion of the compositions corresponding to mixture-producing wells (represented by circles). The values corresponding to fluids produced by steam wells (represented by triangles) tend to be in the upper left section of the distribution, as would be expected from the values of partition coefficients of the isotopic species

between steam and liquid at temperatures above 250 °C.

Fig. 3 presents a plot of the isotopic values, corrected as proposed under the second alternative. Superposition of Figs. 2 and 3 shows that the correction has a substantial effect only for those cases where 20% or more of the feeding mixture was constituted by steam, as is the case of wells A-19, A-5 (sample of 1980) and A-1. The correction tends to reduce the dispersion of the data points corresponding to liquid phase. I also increases the systematic difference between the compositions of liquid and steam phases. The data points for liquid phase show an aproximately linear distribution; the solid line corresponds to a least-squares fit with a correlation coefficient of 0.75.

The uncertainties in the measurement of δD and $\delta^{18}O$ are estimated as $\pm$ 0.5 and $\pm$ 0.05, respectively. The observed differences in isotopic composition of liquid phase are much larger than these error margins, and thus indicate a degree of heterogeneity in the aquifer. As reported by Giggenbach and Quijano (1981), the isotopic compositions of local shallow waters and the geothermal fluids are very different, ruling out the possibility of a direct origin of the latter from local meteoric precipitation. The approximately linear distribution in Fig. 3 suggests the possibility of mixture of two fluids in the aquifer. Extrapolation of the best-fit line gives an intercept with the meteoric line (Craig, 1961) corresponding to an isotopic composition very different than that of any of the analysed local waters. Although there is a considerable scatter in the points along the adjusted line, it can be concluded that available evidence does not support the possibility of mixing of the geothermal fluid with local ground waters.

The wellheads of A-7 and A-8 are on different sides of a fault (see Fig. 1); however, well A-7 is very close to the fault and on the side of inclination of the fault plane, so that it probably intersects it. This is consistent with the two wells being fed by fluid of similar composition. The feeding zone of A-2 is on the other side of the fault, and this well receives fluid of a somewhat different composition. Well A-16D is relatively close to A-2, but separated by an inferred fault. The feeding fluid of A-16D is clearly different than that of the other three wells mentioned above.

The northern and southern sections of the field which have been chosen for exploitation are separated by a zone of high resistivity (Romero and Palma, 1983), and of relatively minor hydrothermal alteration at the surface and shallow levels. Thus, the two sections might appear to be unrelated. However, the available information from deep wells in the middle section show that there is a continuity of hydrothermal alteration at great depth (> 1800 m), which joins the northern and southern sections. This suggests that there is a deep aquifer which spans the entire area of the field (Cathelineau et al, this Proceedings). Well A-4, A-19, A-5 and A-13 are distributed along the Maritaro fault. The fluid feeding well A-4 is similar to that which feeds wells A-7 and A-8 in the southern part of the field. Well A-13, which is on the same side of the Maritaro fault than A-4, receives a fluid of very different composition. However, it should be noted that the feeding zones of these two wells are at very different depths. The slotted liner sections of A-4 and A-13 are at approximately 900-1300 meters and 1650-1850 meters above sea level, respectively. The slotted liner section of A-5, on the other side of the Maritaro fault, is at an intermediate depth (approximately 1400-1800 meters above sea level). The composition of the fluid feeding this well is also intermediate, but closer to that of A-13. Data for well A-19 can not be used to support or disprove this suspected correlation of composition

with depth, because its slotted liner section spans most of the depth range involved (1200-1850 meters above sea level). Clearly, information from more wells located in this area is needed, in order to investigate the possibility of the existence of two aquifers at different depths.

The compositions of steam phases separated at 300°C, 280°C and 260°C from liquid phases with compositions falling in the solid line of Fig. 3, have been calculated. The results fall in the broken lines shown in the same Figure. These calculations assume that the mass of the separated steam is negligible compared to that of the remaining liquid. If this is not so, than the composition of the separated steam will fall in the space bounded by the broken and solid lines, the closer to the latter the higher the fraction of separated steam. The points corresponding to the 1980 and 1982 samples from well A-6 seem to fall just out of the allowable range. However, taking into account the error margin in the determination of deuterium, and the scatter of the linear distribution of liquid phase compositions, these two points might fall in the extreme of the range. The other two points corresponding to samples from steam wells also fall near the extreme of the range, close to the broken lines. This implies that wells A-6 and A-17 are fed by steam separated from a much larger mass of liquid. The large variations with time shown by the composition of fluid produced by A-6, suggests that this well might receive steam from more than one section of the aquifer, at different times.

CONCLUSIONS

The chemical and specific enthalpy data show that there is phase separation in the feeding zones of most of the wells considered. The isotopic composition data shows no evidence of mixing of the geothermal fluid with local meteoric and shallow ground waters. These inferences are consistent with a situation in which the aquifer has no local recharge, although it may have lateral recharge from the low-lying surrounding valley. Under these circumstances, it would be expected that the system be underpressurized and flashing would occur in zones with a high degree of fracturing, as well as in zones of intake of producing wells.

The origin of the heterogeneity of the liquid phase in the reservoir remains obscure. The approximately linear distribution of isotopic compositions suggests a process of mixing of two fluids. Clearly, data from more of the wells in the field is needed in order to draw firmer conclusions in this regard. In particular, it is necessary to investigate the possible correlation of isotopic composition with depth in the northern section of the field.

ACKNOWLEDGMENTS

The work described in this report constitutes part of a project supported by Consejo Nacional de Ciencia y Tecnología de México, contract PIT/EN/NSF/1810. The authors want to express their indebtedness to much of the personnel of the Gerencia de Proyectos Geotermoeléctricos, Comisión Federal de Electricidad for their general support and assistance during the conduction of these studies. Thanks are also due to Bertha Solano, Ma. Eugenia Calderón and Ma. de Lourdes Calderón for expertly typing the manuscript, and to Adrián Patiño for drafting the figures.

REFERENCES

Cathelineau M., Oliver R., Izquierdo G., Garfias A., Nieva D. and Izaguirre O. (1983) "Mineralogy and Distribution of Hydrothermal Mineral Zones in Los Azufres (México) Geothermal Field. This Proceedings.

Craig H. (1961) "Isotopic Variations in Meteoric Waters". Science 133, 1702.

Fournier R.O., and Potter II, R.W. (1982) "A Revised and Expanded Silica (Quartz) Geothermometer". G.R.C. Bull. November, p 3.

Fournier R.O. and Truesdell A.H. (1973) "An Empirical Na-K-Ca Geothermometer for Natural Waters". Geochim. Cosmochim. Acta 37, 1255.

Giggenbach W. and Quijano L. (1981) "Estudio Isotópico de las Aguas del Campo Geotérmico de Los Azufres". Manuscript.

Nieva D., Fausto J.J., González J. and Garibaldi F. (1982) "Flow of Steam into the Feeding Zone of Wells of Cerro Prieto I". Proceedings, Fourth Symposium on the Cerro Prieto Geothermal Field".

Nieva D., and Nieva R. (1982) " A Cationic Composition Geothermometer for Prospection of Geothermal Resources". Manuscript.

Romero J.C., and Palma O. (1983) "Estudios Geoeléctricos en la Zona Geotérmica de Los Azufres, Michoacán". 1ª Reunión Informal Interdisciplinaria de Actividades sobre el Campo Geotérmico de Los Azufres. Resúmenes" Nov. 23-25, 1983. Los Azufres, Mich., México.

Truesdell A.H., D'Amore F., Nieva D., and Pruess K. (1983) "The Origin of Excess Steam in Discharges from Cerro Prieto Geothermal Wells". This Proceedings.

Truesdell A.H., Nathenson M., and Rye R.O. (1977) "The Effects of Subsurface Boiling and Dilution on the Isotopic Compositions of Yellowstone Thermal Waters". J. Geophys. Res. 82, 3694.

SuBJ
GTHm
HPGA

HEAT PUMPS FOR GEOTHERMAL APPLICATIONS: AVAILABILITY AND PERFORMANCE

Quarterly Technical Progress Report

June 7, 1979 - August 31, 1979

Gordon M. Reistad
Department of Mechanical Engineering
Oregon State University
Corvallis, OR 97331

Prepared for

The U.S. Department of Energy under Contract No. DE-FC07-79ID12020

DISCLAIMER

INTRODUCTION

Oregon State University is under contract with the U.S. Department of Energy to carry out a survey of the performance and availability of water source heat pumps. The primary purpose for this work is to obtain information so the role of water source heat pumps in geothermal energy utilization can be evaluated and/or to identify the research needed to accomplish this. The project is of eight months duration.

This report is the first quarterly report, covering activities during the period June through August, 1979. During this period, Dr. Gordon M. Reistad, the project director, spent 0.6 man months on the project and Mr. Paul Means, a Graduate Research Assistant, spent 1.5 man months on the project. During this period, the primary efforts have been directed at (i) surveying the literature, (ii) identifying manufacturers, (iii) obtaining performance data, and (iv) contacting the major manufacturers.

LITERATURE

The literature reveals that interest and activity in the heat pump area has increased sharply in the mid and late 1970's. The activity covers the full range from public interest, increased sales, research and development (both government and industry sponsored), and substantially increased published literature. The primary reasons for this activity stem from (i) an increased awareness of our limited available energy and the heat pump's potential to use this energy more effectively in certain applications, and (ii) the shift towards using electrical power for residential heating as oil and natural gas supplies become increasingly scarce and less reliable*

*Two-thirds of the electrical power generated in the U.S. is from more abundant sources such as coal, nuclear, and hydro power (Comly, et al., 1975).

(Pietsch, 1977 and Comly, et al., 1975).

The emphasis of this report is on water source heat pumps and to a large degree, unitary units. The basic type of heat pump considered here is shown in Figure 1. The major components are 1) a reciprocating compressor unit, typically hermetically sealed, 2) an air side heat exchanger with fan, 3) either a thermostatically controlled expansion valve or more commonly, a capillary tube, 4) a tube in tube water to refrigerant heat exchanger, and 5) a four-way reversing valve. Refrigerant 22 is used almost universally as the working fluid in these heat pump applications. A unitary heat pump is one which has all of these components and associated controls enclosed in one or two factory assemblies. Typical size ranges are from 1.5 to 20 tons.

Heat pump development, as indicated by the published literature, is being advanced in three primary and interrelated areas. These areas are: (i) new and expanding applications, (ii) performance improvement of the existing type units, and (iii) development and evaluation of alternate system designs.

The most widespread application of water source heat pumps for space heating is in the use of groundwater as an energy source for heating single family residences. Such units are also typically used for cooling during the summer months, with the well water then being used as the energy sink. These applications are common in many areas of the country, and efforts to allow heat pumps to use lower temperature water (approaching 40°F) are directed at expanding the areas where these units are viable.

Solar heated water is also being used, on a limited scale, as an energy

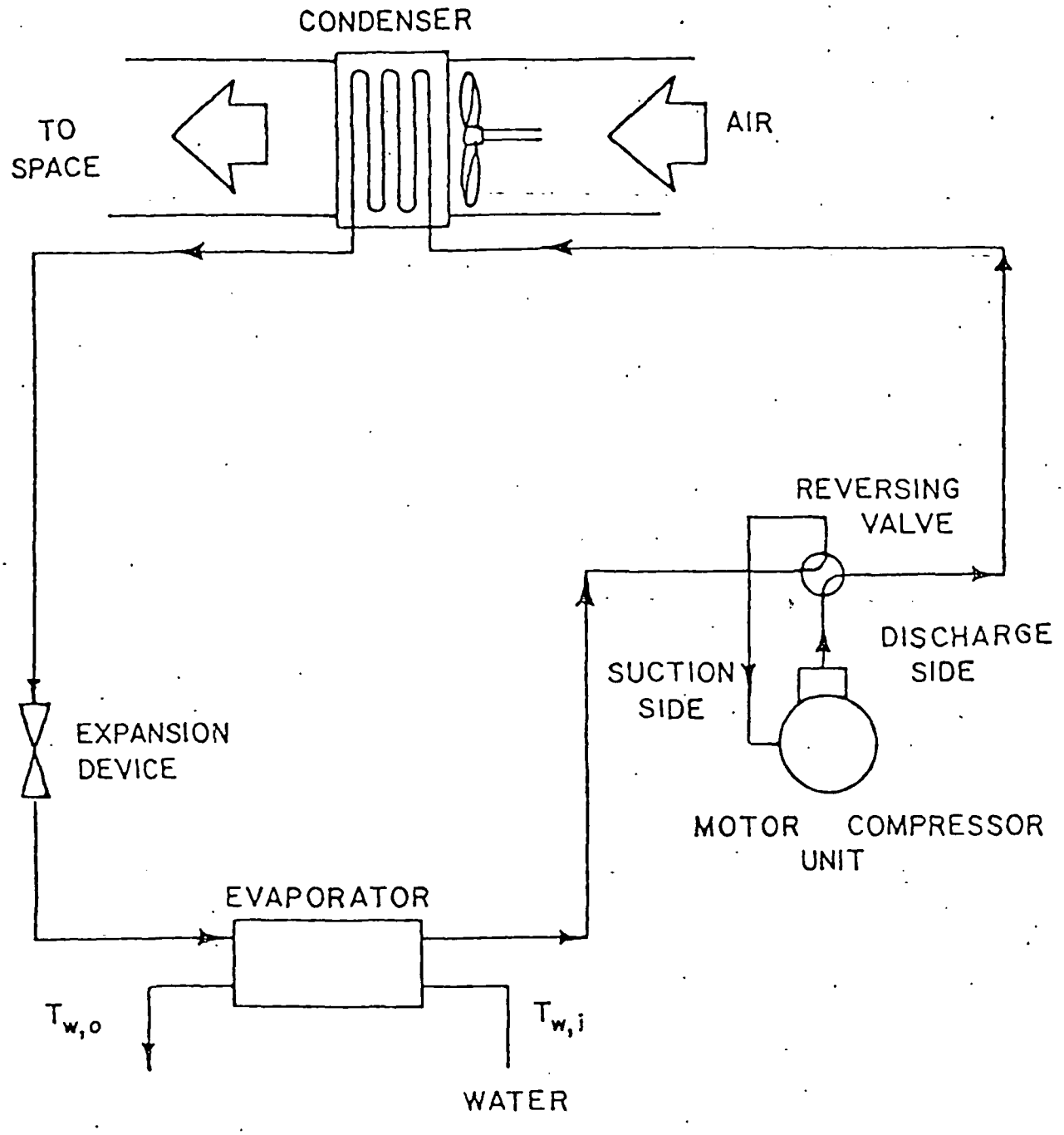

Figure 1. Water source heat pump operating in the heating mode.

source for residential heat pumps. A few of the smaller heat pump manufacturers/suppliers have limited product lines directed at this market. The most activity in this area is in the evaluation of such systems. There is an extensive amount of published literature on this topic, some of which is contradictory as to the real benefit of such a solar-heat pump series system (Andrews, et al., 1978). It has been stressed by some authors that a heat pump with good high temperature performance is essential to obtain the most advantage of such a system (Kush, 1979).

Commerical and industrial water source heat pumps are also common. Commercial installations are usually in the form of distributed systems consisting of a one or two pipe water distribution system with terminal heat pumps. Such units are typically designed to operate in both cooling and heating modes and with water in a restricted temperature range. Industrial applications usually have custom engineered systems.

The published literature on actual water source heat pump performance, specifically Coefficient of Performance in Heating (COPH) as a function of source water temperature, is limited and rather general. The COPH values increase slightly with increasing source temperature up to 60 or 70°F, however, at higher temperatures there is essentially no improvement in COPH. This is in contrast to the theoretical COPH which increases monotonically with increasing source temperature. There are several reports which detail very well the reasons why the actual heat pump performance is so much less than the theoretical (for example, Comly, et al., 1975 and Ambrose, 1974). Although, these reports are directed towards air to air heat pumps much of the discussion is also appropriate for the water source units.

A much larger portion of the heat pump literature deals with perform-

ance improvement techniques. These include compressor capacity control, larger heat exchangers, more controllable expansion devices, and heat only heat pumps to name a few. Analytical methods are often used to show the value of such performance improvement techniques (Gordian Assoc., 1978, Kirshbaum, et al., 1977, and Blundell, 1977).

Many alternative designs have been proposed (usually much more complex than existing units). These include multipressure systems, parallel compression, series compression, and alternative compressor motor power concepts. A limited number of these systems have been tested. More often the performance is based on numerical analysis from which economic evaluations are made (Comly, et al., 1975 and Gordian Assoc., 1978).

MANUFACTURERS

Table 1 shows a list of water to air heat pump manufacturers. A majority of these have been contacted by phone or mail or both and the remainder have been recently mailed a written questionnaire. The table was compiled from information obtained from (i) the Air Conditioning and Refrigeration Institute (ARI), (ii) the ASHRAE Handbook and Product Directory, and (iii) the National Water Well Association. ARI claims that its directory covers 90% of all water source heat pumps manufactured although only about one-third of the companies in Table 1 were found in the directory. This implies that primarily the major manufacturers are certified by ARI and that some of the smaller manufacturers, especially those oriented towards solar assisted heat pumps, are relatively new in the water source heat pump business and/or have limited production. Although 33 companies are listed, they do not necessarily represent 32 different product lines. Some of the companies simply market

Table 1. Water Source Heat Pump Manufacturers

Name and City	Source
Air Conditioning Corporation Greensboro, NC	3
American Air Filter Co., Inc. Louisville, KY	1,2,3
American Solar King Corp. Waco, TX	1
Barkow Manufacturing Co., Inc. Milwaukee, WI	2
Budco Bloomfield, CT	2
Carrier Corporation, Air Conditioning Group Syracuse, NY	1,2,3
Climate Master Products, Inc., Div. Weil McClain Co. Ft. Lauderdale, FL	2
Command Aire Waco, TX	1,2,3
Elm Brook Refrigeration, Inc. Brookfield, WI	2
Florida Heat Pump Corp. (Div. Leigh Products Co.) Pampano Beach, FL	1,2,3
Friedrich Air Conditioning and Refrigeration Co. San Antonio, TX	1,2,3
Heat Controller, Inc. (Div. Addison Products)* Jackson, MI	2,3
Heat Exchangers, Inc., Koldwave Division Skokie, IL	1,2,3
International Environmental Corp. Oklahoma City, OK	1,2
Lear Siegler, Inc., Mammoth Division Holland, MI	1,2,3
Northrup, Inc. Hutchins, TX	1,2,3
Ramada Energy Systems, Inc. Tempe, AZ	2
Singer Co., Climate Control Division Auburn, NY	1,2,3
Solar Energy Research Corp. Longmont, CO	2
Solar Energy Resources Corp.** Miami, FL	1,3
Solar Kinetics Mechanicsburg, OH	2
Spectrum Solar Systems Corp. Pickerington, OH	3

Table 1. Continued

Name and City	Source
Tempmaster International Energy Conservation Systems, Inc. Orlando, FL	2,3
Thermal Energy Transfer Co. Westerville, OH	3
Vanguard Energy Systems San Diego, CA	2,3
Vilter Manufacturing Corp. Milwaukee, WI	2,3
Weatherking (Div. Addison Products) Orlando, FL	2,3
WESCORP, Inc. (Subsidiary of Vaughn Corp.) Andover, MA	3
Westinghouse Electric Corp. Commercial-Industrial Air Conditioning Division Staunton, VA	2
Whalen Co. Baltimore, MD	2,3
Wilcox Manufacturing Corp. Pinellas Park, FL	3
Wormser Scientific Corp. Stamford, CT	2
York Division Borg Warner Corp. York, PA	2,3

Sources

1 - Air Conditioning and Refrigeration Institute, June 1 - November 30, 1979, Directory of Certified Applied Air-Conditioning Products.

2 - 1979 ASHRAE Handbook and Product Directory.

3 - National Water Well Association Listing.

Footnotes

* - Heat Controller, Inc., and Weatherking, Inc., are both divisions of Addison Products Co., Inc., and market identical water source heat pumps.

** - Also identified as "Solar Oriented" Environmental Systems, Inc.

heat pumps manufactured by others under a different name. A few companies that were included in the three sources mentioned, when contacted, said they no longer manufacture water source heat pumps. These companies therefore are not listed in Table 1.

PERFORMANCE

Performance data for water source heat pumps has been obtained from most of the major manufacturers listed in Table 1. The performance values have not been completely compiled at this time, but the data have been examined in several ways.

Water source heat pump performance, in terms of COPH was plotted versus nominal heating capacity for ARI certified units. This data set, shown in Figure 2, is based on rating conditions per ARI Standard 320-76. The plot, which is very similar to that done by Briggs and Shaffer, 1977 shows a wide range of performance between units at any one capacity. There is a slight trend for increased performance with increasing capacity, however this is only a general trend and may not be true for all manufacturers. Comparison of this current data with that presented by Briggs and Shaffer in 1977 shows an average increase in COPH of around 0.2 over the last two years. This increase may not be entirely due to product improvement, however, since the 1979 rating condition is based on a 70°F water source temperature and the 1977 ratings are based on a 60°F water source temperature and, based on manufacturers' data, a majority of the units have slightly better performance with 70°F than 60°F entering water temperature. Also, there is no allowance for the water pumping power in the 1979 ratings while there was some allowance in the 1977 ratings. Examination of certain units does

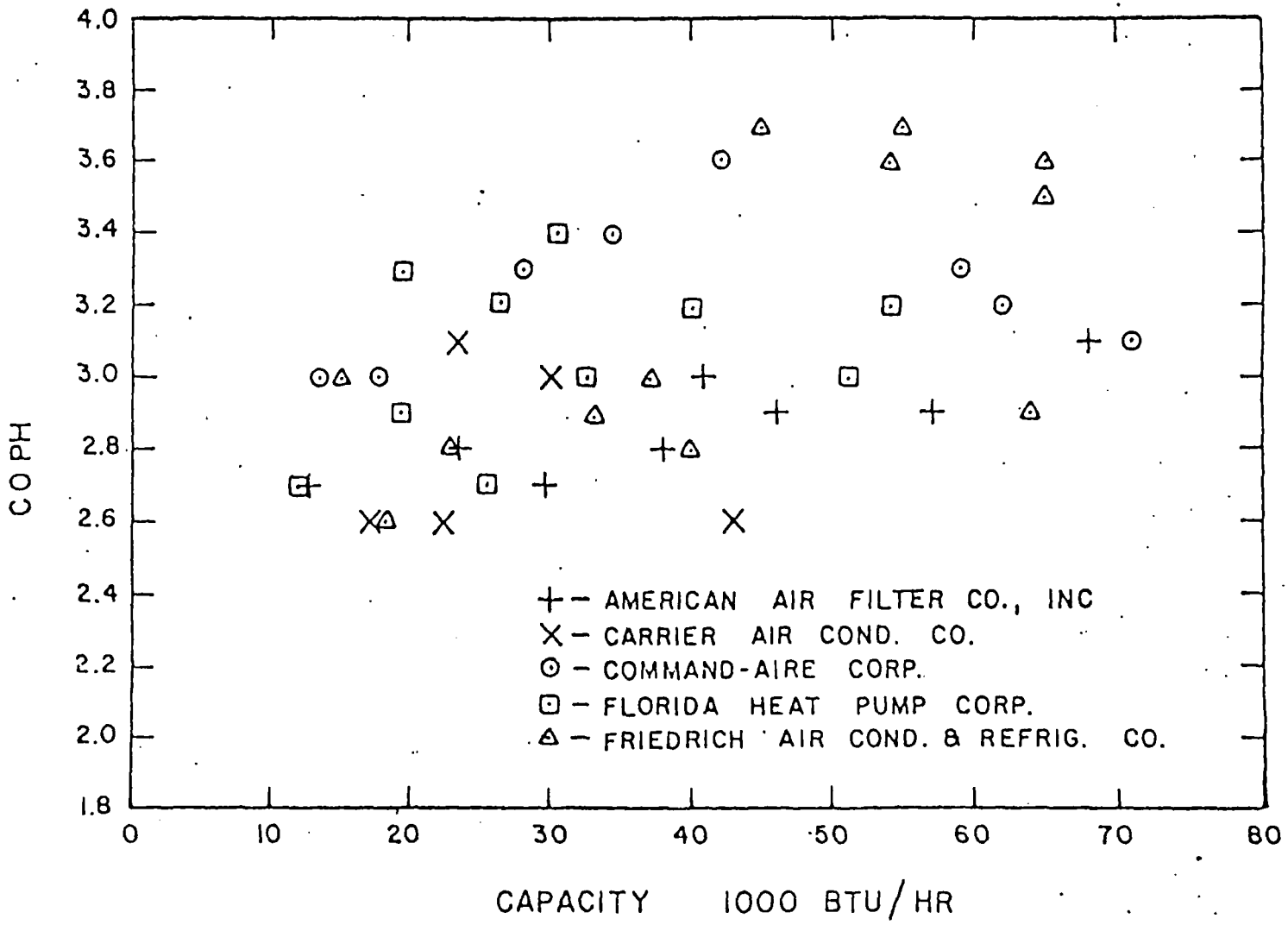

Figure 2a. COPH vs. Capacity for single package water source heat pumps. Data per ARI Standard Ratings, June 1 - Nov. 30, 1979 Directory.

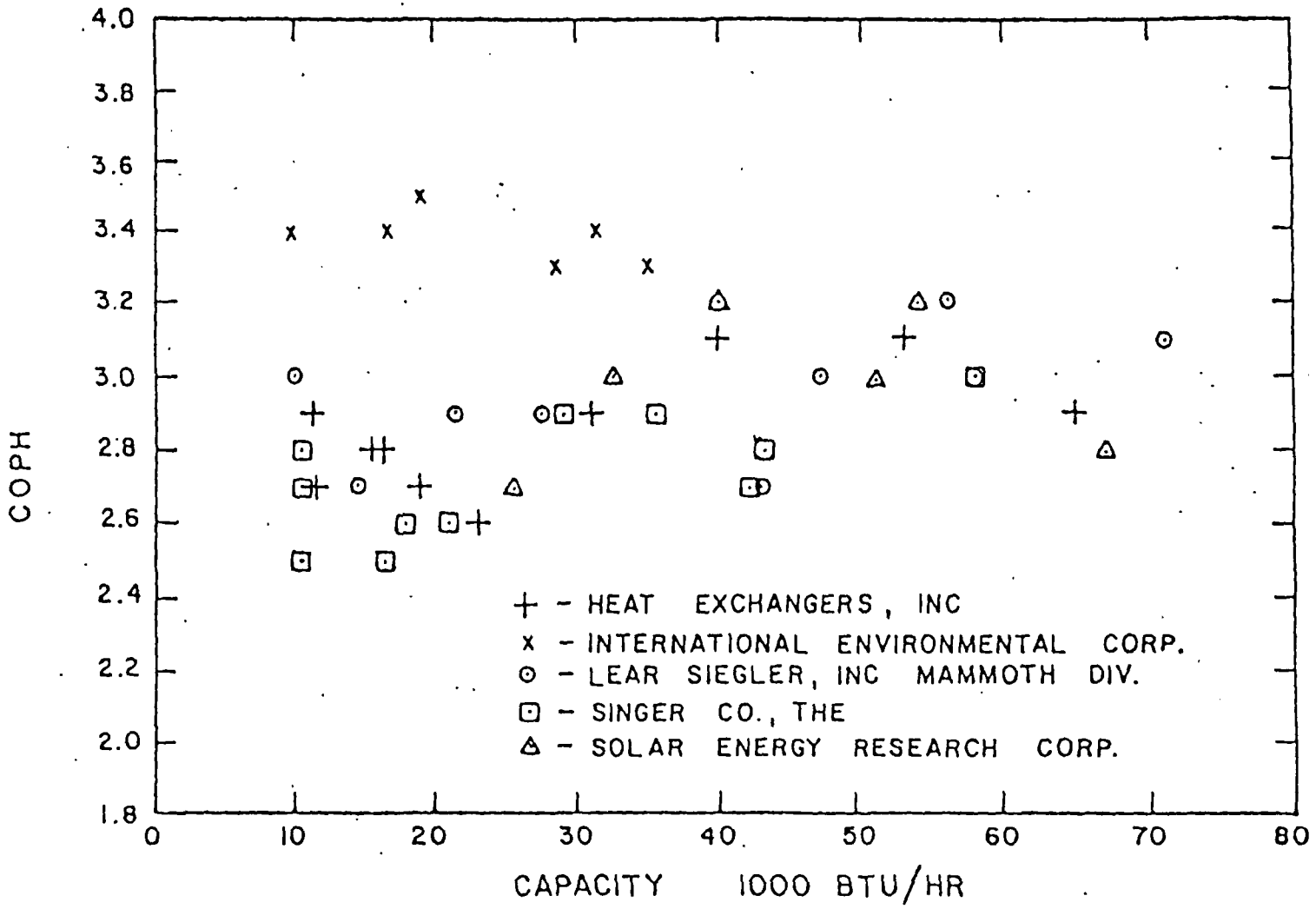

Figure 2b. COPH vs. Capacity for single package water source heat pumps. Data per ARI Standard Ratings, June 1 - Nov. 30, 1979 Directory.

however show substantial improvement since 1977.

A major concern is the water source heat pump performance as a function of water source temperature. Figure 3 shows how the COPH varies with water outlet temperature for five typical mid-sized heat pumps based on manufacturers' data. In Figure 3, the leaving water temperature rather than the entering water temperature was used as the independent variable, because better correlation should result. It is planned to examine several ways of presenting the data for the best utility. Not much variation is evident between the different models at lower outlet water temperatures, however at higher outlet temperatures the difference is pronounced. This is not easily explained without more detailed evaluation of the different units. (A possible explanation is that some manufacturers have calculated performance at higher source temperatures rather than conducting extensive testing. This has been observed in some of the data examined to date.)

CONTACT WITH MANUFACTURERS

Many of the water source heat pump manufacturers listed in Table 1 have been contacted to determine several aspects of their present activity and attitude in regard to water source heat pumps. Those companies which have large scale production of unitary water-source heat pumps and which manufacture their own units were the main ones contacted. Additional companies, both custom water source heat pump manufacturers and traditionally air-to-air heat pump manufacturers that are in the research stage on water-source units, were also contacted. Although the manufacturers in general would not discuss the specifics of their planned developments, they appeared to be willing to discuss the trends of developments and the

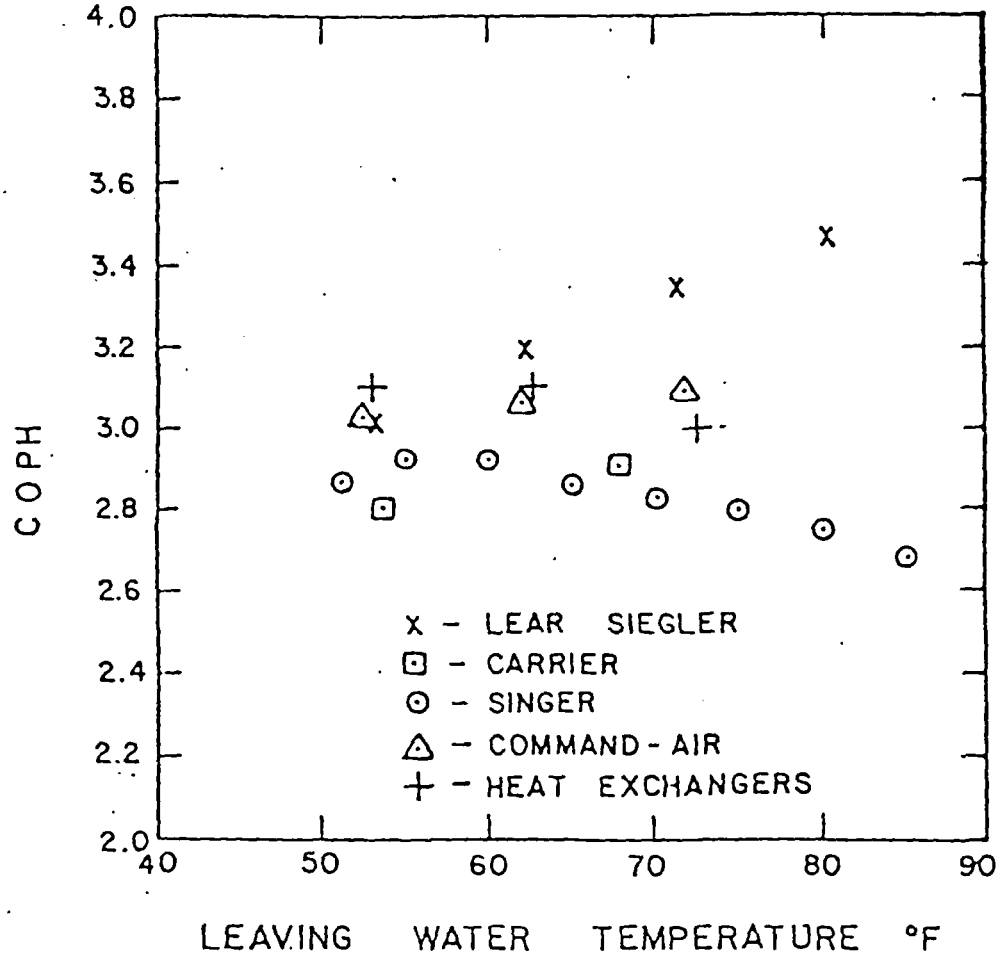

Figure 3. COPH vs. Evaporator exiting water temperature for typical 35000 to 42000 Btu/hr capacity heat pumps.

present position of the company on many aspects that impact present and near-term future products.

The conclusions reached from these discussions are:

- The COPH at ARI rating conditions can be expected to increase slightly over the next few years, at the rate of about 0.1 per year. Most of the companies have a moderate program directed at COPH performance improvement of the water source units. Several companies have quite strong programs in these areas and the performance improvements of their units in the last few years indicate this. Most companies, however, emphasize the cooling performance rather than the heating performance in their system design.
- The entering source water temperature should be less than about 95°F for most of the water source heat pump units primarily because they will shut off on high head pressure as the capacity increases with increasing source water temperature. Some units may be purchased with a special package that regulates the water flow and permits inlet temperatures as high as about 110°F.
- Most of the manufacturers showed little interest in developing a product line directed specifically toward geothermal applications. The primary reasons were (i) they viewed the market as quite limited and (ii) they already have many production lines and they are presently very much bogged down with getting their present units tested under the new DOE guidelines. There are several manufacturers that are very much committed to vigorous programs in water-source heat pump development, and if shown

the need for a product line in the geothermal area would be interested in that application.

- All of the companies contacted indicated that they were not interested in developing a "heating only" water source heat pump. One company said that a decision is near in regard to whether they will or will not start producing a "heating only" air source unit.
- All unitary water-source heat pumps for space heating are presently single stage compression and no change is expected.
- More complex heat pump systems such as hybrid water and air source/sink units are not being seriously considered at this time because great advantage is seen in simplicity and also each different operating mode requires a whole series of additional certification testing. Less significant modifications such as dual compressors are being considered more, but probably will not be commercial for several years.

REFERENCES

Ambrose, E.R., "The Heat Pump: Performance Factor, Possible Improvements," Heating, Piping, and Air Conditioning, Vol. 46, No. 5, pp. 77-82, May, 1974.

Andrews, J.W., E.A. Kush, P.D. Metz, A Solar-Assisted Heat Pump System for Cost-Effective Space Heating and Cooling, Brookhaven National Laboratory Report BNL 50819 UC-59c, March, 1978.

Blundell, C.J., "Optimizing Heat Exchangers for Air to Air Space Heating Heat Pumps in the United Kingdom," Energy Research, Vol. 1, pp. 69-94, 1977.

Briggs, J.B., and C.J. Shaffer, Seasonal Heat Pump Performance for a Typical Northern United States Environment, Idaho National Engineering Laboratory Report TREE-1181, (October, 1977).

Comly, J.B., H. Jaster, and J.P. Quaile, "Heat Pumps - Limitations and Potential," 1st Annual Heat Pump Technology Conference Proceedings, Oklahoma State University, October, 1975.

Gordian Associates, Heat Pump Technology, A Survey of Technical Developments, Market Prospects, and Research Needs, Report HCP/M2121-01 for the U.S. Department of Energy, June, 1978.

Kirshbaum, H.S., and S.E. Veyo, An Investigation of Methods to Improve Heat Pump Performance and Reliability in a Northern Climate, EPRI Report EM-319, (1977).

Kush, E.A., "Experimental Performance Study of a Series Solar Heat Pump," 4th Annual Heat Pump Technology Conference Proceedings, April, 1979.

Pietsch, J.A., "The Unitary Heat Pump Industry - 1952 to 1977," American Power Conference Proceedings, Vol. 39, pp. 816-821, 1977.

SUBJ
GTHM
HTGR

REMARKS FOR

15TH ENERGY TECHNOLOGY CONFERENCE AND EXHIBITION

HIGHER TEMPERATURE GEOTHERMAL RESOURCES: DOMESTIC AND INTERNATIONAL PROJECTS AND TRENDS

DR. CAREL OTTE

PRESIDENT, GEOTHERMAL DIVISION

UNOCAL CORPORATION

FEBRUARY 19, 1988

THANK YOU VERY MUCH, MR. CHAIRMAN.

WITH OIL SO PLENTIFUL AND INEXPENSIVE THESE DAYS, IT IS SOMETIMES DIFFICULT FOR A VITAL ALTERNATIVE ENERGY SOURCE -- LIKE GEOTHERMAL -- TO GET THE ATTENTION IT DESERVES. WHAT WILL LIKELY HAPPEN IS THAT ANOTHER ENERGY CRISIS WILL PUT THE INDUSTRY BACK INTO THE PUBLIC EYE.

I FIRMLY BELIEVE THERE IS ANOTHER ENERGY CRISIS WAITING IN THE WINGS: ANOTHER OPEC BREAKDOWN OR POLITICAL OR ECONOMIC CRISIS WILL BRING IT TO CENTER STAGE AGAIN.

DESPITE THE PRICE AND SUPPLY SWINGS OF FOSSIL FUELS, HOWEVER, GEOTHERMAL ENERGY HAS COME OF AGE OVER THE LAST 25 YEARS.

IN THE UNITED STATES, THE GEOTHERMAL INDUSTRY BEGAN TO DEVELOP RAPIDLY IN THE EARLY SIXTIES, APPROXIMATELY THE SAME TIME THAT THE NUCLEAR INDUSTRY BEGAN TO HIT ITS STRIDE. ALTHOUGH GEOTHERMAL IS STILL YOUNG, IT'S REAL. WE KNOW THE RESOURCE EXISTS IN MANY PLACES. WE KNOW HOW TO FIND IT. AND WE KNOW HOW TO USE IT TO PRODUCE ELECTRICITY AT A COMPETITIVE PRICE.

LET ME TAKE A MOMENT TO DESCRIBE THE GEOLOGICAL CONDITIONS THAT MAKE GEOTHERMAL POSSIBLE. IN CERTAIN PLACES, MAGMA PENETRATES RELATIVELY CLOSE TO THE SURFACE OF THE EARTH AND HEATS UNDERGROUND WATER. THIS MAGMA MOVEMENT OCCURS WHERE THE TECTONIC PLATES -- THE PLATES THAT MAKE UP THE CRUST OF THE EARTH -- ARE BROKEN, OR COLLIDE, OR PULL APART. IT IS HERE, WHERE THE CRUST HAS BEEN WEAKENED, THAT MAGMA CAN RISE FROM THE DEPTHS OF THE EARTH TO HEAT UNDERGROUND RESERVOIRS. MOST OF THE WORLD'S GEOTHERMAL AREAS, THEREFORE, OCCUR ALONG THE BOUNDARIES OF THESE CONTINENTAL AND OCEANIC PLATES.

THE MOST EVIDENT AREA FOR GEOTHERMAL DEVELOPMENT IS ALONG THE PACIFIC RING OF FIRE, A CIRCULAR SPAN OF GEOLOGICAL ACTIVITY THAT EXTENDS VIRTUALLY AROUND THE ENTIRE PACIFIC BASIN: SOUTH AMERICA, CENTRAL AMERICA, THE WESTERN UNITED STATES, INCLUDING ALASKA ... JAPAN, THE PHILIPPINES, INDONESIA AND NEW ZEALAND. THE RESOURCE ALSO EXISTS IN THE RIFT VALLEY OF EAST AFRICA, THE AREAS AROUND THE MEDITERRANEAN AND WHERE THE MID-ATLANTIC RIDGE BREACHES THE OCEAN SURFACE, AS IN ICELAND.

LIKE FOSSIL FUELS, GEOTHERMAL RESOURCES EXIST UNDER ONLY CERTAIN CONDITIONS. GEOLOGISTS, FOR EXAMPLE, HAVE TO FIND PLACES WHERE TRAPPED, UNDERGROUND RESERVOIRS EXIST IN THE SAME PLACE WHERE MAGMA HAS COME CLOSE TO THE EARTH'S SURFACE.

THOSE HEATED UNDERGROUND RESERVOIRS OCCUR WHERE RAINFALL THAT HAS SEEPED DEEP INTO THE EARTH IS WARMED BY THE EARTH'S HEAT. BY DRILLING INTO THOSE ROCK FORMATIONS THAT HOLD HEATED WATER, WE CAN BRING GEOTHERMAL FLUIDS TO THE SURFACE, CAPTURE THE STEAM, AND TRANSPORT IT BY PIPELINE TO AN ELECTRICAL GENERATING STATION WHERE IT TURNS A TURBINE TO PRODUCE ELECTRICITY.

IN TERMS OF PRODUCTION, GEOTHERMAL FLUIDS LOSE TEMPERATURE RAPIDLY WHEN THEY ARE TRANSPORTED ON THE SURFACE, SO ELECTRICAL GENERATING PLANTS MUST BE BUILT NEAR THE RESOURCE, IN CLOSE PROXIMITY TO THE WELLS. THUS, THE POWER IS GENERATED ON SITE, THEN HAS TO BE TRANSMITTED TO LOAD CENTERS. SINCE THE PRIME GEOTHERMAL PROSPECTS IN THE UNITED STATES ARE IN SPARSELY POPULATED AREAS OF THE WEST, TRANSMITTING TO DISTANT LOAD CENTERS ADDS TO THE COST OF DEVELOPMENT.

THE HIGHER TEMPERATURE GEOTHERMAL RESOURCES -- THOSE ABOVE 350 DEGREES FAHRENHEIT -- ARE BEST USED FOR THE PRODUCTION OF ELECTRICITY. LOWER TEMPERATURE RESOURCES ARE BETTER USED FOR DIRECT -- OR NON-ELECTRIC -- APPLICATIONS SUCH AS SPACE HEATING, AGRIBUSINESS, AND INDUSTRIAL PROCESSING.

IN ADDITION TO HIGH TEMPERATURE, A GEOTHERMAL RESOURCE DESIGNATED FOR ELECTRICAL GENERATION MUST BE LARGE ENOUGH AND HAVE FLOW CAPACITY TO PROVIDE A CONSTANT RATE OF STEAM PRODUCTION OVER THE USEFUL LIFE OF A GENERATING PLANT -- NORMALLY 30 YEARS.

THERE ARE TWO TYPES OF GEOTHERMAL RESOURCES: VAPOR- AND LIQUID-DOMINATED. WITH A VAPOR-DOMINATED RESOURCE, THE FLUID IS IN A SINGLE VAPOR OR STEAM PHASE IN THE RESERVOIR. WE DRILL INTO THE RESERVOIR, RELIEVE THE PRESSURE, BRING THE VAPOR TO THE SURFACE, REMOVE THE ROCK DUST AND TRANSPORT THE STEAM BY PIPELINE TO A GENERATING STATION.

A LIQUID-DOMINATED RESOURCE REQUIRES A MORE COMPLEX ABOVE-GROUND TECHNOLOGY. THE MOST WIDELY USED IS A FLASH SYSTEM WHERE THE HOT GEOTHERMAL BRINE PASSES THROUGH PRESSURE-REDUCING VESSELS WHICH CAUSE A PORTION OF THE FLUID TO FLASH INTO A MIXTURE OF STEAM AND BRINE. AFTER SEPARATION, THE REMAINING LIQUID WASTE IS THEN INJECTED BACK INTO THE UNDERGROUND RESERVOIR THROUGH AN INJECTION WELL.

IN THE LOWER TEMPERATURE RANGES, NEAR 350 DEGREES FAHRENHEIT, THE GEOTHERMAL FLUIDS ARE SOMETIMES PUMPED TO THE SURFACE AND CONTAINED UNDER BACK PRESSURE WHILE THE HEAT IS EXTRACTED IN A HEAT EXCHANGER. THE FLUIDS ARE THEN PUMPED BACK INTO THE UNDERGROUND RESERVOIR.

REINJECTION HELPS MAINTAIN RESERVOIR PRESSURE. IT ALSO ELIMINATES THE ENVIRONMENTAL PROBLEM OF DISPOSING OF THE UNUSABLE PORTION OF THE RESOURCE.

ALMOST ALL OF THE WORLD'S GEOTHERMAL RESOURCES ARE LIQUID-DOMINATED -- THAT, UNFORTUNATELY, IS THE NORMAL GEOLOGICAL CONDITION. THE COSTS FOR THE PRODUCTION AND ELECTRICAL GENERATION SYSTEMS NECESSARY WITH A LIQUID-DOMINATED RESOURCE ARE HIGHER. DRILLING INJECTION WELLS AND CONSTRUCTING AND MAINTAINING PIPELINES FOR THE UNUSED RESOURCE ADD SIGNIFICANTLY TO THE COSTS OF RESOURCE DEVELOPMENT.

IN THE UNITED STATES, GEOTHERMAL POWER IS NOW DEVELOPED IN INCREMENTS OF 50 TO 100 MW. THESE APPEAR TO BE OPTIMUM BLOCKS OF POWER FOR THE NUMBER OF WELLS REQUIRED, THE PIPELINE DISTANCE AND SIZE AND COST OF THE TURBINE. AT INCREMENTS OF 100 MW, GEOTHERMAL POWER IS ECONOMICALLY COMPETITIVE WITH ENERGY PRODUCED BY FOSSIL FUEL AND NUCLEAR PLANTS OF ABOUT 1,000 MW SIZE -- THOSE THAT ENJOY THE ADVANTAGE OF ECONOMY OF SCALE. THIS IS THE SIZE PLANT MOST COMMONLY INSTALLED IN THE U.S.

MANY DEVELOPING COUNTRIES CANNOT HANDLE THE LARGE 1000-MW INCREMENTS TO THEIR INSTALLED CAPACITY, AND SMALLER BLOCKS OF FOSSIL POWER ARE UNECONOMIC. THIS MAKES GEOTHERMAL POWER A VERY ATTRACTIVE FORM OF POWER GENERATION IN THOSE DEVELOPING COUNTRIES THAT HAVE THE GEOLOGIC POTENTIAL.

THERE ARE NOW SOME 50 COUNTRIES AROUND THE WORLD ACTIVE OR INTERESTED IN GEOTHERMAL EXPLORATION.

A QUICK REVIEW OF A FEW OF THE WORLD'S GEOTHERMAL DEVELOPMENTS WILL PROVIDE AN OVERVIEW OF THE TYPES OF RESOURCES THAT EXIST, SOME OF THE LIMITATIONS I MENTIONED EARLIER, AND THE DIFFERENT PRODUCTION AND GENERATION TECHNOLOGIES THAT HAVE BEEN DEVELOPED OVER THE LAST 25 YEARS.

THE GEYSERS, NORTH OF SAN FRANCISCO, IS THE WORLD'S LARGEST GEOTHERMAL DEVELOPMENT. THE RESOURCE THERE IS DRY STEAM, A FACTOR THAT HAS ACCOUNTED IN PART FOR ITS RAPID DEVELOPMENT. DRY STEAM REQUIRES A SIMPLE FORM OF CONVERSION TO ELECTRICITY: THE STEAM FLOWS UP THE WELL TO THE SURFACE, TRAVELS THROUGH PIPELINES TO AN ELECTRICAL GENERATING STATION WHERE IT TURNS TURBINES THAT PRODUCE ELECTRICITY. CONDENSATE IS THEN REINJECTED INTO THE RESERVOIR THROUGH AN INJECTION WELL.

THE GEYSERS FIELD HAS BEEN STEADILY DEVELOPED SINCE 1960 BY A NUMBER OF STEAM PRODUCERS AND ELECTRIC UTILITIES. THE ENTIRE FIELD NOW PRODUCES OVER 1800 MEGAWATTS OF GENERATING CAPACITY -- ENOUGH CAPACITY TO SUPPLY A CITY THE SIZE OF SAN FRANCISCO AND OAKLAND COMBINED.

THE GEYSERS IS NOW A MATURE FIELD. WITH THE COMMISSIONING OF ANOTHER POWER PLANT IN THE SUMMER OF 1988, IT APPEARS THAT THE FIELD WILL HAVE BEEN FULLY DEVELOPED.

THE FACT THAT THE GEYSERS IS A DRY STEAM FIELD IS AN EXCEPTION TO THE RULE. ALTHOUGH WE KNOW THERE ARE OTHER SMALLER DRY STEAM FIELDS IN THE WORLD -- AT LARDARELLO IN ITALY, IN NORTHERN TUSCANY, AND IN MATSUKAWA ON HONSHU, THE MAIN JAPANESE ISLAND -- THE BULK OF THE WORLD'S RESOURCES ARE LIQUID-DOMINATED.

NEW ZEALAND, HAS LONG EXPLORED FOR AND DEVELOPED GEOTHERMAL ENERGY. THAT COUNTRY, ONE OF GEOTHERMAL'S PIONEER DEVELOPERS, NOW HAS AN INSTALLED CAPACITY OF 167 MEGAWATTS. THE DISCOVERY OF NATURAL GAS HAD SLOWED GEOTHERMAL DEVELOPMENT, BUT THE NEW ZEALANDERS APPEAR TO HAVE RESUMED DEVELOPMENT OF THEIR GEOTHERMAL RESOURCES.

THE PHILIPPINES, WITH 894 INSTALLED MEGAWATTS, HAS THE SECOND LARGEST GEOTHERMAL DEVELOPMENT IN THE WORLD. TWO PRIMARY GEOTHERMAL FIELDS AT TIWI AND MAK-BAN HAVE BEEN DEVELOPED, EACH WITH 333 MEGAWATTS OF CAPACITY. THERE IS ADDITIONAL POTENTIAL ON THE ISLAND OF LUZON BUT, FOR THE MOMENT, THE LOCAL MARKET FOR ELECTRICITY IS LIMITED DUE TO THE SEVERE ECONOMIC CRISIS. THERE IS A 112-MEGAWATT INSTALLATION ON THE ISLAND OF LEYTE AND A 118-MEGAWATT INSTALLATION ON SOUTHERN NEGROS. REGRETTABLY, BOTH INSTALLATIONS ARE UNDER-UTILIZED.

TODAY, GEOTHERMAL POWER PLANTS IN THE PHILIPPINES REPLACE THE ENERGY EQUIVALENT OF ABOUT EIGHT MILLION BARRELS OF IMPORTED OIL A YEAR. GEOTHERMAL ENERGY NOW PROVIDES OVER 20 PERCENT OF THAT COUNTRY'S ELECTRICAL NEEDS.

POTENTIALLY THE LARGEST OF THE LIQUID-DOMINATED FIELDS IS THE SALTON SEA FIELD IN THE IMPERIAL VALLEY OF SOUTHERN CALIFORNIA. A NUMBER OF STEAM PRODUCERS HAVE BEEN WORKING THERE FOR MORE THAN A DECADE TO DEVELOP THIS RESOURCE.

WHILE THE GEYSERS IS AN EXCEPTION TO THE RULE BECAUSE IT IS A VAPOR-DOMINATED FIELD, THE SALTON SEA RESERVOIR IS AN EXCEPTION BECAUSE IT IS SUCH A HOSTILE LIQUID-DOMINATED RESOURCE.

THE GEOTHERMAL FLUIDS IN THE PHILIPPINES, NEW ZEALAND, JAPAN, TO NAME A FEW, ARE BENIGN IN CHEMICAL COMPOSITION. AS SUCH, THEY DO NOT CAUSE TECHNOLOGICAL PROBLEMS IN THE PRODUCTION PHASE OF THE OPERATION.

WHILE WE HAVE KNOWN THE POTENTIAL OF THE RESOURCE IN THE IMPERIAL VALLEY FOR A LONG TIME, WE HAVEN'T BEEN ABLE TO PRODUCE IT ON A LARGE SCALE BECAUSE OF ITS HIGH SALINITY.

THE RESOURCE IN THE IMPERIAL VALLEY CONTAINS ABOUT TEN TIMES AS MUCH SALT AS SEA WATER. THIS HAS CAUSED EXTREME CORROSION AND THE BUILD-UP OF SCALE DEPOSITS IN WELLS, PIPELINES, AND EQUIPMENT.

NEW METHODS TO PRODUCE FROM THIS HOSTILE RESOURCE HAVE BEEN DEVELOPED AT TWO PILOT PLANTS IN THE AREA. WE HAVE MADE SIGNIFICANT ADVANCES IN IDENTIFYING THE SPECIFIC CAUSES OF CORROSION AND HAVE COME UP WITH METHODS TO MINIMIZE THE DAMAGE IT CAUSES TO EQUIPMENT. RESEARCH STILL CONTINUES IN THE IMPERIAL VALLEY, BUT THE SOLUTIONS WE HAVE COME UP WITH ALREADY ARE INDICATIVE OF HOW THE GEOTHERMAL STEAM PRODUCERS HAVE LEARNED TO COPE WITH A VARIETY OF NATURAL FLUIDS.

MEANWHILE, STEAM PRODUCERS AND UTILITIES ARE NOW WORKING TOWARDS PUTTING THE SALTON SEA FIELD INTO COMMERCIAL OPERATION. MORE THAN 220 MEGAWATTS ARE UNDER CONSTRUCTION OR ARE BEING PLANNED. IN THE EAST MESA AND HEBER FIELDS, 174 MEGAWATTS OF CAPACITY IS INSTALLED OR PLANNED.

JAPAN IS A COUNTRY THAT IMPORTS VIRTUALLY ALL OF ITS OIL, SO IT SHOULD HAVE AN OVERWHELMING INCENTIVE TO DEVELOP INDIGENOUS ENERGY SUPPLIES BEYOND ITS PRESENT 215 MEGAWATTS OF INSTALLED CAPACITY. YET JAPAN IS HAMPERED BY EXTREME ENVIRONMENTAL CONCERNS.

MEXICO IS ONE OF THE WORLD'S LEADING OIL PRODUCERS, YET IT ALSO HAS BECOME THE WORLD'S THIRD LARGEST PRODUCER OF GEOTHERMAL ENERGY. WHILE MEXICO FACES SEVERE ECONOMIC PROBLEMS, IT HAS MANAGED TO DEVELOP 645 MEGAWATTS OF INSTALLED CAPACITY. ITS GEOTHERMAL DEVELOPMENT AT CERRO PRIETO SUPPLIES A SUBSTANTIAL AMOUNT OF ELECTRICAL POWER IN NORTHERN MEXICO.

IN CENTRAL AMERICA, EL SALVADOR PRODUCES 95 MEGAWATTS AND NICARAGUA, WHICH IS EXPANDING ITS DEVELOPMENTS AT MOMOTOMBO, PRODUCES 35 MEGAWATTS. GEOTHERMAL IS A POTENTIAL ENERGY SOURCE FOR SEVERAL CENTRAL AND SOUTH AMERICAN COUNTRIES AS WELL: GUATEMALA, COSTA RICA, CHILE, PERU, BOLIVIA, ECUADOR, COLUMBIA, AND ARGENTINA.

POWER PLANTS IN THE IMPERIAL VALLEY -- AS WELL AS IN OTHER AREAS -- DIXIE VALLEY, NEVADA, COSO HOT SPRINGS -- ALL ARE POSSIBLE BECAUSE OF STANDARD OFFER FOUR CONTRACTS UNDER PURPA. I KNOW THERE IS SOME DEBATE, EVEN CONTROVERSY, CONCERNING THESE CONTRACTS. I BELIEVE, HOWEVER, THAT THE CONCEPT BEHIND THE CONTRACTS IS SOUND BECAUSE IT ENCOURAGES DIVERSIFICATION ... IT IS ONE MORE WAY TO BREAK FROM OUR DEPENDENCE ON HYDROCARBON FUELS. SINCE THESE STANDARD OFFER FOUR CONTRACTS ARE NO LONGER GIVEN, NEW GEOTHERMAL DEVELOPMENTS HAVE TO MEET "AVOIDED" COST STANDARDS.

IT IS MY BELIEF THAT PUBLIC UTILITY COMMISSIONS ARE SHORT-SIGHTED IF THEY DEMAND THAT THE ECONOMICS OF GEOTHERMAL HAS TO MEET OR BE LOWER THAN THE LOWEST COST ALTERNATIVES. USING PURPA CONTRACTS AS AN EXAMPLE, THEY HAVE BEEN EXTREMELY SUCCESSFUL IN ALLOWING FOR LONG-TERM PLANNING FOR ALTERNATIVE ENERGY. THEY HAVE HELPED THE INDUSTRY EXPAND IN A DOWN CYCLE. IN EFFECT, PURPA CONTRACTS HAVE DEREGULATED THE INDUSTRY, CREATING IN THE LONG RUN, A MORE COMPETITIVE FIELD AND A MORE STABLE ENERGY ENVIRONMENT. BECAUSE OF THE NEW PUBLIC UTILITY COMMISSION ATTITUDES, GEOTHERMAL DEVELOPMENTS ARE NOW EXPECTED TO SLOW DOWN.

GENERALLY, A COUNTRY THAT DEVELOPS ALL OF ITS ENERGY RESOURCES OPENS UP ECONOMIC OPTIONS FOR ITSELF. THE MORE OPTIONS, THE HEALTHIER THE ECONOMY.

INDONESIA IS A GOOD EXAMPLE OF A COUNTRY WITH A BROADER OUTLOOK. INDONESIA CURRENTLY PRODUCES OVER 1.3 MILLION BARRELS OF OIL PER DAY. BUT IT IS SIMULTANEOUSLY MOVING AHEAD TO DEVELOP ITS SIGNIFICANT GEOTHERMAL POTENTIAL. ASIDE FROM ITS 142 MEGAWATTS OF INSTALLED GENERATING CAPACITY, ADDITIONAL GEOTHERMAL EXPANSION IS UNDER WAY. INDONESIA IS ALSO EXPLOITING ITS COAL RESOURCES FOR POWER GENERATION.

THE ENERGY POLICY PRACTICED BY INDONESIA -- THAT IS, DEVELOPING AS MANY OF ITS ENERGY RESOURCES AS POSSIBLE -- WILL ALLOW THE GOVERNMENT TO USE LESS OF ITS EXPORTABLE ENERGY -- OIL AND GAS -- FOR DOMESTIC DEVELOPMENT. WHEN THE PRICE OF OIL IS BACK UP AGAIN, SAY IN THE MID-NINETIES, INDONESIA SHOULD HAVE IN PLACE THE GEOTHERMAL POWER PLANTS TO SUPPLY A GOOD PORTION OF ITS ELECTRICITY. WHETHER THE PRICE OF OIL IS HIGH OR LOW, INDONESIA EARNS VALUABLE FOREIGN CURRENCY BY EXPORTING MORE OF ITS OIL. THAT CURRENCY CAN THEN BE USED FOR DOMESTIC DEVELOPMENT PROJECTS.

CONSIDERING THE UNITED STATES' DEPENDENCE ON IMPORTED FUELS, AND OUR NEGATIVE TRADE BALANCE, WE AS A NATION MIGHT BE WISE TO FOLLOW INDONESIA'S EXAMPLE.

WHAT ALL THE PACIFIC RIM COUNTRIES HAVE IN COMMON IS THE OPTION TO EXPAND THEIR INDIGENOUS SOURCES OF ENERGY -- AN OPTION THAT OUGHT TO BE TAKEN ADVANTAGE OF DURING THIS TIME OF LOW OIL PRICES.

MOST PEOPLE ARE SURPRISED WHEN I SAY THAT A LESS COMPETITIVE FORM OF ENERGY, LIKE GEOTHERMAL, OUGHT TO BE DEVELOPED WHEN OIL IS PLENTIFUL AND MUCH CHEAPER. BUT IT IS MY OPINION THAT SOONER OR LATER, ANOTHER ENERGY CRISIS WILL HIT US AND WE MUST BE PREPARED. MANY PREDICT ANOTHER CRISIS IN THE EARLY OR MID-NINETIES. THAT BEING THE CASE, WE SHOULD DEVELOP OUR GEOTHERMAL RESOURCES NOW SINCE IT TAKES FROM SEVEN TO TEN YEARS FROM EXPLORATION TO ON-LINE PRODUCTION.

AND GEOTHERMAL ENERGY WILL COMPETE SUCCESSFULLY. THE TECHNOLOGY IS PROVEN. THE PROSPECTS ARE GOOD. MOST OF THE WORLD'S RESOURCES CAN BE DEVELOPED. WE IN THE UNITED STATES, ALONG WITH SOME OF THE OTHER NATIONS ON THE PACIFIC RIM, HAVE AVAILABLE TO US THE OPTION OF DEVELOPING ALL OF OUR RESOURCES TO DO A BETTER JOB OF PREPARING OURSELVES FOR THE FUTURE.

Table 1

STATUS OF GEOTHERMAL POWER PLANTS-WORLDWIDE (1987)

WORLDWIDE
(Online as of 1987)

COUNTRY	MWe
UNITED STATES	2212
PHILIPPINES	894
MEXICO	655
ITALY	504
JAPAN	215
NEW ZEALAND	167
EL SALVADOR	95
KENYA	45
ICELAND	39
NICARAGUA	35
INDONESIA	142
TURKEY	21
CHINA	15
USSR	11
FRANCE	4
PORTUGAL	3
GREECE	2
TOTAL	5059

AFTER DIPIPPO, 1987

Table 2

SUMMARY OF GEOTHERMAL POWER PLANT CAPACITIES UNITED STATES–1987

	MWe ONLINE	MWe PLANNED
CALIFORNIA		
THE GEYSERS	1918	50
COSO	27	215
SALTON SEA	44	165
HEBER	94	0
EAST MESA	37	50
MAMMOTH	7	38
WENDELL H.S.	1	11
SUBTOTAL	2128	529
NEVADA	58	83
UTAH	23	19
HAWAII	3	13
SUBTOTAL	84	115
TOTAL	2212	644

AFTER DIPIPPO, 1987

SUBJ
GTHM
Hydro
Cost

HYDROTHERMAL COST OF POWER

An important factor in the rate of development of hydrothermal energy for electric power production will be its cost relative to possible alternatives including coal and nuclear. Although numerous forecasts of costs have been made, and will be subsequently discussed, the basic economic data necessary to give credibility to these forecasts is lacking. DOE expects to develop accurate cost and performance information for hydrothermal power through two 50 MWe demonstration plants which have been contracted for under cost-shared industry agreements. These plants will provide detailed capital and operating cost data in addition to serving as institutional path finders and technology demonstrations.

The first of these two plants, a flash steam design, will be constructed and operated by the Public Service Co. of New Mexico (PNW) on a high temperature (550°F) resource at the Baca location in the Valles Caldera in New Mexico. This plant is scheduled for start up in 1982. The second demonstration plant, employing an organic binary cycle design, will be constructed and operated by San Diego Gas and Electric Co. (SDG&E) on a moderate temperature (365°F) resource at Heber in the Imperial Valley of California. The binary plant is scheduled for start up in 1984. Cost of power estimates for these plants as well as western coal and nuclear plants are presented in Table 1.

Source
DOE/DGE annual
report

Table 1

Estimated Busbar Cost of Power (Mille/kwh)*

Start Up	Geothermal	Initial Year of Operation	Levelized Current Dollars	Levelized Constant Dollars
1982	PNM Baca Flash Demo (50% DOE funded plant)	42	62	36
1982	Baca Subsequent unit (no DOE funds)	43	64	36
1985	SDG&E Heber Binary Demo (cost estimates ignore 50% DOE funding)	89	129	75
	Coal			
1982	PNM estimate (San Juan unit 4)	42	62	36
1985	SDG&E estimates (Blythe)	43	64	36
1990	NRC (report NUREC 0480)	55	58	44
	Nuclear			
1985	SDG&E estimate (Sundesert)	**	50	29
1990	NRC	46	61	37

*in year of start-up dollars

**not available

assumptions:

PNM - 80% capacity factor
escalation 7% to 1982

SDG&E - 75% capacity factor
escalation 7% per year to 1985

NRC - 65% capacity factor
5% escalation to 1990
(both coal and nuclear)

This table illustrates the confusion which characterizes comparisons of the cost of power. The calculated (or estimated) generation costs vary with time, capital costs, o&m costs, fuel costs, discount rate, escalation rate and plant capacity factor. Results are presented in three different conventions as noted in the table; first year generation costs, levelized costs in current dollars and levelized costs in constant dollars. The different assumptions cited at the bottom of Table 1 will account for nominal differences in costs by do not obscure the basic conclusions discussed later.

Levelized costs are constant kwh charges over the life of the plant, which result in a present value of revenues precisely equal to the present value of costs. Levelized costs can be calculated in current (as spent) dollars, resulting in a hypothetical cash flow decreasing in real buying power year after year (analogous to a constant home mortgage payment), or levelized costs can be calculated in constant dollars, which would reflect a revenue stream starting at a much lower value and having constant real buying year after year, but increasing in current dollars each year. Neither method would represent actual year by year kwh charges but both methods would generate the same present value and thus either method can be used to determine the relative attractiveness of alternative investments. Initial year costs reflect the kwh charges in that year's dollars which would actually occur in the year of start up to balance revenues with costs. The initial year costs do not represent a proper basis for determining the relative attractiveness of alternatives, as the out year escalation rates (for fuel for example) may cause a system with low initial costs to have a higher present value than another system with high initial costs but which is essentially fuel inflation free.

Table 1 shows that hydrothermal energy is cost competitive with coal and nuclear for high temperature resources (as at Baca), but is measurably more expensive at moderate temperature (as at Heber). PNM estimates that a 30 year hydrothermal plant will produce power at essentially the same cost as a 40 year coal plant. PNM assumes the second plant at the Valles Caldera site will have lower o&m and fuel costs which essentially compensate for the DOE 50% subsidy of the demonstration unit. SDG&E shows their average temperature generation cost estimates to be twice as high for geothermal as coal and 2½ times as high as nuclear. SDG&E projects lower costs for subsequent hydrothermal units but has not attempted to quantify these projections.

The reasons for high costs on the proposed SDG&E binary plant are straightforward. At 365^{o}F, the binary plant requires approximately 2½ times the brine flow rate as the 550^{o}F flash plant. This higher brine flow dictates larger piping, valves and reinjection pumps. The lower temperature necessarily means a 20 percent lower thermal efficiency, which requires approximately 20 percent larger condensers, cooling towers, water circulating pumps and 20 percent more make-up water. In addition, the lower vapor pressure of the 365^{o}F brine causes wells to be low in productivity unless they are pumped. The binary plant will use approximately 5MW of parasitic power for downhole pumps which is not required for the 550^{o}F resource, plus an additional 2MW of parasitic power for injection pumps. Capital costs for downhole pumps add 2½ million dollars in initial cost and will require frequent maintainance and replacement. It is clear as Table 1 indicates, that moderate temperature resource utilization with current technology is not competitive with coal and nuclear.

The dominant cost in hydrothermal energy is that of fuel (hot water and steam) which accounts for 50-75% of the kwh charges. Although hydrothermal energy may be more costly from moderate temperature resources, market penetration might still proceed under certain circumstances because this resource is relatively benign environmentally, and coal and nuclear may be discouraged by state policy (as in California).

High hydrothermal fuel costs can be attributed primarily to high drilling costs, low reservoir temperature (requiring more wells) or low well productivity. The prospect for improving economics through technological progress is excellent, especially for the moderate temperature resources (which constitute 80% of the inferred 140,000 MW recoverable resource). Drilling technology development, reservoir stimulation for the purpose of increasing well flow, downhole pump, and more efficient conversion systems have a realistic potential for cutting moderate temperature costs in half, which is why the development of geothermal technology is an important part of the Federal geothermal program.

[AMERICAN JOURNAL OF SCIENCE, VOL. 277, OCTOBER, 1977, P. 937-981]

TRANSPORT PHENOMENA IN HYDROTHERMAL SYSTEMS: COOLING PLUTONS

D. NORTON and J. KNIGHT

Department of Geosciences, University of Arizona, Tucson, Arizona 85721

ABSTRACT. The nature of heat and mass transport in pluton environments has been described by partial differential equations and simulated by numerical approximations to these equations. A series of heuristic models computed on the basis of these equations describes the general features of fluid circulation in the vicinity of an intrusive igneous body within the upper 10 km of the Earth's crust.

Analysis of these models indicates that fluid circulation is an inevitable consequence of the emplacement of magmas in the crust. The magnitude of this fluid circulation generates convective heat fluxes which predominate over conductive heat fluxes when host rock permeabilities exceed 10^{-14} cm^2. However, cooling rates for the pluton are not significantly shortened unless the pluton permeability is also $> 10^{-14}$ cm^2. The geometries of fluid circulation and isotherms are directly affected by variations in pluton size, width, level of emplacement, and permeability, as well as the distribution of permeable zones in the host rocks. Most striking, however, is the effect of the fluid properties on heat and mass transport. The overall style of fluid circulation is effectively controlled by coincident maxima of the isobaric thermal coefficient of expansion and heat capacity with the viscosity minima in the supercritical region of the H_2O-system.

Waters in natural pluton systems are predicted to move from their points of origin to positions several kilometers away in a few hundred thousand years. This redistribution affects magmatic fluids and fluids in host rocks up to several kilometers away from the pluton. Typically, temperature and pressure changes along the fluid flow paths produce dramatic changes in solvent properties. Hence, the fluid-rock interactions along the pathlines should generate diagnostic mineral assemblages and shifts in isotopic compositions. Average fluid:rock mass ratios of 0.4 are realized over the entire permeable portions of the systems.

This analysis reveals the extent of fluid circulation, and magnitude of convective heat flux over broad crustal regions and along crustal plate boundaries where igneous activity is voluminous may be much greater than heretofore realized.

INTRODUCTION

Heat and mass transport processes associated with the emplacement of magmas into the Earth's crust are continually referred to by geologists in their studies of igneous and volcanic rocks. Inferences as to the temperature and pressure conditions within the crust are made mostly on the basis of conductive heat flow, mineral stability data, and analogies to modern environments. In particular, the crystallization and cooling paths of igneous melt systems are inferred from mineral assemblages and experimentally derived phase diagrams. These methods have led to much understanding of the nature of the crust and subcrustal environment, but they require a considerable extrapolation of information derived from a rather complex process.

Magmatic processes may be described by simple physical laws which relate all relevant variables in a set of coupled partial differential equations. Such a description is appealing, primarily because it provides an analysis that is independent of traditional methods and permits consideration of the process at the crustal scale.

Emplacement of magma bodies into the Earth's crust results in large thermal perturbations which are dispersed by a combination of heat conduction and fluid circulation. Generation of a fluid potential field is

the inevitable consequence of a thermal or solute induced pore fluid density anomaly along a horizontal plane in the crust. Recognition of this fact then raises the question of the extent and nature of fluid flow associated with both thermal and "salinity" anomalies in the crust. The magnitude of fluid flux is directly related to rock permeability and transport properties of the fluid. Geophysical evidence suggests that rocks fail by fracture and have interconnected pore spaces to at least 15 km in the crust, and, therefore, convective heat transport may be considerably more significant on a crustal scale than heretofore realized.

This communication derives the partial differential equations that represent the heat transfer process associated with thermal perturbations in the crust, discusses the physical significance of these equations, presents the numerical approximations to these equations, and analyzes how geologic variations in pluton environments affect the cooling history of the pluton. A series of heuristic cooling models that demonstrate the effect of various initial and boundary values on temperature, pressure, fluid velocities, fluid pathlines, and cooling rates are presented.

Large scale fluid circulation around plutons has been actively discussed by students of mineral deposits since the earliest recognition of vein minerals (Ssu-hsiao, 1250; Van Hise, 1901; and Lindgren, 1907). Stable light isotope distribution in pluton environments suggests that fluid derived locally from the surrounding host rocks and ultimately from the local meteoric waters has circulated through most plutons (Taylor, 1971). On the basis of trace element and mineral occurrences, one predicts that a tremendous mass of fluid is required to achieve the mineralogical and bulk composition changes observed in hydrothermal systems.

Analysis of fluid circulation in the crust by mathematical methods has been a topic of study for many years. Lord Rayleigh's original work (1916) defined the fundamental problem which, together with advances in computing technology, encouraged many subsequent efforts (Wooding, 1957; Holst and Aziz, 1972; Elder, 1967; Donaldson, 1962, 1968; Lister, 1974; Ribando, Torrance, and Turcotte, 1976). The common occurrence of high salinity fluids in shallow crustal environments has also been recognized as a probable cause of fluid circulation (Nield, 1968; Veronis, 1968; Rubin, 1973). These studies have defined many of the basic governing differential equations that describe thermal and solute driven fluid circulation. Howeyer, each has dealt with idealized equations of state for the fluid and rock phases and with uniform properties in dimensionless systems. In order to relate the processes to geologic features, real fluid and rock properties have been used in this study.

Notation

a — volumetric heat sources (cal cm^{-3} $°C^{-1}$)
A — area (cm^2)
C_f — isobaric heat capacity of the fluid (cal g^{-1} $°C^{-1}$)

C_m — heat capacity at constant pressure of the media (cal g^{-1} °C^{-1})
C_p — heat capacity at constant pressure (cal g^{-1} °C^{-1})
D_1 — matrix coefficient in Poisson equation
D_2 — matrix coefficient in Poisson equation
D_3 — matrix coefficient in Poisson equation
E — internal energy (cal g^{-1})
$\bar{g}$ — gravitational force vector (cm sec^{-2})
$\bar{i}$ — unit vector in x-direction
$\bar{j}$ — unit vector in y-direction
K — η divided by k
$\bar{k}$ — unit vector in z-direction
k — permeability (cm^2)
k_m — thermal conductivity (cal (cm sec °C) $^{-1}$)
M — mass (g)
M_f — mass of fluid (g)
M_r — mass of rock (g)
P — pressure (bars)
P_r — reference pressure (bars)
q — thermodynamic heat (cal g^{-1})
q_1 — magnitude of fluid flux in x-direction (g cm^{-2} sec^{-1})
q_2 — magnitude of fluid flux in y-direction (g cm^{-2} sec^{-1})
q_3 — magnitude of fluid flux in z-direction (g cm^{-2} sec^{-1})
Q_{ADV} — nonlinear advection term
$\bar{Q}_{conduction}$ — conductive component of heat flow vector (cal cm^{-2} sec^{-1})
$\bar{Q}_{convection}$ — convective component of heat flow vector (cal cm^{-2} sec^{-1})
$\bar{Q}_n$ — component of heat flow vector normal to the surface (cal cm^{-2} sec^{-1})
Q_P — nonlinear density perturbation term
Q_{total} — total heat flux (cal sec^{-1})
$\bar{r}$ — position vector (cm)
R — arbitrary region
R_a — Rayleigh number
S — surface
t — time (sec)
T — temperature (°C)
T_o — background temperature (°C)
T_r — reference temperature (°C)
$\bar{u}$ — fluid flux vector (g cm^{-2} sec^{-1})
$\bar{u}_x$ — x-component of fluid flux vector (g cm^{-2} sec^{-1})
$\bar{u}_y$ — y-component of fluid flux vector (g cm^{-2} sec^{-1})
$\bar{u}_z$ — z-component of fluid flux vector (g cm^{-2} sec^{-1})
u — variable at known time step
u^* — variable at half time step
u^{p+1} — variable at new time step
$\bar{v}$ — velocity vector (cm sec^{-1})

v_1 — magnitude of velocity in x-direction (cm sec^{-1})
v_2 — magnitude of velocity in y-direction (cm sec^{-1})
v_3 — magnitude of velocity in z-direction (cm sec^{-1})
$\bar{v}_l$ — velocity vector of interest (cm sec^{-1})
$\bar{v}_t$ — tangential velocity vector (cm sec^{-1})
V — volume (cm^3)
w — thermodynamic work (cal g^{-1})
x — cartesian coordinate
y — cartesian coordinate
z — cartesian coordinate
α — coefficient of isobaric thermal expansion ($°C^{-1}$)
β — coefficient of isothermal compressibility (bar^{-1})
Ψ — streamfunction (g cm^{-1} sec^{-1})
ϕ — flow connected porosity
ν — viscosity (cm^2 sec^{-1})
ρ — density (g cm^{-3})
ρ_m — density of the media (g cm^{-3})
γ_1 — boundary equation constant
γ_2 — boundary equation constant
γ_3 — boundary equation constant
∇x — curl

$$\nabla - \frac{\partial}{\partial x} + \frac{\partial}{\partial y} + \frac{\partial}{\partial z}$$

HEAT AND MASS TRANSPORT

Thermal anomalies in the Earth's crust are dispersed by a combination of conductive and convective heat transfer. Thermal energy transfer away from regions of anomalous temperature at depths below 15 to 20 km is apparently by pure conduction, whereas in shallower crustal environments heat transfer by the circulation of fluids augments and, in certain instances, may predominate over conductive heat transfer. Equations sufficiently general to permit a reasonable analysis of temperature distribution and fluid flow in a variety of pluton environments have been developed for a two-dimensional region of the crust into which a thermal energy source has been instantaneously emplaced. The region is treated as a fluid saturated permeable media, and all properties of the fluid phase are described with respect to the H_2O–system and Newtonian mechanisms. Constraints of energy, mass, and momentum conservation are utilized to represent the heat and mass transfer process.

Energy

Energy content of a one component single phase, constant mass system is defined by the first law of thermodynamics:

$$\int_0 (dq - dw) = 0. \qquad (1)$$

For a reversible process, the work done by the system defines a path independent function, E, called internal energy.

$$E(T,P) - E(T_oP_o) = \int_{T_oP_o}^{T,P} [C_p - PV\alpha T]\, dT + [V P\beta - T\alpha]\, dP. \quad (2)$$

For single phase fluid system eq (2) can be simplified to

$$E(T,P) - E(T_oP_o) = \int_{T_oP_o}^{T,P} C_p dT, \quad (3)$$

where C_p may be either the heat capacity of the fluid phase, C_f, or the average heat capacity of the fluid saturated media, C_m. This simplification introduces a few percent error in the energy content of the system in the vicinity of the fluid critical endpoint.

Consider a permeable, temperature anomalous region, R, in the crust at some temperature, T. Thermal energy transferred from this region across the enclosing surface, S, and to the surroundings can be described in terms of the heat flow normal to the surface, $\bar{Q}_n$ [cal cm^{-2} sec^{-1}]. The conduction contribution to total heat flux is proportional to the negative thermal gradient:

$$\bar{Q}_{conduction} = -k_m \nabla T. \quad (4)$$

Fluids flowing across the surface will also transport thermal energy in direct proportion to their heat content and mass flux,

$$\bar{Q}_{convection} = \bar{u}\, C_f T. \quad (5)$$

Total heat flow, $\bar{Q}_n$, is the sum of eqs (4) and (5):

$$\bar{Q}_n = -k_m \nabla T + \bar{u}\, C_f T. \quad (6)$$

Total heat flux is then the product of the infinitesimal area and the heat flow vector integrated over the entire surface:

$$\bar{Q}_{total} = \int_S \bar{Q}_n dA. \quad (7)$$

The heat lost from the entire region is obtained by transforming vector eq (7) into volumetric integrals by means of the Gauss divergence theorem:

$$\bar{Q}_{total} = \int_S \bar{Q}_n dA = \int_R \nabla \cdot \bar{Q}_n\, dV. \quad (8)$$

Combining eqs (6) and (8) results in the general expression for heat loss from the entire region:

$$\bar{Q}_{total} = \int_R (-\nabla \cdot (k_m \nabla T) + \bar{u} \nabla \cdot (C_f T) + C_f T \nabla \cdot \bar{u})\, dV. \quad (9)$$

Several different natural heat sources or sinks, for example, radioactive decay, heat of crystallization, hydrolysis reactions, or mixing reactions, may be contained in the region. Our treatment will focus on the thermal energy associated with magma bodies in the upper portion of the Earth's crust. We consider here a fairly specific formulation which includes a term, a, for volumetric heat sources and sinks in the region. Total thermal energy content in the region is then

$$E_R = \int_R (C_m \rho_m T + aT)\, dV. \tag{10}$$

The rate at which this heat is depleted is merely the derivative of eq (10) with respect to time,

$$\frac{\partial E_R}{\partial t} = -\int_R (C_m \rho_m + a) \frac{\partial T}{\partial t} dV, \tag{11}$$

where the heat capacity and density of the media and the volumetric source or sink term are assumed to be constant with time.

The rate at which heat leaves the region, defined by eq (9), must equal the rate at which heat is depleted within the region, eq (11), in order to maintain conservation of energy. Since eqs (9) and (11) hold for any portion of the region, the volumetric integrals are zero everywhere, and they become

$$(C_m \rho_m + a) \frac{\partial T}{\partial t} + \bar{u} \nabla \cdot C_f T + C_f T\, \nabla \cdot \bar{u} = \nabla \cdot (k_m \nabla T). \tag{12}$$

Eq (12) is the partial differential equation describing thermal energy transport in a one component single fluid phase, constant mass, system undergoing reversible changes.

Conservation of Mass, Divergence of $\bar{u}$

Consider fluid flow through a representative volume in which the velocity vector, $\bar{v}$, is described by

$$\bar{v} = v_1 \bar{i} + v_2 \bar{j} + v_3 \bar{k}. \tag{13}$$

And since $\rho \bar{v} = \bar{u}$, the fluid flux vector is

$$\bar{u} = \rho \bar{v} = q_1 \bar{i} + q_2 \bar{j} + q_3 \bar{k}. \tag{14}$$

For unit volume, ΔV, the fluid flux through face $\Delta x \Delta z$ is

$$q_2 (y)\, \Delta x \Delta z, \tag{15}$$

and the fluid flux leaving the opposite face $(y+\Delta y)$ is

$$q_2 (y+\Delta y)\, \Delta x \Delta z. \tag{16}$$

The difference in fluid flux in the y direction is, therefore, given by the difference between eqs (15) and (16),

$$\Delta q_2 \frac{\Delta V}{\Delta y} = [q_2(y) - q_2(y + \Delta y)]\, \Delta x \Delta z. \tag{17}$$

Similarly, the difference in the mass flux for the other faces can be derived. Therefore, the net mass loss or gain from the entire volume over time Δt is

$$M = \left(\frac{\Delta q_1}{\Delta x} + \frac{\Delta q_2}{\Delta y} + \frac{\Delta q_3}{\Delta z}\right) \Delta V \Delta t. \tag{18}$$

Changes in fluid density or the connected flow porosity (Norton and Knapp, 1977) may produce changes in fluid mass in the volume.

$$M = \frac{\partial \rho \phi}{\partial t} \Delta V \Delta t. \tag{19}$$

Combining eqs (18) and (19) and letting Δx, Δy, Δz, and Δt approach zero give

$$\frac{\partial \rho \phi}{\partial t} = \frac{\partial \bar{u}}{\partial x} + \frac{\partial \bar{u}}{\partial y} + \frac{\partial \bar{u}}{\partial z}, \tag{20}$$

which is the conservation of mass or continuity equation for compressible fluid flow. For steady state flow

$$\nabla \cdot \bar{u} = 0. \tag{21}$$

This conservation of mass equation is used to obtain the conservative form of eq (12).

$$(C_m \rho_m + a) \frac{\partial T}{\partial t} + \bar{u} \nabla \cdot C_f T = \nabla \cdot (k_m \nabla T). \tag{22}$$

Momentum Equations

The necessary condition for no fluid flow, $\bar{u} = 0$, is

$$\rho \bar{u} + \nabla P = 0, \tag{23}$$

which is the familiar equation of hydrostatics. Eq (23) can be written in vector form:

$$\begin{bmatrix} 0 \\ 0 \\ \rho \bar{u} \end{bmatrix} + \begin{bmatrix} \partial P/\partial x \\ \partial P/\partial y \\ \partial P/\partial z \end{bmatrix} = \begin{bmatrix} 0 \\ 0 \\ 0 \end{bmatrix} \tag{24}$$

For no flow conditions, eq (24) requires $\partial P/\partial x = \partial P/\partial y = 0$; that is, pressure can only vary with depth, and fluid density must be constant over any horizontal plane. Ergo, lateral variations in fluid density associated with plutons require fluid flow. The magnitude of this flow is determined by the permeability and fluid viscosity, as indicated by Darcy's Law:

$$\bar{u} = \frac{-k}{\nu} (\rho g + \nabla P). \tag{25}$$

Density perturbations may be due to temperature variation, which is defined by the isobaric constant molality coefficient of thermal expansion,

$$\alpha \equiv \frac{-1}{\rho_o} \left(\frac{\partial \rho}{\partial T}\right)_{P, m_1} \tag{26}$$

or to solute content. Considering for the moment only the thermal effects and that α is not a function of temperature[1], eq (26) is integrated:

$$\rho = \rho_o \left[1 - \alpha (T - T_o)\right], \tag{27}$$

where T_o is the temperature distribution for no flow conditions. The Darcy equation for fluid flow then becomes

$$\bar{u} = \frac{-k}{\nu} \left[\rho_o (1 - \alpha (T - T_o)g) + \nabla P\right]. \tag{28}$$

The gradient in pressure with respect to the z axis is $-\rho_o g$; therefore, eq (28) becomes

$$\bar{u} = \frac{k}{\nu} \left[\alpha T - T_o)g\rho_o + \nabla_{xy} P\right]. \tag{29}$$

Eq (29) describes the mass flow due to a thermal anomaly in the Earth's crust.

Combined Equations

The energy balance, conservation of mass, and momentum equations can be treated in one of several possible ways to obtain a numerical solution. We will utilize the conservative form, where the equations are reduced to two independent scalar quantities, streamfunction and temperature.

The circulation tendency of a fluid around the surface is a vector quantity, defined as the product of the average tangential velocity and the distance around the closed surface,

$$\text{Circulation} = \bar{v}_t ds. \tag{30}$$

From Stokes Theorem we have

$$\int_S (\nabla x\, \bar{v})_n dA = \bar{v}_t ds, \tag{31}$$

where $(\nabla x\, \bar{v})_n$ is the component of $\nabla x\, \bar{v}$ in the direction of a unit vector, $\hat{n}$. Applying the circulation concept to eq (29) gives

$$\nabla x \frac{\nu}{k} \bar{u} = \nabla x (\alpha(T - T_o)g\rho_o) + \nabla x (\nabla_{xy} P) \tag{32}$$

and, since $\nabla_{x,y} P$ is a gradient field and the curl of a gradient field is zero, the fluid flow equation reduces to

$$\nabla x \frac{\nu}{k} \bar{u} - \nabla x (\alpha(T - T_o)g\rho_o) = 0. \tag{33}$$

A packet of fluid circulating through permeable rocks reacts with the enclosing rock mass and changes composition along its flow path. A description of this flow pathline is necessary to study the chemical varia-

[1] α indeed varies considerably with P and T, but this modification will be accounted for later.

tions in time of any given fluid packet. Consider a fluid packet in a permeable media and represent its position at time t_o with position vector r_i, where i denotes the particle of interest. As time varies, movement of the packet and changes in its fluid properties can be followed. The velocity of the packet is simply

$$\bar{v}_i = \frac{dr}{dt}. \tag{34}$$

Transforming to orthogonal coordinates and recalling that the fluid flow $\bar{u}$ is defined by $\bar{u} = \rho\bar{v}$,

$$\frac{\rho dx}{q_x} = \frac{\rho dy}{q_y} = \frac{\rho dz}{q_z} = dt, \tag{35}$$

where eq (35) describes the position after time increment dt.

At every instant in time, dt = 0, fluid flux vectors can be related to the streamfunction, which is tangent to these vectors. The parametric equation for this function in three dimensions is:

$$\frac{dx}{q_x} = \frac{dy}{q_y} = \frac{dz}{q_z}, \tag{36}$$

and in two dimensions eq (36) becomes

$$q_z dy - q_y dz = 0, \tag{37}$$

which is an exact differential equation since $\nabla \cdot q = 0$. Eq (37) defines the streamfunction, which can also be written as an exact differential:

$$d\Psi = \frac{\partial\Psi}{\partial y}dy + \frac{\partial\Psi}{\partial z}dz = q_z dy - q_y dz = 0. \tag{38}$$

This leads to the definition of fluid flux in terms of the streamfunction:

$$q_y = -\frac{\partial\Psi}{\partial z}\,;\; q_z = \frac{\partial\Psi}{\partial y}. \tag{39}$$

Introducing the streamfunction into eq (33) gives

$$\nabla_y x \frac{\nu}{k} \nabla_y\Psi - \nabla_z x \frac{\nu}{k} \nabla_z\Psi - \nabla_y(g\rho_o\,\alpha(T - T_o)) = 0. \tag{40}$$

Eq (40) reduces to the familiar Poisson equation: $\nabla^2\Psi = f(y,z,t)$, if ν/k is constant.

Eq (33) can now be rewritten, and the operator (∇x) expanded with respect to the y–z plane and $K = \nu/k$ substituted.

$$q_y\frac{\partial K}{\partial z} + K\frac{\partial q_y}{\partial z} - q_z\frac{\partial K}{\partial y} - K\frac{\partial q_z}{\partial y} - g\rho_o\frac{\partial(\alpha(T - T_o))}{\partial y} = 0. \tag{41}$$

Combining eq (39) with (41) and rearranging terms give the general momentum equation:

$$\nabla^2\Psi + \frac{1}{K}\frac{\partial K}{\partial z}\frac{\partial \Psi}{\partial z} + \frac{1}{K}\frac{\partial K}{\partial y}\frac{\partial \Psi}{\partial y} = \frac{g\rho_o\partial(\alpha(T - T_o))}{K\,\partial y} \tag{42}$$

Eq (42) is equivalent to

$$\frac{1}{K}\nabla \cdot (K\,\nabla\Psi) = \frac{\rho_o g\partial(\alpha T - T_o)}{K\,\partial y}, \tag{43}$$

which forms the basis of the numerical computation. Extensions to afford for anisotropic and heterogeneous permeability distribution follow directly from eq (40).

In summary, the governing partial differential equations are:

Conservation of Energy:

$$(C_m\rho_m + a)\frac{\partial T}{\partial t} + \bar{u}\nabla \cdot C_f T = \nabla \cdot (k_m \nabla T) \tag{22}$$

Conservation of Mass:

$$\nabla \cdot q = 0 \tag{21}$$

Conservation of Momentum:

$$\nabla^2\Psi + \frac{1}{K}\frac{\partial K}{\partial z}\frac{\partial \Psi}{\partial z} + \frac{1}{K}\frac{\partial K}{\partial y}\frac{\partial \Psi}{\partial y} = \frac{g\rho_o\partial(\alpha(T - T_o))}{K\,\partial y} \tag{42}$$

Dimensionless Forms of Equations

The governing equations contain three dependent quantities — temperature, streamfunction, and fluid flux. The solution can be obtained with eqs (22) and (42) alone, since eq (42) is written in conservative form, that is, eq (42) implicitly includes eq (21). In turn, fluid flux can be computed from the stream function, eq (39).

Modeling of geologic processes with the governing equations derived above requires that the variables be scaled, similar to bench scale model experiments. Scaling permits simulation of processes that occur over hundreds of thousands of years in a few minutes of computer time. Often only the dimensionless variables are reported, generally as a constant Rayleigh number; however, to afford for the equations of state of the fluid and rock utilized in this study, Rayleigh numbers were computed from actual temperatures and pressures at each time increment.

The dimensionless forms of eqs (22) and (42) (see table 1 for definitions) are

$$F\frac{\partial T}{\partial t} + \bar{u}\,\nabla C_f\,T = \nabla \cdot k_m \nabla T \tag{44}$$

$$\frac{1}{K}\nabla \cdot (K\,\nabla\,\Psi) = R_a\,\nabla\,\alpha\,T. \tag{45}$$

TABLE 1
Dimensionless and characteristic values

$$y = yl^* \qquad k = k\,k^*$$

$$z = zl^* \qquad \rho = \underline{\rho}\,\rho^*$$

$$\nabla = (\underline{\nabla}/l^*) \qquad C_f = C_f\,C_f^*$$

$$T = TT^* \qquad k_m = k_m\,k_m^*$$

$$F = 1 + \frac{a}{\rho_m C_m}$$

$$Ra = \frac{gk\,\rho_o\,C_f^*\,T^*\,\alpha^*\,l^*}{\rho\,k_m^*}$$

$$t = \frac{t\,l^{*2}\,\rho_m C_m}{k_m^*} \qquad \alpha = \underline{\alpha}\,\alpha^*$$

$$\bar{u} = \bar{u}\,\frac{k_m^*}{C_f^*\,l^*}$$

$$\Psi = \underline{\Psi}\,\frac{k_m^*}{C_f^*}$$

Starred quantities are characteristic values for the respective parameters; l^* is characteristic height. For all model systems in this paper, $\Psi = \underline{\Psi}\ 3 \times 10^{-4}$ g cm^{-1} s^{-1}.

Approximations of Equations

The dimensionless energy and momentum equations are of the general form

$$\frac{1}{K}\,(\nabla \cdot (C\,\nabla\,u)) = F\,\frac{\partial u}{\partial t} - s \tag{46}$$

where s is the nonlinear advection term in the energy equation or the density perturbation term in the momentum equations, and F is a term in the energy equation that accounts for energy sources or sinks in the domain but is equal to 1 in the momentum equation. The equation is readily solved by the alternating direction implicit method (Peaceman-Rachford, 1955).

The alternating direction implicit method has been modified to include the variable parameter C in eq (46). The modified form of the difference equations is, for the initial one-half time step,

$$F_{ij}\frac{u^*_{ij}-u_{ij}}{\Delta t} = \frac{1}{K_{ij}}(\nabla_y \cdot (C_{ij}\nabla_z u^*_{ij}) + \nabla_z \cdot (C_{ij}\nabla_y u_{ij})) - s_{ij}, \tag{47}$$

and for the final one-half time step,

$$F_{ij}\frac{u_{ij}^{p+1}-u^*_{ij}}{\Delta t} = \frac{1}{K_{ij}}(\nabla_y \cdot (C_{ij}\nabla_y \cdot u^*_{ij}) + (\nabla_z \cdot (C_{ij}\nabla_z u_{ij}^{p+1})) - s_{ij}. \tag{48}$$

The expanded finite difference equations are of the general form:

$$D_1\, u^*_{i-1j} + D_2\, u^*_{ij} - D_3\, u^*_{i+1j} = 0. \tag{49}$$

Eq (49) forms a system of linearly independent equations between the N unknown quantities, u*'s, which is quickly solved by a Gauss elimination method.

Nonlinear Terms

Nonlinear terms, S_{ij}, in the momentum and energy equations are the thermal energy advection and fluid density gradients. The advective transport of thermal energy is given by

$$Q_{ADV} = \bar{u}\,\nabla C_p T, \tag{50}$$

The transportive character of this equation must be maintained in the numerical equations. Therefore, "upwind" differencing equations are used:

for $\bar{u} = > 0$

$$Q_{ADV} = \frac{\bar{u}_{ij}}{\Delta z}(C_{ij}\,(T_{ij} - T_{i-1j}) + T_{ij}\,(C_{ij} - C_{i-1j})); \tag{51}$$

for $\bar{u} = < 0$

$$Q_{ADV} = \frac{\bar{u}_{ij}}{\Delta z}(C_{ij}\,(T_{ij} - T_{i+1j}) + T_{ij}\,(C_{ij} - C_{i+1j})). \tag{52}$$

Perturbations caused by fluid density gradients across an arbitrary horizontal plane in the system from eq (42) can be represented by a central difference equation:

$$Q_P = \frac{Ra_{ij}}{2\Delta y^2}(\alpha_{ij}\,(T_{ij-1} - T_{ij+1}) + T_{ij}\,(\alpha_{ij-1} - \alpha_{ij+1}). \tag{53}$$

Boundaries

Difference equations containing a point on the boundary are approximated with a general, first order, constant coefficient boundary condition equation:

$$\gamma_1\, u + \gamma_2\, \nabla\, u = \gamma_3 \tag{54}$$

For i = 2 this equation gives

$$u_{ij} = \gamma_{3_{2j}} + \frac{\gamma_{2_{2j}}}{2\Delta z}\, u^*_{3j}\left(\gamma_{1_{2j}} + \frac{\gamma_{2_{2j}}}{2\Delta z} \right)^{-1} \tag{55}$$

which may be substituted directly into eq (49).

Convergence and Time Steps

The numerical approximation for eq (22) is of the form

$$\nabla \cdot (k_m \nabla T) = F \frac{\partial T}{\partial t} - s. \tag{56}$$

This requires K_{ij} in numerical eq (46) to be equal to 1. A minor modification of eq (46) gives a solution to momentum eq (45) where $K = \nu/k$ and $C = \nu/k$. The transient term does not appear since energy and momentum equations are coupled, and the time step is made through the energy equation. We, therefore, require a steady-state solution which can be achieved through the relaxation sequence, used by Peaceman and Rachford (1955).

The maximum time step that will produce a convergent and stable numerical solution to the equations has been determined by stability analysis. This analysis shows the numerical solutions are stable, if time increments are constrained by

$$\Delta t < \frac{2}{\Delta z} + \frac{2}{\Delta y} + \frac{|q_z|}{\Delta z} + \frac{|q_y|}{\Delta y}. \tag{57}$$

This step size criteria returns a perfectly stable solution and is used in the steady state iteration to define the maximum step size possible for a given problem (Roache, 1972).

The numerical reliability of the model calculations was checked against analytical functions for pure conductive heat transport and were found to be in reasonable agreement. Exact verification is not possible for complex geometries of the heat source or for the combined convective-conductive heat transfer, since exact analytical solutions to these problems are impossible. The models give reasonable cooling times with respect to pure conduction, and the computed fluid fluxes seem realistic. However, the geologic reliability is entirely dependent on the reliability of the initial and boundary conditions and the equations of state for fluid and rock.

Equations of state.—Any equation of state can be used in conjunction with the numerical equations to represent rock and fluid properties. In this study the fluid properties were approximated by the H_2O–system, and the rock properties by average values for the appropriate rock composition.

Fluid.—The fluid phase transport properties significantly affect the nature of the cooling process. The fluid properties, except for viscosity, were computed directly from equations of state for the H_2O system

which was originally developed by Keenan and Keyes (1969), programmed and provided to us by Helgeson (see Helgeson and Kirkham, 1974, for details). The viscosity values were obtained from equations and tables modified from Bruges, Latto, and Ray (1966).

Rock.—The properties of the permeable media were estimated from standard table values for igneous and sedimentary rocks (Clark, 1966). Permeability data were estimated on the basis of analytical equations which relate fracture frequency and aperture to rock permeability (Norton and Knapp, 1977) and observations (Villas, 1975). The greatest uncertainty between the computed models and actual geologic processes is the woefully inadequate data on rock permeabilities. Bulk rock density and heat capacity are considered constant.

Analyses of Pluton Environments

Heat and mass transport phenomena in pluton environments depend on variations in pluton geometry, rock permeabilities, initial pluton temperature and heat content, fluid properties, and the system boundaries. Effects of these geologic parameters on the cooling process have been analyzed, using the partial differential equations and numerical approximations described above. In a sense, a sequence of heat transport experiments which simulate hypothetical systems have been computed in order to ascertain the effects of various geological parameters on transport phenomena in complex and realistic systems.

The emplacement of an igneous mass into the upper 10 km of the crust was assumed to be rapid with respect to the loss of heat by the body. The assumption was also made that fluid properties in these systems may be approximated by the equation of state for the H_2O–system, even though evidence suggests multicomponent fluids are certainly present. Circulating fluids are assumed not to react with the enclosing host rocks even though geologic evidence suggests that reactions occur. Finally, the two-dimensional domain, represented by 200 to 400 discrete points, is assumed to approximate a vertical section through the actual system. The errors introduced by the numerical approximations to the differential equations are on the order of $(\Delta z^2 + \Delta y^2)$ in space and Δt^2 in time. Overall, these errors in the model system are estimated to be less than 10 percent for the first derivatives, with respect to space and time.

The dependent variables, temperature, streamfunction, pressure, fluid, and heat flux, have been computed for a series of optimized steady state iterations which approximate the transient behavior of the system. Fluid redistribution caused by the cooling process and the temperature-pressure path that these fluids are subjected to is also summarized for a series of heuristic models, P1-P8.

Permeability.—Heat is transported in pluton environments by fluid convection and by thermal conduction. In the first portion of this communication, fluid circulation was shown to be an inevitable consequence of emplacement of dikes, stocks, and batholiths into fluid bearing host rocks. Although the magnitude of the thermal flux in such systems is a

linear function of rock permeability for low fluxes, it becomes nonlinear in systems that more closely approximate pluton environments. Therefore, relative contributions of conductive and convective heat transfer to the cooling process were compared.

The magnitude, distribution, and variation of bulk rock permeability with time affect the nature of heat transfer in the model systems. Permeability data on fractured crystalline rocks are not available; therefore, estimates have been based on a simple planar fracture model and on field observations. These considerations, together with interpretations of electrical resistivity and seismic data measured on the upper crust, indicated that bulk rock permeabilities were large enough to permit fluid circulation around hot plutons to depths of 10 to 20 km (Norton and Knapp, 1977). Therefore, we analyzed a sequence of systems whose initial conditions covered a reasonable range in bulk rock permeabilities.

Magnitude.—Systems in which host rocks have permeabilities of 10^{-17} cm^2, nanodarcy, or smaller and are saturated with a fluid whose properties are approximated by the H_2O–system apparently cool by pure conductive heat transfer since the fluid fluxes are $< 10^{-9}$ g cm^{-2} sec^{-1}. Pluton model P1 (fig. 1) is analogous to these types of systems.

Conductive heat transfer from a pluton produces isotherms that tend to be subparallel to the side and top contacts of the pluton and that have a broad convex upward form in rocks above the plutons. As we shall demonstrate in subsequent models, this pattern is unique to a system dominated by pure conductive cooling. The maximum vertical conductive heat flux is realized at the top contact between the pluton and host rocks at time = 0 yrs and decreases exponentially with increasing time (fig. 2).

The temperature maxima migrates upward from the P1 pluton top at 2 cm/yr during the initial 5×10^4 yrs and decreases to 0.5 cm/yr at 2×10^5 yrs (fig. 3). Thus, the initial condition of instantaneous emplacement of the pluton is reasonable for plutons that intrude into the upper crust at a rate $\geq$ 2 cm/yr. As a result of the relatively slow upward migration of thermal energy from the pluton, the 50°C isotherm is not displaced until 5×10^5 yrs after emplacement. Thermal decay of P1 is similar to the thermal decay predicted by Lovering (1935) and Jaeger (1968) using analytic solutions of the heat conduction equation. Their solutions predict the average pluton temperature decreases to 0.3 of the initial anomaly at 5.8×10^6 yrs, whereas our model predicts a decrease to 0.2 of the initial anomaly. The discrepancy is due to heat loss through the pluton top in our model, which was not accounted for in their analytic models, and, undoubtedly, to numerical differences.

The transition from conduction to convection dominated heat transfer occurs in systems where the fluid flux is $\geq 10^{-8}$ g/cm^2 sec, if the heat content of the fluid is $\sim$ 100 cal/g. Host rock permeabilities $> 10^{-14}$ cm^2 and several kilometers tall thermal perturbations produce this magnitude of fluid flux. Models P2 and P3 demonstrate the transition

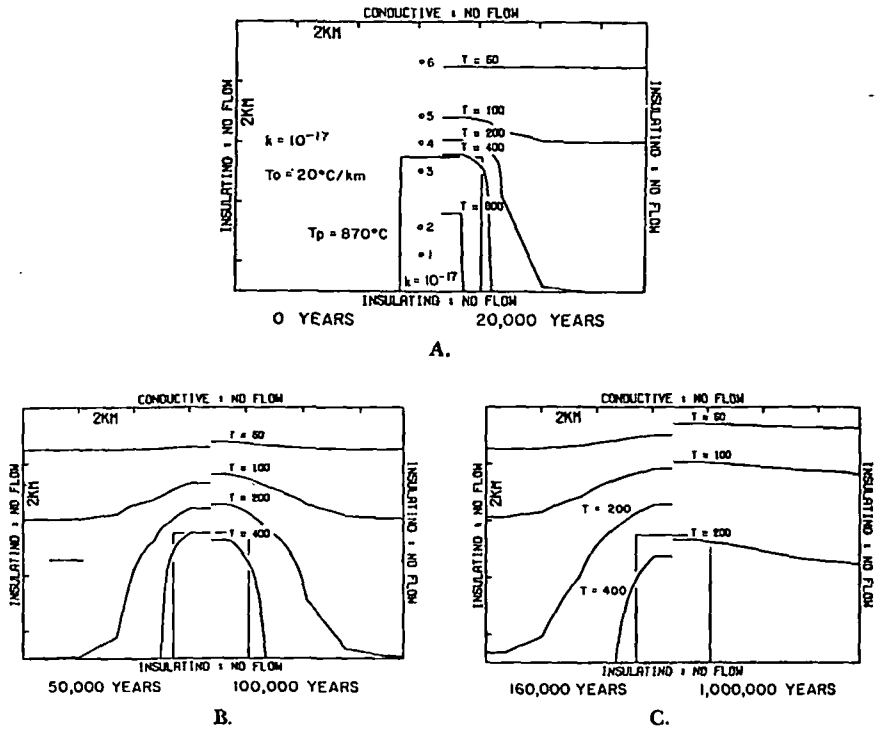

Fig. 1. Two-dimensional cross section of a pluton, P1, and surrounding host rocks. (A) Boundary conditions and (left) initial conditions are depicted for an impermeable pluton emplaced at 870°C into uniform permeability host rocks, $k = 10^{-17}$ cm². Initial temperatures of the host rocks were defined by 20°C temperature at the top boundary and a thermal gradient of 20°C/km. The domain was represented by 100 grid points at regular intervals, $\Delta z = 0.9$ km and $\Delta y = 1.35$ km, and the cooling process was approximated by equations in text at discrete time intervals. (A) Steady state temperature distribution (right half) at elapsed time of 2×10^4 yrs. (B) Steady state temperature distribution in P1 at elapsed times of 5×10^4 yrs (left) and 10^5 yrs (right), (C) Steady temperature distribution in P1 at elapsed times of 1.6×10^5 yrs (left) and 10^6 yrs (right). Note that sharp inflections in all contoured functions are a consequence of the discretization interval and the interpolation function used in the contouring algorithm.

from conductive to convective dominated heat transport for systems containing impermeable plutons and uniformly permeable host rocks.

P2 is characterized by a host rock permeability equal to 10^{-14} cm² and has a total heat flux at the pluton top, which is on the average 10 percent greater than in P1, although the differences in isotherm distributions in the two systems are barely discernible. Vertical convective heat flux in P2 increases from zero at $t = 0$ to 0.5 HFU at 5×10^3 yrs, remains at this value until 10^5 yrs, then decreases gradually to 0.1 HFU at 2×10^5 yrs. Systems with permeabilities $> 10^{-14}$ cm² or with taller thermal anomalies than P2 are characterized by larger convective thermal fluxes because of the direct dependence of fluid flux on vertical extent of the initial anomaly and permeability.

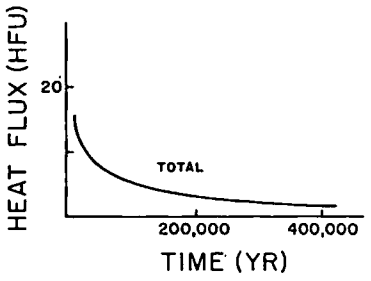

Fig. 2. Conductive heat flux in P1 as a function of time at top of pluton, 1 HFU = 10^{-6} cal cm^{-2} sec^{-1}. Thermal conductivity of 3×10^{-3} cal cm^{-1} sec^{-1} $°C^{-1}$ was assumed for all rocks in the system.

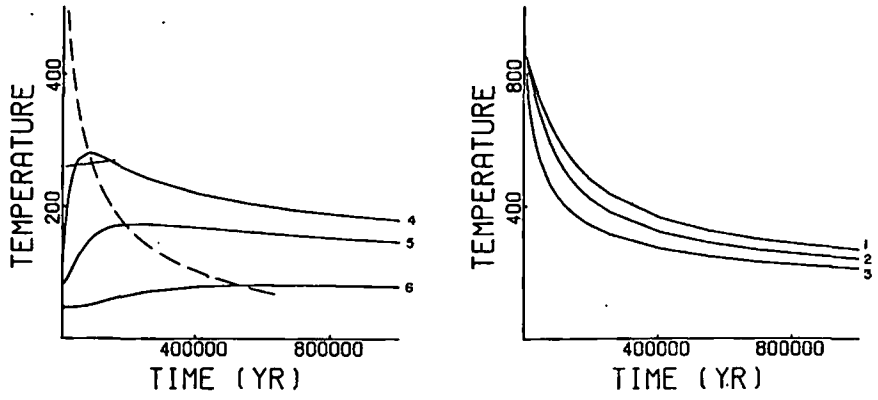

Fig. 3. Temperature as a function of time in P1 at fixed positions (left) 4, 5, and 6, fig. 1A, above top of pluton, 0.45, 1.4, and 3.2 km, respectively, and (right) within pluton at positions 1, 2, and 3, below top of pluton, 2.3, 1.4, and 0.45 km, respectively. Dashed line defines upward migration of temperature maxima with time.

Permeabilities in host rocks and plutons of 10^{-11} and 10^{-14} cm^2, respectively, cause convection to dominate the heat transfer process, P3 (fig. 4).

Fluid circulation in P3 is restricted to host rocks adjacent to and above the side contacts of the pluton (left half of fig. 4, B–D). The relatively lower permeability pluton acts as a barrier to fluid flow (left half of fig. 4B and table 2).[2]

Thermal energy is transferred upward into the overlying host rocks as the fluid circulation cells shift upward (fig. 4B–D). Although the streamfunction reaches a maximum at $\sim 10^5$ yrs, (fig. 4C), the gradient in the streamfunction near the symmetry plane of the system and at the side contacts of the pluton is a maximum at 1.6×10^5 yrs. The maximum fluxes range from 1 to 40×10^{-8} g/cm^2 sec (table 1) and occur directly above the pluton where T~300°C and P~250 bars. Although these fluid

[2] As defined in eq (40), the streamfunction is tangent to the instantaneous fluid flux vectors, and the gradient in the streamfunction defines the mass flux normal to that gradient.

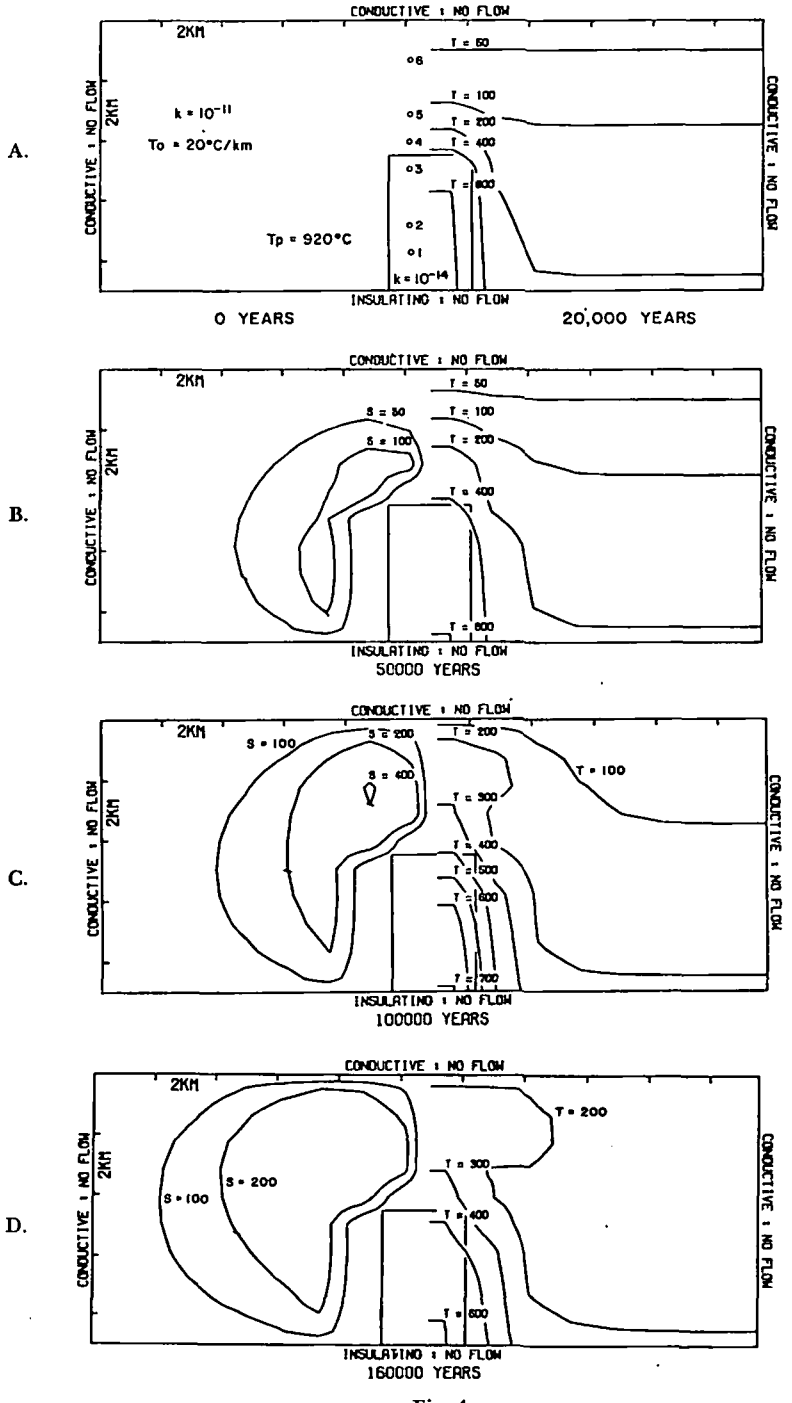
A.
CONDUCTIVE : NO FLOW
2KM
T = 50
T = 100
T = 200
T = 400
T = 800
k = 10⁻¹¹
To = 20°C/km
Tp = 920°C
k = 10⁻¹⁴
CONDUCTIVE : NO FLOW
2KM
CONDUCTIVE : NO FLOW
INSULATING : NO FLOW
0 YEARS
20,000 YEARS
B.
CONDUCTIVE : NO FLOW
2KM
S = 50
S = 100
T = 50
T = 100
T = 200
T = 400
T = 800
CONDUCTIVE : NO FLOW
2KM
CONDUCTIVE : NO FLOW
INSULATING : NO FLOW
50000 YEARS
C.
CONDUCTIVE : NO FLOW
2KM
S = 100
S = 200
S = 400
T = 200
T = 100
T = 300
T = 400
T = 500
T = 600
T = 700
CONDUCTIVE : NO FLOW
2KM
CONDUCTIVE : NO FLOW
INSULATING : NO FLOW
100000 YEARS
D.
CONDUCTIVE : NO FLOW
2KM
T = 200
S = 200
S = 100
T = 300
T = 400
T = 600
CONDUCTIVE : NO FLOW
2KM
CONDUCTIVE : NO FLOW
INSULATING : NO FLOW
160000 YEARS

Fig. 4.

TABLE 2

Fluid fluxes in P3 ($g\ cm^{-2}\ sec^{-1} \times 10^8$)

Position	time yrs =	2×10^4	5×10^4	1.6×10^5
Side contact (lower 3.6 km)				
q_y		0.07	1.	1.
q_s		5	12	25
Above top contact				
q_y		3	21	40
q_s		7	14	31

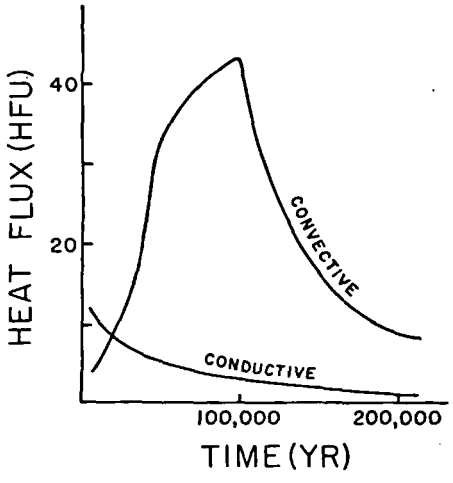

Fig. 5. Conductive and convective heat flux in P3 as a function of time at top of pluton. Thermal conductivity of 3×10^{-3} cal cm^{-1} sec^{-1} $°C^{-1}$ was used for all rocks, whereas heat capacity of fluid was determined from temperature, pressure, and the equation of state for H_2O.

fluxes are relatively small compared with shallow groundwater systems, where fluxes are 10^{-4} cm sec^{-1}, the persistence of the hydrothermal system over 2×10^5 yrs results in the circulation of a large total fluid mass.

Heat flux is directly related to the magnitude of fluid circulation. Although within the pluton heat transfer is by conduction, along the pluton margins and in the overlying host rocks convection predominates. Conductive flux at the pluton top is largest at t = 0 yrs and decreases with time (fig. 5). Convective flux increases from zero at t = 0 to a maximum of 45 HFU at slightly less than 10^5 yrs, then decreases to 10 HFU

← Fig. 4. Two-dimensional cross section of system P3 depicting boundary conditions and (left): (A) initial conditions for pluton emplaced, at an initial temperature of 920°C, into uniform permeability, $k = 10^{-11}$ cm^2, host rocks. Pluton permeability is set at maximum permeability at which conduction dominates heat transfer out of the pluton. Initial temperatures of host rocks were defined by 20°C temperature at the top boundary and a thermal gradient of 20°C/km. The domain was represented by 200 grid points at regular intervals, $\Delta z = 0.9$ km and $\Delta y = 1.35$ km. (B–D) Steady state dimensionless streamfunction representing counter-clockwise fluid circulation at (B) 5×10^4 yrs, (C) 10^5 yrs, (D) 1.6×10^5 yrs; (right) temperature distribution at (A) 2×10^4 yrs, (B) 5×10^4 yrs, (C) 10^5 yrs, (D) 1.6×10^5 yrs.

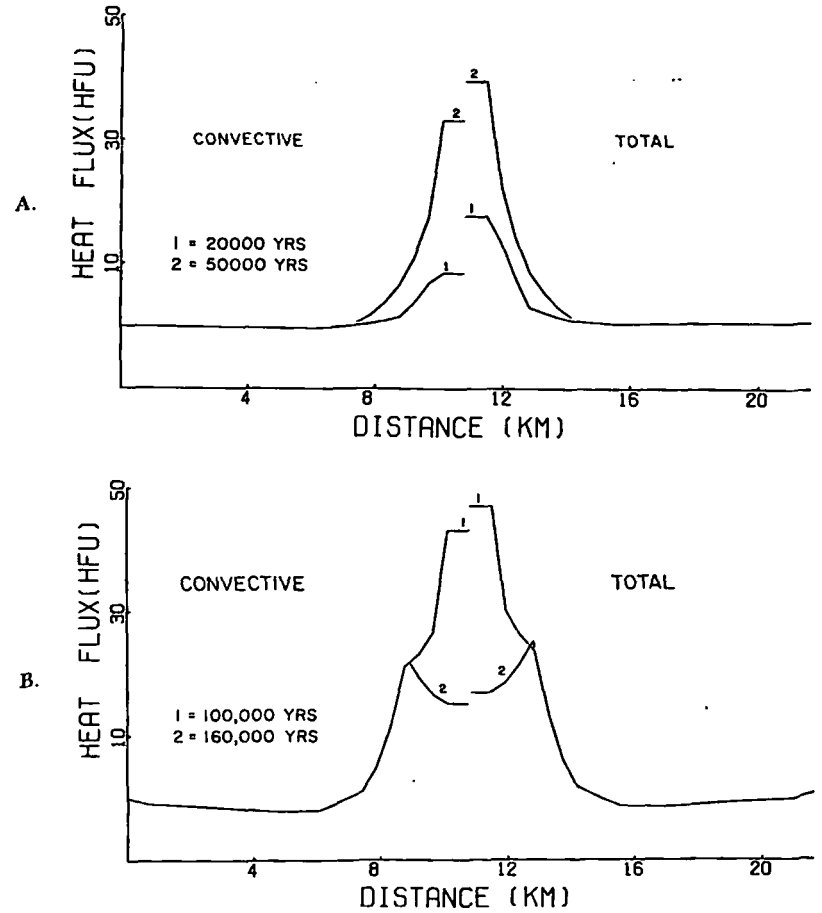

Fig. 6. Vertical component of convective and total heat fluxes as a function of distance along a horizontal plane coincident with the top of P3 pluton at elapsed times of (A) 2×10^4 yrs and 5×10^4 yrs, and (B) 10^5 yrs and 1.6×10^5 yrs.

at 2×10^5 yrs. The total heat flux across the pluton top decreases as the top portion cools. However, the large thermal gradient associated with the side contacts maintains the large heat flux in this region (fig. 6).

Convective heat flux is a nonlinear function of permeabilities, increases rapidly at 10^{-14} cm^2, becomes greater than the conductive heat flux function at 10^{-13} cm^2, then increases at a decreasing rate through P3 such that as permeability becomes infinite the heat flux becomes constant, as required by free convection in a single phase system (fig. 7).

Isotherms in P3 are more convex upward than in P1 and P2 and are displaced closer to the surface and inward toward the side contacts at comparable cooling times. This suggests that the distribution of temperature diagnostic mineral assemblages and fluid inclusions around the side contacts of plutons are useful in ascertaining the relative magnitude

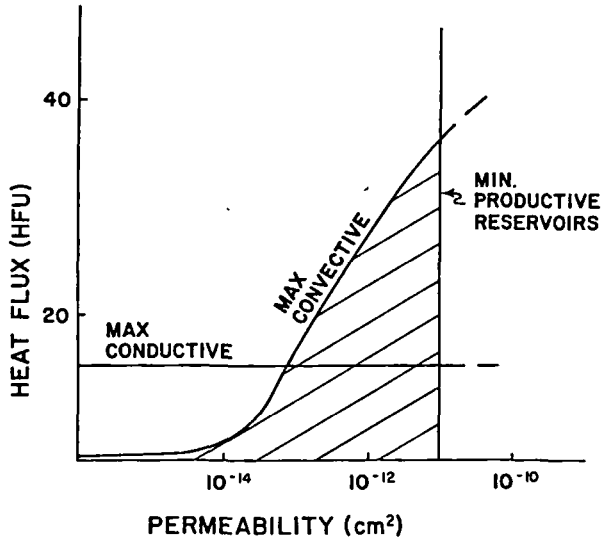

Fig. 7. Maximum vertical heat fluxes calculated at top of pluton as a function of host rock permeability, showing maximum model values for convection and conduction. At point $k = 10^{-14}$ cm^2 convective heat flux is approximately 10 percent of total heat flux. The minimum permeability at which geothermal fluids are produced is represented by the vertical line at $k = 10^{-11}$ cm^2 or about 1 millidarcy permeability.

of convective and conductive heat fluxes. At elapsed time = 1.6×10^5 yrs, the 200°C isotherm is shifted toward the pluton with respect to P1. The relatively large vertical heat flux transports thermal energy to the top boundary faster than it can be dispersed through the conductive but impermeable surface, and horizontal fluxes associated with the upward migrating circulation cells produce a plumose pattern in the isotherms (right half of 4C and D). As a result, regions of uniform temperature much broader than the thermal source are produced.

Temperatures in the P3 pluton decrease in a similar manner to the P1 and P2 plutons, since they are cooling essentially by conduction, (figs. 8A and 3); however, the rate of temperature decrease in P3 is greater as a result of increased heat transfer away from the boundaries caused by fluid circulation. Temperature variations with time in the overlying host rocks are complex (fig. 8A), especially when compared to P1 (fig. 3). This complexity is apparently a manifestation of the transport properties of the circulating fluid, the relative rate of conductive and convective heat flux, and numerical effects. The first temperature maxima at $t = 4 \times 10^5$ yrs occurs in response to convection along the pluton margins and conduction from the pluton. This maxima is analogous to the maxima in P1, except it occurs at smaller elapsed time and is greater in magnitude. The temperature in both systems gradually decreases after this maxima (fig. 3); however, in P3 the temperature increases to a second maxima. These temperature fluctuations with time may be caused by the fluid transport properties. As the fluid column

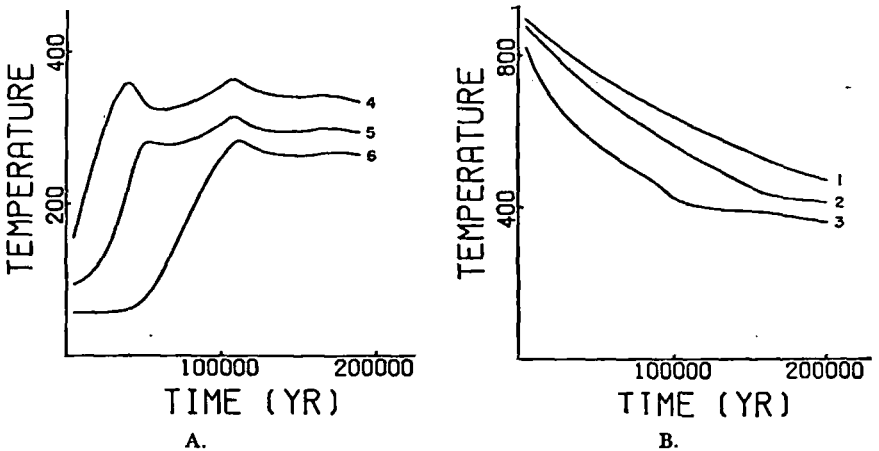

Fig. 8. Temperature as a function of time in system P3 at positions (A) 4, 5, and 6, above top of pluton, 0.45, 1.3, and 3.2 km, respectively, and (B) 1, 2, and 3, below top of pluton, 3.2, 2.3, and 0.45 km, respectively.

above point 4 is heated, fluid density decreases, and, consequently, pressure decreases. Viscosity, thermal coefficient of expansion, and heat capacity of the fluid, therefore, increase, but alpha increases more rapidly than viscosity or heat capacity (paths A and B, fig. 9).

Supercritical-fluid phase properties near the H_2O–system critical end point are continuous and show coincidence of C_p and α maxima and near coincidence of the viscosity minimum in the fluid properties.[3] This maximizes the heat flux at temperatures between 350° to 550°C (fig. 10). Over this temperature range bouyancy forces and heat transport properties are maximized, and the viscous drag force is minimized. Therefore, as conditions in a hydrothermal system cross the extrema in fluid properties from low to high temperature or from high to low pressure, the fluid's heat transport capability first increases then decreases. Therefore, small fluctuations in pressure and temperature may produce large variations in transport properties and cause multiple thermal pulses. Furthermore, in systems whose temperature and pressure conditions do intersect the two-phase surface, the broad oscillations in the temperature-time plot become sharp discontinuities. However, the numerical approximation of the differential equations has contributed an unknown amount to this phenomena. Clearly, the finite difference approximation of alpha across its maxima requires small differential pressure and temperature values. Therefore, we feel that the overall nature of the temperature time plots is realistic but that smaller time period oscillations may be numerical artifacts.

Broad aspects of the temperature-pressure variations in the system define some physical constraints on the development of a two-phase,

[3] The analogous feature is realized in NaCl–H_2O systems, only it is shifted to higher temperatures and pressures because of the corresponding shift in the critical end point.

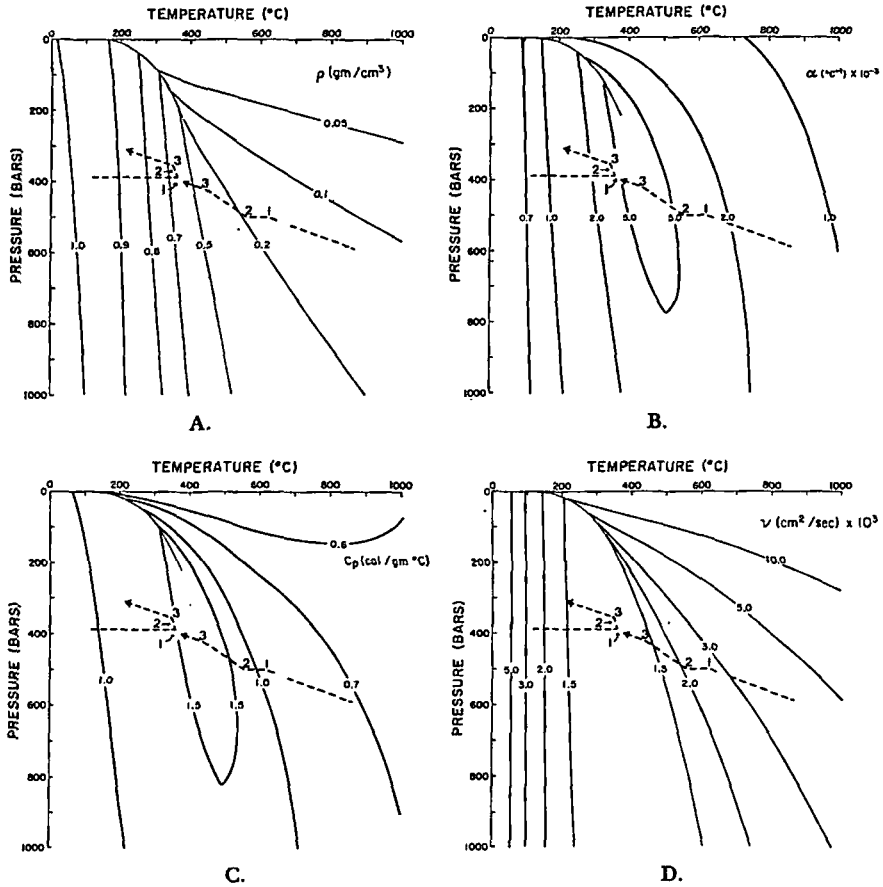

Fig. 9. Temperature-pressure projections of liquid-vapor surface and transport properties of phases in H_2O-system depicting transient temperature and pressure conditions at a position in host rocks 0.45 km above P3 pluton, left dashed line, and 0.45 km below pluton top, right dashed line. Numbers on the dashed lines correspond to maxima on the temperature versus time plot at position 4 in figure 8A. Temperature-pressure variations are shown relative to transport properties: (A) density, ρ, (B) isobaric thermal coefficient of expansion, α, (C) heat capacity at constant pressure, C_p, and (D) viscosity, ν.

liquid-vapor, region. Plutons that are emplaced at depths where the confining pressure is greater than the critical end point pressure do not develop a two-phase system by simple upward transfer of heat. This is evident if we examine the derivative fluid properties along the maximum, for example, for α and C_p, from 1 kb and 450°C to the critical end point (fig. 10). Both α and C_p increase, thereby increasing the transport capability of the fluid and preventing the system's conditions from reaching the two-phase surface.

Stratified.—Plutons emplaced into the upper 10 km of the crust often intrude stratified rocks. Volcanic or sedimentary rock sequences inevitably

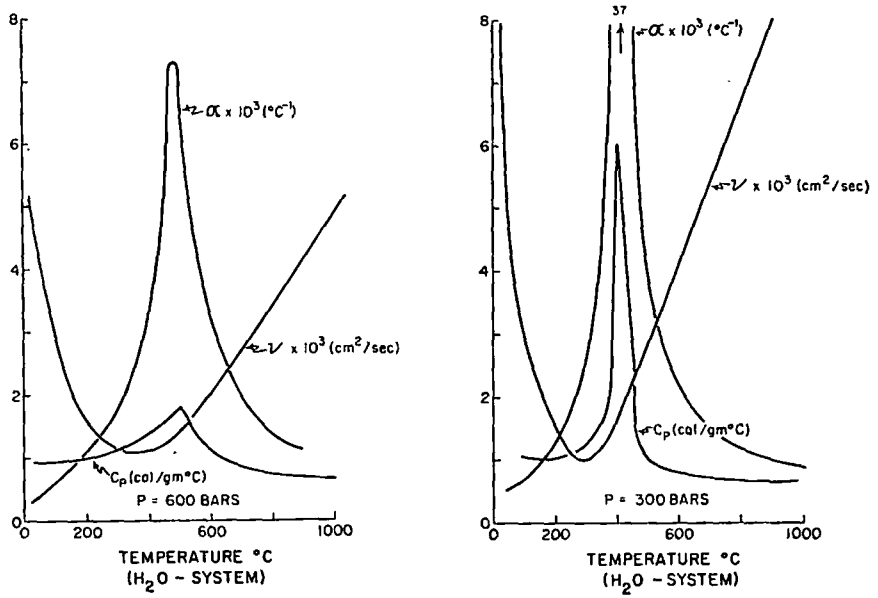

Fig. 10. Thermodynamic and transport properties of supercritical fluid in the H_2O system. The variation of the isobaric coefficient of thermal expansion, α, isobaric heat capacity, C_p, and viscosity, ν, with temperature at (A) 600 bars and (B) 300 bars pressure.

have vertical variations in permeability that may affect the style of fluid circulation and, consequently, the pluton's cooling history. This type of system is simulated by P4, which consists of a pluton intruded into a layered stratigraphic sequence (fig. 11).

Stratified rocks confine fluid circulation to the more permeable layers (fig. 12). Streamlines are refracted at permeability discontinuities, but since the streamlines are developed into circular like cells, the refraction often does not appear to coincide with the actual physical

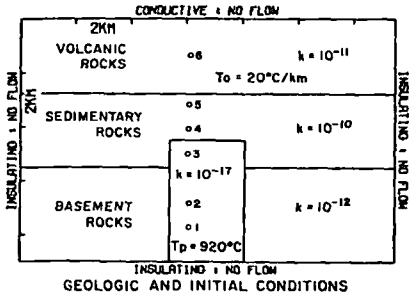

Fig. 11. Two-dimensional cross section of a pluton, P4, and stratified host rocks. Boundary conditions and (left) geologic conditions are depicted for an impermeable pluton emplaced at 920°C; (right) initial conditions depicted for a temperature of 20°C at the top boundary and a thermal gradient of 20°C/km. Constant permeability was maintained in the host rocks, but stepwise permeability increases were included for the upper portion of the pluton in order to simulate fracturing. The domain was represented by 160 grid points at regular intervals, $\Delta z = 0.9$ km and $\Delta y = 1.35$ km.

boundary. This style of fluid circulation accentuates the displacement of isotherms toward the sides of the pluton (right half of 12D; right half of 13A). The plumose outline of isotherms noted in P3 is not as well developed in P4, nor do the isotherms reach as near to the surface. The thermal energy dispersed laterally into the permeable unit is redispersed by conduction and results in a very broad doming of the isotherms in the upper portion of the system (see 100°C, right half of fig. 12A).

Time.—The effective stresses associated with the emplacement of magmas, their crystallization, and concomitant heating of the surrounding host rocks produce systematic and relatively abundant fractures in plutons and host rocks. Although the distribution of fracturing in time is poorly known, the crosscutting relationships observed in natural systems suggest a complex sequence of fracturing events. Crystallization of fluid bearing magmas may release substantial mechanical energy; therefore, the P4 pluton's permeability was increased early in its cooling history to simulate fracturing. Permeability variations were chosen arbitrarily, but the time of fracturing was chosen when the temperature decreased to ~ 860°C. Fracturing was approximated by an instantaneous increase in permeability.

The upper 0.9 km portion of the pluton was fractured at t = 1250 yrs, and permeability was increased to 10^{-11} cm^2 (left half of fig. 13A).

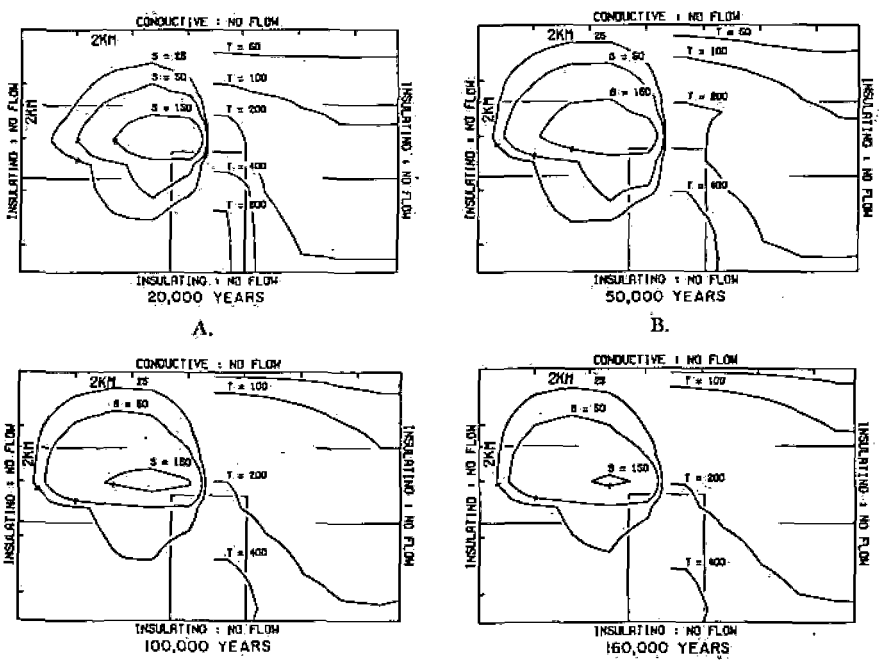

Fig. 12. Steady state (left) dimensionless streamfunction and (right) temperature distribution in system P4.—Horizontal broken lines depict stratified permeability boundaries, (A) at 2×10^4 yrs, (B) at 5×10^4 yrs, (C) at 10^5 yrs, (D) at 1.6×10^6 yrs.

Comparison of the pre-fracture fluid circulation at t = 1200 yrs (left half of fig. 13B) with the post-fracture pattern at t = 2000 (left half of fig. 13C)-illustrates both the deeper penetration of flow into the pluton and increasing fluid fluxes (table 2). A second fracture event at t = 5000 yrs (right half of fig. 13D) increased permeability to 10^{-10} cm² in the upper 0.9 km of the pluton and to 10^{-12} cm² in the next lower 1.8 km. Again the fluid circulation at t = 5 × 10^3 yrs (left half of fig. 13D) and at t = 2 × 10^4 yrs (left half of fig. 12A) illustrates the effect of the permeability increase.

The two increases in pluton permeability over 5 × 10^3 yrs have a dramatic effect on the fluid flux and thermal decay of the pluton (fig. 14). Specifically, the upper 0.9 km of the pluton cools at 0.12°C/yr for 5000 yrs, and the next lower 1 km cools at 0.02°C/yrs for 17500 yrs; thereafter temperature decreases at 10^{-4}°C/yr in both regions. Consequently, the temperature in the upper 2 km averages 260°C for 2 × 10^5 yrs. The coincidence of emplacement into shallow portions of the crust and thorough fracturing of the pluton rapidly cools the entire body to temperatures between 200° to 400°C.

Increased permeability increases fluxes in both the vertical and horizontal directions such that the thermal energy is more quickly dispersed.

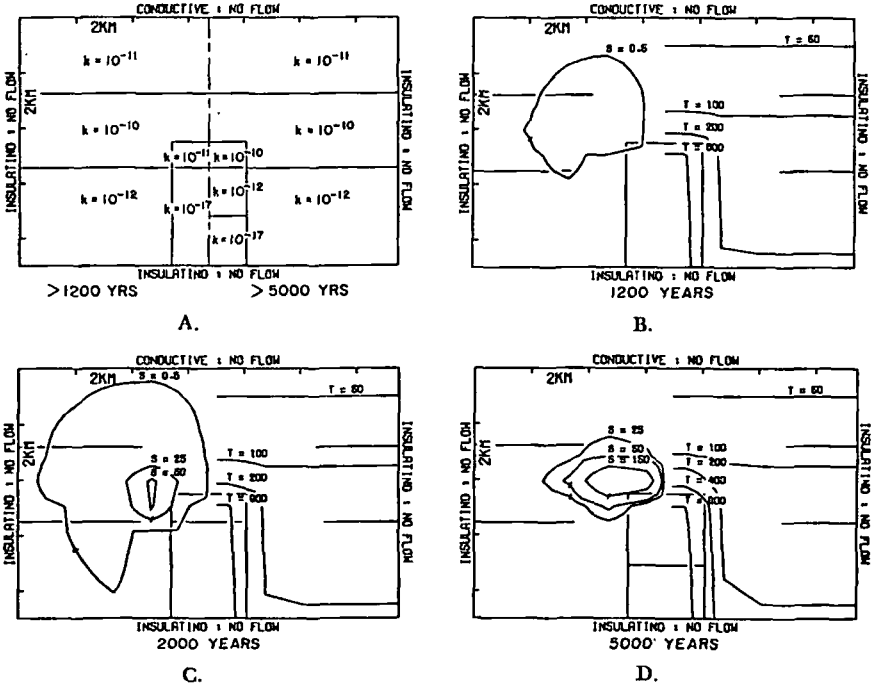

Fig. 13. Thermal history of P4 during short elapsed times when pluton permeability was increased to simulate fracturing. (A) Permeability distribution in systems (left) 1200 yrs < t < 5000 yrs (right). (B–D) Steady state (left) dimensionless streamfunction and (right) temperature distribution in system P4. Horizontal broken lines in host rocks and horizontal solid lines in pluton depict stratified permeability boundaries at (B) 1200 yrs, (C) 2000 yrs, (D) 5000 yrs.

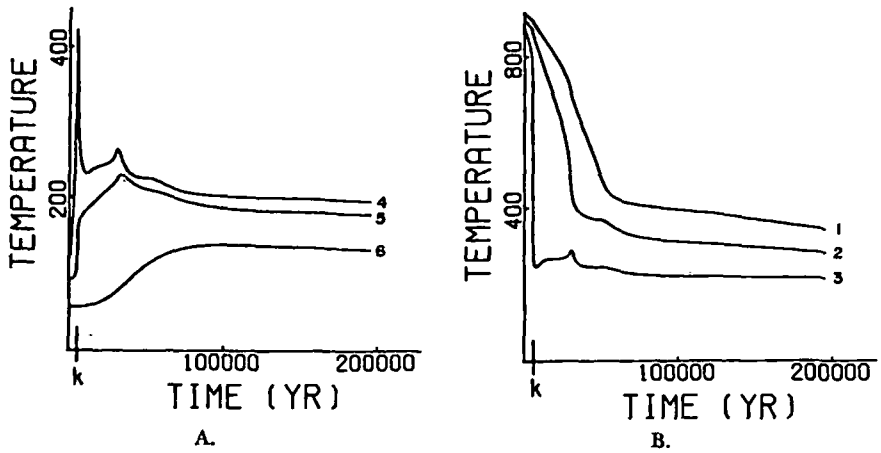

Fig. 14. Temperature as a function of time in system P4 at fixed points (A) 4, 5, and 6, above top of pluton, 0.45, 1.3, and 3.2 km, respectively, and (B) 1, 2, and 3, below top of pluton, 3.2, 2.3, and 0.45 km, respectively. Symbol k denotes approximate times at which pluton permeability was increased in order to simulate fracturing.

However, the thermal history at a position 4 km above the pluton does not reveal evidence of the pluton fracturing.

Fracture zone.—Conditions where igneous activity is most common are conducive to the formation of numerous fractures, both within the pluton and in host rocks. The effects of fracture controlled permeability within host rocks over the top of the pluton were analyzed using model P5 (fig. 15A).

Fluid circulation is confined to the permeable zone above the pluton. The streamline pattern also differs from previous models, because the system boundaries are open to fluid flow (figs. 15B–D). Circulation cells, centered within the fracture zone, reduce the broad isotherm surface observed in previous systems to a much narrower and larger amplitude surface confined to the fracture zone. The broader low amplitude doming of the isotherms is primarily the result of conduction heat away from the fracture zone (right half of fig. 15D). Temperature variation with time within the pluton follows a normal conductive cooling pattern, except that the upper 1 km of the pluton is cooled at an increased rate by fluid circulation.

Temperatures within the fracture zone are similar in distribution but lower in magnitude than previous systems: Lower values of temperature, relative to model P3, are a result of the narrow, large permeability fracture zone and the height of the thermal anomaly in the fracture zone (figs. 16 and 8). However, the temperature-time curves are quite similar in magnitude to P4 (fig. 14), illustrating the common effect of increased permeability.

Pluton geometry.—The vertical extent of the pluton exposed to permeable host rocks determines the lateral extent of the fluid circulation. This effect was simulated by model P6, where the vertical exposure of the pluton was decreased to 2.7 km by introducing a layer of 10^{-17}

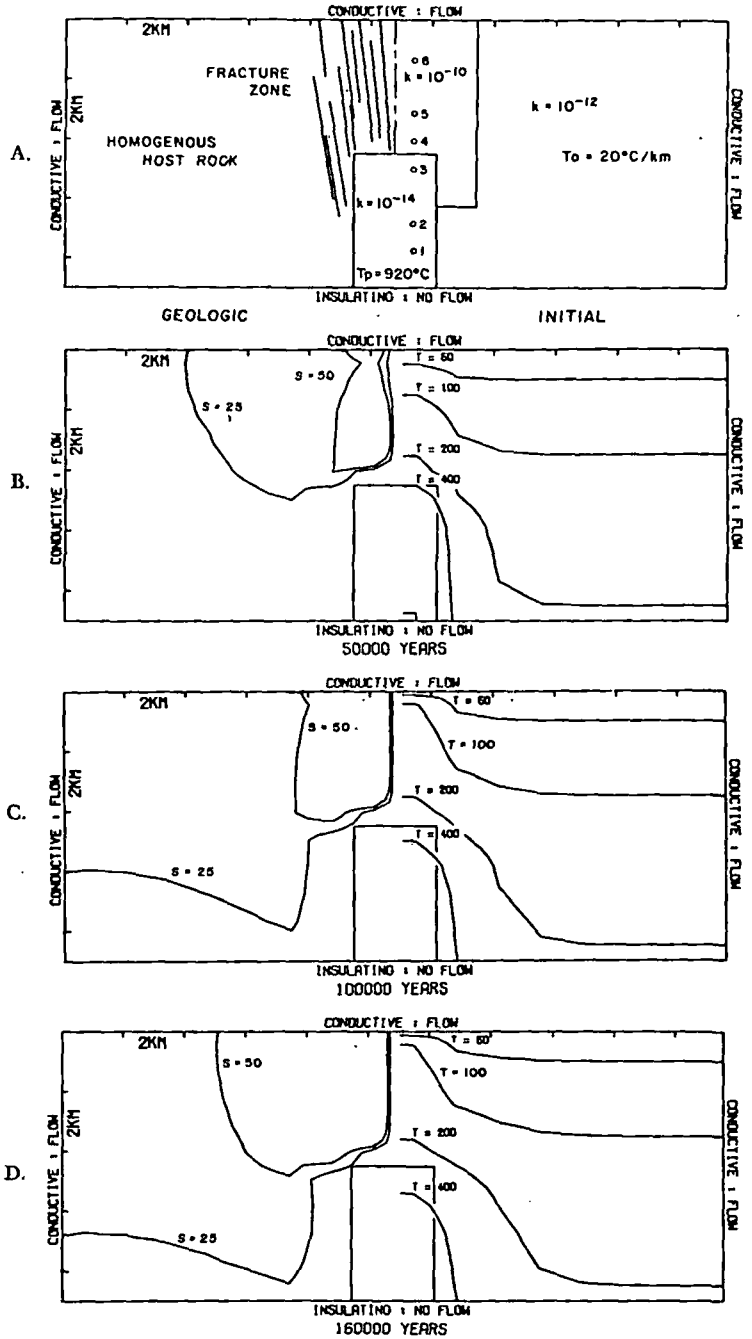

Fig. 15. Two-dimensional cross section of system P5 depicting boundary conditions and (A) initial (left) and geologic (right) conditions for anomalously high permeability zones directly over the top of pluton. Pluton is emplaced at 920°C into host rocks whose temperatures are defined by 20°C top boundary temperature and a 20°C/km thermal gradient. The domain was represented by 160 grid points at regular intervals, $\Delta z = 0.9$ km and $\Delta y = 1.35$ km. (B–D) Steady state (left) dimensionless streamfunction at (B) 5×10^4 yrs, (C) 10^5 yrs, (D) 1.6×10^5 yrs; (right) temperature distribution at (B) 5×10^4 yrs, (C) 10^5 yrs, (D) 1.6×10^5 yrs.

cm² permeability across the base of the domain (fig. 17A). In the upper portion of the system heat is transferred away from the pluton by convection. Fluid circulation is centered over the side contact and 1 km above the top of the pluton at 5×10^5 yrs and migrates upward 1 km by $t = 1.6 \times 10^5$ yrs (fig. 17, B–D). However, in P3, fluid circulation is centered in the host rocks laterally away from the side contact, as well as above the top contact (fig. 4, B–D). The height of the circulation cells is less in P6 than in P3, and the lateral extent of the cells is also proportionately smaller. The ratio of the cell widths is approximately equal to the ratio of the effective pluton heights for the two systems. Therefore, plutons with the larger effective heights will cause fluid circulation a greater distance from their side contacts.

The convective heat flux at $t = 2 \times 10^4$ yrs is equivalent over the plutons in both P3 and P6, but P6 has 10 percent greater flux along its side margins (figs. 6A and 18). This difference increases to 50 percent between 5×10^4 yrs and 10^5 yrs, then decreases to 45 percent at 1.6×10^5 yrs (fig. 19). These differences between the two systems are also evident in the temperature variations with time, although the initial temperature increase above the pluton tops is nearly identical, figures 20 and 8. The second inflection point in each of the temperature-time curves is shifted to earlier times and is of lower magnitude for the shorter pluton.

Level.—Plutons emplaced at levels < 2.2 km generate initial conditions that include two-phase fluid flow with respect to H_2O–systems; those emplaced at increasing depth greater than 2.2 km generate thermal anomalies that are proportionately more extended in the vertical direction. The theory and numerical equations used in this study do not afford for two-phase flow; therefore, the effect of pluton emplacement at depths greater than 2.2 km was examined. The effective height of pluton P7 in permeable rocks is 2.7 km, equivalent to P6, but P7 is 6.3 km deep (left half of fig. 21A).

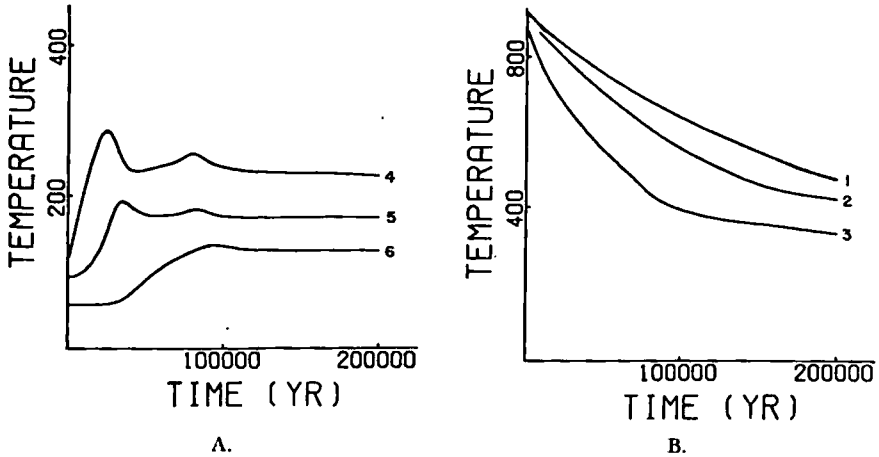

Fig. 16. Temperature as a function of time in system P5 at fixed positions (A) 4, 5, and 6, above top of pluton, 0.45, 1.3, and 3.2 km, respectively, and (B) 1, 2, and 3, below top of pluton, 3.2, 2.3, and 0.45 km, respectively.

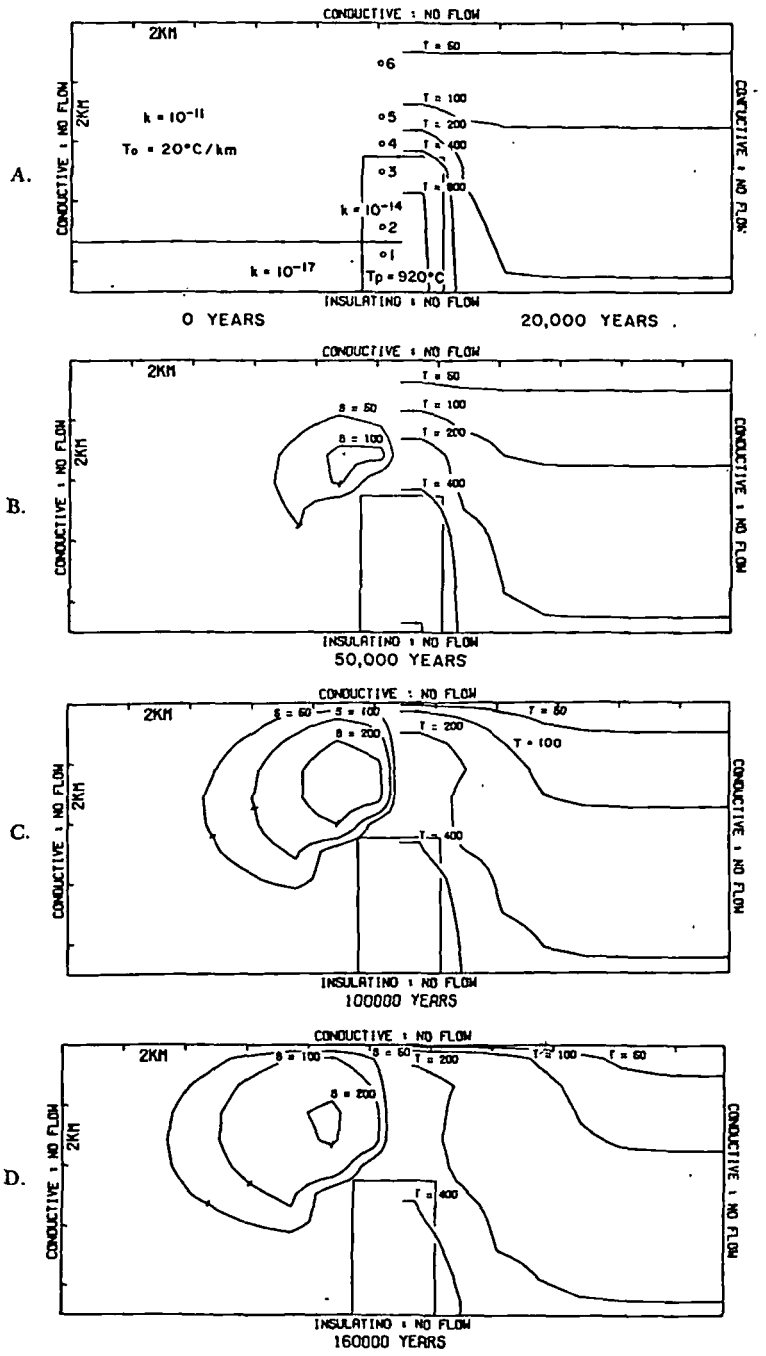

Fig. 17. Two-dimensional cross section of system P6 depicting boundary conditions and (left): (A) initial conditions for pluton identical to P3 except for low permeability layer at base of system. (B–D) Steady state dimensionless streamfunction at (B) 5×10^4 yrs, (C) 10^5 yrs, (D) 1.6×10^5 yrs; (right) temperature distribution at (A) 2×10^4 yrs, (B) 5×10^4 yrs, (C) 10^5 yrs, (D) 1.6×10^5 yrs.

Fluid circulation is similar initially around plutons P7 and P6 since the thermal perturbation with respect to the surroundings is similar (left half of fig. 21B). However, as the thermal anomaly from P7 becomes dispersed over the 6.3 km between the top of the pluton and the surface, larger circulation cells develop (left half of fig. 17D and left half of fig. 21D). This extension of the anomaly results in a plumose isotherm pattern similar to the taller and shallower pluton in P3 but is less extensive in width and height because of the lower total energy content of the P7 pluton (right half of figs. 21C, 21D, and 4D).

Width.—A batholith size pluton was simulated with model P8 (fig. 23). Fluid circulation in P8 is similar to other systems but is upward along the side contacts of the relatively impermeable pluton around the top corner and upward from the top contact (left half of figs. 23D–F).

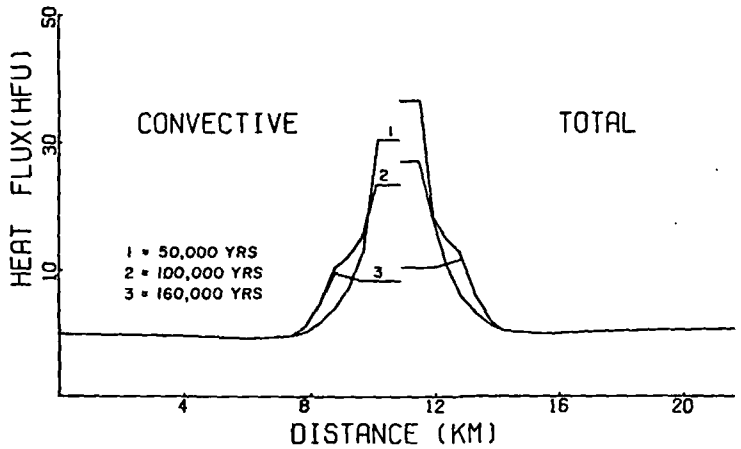

Fig. 18. Vertical component of convective and total heat fluxes as a function of distance along a horizontal plane coincident with the top of P6 pluton at elapsed times of 5×10^4 yrs, 10^5 yrs, and 1.6×10^5 yrs.

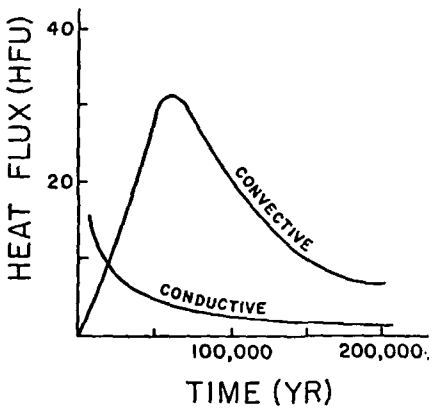

Fig. 19. Maximum convective and conductive heat fluxes as a function of time at top of P6 pluton.

This flow style eventually generates a secondary thermal perturbation due to the width of the pluton (right half of fig. 23F). The effect of the pluton width is to delay the development of fluid circulation over the top of the batholith. Therefore, upward displacement of isotherms is less over the pluton top than at its sides (right half of figs. 23D–F). This lateral temperature perturbation produces secondary circulation cells. These circulation cells further accentuate the temperature anomaly by depressing the isotherms in the central downflow zone (right half of fig. 23F). The secondary cells eventually dominate over the fluid circulation along the side contacts (left half of fig. 23F), and circulation breaks up into 4 Bénard-like cells (Bénard, 1901). As a consequence of this circulation pattern, a 60 km^2 region over the top of the batholith remains at 400°C for 10^6 yrs.

Undoubtedly, the perfectly flat top pluton which extends for 54 km is geologically unreasonable. However, it does indicate an extreme condition which, together with the stock sized plutons in previous models, can be used to analyze the nature of heat transport from a batholith sized body which may have stocks protruding from its upper boundary or for a broad convex topped batholith. Batholiths with convex tops tend to decrease the tendency for secondary cells to develop. Irregular topography, consisting of apical stocks on the batholith top, will develop secondary convective cells around each topographic feature.

Relative cooling rates.—Differences in the cooling rates are insignificant for systems for which pluton size and permeability are equal (table 3). Although large fluid flux occurs along the margins of systems P3 and P6, this does not increase the cooling rate of the pluton significantly. Fluid circulation has its greatest effect in redistributing the thermal energy upward toward the surface as opposed to laterally away from the

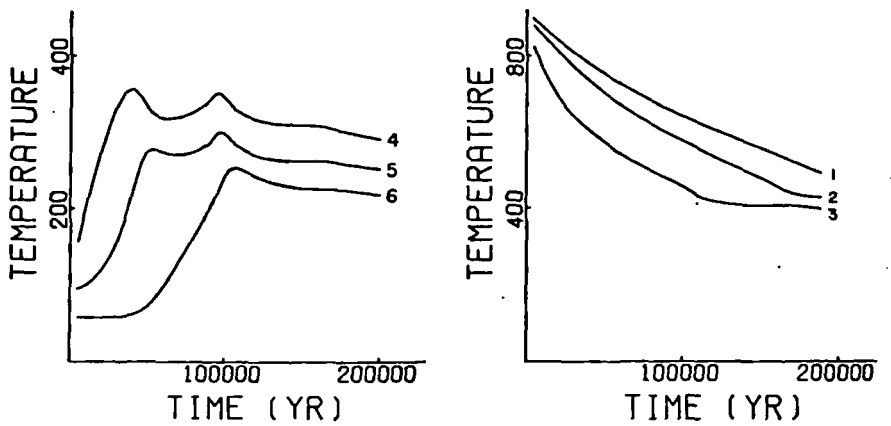

Fig. 20. Temperature as a function of time in system P6 at fixed positions (A) 4, 5, and 6, above top of pluton, 0.45, 1.3, and 3.2 km, respectively, and (B) 1, 2, and 3, below top of pluton, 3.2, 2.3, and 0.45 km, respectively.

Fig
and (A)
form P
system
1.35 km
(C) 10^5
5×10^4

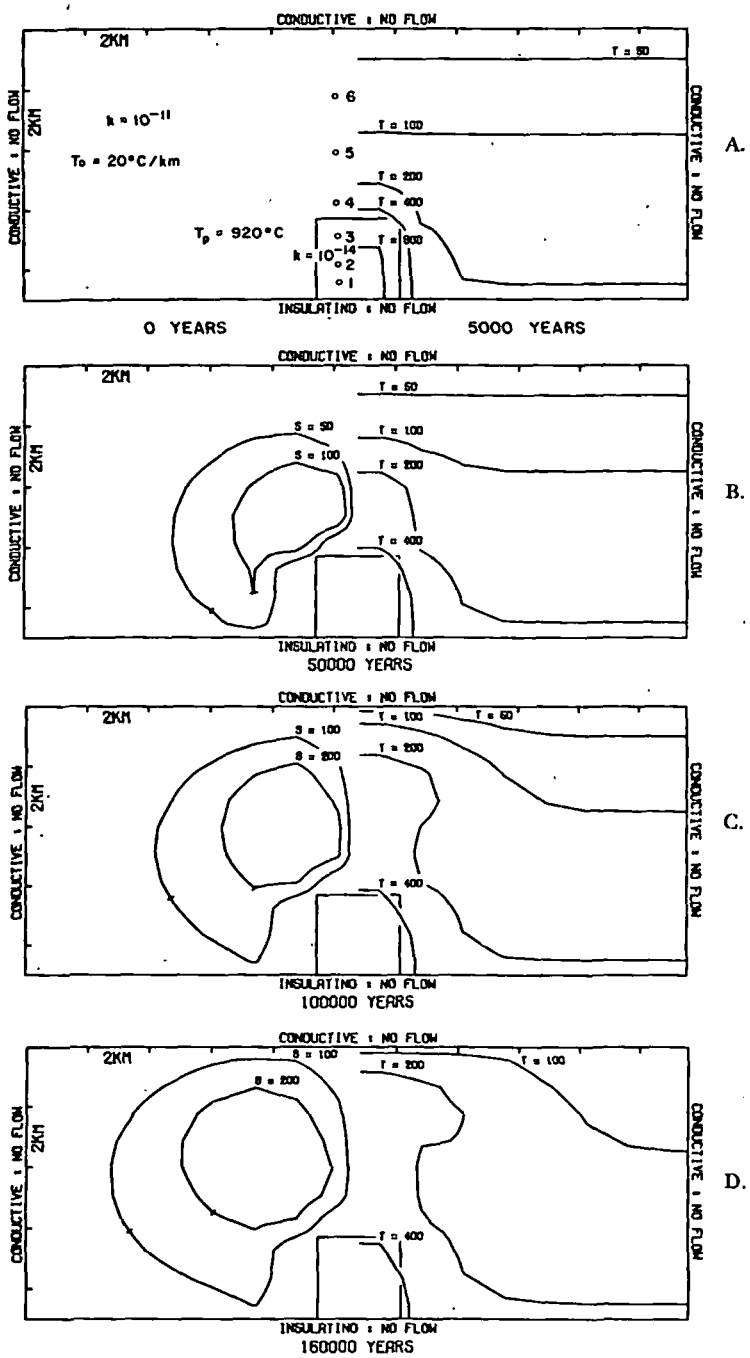

Fig. 21. Two-dimensional cross section of system P7 depicting boundary conditions and (A) initial conditions (left) for a 2.7 km tall pluton emplaced at 920°C into uniform permeability host rocks. Host rock temperature and permeability are same as system P3. The domain was represented by 160 grid points, Δz = 0.9 km and Δy = 1.35 km. (B–D) Steady state (left) dimensionless streamfunction at (B) 5×10^4 yrs, (C) 10^5 yrs, (D) 1.6×10^5 yrs; (right) temperature distribution at (A) 5×10^3 yrs, (B) 5×10^4 yrs, (C) 10^5 yrs, (D) 1.6×10^5 yrs.

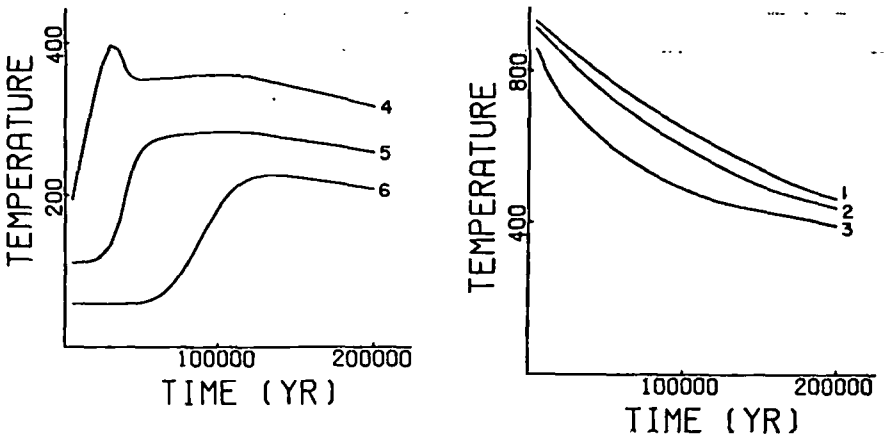

Fig. 22. Temperature as a function of time in system P7 at fixed points (A) 4, 5, and 6, above top of pluton, 0.45, 1.3, and 3.2 km, respectively, and (B) 1, 2, and 3, below top of pluton, 3.2, 2.3, and 0.45 km, respectively.

pluton. Plutons with permeabilities 10^{-14} cm^2 tend to cool much more rapidly than their relatively impermeable counterparts, compare P4 with P3.

Fluid redistribution.—The redistribution of large quantities of fluid is a direct consequence of fluid circulation in pluton environments. This redistribution and concomitant changes in temperature and pressure give rise to an overall irreversible chemical interaction between fluids and minerals. The purpose of this section is to examine some of the features of fluid redistribution in model systems.

Fluid circulation is represented by the distribution of streamlines in each of the systems; however, of more direct interest to mass transport computations is the actual distance and path along which a given fluid packet moves during the thermal event. These fluid pathlines, as defined by eq (36), are analogous to a time exposure of a single fluid packet as it circulates through the system. Pathlines for fluid packets whose origins are in various portions of a system are dependent on the rock permeability and proximity of the path origin to the thermal anomaly (figs. 24, 26, 28, 30, and 32). Fluids initially in the upper portions of low permea-

TABLE 3

Pluton cooling rates

System	Fraction of initial anomaly after 2×10^5 yrs	
P1	0.4	conduction
P3	0.4	convection in host rocks
P4	0.2	permeable pluton
P5	0.4	fracture zone in host rocks
P6	0.4	less exposed in impermeable rocks
P7	0.3	shorter and deeper pluton
P8	0.8*	batholith

* 0.45 after 1.2×10^6 yrs

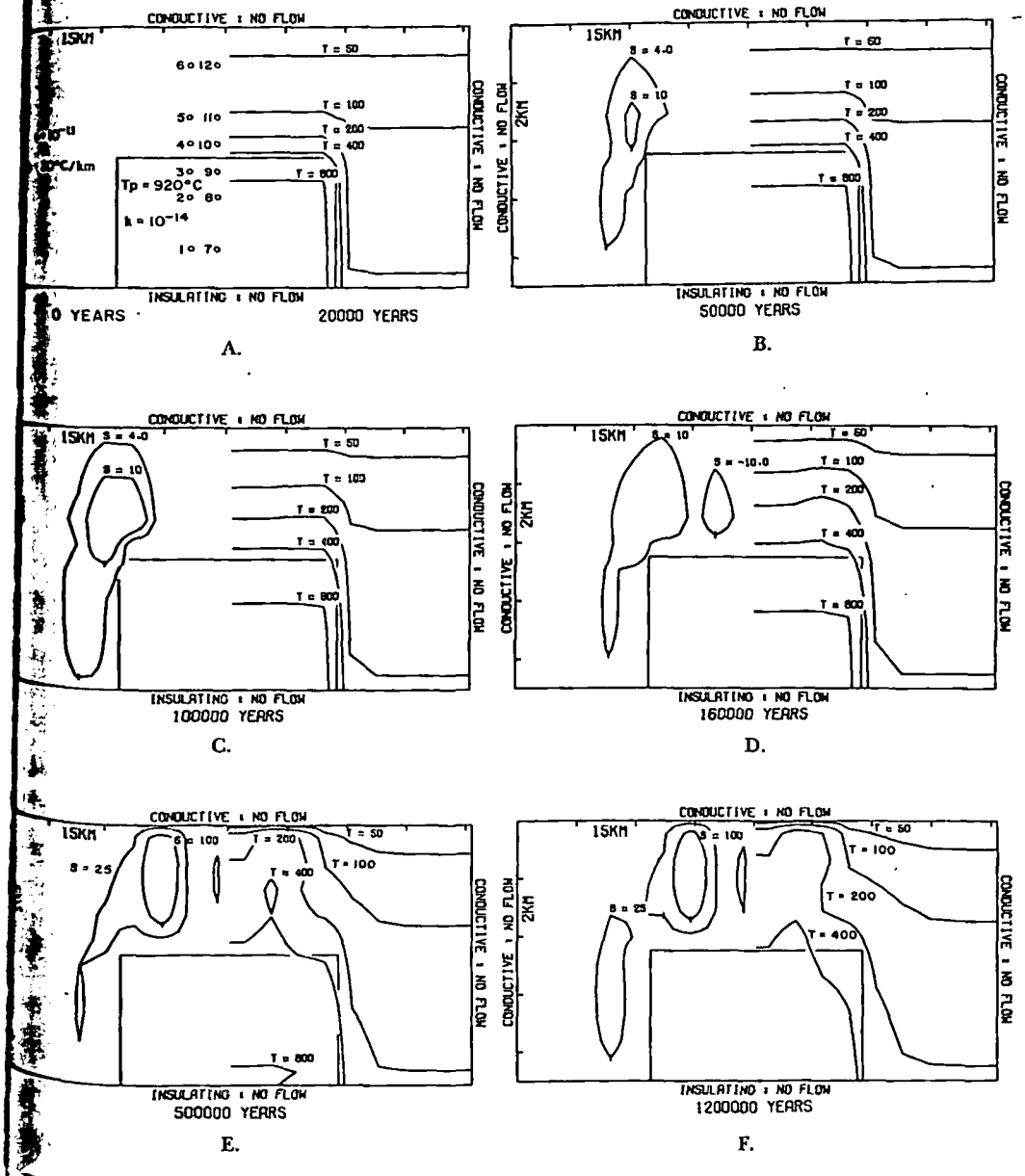

Fig. 23. Two-dimensional cross section of system P8 depicting boundary conditions and (A) initial conditions (left) for batholith size intrusive emplaced into domain with conditions similar to P3. The domain is represented by 180 grid points, $\Delta z = 0.9$ km and $\Delta y = 6.75$ km. (B–D) Steady state (left) dimensionless stream function at (B) 5×10^4 yrs, (C) 10^5 yrs, (D) 1.6×10^5 yrs, (E) 5×10^5 yrs, (F) 1.2×10^6 yrs; (right) temperature distribution at (A) 2×10^4 yrs, (B) 5×10^4 yrs, (C) 10^5 yrs, (D) 1.6×10^5 yrs, (E) 5×10^5 yrs, (F) 1.2×10^6 yrs.

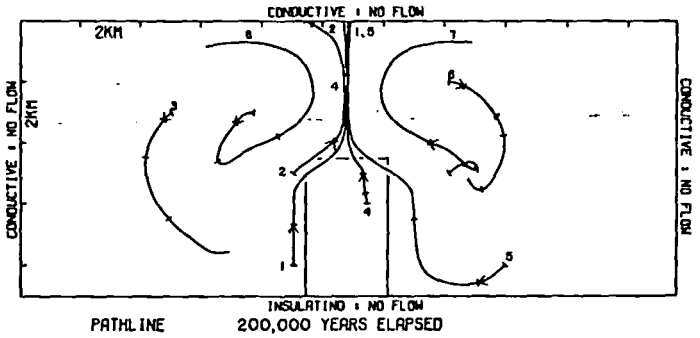

Fig. 24. Examples of fluid pathline in system P3 representing the redistribution of fluids caused by the thermal anomaly. Arrows indicate direction of fluid motion; tic marks occur every 5×10^4 yrs.

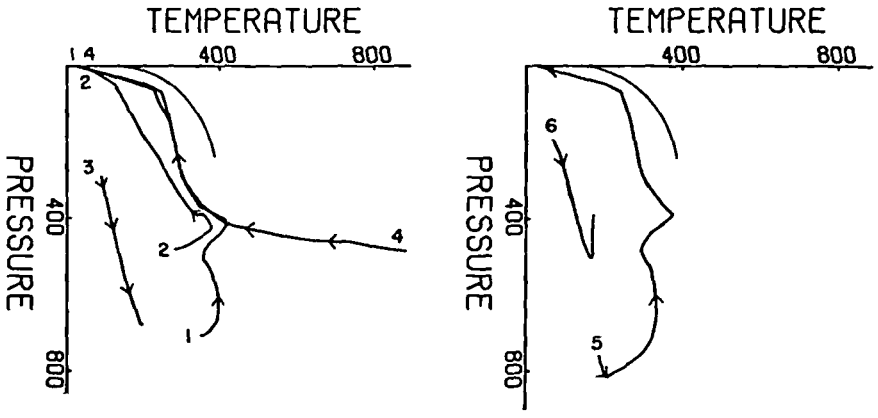

Fig. 25. Pressure-temperature path of fluid packets that circulate along paths in system P3 (fig. 24). Paths are shown with respect to liquid-vapor surface in H_2O system.

bility plutons flow relatively short distances in the initial 10^5 yrs (for example, 1 km in systems P3, P5–P7, figs. 24, 28, 30, and 32). During the subsequent 10^5 yrs fluid circulation increases enough in the upper portions of the pluton to transport fluid packets several km into the overlying host rocks. Fluids initially in larger permeability plutons are transported completely out of the pluton in the initial 10^5 yrs (fig. 26). As a result, this fluid is replaced by fluid packets circulating along pathlines into the sides of the pluton.

Fluids initially in host rocks several km away from the pluton convect toward and into the pluton (fig. 24). The pathlines trend along the side contacts of low permeability plutons, whereas they flow into the plutons with larger permeability (fig. 26). As the fluids move horizontally toward the pluton, the circulation center migrates upward in the system. Therefore, pathlines with origins above the pluton tend to form upward looping spirals. Stratified permeabilities restrict pathline movement to

the larger permeability units. In P4 layered units force the circulation toward the pluton (fig. 26), and, since P4 is a relatively permeable pluton, fluid packets then circulate through the pluton.

Fracture zones effectively channel the fluid up through the fracture zone. Pathlines in the vertical fracture zone are proportionately longer than those in the adjacent, less permeable rocks (fig. 28). Transit time for these packets from the top of the pluton to the surface is 10^5 yrs.

Changes in temperature and pressure along fluid pathlines describe a path through the H_2O system along which the solvent properties of the fluid may be described and define the intensive variables required to calculate mass transfer between fluid and rock. Packets of supercritical fluid, whose temperatures are in the critical endpoint region, are subjected to drastic changes in thermodynamic and electrostatic properties (figs. 25, 27, 29, 31, and 33). Extreme variations in thermodynamic behavior of the solvent along these paths are apparent from the work by Helgeson and Kirkham (1974a,b).

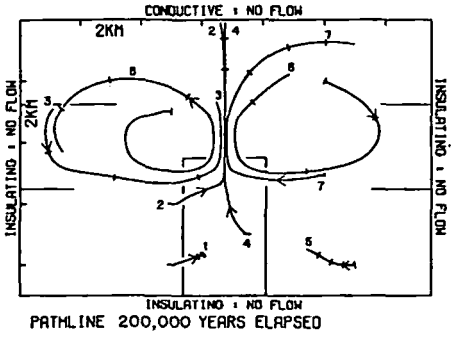

Fig. 26. Examples of fluid pathline in system P4 representing the redistribution of fluids caused by the thermal anomaly. Arrows indicate direction of fluid motion; tic marks occur every 5×10^4 yrs.

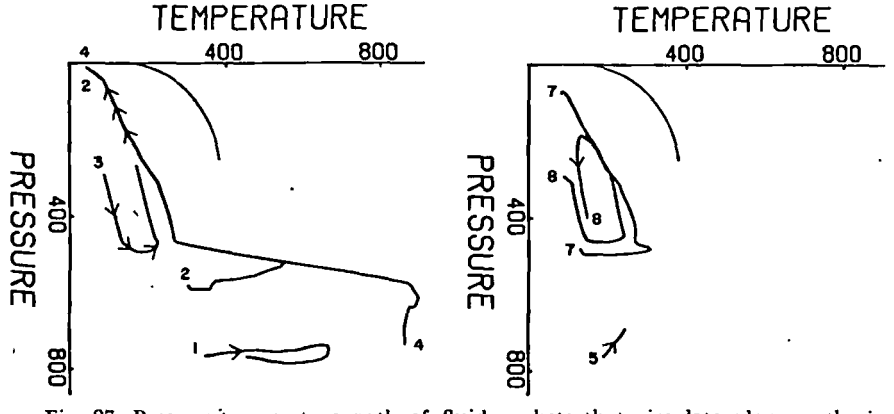

Fig. 27. Pressure-temperature path of fluid packets that circulate along paths in system P4 (fig. 26). Paths are shown with respect to liquid-vapor surface in H_2O system.

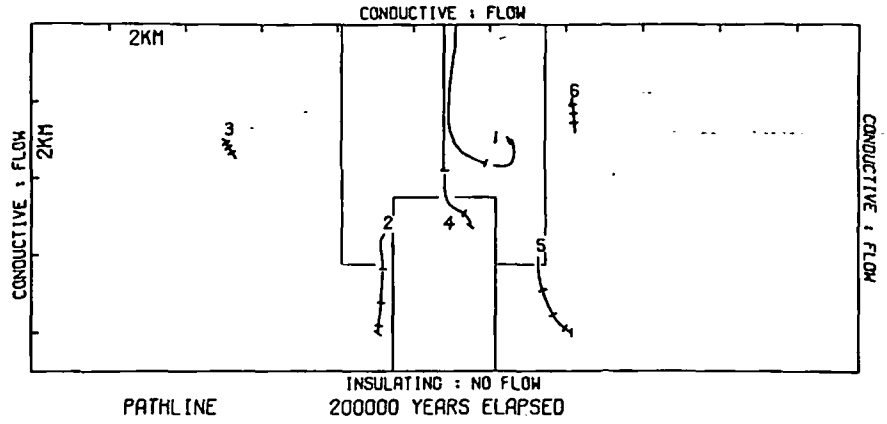

Fig. 28. Examples of fluid pathline in system P5 representing the redistribution of fluids caused by the thermal anomaly. Arrows indicate direction of fluid motion; tic marks occur every 5×10^4 yrs.

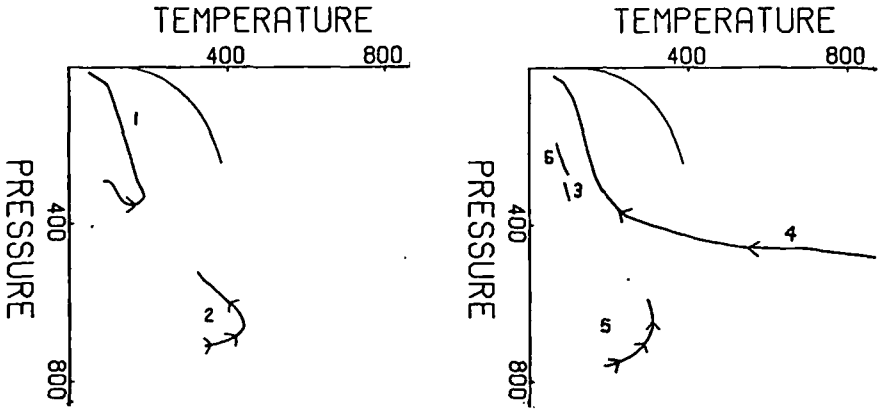

Fig. 29. Pressure-temperature path of fluid packets that circulate along paths in system P5 (fig. 28). Paths are shown with respect to liquid-vapor surface in H_2O system.

Enormous quantities of fluid are circulated through pluton environments where thermal convection is the predominant cooling process. The total mass of fluid circulating through a unit area, integrated over a time interval of 2×10^5 yrs for each system (table 4), is considerably less for low permeability plutons than for the fractured plutons.

The mass of fluid that flows during time interval t_2–t_1, through an area, A, normal to a fluid pathline is defined by

$$M_f = A \int_{t_1}^{t_2} \rho_f \bar{v} dt, \qquad (58)$$

where $\bar{v}$ is the Darcy velocity and ρ_f is the density of the fluid. The mass

of rock exposed to the circulating mass of fluid is defined in terms of the true velocity, $\bar{v}_t$, of the fluid:

$$M_r = A\,(1-\phi)\int_{t_1}^{t_2} \rho_r \bar{v}_t dt, \tag{59}$$

where ϕ is the flow porosity and ρ_r is the density of the rock. The mass ratio of circulating fluid to rock contacted by the fluid is the ratio of eqs (58) and (59), if the average fluid velocity over the time interval is used:

$$\frac{M_f}{M_r} = \frac{\phi}{1-\phi}\,\frac{\int_{t_1}^{t_2} \rho_f dt}{\int_{t_1}^{t_2} \rho_r dt}, \tag{60}$$

since the true velocity is related to the Darcy velocity by

$$\bar{v}_t = \frac{\bar{v}}{\phi}. \tag{61}$$

The rock density is nearly constant over temperature ranges realized in pluton environments, and the fluid density varies from 0.2 to 0.9 g cm^{-3}. Therefore, fluid-rock mass ratios are approximately

$$\frac{M_f}{M_r} \approx \frac{\phi\,\rho_f}{(1-\phi)\,\rho_r}. \tag{62}$$

TABLE 4

Mass of fluid circulated through systems (g cm^{-2} × 10^5)

Position	System P3	P4	P5	P6	P7
1	0.3	0.02	0.3	trace	trace
2	0.5	4	0.4	0.5	0.4
3	0.7	24	0.6	0.5	0.5
4	22	35	20	15	20
5	33	27	30	15	20
6	24	5	20	20	20

TABLE 5

Fluid:rock mass ratios

Position	P3	P4	P5	P6	P7
1	0.05	0.1	0.06	0.07	0.1
2	0.08	0.16	0.1	0.1	0.1
3	0.1	0.3	0.1	0.1	0.1
4	0.25	0.31	0.31	0.26	0.25
5	0.28	0.32	0.33	0.3	0.28
6	0.30	0.33	0.34	0.3	0.30

The effective mass ratio (table 5), defined by eq (60), permits computation of fluid-rock reactions from the viewpoint of a circulating or stagnant fluid. In rocks where the fluid flow is confined to fractures, the flow porosity may be on the order of 10^{-4} to 10^{-5} (Norton and Knapp, 1977); and, therefore, the $(1-\phi)$ term in the denominator is $\cong 1$, and the effective mass ratio is on the order of the flow porosity, since $\rho_r \cong 2.73$ g cm^{-3}. These mass ratios are exceedingly small compared to those predicted from stable light isotope data on hydrothermal systems (Taylor, 1971). The reason for this discrepancy is obvious, since eq (60) defines the mass of rock contacted by a circulating mass of fluid, whereas the isotopic data estimates the integrated effect of all fluid packets circulating through an arbitrary rock mass.

The total mass of fluid that circulates through an arbitrary mass of rock, at a fixed position in a hydrothermal system, is normally used in predicting the amount of isotopic or other chemical exchange that occurs

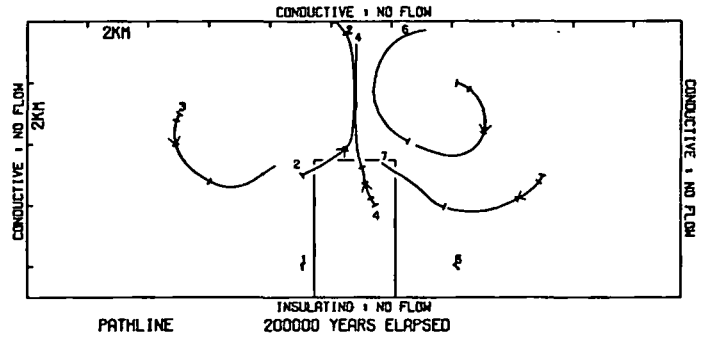

Fig. 30. Examples of fluid pathlines in system P6 representing the redistribution of fluids caused by the thermal anomaly. Arrows indicate direction of fluid motion; tic marks occur every 5×10^4 yrs.

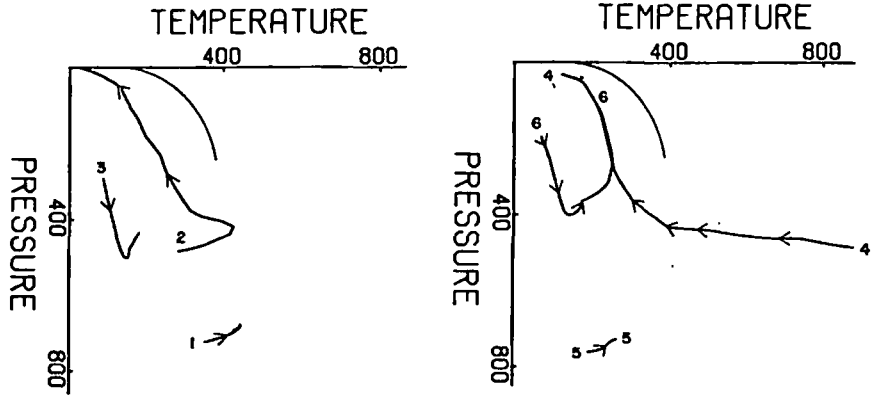

Fig. 31. Pressure-temperature path of fluid packets that circulate along paths in system P6 (fig. 30). Paths are shown with respect to liquid-vapor surface in H_2O system.

between fluid and rock. The amount of fluid flowing through rock volume, V, is

$$M_f = \int_{t_1}^{t_2} A\bar{v}\rho_f dt, \tag{63}$$

where A is the cross-sectional area of the rock volume that is normal to the Darcy velocity vector, $\bar{v}$. The fluid-rock mass ratio in this case is defined by

$$\frac{M_f}{M_r} = \frac{\int_{t_1}^{t_2} A\bar{v}\rho_f dt}{\rho_r V}. \tag{64}$$

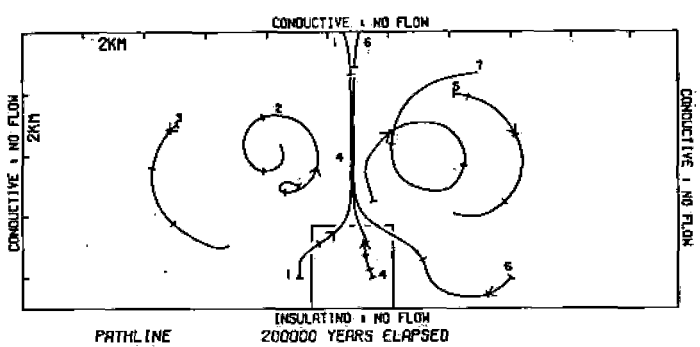

Fig. 32. Examples of fluid pathline in system P7 representing the redistribution of fluids caused by the thermal anomaly. Arrows indicate direction of fluid motion; tic marks occur every 5×10^4 yrs.

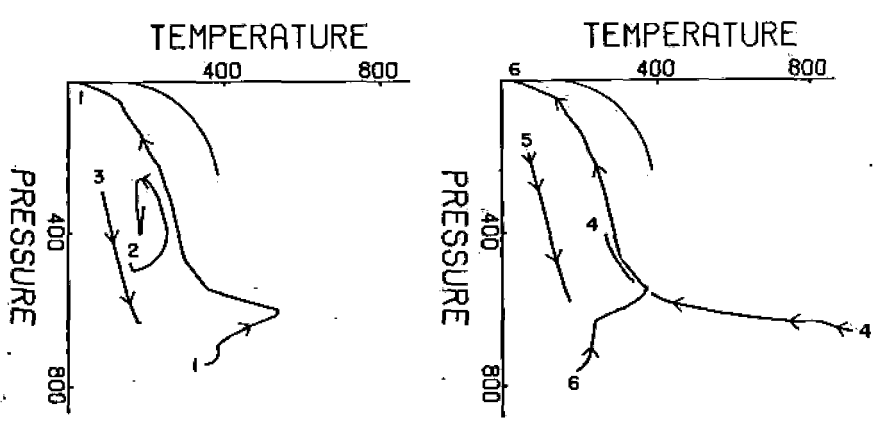

Fig. 33. Pressure-temperature path of fluid packets that circulate along paths in system P7 (fig. 32). Paths are shown with respect to liquid-vapor surface in H_2O system.

This ratio is essentially the integrated amount of fluid passing through the rock. Ratios computed from eq (64) for the model systems range from positive infinity, for infinity thin rock wafers, to values on the order of 0.5 when the rock volume is the entire thermal anomaly. Circulation of reactive fluids through these environments can not be adequately simulated by the numerical equation used for the circulation of inert fluids but requires explicit equations for exchange, reaction, diffusion, and advection of components, as suggested in Norton and Knapp (1977). Simulation of these types of systems will be the topic of a future communication.

CONCLUSIONS

Spatial and temporal variations in fluid flow and heat flux in a sequence of simplified geologic systems indicate that bulk rock permeabilities in host rocks around hot plutons that are $\geqq 10^{-14}$ cm^2 result in convection of thermal energy upward along the sides of the pluton and toward the surface. However, only in those systems that contain permeable plutons is the cooling rate increased. The rather small variation in permeability over which the transition from conductive to convective heat transfer occurs and the relatively low threshold value of permeability required for significant convective heat transfer suggest that heat transfer by circulating fluids may be significant over very broad crustal regions where temperature perturbations occur within the crust. Temperature conditions around plutons that cool by convective heat transfer are substantially different from their conductive dominated equivalents. Large volumes of rock above shallow plutons remain at nearly constant temperature for very long periods of time. The temperature is nominally in the range of 200° to 400°C for the upper crust. This feature and the circulation of large masses of fluid from considerable distances away from the thermal anomaly undoubtedly affect the thermal metamorphism and hydrothermal alteration of rocks in the pluton's vicinity.

Heuristic models of hot pluton environments suggest that fluid circulation is an integral part of their cooling process. Major features of the hydrothermal system noted in these models are undoubtedly evident in their natural analogs. Particularly, the composition and distribution of mineral assemblages shift in both stable and radiometric isotope abundances, and the composition and filling temperatures of fluid inclusions should reflect the style and duration of fluid circulation. However, these data must have been collected with cognizance of the system's flow channels.

Fluids circulate from one rock, temperature, and pressure environment into another along pathlines defined by the fluid potential field and through fracture controlled channels. The fluid flux ranges from 10^{-4} to 10^{-8} gr^{-2} sec^{-1}, and the surface area of minerals exposed along the flow channels is relatively large compared to the amount of fluid in the flow channel. Recalling the porosity model of Norton and Knapp (1977), it is apparent that the circulating bulk fluid may be in direct contact with

only a small portion of the rock in the permeable media, but the mass of fluid to rock ratios is large. As a consequence of the above features, the fluids being redistributed in natural systems will be grossly out of equilibrium with the bulk rock as they flow along the pathlines, although they may have initially been equilibrated with the bulk rock at their initial location. Therefore, if the overall irreversible nature of the reactions between circulating fluids and rocks, the nature of fracture controlled permeability, and the magnitude and direction of fluid flux are accounted for, the geochemical history of pluton environments can be defined.

Hydrothermal alteration phases and stable light isotope distributions have already been interpreted as indicating a style of fluid circulation similar to that indicated by our physical analysis (Helgeson, 1970; Taylor, 1971; and Norton, 1972). Indications that other chemical data may reflect this circulation process are evident. We wish to call attention to the fact that although shifts in chemical composition do indicate fluid redistribution and that in certain instances the direction of fluid flow can be implied, ultimately fluids are shifted into chemical equilibrium with the mineral phases along the flow channel. Subsequently, the fluid and mineral chemistry will not reflect a chemical shift in all or any of the chemical parameters.

Fluid circulation may have played a significant role in regions of the crust where magmatic and volcanic activity is most voluminous, such as along the crustal plate boundaries. The tectonic setting of both convergent and divergent plate boundaries is such that abundant fracturing of host rocks typically accompanies the igneous events. As a result, these environments probably have sufficiently large permeabilities to permit fluid circulation. Fluid circulation, total heat flux, and, consequently, the heat transfer through Earth's crust may be significantly greater than heretofore recognized. One manifestation of this voluminous fluid circulation is the large thicknesses of volcanic rocks that have been hydrothermally altered. Very clearly, our notions of heat flux are in error by perhaps as much as a factor of ten at plate boundaries, since geophysical surveys have probably not measured the convective component.

The divergent plate environment along oceanic ridges is an equally dramatic example of the potential significance of fluid circulation. Consider that the rate of seafloor spreading is proportional to the mass of igneous melt emplaced at the spreading center and further hypothesize that only the upper 2 km of the ridge environment has a permeability greater than 10^{-14} cm^2. Then, by analogy to the models presented above, a mass of fluid equivalent to the entire ocean system has been circulated through the spreading centers, over 2×10^8 yrs, if one assumes an average of 5 cm are added to the crust every year along the strike length of the mid-ocean ridges.

Finally, igneous bodies have interacted with a quantity of fluid nearly equivalent to their mass since permeabilities $\geq 10^{-14}$ cm^2 appear to be reasonable values for many plutons in the shallow crust.

ACKNOWLEDGMENTS

This research was supported by NSF Grants GS-41136 and EAR74-03515 A01 and by matching computer funds from the University of Arizona Computer Center. Additional funds were provided in the early stages by the Universities of Utah and Arizona. The study has benefited from the suggestions and assistance from many of our colleagues, but in particular we are indebted to R. Knapp, R. N. Villas, T. Gerlach, H. Hardee, and D. W. Larson. The study was conceived when H. C. Helgeson pointed out that an early cartoon drawn by the principal author could be quantified, and the study has continually benefited from his critical comments. We are also grateful to H. C. Helgeson and David Kirkham for providing programs to compute equation of state properties in the H_2O–system. We wish to acknowledge the guidance from Lawrence Cathles during the early stages of program development. We wish to thank Lynn McLean for many improvements in the manuscript.

REFERENCES

Bear, Jacob, 1972, Dynamics of fluids in porous media: New York, Am. Elsevier, 764 p.

Bianchi, L., and Snow, D. T., 1969, Permeability of crystalline rocks interpreted from measured orientations and apertures of fractures: Jodphur, Rajasthan, Arid Zone Research Assoc. of India, Annals of Arid Zone, v. 8, no. 2, p. 231-245.

Bénard, M., 1901, Les tourbillons cellulaires dans une nappe liquide transportant de la chaleur par convection en régime permanent: Am. Chim. Phys., v. 23, p. 62-144.

Bruges, E. A., Latto, B., and Ray, A. K., 1966, New correlations and tables of the coefficient of viscosity of water and steam up to 1000 bar and 1000°C: Internat. Jour. Heat and Mass Transfer, v. 9, p. 465-480.

Clark, S. P., Jr., ed., 1966, Handbook of Physical Constants, rev. ed.: New York, Geol. Soc. America Mem. 97, 587 p.

Donaldson, I. G., 1962, Temperature gradients in the upper layers of the earth's crust due to convective water flows: Jour. Geophys. Research, v. 67, no. 9, p. 28-48.

———— 1968, The flow of stream water mixtures through permeable beds: a simple simulation of a natural undisturbed hydrothermal region: New Zealand Jour. Sci., v. 11, no. 1, p. 3-23.

Elder, J. W., 1965, Physical processes in geothermal areas, *in* Lee, W. H. K., ed., Terrestrial Heat Flow: Am. Geophys. Union, Geophys. Mon. Ser. 8, 276 p.

———— 1967, Steady free convection in a porous medium heated from below: Jour. Fluid Mechanics, v. 27, p. 29-84.

Helgeson, H. C., 1970, A chemical and thermodynamic model of ore deposition in hydrothermal systems: Mineralog. Soc. America Spec. Paper 3, p. 155-186.

Helgeson, H. C., and Kirkham, D. H., 1974a, Theoretical predictions of the thermodynamic behavior of aqueous electrolytes at high pressures and temperatures; I: Summary of the thermodynamic/electrostatic properties of the solvent: Am. Jour. Sci., v. 274, p. 1089-1198.

———— 1974b, Theoretical predictions of the thermodynamic behavior of aqueous electrolytes at high pressures and temperatures; II: Debye-Huckel parameters for activity coefficient and relative partial molal properties of the source: Am. Jour. Sci., v. 274, p. 1199-1261.

Holst, P. H., and Aziz, K., 1972, Transient three-dimensional natural convection in confined porous media: Internat. Jour. Heat and Mass Transformation, v. 15, p. 73-90.

Jaeger, J. C., 1968, Cooling and solidification of igneous rocks, *in* Hess, H., ed., Basalts, v. II: New York, John Wiley & Sons, Inc., p. 504-535.

Keenan, J. H., and Keyes, F. G., 1969, Steam Tables: New York, John Wiley & Sons, 162 p.
Lindgren, W., 1907, The relation of ore deposition to physical conditions: Econ. Geology, v. 2, p. 105-127.
Lister, C. R. B., 1974, On the penetration of water in hot rock: Astron. Soc. Jour. Geophys. Research, v. 39, p. 465-509.
Lovering, T. S., 1935, Theory of heat conduction applied to geological problems: Geol. Soc. America Bull., v. 46, p. 69-94.
Nield, D. A., 1968, Onset of thermohaline convection in a porous medium: Water Resources Research, v. 4, p. 553-560.
Norton, D., 1972, Concepts relating anhydrite deposition to solution flow in hydrothermal systems: Internat. Geol. Cong., 24th, Montreal 1972, sec. 10, p. 237-244.
Norton, D., and Knapp, 1977, Transport phenomena in hydrothermal systems: The nature of rock porosity: Am. Jour. Sci., v. 277, p. 913-936.
Peaceman, D. W., and Rachford, H. H., Jr., 1955, The numerical solution of parabolic and elliptic differential equations: Soc. Indust. Appl. Math. Jour., v. 3, no. 1, p. 28-41.
Rayleigh, Lord, 1916, On convection currents in a horizontal layer of fluid, when the higher temperature is on the underside: Philos. Mag., ser. 6, v. 32, p. 529-545.
Ribando, R. J., Torrance, K. B., and Turcotte, D. L., 1976, Numerical models for hydrothermal circulation in the oceanic crust: Jour. Geophys. Research, v. 81, p. 3007-3012.
Roache, Patrick J., 1972, Computational Fluid Dynamics: Albuquerque, N.M., Hermosa Publishers, 434 p.
Rubin, H., 1973, Effect of nonlinear stabilizing salinity profiles on thermal convection in a porous medium layer: Water Resources Research, v. 9, p. 211-221.
Schmidt, E., 1969, Properties of Water and Steam in SI-Units: New York, Springer-Verlag, 205 p.
Ssu-hsiao, C., 1250, *in* Brower, ed., Of All Things Most Yielding: San Francisco, California, McGraw Hill, Friends of the Earth, 128 p.
Taylor, H. P., Jr., 1971, Oxygen isotope evidence for large-scale interaction between meteoric ground waters and Tertiary granodiorite intrusions, Western Cascade Range, Oregon: Jour. Geophys. Research, v. 76, p. 7755-7873.
Van Hise, C. R., 1901, Some principles controlling the deposition of ores: Am. Inst. Min. Eng. Trans., v. 30, p. 27.
Veronis, G., 1968, Effect of stabilizing gradient of solute on thermal convection, Jour. Fluid Mech., v. 34, p. 315-336.
Villas, N. R., ms, 1975, Fracture analysis, hydrodynamic properties, and mineral abundance in altered igneous rocks at the Mayflower Mine, Park City District, Utah: Ph.D. dissert., University of Utah, Salt Lake City, 253 p.
Wooding, R. A., 1957, Steady state free thermal convection of liquid in a saturated permeable medium: Jour. Fluid Mech., v. 2, p. 273-285.

Ann. Rev. Earth Planet. Sci. 1978. 6:229-50

HYDROTHERMAL ALTERATION IN ACTIVE GEOTHERMAL FIELDS

P. R. L. Browne
New Zealand Geological Survey, Box 30368, Lower Hutt, New Zealand

INTRODUCTION

In the fall of 1929 the Carnegie Institution drilled a 124-m well in the Upper Geyser Basin of Yellowstone National Park. Cores from this well and a subsequent well at Norris Basin were studied by Fenner (1934, 1936), who published the first detailed accounts of subsurface hydrothermal alteration in an active geothermal system. Of course, it had long been known from studies of hot springs and ore deposits that thermal fluids can react with the rocks they contact so that both change their compositions. Active geothermal systems, however, are places where these reactions are occurring now and where it is often possible to make direct physical and chemical measurements. Thus they may be regarded as large-scale, uncontrolled, open-end natural experiments. But because there still usually remain several unknown variables—such as the duration of thermal activity or the composition of the fluid before it enters the system—studies of alteration in geothermal samples complement, rather than replace, low-temperature mineral-stability experiments.

This chapter is a survey of hydrothermal alteration in several geothermal systems recently explored by drilling. It is selective in that it usually mentions only papers published since about 1968, and it excludes discussion of ore minerals since these have been described elsewhere (White 1967, Weissberg et al 1978). Also excluded are submarine thermal systems (e.g. Ridge 1973), geopressured sedimentary basins (e.g. Carpenter et al 1974), and accounts of alteration at Steamboat Springs, Nevada (Schoen & White 1965, 1968, Sigvaldason & White 1961, 1962, White 1968), Pauzhetsk, Kamchatka (Naboko 1970, 1976), Tahuangtsui, Taiwan (Chen 1966, 1967), Wairakei (Steiner 1953, 1955, 1968, 1970), and Waiotapu (Steiner 1963). Many aspects of geothermal systems are discussed in three massive volumes forming the proceedings of a United Nations conference (1976), and an extensive bibliography is also now available (ERDA 1976).

0084-6597/78/0515-0229$01.00

HYDROTHERMAL MINERALS

A very wide range of hydrothermal minerals has been recognised in active geothermal systems (Table 1). Many occur in low-grade metamorphic rocks and hydrothermal ore deposits, but some are rare [e.g. buddingtonite (Erd et al 1964)] or perhaps unexpected at low temperatures [e.g. aegirine and lepidolite (Honda & Muffler 1970, Bargar et al 1973)]. Wairakite, a calcium zeolite, is the best known mineral first found in cores from an active geothermal field (Steiner 1955, Coombs 1955).

Several factors affect the formation of hydrothermal minerals and these vary in

Table 1 Some hydrothermal minerals in selected geothermal fields[a]

	Imperial Valley, California[a]	Yellowstone, Wyoming	The Geysers, California	Pauzhetsk, Kamchatka	Matsukawa, Japan	Otake, Japan	Tongonan, Philippines	Kawah Kamojang, Java	N.Z. Volcanic Zone	El Tatio, Chile	Low temp. Iceland	High temp. Iceland	Larderello, Italy
Allophane				x									
Quartz	x	x	x	x	x	x	x	x	x	x	r?	x	x
Cristobalite		x		x	x	x	x	x	x	x			
Kaolin group	d	x	x	x	x	x	x	x	x	x			
Montmorillonite	d	x		x	x	x	x	x	x	x	x	x	
Interlayered illite-mont.	x			x	x	x	x	x	x		x	x	
Illite	x	x	x	x	x	x	x	x	x	x			
Biotite	x			x					x				
Chlorite	x	x	x	x	x	x	x	x	x	x	?	x	x
Celadonite		x		x						x	x		
Alunite			x	x	x	x	x		x				
Anhydrite	x			x	x	x	x	x	x	x		x	x
Sulfur			x	x	x		x		x				
Pyrophyllite					r	x	r	r					
Talc	x						x						
Diaspore					x	x		x					
Calcite	x	x	x	x	x	x	x	x	x	x	x	x	x
Aragonite	x[b]						x[b]		x[b]				
Siderite			x	x			x		x	x			
Ankerite	x			x								x	
Dolomite	d												
Analcime		x		x					x		x	x	
Wairakite	x		x	x		x	x	x	x			x	x
Gmelinite											x		
Gismondine											x		

Table 1 (*continued*)

	Imperial Valley, California[a]	Yellowstone, Wyoming	The Geysers, California	Pauzhetsk, Kamchatka	Matsukawa, Japan	Otake, Japan	Tongonan, Philippines	Kawah Kamojang, Java	N.Z. Volcanic Zone	El Tatio, Chile	Low temp. Iceland	High temp. Iceland	Larderello, Italy
Erionite		x											
Laumontite		x		x	x	x			x	x	x	x	
Phillipsite				x									
Scolecite				x							x		
Chabazite				x							x		
Thomsonite				x							x		
Clinoptilolite		x					x						
Heulandite		x		x		x	x		x		x	x	
Stilbite											x	x	
Mordenite		x		x					x		x	x	
Prehnite	x			x					x		r?	x	
Amphibole	x			x			x					x	
Garnet	x			?								r	
Epidote	x			x		x	x	x	x		r	x	x
Clinozoisite									x				
Pectolite		x							x[b]				
Sphene	x			x			x	x	x				
Adularia	x	x	x	x		x	x	x	x	x			x
Albite	x			x		x	x	x	x			x	
Rutile				x	x	x							
Leucoxene			x	x	x		x		x				
Magnetite							x						
Hematite	x	x		x			x	x	x	x	x		
Pyrite	x	x	x	x	x	x	x	x	x	x	x	x	
Pyrrhotite	x						x		x				
Marcasite							x		x				
Base-metal sulfides	x						x		x				
Fluorite		x						x					

References: Imperial Valley: Skinner et al 1967, Muffler & White 1969, Bird & Elders 1976, Kendall 1976b, Reed 1976, Browne & Elders 1976. Yellowstone: Fenner 1936, Honda & Muffler 1970, Bargar et al 1973, Keith & Muffler 1978, Keith et al 1978. The Geysers: Steiner 1958, McNitt 1964. Pauzhetsk: Naboko 1970. Matsukawa: Sumi 1968. Otake: Hayashi 1973. Tongonan: C. P. Wood, unpublished observations. Kawah Kamojang: Browne, unpublished observations. N.Z. Volcanic Zone: Steiner 1953, 1963, 1968, Browne & Ellis 1970, Browne, unpublished observations. El Tatio: Browne, unpublished observations. Iceland: Sigvaldason 1963, Tómasson & Kristmannsdóttir 1972, 1976, Kristmannsdóttir & Tómasson 1976a, b, c, Kristmannsdóttir 1976. Larderello: Marinelli 1969.

Note: d = detrital, r = relict.

[a] includes Cerro Prieto, Baja California, Mexico.

[b] deposited in discharge pipes and channels.

relative importance from field to field. Some are so intimately related that it is often impossible to separate one factor from another. The factors are: (*a*) temperature, (*b*) pressure, (*c*) rock type, (*d*) permeability, (*e*) fluid composition, and (*f*) duration of activity. This list is similar to several suggested from work on ore deposits, but geothermal studies have demonstrated that permeability and fluid composition are usually at least as important as temperature.

Temperature

Most liquid-dominated systems explored so far have reservoir temperatures below about 280°C, but several people have reported maxima above 300°C [including the Salton Sea, California at 360°C (Palmer 1975), Cerro Prieto, Mexico at 388°C (Mercado 1969) or 371°C (Mercado 1976), and Tongonan, Philippines at 324°C (C. P. Wood, personal communication)]. Vapor-dominated systems have maximum temperatures after exploitation of 236°C (White et al 1971).

Except for epidote, ortho, ring, and chain silicates are uncommon alteration minerals in active geothermal systems, but where present, usually occur at high temperatures. Hydrothermal garnet and tremolite are known from the Salton Sea (Muffler & White 1969, Kendall 1976b), and tremolite also occurs at Tongonan (C. P. Wood, personal communication). An unspecified amphibole is present at one of the Icelandic fields (Kristmannsdóttir 1976), and all its occurrences are where well temperatures exceed 280°C, but garnet is present only above 320°C. Epidote occurs at several fields (Table 1), usually above 240–260°C but in some (Seki 1972), such as at Reykjavik (Sigvaldason 1963), it apparently occurs down to 120°C. Possibly here, however, it is a relict formed when temperatures were higher.

Pyrophyllite and talc also form at high temperatures, but the former is considered to be relict at Kawah Kamojang, Indonesia and in several of the Japanese fields (Sumi 1968). The distribution of clay minerals is also temperature dependent (Browne & Ellis 1970, Muffler & White 1969, Steiner 1968). In the New Zealand fields surface kaolinite, formed at low pH, does not persist above about 60°C, although dickite is known in one well where measured temperatures are from 140 to 150°C. With increasing depth and temperature, the usually dominant clay, Ca-montmorillonite, becomes increasingly interstratified with illite, to become interlayered illite-montmorillonite, but above about 220°C, illite plus chlorite is the typical clay-mineral assemblage. Of course, the apparent temperature dependence of the clays is aided by the near-uniform composition of fluids throughout these fields (Browne & Ellis 1970, Mahon & Finlayson 1972)—a condition not always met elsewhere.

As expected, the distribution of zeolites is strongly temperature dependent, and this is well illustrated by Icelandic and Japanese work (summarized later), although the greatest range of zeolites is at Pauzhetsk (Naboko 1970). Typical zonation in the New Zealand fields is mordenite-laumontite-wairakite, with mordenite forming near 50°C and wairakite usually above 215°C, but occasionally as low as 140°C (Browne & Ellis 1970, Steiner 1953, 1968). Cristobalite and siderite frequently occur below 100°C, but several minerals, including pyrite, calcite, and chlorite, form readily at both low and high temperatures.

Pressure

Fluid pressures in geothermal areas are low and seldom exceed 200 bars. In liquid-dominated fields they are usually close to, or slightly above, hot hydrostatic, but occasionally, where self-sealing has occurred—for example at Yellowstone—they must have exceeded lithostatic pressure (Muffler et al 1971). In vapor-dominated systems, fluid pressures are typically well below hydrostatic (White et al 1971). Over the drilled depths pressure has little *direct* affect on hydrothermal alteration, other than to influence the induration and lithification of sediments. However, *change* of fluid pressure can affect fluid composition. This is most obvious where boiling occurs and CO_2 is lost; zones of subsurface boiling are often characterized by hydrothermal quartz, K-feldspar and bladed calcite (Browne & Ellis 1970, Keith & Muffler 1978, Keith et al 1978). The effect of pressure on the K-mica–K-feldspar equilibrium results in a given solution being more alkaline at high pressure. Fluids released from high-pressure control, therefore, have a tendency to deposit K-feldspar (Ellis & McFadden 1972).

Rock Type

The parent rock influences hydrothermal alteration mainly through the control of permeability by texture and porosity. The initial mineralogy of the reservoir rocks seems to have little affect on equilibrium alteration assemblages above about 280°C. For example, albite, K-feldspar, chlorite, Fe-epidote, calcite, quartz, illite, and pyrite are the typical stable assemblage in basalts of Iceland, sandstones of the Imperial Valley, rhyolites of New Zealand, and andesites of Indonesia. At lower temperatures, however, the nature of the parent material clearly influences the alteration product. High-silica zeolites, such as mordenite, are common in rhyolitic fields at Yellowstone (Honda & Muffler 1970) and New Zealand (Browne & Ellis 1970, Steiner 1968), whereas lower silica zeolites, e.g. chabazite, thomsonite, scolecite, occur in the basalts of Iceland and andesites of Kamchatka (Kristmannsdóttir & Tómasson 1976c, Naboko 1970).

Permeability

Studies on alteration in geothermal fields have clearly recognized the important control of permeability on hydrothermal mineral deposition. Mineral reactions are seldom isochemical and extensive alteration and hydration needs more than pore water to proceed. In many cases, at least carbonate and sulfide species must be added to rocks from solutions.

In rocks of low permeability, equilibrium between rocks and the reservoir fluid is seldom achieved and primary minerals or glass can persist to high temperatures. For example, dense welded tuffs at Broadlands, Wairakei, and Yellowstone have locally remained little changed, even at high temperatures, because fluid access is too difficult (Browne & Ellis 1970, Keith et al 1978). The marked zoning of hydrothermal minerals about fluid channels in several Japanese geothermal fields clearly shows structural control of alteration and demonstrates how intensity and type of alteration reflect permeability (Sumi & Takashima 1976). Permeable fissure channels at Wairakei, Broadlands, Waiotapu, Kawerau (all in New Zealand),

and Tongonan, Philippines are characterized by vein adularia, usually together with quartz and calcite (Steiner 1968, Browne 1970). Browne (1970) showed that at Broadlands there is an approximate relationship between the nature of feldspars in aquifer rocks and the measured well permeabilities; in order of increasing permeability the feldspars are: primary andesine, albite, albite + adularia, adularia. Thus rocks from highly permeable zones are often increased three- to fourfold in K_2O.

Isotopic analysis of hydrothermal minerals also gives information about reservoir hydrology (Blattner 1975, Coplen et al 1975, Clayton et al 1968, Clayton & Steiner 1975, Eslinger & Savin 1973, Kendall 1976a, b, Olson 1976). Kendall's (1976b) study, for example, shows that the carbon and oxygen isotopic composition of minerals from the Salton Sea reflects variations in reservoir permeability, and she was able to relate depletion of O^{18} in calcite with zones of high permeability as indicated by Saraband logs.

Fluid Composition

This was recognized by Fenner (1934) as a factor in hydrothermal alteration at Yellowstone. However, only in the last few years has it been realized how close, in fact, is the relationship between fluid chemistry and alteration mineralogy. Successful use of the silica geothermometer to estimate deep temperatures depends on silica in the fluids being in equilibrium with a silica mineral, usually quartz

Table 2 Concentration (mg/kg) in waters separated from discharge at atmospheric pressure

Drillhole No.	Depth (m)	Source Temp (°C)	pH (15–25°)	Li	Na	K	Rb	Cs	Mg	Ca
Salton Sea IID No. 2[a]	1776	332	—	210	53,000	16,500	70	20	10	28,800
Cerro Prieto[a] M.8	1300	305	5.43	10.9	4730	1180	—	—	0.2	272
Yellowstone Y-3	157	194	8.1	3.5	270	11	—	—	0.02	1.26
Matsukawa T1	162	100	2.8	—	—	—	—	—	2.1	12.0
Otake No. 9	550	220–240	8.1	5.15	936	131	—	—	0.2	12.3
Otake 11-2	720	240–270	3.4	7.03	1186	228	—	—	0.47	15.0
Wairakei 44	695	260	8.4	14.2	1320	225	2.8	2.5	0.03	17
Broadlands 10	1092	260	8.6	9.5	910	143	1.1	1.4	0.05	1.1
Seltjarnarnes S-4	2050	114	—	—	362	10	—	—	0.09	132
Hveragerdi G-3	650	216	9.6	0.3	212	27	0.04	<0.02	0.0	1.5
El Tatio 7	867	262	7.0	45.2	4840	830	0.6	17.4	0.16	211

[a] Helgeson 1968a
[b] Reed 1976
[c] Bargar et al 1973
[d] Sumi 1968
[e] Hayashi 1973
[f] Ellis 1967

(Mahon 1966, 1976, Fournier & Rowe 1966, Fournier 1973, Arnórsson 1975). Similarly, the Na-K and Na-K-Ca geothermometers require that the solutions be in equilibrium with albite and K-feldspar (Ellis & Mahon 1967, Fournier & Truesdell 1973, Truesdell 1976).

Several significant papers on experimental and thermodynamic work have greatly increased our understanding of hydrothermal alteration (Hemley et al 1969, Hemley & Jones 1964, Helgeson 1967, 1968b, 1970, 1971, Helgeson et al 1969a, b). For example, the experimentally derived activity diagram for equilibrium in the system K_2O–Na_2O–Al_2O_3–SiO_2–HCl–H_2O at 260°C (Figure 1), shows the relationships between several mineral phases and water of Broadlands composition (Browne & Ellis 1970); as expected from minerals in the cores, this water is in near equilibrium with K-feldspar (adularia), albite, and K-mica (illite).

By using petrographic studies of cores and analyses of well fluids and well temperatures, diagrams for other element combinations can be constructed. For example, the mineral stability diagram for calcium and potassium minerals (Figure 2) shows that the deep 260°C water at Broadlands has a composition close to equilibrium with K-mica, K-feldspar, wairakite, and calcite and emphasizes the critical role of CO_2 in determining the stability of calcium phases. Where CO_2 concentrations are high, as at Broadlands (0.15 moles), calcite tends to deposit at the expense of epidote (zoisite) or wairakite during steam separation. A close

for selected geothermal fluids

F	Cl	Br	I	SO_4	SiO_2	B	NH_3	CO_2	H_2S	Ref.
—	155,000	—	—	S = 30	400	390	—	500	—	a
—	9040	—	—	9	590	12	11.6	2580	624	b
30	278	—	—	19.1	—	3.6	—	HCO_3-177	—	c
—	4.1	—	—	176	30	—	1.9	—	45.4	d
4.6	1474	3.4	0.3	136	665	32	—	40.7	—	e
1.5	1941	5.6	0.4	318	626	36	—	0.0	—	e
8.3	2260	6.0	0.3	36	690	29	0.15	19	1.0	f
6.2	1244	3.6	0.1	12	635	55	1.2	(CO_3 = —HCO_3—)553	—	g
0.95	554	—	—	209	101	—	—	17	—	h
1.9	197	0.45	0.0	61	480	0.6	0.1	55	7.3	f
3.0	8790	—	—	30	766	203	2.3	5.4(HCO_3-40)	—	i

[a] Browne & Ellis 1970
[b] Tómasson & Kristmannsdóttir 1976
[c] Cusicanqui et al 1976
[d] Corrected for steam loss

relationship between fluid composition and alteration (Tables 1 and 2) is seen in several Japanese fields including Otake. Here near-neutral pH waters form quartz, K-mica, heulandite, wairakite, albite, and adularia, whereas deep low pH fluids produce alunite (Hayashi 1973) in accord with the experimentally derived relations of Hemley et al (1969).

Little has so far been published on alteration in vapor-dominated fields, but the occurrence of wairakite at The Geysers (Steiner 1958) and epidote, adularia, quartz, calcite, and zeolites at Larderello (Marinelli 1969) indicates that a liquid was (or is) present in both fields. However, in rocks affected by steam, pyrrhotite may form in preference to pyrite (Browne & Ellis 1970), and clays, especially kaolinite or montmorillonite, may be more abundant under such conditions.

Duration

Much has yet to be learnt about the age and evolution of geothermal systems, but available evidence suggests they are long lived (Grindley 1965, Browne 1971, White 1974, Sumi & Takashima 1976). Steamboat Springs, for example, has been active, at least intermittently, for 1 million, and probably as long as 3 million years. During such long periods geothermal activity changes in both intensity and location, although many changes will be due to events not directly related to thermal

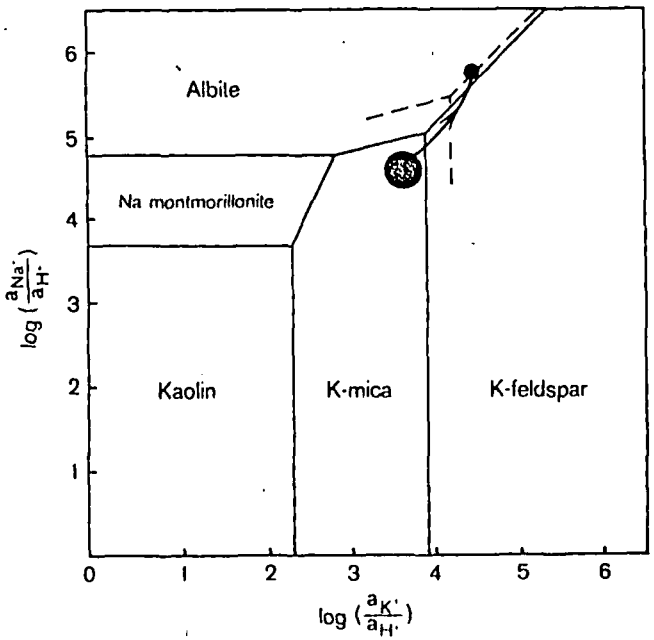

Figure 1 Phase diagram for sodium and potassium in terms of ion activity ratios at 260°C with quartz present. Solid circle plots Broadlands water composition and arrow shows trend with steam loss; dotted lines indicate positions of phase boundaries at 230°C (Browne & Ellis 1970).

activity, such as erosion, earth movement, or volcanic activity. Self-sealing, however, occurs at the tops and margins of fields where cooling waters deposit quartz, or less commonly zeolites (Bird 1975, Elders & Bird 1976, Keith et al 1978). Shifts in activity have long been recognized at Yellowstone from the migration of thermal features, and surficial activity has been extinguished at Matsukawa (Sumi & Takashima 1976) and, locally, Wairakei. Kristmannsdóttir & Tómasson (1976a) concluded that the Nesjavellir (Iceland) thermal field is shifting north and the minerals have not yet adjusted to the new higher temperatures. By contrast, cooling has been recognized at Kawah Kamojang and at Matsukawa (Sumi 1968), where pyrophyllite and diaspore are thought to be relicts from temperatures above 310°C, compared with 150–250°C at present.

Several proposed geothermometric methods have been tested on samples from geothermal areas. They include: aluminum-in-quartz (Hayashi 1973, Browne & Wodzicki 1977), sphalerite compositions (Browne & Lovering 1973), sulfur isotope fractionation between coexisting sulfide pairs (Browne et al 1975), oxygen isotope fractionation between hydrothermal carbonates and silicates (Blattner 1975, Eslinger & Savin 1973, Coplen et al 1975), and fluid inclusions (Browne et al 1976, Browne & Elders 1976, Hoagland 1976b). The last two methods appear to be the most useful in their applications to geothermal systems.

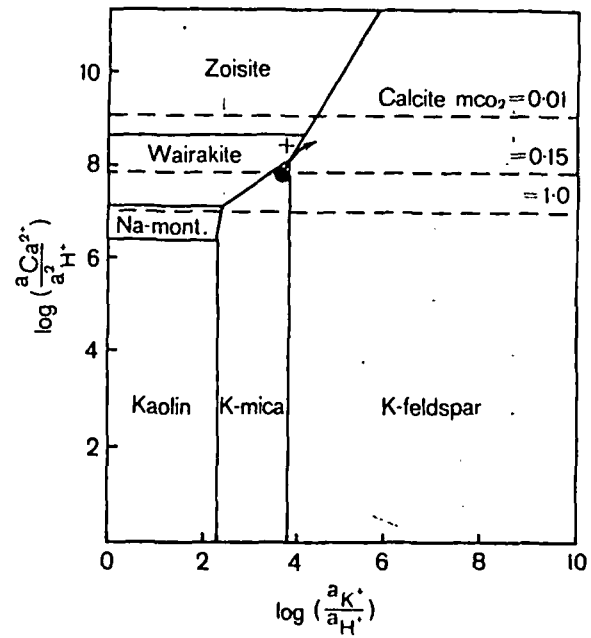

Figure 2 Phase diagram for potassium and calcium minerals in terms of ion activity at 260°C with quartz present; m = moles. Circle plots Broadlands and cross Wairakei water compositions; arrow shows trend with steam loss (Browne & Ellis 1970, Ellis & Mahon 1977).

The homogenization temperatures of 177 primary fluid inclusions in hydrothermal quartz and sphalerite crystals from seven Broadlands wells varied between 201° and 293°C; they ranged from 13°C below to 37°C above well temperatures but averaged 8°C above. One hundred and ninety-eight secondary or pseudosecondary inclusions, which had a wider temperature spread than the primary ones, gave filling temperatures that averaged 6°C below corresponding well temperatures. This close agreement between filling and measured temperatures indicates either that there has long been a stable thermal system at Broadlands or that the crystals and their inclusions are modern.

By contrast, fluid inclusions in calcite from Holtz No. 1 well at Heber, California appear to record two former thermal events; at 1525 m these were at 212±9°C and 235±5°C (Browne & Elders 1976), whereas present reservoir temperatures are probably about 190°C (Renner et al 1975). At well 6–1 East Mesa, homogenization temperatures show that the fluid inclusions formed 15–20°C above present well temperatures (Hoagland 1976b).

To date, there have been few measurements of the freezing temperatures of inclusions to attempt estimates of past fluid salinities, but such studies are likely to be extremely fruitful. In one study freezing temperatures were measured in 33 primary and 60 secondary (pseudosecondary) inclusions in eight hydrothermal quartz and one sphalerite crystal (Browne et al 1976) from Broadlands. The observed freezing point depressions (0.1 to 0.8°C) appear too large if only the dissolved salts in the deep waters (3000 ppm) are considered, but are in agreement with the present-day Broadlands water compositions when the range of downhole CO_2 compositions (0.1–0.3 moles) is included in the calculations.

HYDROTHERMAL ALTERATION IN SELECTED AREAS

Examples of hydrothermal alteration in geothermal fields recently studied show, in more detail, the variability of these usually interrelated factors.

Imperial and Mexicali Valleys, Western North America

Several geothermal fields have been recognized in the Imperial Valley of Southern California and its extension southward into the Mexicali Valley, Baja California. Drilling has so far taken place at the Salton Sea, Brawley, Heber, The Dunes, East Mesa, and Cerro Prieto. The main structural feature, the Salton Trough, is a depression filled with up to 7000 m of poorly sorted Colorado River detritus which form sandstones, shales, siltstones, and minor conglomerates (Biehler et al 1964, Muffler & Doe 1968). Five small young rhyolite domes occur at the Salton Sea, rhyodacite reaches the surface at Cerro Prieto, and minor intrusive basalts have been penetrated by wells at the Salton Sea (Robinson et al 1976) and Heber (Browne & Elders 1976).

The northernmost field, the Salton Sea, is the most famous, and here wells encountered brines with over 250,000 ppm dissolved solids (Table 2) at temperatures up to 360°C (Helgeson 1968a, Randall 1974, Palmer 1975). Salinities at the other fields are much lower and are about 50,000 ppm at Brawley, 2000 to 30,000 ppm at East Mesa, and about 17,000 ppm at Cerro Prieto. Copper- and silver-rich scales deposited from brines (Skinner et al 1967) discharged from the Salton Sea and their precipitation has been considered thermodynamically by Miller et al (1977). Alteration in cores and (mainly) cuttings from several drill holes here have been described by Muffler & White (1968, 1969), Keith et al (1968), Muffler & Doe (1968), and Kendall (1976b); mineral isotope studies have been made by Clayton et al (1968) and Kendall (1976a, b).

Muffler & White (1969) showed that the sediments, which contain detrital quartz, calcite, K-feldspar, plagioclase, montmorillonite, illite, dolomite, and kaolinite, gradually convert, in response to increasing temperatures, to an assemblage above 300°C of quartz, Fe-epidote, chlorite, K-feldspar, albite ± K-mica, pyrite, sphene, sphalerite, and hematite. Detrital montmorillonite below 100°C converts to illite-montmorillonite and then to K-mica below 210°C; ankerite can form as low as 120°C, and chlorite, calcite, and CO_2 are produced below 180°C in response to reaction between dolomite, ankerite, and kaolinite plus Fe^{2+} added from the brine. Fe-epidote and K-feldspar are abundant above 290°C, but calcite disappears at about this temperature. Temperature is thought to be the main control on the formation of this low-grade greenschist mineral assemblage, although lithostatic pressure influences induration and lithification so that rock densities increase from below 2.0 at the surface to 3.0 at 1500 m. Muffler & White (1968, 1969) considered that high CO_2 activity relative to H_2O precluded zeolite formation and favored carbonate precipitation. An interesting aspect of this is that the CO_2 at shallow levels has probably been released from deeper reactions between dolomite and kaolinite (150–200°C) and transformation of calcite into epidote (300–320°C). Kendall (1976b) has given a detailed description of alteration in three wells (Magmamax 2 and 3, Woolsey 1). As well as recognizing hydrothermal biotite, tremolite, garnet, and a high-temperature expanding smectite, she showed that there has been extensive oxygen and carbon isotope exchange between brines and carbonates down to 100–150°C; both detrital and authigenic quartz in sandstones have exchanged oxygen at 290°C generally confirming the conclusions of Clayton et al (1968). Kendall, however, attributes downwell variations in O^{18} to incomplete isotope exchange between fluid and rock caused by differences in reservoir permeability.

Hoagland (1976a, b) and Hoagland & Elders (1978) have described the alteration and Coplen (1976) measured the isotopic ratios of minerals from an 1830 m deep well at East Mesa, which has a maximum temperature of 188°C. The vertical extent of the reservoir can be defined by its alteration and, using thermochemical evaluation of aqueous species and petrographic observations, two distinct hydrothermal events were recognized. During the earlier event, quartz, pyrite, illite, Fe-chlorite, and rare adularia deposited in sandstone, as less porous siltstones and shales altered to illite and chlorite; however, detrital kaolin, montmorillonite, and interlayered clays persisted. Fluid inclusion measurements show that this occurred 15–20°C above present temperatures. Fluids responsible may have been similar to the sodium chloride brine with 26,900 ppm dissolved solids that discharged from a deeper (2200–2450 m) aquifer reached by a drill hole

400 m to the east. Later, cold water entered the system laterally and, on heating, partly dissolved the silicates and precipitated abundant calcite. Thermochemical calculations show that this may have been of the same composition as sodium bicarbonate–chloride fluid (2380 ppm dissolved solids) which discharges from the well and derives from 1660–1800 m. This fluid is in chemical, but apparently not isotopic (Coplen 1976), equilibrium with kaolinite, calcite, and montmorillonite rather than potassium silicates or dolomite.

A 612-m-deep well at the margin of the Dunes thermal area provides a good example of self-sealing (Bird 1975, Bird & Elders 1976, Coplen et al 1975, Elders & Bird 1976). In the upper 300 m, seven zones of dense quartzite have formed by episodic reaction between permeable sandstones and laterally moving sodium chloride fluids containing up to 3000 ppm dissolved solids. After the porosity of the sandstones was reduced, water flowed by way of fractures where quartz, adularia, pyrite, calcite, and hematite were deposited. Hydrothermal alteration has increased both the bulk densities of aquifer rocks (from 2.2 to 2.6 gm cm^{-3}) and their SiO_2 (35–50% above initial content) and K_2O (90–130%) relative to Al_2O_3. The temperature profile shows maxima of 110°C at 110 m and 104°C at 285 m, below which there is a reverse gradient. Further, the isotopic compositions of quartz-water, alkali feldspar-water and calcite-water pairs (Coplen et al 1975) show that temperatures here have never exceeded 130°C.

By contrast, temperatures as high as 388°C have been recorded at Cerro Prieto (Mercado 1969), although 370°C is more usual (Mercado 1976). More than 30 wells have been drilled to between 500 and 2630 m, but unlike the other very hot field, Salton Sea, deep fluids (Table 2) have salinities of only about 17,000 ppm (Mercado 1969). The two main factors affecting the formation and distribution of hydrothermal minerals here are temperature and fluid composition (Reed 1976). Kaolinite, montmorillonite, and illite-montmorillonite do not occur above 160°C, nor dolomite above 210°C, but chlorite and illite-chlorite form above 145°C, wairakite above 240°C, and epidote above 255°C. Authigenic orthoclase increases in abundance above 300°C, in accordance with thermodynamic calculations (Reed 1976) based on the composition of reservoir water, but is not easily distinguished in the cuttings from detrital orthoclase or microcline.

Yellowstone, U.S.A.

Because of environmental constraints, no deep drilling is normally allowed within Yellowstone National Park—one of the world's most famous and spectacular thermal areas. However, in 1967–1968 13 shallow diamond-core wells were drilled as part of a comprehensive scientific project by the U.S. Geological Survey. A major strength of this work, following the example of Fenner (1934, 1936) and Allen & Day (1935), is the close integration of geological, petrologic, and geochemical methods. Although the deepest well (Y-12) is only 329.6 m deep and most are near 150 m deep, both the drilling and the wells were closely monitored, so that an excellent physical record was obtained (White et al 1975). In addition, the near completeness of core recovery (usually above 90%) has made possible the most detailed work so far on hydrothermal alteration in an active geothermal

system. Alteration studies have now been completed for wells Y-1 (Honda & Muffler 1970), Y-5 (Keith & Muffler 1978), Y-7, and Y-8 (Keith et al 1978). Less detailed information from Y-3 (Bargar et al 1973) and Y-11 (White et al 1971) is also available.

Wells in the Upper Geyser Basin (Y-1, Y-7, Y-8, and Fenner's C-1) penetrated sandstone, siltstone, and conglomerate mainly composed of rhyolitic detritus overlying rhyolite; Y-5, in Midway Geyser Basin, was drilled, for the most part, into densely welded rhyolitic ash flow tuff. Maximum well temperatures are: 171°C in Y-1, 170°C in Y-5, 143°C in Y-7, and 170°C in Y-8.

Several minerals not previously known in geothermal systems have been recognized. For example, acgirine occurs in Y-1 where the well temperature is 160°C and in Y-3 it also coexists, in the core from 23.8 to 28.5 m at temperatures of 130–140°C, with quartz, pectolite, montmorillonite, analcime, ?albite, and lepidolite (with 7.5% Li_2O). Fluids depositing these minerals (Table 2), although dilute, have high Li/K ratios (1.8) and low Cl/F ratios (about 5).

Factors affecting hydrothermal alteration at Yellowstone vary in importance from well to well and are not easily separated. The nature of the starting material is important in Y-1, Y-7, and Y-8 where detrital obsidian alters readily, but coexisting lithoidal rhyolite of essentially the same composition remains unchanged. The dense, welded ash-flow tuff in Y-5 shows only incipient alteration (to montmorillonite) as its devitrification products, quartz and sanidine, are more stable than glass so that hydrothermal minerals are here more abundant than in Y-5. Obsidian clasts in Y-7 and Y-8 alter, first nearly isochemically, to ?metastable potassic clinoptilolite (K_2O up to 5.7%) and then to analcime plus K-feldspar.

Temperature is important but its effect is often equivocal and difficult to distinguish from fluid composition or variations in permeability. Obsidian in Y-1 is completely replaced above 85°C, but persists to 170°C in Y-8 because of lower permeability in the vitrophyric flow breccia, which indicates that through-going solutions are needed here for even devitrification to occur. Opal occurs only below 43°C in Y-5 and near 104°C in Y-1, whereas in this well β-cristobalite is not present above 115°C. Erionite is present in cores from several wells where temperatures are below 110°C. Differences in fluid composition, especially SiO_2 activity, rather than temperature, evidently account for the observed distribution of clinoptilolite, mordenite, and α-cristobalite and the quartz-analcime association in Y-1. Subsurface boiling caused changes in fluid pH through loss of CO_2, thereby resulting in deposition of adularia in wells C-1 and Y-13 and bladed calcite in Y-8 and Y-5. The Yellowstone work, however, confirms the important effect of permeability in determining the extent and type of hydrothermal alteration in geothermal systems. For example, K-feldspar, quartz, mordenite, and celadonite have formed in permeable zones of Y-8, but in deeper impermeable parts of this well glass persists. Further, mineral deposition in pore spaces of a correlated unit in the 130 m between the sites of Y-7 and Y-8, the latter of which is thought to be closer to the upflow zone, has caused self sealing, so that there is now a pressure differential of .015 bar m^{-1} between the two wells.

These two wells also provide a good record of relationships among silica

minerals in a geothermal field. X-ray—amorphous opal dominates in superficial sinter and also forms near-surface cement, whereas α- and β-cristobalite have irregular distributions at greater depth. In Y-7, β-cristobalite occurs mainly in veinlets and the α-form is in the groundmass, but cores from Y-8, the hotter well, contain quartz and chalcedony. This suggests that the distribution of silica minerals is controlled primarily by temperature. From a study of veinlets, Keith et al (1978) found that the silica forms, deposited from oldest to youngest, were quartz, chalcedony, α-cristobalite, β-cristobalite and opal; this is also the order of decreasing stability and increasing solubility with respect to water of constant temperature (Fournier 1973, Arnórsson 1975). Keith et al (1978) concluded that water from the wells is strongly supersaturated with respect to quartz, chalcedony, and α-cristobalite; is slightly undersaturated relative to β-cristobalite; and is undersaturated above 80°C with respect to opal. However, fluids in the reservoir itself are just saturated with quartz. Their suggested model is one in which ascending silica-rich water penetrates aquifers which, through self-sealing, become partially closed systems; the trapped pore water then becomes progressively lower in SiO_2 as more stable silica minerals are successively reconstituted from the earlier deposited phases.

Japan

Japan has about one hundred geothermal systems, excluding fumaroles on the craters of active volcanoes (Sumi & Takashima 1976). Several fields have been investigated by exploratory drilling and numerous accounts of their alteration have been published recently; space, however, permits mention of only a few.

Most Japanese geothermal systems, and indeed, many in the west Pacific, are associated with late Cenozoic andesite-dacite volcanic centers where there is usually a strong structural control on hydrology. A characteristic feature of their alteration is marked surface zonation; typically, between 3 and 10 alteration zones can be clearly recognized (Sumi & Takashima 1976). This, and the rarity of zone overlaps, shows that thermal episodes were commonly single events in contrast with many systems where mineral zoning, even when recognizable, is irregular. However, cross sections of alteration in several Japanese fields, such as Matsukawa (Sumi 1968), show more complicated zoning in the subsurface than is evident at the surface. Sulfates (particularly alunite) and kaolin are common, and pyrophyllite and zeolites occur in several fields (Hayashi & Fujino 1976, Hayashi & Yamasaki 1976, Sumi & Takashima 1976, Takashima 1971, Yamada 1976, Yoshida 1974, Yoshida et al 1976). An example of calcium zeolite formation is at Katayama, Onikobe where the zonation, with increasing depth and temperature, is mordenite-laumontite (± yugawaralite, analcime)—wairakite (Seki et al 1969, Seki & Okumuru 1968). However, the transition temperatures between laumontite and wairakite (75°C to 175°C in four wells) seem to be below the usual formation temperatures of wairakite (about 220°C), possibly because water pressures at Katayama are low. However, it is not clear that the measured well temperatures are the same as those that prevailed before drilling. Yamada (1976) suggests that α-cristobalite occurs in the vapor zone at shallow depths, but zeolite alteration results from

reaction between andesite and mildly alkaline solutions. Near the bottom of one 1200-m well (GO-10), however, quartz and kaolin have deposited from acid chloride solutions.

Another field where alteration shows a close dependence on fluid composition is at Otake, north-central Kyushu (Hayashi et al 1968, Hayashi 1973, Hayashi & Fujino 1976, Hayashi & Yamasaki 1976, Yamasaki & Hayashi 1976), where two chemically distinct fluids (Table 2) have deposited minerals zoned about fractures. In the Otake area itself deep waters are neutral to alkaline but wells at Hatchobaru, 3 km south, encountered fluids with a pH between 3.4 and 4.6. Hayashi (1973) classifies the alteration into five types (Table 3), based on the composition of the altering fluids, and subdivides further depending on measured well temperatures and fluid pressures. However, the temperatures in many wells were measured only a few days, or even hours, after drilling, so that they are unlikely to be quite the same as the temperatures of mineral deposition. Where acid fluids prevail, Type B alteration is conspicuous and Type D either occurs at shallow levels or where reaction is incomplete. By contrast, at Otake itself, mildly alkaline fluids have restricted Type B alteration but Types D and E are widespread. Major element analysis (Hayashi 1973) shows that massive amounts of SiO_2 were added to rocks with alteration of Type A, but during formation of Types B and C, SiO_2,

Table 3 Classification of hydrothermal alteration in the Otake geothermal area (after Hayashi 1973)

Type	Minerals*	Fluid	Temperature (°C)	P_{fluid} (bars)
A	crist	strong acid	< 100	< 15
	quartz	acid	100 to 230	30 to 50
B	alunite + crist	strong acid	< 100	< 15
	alunite + quartz	strong acid	100 to 230	15 to 50
C	kaol + crist	acid	< 100	< 15
	kaol + quartz	acid	100 to 200	< 30
	dickite + py + quartz	acid	150 to 250	< 60
	py + quartz	acid	> 230	> 50
D	mont + crist	weak acid	< 100	< 15
	mont S/M + quartz	weak acid	100 to 200	< 30
	ch + S/M + quartz	weak acid	150 to 250	< 60
	S + quartz	neutral	> 230	> 50
E	heul + crist	neutral	< 100	< 15
	laum + wair + quartz	neutral	100 to 200	< 30
	albite + quartz	weak alkaline	150 to 250	< 60
	adularia + quartz	weak alkaline	> 230	> 50

* Abbreviations are as follows: crist, cristobalite; kaol, kaolinite; py, pyrophyllite; mont, montmorillonite; ch, chlorite; S/M sericite-montmorillonite; S, sericite; heul, heulandite; laum, laumontite; wair, wairakite.

Al_2O_3, and TiO_2 are nearly immobile, as are Fe_2O_3, CaO, and Mgo during formation of Types D and E; however, Na_2O and K_2O are the most mobile constituents.

The Matsukawa field, northern Honshu, also has zoned surface alteration (Sumi 1968, 1969, Sumi & Takashima 1976) that extends over an area of 7 by 1.5 km. It is elongated about fissures so that structural control of fluid flow and alteration is obvious. From the margin inward four alteration zones are characterized by saponite plus chlorite, montmorillonite, kaolin, and alunite, but other hydrothermal minerals present include laumontite, calcite, and anhydrite in the chlorite zone, calcite, anhydrite, and quartz in the montmorillonite zone, and quartz in both the kaolin and alunite zones. A far smaller zone of pyrophyllite, usually with diaspore, zunyite, andalusite, quartz and anhydrite, which is overlapped by three other zones, is thought to be relict alteration formed above about 310°C, whereas present well temperature maxima are near 230 to 250°C (Sumi 1968, Truesdell 1976). When first opened, the wells typically discharged wet steam of low pH (about 5) and high sulfate contents (Table 2). Zoning from alunite-quartz at the center to outer kaolin is consistent with acid (at 200°C pH below 4) solutions moving outwards from channels and becoming more alkaline by reaction with reservoir rocks.

Iceland

Work on hydrothermal alteration in geothermal fields of Iceland has several important aspects: (*a*) it provides the best examples of reactions between thermal fluids and basalts, (*b*) there is extensive zeolitisation, especially in the low temperature (< 150°C) fields, (*c*) in the Reykjanes area the thermal fluid is modified sea water (Kristmannsdóttir 1975, 1976, Kristmannsdóttir & Tómasson 1976a, b, c, Sigvaldason 1963, Tómasson & Kristmannsdóttir 1972, 1976).

Reservoir rocks are basalt, basaltic hyaloclastites and minor dolerite. Glass readily alters first to opal, smectite, calcite, or a zeolite, and then to mixed-layer clays, although where permeability is low it persists to 200°C. Olivine is the most unstable mineral and it and pyroxene are often partly replaced by smectite-illite or chlorite. Complete replacement of plagioclase by epidote or albite is also rare, indicating that disequilibrium between fluids and rocks is usual. Factors controlling alteration are rock type, water composition, permeability, temperature, and the age of the system—although the first two are less important.

The high-temperature (up to 298 ± 4°C) fields occur in areas of active volcanism and, except for potash enrichment in some permeable zones at Reykjanes, alteration is near isochemical involving hydration and oxidation. Clays are abundant but poorly crystalline; iron-rich saponite, present below 200°C, is replaced by mixed-layer chlorite-smectite in the range 200° to 230°C and chlorite above 230°C. Zeolites are common below 230°C, but thermal gradients are so steep that a distinct temperature zoning cannot be readily detected. Epidote is abundant above 260°C and an amphibole (of unspecified composition) occurs locally where temperatures exceed 280°C. In the Nesjavellir field, prehnite is present above 250°C and calcite alternates in abundance with the zeolites. Well fluids are rich in carbonate (1355 ppm CO_2 equivalent) and sulfide (311 ppm), and consequently

carbonate and sulfide minerals dominate the deep alteration. However, the observed hydrothermal minerals were not formed at the measured well temperatures because activity is shifting north and there has not been time for minerals to adjust to the higher temperature regime.

A high-temperature system in the Reykjanes area, southwest Iceland, is only one of several fields (Truesdell 1976) in which modified sea water is the thermal fluid, but it has the best record of alteration minerals formed from its reaction with reservoir rocks. Hydrothermal minerals are crudely zoned according to temperature (which reaches 300°C): (*a*) montmorillonite–zeolite–calcite zone; (*b*) mixed-layer clay–prehnite zone; (*c*) chlorite–epidote zone. These minerals occur in many fields in Iceland and elsewhere, although fluid compositions vary greatly, leading Tómasson & Kristmannsdóttir (1972) to conclude that permeability, porosity, and especially temperature are the main controls of hydrothermal alteration. Anhydrite, deposited when sea water heated, has an irregular distribution that may be due to about 20 to 30 sea water invasions which occurred when the usually impermeable boundaries of the field were ruptured by tectonic events.

Alteration in low-temperature (below 150°C at 1000 m) fields expands the smectite-zeolite zone of the hotter areas and confirms the control of temperature on zeolite distribution. Kristmannsdóttir (1976) distinguishes four zones characterised by: (*a*) chabazite, opal, calcite ± levyne and stable to about 80°C; (*b*) mesolite-scolecite present from 80 to 90°C; (*c*) stilbite occurring between 100 and 120°C; and (*d*) laumontite above 120°C. Smectites occur at shallow depths typically coexisting with chlorite from about 180°C, although both "swelling" chlorite and random mixed-layered clays are also present. However, prehnite, epidote, quartz, and possibly chlorite in at least two low temperature fields are thought to be relicts from an earlier hotter regime.

THE FUTURE

No simple enumeration of factors affecting hydrothermal alteration can yet account for all the observed complications. With new or greatly expanded drilling programs in many parts of the world, however, much more will be learnt (and, hopefully published) so that it may soon be possible to isolate more confidently the effects of a single factor without distorting the general pattern.

Observations made so far confirm the important effect of temperature in the formation of hydrothermal mineral assemblages, but also demonstrate the critical role of permeability. Geochemical studies of thermal fluids have made a major contribution to knowledge of the intimate relationship between fluid composition and mineral deposition. However, few attempts have yet been made to interrelate the distribution of minor and trace elements in rocks, minerals, and fluids. Reasons why so many hydrothermal minerals occur in geothermal fields are still sought: possibly some phases are metastable, or stabilized by the substitution of minor or trace elements. Fluid inclusion measurements have great promise in helping unravel the evolution of geothermal systems, particularly when used in conjunction with a thermodynamic model for mineral deposition, such as that suggested by Helgeson

(1970). Experimental mineral syntheses and thermodynamic calculations of mineral equilibria should help clarify low-temperature phase relations, especially if the effects of solid solution are also considered.

Other rewarding approaches for some fields would be to evaluate quantitively mass transfer between fluid and solid phases; such studies, however, need careful, detailed petrologic and geochemical analysis of altered and unaltered rock samples.

Although an understanding of hydrothermal alteration in active geothermal systems will add greatly to our knowledge of low-grade metamorphism and hydrothermal ore deposition, much already known about these subjects could also be usefully applied to predict the evolution, and conditions, in geothermal reservoirs below drilling depth.

Acknowledgments

I am grateful for the helpful comments of W. A. Elders, A. J. Ellis, J. H. Lowery, W. A. Watters, B. G. Weissberg, D. E. White and C. P. Wood, and I also thank Mrs. M. Ruthven for typing and Mrs. P. Williams for drawing the two figures.

Literature Cited

Allen, E. T., Day, A. L. 1935. The hot springs of the Yellowstone National Park. *Carnegie Inst. Washington Publ. 466*, 525 pp.

Arnórsson, S. 1975. Application of the silica geothermometer in low temperature hydrothermal areas in Iceland. *Am. J. Sci.* 725:763–84

Bargar, K. E., Beeson, M. H., Fournier, R. O., Mufller, L. J. P. 1973. Present-day deposition of lepidolite from thermal waters in Yellowstone National Park. *Am. Mineral.* 58:901–04

Bichler, S., Kovach, R. L., Allen, C. R. 1964. Marine geology of the Gulf of California. *Am. Assoc. Petrol. Geol. Mem.* 3:126–43

Bird, D. K. 1975. Geology and geochemistry of the Dunes hydrothermal system, Imperial Valley of California. *Inst. Geophys. Planet. Phys.—Univ. Calif. Riverside Rep.* 75–2. 123 pp.

Bird, D. K., Elders, W. A. 1976. *Proc. 2nd U.N. Symp. Dev. Use Geotherm. Resour. 1975.* 1:285–95. San Francisco: United Nations 844 pp.

Blattner, P. 1975. Oxygen isotopic composition of fissure-grown quartz, adularia, and calcite from Broadlands geothermal field, New Zealand. *Am. J. Sci.* 275: 785–800

Browne, P. R. L. 1970. Hydrothermal alteration as an aid in investigating geothermal fields. *Geothermics.* Spec. Issue 2:564–70

Browne, P. R. L. 1971. Mineralization in the Broadlands geothermal field, Taupo volcanic zone. *Soc. Min. Geol. Jap.* Spec. Issue 2:64–75

Browne, P. R. L., Elders, W. A. 1976. *Geol. Soc. Am. Boulder 793* (Abstr.)

Browne, P. R. L., Ellis, A. J. 1970. The Ohaki-Broadlands hydrothermal area, New Zealand: Mineralogy and related geochemistry. *Am. J. Sci.* 269:97–131

Browne, P. R. L., Lovering, J. F. 1973. Composition of sphalerites from the Broadlands geothermal field and their significance to sphalerite geothermometry and geobarometry. *Econ. Geol.* 68:381–87

Browne, P. R. L., Rafter, T. A., Robinson, B. W. 1975. Sulphur isotope ratios of sulphides from the Broadlands Geothermal Field, New Zealand. *N.Z. J. Sci.* 18:35–40

Browne, P. R. L., Roedder, E., Wodzicki, A. 1976. In *Proc. Int. Symp. Water-Rock Interaction 1974*, ed. J. Čadek, T. Pačes, pp. 140–9. Prague: Geol. Surv. 463 pp.

Browne, P. R. L., Wodzicki, A. 1977. The aluminium-in-quartz geothermometer. *N.Z. Dep. Sci. Ind. Res. Bull.* 218:35–36

Carpenter, A. B., Trout, M. L., Pickett, E. L. 1974. Preliminary report on the origins and chemical evolution of lead- and zinc-rich oil field brines in Central Mississippi. *Econ. Geol.* 69:1191–1206

Chen, C. H. 1966. Preliminary exploration of geothermal steam in Tatun volcanic region, Taiwan, Republic of China. *Ministry Economic Affairs.* 6 pp.

Chen, C. H. 1967. Exploration of geothermal steam in Tahuangtsui thermal area, Tatun volcanic region, north Taiwan. *Ministry Economic Affairs.* 23 pp.

Clayton, R. N., Mufller, L. J. P., White, D. E. 1968. Oxygen isotope study of calcite and silicates of River Ranch No. 1 Well, Salton Sea geothermal field, California. *Am. J. Sci.* 266:968–79

Clayton, R. N., Steiner, A. 1975. Oxygen isotope studies of the geothermal system at Wairakei, New Zealand. *Geochim. Cosmochim. Acta* 39:1179–86

Coombs, D. S. 1955. X-ray observations on wairakite and non-cubic analcime. *Mineral. Mag.* 30:699–708

Coplen, T. B. 1976. Cooperative geochemical resource assessment of the Mesa geothermal system. *Inst. Geophys. Planet. Phys.—Univ. Calif. Riverside Rep. 76–1.* 97 pp.

Coplen, T. B., Kolesar, P., Taylor, R. E., Kendall, C., Mooser, C. 1975. Investigations of the Dunes geothermal anomaly, Imperial Valley, California, Part IV. *Inst. Geophys. Planet. Phys.—Univ. Calif. Riverside Rep. 75–20.* 42 pp.

Cusicanqui, H., Mahon, W. A. J., Ellis, A. J. 1976. See Bird & Elders 1976, pp. 703–11

Elders, W. A., Bird, D. K. 1976. See Browne, Roedder & Wodzicki 1976, pp. 150–57

Ellis, A. J. 1967. In *Geochemistry of Hydrothermal Ore Deposits*, ed. H. L. Barnes, pp. 465–514. New York: Holt, Rinehart & Winston. 670 pp.

Ellis, A. J., McFadden, I. M. 1972. Partial molal volumes of ions in hydrothermal solutions. *Geochim. Cosmochim. Acta* 36: 413–26

Ellis, A. J., Mahon, W. A. J. 1967. Natural hydrothermal systems and experimental hot water/rock interactions (Part II). *Geochim. Cosmochim. Acta* 31:519–38

Ellis, A. J., Mahon, W. A. J. 1977. *Chemistry and Geothermal Systems.* New York: Academic

Energy Research and Development Administration. 1976. *A Bibliography of Geothermal Resources—Exploration and Exploitation.* 617 pp.

Erd, R. C., White, D. E., Fahey, J. J., Lee, D. E. 1964. Buddingtonite, an ammonium feldspar with zeolitic water. *Am. Mineral.* 49:831–50

Eslinger, E. V., Savin, S. M. 1973. Mineralogy and oxygen isotope geochemistry of the hydrothermally altered rocks of the Ohaki-Broadlands, New Zealand geothermal area. *Am. J. Sci.* 273:240–67

Fenner, C. N. 1934. *Trans. Am. Geophys. Union, 15th Meet., Washington.* Pt. 1. pp. 240–43

Fenner, C. N. 1936. Bore-hole investigations in Yellowstone Park. *J. Geol.* 44:225–315

Fournier, R. O. 1973. *Proc. Symp. Hydrogeochem. Biogeochem.* 1:122–39

Fournier, R. O., Rowe, J. J. 1966. Estimation of underground temperatures from the silica content of water from hot springs and wet-steam wells. *Am. J. Sci.* 264: 685–97

Fournier, R. O., Truesdell, A. H. 1973. An empirical Na-K-Ca geothermometer for natural waters. *Geochim. Cosmochim. Acta* 37:1255–75

Grindley, G. W. 1965. The geology, structure, and exploitation of the Wairakei geothermal field, Taupo, New Zealand. *N.Z. Geol. Surv. Bull. 75.* 131 pp.

Hayashi, M. 1973. Hydrothermal alteration in the Otake geothermal area, Kyushu. *J. Japan Geotherm. Energy Assoc.* 10:9–46

Hayashi, M., Fujino, T. 1976. See Bird & Elders 1976, pp. 407–14

Hayashi, M., Yamasaki, T. 1976. See Browne, Roedder & Wodzicki 1976, pp. 158–69

Hayashi, M., Yamasaki, T., Matsumoto, Y. 1968. Secondary minerals of drilling cores from test borings T-1 and T-2 in the Otake geothermal area, Kujyu volcano group, Kyushu. *J. Japan Geotherm. Energy Assoc.* 17:93–8 (In Japanese with English abstr.)

Helgeson, H. C. 1967. In *Researches in Geochemistry*, ed. P. H. Abelson. 2:362–404 New York: Wiley. 663 pp.

Helgeson, H. C. 1968a. Geologic and thermodynamic characteristics of the Salton Sea geothermal system. *Am. J. Sci.* 266:129–66

Helgeson, H. C. 1968b. Evaluation of irreversible reactions in geochemical processes involving minerals and aqueous solutions—1. Thermodynamic relations. *Geochim. Cosmochim. Acta* 32:853–77

Helgeson, H. C. 1970. A chemical and thermodynamic model of ore deposition in hydrothermal systems. *Mineral. Soc. Am. Spec. Pub.* 3:155–86

Helgeson, H. C. 1971. Kinetics of mass transfer among silicates and aqueous solutions. *Geochim. Cosmochim. Acta* 35: 421–69

Helgeson, H. C., Garrels, R. M., Mackenzie, F. T. 1969a. Evaluation of irreversible reactions in geochemical processes involving minerals and aqueous solutions. Applications. *Geochim. Cosmochim. Acta* 33:455–81

Helgeson, H. C., Brown, J. H., Leeper, R. H. 1969b. *Handbook of Theoretical Activity Diagrams Depicting Chemical Equilibria in Geologic Systems Involving an Aqueous Phase at One Atm. and 0° to 300°C.* San Francisco: Freeman. 253 pp.
Hemley, J. J., Hostetler, P. B., Gude, A. J., Mountjoy, W. T. 1969. Some stability relations of alunite. *Econ. Geol.* 64: 599–612
Hemley, J. J., Jones, W. R. 1964. Chemical aspects of hydrothermal alteration with emphasis on hydrogen metasomatism. *Econ. Geol.* 59: 538–69
Hoagland, J. R. 1976a. *Geol. Soc. Am. Boulder 919* (Abstr.).
Hoagland, J. R. 1976b. *Petrology and geochemistry of hydrothermal alteration in borehole Mesa 6-2, East Mesa geothermal area, Imperial Valley, California.* M.S. thesis. Univ. Calif. Riverside. 90 pp.
Hoagland, J. R., Elders, W. A. 1978. The evolution of the East Mesa hydrothermal system, California, U.S.A. In *Proc. 2nd Int. Symp. Water-Rock Interaction, Strasbourg, 1977.* 10 pp. In press
Honda, S., Muffler, L. J. P. 1970. Hydrothermal alteration in core from research drill hole Y-1, Upper Geyser Basin, Yellowstone National Park, Wyoming. *Am. Mineral.* 55: 1714–37
Keith, T. E. C., Muffler, L. J. P., Cremer, M. 1968. Hydrothermal epidote formed in the Salton Sea geothermal system, California. *Am. Mineral.* 53: 1635–44
Keith, T. E. C., Muffler, L. J. P. 1978. Minerals produced during cooling and hydrothermal alteration of ash flow tuff from Yellowstone drillhole Y-5. Submitted to *J. Volcanol. Geotherm. Res.*
Keith, T. E. C., White, D. E., Beeson, M. H. 1978. Hydrothermal alteration and self-sealing in Y-7 and Y-8 drillholes in northern part of Upper Geyser Basin, Yellowstone National Park, Wyoming. *USGS Prof. Pap. 1054-A.* In press
Kendall, C. 1976a. *Geol. Soc. Am. Boulder 952* (Abstr.)
Kendall, C. 1976b. *Petrology and stable isotope geochemistry of three wells in the Buttes area of the Salton Sea geothermal field, Imperial Valley, California, U.S.A.* M.S. thesis. Univ. Calif. Riverside Rep. UCR/IGPP–76/17. 211 pp.
Kristmannsdóttir, H. 1975. Clay minerals formed by hydrothermal alteration of basaltic rocks in Icelandic geothermal fields. *Geol. Fören. Stockholm Förh.* 97: 289–92
Kristmannsdóttir, H. 1976. See Bird & Elders 1976, pp. 441–45
Kristmannsdóttir, H., Tómasson, J. 1976a. See Browne, Roedder & Wodzicki 1976, pp. 170–77
Kristmannsdóttir, H., Tómasson, J. 1976b. Hydrothermal alteration in Icelandic geothermal fields. *Soc. Sci. Islandica* 5: 167–75
Kristmannsdóttir, H., Tómasson, J. 1976c. *Zeolite Zones in Geothermal Areas in Iceland.* Presented at Zeolite Meet., 1976, Tucson.
Mahon, W. A. J. 1966. Silica in hot water discharged from drillholes at Wairakei, New Zealand. *N.Z. J. Sci.* 9: 135–44
Mahon, W. A. J. 1976. See Bird & Elders 1976, pp. 775–83
Mahon, W. A. J., Finlayson, J. B. 1972. The chemistry of the Broadlands geothermal area, New Zealand. *Am. J. Sci.* 272: 48–68
McNitt, J. R. 1964. Geology of the Geysers thermal area. *Proc. U.N. Conf. New Sources Energy 1961* 2: 292–301
Marinelli, G. 1969. Some geological data on the geothermal areas of Tuscany. *Bull. Volcanol.* 33: 319–34
Mercado, S. 1969. Chemical changes in geothermal well M-20, Cerro Prieto, Mexico. *Geol. Soc. Am. Bull.* 80: 2623–29
Mercado, S. 1976. See Bird & Elders 1976, pp. 487–95
Miller, D. G., Piwinskii, A. J., Yamauchi, R. 1977. The use of geochemical-equilibrium computer calculations to estimate precipitation from geothermal brines. *Univ. Calif. Livermore Rep. 52197.* 35 pp.
Muffler, L. J. P., Doe, B. R. 1968. Composition and mean age of detritus of the Colorado river delta in the Salton Trough, southeastern California. *J. Sediment. Petrol.* 38: 384–99
Muffler, L. J. P., White, D. E. 1968. Origin of CO_2 in the Salton Sea geothermal system, southeastern California, U.S.A. *23rd Int. Geol. Congr.* 17: 184–95
Muffler, L. J. P., White, D. E. 1969. Active metamorphism of Upper Cenozoic sediments in the Salton Sea geothermal field and the Salton Trough, southeastern California. *Geol. Soc. Am. Bull.* 80: 157–82
Muffler, L. J. P., White, D. E., Truesdell, A. H. 1971. Hydrothermal explosion craters in Yellowstone National Park. *Geol. Soc. Am. Bull.* 82: 723–40
Naboko, S. I. 1970. Facies of hydrothermally altered rocks of Kamchatka-Kurile volcanic arc. *Pac. Geol.* 2: 23–27
Naboko, S. I. 1976. See Browne, Roedder & Wodzicki 1976, pp. 184–95

Olson, E. R. 1976. *Geol. Soc. Am. Boulder 1036* (Abstr.)
Palmer, T. D. 1975. Characteristics of geothermal wells located in the Salton Sea geothermal field, Imperial County, California. *Univ. Calif. Livermore Rep. 51976.* 54 pp.
Randall, W. 1974. *An analysis of the subsurface structure and stratigraphy of the Salton Sea geothermal anomaly, Imperial Valley, California.* PhD thesis. Univ. Calif. Riverside. 92 pp.
Reed, M. J. 1976. See Bird & Elders 1976, pp. 539–47
Renner, J. L., White, D. E., Williams, D. L. 1975. *Assessment of geothermal resources of the United States—1975.* U.S. Geol. Surv. Circ. 726: 5–57
Ridge, J. D. 1973. Volcanic exhalations and ore deposition in the vicinity of the sea floor. *Miner. Deposita* 8: 332–48
Robinson, P. T., Elders, W. A., Muffler, L. J. P. 1976. Quaternary volcanism in the Salton Sea geothermal field, Imperial Valley, California. *Geol. Soc. Am. Bull.* 87: 347–60
Schoen, R., White, D. E. 1965. Hydrothermal alteration in GS-3 and GS-4 drillholes, Main Terrace, Steamboat Springs, Nevada. *Econ. Geol.* 60: 1411–21
Schoen, R., White, D. E. 1968. Hydrothermal alteration of basaltic andesite and other rocks in drillhole GS-6, Steamboat Springs, Nevada. *U.S. Geol. Surv. Prof. Pap.* 575–13: 110–19
Seki, Y. 1972. Lower grade stability limit of epidote in the light of natural occurrences. *J. Geol. Soc. Jpn.* 78: 405–13
Seki, Y., Okumuru, K. 1968. Yugawaralite from Onikobe active geothermal area, northeast Japan. *J. Jpn. Assoc. Miner. Petrol. Econ. Geol.* 60: 27–33
Seki, Y., Onuki, H., Okumura, K., Takashima, I. 1969. Zeolite distribution in the Katayama geothermal area, Onikobe, Japan. *Jpn. J. Geol. Geogr.* 40: 63–79
Sigvaldason, G. E. 1963. Epidote and related minerals in two geothermal drill holes, Reykjavik and Hveragerdi, Iceland. *U.S. Geol. Surv. Prof. Pap. 450-E*, pp. 77–9
Sigvaldason, G. E., White, D. E. 1961. Hydrothermal alteration of rocks in two drillholes at Steamboat Springs, Nevada. *U.S. Geol. Surv. Prof. Pap. 424-D*, pp. 116–22
Sigvaldason, G. E., White, D. E. 1962. Hydrothermal alteration in drillholes GS-5 and GS-7, Steamboat Springs, Nevada. *U.S. Geol. Surv. Prof. Pap. 450-D*, pp. 113–17
Skinner, B. J., White, D. E., Rose, H. J., Mays, R. E. 1967. Sulfides associated with the Salton Sea geothermal brine. *Econ. Geol.* 62: 316–30
Steiner, A. 1953. Hydrothermal rock alteration at Wairakei, New Zealand. *Econ. Geol.* 48: 1–13
Steiner, A. 1955. Wairakite, the calcium analogue of analcime, a new zeolite mineral. *Mineral. Mag.* 30: 691–98
Steiner, A. 1958. Occurrence of wairakite at the Geysers, California. *Am. Mineral.* 43: 781
Steiner, A. 1963. Waiotapu geothermal field. *N.Z. Dep. Sci. Ind. Res. Bull.* 155: 26–34
Steiner, A. 1968. Clay minerals in hydrothermally altered rocks at Wairakei, New Zealand. *Clays Clay Miner.* 16: 193–213
Steiner, A. 1970. Genesis of hydrothermal K-feldspar (adularia) in an active geothermal environment at Wairakei, New Zealand. *Mineral. Mag.* 37: 916–22
Sumi, K. 1968. Hydrothermal rock alteration of the Matsakawa geothermal area, northeast Japan. *Geol. Surv. Jpn. Rep.* 225: 42 pp.
Sumi, K. 1969. Zonal distribution of clay minerals in the Matsukawa geothermal area, Japan. *Int. Clay Conf. Tokyo.* pp. 501–12
Sumi, K., Takashima, I. 1976. See Bird & Elders 1976, pp. 625–34
Takashima, I. 1971. Hydrothermal rock alteration in Takenoyu geothermal area, Kumamoto Prefecture, Japan. *Jpn. Geol. Surv. Bull.* 23: 26–32 (In Japanese with English abstr.)
Tómasson, J., Kristmannsdóttir, H. 1972. High temperature alteration minerals and thermal brines, Reykjanes, Iceland. *Contrib. Mineral. Petrol.* 36: 123–34
Tómasson, J., Kristmannsdóttir, H. 1976. See Browne, Roedder & Wodzicki 1976, pp. 243–49
Truesdell, A. H. 1976. See Bird & Elders 1976, pp. liii–lxxix
United Nations 1976. *Proc. 2nd U.N. Symp. Dev. Use Geotherm. Res. 1975.* 3 vols. San Francisco: U.N. 2466 pp.
Weissberg, B. G., Browne, P. R. L., Seward, T. M. 1978. In *Geochemistry of Hydrothermal Ore Deposits*, ed. H. L. Barnes. New York: Wiley. 2nd ed.
White, D. E. 1967. See Ellis 1967, pp. 575–631
White, D. E. 1968. Hydrology, activity, and heat flow of the Steamboat Springs thermal system, Washoe County, Nevada. *U.S. Geol. Surv. Prof. Pap. 458-C.* 109 pp.
White, D. E. 1974. Diverse origins of hydro-

thermal ore fluids. *Econ. Geol.* 69: 954–73
White, D. E., Fournier, R. O., Muffler, L. J. P., Truesdell, A. H. 1975. Physical results of research drilling in thermal areas of Yellowstone National Park, Wyoming. *U.S. Geol. Surv. Prof. Pap.* 892. 70 pp.
White, D. E., Muffler, L. J. P., Truesdell, A. H. 1971. Vapor-dominated hydrothermal systems compared with hot-water systems. *Econ. Geol.* 66:75–97
Yamada, E. 1976. See Bird & Elders 1976, pp. 665–72
Yamasaki, T., Hayashi, M. 1976. See Bird & Elders 1976. pp. 673–84
Yoshida, T. 1974. Alteration zones in the Kirishima geothermal area. *J. Jpn. Geotherm. Energy Assoc.* 11:35–40 (In Japanese with English abstr.)
Yoshida, T., Higuchi, K., Yahara, K. 1976. Alteration of rocks by geothermal activities in Satsuma Iwao-jima island, Kayoshima Prefecture, Japan. *J. Jpn Geotherm. Energy Assoc.* 13:9–19 (In Japanese with English abstr.)

Economic Geology
Vol. 72, 1977, pp. 1471–1504

SUBJ
GTHM
Hydro
IMT

Irreversible Mass Transfer between Circulating Hydrothermal Fluids and the Mayflower Stock

R. N. Villas and D. Norton

Abstract

Heat and mass transport processes related to the Mayflower stock in the Park City district, Utah, have been simulated using calculations based on geological observations and numerical methods which approximate convective and conductive heat transfer in permeable media. Permeability and flow porosity values for the Mayflower stock were estimated on the basis of a planar fracture model and data on the abundances and apertures of continuous fractures. Estimated permeabilities ranged from 4×10^{-9} to 10^{-7} cm^2 and were hypothesized to represent initial permeabilities at the onset of the hydrothermal fluid circulation. An estimated fluid mass of 10^{13} kg/km strike length of the stock circulated through the upper 1.5 km of the Mayflower stock in 1.8×10^5 years of cooling, thereby reducing the thermal anomaly to 0.3 of its initial value. Temperatures decreased rapidly in the permeable portions of the stock, as a result of convective transfer of heat, but remained at 350° to 250°C in the upper 1.5 km for approximately 7×10^4 years subsequent to fracturing of the stock. Fluids in the host rocks flowed toward and often into the stock from distances about 5 km away from the stock side contact. Irreversible mass transfer between these circulating fluids and the Mayflower stock altered the stock to mineral assemblages which reflect the chemical composition of the rocks through which the fluids circulated, the pressure and temperature conditions along the flow paths, and initial composition of the fluids.

Simulation of the heat transport processes in the Mayflower system provides an initial approximation of the temperature, pressure, and fluid fluxes that may have been realized in the natural system. These data allow the mineral content of the altered Mayflower rocks to be predicted from mass transfer computations. Irreversible mass transfer reactions between the unaltered Mayflower rocks and solution compositions derived initially from fluid inclusion data were computed at discrete temperatures over the interval from 300° to 150°C. The alteration processes in the Mayflower stock were thus simulated by a sequence of isothermal reactions over the cooling history of the stock. The mineral content of the altered igneous rocks exposed in the Mayflower mine was determined by least-square treatment of bulk chemical compositions of rocks and mineral phases and was used to test the validity of coupling existing theoretical models of mass and heat transfer. The assumed solution compositions, prevalent temperature and pressure during the hydrothermal processes, and the estimated mass of fluids that circulated through the upper 1.5 km of the Mayflower stock as it cooled predicted masses of the mineral assemblages similar to those measured in the altered Mayflower igneous rocks.

The determined mineral modes disclose two broad zones over the north-south cross section of the mine: a lateral zone characterized by an increase of K-feldspar (3–15 wt %), kaolinite (0–10 wt %), and quartz (12–24 wt %), and a decrease of andesine (55–25 wt %) toward the main veins; and a vertical zone characterized by higher concentrations of K-feldspar, kaolinite, anhydrite, and pyrite below the 2,400-ft mine level, and calcite-quartz and biotite above. Gains and losses for elemental components indicate an overall loss (in grams of components per cm^2 of rock) of Si (0.009), Al (0.050), Na (0.032), and Ca (0.011) and an overall gain of Mg (0.026), K (0.020), S (0.038), SO_3 (0.037), and CO_2 (0.007). A relatively small gain of Fe (0.006) is the result of decrease in bulk density caused by the dissolution of igneous mafic minerals to produce pyrite, as evidenced by the shift from an annitic to a phlogopitic biotite during the hydrothermal event.

This analysis of the Mayflower hydrothermal system suggests that the original igneous minerals were altered by acid-sulfate, Na-K-rich solutions at moderate temperatures, < 400°C, and pressures, ≤ 1 kb. These solutions added large masses of Mg, K, S, and C to the stock and, concomitantly, altered the original igneous minerals. In order to account for the observed masses and compositions of alteration products, fluid fluxes on the order of 10^{-7} g/cm^{2}s are required for at least 2×10^5 years. This large mass ($\sim 10^{16}$ g/km^2 of area) of hydrothermal fluid was evidently derived from a variety of environments within and around the stock.

Introduction

TERTIARY plutons in the Cottonwood-Park City area, Utah, have intruded folded metamorphic and sedimentary units of Precambrian to Jurassic age. These intrusive rocks range in composition from quartz monzonite to quartz diorite and include the Little Cottonwood, Alta, and Clayton Peak stocks in the Cottonwood area and the Pine Creek, Mayflower, Ontario, Valeo, Flagstaff, and Glencoe stocks in the Park City district. This series of igneous events distributed over several millions of years were characterized by magma temperatures of approximately 850° ± 50°C. Each discrete intrusive body was apparently emplaced at approximately the same depth in the crust (<10 km below the surface), and its thermal energy was dispersed by conductive heat transfer and convective flow of aqueous solutions through the stock-host rock environment. The shallow depths of emplacement of these bodies into water-saturated permeable rocks suggest that convective fluid flow contributed significantly to the transport of heat and mass.

The emplacement of these relatively shallow-seated heat sources, and the subsequent fracturing that occurred in the Cottonwood-Park City area in Tertiary times, generated the physical conditions appropriate for fluid circulation that resulted in chemical reactions between original igneous materials and the circulating fluids, ultimately forming ore deposits and extensive hydrothermal alteration in the area.

Numerical simulation of heat transfer and chemical reaction between fluids and rocks at elevated temperature and pressure (Helgeson et al., 1970; Norton, 1972; Norton and Knight, 1977) suggests several parameters that must be documented in order to predict the nature of mineral deposition in pluton environments. The purpose of this communciation is to present the results of preliminary studies whose objectives were to develop and test methods useful in quantifying these parameters. The first section of this paper analyzes the thermal and hydrodynamic aspects of the problem; the second section analyzes the hydrothermal alteration and mineral deposit formation.

Geology of the Cottonwood-Park City Area

The Cottonwood-Park City area is located in the central northern part of the State of Utah, approximately 50 km southeast of Salt Lake City, at the intersection of the north-south-trending Wasatch Range and the east-west-trending Uinta Range. This region, in which rocks from Precambrian to

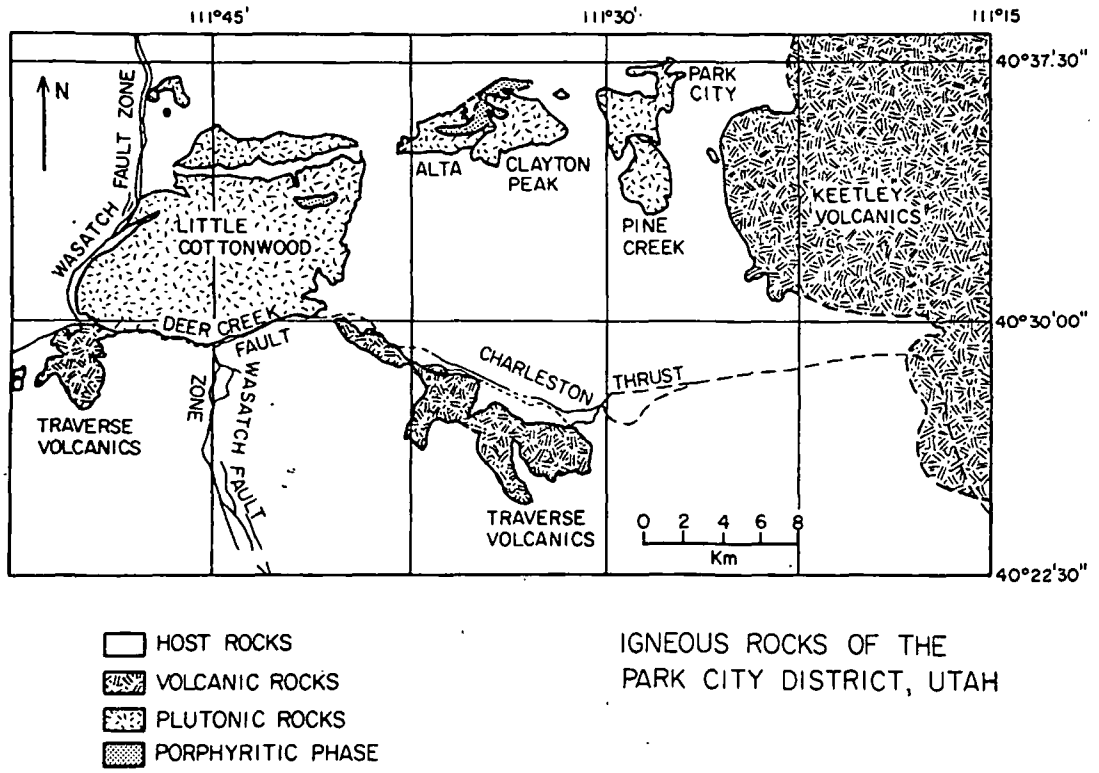

FIG. 1. Distribution of Tertiary igneous rocks in the Cottonwood-Park City area, Utah (modified after Crittenden et al., 1973).

aternary age crop out, has undergone two major lifts: the Uinta on the east and the Cottonwood the west. Gneiss, quartzite, and schist make up ost of the Precambrian terrains and occupy the ntral parts of the above-mentioned uplifts. Paleoic sedimentary rocks, which flank both uplifts, are rgely composed of limestone, dolomite, and sandone and their altered equivalents. Mesozoic rocks op out away from the uplifts and include conomerate, sandstone, shale, and limestone. Cenoic rocks are irregularly distributed and include oth intrusive and extrusive igneous rocks and sedientary units. Tertiary plutonic intrusions occur long a line coincident with the east-west trend of he Uinta axis. The Eocene-Oligocene equivalents f these plutonic rocks occur on the east (Keetley olcanics) and on the west and south of the area Traverse volcanics).

Intrusve rocks in the Cottonwood-Park City area ccur as dikes and stocks discordantly emplaced nto metamorphic and/or sedimentary host rocks (Fig. 1). They include, from west to east: the Little Cottonwood, Alta, Clayton Peak, and Pine Creek stocks and a composite intrusion comprising the Mayflower, Ontario, Valeo, Flagstaff, and Glencoe stocks (Bromfield et al., 1974), collectively called the Park City stock. These intrusions range in composition from quartz monzonite to quartz diorite, with these same variations frequently found within individual intrusions. Major mineral constituents are plagioclase (oligoclase-andesine), orthoclase, quartz, biotite, and hornblende, which vary in abundance from stock to stock. The Little Cottonwood, Clayton Peak, and Alta stocks are composed of coarse-grained rocks, in marked contrast with the Pine Creek and Park City stocks which are porphyritic and generally have an aphanitic or fine- to medium-grained groundmass. The Alta stock, however, displays a porphyritic phase which appears to intrude an enclosing nonporphyritic phase.

Chemical analyses of these intrusive rocks (Table 1) suggest a trend in silica content increasing to the west, although among the porphyritic intrusions the silica content is more or less constant. Radiometric dating of the igneous rocks indicates that magmatic activity in the area lasted a maximum of 17 m.y. in Oligocene-Miocene times and that the stocks become progressively younger to the west (Crittenden et al., 1973).

Several continuous fissures 4 km or more in length have been recognized in the Park City district (Fig. 2). They are normal faults that strike east-northeast–west-southwest and dip either northwest or southeast. The most prominent of these fissures is the Daly-Ontario-Hawkeye which extends

TABLE 1. Chemical Compositions of Igneous Rocks in the Cottonwood-Park City Area

	L. Cotton-wood (1)	Alta (1)	Alta (1)	Alta (5)	Alta* (1)	Alta* (5)	Clayton Peak (4)	Clayton Peak (3)	Pine Creek (3)	May-flower (2)	Ontario (3)	Flag-staff (3)
SiO_2	67.02	65.27	62.16	63.92	63.43	63.70	59.35	61.40	60.70	61.11	60.80	59.50
Al_2O_3	15.78	15.75	17.17	16.13	15.93	15.89	16.36	17.90	17.50	18.20	16.70	17.20
Fe_2O_3	1.56	2.31	2.26	2.03	2.61	2.09	2.90	2.90	3.05		3.96	2.66
FeO	2.80	1.85	2.78	2.43	2.31	1.97	3.36	2.06	1.89	3.93†	1.20	2.54
MgO	1.09	1.62	1.81	1.90	2.27	1.73	3.08	2.22	2.49	3.04	1.81	2.93
CaO	3.31	4.09	4.70	4.50	4.33	4.07	5.03	4.30	4.60	5.10	3.15	3.09
Na_2O	3.85	3.92	3.96	3.77	3.66	3.85	3.73	4.48	4.46	3.94	5.39	4.26
K_2O	3.67	3.25	3.58	3.24	3.49	3.19	3.85	2.40	2.54	2.95	3.60	2.37
H_2O^-	0.29	0.21	0.03	0.01	0.27	0.03	0.28	0.72	0.36		0.44	0.47
H_2O+	0.63	0.53	0.60	0.44	0.74	0.49	0.64	1.64	0.64		0.73	2.32
TiO_2	0.37	0.55	0.53	0.61	0.62	0.53	0.87			0.82		
ZrO_2	0.04	0.02	0.01		0.03		0.03					
P_2O_5	0.26	0.25	0.17	0.31	0.16	0.25	0.44					
S	0.03		0.04					0.02	n.d.	0.12	0.07	n.d.
MnO	0.02	0.10	0.06	0.08	0.09	0.07	0.07			0.10		
CO_2		Trace			Trace					0.48		
BaO	0.13	0.11	0.17		0.15		0.16					
Cl		0.01			0.05		0.05					
FeS_2		0.02					0.02					
SrO		0.05					0.05					
SO_3										0.58		
Total	100.85	99.91	100.03	99.37	100.17	99.86	100.29	100.00	98.20	100.37	97.80	97.30

* Porphyritic phase.
† Total Fe as FeO.
n.d. = none detected.
References: (1) Calkins and Butler, 1943; (2) Villas, 1975; (3) Norton, unpub. data; (4) Boutwell, 1912; and (5) Wilson, 1961.

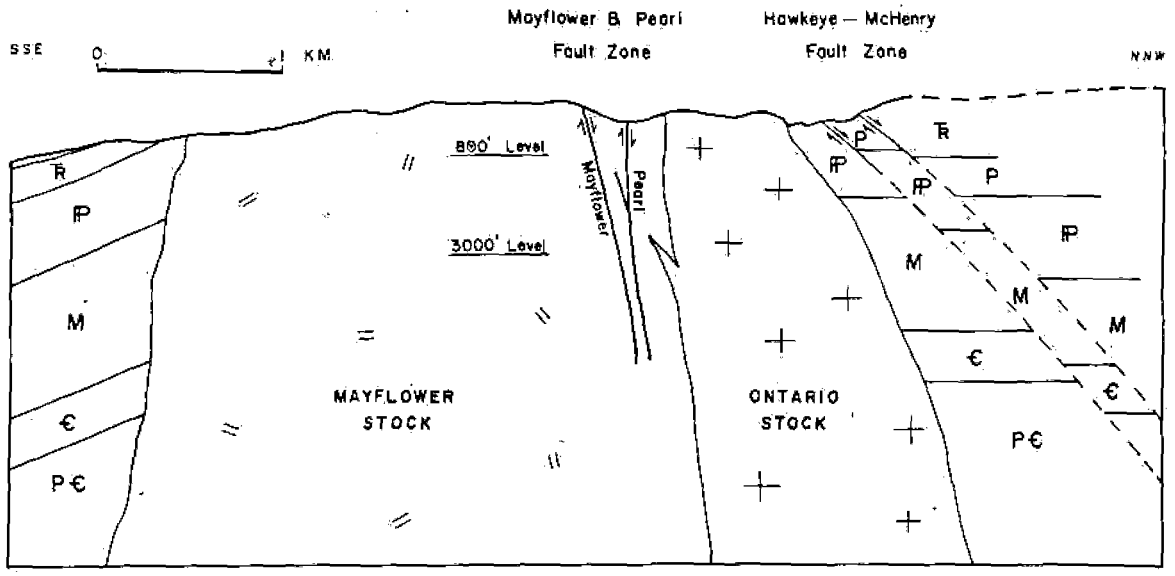

FIG. 2. Schematic north-northwest–south-southeast cross section of the Mayflower stock showing major geological features. Sedimentary units are represented with their maximum thickness. T = Triassic, P = Permian, P = Pennsylvanian, M = Mississippian, ∈ = Cambrian, and, P∈ = Precambrian.

for approximately 10 km from east of the Keetley volcanics to west of the Clayton Peak stock. Other regionally less continuous fissures, but locally important because of their associated ore deposits, are the Mayflower-Pearl, Naildriver, Back Vein, Crescent, and Massachusetts. Southeast-dipping faults, ranging from N 25° E to almost east-west, generally exhibit wider scatter in their strike directions than northwest-dipping faults; angles of dip vary from moderate (45°–55°) to steep (80°–90°) (Fig. 2).

An irregular pattern of fracturing in the host rocks between the Little Cottonwood stock and the Clayton Peak-Alta complex is indicated on the Dromedary Peak (Crittenden, 1965) and Brighton (Baker et al., 1966) geologic maps, but fractures apparently do not extend into the plutons. Their maps show that fractures, up to 1 km long and aligned parallel to the major fissures of the adjacent Park City district, transect the central portions of the Little Cottonwood stock. Likewise, most dikes cutting through the host rocks and plutons in the Cottonwood area follow the major fissure directions of that district. Similar structural relations, with fractures displaying two prominent sets, one along N 80° E directions and the other along N 25°–50° E directions, are present in the Alta stock. Fracture abundances in the Alta stock were estimated between one and three fractures per meter (Wilson, 1961). Similarly, reconnaissance observations of the fracture abundance in the Little Cottonwood and Clayton Peak stocks have revealed local zones where fracture abundances are approximately one fracture per meter.

The Mayflower Pluton

The hydrothermal systems in the Cottonwood-Park City area that developed as a consequence of emplacement of igneous intrusions can be simulated if hydrodynamic parameters are available. These properties were estimated for the Mayflower stock, which is well exposed in the extensive underground workings of the Mayflower mine, as described below.

The Mayflower pluton is the easternmost intrusion of the composite Park City stock, which has been emplaced into a sequence of intercalated clastic and carbonate units of Precambrian to Jurassic age. The post-Devonian formations include most of the carbonate beds and form a relatively thin cover overlying much thicker Precambrian and Cambrian strata. All of these sedimentary units have been broadly folded into the north-plunging Park City anticline, which has been truncated by intrusive rocks on its southern extension. Fissures developed in the area along east-northeast–west-southwest directions and localized the base metal ore deposits of the Park City mining camp.

The Mayflower pluton is exposed in the Mayflower mine between the 800-ft and 3,000-ft levels (Fig. 3). Underground workings show the Mayflower pluton in contact with sedimentary formations from the Mississipian Gardison limestone on the bottom of the Pennsylvanian Weber quartzite, on the surface (Quinlan and Simos, 1968), and with rocks

of two other stocks: the Ontario and the Valeo. Crosscutting relations between the Mayflower and the Ontario stocks show the former to be older, but age relationships to the Valeo stock are not evident.

Economic mineralization in the Mayflower stock occurs along the Mayflower-Pearl fault zone and consists of fissure-filling Pb-Zn sulfides with important amounts of gold, copper, and silver. Mine production has come primarily from veins in igneous host rocks; only about 20 percent of the production has been provided by veins and replacement deposits in sedimentary host rocks (Barnes and Simos, 1968).

Orientation, continuity, frequency, and aperture of fractures were determined for the Mayflower stock to serve a twofold objective: (1) analysis of the tectonic history of the stock with the hope of disclosing possible relationships with the major fissure zones of the Park City district; and (2) estimation of hydrodynamic properties on the basis of fracture continuity, frequency, and aperture.

Interpretation of the fracture pattern of the Mayflower stock with regard to the district structural framework was based on an analysis of 1,100 fracture planes, mostly shear, derived from Hecla Mining Company maps, together with fracture orientation data obtained during this study. The results of this analysis reveal that two prominent sets of fractures developed in the Mayflower stock (Figs. 4A and 4B). One set trends northeast-southwest, dipping either northwest or southeast; the other is northwest-southeast trending and dips dominantly southwest. The steep-dipping character of both fracture sets is evident from the stereogram plot of poles. For purposes of subsequent discussion, the representative structural attitudes of these two sets were considered to be N 50° E/80° NW and N 50° W/80° SW.

The northeast-trending fissure system in the Mayflower pluton is subparallel to the major fissure systems in the district (Figs. 2, 4A, and 4B). However, the northwest-trending fissures in the Mayflower pluton do not have recognized counterparts on a district scale. These fracture sets in the pluton are considered conjugate shear fractures developed during the pluton emplacement and cooling processes (Villas, 1975). The contemporaneity of the two sets is evidenced by the lack of significant offset of one fracture set by the other and the fact that both sets contain similar alteration mineralogy. The conjugate shear angle (2θ) of these two sets is approximately $80° \pm 5°$, measured from the stereograms (Figs. 4A and 4B). Failure under conditions of low coefficient of internal friction, $[\mu = \tan (90° - 2\theta)]$, as indicated by the Navier-Coulomb's or Mohr's criterion of failure, is consistent with failure at high temperature and high confining pressure (Heard, 1967).

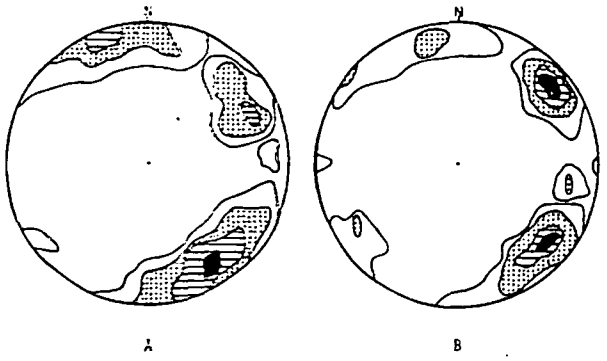

FIG. 4. Percent plot of the poles of fractures in the Mayflower and Ontario stocks. One percent counting areas. Lower hemisphere projection on equal area net. A. Approximately 1,100 sheer planes compiled from mine maps (all levels below the 700-ft level). Dark areas, 5.5 to 7.5 percent; hachured areas, 3.4 to 5.5 percent, dotted areas, 1.5 to 3.5 percent, and blank encircled areas, 0.5 to 1.5 percent. B. 21,061 poles of mineralized fractures (800-ft, 1,380-ft, 1,505-ft, 1,775-ft, 2,005-ft 2,200-ft, 2,600-ft, 2,800-ft, and 3,000-ft levels). Dark areas, 8.0 to 11.0 percent; hachured areas, 5.0 to 8.0 percent; dotted areas, 2.0 to 5.0 percent; and black encircled areas, 0.8 to 2.0 percent.

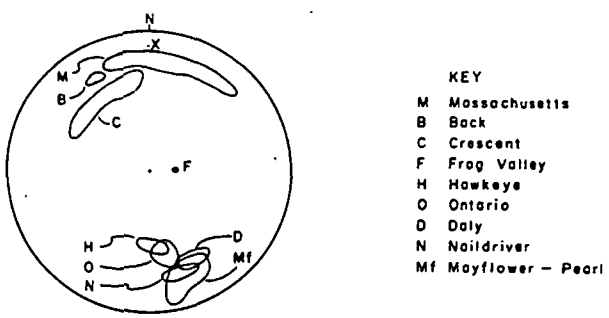

FIG. 3. Lower hemisphere stereographic plot of the poles of the major fissure zones present in the Park City district. Encricled areas delimit the variation of fissure attitude; X represents the axis of the Park City anticline.

Fluid flowpaths through fractured media are principally along continuous fractures which are usually present in the crystalline rocks, and an analysis of hydrothermal fluid flow through these rocks coupled with the reactions that occur between fluids and rocks requires consideration of those fracture properties which define rock permeability (Norton and Knapp, 1977). If the fractures are considered to consist of equidistant, planar, parallel plates of infinite extent, as proposed by Snow (1968, 1970), then the permeability (k, in cm^2, 10^{-8} cm^2 = 1 darcy) of a single set of fractures is given by:

$$k = \frac{n d_1^3}{12} \qquad (1)$$

where the abundance of continuous fractures (n, in cm^{-1}) and their apertures (d_1 in cm) need to be known. The flow porosity (ϕ) per unit length of

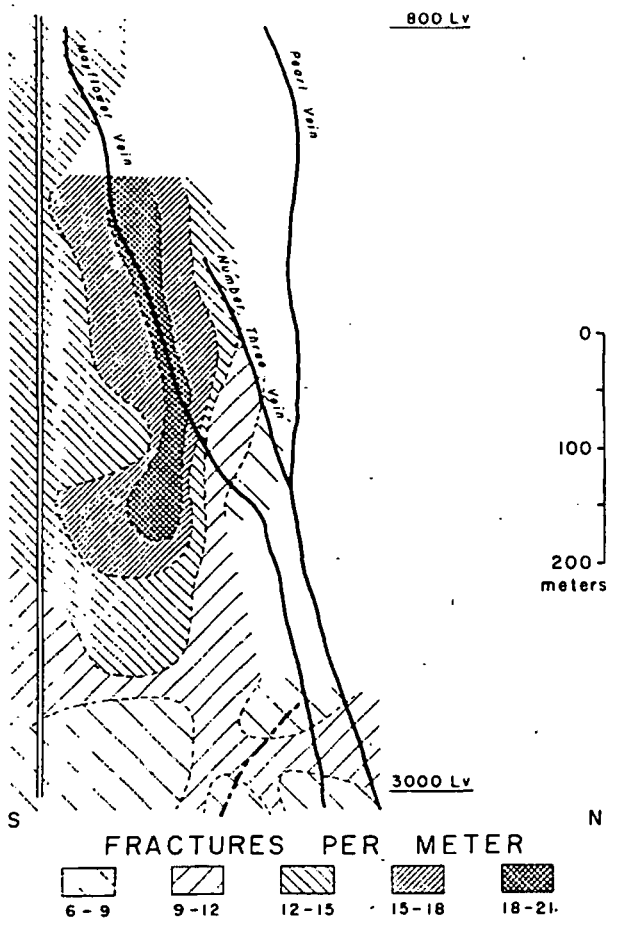

FIG. 5. Fracture abundance (n) distribution in a portion of the Mayflower stock showing the substantial decrease of n below the 2,600-ft level and zones of higher fracture density related to the Mayflower vein in the upper levels.

fracture for the corresponding case of equation (1) can be written as

$$\phi = nd_i. \qquad (2)$$

Fracture abundance and aperture were, therefore, measured and used with equation (1) to estimate the flow porosity and permeability of the Mayflower pluton. The abundance of continuous fractures (cf. Villas, 1975, for methods) over a north-south cross section of the Mayflower mine ranges from six fractures per meter to 21 fractures per meter (Fig. 5). These values are generally greater than those for all other stocks in the Cottonwood-Park City area, which are generally in the order of 0.6 to 3.0 fractures per meter. Larger fracture abundances in the Mayflower stock occur on the upper levels of the mine in the vicinity of the Mayflower vein, notably between the 1,380-ft and 2,005-ft levels where they occur symmetrically on either side of the vein. A substantial decrease in fracture abundance occurs below the 2,600-ft level.

The continuous fractures mapped in the Mayflower pluton were partially or totally filled with alteration minerals. Although present-day openings are most likely the net effect of mineral dissolution and precipitation, these openings are the only remaining indication of what the fracture apertures were during the alteration processes. Fracture aperture data for the Mayflower pluton refer to present-day openings and are assumed to represent the fracture aperture at the onset of the hydrothermal fluid circulation. In the absence of a more adequate way to quantify paleofracture apertures, this approach is considered to provide a reasonable initial estimate. Fracture aperture values measured in this manner range from 40 to 270 μm and average 145 μm (Villas, 1975). On some levels where the average aperture values are rather uniform, on the order of 150 μm $\pm$ 30 μm, no systematic variations in apertures with depth or lateral extent were found.

The geometry and distribution of pores define the contact area between fluids and reactant minerals—a critical parameter in understanding the mass transfer between reactant minerals and aqueous solutions. It is necessary, therefore, to discriminate the major

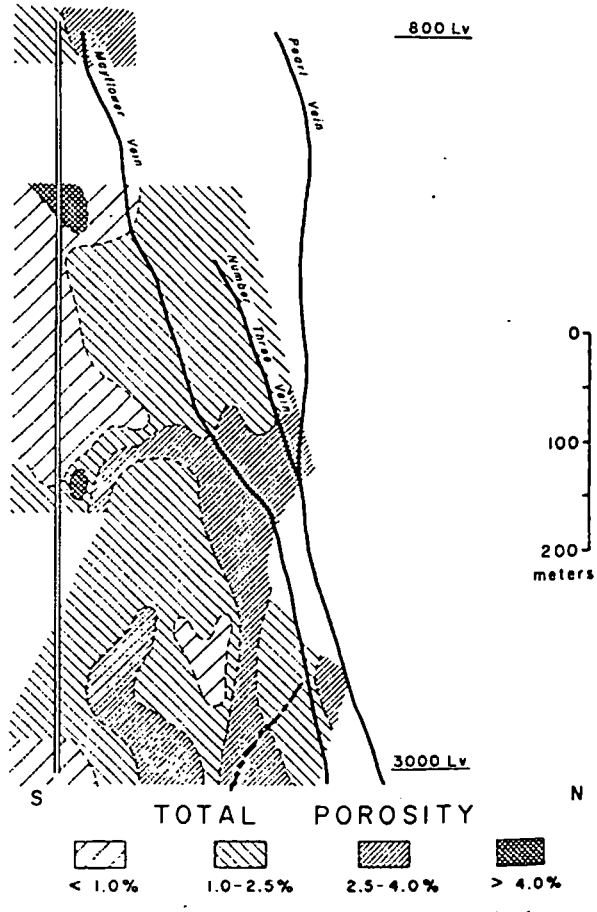

FIG. 6. Distribution of total porosity (ϕ_T) in the Mayflower stock.

contributing parts of the rock porosity. The nature of pores can be related to specific porosities,

$$\phi_T = \phi_F + \phi_D + \phi_R \quad (3)$$

where ϕ_T is the total porosity of the rock, and ϕ_F is the flow porosity which refers to open spaces along fractures where aqueous ions are transported primarily by fluid; ϕ_D is the diffusion porosity and includes those pores or dead-end fractures conected to flow chanels. This latter type of fluid-saturated void constitutes the channels through which ions are transported, primarily by diffusion. ϕ_R is the residual porosity which is associated with pores not connected to flow or diffusion channels, such as fluid inclusion voids, mineral grain boundaries, and submicroscopic cracks (Norton and Knapp, 1977).

Total porosity of a rock can be obtained from

$$\phi_T = 1 - \frac{\rho_\beta}{\rho_\gamma} \quad (4)$$

where ρ_β and ρ_γ are the bulk and grain densities of the rock, respectively. Values of total porosity for the Mayflower pluton fall in the range of 0.4 to 6.0 percent. Average total porosities for rocks along traverses oriented along east-northeast–west-southwest directions, at approximately 15 m south of the Mayflower vein, are the highest values (3.20%, 4.50%, and 2.70% for the 2,005-ft, 2,200-ft, and 2,600-ft levels, respectively), whereas those along north-south traverses on these same levels reveal average porosities of 2.20, 2.00, and 1.20 percent, respectively. The east-northeast–west-southwest traverses correspond to altered zones where clay minerals are most abundant. The distribution of total porosity values over a north-south cross section of the mine (Fig. 6) indicates that the higher values occur below the 2,005-ft level.

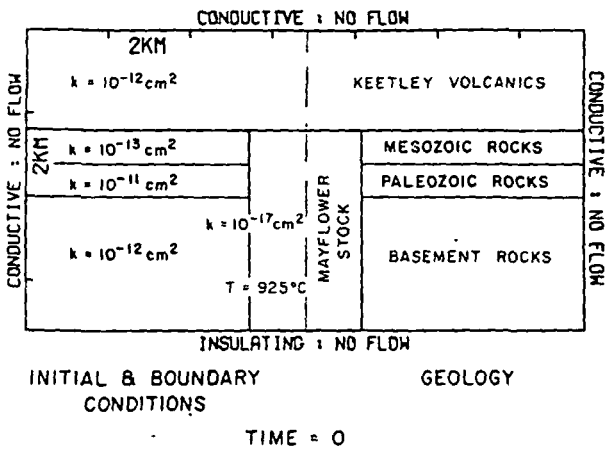

FIG. 7. Geology and initial boundary conditions used for the two-dimensional cooling model of the Mayflower stock.

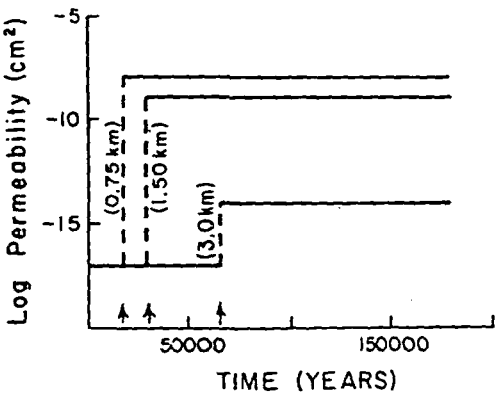

FIG. 8. Variation of permeability (k) with time throughout section down to 0.75, 1.50, and 3.0 km below the top of the Mayflower stock.

The directional permeabilities of the Mayflower pluton were computed with respect to the N 50°0 E/80° NW and the N 50° W/80 SW structural planes and were calculated from equation (1). Values range from $<10^{-14}$ to 7×10^{-8} cm² for fractures oriented along the N 50° E/80° NW direction and from $<10^{-14}$ to 5×10^{-5} cm² for the N 50° W/80 SW plane. These results are in reasonable agreement with reported values of permeabilities for fractured plutonic rocks. Permeabilities ranging from 10^{-10} to 1.7×10^{-7} cm² have been measured in quartz-porphyry stocks, although most reported values occur in the 10^{-10} to 10^{-9} cm² range (Cadek et al., 1968). This lower permeability range was attributed to the fact that those stocks are not as abundantly fractured and/or that the fractures observed are filled with alteration minerals.

Simulation of the Hydrothermal System Related to the Mayflower Stock

The hydrothermal system associated with the emplacement of the Mayflower and Little Cottonwood stocks has been simulated in order to predict the style of fluid circulation related to these intrusions. The large permeability of the Mayflower stock requires that convective fluid flow was the dominant mechanism of heat transport during its thermal history. By contrast, the Little Cottonwood stock is characterized by very large fracture spacings and, hence, low permeability, and appears to have cooled predominantly by conduction.

The system was simulated by methods which utilize numerical approximations of differential equations which describe the process of heat and mass transport around cooling plutons (Norton and Knight, 1977). The computational program affords for both conductive and convective heat transfer mechanisms in a two-dimensional framework, thermodynamic properties of the circulating fluid (H_2O system) in the

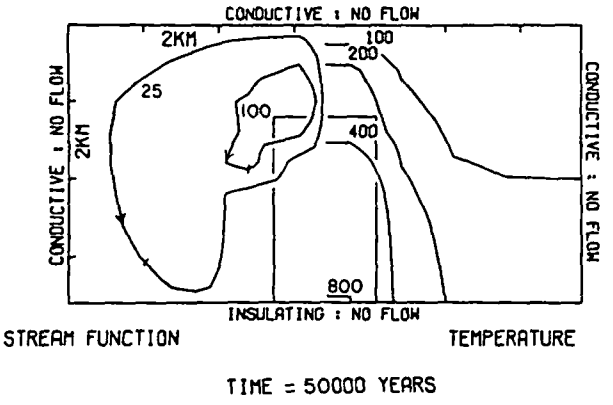

FIG. 9. Steady state (A) streamfunction and (B) isotherms in the Mayflower system at 5×10^4 years of cooling.

P-T region of interest, and variable permeabilities and thermal conductivities at each grid point of the domain.

Simplified geologic cross sections combined with estimates of permeabilities for the different rock units and temperature of the heat source define a possible set of initial conditions at the time of emplacement of the Mayflower stock (Fig. 7). Emplacement of the intrusion into water-saturated host rocks was assumed to be instantaneous. The initial temperature of the stock was set to 925°C, and the surrounding rocks were set to temperatures appropriate for a geothermal gradient of 20°C/km. Heat of crystallization, for water pressures compatible with the depths of emplacement, was included in the heat equations. The size and shape of the stocks were assigned on the basis of geologic cross sections and constraints imposed by the numerical approximations which utilize discrete points to approximate the differential equations. A thermal conductivity of 3.0×10^{-3} cal/cms °C was assumed for all rocks. The systems were analyzed for conductive boundary conditions, except for the lower boundary which was insulating, and impermeable flow boundary conditions were used.

Host rock permeabilities were assigned on the basis of notions of permeabilities of stratified sequences comparable to the varied lithologies in the Cottonwood-Park City area. Stock permeabilities, however, were estimated on the basis of observed fracture characteristics, as previously discussed. Initial permeabilities of the magma at the time of emplacement were assumed to be 10^{-17} cm^2. To account for variation of permeability with time, fracturing was simulated by instantaneously increasing the permeabilities as the stocks cooled below solidus temperatures, i.e., 750°C.

The style of fluid circulation caused by the emplacement of the Mayflower stock has been predicted on the basis of estimated permeabilities, as discussed earlier. Three episodes of fracturing were simulated as the stock cooled below 750°C, approximately the solidus temperature of this system. Each of these episodes was assumed to affect progressively lower zones of the stock (Fig. 8). Fractures developed during the first episode were considered to extend arbitrarily into the host rock for distances of 1.5 km away from the top and upper 0.75-km margins of the stock, and the host rock permeabilities were increased one order of magnitude relative to their initial values. Partial or total filling of fractures with alteration minerals is evident and indicates that rock permeabilities have actually decreased with time. Although this decrease may have had a substantial effect on the style of flow, it was not accounted for in this analysis.

Subsequent to fracturing, relatively large amounts of fluids circulated through the domain, with the exception of the impermeable lower half of the stock. As gradients in the streamfunction increased (Figs. 9 to 11), convection cells, initially centered

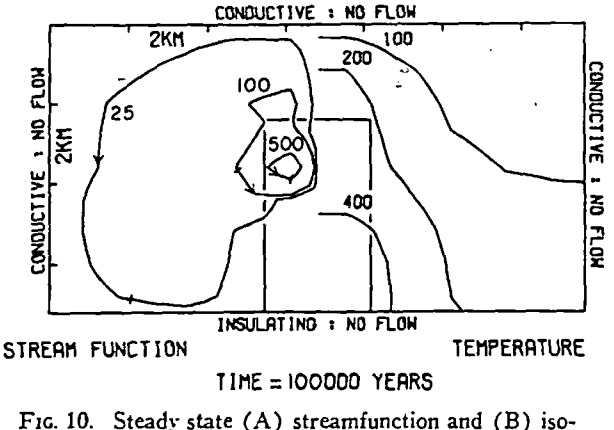

FIG. 10. Steady state (A) streamfunction and (B) isotherms in the Mayflower system at 10^5 years of cooling.

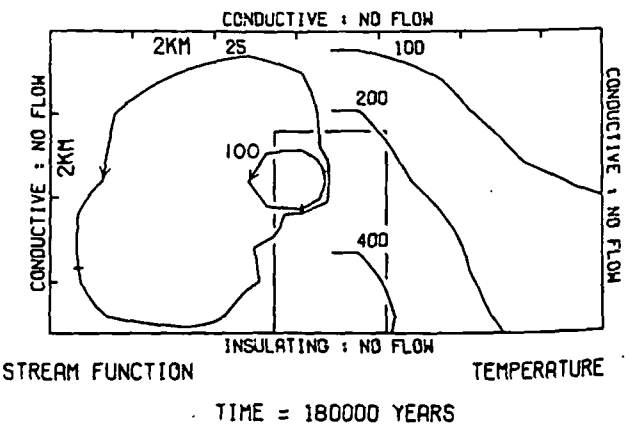

FIG. 11. Steady state (A) streamfunction and (B) isotherms in the Mayflower system at 1.8×10^5 years of cooling.

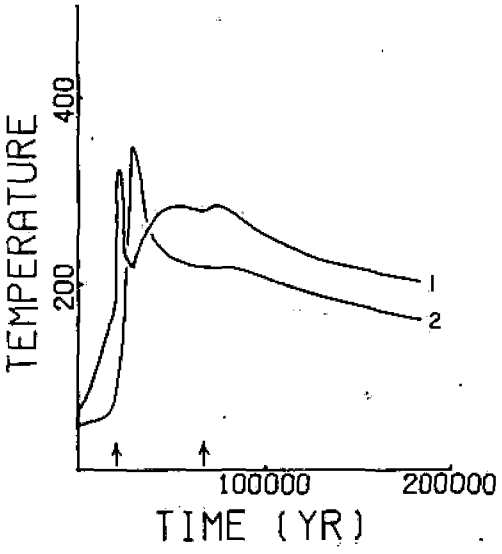

FIG. 12. Average temperature of a 2-km² region as a function of time in the Mayflower systems at fixed positions, 0.4 and 1.2 km, above top of the stock, 1 and 2, respectively. Arrows show times at which permeability was increased.

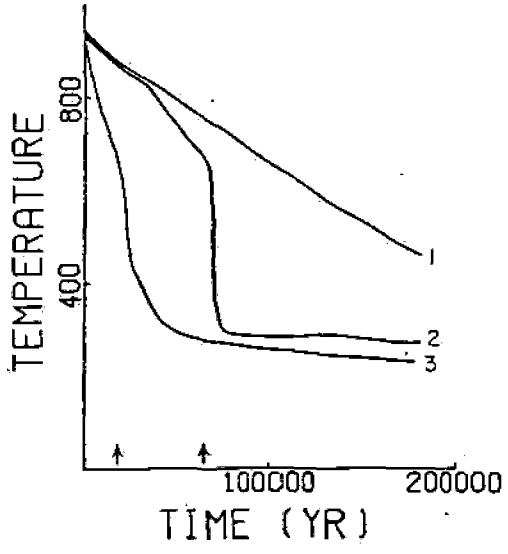

FIG. 13. Average temperature for 2 km² as a function of time in the Mayflower system at fixed positions, 3.6, 2.0, and 0.4 km, below top of the stock, 1, 2, and 3, respectively. Arrows show times at which permeability was increased.

in the host rocks, shifted to the more permeable zones of the stock where the largest flow velocities occurred at approximately $t = 7 \times 10^4$ years, decreasing gradually thereafter. Fluid fluxes in the carbonate layers ranged from 10^{-8} to 10^{-9} g/cm²s at $t = 1.5 \times 10^5$ years to 10^{-7} to 10^{-9} g/cm²s at $t = 1.8 \times 10^5$ years with values, at a given time, increasing toward the stock side contact. In the shaly formations immediately above, fluid fluxes increased from an average of 5×10^{-9} g/cm²s before the first fracture event to an average of 10^{-8} g/cm²s, which persisted for most of the cooling of the stock subsequent to that event. Magnitudes of fluid fluxes varied significantly with time inside the stock. The more permeable upper half witnessed fluxes four to five orders of magnitude greater than those in the lower half, which were in the order of 10^{-12} g/cm²s. However, after the third fracture event, at $t = 6.5 \times 10^4$ years, fluid fluxes ranged from 10^{-7} to 10^{-9} g/cm²s in the upper 4 km of the stock, with values increasing with time.

The high permeabilities in the domain caused a convection-dominated system in which large amounts of fluids flowed through the heat source, thereby reducing its thermal energy to about 40 percent of the initial value after only 10^5 years of cooling. Convective heat flux at 0.25 km above the stock top reached maximum values of 11, 7, and 5 HFU at approximately 2×10^4 years after each fracture episode and was at least four times higher than the conductive heat flux during at 1.2×10^5-year period of cooling.

The heat transferred across the stock margins increased the temperature of a 1.2-km-thick pile of host rocks above the stock at an average rate of 9×10^{-3} °C/year. At approximately $t = 3 \times 10^4$ years temperatures had risen to a maximum of 350°C in those rocks which subsequently cooled at an average rate of 6×10^{-4} °C/year (Fig. 12). By $t = 1.8 \times 10^5$ years only a 0.5 km of overlying rocks was still heated above 200°C. Abundant fluid circulation into the upper stock margin and along the stock-host rock contacts inhibited a significant outward displacement of the 200°C isotherm. Inside the stock temperatures dropped very rapidly in the fractured zones (Fig. 13). The 800°C isotherm was displaced at an average rate of 12 cm/year, which was 3.5 times as high as the average displacement of the 400°C isotherm in corresponding periods of time. The upper 2 km of the stock was thus maintained at average tempera-

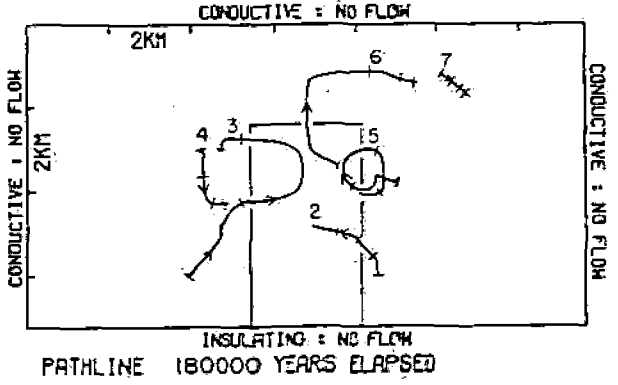

FIG. 14. Fluid pathlines in the Mayflower system representing redistribution of fluids during 1.8×10^5 years of cooling. Tick marks on path occur at $t = 0$ and every 6×10^4 years.

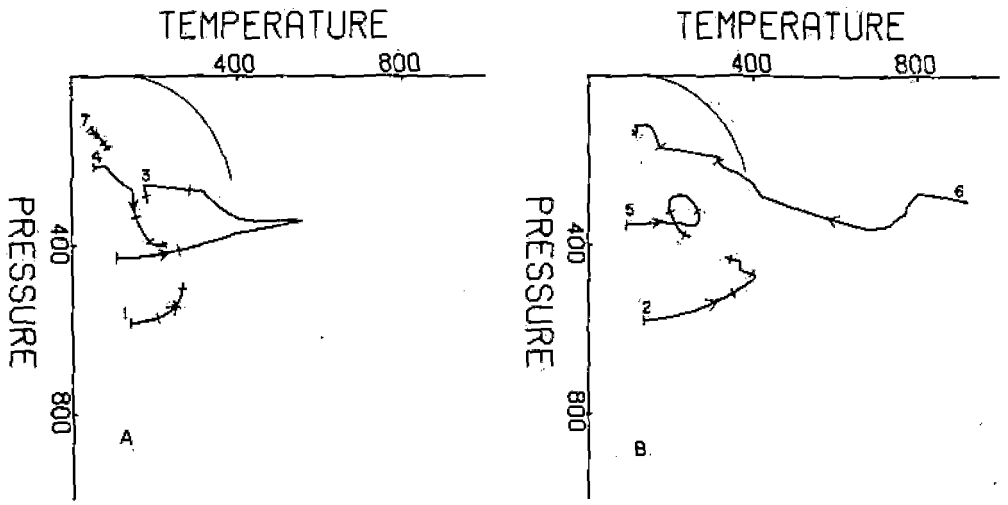

FIG. 15, A, B. Pressure-temperature conditions along pathlines in the Mayflower system, Figure 14, with respect to two-phase surface in H_2O-system. Tick marks on path occur at 6×10^4-year increments.

tures of 270°C, subsequent to the last fracture event at $t = 6.5 \times 10^4$ years, while the lower third of the stock continued to cool at a rate of 2.60×10^{-3} °C/year.

The analysis of fluid distribution in and around the Mayflower stock during its cooling provides important evidence to understanding the nature of the mineral assemblages observed in the altered rocks of have been chosen as representative of both the extent the Mayflower mine. Pathlines of seven fluid packets have been chosen as representative of both the extent to which fluids moved through contrasting chemical and mineralogical environments (Fig. 14) and the variation in pressure and temperature that those fluids experienced along their paths (Figs. 15a and 15b). Fluid packets that started in the basement rocks at different depths and distances from the stock-side contacts showed distinct pathlines during a cooling period of 1.8×10^5 years. Fluids associated with pathline 1 did not penetrate the stock, whereas those associated with pathline 2 crossed the stock margin at $t = 10^5$ years and moved 1.5 km into the stock interior. The paths of fluid packets 1 and 2 in P-T space are similar, but the fluid packets of pathline 2 were heated to higher temperatures (up to 400°C) and subjected to lower pressures (down to 425 bars). The fluid packet represented by pathline 3 crossed the stock margin at $t = 7.5 \times 10^4$ years and moved for 3 km through the stock at which point it moved to the Mesozoic shaly formation-stock contact. The fluids then circulated for over 6×10^4 years through those formations, heading toward the carbonate rocks immediately below. Along this path the temperature increased from 110° to 560°C then decreased to 180°C as fluids moved away from the stock interior. The corresponding pressure change reached a maximum of about 170 bars (Fig. 15a). The fluid packet of pathline 4, which originated in the shaly formations, moved downward through the more permeable carbonate rocks and then into the basement rocks. Both pressure and temperature increased along this path to a maximum of 400 bars and 230°C. Pathline 5 describes the path of a fluid packet residing initially in the carbonate rocks at approximately 1 km from the stock side contact. Fluids entered the stock at a depth of 4 km and moved upward inside the stock for about 1.6 km, crossing the stock-Mesozoic shale contact at approximately $t = 10^5$ years. Fluids continued to move through the shaly formations, then toward the underlying carbonate rocks to enter the stock again along the carbonate-basement rock contact at $t = 1.8 \times 10^5$ years. Fluid temperature increased isobarically to about 260°C at the stock margin, and for a period of approximately 1.4×10^5 years temperature and pressure first decreased and then increased as fluids moved out of and into the heat source. The fluid packet associated with pathline 6 crossed the upper stock contact at $t = 2 \times 10^4$ years, moving into the overlying volcanic rocks in the subsequent 1.6×10^5 years of cooling, first upward for about 1 km then laterally for about 2.5 km. The fluid packet underwent a 625°C decrease in temperature over an initial 6×10^4-year period of cooling, continuing to cool thereafter at a much slower rate. Fluid pressure increased for a short period of time, but the overall trend was a gradual decrease from 300 bars initially to 120 bars at $t = 1.8 \times 10^5$ years. Fluids represented by pathline 7, with origin in the volcanic rocks at a distance of 2.3 km from the stock upper corner, flowed only a relatively short distance and without changing pressure or temperature.

Irreversible Mass Transfer between Circulating Fluid and the Mayflower Stock

The composition and relative amounts of product minerals derived from solution-rock interactions depend upon time- and space-dependent parameters such as temperature, pressure, fluid flux, and fluid and rock compositions. The extent of alteration is measured by the distribution and abundance of alteration minerals and the gains or losses of components relative to the unaltered rock.

Mineral abundances were calculated from the chemical compositions of rocks and minerals. These data were obtained on samples collected in a region near the top of the Mayflower stock over a vertical depth of approximately 700 m and a lateral distance of about 300 m south of the Mayflower vein.

The Mayflower stock is the predominant rock unit exposed within the underground limits of the Mayflower mine. Its composition ranges from diorite to granodiorite, but it generally falls into the quartz diorite category. The Mayflower rocks are porphyritic with phenocrysts of andesine, biotite, quartz, hornblende, and K-feldspar. The groundmass is aphantic to fine grained and exhibits basically the same mineralogy. Subhedral to anhedral andesine phenocrysts show zoning, but enrichment in albite content is nonuniform toward the phenocryst edges. Andesine is the most abundant phenocryst and is the major component of the groundmass. The most common alteration products replacing andesine are kaolinite, sericite, epidote, calcite, anhydrite, and chlorite.

Biotite is present in varying amounts and constitutes the second most abundant phenocryst in the rocks. In the groundmass it occurs as scattered flakes less than 0.5 mm in length. In some instances biotite is found replacing hornblende. Most samples contain clusters of fine-grained biotite, about 0.1 mm long, apparently the result of alteration of earlier biotite phenocrysts. The most common alteration products of biotite are chlorite, epidote, fine-grained calcite, and sphene.

Hornblende has an occurrence similar to that of the biotite with which it is usually associated. Generally, it is present as an accessory mineral, although in a few cases it comprises up to 15 percent of the rock volume. It appears usually in subhedral crystals, commonly altered to chlorite.

Quartz exists both as phenocrysts and small grains in varying amounts and has been introduced along with the veinlets that transect the rock. In general, it forms small anhedral equant crystals, especially in the groundmass.

K-feldspar occurs rarely as phenocrysts. When present, it shows anhedral crystals of orthoclase or microcline slightly altered to kaolinite or sericite. In the groundmass it is more abundant, especially as a hydrothermal alteration product. Augite, apatite, sphene, and zircon occur as accessories.

The Ontario stock is exposed only on the 2,800-ft and 3,000-ft levels of the Mayflower mine. The Ontario rocks are porphyritic, although some facies are nearly equigranular, and their composition ranges from quartz monzonite to quartz diorite. Petrographically, the Mayflower and Ontario stocks look alike; their minerals display essentially the same textural characteristics, except that some plagioclase phenocrysts in the Ontario rocks have a myrmekitic intergrowth of quartz.

The Valeo porphyry rocks are exposed in the west side of the mine between the 800-ft and 1,270-ft levels, forming a thick sill-like body between sedimentary walls. It reappears on the 2,005-ft level as small dikes or tongue-shaped intrusions cutting through calcareous units. These rocks have a distinctive porphyritic texture with phenocrysts of oligoclase-andesine and quartz (some with rounded outlines) embedded in a fine-grained groundmass. Plagioclase phenocrysts are tabular, reaching up to 1 cm in length. Mafic minerals, particularly biotite, are present as scattered small crystals but are not abundant. K-feldspar occurs in larger amounts than in the other two stocks, and some grains are perthitic. Pyrite, kaolinite, sericite, calcite, and chlorite are the principal alteration minerals found in the Valeo stock.

The chemical and mineral compositions of the igneous rocks were quantitatively determined on samples representing a depth of about 670 m (between the 800-ft and the 3,000-ft levels), and a lateral distance of 2.0 km along drifts and crosscuts was examined, of which 1.4 km was sampled along north-south directions. The remaining 0.6 km was mapped in laterals parallel to the Mayflower-Pearl system along east-northeast–west-southwest directions. Observations were made and samples collected over 15-m intervals or less. Continuous rock chip samples covered the whole extension of each interval; a few were restricted to the immediate vicinity of veins. In addition, 305 m of core samples from a vertical diamond drill hole located near the shaft on the 3,000-ft level were studied.

One hundred and thirty samples were chemically analyzed for all major components except chemically bound water (Table 2). Si, Al, Fe (total iron as Fe^{2+}), Mg, Ca, Na, K, Mn, and Ti were determined by X-ray fluorescence spectroscopy, whereas sulfur (both sulfide and sulfate) was determined with a LECO automatic titrator. Carbon dioxide was determined with a selective collecting-gas system adapted to a LECO induction furnace (cf. Villas, 1975, for analytical procedures).

TABLE 2. Grain and Bulk Densities, Porosity, and Bulk Chemical Composition of the Igneous Rocks of the Mayflower Mine

	G/CM**3		PER CENT	WEIGHT PER CENT												
SAMPLE	GRDENS	BKDENS	PRSTY	SIO2	AL2O3	FEO	MGO	CAO	NA2O	K2O	S	CO2	MNO	SO3	TIO2	TOTAL
MF-0801	2.821	2.78	1.45	58.20	16.70	4.25	3.61	5.60	3.67	3.27	0.58	1.32	0.15	0.19	0.86	98.40
MF-0802	2.819	2.79	1.03	54.40	17.40	4.85	4.18	7.01	3.30	2.77	0.93	1.87	0.20	0.22	0.95	98.08
MF-0803	2.849	2.74	3.83	56.50	17.60	4.43	4.31	6.08	3.56	2.55	0.34	1.21	0.13	0.22	0.95	97.88
MF-0804	2.885	2.75	4.68	57.00	18.00	4.97	3.90	5.97	3.62	2.61	0.81	1.49	0.12	0.00	0.93	99.42
MF-1301	2.761	2.70	2.21	61.50	17.20	3.67	2.50	4.74	3.27	3.62	0.47	1.31	0.17	0.02	0.69	99.16
MF-1302	2.785	2.73	1.97	61.50	17.20	3.89	2.50	4.00	3.16	3.72	0.41	0.70	0.29	0.00	0.71	98.08
MF-1303	2.754	2.70	1.96	61.50	15.30	3.92	2.30	4.04	2.87	3.43	1.74	1.07	0.35	1.02	0.53	98.07
MF-1304	2.759	2.73	1.05	61.70	17.20	4.18	2.77	3.81	3.03	3.92	0.84	0.66	0.30	0.11	0.74	99.26
MF-1306	2.827	2.70	4.49	59.10	16.70	4.00	2.52	5.62	3.58	2.95	0.60	1.12	0.10	0.35	0.73	97.37
MF-1501	2.811	2.78	1.10	60.40	17.10	3.72	2.78	4.87	3.10	3.15	0.20	1.19	0.11	0.16	0.72	97.50
MF-1502	2.825	2.75	2.65	59.70	16.80	3.78	2.71	4.53	3.24	3.05	1.22	1.64	0.12	0.00	0.66	95.85
MF-1503	2.746	2.71	1.31	60.30	16.50	3.82	2.79	3.92	3.10	3.33	0.81	0.89	0.38	0.17	0.62	96.63
MF-1504	2.759	2.72	1.41	61.50	16.20	4.14	2.72	3.93	2.98	3.65	0.85	0.90	0.33	0.15	0.67	98.02
MF-1505	2.821	2.75	2.52	59.40	17.50	4.40	3.32	5.36	3.52	3.05	0.24	0.42	0.10	0.13	0.94	98.38
MF-1506	2.681	2.61	2.65	43.50	13.50	4.59	1.74	19.74	1.44	2.34	1.11	9.81	0.38	2.17	0.48	100.80
MF-1701V	2.765	2.72	1.63	56.90	13.30	7.53	1.74	4.42	1.90	2.55	6.18	2.52	0.39	1.49	0.49	99.41
MF-1702	2.795	2.76	1.25	58.20	16.80	5.16	3.39	3.68	2.41	4.30	1.40	0.97	0.51	0.33	0.80	97.95
MF-1703	2.755	2.72	1.27	57.40	17.80	4.36	3.37	4.76	3.24	3.44	0.27	1.03	0.23	0.67	0.83	97.40
MF-1704	2.780	2.74	1.44	58.80	17.90	4.27	3.60	4.74	3.36	3.37	0.40	0.72	0.19	0.20	0.83	98.38
MF-1705	2.777	2.74	1.33	58.30	17.30	4.44	3.52	4.52	2.96	3.69	0.49	0.67	0.35	0.33	0.77	97.34
MF-1706	2.750	2.71	1.45	54.70	16.50	4.10	2.89	7.80	2.53	3.49	1.74	4.77	0.26	0.00	0.57	99.35
MF-1707	2.798	2.75	1.72	56.70	17.50	4.29	3.39	6.20	3.04	3.09	0.43	1.66	0.24	0.30	0.82	97.66
MF-1708	2.794	2.74	1.93	55.00	15.90	4.22	3.23	7.79	2.79	2.84	0.82	2.67	0.21	0.75	0.78	97.00
MF-1709	2.784	2.73	1.94	57.50	17.20	4.39	3.45	6.06	3.27	2.96	0.22	0.96	0.13	0.24	0.85	97.23

TABLE 2—(*Continued*)

	G/CM**3		PER CENT	WEIGHT PER CENT

TABLE 2—(*Continued*)

	G/CM**3		PER CENT	WEIGHT PER CENT											
SAMPLE	GRDENS	BKDENS	PRSTY	SIO2	AL2O3	FEO	MGO	CAO	NA2O	K2O	S	CO2	MNO	SO3	TIO2	TOTAL
MF-1710	2.774	2.76	0.50	58.70	16.90	4.45	3.60	5.18	3.21	3.03	0.49	0.69	0.12	0.01	0.84	97.22
MF-1711	2.791	2.72	2.54	61.60	17.70	4.26	2.96	4.90	3.79	3.25	0.27	0.40	0.10	0.17	0.82	100.22
MF-1712	2.735	2.71	0.91	58.90	17.20	4.34	3.17	5.83	3.41	2.99	0.98	1.74	0.10	0.11	0.77	99.54
VL-2001	2.733	2.70	1.21	63.00	17.70	1.96	2.70	2.48	2.70	6.01	1.09	0.96	0.16	0.00	0.45	99.21
VL-2002	2.664	2.59	2.78	62.10	18.40	2.02	3.54	2.20	2.33	6.07	1.34	.84	.14	0.00	.46	99.44
MF-2001	2.793	2.67	4.40	59.10	18.10	3.47	2.71	4.10	3.04	3.57	0.96	1.25	0.15	0.84	0.64	97.93
MF-2002	2.834	2.77	2.26	60.20	18.00	3.53	2.36	3.58	3.07	3.82	1.43	1.09	0.16	0.13	0.59	97.96
MF-2003	2.788	2.74	1.72	53.60	16.80	5.03	4.36	6.50	2.16	3.61	1.38	2.76	0.65	0.48	0.64	97.97
MF-2004	2.687	2.59	3.61	58.10	17.30	4.97	3.86	3.16	2.16	3.86	1.47	1.15	0.52	0.42	0.74	97.71
MF-2005	2.774	2.74	1.23	61.30	17.50	3.89	3.42	3.68	3.70	3.25	0.90	0.60	0.12	0.46	0.72	99.54
MF-2006	2.868	2.76	3.77	55.70	17.20	4.91	4.88	5.22	3.24	2.74	0.66	0.40	0.10	1.14	1.00	97.19
MF-2007	2.836	2.76	2.68	53.58	17.40	4.87	4.53	6.36	3.04	2.88	1.00	0.75	0.08	2.58	0.92	97.99
MF-2008	2.798	2.78	0.64	53.66	16.80	4.75	4.32	6.31	3.01	2.61	1.08	0.68	0.06	2.51	0.87	96.66
MF-2009	2.797	2.74	2.04	51.43	16.00	3.91	4.17	8.26	2.76	2.18	2.28	1.11	0.09	3.86	0.60	96.65
MF-2010	2.744	2.73	0.51	52.36	16.20	4.89	4.67	6.96	2.84	2.42	2.82	1.45	0.06	3.18	0.64	98.49
MF-2011	2.824	2.74	2.97	59.20	16.70	4.96	3.15	3.69	2.41	3.70	1.37	1.30	0.72	0.00	0.72	97.92
MF-2012	2.791	2.73	0.76	60.17	15.50	4.98	2.90	3.92	1.93	3.70	2.27	1.70	0.63	0.89	0.60	99.19
MF-2013	2.798	2.74	2.87	56.40	17.50	4.34	3.29	5.36	3.65	3.19	0.24	0.64	0.15	0.40	0.76	97.92
MF-2014	2.764	2.72	1.59	57.90	16.90	4.07	3.43	5.17	3.06	3.66	0.73	1.12	0.25	0.35	0.76	97.40
MF-2015	2.854	2.76	3.29	58.10	17.60	4.34	4.11	5.73	3.21	2.94	0.28	0.87	0.15	0.00	0.90	98.23
MF-2016	2.782	2.73	1.87	59.50	17.50	4.28	4.04	5.79	3.21	2.98	0.16	0.97	0.12	0.67	0.89	100.11
MF-2017	2.777	2.71	2.41	59.50	18.00	4.27	3.43	6.14	3.35	3.08	0.22	1.32	0.12	0.00	0.88	100.31
MF-2018	2.822	2.75	2.55	61.10	18.20	3.93	3.04	5.10	3.94	2.95	0.12	0.48	0.10	0.58	0.82	100.36
MF-2001				59.90	16.80	3.10	2.08	4.65	2.19	3.80	1.49	2.10	0.34	.76	.49	97.70

TABLE 2—(*Continued*)

	G/CM**3		PER CENT	WEIGHT PER CENT											
SAMPLE	GRDENS	BKDENS	PRSTY	SIO2	AL2O3	FEO	MGO	CAO	NA2O	K2O	S	CO2	MNO	SO3	TIO2	TOTAL
MF-2202	2.761	2.65	4.02	62.48	18.27	3.00	3.00	3.38	3.79	3.11	0.80	0.53	0.08	0.65	0.60	99.69
MF-2203	2.784	2.64	5.17	59.93	17.30	5.19	4.07	4.06	4.16	3.31	1.48	0.50	0.12	1.24	0.79	99.16
MF-2004				59.10	18.40	4.52	4.64	4.37	4.08	2.51	0.53	0.70	0.18	0.42	0.76	100.31
MF-2205	2.781	2.71	2.55	55.70	17.60	5.16	4.85	4.91	2.77	3.25	1.25	0.83	0.31	0.87	0.74	98.24
MF-2206	2.800	2.74	2.14	57.10	18.00	4.51	3.79	5.72	4.16	2.40	0.57	0.57	0.07	2.02	0.75	99.66
MF-2207	2.753	2.72	1.20	57.40	17.80	4.30	3.49	5.78	3.76	2.69	0.64	0.54	0.07	2.04	0.81	99.32
MF-2208	2.793	2.76	1.18	56.60	16.30	4.26	3.54	6.56	3.06	2.36	1.00	0.77	0.10	3.10	0.67	98.32
MF-2209	2.894	2.85	1.52	53.54	15.30	3.97	4.61	9.44	2.92	1.71	1.09	1.95	0.07	4.59	0.56	99.75
MF-2210	2.772	2.70	2.60	54.90	17.20	4.96	4.32	6.94	3.57	2.47	0.59	1.00	0.10	0.79	0.96	97.80
MF-2211	2.766	2.64	4.56	54.40	17.30	4.81	4.46	7.97	3.43	1.91	0.60	0.53	0.12	0.71	1.04	97.28
MF-2212	2.760	2.75	0.36	57.10	18.00	4.64	4.14	6.11	4.45	2.70	0.27	0.45	0.12	0.32	0.98	99.28
MF-2213	2.801	2.77	1.11	55.80	17.40	4.99	4.43	6.70	3.36	2.75	0.23	0.76	0.12	0.38	1.00	97.92
MF-2214	2.778	2.72	2.09	56.60	17.30	5.23	4.36	6.12	3.36	2.95	0.44	0.84	0.14	0.06	1.08	98.48
MF-2601	2.727	2.63	3.56	60.70	17.46	4.95	3.11	3.18	3.43	2.90	2.48	0.45	0.05	0.51	0.66	99.88
MF-2602	2.709	2.61	3.65	60.90	17.95	4.36	3.15	3.19	3.94	2.61	2.03	0.49	0.35	0.34	0.67	99.98
MF-2603	2.824	2.74	2.97	60.10	17.57	5.38	3.15	3.17	3.57	2.62	2.70	0.36	0.05	0.79	0.68	100.14
MF-2604	2.834	2.72	4.02	60.03	16.99	5.37	3.40	3.85	3.58	2.62	2.67	0.37	0.05	1.20	0.65	100.78
MF-2605	2.785	2.72	2.33	57.60	17.00	5.32	3.23	4.34	3.79	2.70	2.67	0.53	0.07	1.20	0.62	99.07
MF-2606	2.755	2.69	2.36	59.23	17.09	4.63	3.11	4.13	3.79	2.91	2.24	0.47	0.05	1.52	0.63	99.80
MF-2607	2.775	2.72	1.98	59.10	17.18	5.08	3.47	3.56	3.14	2.49	2.47	0.69	0.05	2.07	0.69	99.99
MF-2608	2.776	2.72	2.02	60.10	16.51	4.60	4.11	3.91	3.21	2.88	2.05	0.28	0.05	1.14	0.75	99.59
MF-2609	2.813	2.71	3.66	60.06	16.69	5.46	3.96	2.94	3.14	3.04	2.62	0.36	0.06	0.39	0.73	99.45
MF-2610	2.801	2.63	6.10	58.10	17.20	6.61	3.38	3.20	3.00	3.45	3.43	0.35	0.05	0.89	0.82	100.48
MF-2611	2.782	2.66	4.39	59.17	17.41	5.93	4.39	2.65	3.21	2.88	2.48	0.49	0.06	0.70	0.74	100.11

TABLE 2—(*Continued*)

G/CM**3 PER CENT WEIGHT PER CENT

TABLE 2—(*Continued*)

	G/CM**3		PER CENT	WEIGHT PER CENT										
SAMPLE	GRDENS	BKDENS	PRSTY	SIO2	AL2O3	FEO	MGO	CAO	NA2O	K2O	S	CO2	MNO	SO3	TIO2	TOTAL
MF-2612	2.779	2.75	1.04	59.57	16.64	5.82	3.72	3.29	3.94	2.54	2.27	Ø.23	0.05	1.10	0.72	99.89
MF-2613	2.756	2.72	1.31	57.74	16.12	5.39	3.47	5.51	3.53	2.69	2.40	0.57	0.04	2.90	0.64	101.00
MF-2614	2.782	2.74	1.51	58.88	16.18	4.66	2.90	4.89	3.72	3.13	2.00	0.43	0.04	2.90	0.64	100.37
MF-2615	2.832	2.75	2.90	55.80	16.30	5.30	3.47	6.00	3.65	2.90	2.27	0.40	0.04	3.19	0.63	99.95
MF-2616	2.765	2.75	0.54	57.50	17.50	4.73	3.29	5.07	3.57	2.88	1.98	0.33	0.04	2.62	0.66	100.17
MF-2617	2.835	2.78	1.94	59.85	16.99	4.13	3.43	4.41	3.94	2.99	1.24	0.63	0.05	1.67	0.68	100.01
MF-2618	2.727	2.64	3.19	62.90	17.95	3.07	2.04	3.73	3.50	3.55	0.64	0.42	0.06	1.10	0.57	98.54
MF-2619	2.768	2.62	5.35	61.25	17.66	4.55	2.65	3.18	2.99	3.52	1.50	0.47	0.09	0.71	0.63	99.20
MF-2620	2.811	2.69	4.30	60.45	17.02	4.49	2.53	3.95	3.35	3.66	1.33	0.58	0.11	1.33	0.61	99.41
MF-2621	2.811	2.79	0.74	61.10	17.10	4.06	2.29	4.08	3.21	3.29	1.75	0.38	0.07	1.72	0.54	99.59
MF-2622	2.742	2.69	1.90	61.40	17.20	2.93	2.22	4.58	3.86	3.10	0.75	0.36	0.08	0.86	0.58	97.92
MF-2623	2.728	2.70	1.03	60.55	17.55	4.00	2.72	4.29	4.37	2.49	1.30	0.45	0.06	1.52	0.56	99.86
MF-2624	2.735	2.63	3.84	58.50	16.90	3.01	2.61	5.84	3.14	2.80	0.90	0.64	0.10	3.39	0.56	98.39
MF-2625	2.724	2.70	0.80	61.60	18.00	3.14	2.11	4.53	3.79	3.06	0.82	0.57	0.08	1.50	0.55	99.75
MF-2626	2.830	2.73	3.53	54.80	16.90	4.22	2.90	6.60	4.01	2.46	1.22	0.47	0.06	3.63	0.66	97.93
MF-2627	2.797	2.72	2.75	61.70	17.40	3.07	1.65	5.11	2.99	3.40	1.20	1.18	0.11	2.21	0.54	100.64
MF-2628	2.753	2.65	3.95	62.10	17.00	3.12	1.97	3.96	2.55	3.98	1.34	Ø.83	Ø.14	1.86	Ø.51	100.16
MF-2629	2.755	2.74	0.54	56.30	15.90	3.03	2.79	7.02	2.84	3.24	1.06	1.33	0.05	5.43	0.59	99.58
MF-2630	2.797	2.74	2.04	59.86	16.79	4.52	3.34	4.04	2.74	3.50	2.10	1.52	0.17	0.46	0.72	99.76
MF-2631	2.769	2.75	0.69	55.70	17.70	3.02	3.15	6.28	3.50	2.44	1.03	0.83	0.05	2.83	0.80	98.13
MF-2632	2.787	2.76	0.97	56.30	17.60	3.60	2.76	6.25	3.57	2.75	1.17	0.64	0.11	2.80	0.70	98.25
MF-2633	2.824	2.76	2.27	55.10	17.40	3.95	3.97	7.12	3.28	2.73	1.06	1.06	0.10	1.76	0.87	98.40
MF-2634	2.804	2.78	0.86	53.30	17.30	5.29	4.61	6.03	2.29	2.65	2.51	0.67	0.06	2.37	0.86	97.94
MF-2801	2.782	2.72	2.23	54.21	17.65	5.34	2.75	5.28	1.68	4.13	2.84	2.13	0.34	1.80	0.53	98.68

TABLE 2—(*Continued*)

	G/CM**3		PER CENT	WEIGHT PER CENT											
SAMPLE	GRDENS	BKDENS	PRSTY	SIO2	AL2O3	FEO	MGO	CAO	NA2O	K2O	S	CO2	MNO	SO3	TIO2	TOTAL
MF-2802	2.790	2.70	3.23	59.30	17.10	3.43	2.83	4.75	2.92	2.91	1.28	0.66	0.06	2.06	0.66	97.96
MF-2803	2.813	2.75	2.24	56.60	16.50	3.98	3.40	5.91	3.21	2.79	1.49	0.66	0.06	3.90	0.60	99.10
MF-2804	2.819	2.78	1.38	56.20	17.20	4.92	4.75	5.59	3.87	2.61	2.53	0.60	0.04	1.93	0.80	101.04
MF-2805	2.799	2.76	1.39	51.70	15.70	6.85	4.33	6.67	2.97	2.78	3.79	1.77	0.24	1.87	0.80	99.47
MF-2806	2.829	2.78	1.73	55.50	16.40	5.51	4.61	5.91	2.92	2.49	2.07	0.62	0.06	2.42	0.74	99.25
MF-2807	2.822	2.76	2.20	56.80	16.32	4.86	5.25	5.63	3.14	2.83	1.39	1.32	0.06	2.57	0.79	100.96
MF-2808	2.775	2.76	0.54	56.20	15.90	5.38	4.50	5.57	3.06	2.55	2.84	0.66	0.07	1.79	0.73	99.25
MF-2809	2.789	2.67	4.27	55.16	16.00	5.54	5.28	5.61	3.21	2.57	2.13	0.56	0.11	2.78	0.81	99.76
MF-2810	2.811	2.78	1.10	52.60	14.90	7.06	4.85	6.17	2.72	2.81	3.85	0.90	0.11	2.77	0.83	99.57
MF-2811	2.794	2.76	1.22	55.70	15.90	5.63	5.89	5.89	3.28	2.39	1.48	0.61	0.06	1.85	0.88	99.56
ON-2801	2.754	2.70	1.96	61.30	17.50	3.25	2.36	4.24	3.21	3.94	1.32	0.77	0.12	1.76	0.57	100.34
ON-2802	2.697	2.63	2.48	62.30	18.30	3.30	2.26	2.96	3.43	3.70	1.36	0.43	0.05	0.90	0.59	99.58
ON-2804	2.927	2.84	2.97	59.60	17.60	5.63	2.90	2.69	2.55	3.62	2.94	0.38	0.12	0.82	0.59	99.44
MF-3001	2.845	2.76	2.99	55.32	16.00	5.45	4.06	5.53	3.52	2.81	2.12	0.28	0.05	2.50	0.77	98.41
MF-3002	2.808	2.77	1.35	56.86	16.14	4.93	4.04	5.70	3.72	2.57	1.79	0.33	0.05	1.40	0.76	98.29
MF-3003	2.817	2.74	2.73	54.90	14.90	6.07	4.16	5.68	3.38	2.87	2.84	0.43	0.05	2.62	0.74	98.64
MF-3004	2.815	2.75	2.31	55.80	15.40	5.16	4.16	5.82	3.55	2.52	1.62	1.20	0.05	2.59	0.75	98.62
MF-3005	2.873	2.78	3.24	54.70	14.80	6.23	3.96	5.70	3.43	2.80	3.24	0.48	0.09	2.80	0.69	98.92
MF-3006	2.771	2.74	1.12	54.90	15.40	5.92	4.89	6.43	3.38	2.47	1.36	0.40	0.06	2.85	0.79	98.85
MF-3007	2.792	2.75	1.50	52.70	15.60	6.91	5.38	5.98	3.18	2.54	3.54	0.70	0.10	2.00	0.80	99.43
MF-3008	2.795	2.77	0.89	53.70	16.50	5.65	5.66	5.83	2.81	3.04	1.64	0.59	0.10	2.12	0.94	98.58
MF-3009	2.822	2.76	2.20	53.90	17.10	5.78	5.84	6.07	3.33	2.78	1.78	0.52	0.09	1.53	0.89	99.61
ON-3001	2.882	2.79	3.19	58.90	17.70	4.56	2.95	4.49	3.36	3.26	1.81	0.46	0.09	0.41	0.63	98.62
ON-3002	2.785	2.68	3.77	60.60	17.20	3.32	2.52	4.27	3.41	3.55	1.14	0.51	0.06	1.25	0.58	98.41

TABLE 2—(*Continued*)

	G/CM**3		PER CENT	WEIGHT PER CENT											
SAMPLE	GRDENS	BKDENS	PRSTY	SIO2	AL2O3	FEO	MGO	CAO	NA2O	K2O	S	CO2	MNO	SO3	TIO2	TOTAL
ON-3003	2.769	2.70	2.49	61.70	16.90	3.21	2.24	4.21	2.71	4.44	1.27	1.04	0.13	0.90	0.59	99.34
ON-3004	2.834	2.76	2.61	60.70	16.70	3.20	2.24	4.52	3.06	4.32	1.66	1.16	0.17	1.77	0.55	100.05
ON-3005	2.750	2.69	2.18	59.80	18.10	3.91	2.25	3.75	2.33	5.17	2.24	1.19	0.14	0.27	0.58	99.71
ON-3005V				58.10	17.60	4.59	2.31	3.08	2.02	5.04	3.27	1.29	0.18	1.22	0.58	99.28
ON-3006	2.776	2.72	2.02	59.50	16.80	3.45	2.71	4.55	3.47	4.07	1.15	0.56	0.10	1.88	0.53	98.77
ON-3007	2.753	2.72	1.20	57.90	17.30	5.28	3.32	4.25	2.13	3.74	2.00	1.06	0.35	1.36	0.59	99.28
DDH-216	2.794	2.78	0.50	55.80	16.10	4.09	5.35	6.35	4.23	2.45	0.50	0.38	0.06	2.95	0.80	99.06
DDH-350	2.803	2.78	0.82	56.20	16.60	4.23	5.03	6.06	3.72	2.75	0.77	0.36	0.08	1.14	0.83	97.77
DDH-639	2.753	2.70	1.93	62.00	17.30	2.86	2.26	4.38	4.37	2.54	0.28	0.33	0.05	1.36	0.60	98.33
DDH-770	2.747	2.70	1.71	62.10	17.20	3.34	1.33	3.33	3.59	3.34	1.26	0.35	0.04	1.39	0.49	97.76
DDH-992	2.856	2.77	3.01	55.10	16.40	5.31	5.10	6.05	3.21	2.64	1.16	0.30	0.05	3.53	0.70	99.03

TABLE 3. Estimated Composition of the Unaltered Mayflower and Ontario Stocks

	Mayflower[1]		Ontario
	Calculated	MF-2018†	
	Weight percent		
SiO_2	59.40	61.10	60.80
Al_2O_3	20.60	18.20	16.70
FeO	4.30*	3.93	1.20
Fe_2O_3	—	—	3.96
MgO	1.90	3.04	1.81
CaO	5.90	5.10	3.15
Na_2O	4.90	3.94	5.39
K_2O	2.10	2.95	3.60
S	—	0.12	3.60
H_2O†	0.45	—	0.73
H_2O	—	—	0.44
CO_2	—	0.48	—
SO_4	—	0.58	—
MnO	0.05	0.10	—
TiO_2	0.40	0.10	—
Total	100.00	100.36	97.80
Bulk density	2.69	2.75	

[1] Villas, 1975.
† Least altered Mayflower rock sampled.
* Total iron as FeO.

Unaltered specimens of igneous rocks were not found in the mine. Therefore, estimates of their original chemical compositions became necessary to determine the extent to which hydrothermal fluids reacted with the igneous rocks.

Chemical compositions of the unaltered Mayflower rocks were, on the other hand, approximated from modal analysis of the least altered samples and from the chemical compositions of primary minerals, with the exception of igneous biotite. Mineral modes for the unaltered rocks were estimated as follows: andesine, 69 ± 5 percent; orthoclase, 5 ± 2 percent; quartz, 10 ± 3 percent; biotite, 12 ± 3 percent; hornblende, 3 ± 1 percent; and magnetite, 1 ± 0.5 percent. The corresponding calculated chemical composition is given in Table 3. Iron was assumed to be conserved in the system, implying that iron-bearing alteration phases were primarily formed with iron derived from the dissolution of igneous mafic minerals and magnetite. Because the mole fraction, N, of annite and phlogopite in present-day biotite ($N_{ann} = 0.36$ and $N_{phl} = 0.64$) would fall short of accounting for the observed amounts of iron in the altered Mayflower rocks, the igneous biotite was assumed to correspond to 7 weight percent annite and 5 weight percent phlogopite. These values fix the igneous biotite composition, making it equivalent to the member of the biotite solid solution series characterized by 58 weight percent annite and 42 weight percent phlogopite (or $N_{ann} = 0.53$ and $N_{phl} = 0.47$). The more magnesian character found for hydrothermal biotites in other areas (Beane, 1974; Jacobs and Parry, 1976) adds qualitative evidence to support these assumptions.

Mineral Assemblages

Andesine, quartz, orthoclase, biotite, and hornblende are the major primary minerals of the unaltered counterparts of the stocks exposed in the Mayflower mine. The alteration assemblages of these stocks, on the other hand, are much more varied, but only a few minerals occur in significant quantities over the studied vertical section of the mine. The most abundant alteration products are kaolinite, K-feldspar, quartz, biotite, chlorite, anhydrite, calcite, and pyrite. Minor alteration components include actinolite, epidote, salite, zeolite, rhodochrosite, schorlite, and magnetite, which locally are abundant, especially as vein-filling minerals. Sericite, although ubiquitous, is not abundant except locally in the immediate vicinity of the main vein system. Albite, likewise, is not widespread but is a major hydrothermal mineral in the range of two to five meters from the Mayflower vein. Montmorillonite was not found in this study, but it has been reported to occur ubiquitously in small amounts above the 800-ft level (Williams, 1952).

Chemical Compositions of the Mineral Phases

Only silicate minerals that usually exhibit significant compositional variation, e.g., members of solid solution series, were analyzed. Grains of biotite, chlorite, hornblende, actinolite, epidote, salite, augite, plagioclase, and K-feldspar in carbon-coated polished thin sections were examined with an electron microprobe. Chemical determinations were made for nine major elements, Si, Al, Fe (total iron as Fe^{2+}), Mg, Ca, Na, K, Ti, and Mn (Table 4). Biotite analyses also include F, Cl, and Ba, while Ca, Na, and K were the only elements determined in feldspar grains. Eighteen microprobe sections were prepared from samples collected in all levels of the mine studied. As a rule, mineral compositions determined from a mount were taken as representative for the level from which the sample came. On levels where more than one sample was analyzed, determined mineral compositions were assigned to the intervals closest to the sampling site. The minerals analyzed show remarkably uniform compositions despite their spatial distribution in the cross section of the mine and their mode of occurrence.

Mineral Abundance Determinations

The relative amounts of reactant and product minerals composing the igneous rocks of the Mayflower mine were calculated using a least squares regression

TABLE 4. Structural Formulas of Minerals Used in Mass Abundance Calculations, Mayflower, Ontario, and Valeo Stocks

MINERAL	SI	AL	FE	MG	CA	NA	K	MN	TI	RA	O	H2O
						GRAM ATOM / MOLE						
ANALYSED WITH THE ELECTRON MICROPROBE												
BIOTITE												
MF-0801	2.84	1.13	0.96	1.56	0.01	0.04	0.84	0.02	0.29	0.05	11.0	1.0
MF-1306	2.89	1.10	0.97	1.73	0.01	0.03	0.85	0.02	0.20	0.01	11.0	1.0
MF-1504	2.81	1.21	0.92	1.75	0.01	0.03	0.86	0.02	0.20	0.02	11.0	1.0
MF-1708	2.90	1.09	0.95	1.71		0.02	0.90	0.01	0.21		11.0	1.0
MF-2011	2.84	1.18	0.93	1.77		0.04	0.80	0.01	0.21	0.01	11.0	1.0
MF-2201	2.85	1.23	0.90	1.60	0.01	0.04	0.85	0.01	0.23	0.02	11.0	1.0
MF-2204	2.88	1.09	0.96	1.78	0.01	0.04	0.87	0.01	0.19	0.01	11.0	1.0
MF-2206	2.90	1.10	0.97	1.71	0.01	0.03	0.87	0.02	0.19	0.01	11.0	1.0
MF-2211	2.83	1.18	1.01	1.54	0.02	0.04	0.89	0.02	0.23	0.04	11.0	1.0
MF-2603	2.77	1.30	1.20	1.53	0.01	0.05	0.87	0.02	0.21	0.03	11.0	1.0
MF-2634	2.79	1.18	0.87	1.85	0.02	0.04	0.86	0.01	0.21	0.01	11.0	1.0
MF-2802	2.84	1.21	0.86	1.58	0.04	0.04	0.86		0.29	0.01	11.0	1.0
MF-3005	2.83	1.18	1.02	1.59	0.01	0.04	0.92	0.01	0.22	0.02	11.0	1.0
DDH-177	2.80	1.20	0.79	2.00	0.02	0.03	0.84	0.01	0.17	0.01	11.0	1.0
DDH-812	2.79	1.26	0.99	1.64		0.05	0.87	0.01	0.20	0.02	11.0	1.0
ON-3005	2.74	1.28	0.97	1.66		0.04	0.88	0.01	0.24	0.02	11.0	1.0
VL-2002	2.73	1.29	0.36	2.51		0.02	0.84	0.01	0.14		11.0	1.0
CHLORITE												
MF-0801	5.87	4.20	3.29	6.51	0.05	0.04		0.07	0.01		28.0	8.0
MF-0801V	5.84	4.25	2.91	6.91	0.03	0.05		0.05			28.0	8.0
MF-0804	5.80	4.08	2.59	7.54	0.03	0.05		0.03	0.01		28.0	8.0
MF-1306	5.76	4.21	3.36	6.77	0.03	0.04		0.03	0.01		28.0	8.0
MF-1504	5.73	4.13	3.22	6.97	0.02	0.04	0.01	0.04	0.02		28.0	8.0
MF-1708	5.77	4.18	3.41	6.63	0.02	0.02	0.03	0.07	0.01		28.0	8.0
MF-2011	5.76	4.20	3.48	6.59	0.03	0.04	0.01	0.04	0.08		28.0	8.0
MF-2201	5.83	4.46	3.58	5.86	0.02	0.01	0.01	0.17	0.01		28.0	8.0
MF-2204	5.89	4.06	3.45	6.52	0.04	0.06	0.01	0.07	0.01		28.0	8.0
MF-2206	5.73	4.13	3.53	6.61	0.02	0.02	0.01	0.13	0.01		28.0	8.0
MF-2211	5.82	4.18	3.54	6.37	0.06	0.04	0.01	0.07	0.01		28.0	8.0
MF-2603	5.58	4.46	3.01	7.05	0.02	0.04	0.01	0.06			28.0	8.0
MF-2634	5.74	4.20	3.55	6.54	0.05	0.04		0.05	0.01		28.0	8.0
MF-2802	5.74	4.30	3.56	6.43	0.03	0.02		0.02	0.01		28.0	8.0
MF-3005	5.85	4.23	3.66	6.19	0.04	0.05	0.04	0.05	0.01		28.0	8.0
DDH-177	5.85	4.02	3.53	6.62	0.04	0.03	0.02	0.04	0.01		28.0	8.0
DDH-177V	5.86	4.04	4.01	6.10	0.07	0.01		0.05			28.0	8.0

TABLE 4—(*Continued*)

	SI	AL	FE	ME	CA	NA	K	MN	TI	RA	O	H2O
DDH-812	5.48	4.42	3.48	6.80	0.02	0.03	0.01	0.06	0.01		28.0	8.0
ON-3005	5.51	4.39	3.74	6.55	0.02	0.01	0.02	0.05	0.01		28.0	8.0
VL-2002	5.54	4.15	1.75	8.39	0.01	0.02	0.02	0.17	0.01		28.0	8.0
ACTINOLITE												
MF-0301	7.79	0.39	1.24	3.55	1.87	0.10	0.02	0.08	0.02		23.0	1.0
MF-1306	7.40	0.89	1.65	3.01	1.78	0.24	0.09	0.07	0.10		23.0	1.0
MF-2011	7.51	0.76	1.33	3.47	1.77	0.18	0.07	0.04	0.04		23.0	1.0
MF-2204	7.49	0.62	1.46	3.49	1.91	0.17	0.05	0.04	0.04		23.0	1.0
MF-2206	7.61	0.65	1.37	3.39	1.82	0.16	0.05	0.07	0.03		23.0	1.0
MF-2211	7.41	0.75	1.50	3.28	1.72	0.22	0.07	0.07	0.11		23.0	1.0
MF-2634	7.60	0.52	1.55	3.39	1.97	0.09	0.03	0.03	0.01		23.0	1.0
MF-3005	7.71	0.51	1.19	3.54	1.88	0.11	0.05	0.05	0.04		23.0	1.0
DDH-177	7.57	0.65	2.08	2.69	1.96	0.13	0.04	0.03	0.01		23.0	1.0
EPIDOTE												
MF-0801	3.22	2.06	0.90	0.01	2.03	0.01		0.02			12.5	0.5
MF-1306	3.10	2.16	0.99	0.01	1.98	0.01	0.01	0.02	0.01		12.5	0.5
MF-2011	3.60	2.20	0.96	0.01	2.05	0.01	0.01	0.01	0.02		12.5	0.5
MF-2204	3.12	2.22	0.76	0.01	2.13	0.01		0.02			12.5	0.5
MF-2603	3.10	2.21	0.90		2.06	0.01		0.01			12.5	0.5
MF-2634	3.22	2.02	0.99	0.01	2.01			0.01			12.5	0.5
MF-2802	3.01	2.24	0.98	0.01	2.01	2.10	0.01	0.01	0.01		12.5	0.5
DDH-177	3.16	2.05	1.03	0.03	2.02			0.01			12.5	0.5
SALITE												
MF-0801	1.96	0.05	0.27	0.80	0.88	0.03		0.02	0.06		6.0	
MF-2204	1.95	0.05	0.24	0.80	0.96	0.03		0.02	0.03		6.0	
AUGITE												
MF-1708	1.98	0.05	0.29	0.76	0.86	0.04		0.01	0.01		6.0	1.0
HORNBLENDE												
MF-1708	6.20	2.10	1.24	3.54	1.77	0.60	0.21	0.03	0.23		23.0	1.0
MF-3005	6.45	1.96	1.77	2.79	1.90	0.38	0.21	0.02	0.18		23.0	1.0
PLAGIOCLASE												
MF-0804	2.59	1.42			0.41	0.57	0.01				8.0	
MF-1306	2.58	1.42			0.42	0.56	0.02				8.0	
MF-1504	2.56	1.44			0.44	0.55	0.01				8.0	
MF-1708	2.60	1.40			0.40	0.59	0.01				8.0	
MF-2011	2.60	1.40			0.40	0.59	0.01				8.0	
MF-2206	2.64	1.36			0.36	0.63	0.02				8.0	
MF-2603	2.64	1.36			0.36	0.62	0.02				8.0	

TABLE 4—(*Continued*)

	SI	AL	FE	MG	CA	NA	K	MN	TI	RA	O	H2O
MF-2802	2.66	1.34			0.34	0.64	0.02				8.0	
MF-3005	2.59	1.41			0.41	0.58	0.01				8.0	
DDH-812	2.63	1.37			0.37	0.61	0.01				8.0	
ON-3005	2.64	1.36			0.37	0.61	0.02				8.0	
VL-2002	2.68	1.32			0.32	0.66	0.02				8.0	
K-FELDSPAR												
MF-0804	2.99	1.01			0.01	0.12	0.87				8.0	
MF-1306	2.99	1.01			0.01	0.12	0.88				8.0	
MF-1708	2.99	1.01			0.01	0.14	0.85				8.0	
MF-2011	2.99	1.01			0.01	0.12	0.87				8.0	
MF-2206	2.99	1.01			0.01	0.13	0.86				8.0	
MF-2802	3.00	1.00			0.01	0.17	0.83				8.0	
MF-3005	3.00	1.00				0.12	0.88				8.0	
DDH-812	3.00	1.00			0.01	0.12	0.88				8.0	
ON-3005	2.99	1.01			0.01	0.12	0.87				8.0	
VL-2002	3.00	1.00				0.10	0.90				8.0	

procedure. The mass concentration, X_i, of the i^{th} element in a rock is determined by the relationship between the mass abundances of the n mineral phases, m_j, and the concentrations of the i^{th} element in the j^{th} mineral, $C_{i,j}$.

$$X_i = \sum_{j=1}^{n} m_j C_{i,j}. \tag{5}$$

A set of such equations can be written to represent the k rock-forming elements where $n \leq k$ is a required condition. The set of equations has the form:

$$\begin{aligned} m_1C_{11} + m_2C_{12} \ldots + m_jC_{1j} &= X_1 \\ m_2C_{21} + m_2C_{22} \ldots + m_jC_{1j} &= X_2 \\ \vdots \qquad\qquad\qquad\qquad\quad &\vdots \\ m_1C_{k1} + m_2C_{k2} \ldots + m_jC_{kj} &= X_k. \end{aligned} \tag{6}$$

In matrix notation, equation (6) becomes

$$mC = X \tag{7}$$

where C contains the chemical composition of the mineral phases, X the chemical composition of the rocks, and m the mineralogical composition of the sample. If the number of minerals is equal to the number of elements analyzed, i.e., if $n = k$, there will usually be a unique solution to (7). Hydrothermally altered rocks are generally disequilibrium assemblages; thus, the number of phases is not constrained to be less than or equal to the number of components. However, the number of major phases is commonly observed to be less than the components, and equation (7) is overdetermined. The solution to (7) is obtained by a least squares approximation in which the sum of the square of the difference between actual whole-rock chemical data and the value of X_i computed from (7) are minimized. Additional constraints are imposed whereby $\Sigma m_i = 1.0$, negative values of m_i are not allowed, and the solution is allowed, and the solution is weighted according to the estimated absolute error in the analytical data. Practical use of this method requires the selection of a representative mineralogy in terms of major minerals in order to obtain the best mineral fit from the computations.

Distribution of Major Mineral Constituents in the Altered Rocks

The thermal anomaly accompanying the emplacement of the Mayflower and Ontario stocks was largely dissipated by movements of fluids along open continuous fractures present in both igneous and adjacent rocks, as discussed previously. Observations in the fractured igneous rocks of the Mayflower mine reveal that permeable fractures are commonly filled with product minerals and enveloped by discrete halos of alteration phases (1–2 cm wide). As a result, large volumes of the stocks appear to have survived as relatively unaltered blocks of rock bounded by flow fractures. Diffusion channels cut

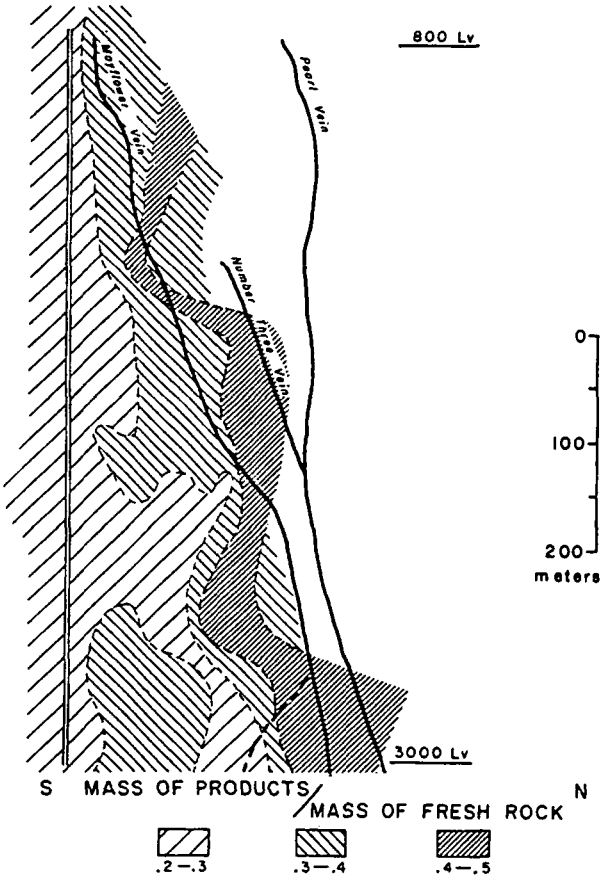

FIG. 16. Distribution of mass of alteration products in relation to mass of unaltered rocks in a portion of the Mayflower stock.

across these blocks as evidenced by tortuous alteration paths on the order of millimeters in width.

From this general picture, one is led to expect a major control of the flow fractures on the distribution of reactant and product minerals composing the altered Mayflower and Ontario stocks. The best evidence of this control comes from the overall mass distribution, as determined by regression, of the major minerals of the stock over a north-south cross section of the mine (Fig. 16), showing that the ratio of altered to unaltered assemblages increases toward the main vein system. Control on the distribution of individual minerals is evident for andesine, K-feldspar, kaolinite, and quartz (Figs. 17 to 20), the last three increasing in abundance toward the major veins. Andesine, the quantitatively most important reactant mineral, was more thoroughly destroyed in the vicinity of the major veins than in any other zone sampled. Biotite, chlorite, pyrite, anhydrite, and calcite distributions (Figs. 21 to 25), on the other hand, do not seem to depend on the main veins, although below the 2,600-ft level a lateral zoning is apparent, with biotite and chlorite increasing in abundance away from the Mayflower vein.

The distribution of the major minerals also disclosed a vertical zoning with calcite and quartz being more abundant above the 2,400-ft level of the mine and pyrite, anhydrite, K-feldspar, kaolinite, biotite, and chlorite more abundant below. The change in the relative abundance of anhydrite and calcite with depth may reflect an increase in the $a_{CO_3^{2-}}/a_{SO_4^{2-}}$ ratio in the solutions which favored the precipitation of calcite as the CO_2 pressure increased. This chemical change may have been a consequence of solutions flowing from quite distinct sedimentary sequences, below and above the horizons that mark the upward transition from more clastic to more calcareous formations. This transition occurs at a depth corresponding approximately to the 2,400-ft level (Fig. 26). As a result, the inflow of solutions that might have been in equilibrium with carbonate rocks was largely favored at depths above that level, and precipitation of calcite occurred as the relatively high CO_3 solutions moved into the pluton. Likewise, SO_4^{2-}-rich solutions, possibly in equilibrium with the basement rocks, might have entered the system from below to cause the observed vertical zoning, with

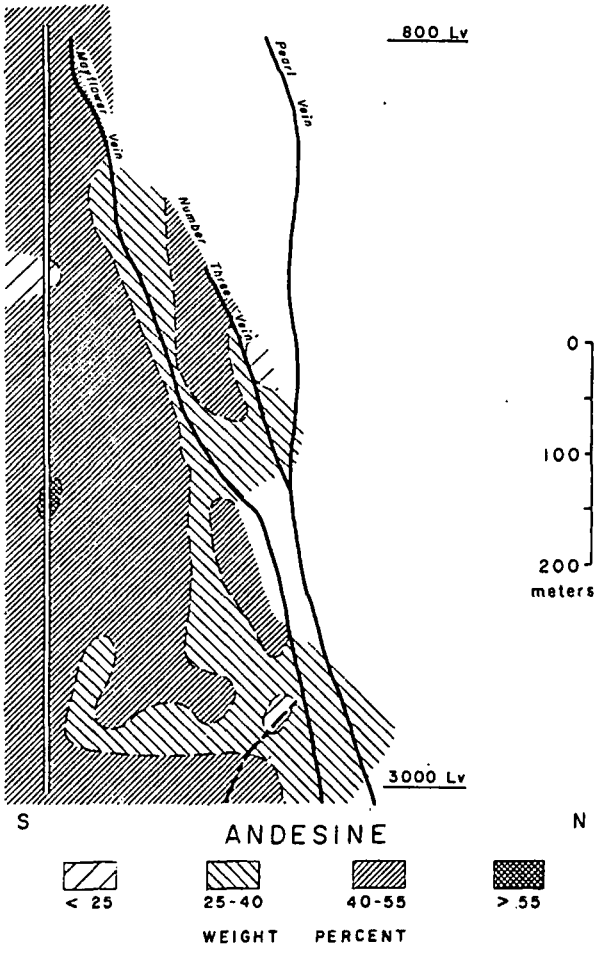

FIG. 17. Distribution of andesine in the Mayflower stock.

sulfate largely consumed at greater depths as anhydrite precipitated. Equilibrium relations show that at lower reaction temperatures, for a given CO_2 pressure and SO_4^{2-} constant, calcite has its stability field expanded over that of anhydrite, suggesting that temperature may have also contributed to larger ratios of calcite to anhydrite at shallower depths. Pyrite was found to be more abundant below the 2,600-ft level at some distances south of the Mayflower vein.

A collective picture of the variational trends of the major minerals is shown along north-south traverses on the 2,800-ft level across the Mayflower-Ontario contact (Fig. 27); it relates the abundances of reactant and product phases with distance from the main vein structure.

Gains and Losses of Components

The comparison between altered and unaltered compositions of rock samples affords a quantitative estimate of the irreversible reactions that took place between hydrothermal solutions and rocks. The extent of these reactions in the Mayflower mine is indicated by the variation of ratios between the masses of product and reactant minerals, which shows that the greatest change in mineralogy occurred in the regions closer to the Mayflower vein (Fig. 16). From data on chemical and mineralogical compositions of altered and unaltered rocks, the overall mass transfer in the stocks could be appraised in terms of gains and losses of both minerals and components. Bulk densities were determined on all samples in order to compute gains and losses. Lack of visible microscopic or megascopic deformational features in the altered zones of the Mayflower and Ontario stocks is supporting evidence that no significant volume change took place during alteration so that densimetric percentages could be used to represent rock compositions without introducing errors. Bulk density variations resulting from the hydrothermal processes were thus caused by the addition or removal of mass from the rocks.

Mineral abundances and gains and losses of minerals and major elemental components in the Mayflower stock, determined by regression, are sum-

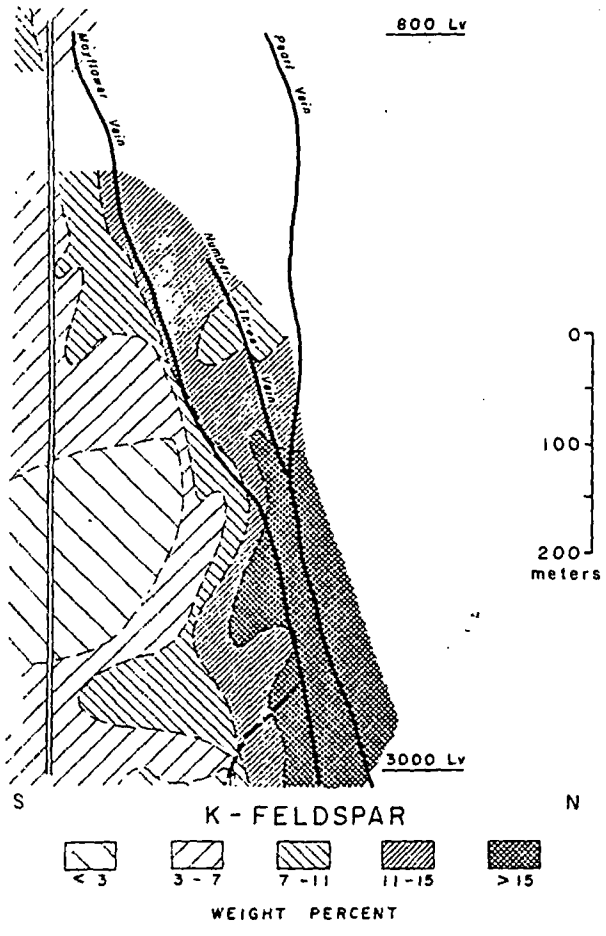

FIG. 18. Distribution of K-feldspar in the Mayflower stock.

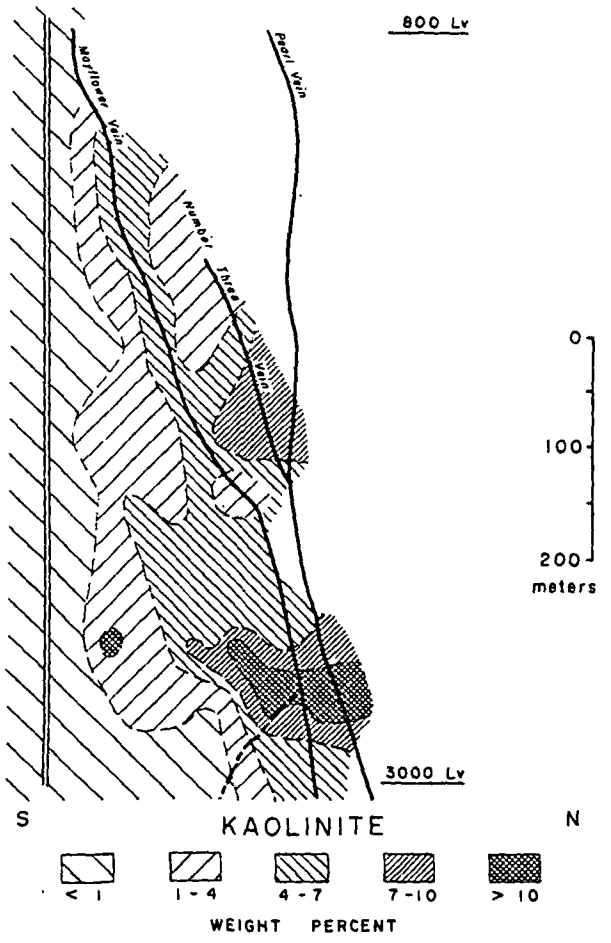

FIG. 19. Distribution of kaolinite in the Mayflower stock.

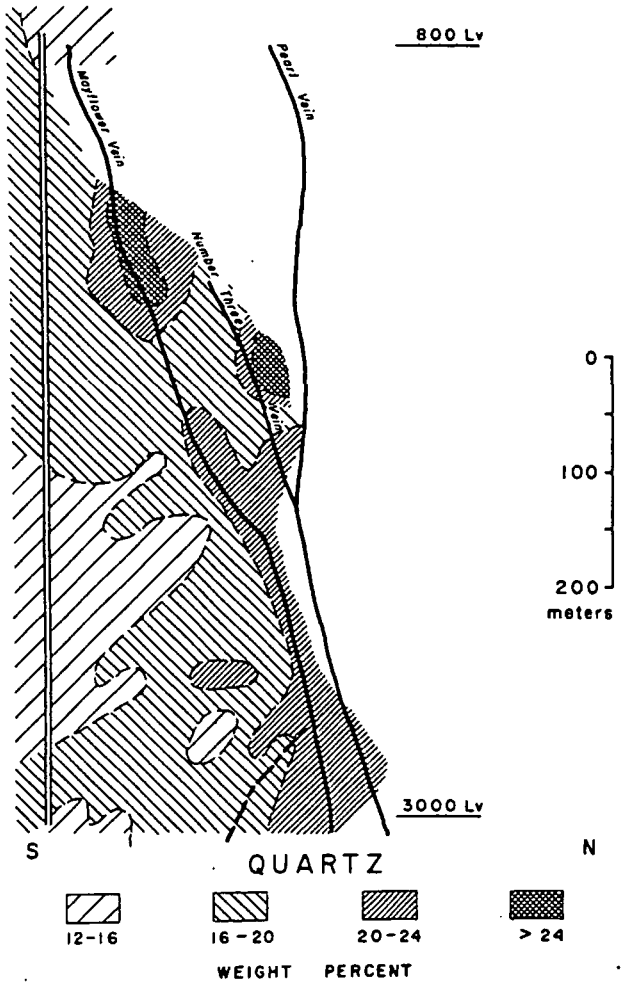

FIG. 20. Distribution of quartz in the Mayflower stock.

marized in Table 5. Gains and losses of minerals are reported either as the range of variation for all sampled traverses or as the average mass balance for distinct altered blocks in the north-south cross section (Fig. 28). Gains and losses of elemental components are shown as average values in either case. The division of the vertical section into blocks of alteration was based on the distribution of relative amounts of major minerals and was done in order to compare systematically the observed mass transfer with that predicted by theoretical computations. Average mineral masses are also presented, and their variation from block to block reiterates the earlier recognition of a broad zone of alteration in the mine.

From the mineralogical gain and loss tabulation, it can be seen that greater masses of andesine were destroyed than any other reactant mineral, followed by igneous biotite and hornblende. The other reactant phases were either consumed or reequilibrated with the hydrothermal solutions but were subsequently added to the rocks as alteration products. Anhydrite, calcite, pyrite, kaolinite, chlorite, and albite occur exclusively as alteration products. The original mass of hornblende (0.08 g/cm³) was assumed to be totally consumed during alteration, despite its preservation in some rock pulps (generally in amounts less than 1%, a condition that excludes it from the mineral abundance calculations). Similarly, the igneous biotite (0.32 g/cm³) was assumed to be completely destroyed or reequilibrated to the composition of the present hydrothermal biotite. Hence, the values of hornblende and igneous biotite appear as losses equivalent to their respective original amounts, regardless of the alteration zone to be considered.

The mass balance for the sampled rocks indicates an overall loss of Si, Al, Na, and Ca and an overall gain of Fe (total), Mg, K, S, C, and Ti. Large quantities of sulfide and sulfate were added to the altered rocks from the hydrothermal solutions by reaction with indigenous iron and calcium in the wall rocks. The latter were almost exclusively deposited

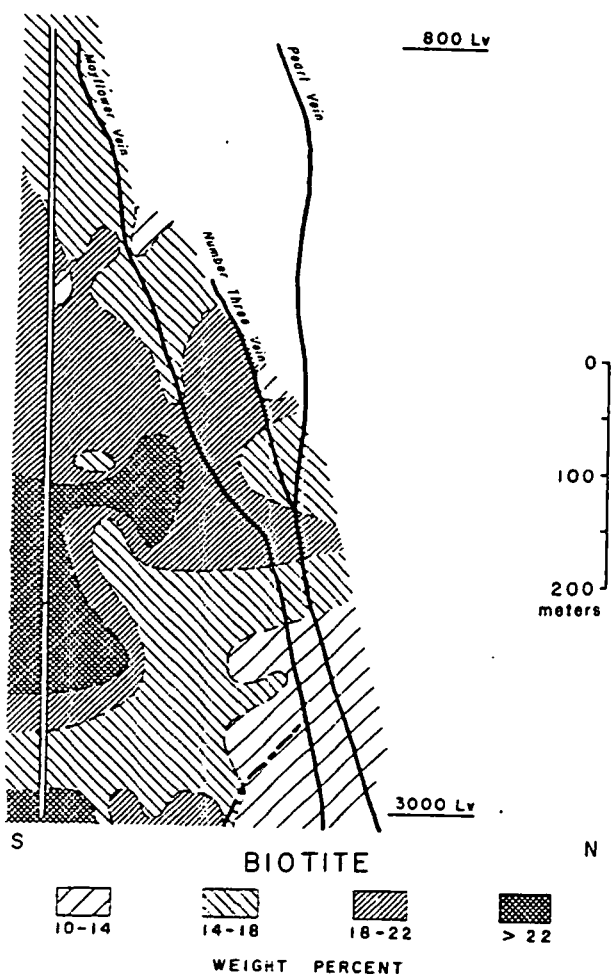

FIG. 21. Distribution of biotite in the Mayflower stock.

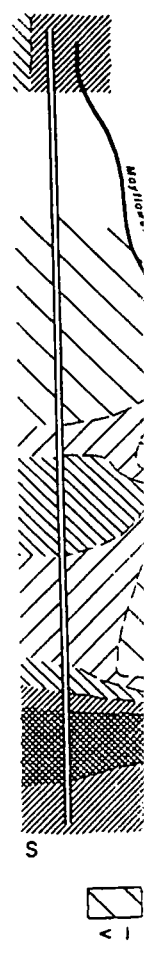

FIG. 22.

in the ore zone as sulfides. A portion of the total sulfur was in the form of sulfate which was incorporated into the altered rocks mainly as anhydrite. Considerable addition of CO_3^{2-} was also evident, as the widespread occurrence of calcite indicates.

Comparison of Predicted with Observed Mineral Abundances

Circulation of fluids along pathlines between different chemical environments apparently resulted in the mineral abundances and elemental gains and losses that were measured. As a fluid packet circulates from one chemical environment into another, mass transfer occurs between the fluid and rock along its flow path. On the basis of the conditions predicted by the heat transfer calculations and an estimation of initial solution concentrations, the alteration process can be simulated by theoretical methods. Helgeson et al. (1970) describe methods which simulate the overall mass transfer resulting from irreversible reactions between a fixed quantity of aqueous solution and initial reactant mineral assemblages. Equilibrium conditions are defined by a set of differential equations describing the laws of mass action and mass and charge balances at a fixed temperature and pressure, and the overall irreversible reaction is approximated by the derivatives of these variables with respect to the reaction progress.

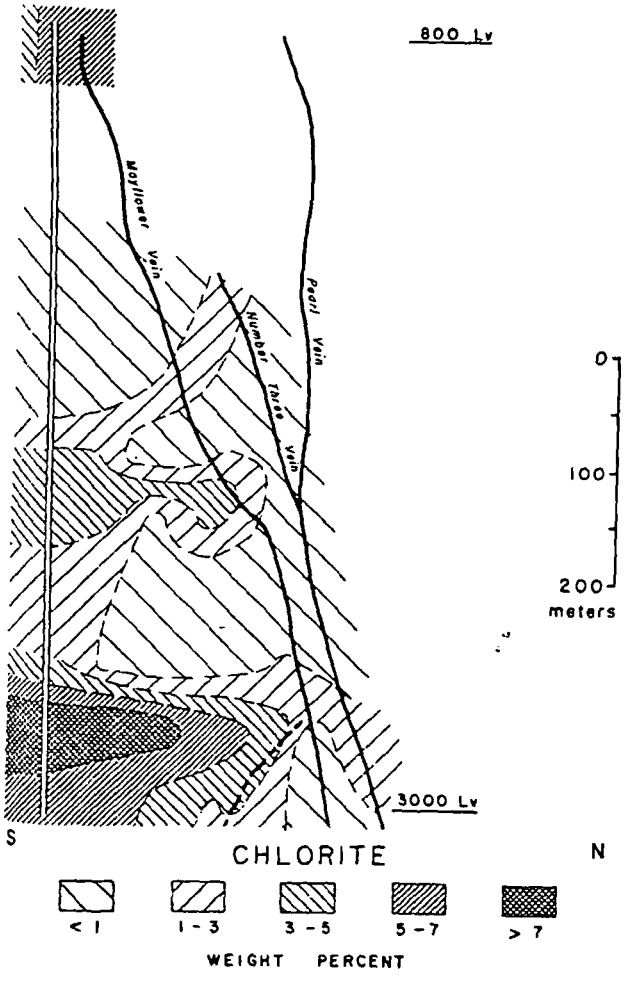

FIG. 22. Distribution of chlorite in the Mayflower stock.

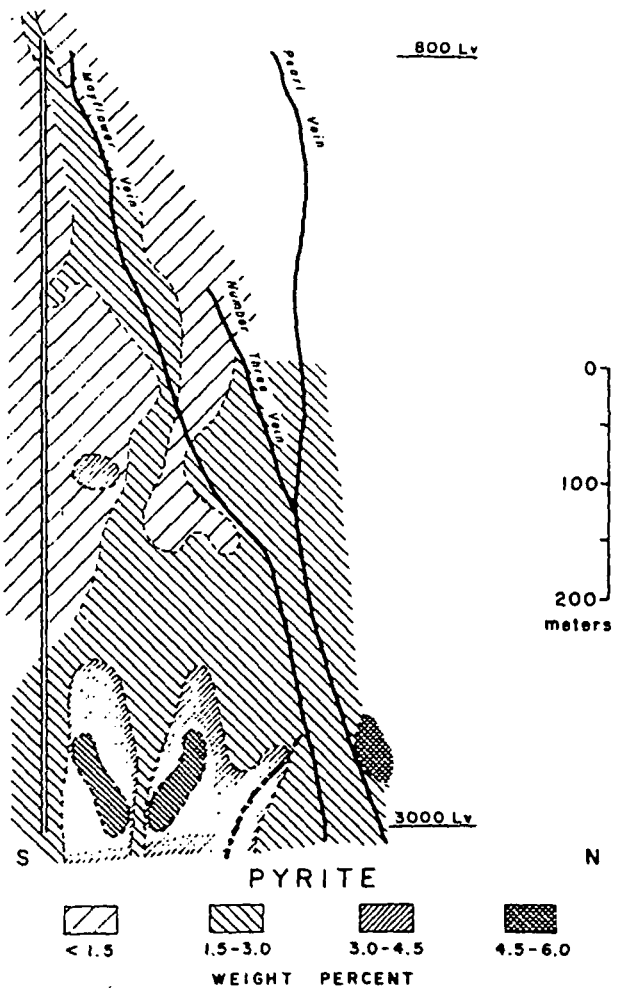

FIG. 23. Distribution of pyrite in the Mayflower stock.

The thermal regime of the igneous wall rocks and fluids that prevailed over discrete periods of time during the cooling history of the Mayflower stock was used to define conditions for which the fluid-rock reactions were simulated. The heat flow computations predict that during the major portion of the cooling process temperatures were in the 150° to 400°C range, but the thermodynamic data for the mass transfer computations was only available for 25° to 300°C and 1 bar; therefore, fluid-rock reactions could be simulated only at a sequence of discrete temperatures between 300° and 150°C. Modeling of the cooling history of the Mayflower stock has shown that its top regions remained at temperatures significantly above 300°C only for the initial 1.5×10^4

alteration of the Mayflower stock are presented in Table 6. These solutions were selected on the basis of observed mineral assemblages, gains and losses of elemental components, and inferred compositions of circulating fluids. Additional initial conditions included: (1) oxygen fugacity fixed at a given temperature for the pyrite-magnetite and pyrite-hematite pairs which were commonly observed in the alteration assemblages; (2) starting solutions in equilibrium with quartz and pyrite; (3) CO_2 pressure fixed at an upper limit of 10 bars; (4) $CO_2(g)$ as a reactant only at temperatures below 200°C; and (5) reaction rates of reactant solid phases proportional to their original mole fractions in the unaltered rocks.

Results of Mass Transfer Calculations

The irreversible reaction paths between solutions and the unaltered equivalents of the Mayflower rocks are represented in activity-activity diagrams which depict the stability fields of minerals and the compositions of the solutions that coexist with these minerals. The composition of the starting solution at 300°C is in equilibrium with both pyrite and quartz and projects onto the microcline stability field (Fig. 29). Incremental masses of reactants dissolved in the solution caused its composition to shift initially toward

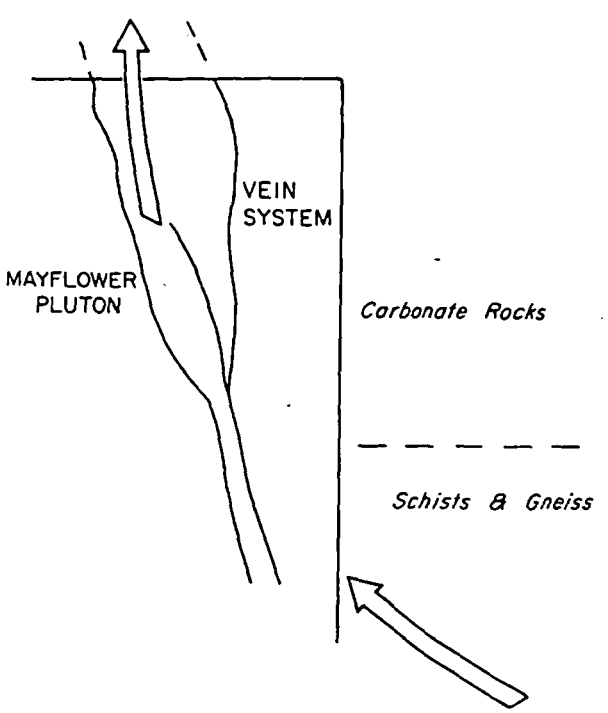

FIG. 26. Schematic north-south cross section of the vein system in the Mayflower stock, showing major types of host rocks and direction of fluid flow. The upward transition from clastic to calcareous rocks occurs at a depth corresponding approximately to the 2,400-ft level of the mine.

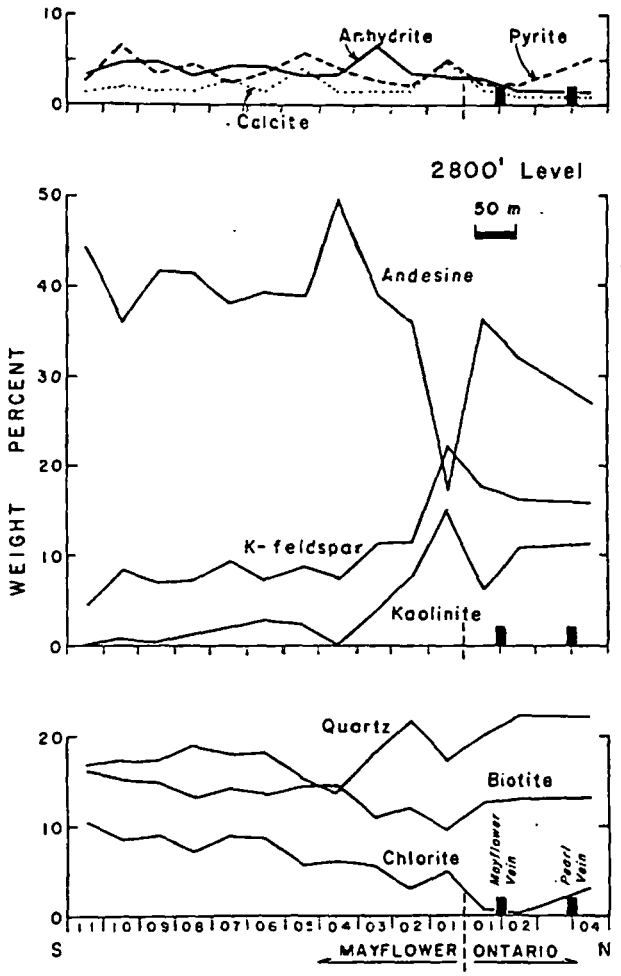

FIG. 27. Lateral variation of the abundance of the major mineral constituents of the Mayflower and Ontario stocks with respect to the vein system on the 2,800-ft level.

higher $a_{Mg^{2+}}/a^2_{H+}$ ratios at an essentially constant $a_{Fe^{2+}}/a^2_{H+}$ ratio, since the solution was enriched in Mg as a result of dissolution of igneous biotite, whereas the Fe derived from the destruction of biotite and magnetite was consumed by the production of pyrite. This portion of the reaction path was followed by precipitation of anhydrite, then by muscovite, Figure 30. However, near the Mg-montmorillonite-phlogopite boundary, muscovite ceased being produced. The solution next equilibrated with Mg-montmorillonite but then undersaturated with respect to quartz and, at the same time, started precipitating phlogopite. Further dissolution of igneous biotite and simultaneous precipitation of phlogopite and Mg-montmorillonite maintained the $a_{Mg^{2+}}/a^2_{H+}$ ratio constant, shifting the solution composition toward equilibrium with biotite. In the process, Mg-montmorillonite, phlogopite, and pyrite became undersaturated, favoring the precipitation of Mayflower biotite and Ca-montmorillonite. By the time overall

TABLE 5. Mineral Abundances and Gains and Losses of Minerals and Elemental Components in the Mayflower Stock

Minerals	Mineral abundances					Gains and losses					Range of variation for all traverses	
	Grams of minerals/cm³ of rock										Gains	Losses
	Block 1	Block 2	Block 3	Block 4	Block 5	Block 1	Block 2	Block 3	Block 4	Block 5		
Andesine	0.98	1.19	1.25	1.08	1.24	−0.92	−0.72	−0.70	−0.86	−0.60		0.17–1.04
K-feldspar	0.41	0.16	0.18	0.33	0.17	0.27	0.03	0.00	0.18	0.03	0.47 to	0.13
Quartz	0.54	0.47	0.43	0.58	0.44	0.26	0.20	0.21	0.28	0.21	0.00–0.46	
MF-biotite	0.35	0.47	0.49	0.52	0.51	0.35	0.47	0.49	0.52	0.51	0.26–0.70	
Pyrite	0.08	0.11	0.05	0.05	0.04	0.08	0.11	0.05	0.05	0.04	0.06–0.18	
Calcite	0.05	0.04	0.05	0.09	0.06	0.05	0.04	0.05	0.09	0.06	0.01–0.60	
Anhydrite	0.08	0.10	0.08	0.02	0.06	0.08	0.10	0.08	0.02	0.06	0.00–0.24	
Chlorite	0.05	0.18	0.05	0.03	0.05	0.05	0.18	0.05	0.03	0.05	0.00–0.29	
Kaolinite	0.18	0.01	0.11	0.14	0.05	0.18	0.01	0.11	0.14	0.05	0.00–0.41	
Magnetite	—	—	—	0.01	0.02	−0.03	−0.03	−0.03	−0.02	−0.01		0.00–0.03
Hornblende*	—	—	—	—	—	−0.08	−0.08	−0.08	−0.08	−0.08		0.08
Biotite*	—	—	—	—	—	−0.32	−0.32	−0.32	−0.32	−0.32		0.32
Albite	—	—	—	—	—	—	—	—	—	—	0.00–0.43	
Grain density	2.72	2.73	2.69	2.85	2.64							

Elements	Gains and losses					Average for all traverses	
	Grams of components/cm³ of rock					Gains	Losses
Si	0.010	−0.040	−0.026	0.000	−0.032		0.009
Al	−0.043	−0.061	−0.044	−0.052	−0.050		0.049
Fe(total)	−0.009	0.028	0.003	0.002	0.004	0.006	
Mg	0.011	0.049	0.032	0.021	0.028	0.026	
Ca	−0.024	0.002	0.010	−0.024	0.023		0.011
Na	−0.035	−0.031	−0.031	−0.041	−0.034		0.032
K	0.032	0.014	0.015	0.032	0.017	0.021	
S	0.043	0.068	0.027	0.034	0.024	0.038	
C	0.006	0.005	0.007	0.011	0.011	0.007	
SO_3	0.048	0.062	0.051	0.011	0.031	0.037	
Ti	0.009	0.013	0.013	0.012	0.013	0.010	

* Hornblende was assumed to be totally destroyed for purposes of computing mineral abundances of major minerals. Igneous biotite was assumed to be destroyed or reequilibrated to hydrothermal biotite (MF-biotite).

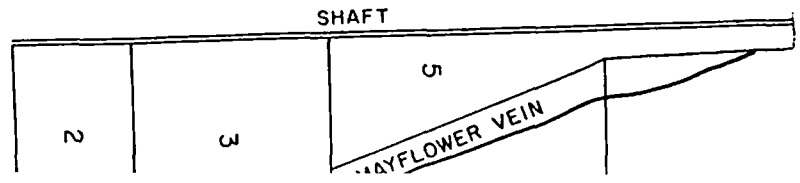

FIG. 28. Bloc
cross section in t
basis of abundan
4).

equilibrium w
were destroye
formed per ki
pH from 4.5 t
The startin
initially in

T

Sp

Al³⁺
K⁺
Na⁺
Ca²⁺
Mg²⁺
Fe²⁺
Cu⁺
H_4SiO_4
S^{2-}
SO_4^{2-}
CO_3^{2-}
Cl^-

Initial
Final p
True lo

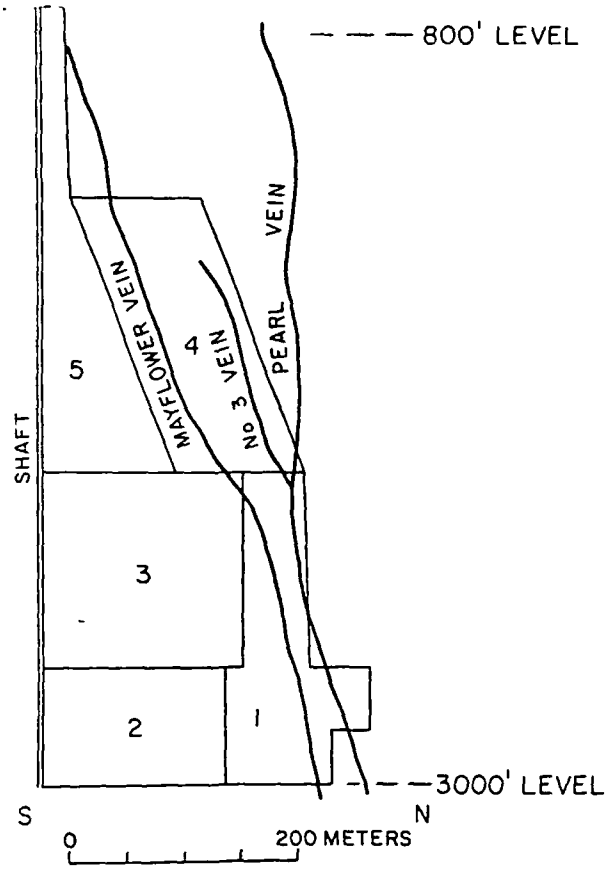

FIG. 28. Blocks of alteration over a north-south 670 m cross section in the Mayflower stock that were defined on the basis of abundances of major alteration products (see Table 4).

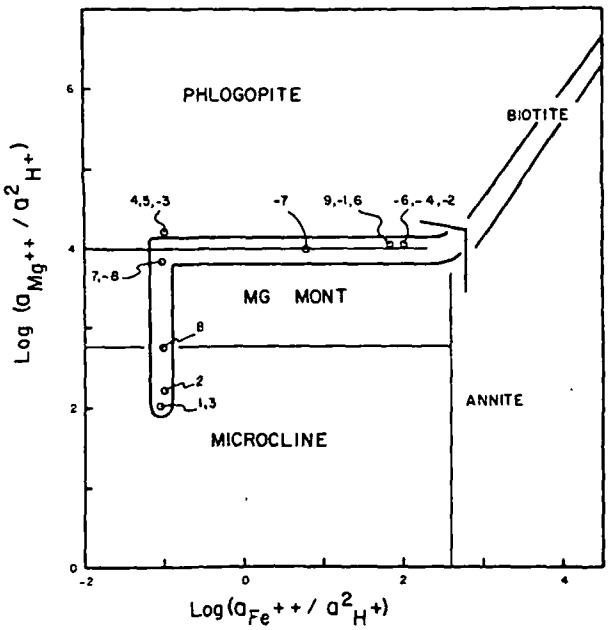

FIG. 29. Activity diagram for the system MgO-FeO-K_2O-Al_2O_3-SiO_2-HCl-H_2O at 300°C and 1 bar. Activity of solid phases and H_2O are equal to one; equilibrium reactions were balanced on aluminum. Log $a_{H_4SiO_4} = -1.94$, quartz saturation and log $(a_{K^+}/a_{H^+}) = 4.0$. Reaction path at 300°C (refer to Fig. 30) on activity diagram shows the shift in solution composition as the reaction progressed. The tail of the arrow represents the composition of the starting solution, whereas the small circles mark the positions at which a product phase either started (positive numbers) or ceased (negative numbers) precipitating out of the solution. Mg-mont = magnesium-montmorillonite. Biotite represents stability field for biotite found in the Mayflower altered igneous rocks.

equilibrium was reached, 130 g of reactant phases were destroyed, and 150 g of product phases were formed per kilogram of water, with a net change in pH from 4.5 to 4.7, Table 7.

The starting solution at 200°C (Fig. 31) was initially in equilibrium with quartz, pyrite, and Ca-montmorillonite. As reactants dissolved, the solution composition shifted parallel to the Ca-montmorillonite–Na-montmorillonite boundary. The solution then equilibrated with calcite, whose saturation surface for a CO_2 fugacity of 9.5 bars was reached at log $(a_{Ca^{2+}}/a^2_{H^+}) = 7.47$ and after 0.57 g of andesine

TABLE 6. Initial Solution Compositions for Path Reactions at Different Temperatures (molality)

Species	300°C	250°C	200°C	150°C
Al^{3+}	1.0×10^{-9}	1.0×10^{-9}	1.0×10^{-9}	1.0×10^{-9}
K^+	2.5	2.5	2.5×10^{-2}	2.5×10^{-2}
Na^+	3.2	3.2	3.2×10^{-1}	3.2×10^{-1}
Ca^{2+}	2.2×10^{-3}	1.3×10^{-3}	1.3×10^{-3}	1.3×10^{-3}
Mg^{2+}	3.7×10^{-6}	3.7×10^{-6}	3.7×10^{-5}	3.7×10^{-5}
Fe^{2+}	7.4×10^{-10}	2.6×10^{-10}	1.0×10^{-9}	1.0×10^{-7}
Cu^+	1.0×10^{-3}	1.0×10^{-3}	1.0×10^{-7}	1.0×10^{-6}
H_4SiO_4	1.2×10^{-2}	7.8×10^{-3}	4.5×10^{-3}	2.1×10^{-3}
S^{2-}	8.0×10^{-2}	2.4×10^{-2}	1.0×10^{-3}	1.0×10^{-6}
SO_4^{2-}	9.5×10^{-3}	5.6×10^{-2}	2.8×10^{-2}	2.5×10^{-2}
CO_3^{2-}	1.0×10^{-3}	1.0×10^{-3}	7.8×10^{-2}	7.7×10^{-2}
Cl^-	4.4	4.4	4.7×10^{-1}	3.5×10^{-1}
Initial pH	4.50	4.40	4.50	4.50
Final pH	4.68	4.82	6.25	6.56
True ionic strength	5.32	5.36	0.54	0.32

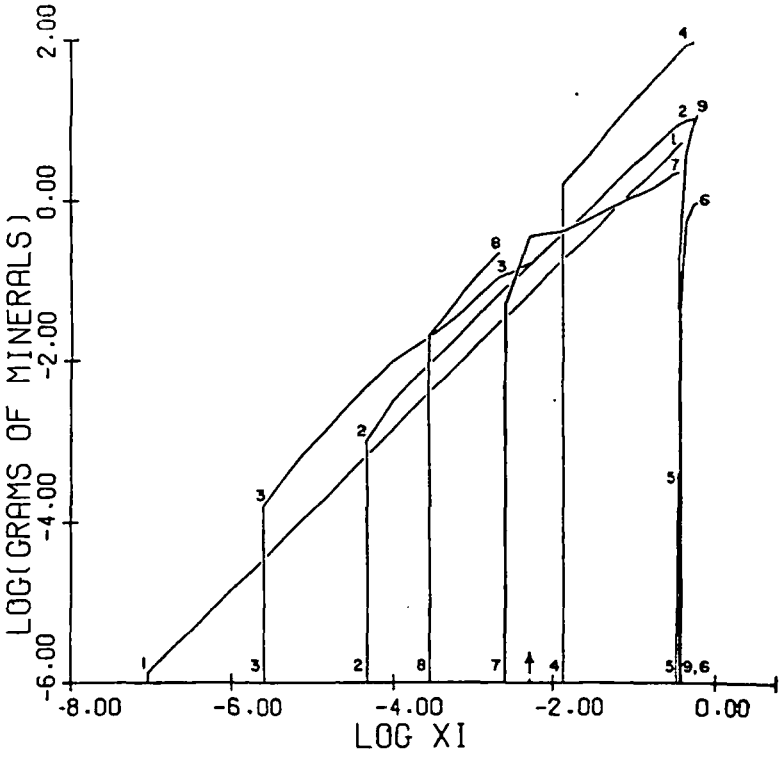

FIG. 30.—Masses of alteration minerals produced, per 1,000 g of solution, as a function of reaction progress during reaction of unaltered Mayflower igneous assemblages and solutions at 300°C. Arrow marks position with respect to reaction progress when phlogopite equilibrated with the solution. Indices refer to curves that represent precipitation of alteration minerals in systems where 1 = pyrite, 2 = anhydrite, 3 = quartz, 4 = microcline, 5 = phlogopite, 6 = Ca-montmorillonite, 7 = Mg-montmorillonite, 8 = muscovite, and 9 = biotite. Calculations based on thermodynamic data from Helgeson (1969).

per kilogram of water had been destroyed. Calcite equilibration constrained the solution composition to shift along the calcite saturation surface. Increases of H in log a_{Na^+}/a_{H^+} relative to log $a_{Ca^{2+}}/a^2_{H^+}$ changed the solution composition toward the Ca-montmorillonite–Na-montmorillonite low albite phase equilibrium point. Phlogopite and alteration muscovite became stable, but Ca-montmorillonite ceased precipitating. The solution then equilibrated with Na-montmorillonite and low albite, at which time only 22 g of product phases had been formed. Thereafter, as the reaction progressed, significantly larger mass transfer occurred and, when overall equilibrium was attained, 166 g of products had been precipitated as opposed to 163 g of reactants destroyed per kilogram of water (Fig. 32 and Table 7).

The saturation surface of anhydrite shifted as calcite precipitated, from a position at log $(a_{Ca^{2+}}/a^2_{H^+}) = 8.2$ when the solution first saturated with calcite to a position at log $(a_{Ca^{2+}}/a^2_{H^+}) = 9.8$ by the time

TABLE 7. Irreversible Mass Transfer at 300°C and 200°C

	Reactants 300°C		Reactants 200°C	
	Log mass destroyed	Log mass produced	Log mass destroyed	Log mass produced
Magnetite	0.2	—	−2.0	0.8
Quartz	1.5	−0.8	−4.7	0.7
Microcline	−0.8	2.1	1.0	—
Annite	1.0	—	1.1	—
Phlogopite	0.9	−3.4	−0.8	−0.9
Mayflower plagioclase	1.9	−7.6	2.1	—
Carbon dioxide			1.0	−8.4
Initial pH	4.5		4.5	
Final pH	4.7		6.3	

overall equilibrium was attained. At 200°C production of calcite prevented the solution from saturating with respect to anhydrite. This may partly explain the occurrence of larger masses of calcite than anhydrite in the shallower depths of the mine, as discussed earlier. The style of mass transfer between the aqueous phase and rock for reactions simulated at other temperatures (250° and 150°C) is similar to that documented for 300° and 200°C.

Comparison of Measured and Predicted Mineral Abundances

Predicted gains and losses of minerals were estimated from the amounts of minerals produced or destroyed on the basis of the mass transfer computations and from mass fluxes derived from analysis of fluid flow associated with the initial 1.8×10^5 years of cooling of the Mayflower stock. The mass flux estimates apply to the upper 1.5 km of the stock, whose temperatures remained at 350° to 300°C, 300° to 250°C, 250° to 200°C, and 200° to 150°C for periods of approximately 10^4, 6×10^4, 1.8×10^5, and 2.0×10^5 years, respectively. The last two periods were linearly extrapolated from the initial 1.8×10^5 years of cooling. Mass fluxes corresponding to these time intervals (Table 8) refer to the mass of fluids that flowed through a volume of rock with length measured vertically on the cross section of the stock.

Densimetric amounts of minerals (M_p, in grams of minerals per cm³ of rock) produced or destroyed in the computed irreversible reactions were calculated from

$$M_p = \frac{Wq\Delta t}{l} 10^{-3} \qquad (8)$$

where W is the computed amount of mineral produced or destroyed per kilogram of water, q is the total mass flux in g/cm²s, Δt is the time interval in seconds, and l, in cm, is the flow path length through a given volume of rock.

The predicted and observed gains and losses of minerals (Fig. 33 and Table 9) show a remarkable agreement for most minerals, considering the nature of the approximations made in the theoretical predictions and error in the observed data. The theory indicates much more microcline was added to the initial rock than was detected in the measurement. Conversely, the theory predicted quartz was removed from the rock, but in reality the quartz content increased. One possible explanation is the somewhat unusually large Na/K ratios in the initial solution. These ratios were estimated from the occurrence of halite and sylvite in the fluid inclusions (Nash, 1973) and may be too high since a decrease in potassium in the original solution would lead to the formation of less microcline and, consequently, more quartz. Chlorite was approximated by clinochlore because thermodynamic data do not exist on chlorites with a composition similar to those found in the altered Mayflower igneous rocks, which may explain the fact that chlorite did not appear as a product phase in the computed irreversible reactions. Similarly, end members of the montmorillonite group were included as possible product phases in the irreversible reactions, due to a lack of thermodynamic data on intermediate members. This necessary approximation, together with the uncertainty in the end-member data, most likely stabilized the montmorillonites over other phases, causing large predicted amounts of these clays. As a result, these clays were equated to observed amounts of kaolinite.

The predicted mass abundances clearly indicate that many of the limitations imposed by the very simple coupling of the fluid flow and irreversible mass

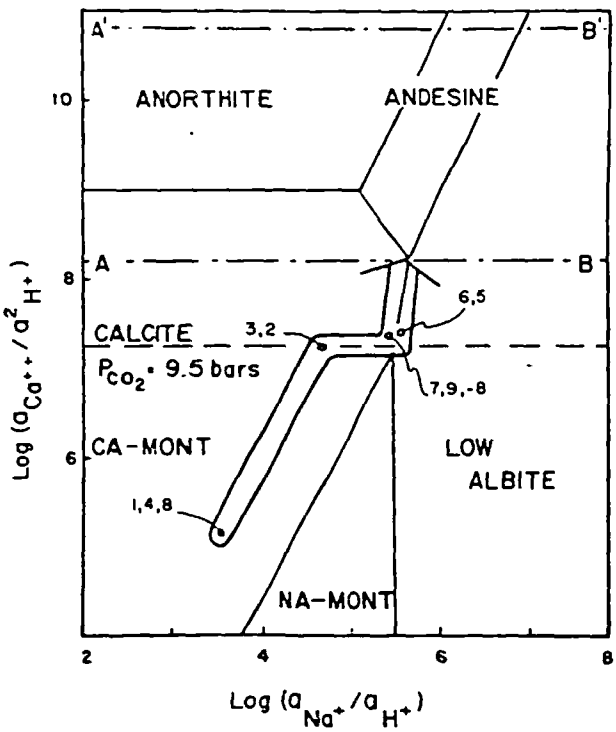

FIG. 31. Activity diagram for the system MgO-FeO-K_2O-Al_2O_3-SiO_2-HCl-H_2O at 200°C and 1 bar. Activity of solid phases and H_2O are equal to one; equilibrium reactions were balanced on aluminum. Log $a_{H_4SiO_4} = -2.35$, quartz saturation. Reaction path at 200°C (refer to Fig. 32) on activity diagram shows the shift in solution composition as reaction progressed. The tail of the arrow represents the composition of the starting solution, whereas the small circles mark the positions at which a product phase either started (positive numbers) or ceased (negative numbers) precipitating out of solution. A-B and A'-B' are the saturation surfaces for anhydrte at ξ values where calcite started precipitating and at the time the system attained overall equilibrium, respectively.

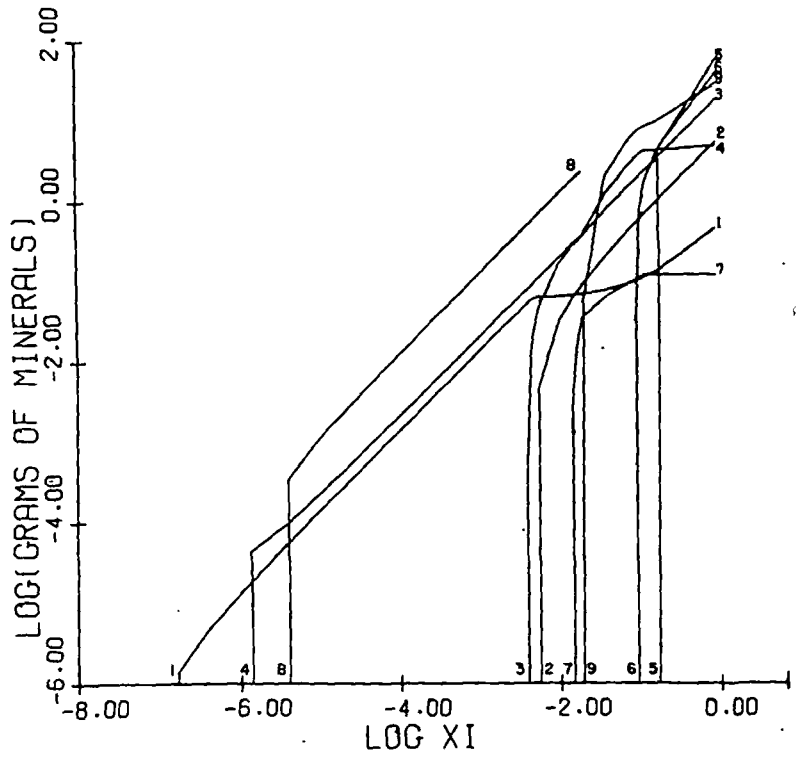

FIG. 32. Masses of alteration minerals produced, per 1,000 g of solution, as a function of reaction progress during reaction of unaltered Mayflower igneous rocks and solutions at 200°C. Indices refer to curves that represent precipitation of alteration minerals in open systems where 1 = pyrite, 2 = magnetite, 3 = calcite, 4 = quartz, 5 = low albite, 6 = Na-montmorillonite, 7 = phlogopite, 8 = Ca-montmorillonite, and 9 = muscovite. Calculations based on thermodynamic data from Helgeson (1969).

transfer theories must be accounted for in order to use transport theory to predict the mass abundance and distribution of phases in hydrothermal systems. But, for a first order approximation, the results are quite encouraging.

Conclusions

The igneous event that produced the Mayflower stock resulted in the development of abundant continuous fractures within the stock as it cooled below solidus temperatures. This fracturing generated permeabilities in the darcy range and allowed relatively large masses of fluids to circulate in and out of the stock. This convective transfer of heat cooled the entire stock to 0.3 of the initial thermal anomaly in 1.8×10^5 years, which is approximately 1.5 times faster than if the rock were impermeable and cooled by pure conduction. A large mass of hydrothermal fluid, 10^{13} kg per km of strike length, flowed through the upper 1.5-km portion of the stock during this same time period. These fluids circulated from a variety of rock environments, and along their pathlines they encountered variations in temperature and pressure. Irreversible mass transfer between these fluids and the Mayflower stock altered the stock to mineral assemblages that reflect the chemical composition of the rocks through which the fluids circulated, the pressure and temperature conditions along the flow paths, and initial composition of the fluids.

The heat and mass transport model of the Mayflower system provides a first order approximation

TABLE 8. Mass Fluxes that Prevailed in the Upper 1.5 Km of the Mayflower Stock during Cooling

	Time intervals (years)			
	10,000	60,000	180,000	200,000
Temperature range	350°–300°C	300°–250°C	250°–200°C	200°–150°C
Mass fluxes (g/cm^2 s)	1.6×10^{-7}	1.8×10^{-7}	4.0×10^{-8}	2.0×10^{-8}

of the temperature, pressure, and fluid fluxes that may have been realized in the natural system. These variables in turn define the conditions under which alteration and mineralization of the Mayflower stock occurred.

An analysis of the Mayflower hydrothermal system was based on quantitative data on the mineralogy and fluid inclusions combined with theoretical predictions of mass transfer and analysis of fluid flow in and around the Mayflower stock. The assumed solution compositions, prevalent pressure and temperature during the hydrothermal process, and the estimated amounts of fluids that circulated through the upper 1.5 km of the Mayflower stock as it cooled, predict the formation of mineral assemblages in masses similar to those found in the altered Mayflower igneous rocks. The mass transfer that resulted from irreversible reactions between the circulating fluids and the igneous rocks added relatively large amounts of S, C, K, Mg, and H_2O to the stock. The vertical zoning characterized by larger masses of calcite than anhydrite above the 2,400-ft level of the mine may reflect precipitation from fluids that circulated through different stratigraphic horizons and entered the stock at different depths. Fluids derived from the stratigraphically upper-carbonate host rocks were enriched in CO_3^{2-} content which favored the precipitation of calcite upon reaction with the andesine of the stock. Decrease in temperature and increase in CO_2 pressure further favored the precipitation of calcite over anhydrite in the shallower depths of the mine.

This analysis of the Mayflower hydrothermal system suggests that the original igneous minerals were altered by acid-sulfate solutions at moderate temperatures, <400°C, and pressures <1 kb. In order to account for the observed masses and compositions of alteration products, fluid fluxes on the order of 10^{-7} g/cm²s⁻¹ are required for at least 2×10^5 years. Although the hypothetical solution contained on the order of 50 ppm total copper, only small amounts of chalcopyrite were precipitated along the

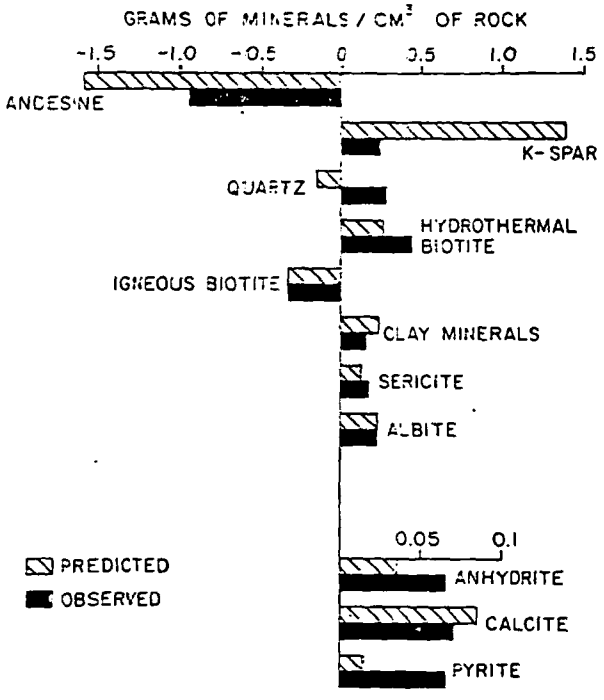

FIG. 33. Comparison between observed mineral gains and losses in the Mayflower stock and those predicted on the basis of irreversible mass transfer calculations between 300°C and 150°C and fluid-flow computations.

TABLE 9. Predicted Gains and Losses of Minerals on the Basis of Irreversible Mass Transfer Calculations between 300° and 150°C and Fluid-Flow Computations

	Length = 700 m (vertical section)				Total predicted	Total observed blocks 1 & 4
Temperature	300°C	250°C	200°C	150°C		
Mineral	Grams of minerals/cm² of rock					
Andesine	-6.1×10^{-2}	-9.4×10^{-1}	-4.2×10^{-1}	-1.6×10^{-1}	-16×10^{-1}	-9×10^{-1}
K-feldspar	8.5×10^{-2}	1.35	-3.2×10^{-2}	-1.2×10^{-2}	14×10^{-1}	2×10^{-1}
Quartz	-2.0×10^{-2}	-3.4×10^{-1}	1.7×10^{-2}	1.8×10^{-1}	-1.6×10^{-2}	3×10^{-1}
Anhydrite	0.8×10^{-2}	3.5×10^{-2}	trace	—	4×10^{-2}	7×10^{-2}
Calcite	—	0.1×10^{-4}	6.3×10	2.3×10^{-2}	9×10^{-2}	7×10^{-2}
MF-biotite	0.9×10^{-2}	2.3×10^{-1}	—	2.0×10^{-2}	3×10^{-1}	4×10^{-1}
Ig. biotite	-1.2×10^{-2}	-2.3×10^{-1}	-4.4×10^{-2}	-2.8×10^{-2}	3×10^{-1}	3×10^{-1}
Pyrite	0.4×10^{-2}	0.8×10^{-2}	1.6×10^{-2}	trace	1×10^{-2}	7×10^{-2}
Clay minerals[1]	2.5×10^{-2}	—	1.4×10^{-1}	8.7×10^{-2}	2×10^{-1}	2×10^{-1}
Magnetite	-1.0×10^{-3}	-2.9×10^{-3}	1.9×10^{-2}	3.4×10^{-2}	2×10^{-2}	-3×10^{-2}
Sericite	1.7×10^{-4}	3.5×10^{-4}	2×10^{-1}	3.1×10^{-2}	1×10^{-1}	2×10^{-1}*
Low albite	—	—	1.9×10^{-1}	2.8×10^{-2}	2×10^{-1}	2×10^{-1}†
Chlorite	—	—	—	—	—	4×10^{-2}
Chalcopyrite			trace	trace		trace

[1] Clay minerals comprise kaolinite and montmorillonites. The observed values refer only to kaolinite.
* Value for sample MF-2801 on the 2,800-ft mine level at about 60 m south of the Mayflower vein.
† Average value of 360 m of sample along the Mayflower vein on the 2,600-ft level.

Economic Geology
Vol. 72, 1977, pp.

reaction path. Therefore, the effluent fluids from the stock still contained sufficient copper to produce a significant quantity of copper sulfide in the overlying host rocks.

This heuristic model of the Mayflower hydrothermal system summarizes the nature of processes which prevailed during the cooling of the stock and accounts for many of the observed geologic features. More importantly, we wish to communicate the utility of combining field observation and computer models of process to extend understanding of the processes attending formation of mineral deposits.

Acknowledgments

This research was supported by NSF Grant GA41136 and funds from the Research Corporation to Denis Norton. Financial assistance in the early stages was provided by the Research Fund of the Geology and Geophysics Department of the University of Utah, which also financed the analytical work with X-ray equipment and electron microprobe. We are grateful for valuable suggestions given by R. E. Beane, Jerry Knight, and John Delaney. A special thanks goes to Lynn McLean who greatly improved this manuscript. The data for this study were collected with the cooperation and assistance of numerous hard-rock miners, the Hecla Mining Company, and John Simos; the data were analyzed with the cooperation and assistance of the University of Arizona Computer Center staff; we thank them for their help and patience.

Department of Geosciences
University of Arizona
Tucson, Arizona 85721

Present Address:
R. N. V.
Núcleo de Ciências Geofísicas E. Geologicas
Universidade Do Pará
Belém Pará, Brazil

April 28, 1976; March 8, 1977

REFERENCES

Baker, A. A., Calkins, F. C., Crittenden, M. D., Jr., and Bromfield, C. S., 1966, Brighton Quadrangle, Utah: U. S. Geol. Survey, Geol. Quad. Map.

Barnes, M. P., and Simos, J. G., 1968, Ore deposits of the Park City district, with a contribution on the Mayflower lode, *in* Ridge, J. F., ed., Ore deposits of the United States, 1933–1967, (Graton-Sales vol.): New York, Am. Inst. Mining Metall. Petroleum Engineers, p. 1002–1126.

Beane, R. E., 1972, A thermodynamic analysis of the effect of solid solution of the hydrothermal stability of biotite: Unpub. Ph.D. thesis, Northwestern Univ., 195 p.

—— 1974, Biotite stability in the porphyry copper environment: Econ. Geol., v. 69, p. 241–256.

Boutwell, J. M., 1912, Geology and ore deposits of the Park City district, Utah, with contributions by L. H. Woolsey: U. S. Geol. Survey Prof. Paper 77, 231 p.

Brace, W. F., Walsh, J. B., and Frangos, W. T., 1968, Permeability of granite under high pressure: Jour. Geophys. Research, v. 73, p. 2225–2236.

Bromfield, C. S., Baker, A. A., and Crittenden, M.D., Jr., 1970, Heber Quadrangle, Wasatch and Summit Counties, Utah: U. S. Geol. Survey, Geol. Quad. Map.

Burnham, C. W., and Davis, N. F., 1971, The role of H_2O in silicate melts I. P-V-T relations in the system $NaAlSi_3O_8$-H_2O to 10 kilobars and 1,000°C: Am. Jour. Sci., v. 270, p. 54–79.

Burnham, C. W., Holloway, J. R., and Davis, N. F., 1969, Thermodynamic properties of water to 1,000°C and 10,000 bars: Geol. Soc. America Spec. Paper 132, 96 p.

Cadek, J., Hazdrova, M., Kacura, G., Krasny, J., and Malkovsky, M., 1968, Hydrogeology of the thermal waters at Teplice and Usti nad Labem: Sbornik Geologickych Ved Hydrology Inzenyraska Geologie, Rada Hig. Sv.6 (summary in English).

Calkins, F. C., and Butler, B. S., 1943, Geology and ore deposits of the Cottonwood-American Fork area, Utah, with contributions by V. C. Heikes: U. S. Geol. Survey Prof. Paper 201, 152 p.

Crittenden, M. D., Jr., 1965, Dromedary Peak Quadrangle, Utah: U. S. Geol. Survey, Geol. Quad. Map.

Crittenden, M. D., Jr., Stackless, J. S., Kistler, R. W., and Stern, T. W., 1973, Radiometric dating of intrusive rocks in the Cottonwood area, Utah: U. S. Geol. Survey Jour. Research, v. 1, p. 173–178.

Goranson, R. W., 1938, Silicate-water systems: Phase equilibria in the $NaAlSi_3O_8$-H_2O and $KAlSi_3O_8$-H_2O systems at high temperatures and pressures: Am. Jour. Sci., 5th ser., v. 35A, p. 71–91.

Heard, H. C., 1967, The influence of environment on the brittle failure of rocks, *in* Failure and breakage of rocks, Eighth symposium on rock mechanics: New York, Am. Inst. Mining Metall. Petroleum Engineers, p. 82–93.

Helgeson, H. C., 1969, Thermodynamics of hydrothermal systems at elevated temperatures and pressures: Am. Jour. Sci., v. 267, p. 729–804.

—— 1970, A chemical and thermodynamic model of ore deposition in hydrothermal systems: Mineralog. Soc. America Spec. Paper 3, p. 155–186.

Helgeson, H. C., Brown, T. H., Nigrini, A., and Jones, T. A. 1970, Calculation of mass transfer in geochemical processes involving aqueous solutions: Geochim. et Cosmochim. Acta, v. 34, p. 569–592.

Jacobs, D. C., and Parry, W. T., 1976, A comparison of the geochemistry of biotite from some Basin and Range stocks: Econ. Geol., v. 71, p. 1029–1035.

Nash, T. J., 1973, Geochemical studies in the Park City district; I, Ore fluids in the Mayflower mine: Econ. Geol., v. 68, p. 34–51.

Norton, D. L., 1972, Concepts relating anhydrite deposition to solution flow in hydrothermal systems: Internat. Geol. Cong., 24th Montreal, sect. 10, p. 237–244.

Norton, D. L., and Knapp, R., 1977, Transport phenomena in hydrothermal systems: Nature of porosity: Am. Jour. Sci., v. 277, p. 913–936.

Norton, D. L., and Knight, J., 1977, Transport phenomena in hydrothermal systems: Cooling plutons: Am. Jour Sci., v. 277, p. 937–981.

Quinlan, J. J., and Simos, J. G., 1968, The Mayflower mine, in Park City district, Utah, *in* Erickson, A. J., ed., Guidebook no. 22: Geol. Soc. Utah, p. 40–55.

Robie, R. A., and Waldbaum, D. R., 1968, Thermodynamic properties of minerals and related substances at 298.15° K (25°C) and one atmosphere (10^5 bars) pressure and at higher temperatures: U. S. Geol. Survey Bull. 1259, 256 p.

Snow, D. T., 1968, Rock fracture spacings, openings, and porosities: Jour. Soil Mech. Foundations Div., Am. Soc. Civil Engineers, v. 94, p. 73–91.

—— 1970, The frequency and apertures of fractures in rocks: Internat. Jour. Rock Mech. Mining Sci., v. 7, p. 23–40.

Villas, R. N., 1975, Fracture analysis, hydrodynamic properties, and mineral abundance in altered igneous rocks at the Mayflower mine, Park City District, Utah: Unpub. Ph.D. thesis, Univ. Utah, 254 p.

Williams, N. C., 1952, Wall-rock alteration, Mayflower mine, Park City, Utah: Unpub. Ph.D. thesis, Columbia Univ., 58 p.

Wilson, J. C., 1961, Geology of the Alta stock, Utah: Unpub. Ph.D. thesis, California Inst. Technology, 236 p.

[AMERICAN JOURNAL OF SCIENCE, VOL. 277, OCTOBER, 1977, P..913-936]

American Journal of Science

OCTOBER 1977

TRANSPORT PHENOMENA IN HYDROTHERMAL SYSTEMS: THE NATURE OF POROSITY

D. NORTON and R. KNAPP

Department of Geosciences,
University of Arizona, Tucson, Arizona 85721

ABSTRACT. Porosity of rocks may be described by $\phi_{Total} = \phi_{Flow} + \phi_{Diffusion} + \phi_{Residual}$. Laboratory experiments indicate that total porosities of fractured rocks in hydrothermal systems range from 0.2 to 0.01, and diffusion porosities range from 10^{-3} to 10^{-6}. Synthesis of data from the literature and field observations of fracture characteristics indicate that flow porosities range from 10^{-4} to 10^{-6}. Therefore, the major portion of total porosity in pluton environments is due to residual pores not interconnected to either flow or diffusion porosity.

Permeability may be defined as a function of the abundance and geometry of continuous flow channels. Our observations suggest that a planar fracture model is a reasonable first order approximation for fractures in pluton environments. An analysis of aperture, abundance, and continuity indicates permeabilities on the order of 10^{-14} cm^2 may characterize large regions of the crust.

The proposed porosity model affords for the definition of the interface between circulating hydrothermal fluids and reactant minerals in a manner consistent with the physical phenomena and with the partial differential equations that describe advection-diffusion-reaction processes.

NOTATION

- A — area (cm^2)
- A_i — volumetric source of i^{th} component
- b — half the fracture aperture (cm)
- B — coordinate of fracture aperture (cm)
- d — fracture aperture (cm)
- D_{ik} — diffusion coefficient of the i^{th} ion due to a concentration gradient of the k^{th} ion (kgH_2O cm^{-1} sec^{-1})
- f — fracture frequency (cm fracture^{-1})
- F_D — fluid driving force (g cm sec^{-2})
- F_r — fluid resistive force (g cm sec^{-2})
- k — permeability (cm^2)
- l — unit length (cm)
- m_i — molality of the i^{th} component (moles kgH_2O^{-1})
- M_i — moles of the i^{th} component
- n — fracture abundance (fractures cm^{-2})
- Q — volumetric flow rate (cm^3 sec^{-1})
- S — surface area (cm^2)
- S_i — summation of component fluxes for the i^{th} ion (mols cm^{-2} sec^{-1})
- t — time (sec)
- $\bar{u}_i$ — flux of the i^{th} component (moles cm^{-2} sec^{-2})

$\bar{v}$ — fluid velocity (cm sec^{-1})
V — representative elemental volume (cm^3)
δ_c — width of concentration boundary layer (cm)
δ_o — width of laminar flow profile (cm)
η — viscosity (g cm^{-1} sec^{-1})
ν — viscosity (cm^2 sec^{-1})
ρ — fluid density (g cm^{-3})
ρ_β — bulk density (g cm^{-3})
ρ_γ — grain density (g cm^{-3})
σ — shear stress (g cm^{-1} sec^{-2})
τ — tortuosity of pores
ϕ_D — total diffusion porosity
ϕ_F — flow porosity
ϕ_R — residual porosity
ϕ_T — total porosity
ϕ'_D — equal to the directional diffusion porosity divided by τ
$\bar{\phi}$ — equal to ϕ'_D/ϕ_D
Ω — fluid potential (g cm^{-1} sec^{-2})
∇ — operator, $\frac{\partial}{\partial x} + \frac{\partial}{\partial y} + \frac{\partial}{\partial z}$ (cm^{-1})

INTRODUCTION

The interface between circulating aqueous solutions and reactant mineral phases is defined by the relative distribution of solution filled pores and minerals. This interface is a controlling factor in the chemical mass transfer that typically occurs between minerals and solutions in geochemical systems. Conceptual models that have been developed for the sedimentary rock environment (Fatt, 1956) neither adequately describe low total porosity and systematically developed fractures characteristic of igneous rocks nor do they account for the distribution of alteration minerals found in hydrothermal systems. Alteration minerals in hydrothermal systems occur both along and adjacent to continuous fractures. The compositions and assemblages of these minerals do not change over distances of meters to hundreds of meters parallel to the fractures, whereas abrupt changes occur normal to the fracture plane over distances of only millimeters to tens of centimeters. In rocks where the fracture sets are sufficiently close-spaced, the alteration zones may overlap, thereby producing a continuous zone of alteration products normal to the adjacent fractures. These aspects of mineral distributions suggest that the two principal modes of aqueous ion transport are by fluid flow along fractures and by aqueous diffusion away from the fractures.

The reaction between circulating fluids and their host rocks and the diffusion of aqueous ions to and away from flow channels may be described in terms of partial differential equations. Since the distribution of alteration mineral products predicted by the numerical solution to

these equations depends directly on the
porosity model was developed.

Porosity model.—The total porosit
represented by

$$\phi_T = \phi_F + \phi_D$$

ϕ_F is the effective flow porosity and repr
the dominant mode of fluid and aque
flow; ϕ_D is the diffusion porosity and
which the dominant mode of transpo
aqueous phase (Garrels, Dreyer, and H
porosity and represents those pores nc
geometry and distribution of these pore
crops (pl. 1) where one can readily obse
and less continuous sets, ϕ_D. These fi
laboratory measurements that define to
ity, suggest the porosity distribution in
schematically represented by figure 1.

TOTAL POROS

The total porosity of a rock is defined

$$\phi_T = 1 - \frac{\rho}{\rho}$$

where ρ_β is the dry rock bulk density o
mined by standard immersion techniqu
determined on a finely ground sample
minimum pore diameter. The porosity c
measure of the total pore volume in ro
porosity types. Partial or total saturation
introduce errors on the order of 2 percen
in the ≤ 0.05 porosity range.

FLOW POROSI

The flow porosity of fractured rocks i
that constitutes rock permeability. Conti
environments include planar features su
bedding planes in layered host rocks. A si
on open-smooth-walled fractures appears
proximation of permeability.

Fluid flow in natural systems is charac
which is the basis for development of
characteristics to rock permeability. Follc
Weist (1969), Snow (ms, 1970), and Maini (
volume, V, is chosen such that it contain
the x-y coordinate axis. A functional e
dimensional fluid velocity at any point in

these equations depends directly on the nature of porosity, the following porosity model was developed.

Porosity model.—The total porosity in fractured media, ϕ_T, may be represented by

$$\phi_T = \phi_F + \phi_D + \phi_R; \tag{1}$$

ϕ_F is the effective flow porosity and represents those pores through which the dominant mode of fluid and aqueous species transport is by fluid flow; ϕ_D is the diffusion porosity and represents those pores through which the dominant mode of transport is by diffusion through the aqueous phase (Garrels, Dreyer, and Howland, 1949); ϕ_R is the residual porosity and represents those pores not connected to ϕ_F or ϕ_D. The geometry and distribution of these pore types is apparent in many outcrops (pl. 1) where one can readily observe continuous fracture sets, ϕ_F, and less continuous sets, ϕ_D. These field observations, together with laboratory measurements that define total diffusion and residual porosity, suggest the porosity distribution in these types of outcrops can be schematically represented by figure 1.

TOTAL POROSITY

The total porosity of a rock is defined by

$$\phi_T = 1 - \frac{\rho_\beta}{\rho_\gamma} \tag{2}$$

where ρ_β is the dry rock bulk density of a representative sample determined by standard immersion techniques, and ρ_γ is the grain density, determined on a finely ground sample with a grain size less than the minimum pore diameter. The porosity determined in this manner is a measure of the total pore volume in rock, if the sample represents all porosity types. Partial or total saturation of the pores with fluid would introduce errors on the order of 2 percent of the total porosity for rocks in the ≤ 0.05 porosity range.

FLOW POROSITY

The flow porosity of fractured rocks is that portion of the total rock that constitutes rock permeability. Continuous pore features in pluton environments include planar features such as faults, joints, cracks, or bedding planes in layered host rocks. A simple flow porosity model based on open-smooth-walled fractures appears to be a reasonable first approximation of permeability.

Fluid flow in natural systems is characterized by laminar flow (fig. 2), which is the basis for development of equations that relate fracture characteristics to rock permeability. Following the formulations of De-Weist (1969), Snow (ms, 1970), and Maini (ms), a representative elemental volume, V, is chosen such that it contains a single fracture parallel to the x-y coordinate axis. A functional expression is derived for one-dimensional fluid velocity at any point in the fracture cross section from

PLATE 1

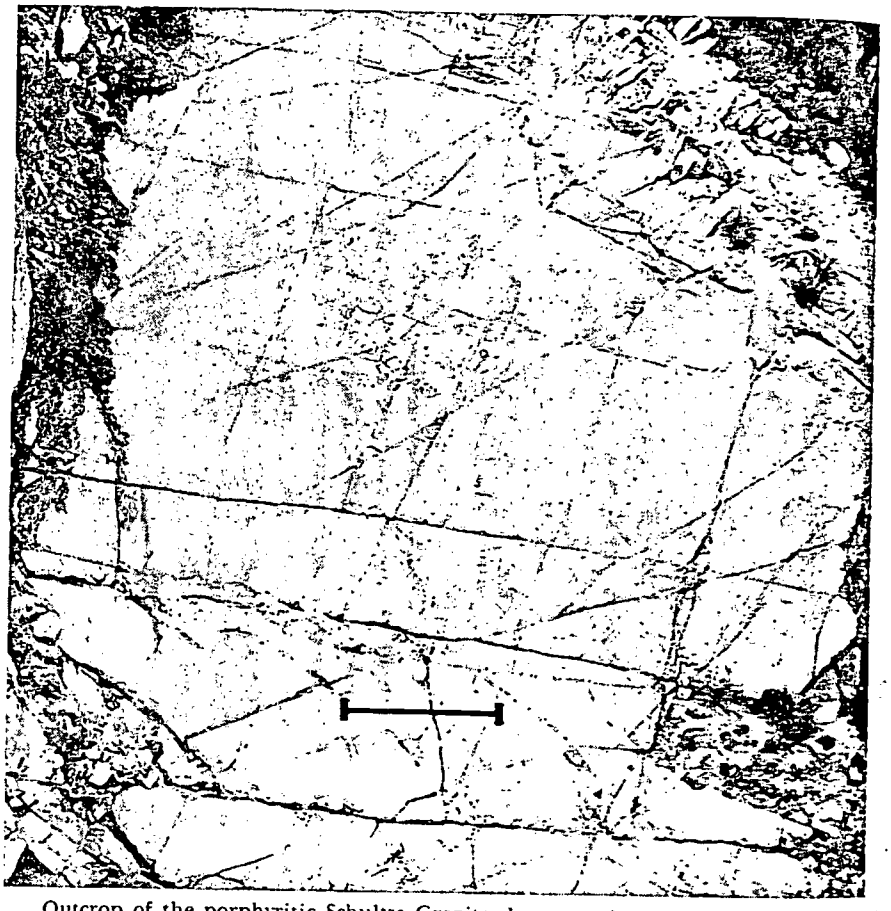

Outcrop of the porphyritic Schultze Granite demonstrating the geometry and distribution of flow and diffusion porosity. Continuous fractures, which cross cut outcrop, represent flow channels, and discontinuous fractures represent diffusion porosity. Scale bar is 5 m.

the differential equation describing the flow. This function is then used to find the mass flow along the fracture by integrating the velocity function over the fracture opening.

Steady state flow conditions require equality between the fluid driving force, F_d, and the resistive viscous force, F_r. The driving force is determined by the gradient in fluid potential and the area on which the force acts:

$$F_d = lA\nabla\Omega. \tag{3}$$

The resistive force is due to shear stress acting on the surface area, S, of the fracture walls:

$$F_r = \sigma S. \tag{4}$$

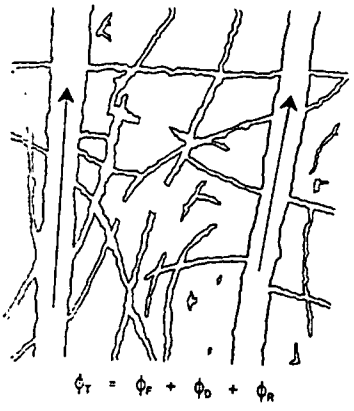

Fig. 1

Fig. 1. Schematic representation o
relationships between residual pores, ϕ
arrows denote an arbitrarily chosen dir
from these two flow channels either hav
cant fluid flow or are discontinuous; t
abundances are not shown.

Fig. 2. The laminar flow profile in
the walls. f is the fracture spacing and
of integration in eq (9).

where $S = 2l$, and l is the unit
volume. The shear stress in a visc
by:

$$\sigma =$$

where b = ½ fracture aperture (cn
force acts is orthogonal to the dire

$$A$$

Combining eqs (3-6), we have a
velocity and distance from the frac

$$d\bar{v} = -$$

Integrating eq (7) and evaluating t
when b = B gives the velocity p
fracture:

$$\bar{v} = \frac{\nabla}{2\eta}$$

This parabolic flow profile develop
for fluid velocities less than 10 cm/
subsequent discussions that this flow
systems.

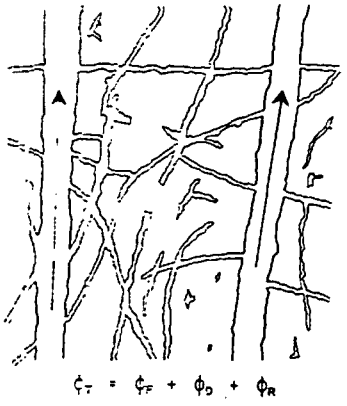

Fig. 1

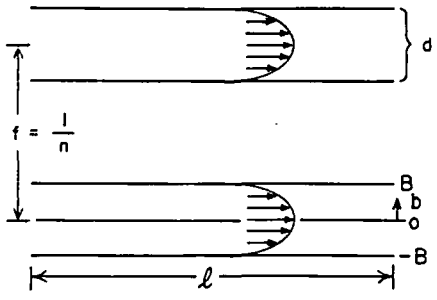

Fig. 2

Fig. 1. Schematic representation of constituent porosities showing the geometric relationships between residual pores, ϕ_R, diffusion pores, ϕ_D, and flow pores, ϕ_F. The arrows denote an arbitrarily chosen direction of fluid flow in ϕ_F. The pores extending from these two flow channels either have apertures that are too small to permit significant fluid flow or are discontinuous; therefore, all these pores are ϕ_D. The relative abundances are not shown.

Fig. 2. The laminar flow profile in planar fractures due to viscous drag forces at the walls. f is the fracture spacing and d the aperture. B and $-B$ represent the limits of integration in eq (9).

where $S = 2l$, and l is the unit length of the representative elemental volume. The shear stress in a viscous fluid is related to the fluid velocity by:

$$\sigma = -\eta \frac{d\bar{v}}{db}, \tag{5}$$

where $b = \frac{1}{2}$ fracture aperture (cm). The area on which the fluid driving force acts is orthogonal to the direction of flow in the fracture:

$$A = 2b \tag{6}$$

Combining eqs (3-6), we have a differential equation in terms of fluid velocity and distance from the fracture wall:

$$d\bar{v} = -b \frac{\nabla \Omega}{\eta} db. \tag{7}$$

Integrating eq (7) and evaluating the integration constant by using $\bar{v} = 0$ when $b = B$ gives the velocity profile across the aperture of a single fracture:

$$\bar{v} = \frac{\nabla \Omega}{2\eta} (B^2 - b^2). \tag{8}$$

This parabolic flow profile develops in less than 1 m along the fracture for fluid velocities less than 10 cm/sec, and we will, therefore, assume in subsequent discussions that this flow profile is fully developed in geologic systems.

The volumetric flow rate from a single fracture is defined by first considering the flow velocity through an incremental cross-sectional area of the fracture and then integrating this expression over the fracture opening orthogonal to the flow direction (fig. 2).

$$Q = \int_{-B}^{B} \frac{l \nabla \Omega}{2\eta} (B^2 - b^2)\, db. \tag{9}$$

Integrating eq (9) gives the flow rate,

$$Q = \frac{-2B^3 \nabla \Omega}{3\eta} \tag{10}$$

per unit length, l, of a single fracture. Substituting the aperture of the fracture into (10) gives the volume flow rate from n such parallel fractures

$$Q = \frac{-nd^3 \nabla \Omega}{12\eta}. \tag{11}$$

The general statement of Darcy's Law for flow through porous media is (Hubbert, 1940):

$$Q = \frac{-k \nabla \Omega}{\eta}, \tag{12}$$

and k is a factor describing the shape and length characteristics of the flow passages. By analogy of (12) to (11) we see this intrinsic rock parameter, permeability, for fracture controlled flow is:

$$k = \frac{nd^3}{12}. \tag{13}$$

Fracture sets in natural systems are not precisely represented by this model; however, anisotropic characteristics of the fractures may be formulated into a tensor form:

$$Q = -\frac{k_{ij}}{\eta} \nabla \Omega, \tag{14}$$

where k_{ij} is the permeability tensor in which the subscript i relates to the fluid flow direction, and j relates to the potential gradient direction.

The porosity of the flow channels is also related to the fracture aperture and abundance, where

$$\phi_F = nd \tag{15}$$

for a single parallel fracture set.

Field observations of abundance and aperture on parallel fracture sets, together with eq (13), permit permeability estimates to be made. Abundances of fractures in plutons vary from 0.5 fracture/cm in some ore deposits (Bingham, Utah) to 10^{-3} fractures/cm in unaltered igneous bodies (Villas, ms; Bianchi and Snow, 1969). Aperture variations, which

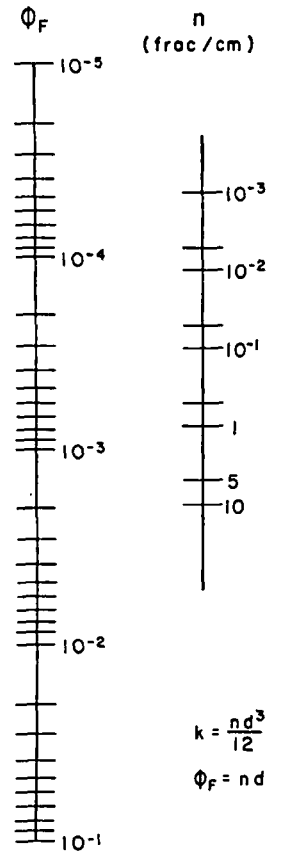

Fig. 3. Graphical solution to eqs (13) a
5×10^{-5} to 2×10^{-2} cm, whereas fractur
10^{-3}/cm. With $d = 10^{-4}$ cm and $n = 5 \times$
10^{-3} md where 10^{-11} cm^2 = 1 millidarcy.

have the greatest effect on permeabi
may range from 5×10^{-5} to $2 \times$
apertures and abundances are large
straints on the magnitude of flow po
to a single fracture set, compare eqs
tion (fig. 3). The maximum range in
10^{-8}. Values estimated by Villas (m
from 2×10^{-3} to 3×10^{-5}. The c
Mayflower diorite are in the range
porosity and the total porosity of the
10^{-2}, respectively (Pratt and others,
the flow porosities are generally a sn
even though precise limits can not b

Measurements of permeability b
nificantly different values. In genera

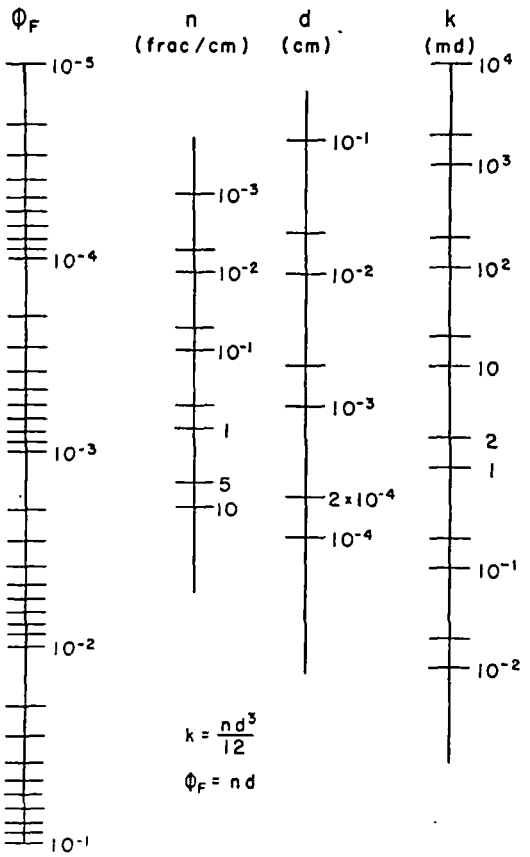

Fig. 3. Graphical solution to eqs (13) and (15). Aperture estimates, d, range from 5×10^{-5} to 2×10^{-2} cm, whereas fracture abundances, n, range from 5×10^{-1} to 10^{-3}/cm. With $d = 10^{-4}$ cm and $n = 5 \times 10^{-1}$/cm, $\phi_F = 5 \times 10^{-5}$ and $k = 4 \times 10^{-5}$ md where 10^{-12} cm^2 = 1 millidarcy.

have the greatest effect on permeability but are the least well known, may range from 5×10^{-5} to 2×10^{-2} cm. Though these ranges in apertures and abundances are large, they place some interesting constraints on the magnitude of flow porosity when examined with respect to a single fracture set, compare eqs 13 and 15 and their graphical solution (fig. 3). The maximum range in flow porosity is from 10^{-2} to 5×10^{-5}. Values estimated by Villas (ms) on the Mayflower Pluton range from 2×10^{-3} to 3×10^{-5}. The comparable total porosities for the Mayflower diorite are in the range of 0.01 to 0.03. Similarly, the flow porosity and the total porosity of the Sherman Granite are 5×10^{-6} and 10^{-2}, respectively (Pratt and others, 1974). We, therefore, conclude that the flow porosities are generally a small fraction of the total porosities, even though precise limits can not be established.

Measurements of permeability by different methods often yield significantly different values. In general, in-situ measurements of permea-

bility on large representative blocks of fractured rock indicate values in the range of 10^{-12} to 10^{-8} cm^2 (table 1). An in-situ experiment conducted on the Sherman Granite determined the permeability of this rock to be 10^{-11} cm^2, whereas the permeability determined on intact core samples is about 2 to 3 orders of magnitude lower. Laboratory measurements of intact core samples of limestones, dolomites, and granites (table 1) also indicate very low values of permeability. Clearly, the permeability of rocks in hydrothermal systems is a poorly known quantity.

Estimates of rock permeabilities in the Earth's crust rely on deep drill holes, 10 km in sedimentary basins and 4 to 5 km in crystalline rocks, abundance and aperture of continuous fractures, electrical resistivity profiles, elastic properties of intact rock samples, and seismic data. These various lines of indirect evidence suggest that permeabilities to depths of 10 to 15 km may be significantly greater than 10^{-14} cm^2. Whereas laboratory measurements indicate that a pressure increase from 1 bar to 1 kb produces a $10^{1.5}$ decrease in permeability (Brace, Walsh, and Frangos, 1968), seismic hypocentral data suggest that brittle rock failure and transient fractures occur at depths to at least 15 to 20 km. The persistence of continuous fractures filled with conductive pore fluids at considerable depths is further indicated by relatively high electrical conductivities in the middle to upper crust (Plauff, 1966; Jackson, 1966; Keller, Anderson, and Pritchard, 1966; and Brace, 1971).

The permeability of fractured crystalline rocks is due to continuous fractures, and, even though the rock mass between these channels has a

TABLE 1

Some permeability measurements on crystalline rocks

Rock type	k(cm^2)	ϕ_P	Method	Reference
Hardhat-granite	10^{-0}-10^{-12}		pump	Boardman and Skrey 1966
Sherman-granite	10^{-11}	2×10^{-5}	pump	Pratt and others, 19
Sherman-granite	$< 10^{-14}$		core	Pratt and others, 19
Quartz porphyry	$\sim 10^{-11}$		pump	Cadek and others, 19
Gneiss-schist	5×10^{-11}		pump test in fractured zone	Marine, 1966
Gneiss-schist	5×10^{-14}		pump (without fractures)	Marine, 1966
Gneiss-schist	10^{-15}		core	Marine, 1966
Metabasalt	2×10^{-6}		pump	Davis, 1969
Schist	1.4×10^{-6}		pump	Davis, 1969
Quartz diorite	10^{-7} to 3×10^{-10}	2×10^{-3} to 3×10^{-5}	planar fracture model	Villas, ms.
Granite	10^{-4} to 10^{-10}	5×10^{-2} to 4×10^{-5}	planar fracture model	Bianchi and Snow, 19
Welded tuff	$< 2\times10^{-16}$		pump	Winograd, 1971
Bedded tuff	10^{-10}-10^{-12}		pump	Winograd, 1971
Granite	10^{-14}-10^{-17}		core*	Brace, Walsh, and Frangos, 1968
Limestone	2×10^{-15}		disk	Ohle, 1951
Dolomite	10^{-10}		disk	Ohle, 1951
Volcanic (clastics)	10^{-8}-6×10^{-12}		drawn down	Grindley, 1965

* Measured as a function of effective pressure

relatively high total porosity, its effecti
is also evidenced by the above observa
drothermal alteration minerals along th
alteration minerals occur in veins in o
systems clearly demonstrates the nature
The widespread chemical alteration o
further attests to the relatively large pe
crust.

The importance of deducing broad
relates directly to studies of the mass m
the crust. Permeabilities greater than
circulation of fluids in pluton environ
regions of the crust (Norton and Knigh
in fractured igneous rocks, and possibly
apparently a small fraction of the total
true velocity of particles within a flow
magnitude greater than the superficial v

$$\bar{v}_{true} = \frac{\bar{v}_D}{\phi}$$

DIFFUSION PO

The nature of diffusion porosity is
region, R, within which the transport
flow is insignificant with respect to dif
tions may occur in regions characteri
small aperture fractures, or discontinuo
typically bounded by continuous sets o
flow channels in the overall system (fig.

The diffusional flux of the i^{th} ion f
flux vector normal to an incremental are

$$\bar{u}_i = -\phi'_D \sum_k D_i$$

where ϕ'_D is the ratio of the diffusion por
flux vector to the tortuosity, τ, of the p
the k^{th} ion in molality, and D_{ik} is the d
due to the gradient in concentration of t
ion leaving the region, with respect to th
integral of the divergence of $\bar{u}_i$,

$$\frac{\partial M_i}{\partial t} = \int_R \text{div}$$

whereas the change in the amount of
within the region as a function of time, i

$$\frac{\partial M_i}{\partial t} = \int_R \rho\phi_D (1 +$$

relatively high total porosity, its effective permeability is nil. This fact is also evidenced by the above observations and the distribution of hydrothermal alteration minerals along the walls of fractures. The fact that alteration minerals occur in veins in ore deposits and active geothermal systems clearly demonstrates the nature of fracture controlled fluid flow. The widespread chemical alteration of rocks in hydrothermal systems further attests to the relatively large permeability of rocks in the Earth's crust.

The importance of deducing broad scale permeabilities of the crust relates directly to studies of the mass movement of aqueous solutions in the crust. Permeabilities greater than 10^{-14} cm^2 are conducive to the circulation of fluids in pluton environments and perhaps over broader regions of the crust (Norton and Knight, 1977). Also, since flow porosity in fractured igneous rocks, and possibly in fractured rocks in general, is apparently a small fraction of the total rock porosity, 10^{-1} to 10^{-5}, the true velocity of particles within a flow fracture, eq (8), will be orders of magnitude greater than the superficial velocity.

$$\bar{v}_{true} = \frac{\bar{v}_{Darcy}}{\phi_F} \tag{16}$$

DIFFUSION POROSITY

The nature of diffusion porosity is apparent, if we consider a typical region, R, within which the transport of aqueous components by fluid flow is insignificant with respect to diffusional transport. These conditions may occur in regions characterized by discontinuous fractures, small aperture fractures, or discontinuous pores. This type of region is typically bounded by continuous sets of fractures which constitute the flow channels in the overall system (fig. 1).

The diffusional flux of the i^{th} ion from the region is defined by the flux vector normal to an incremental area of the region's surface, S,

$$\bar{u}_i = -\phi'_D \sum_k D_{ik} \nabla m_k \tag{17}$$

where ϕ'_D is the ratio of the diffusion porosity coincident with the normal flux vector to the tortuosity, τ, of the pores, m_k is the concentration of the k^{th} ion in molality, and D_{ik} is the diffusion coefficient of the i^{th} ion due to the gradient in concentration of the k^{th} ion. The amount of the i^{th} ion leaving the region, with respect to the volume, is given by the volume integral of the divergence of $\bar{u}_i$,

$$\frac{\partial M_i}{\partial t} = \int_R \text{div } \bar{u}_i dV, \tag{18}$$

whereas the change in the amount of the i^{th} aqueous ion contained within the region as a function of time, is given by,

$$\frac{\partial M_i}{\partial t} = \int_R \rho \phi_D (1 + A_i) \frac{\partial m_i}{\partial t} dV, \tag{19}$$

where ϕ_D is the total diffusion porosity, and A_i is a volumetric source or sink of the i^{th} ion which, in effect, describes the irreversible mass transfer between the aqueous and solid phases. The amount leaving and amount depleted must be equal; therefore, eqs (18) and (19) are equal. Since the integrals hold for any subregion in R, the integrals can be eliminated. Eqs (18) and (19) are combined to describe the conservation of the i^{th} aqueous species in R:

$$\rho\phi_D (1 + A_i) \frac{\partial m_i}{\partial t} = \nabla \cdot \phi'_D \sum_k D_{ik} \nabla m_k. \tag{20}$$

The magnitude and distribution of the directional diffusion porosity, ϕ'_D, as defined by eq (17), have been measured on a variety of rocks. The total diffusion porosity is determined by experiments where $A_i = 0$ and $k = 1$ and are calculated by rearranging (20).

$$\frac{\partial m_i}{\partial t} = \rho D_i \bar{\phi} \nabla^2 m_i, \tag{21}$$

where

$$\bar{\phi} = \frac{\phi'_D}{\phi_D} \tag{22}$$

Eq (21) is then solved numerically to yield $\bar{\phi}$, which substituted in eq (22) gives ϕ_D.

Experimental apparatus modified from Garrels, Dreyer, and Howland (1949) was used to obtain the diffusion porosity data (Knapp, ms). Rock wafers, 1.0 to 2.5 cm in radius and from about 0.2 to 1.0 cm thick, are embedded with epoxy in Plexiglas plugs, so that only the circular surfaces are exposed. The samples are then saturated by drawing 10^{-4} N KCl solution through the wafer for at least 24 hrs. Microscopic examination of the wafers serves to check the epoxy seal for leakage and the rock for any induced fractures.

The plug with the saturated rock is next placed in a Plexiglas diffusion cell; the cell is filled with a measured amount (usually 60 ml) of 10^{-4} N KCl solution, and electrodes are inserted into the cell. The entire assemblage is placed in a thermally insulated, 25°C, tank containing about 10 l of 1 N KCl solution, which sets up an activity gradient across the rock wafer. Care is taken to minimize any fluid potential gradient between the cell and the tank to a negligible value. The concentration change is monitored by conductometric methods.

The experimental error in these measurements is difficult to define precisely. But, based on ϕ'_D measured on adjacent samples of apparently homogeneous and isotropic rocks, the precision is between 4 and 30 percent (Knapp, ms). Though this upper limit is fairly large, it does not seriously affect the conclusions derived from the experimental data.

The results of experiments indicate that the diffusion porosity is on the order of 10^{-3} to 10^{-4} (fig. 4). Furthermore, the diffusion porosity is

a very small fraction of the total rock
Total rock porosities in the samples
(fig. 6).

Of all the rocks examined dur
volcanic rocks have the largest tota
and ϕ'_D values, from 10^{-2} to 10^{-3} (fi
have a fairly narrow range of total p
to less than 10^{-2}, whereas the ϕ'_D v

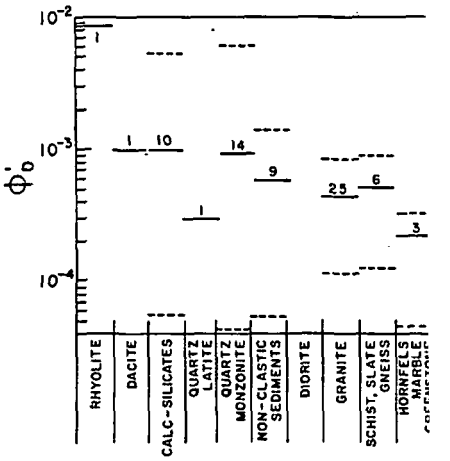

ROCK TYPE

Fig. 4

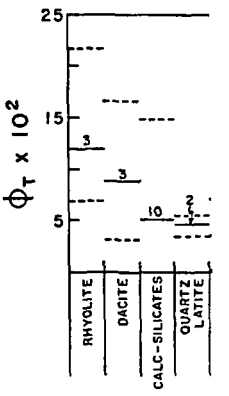

ROC

Fig

Fig. 4. Mean values, solid lines, and ra
various rock types examined in this stud
determinations for each rock type.

Fig. 5. The percentage of the total po
lines are mean values, and the dashed lin
denote the number of determinations for eac

Fig. 6. Total porosity values for the var
mean values, and the dashed lines the ra
number of determinations for each rock type

a very small fraction of the total rock porosity, since $\phi'_D \approx 0.04\ \phi_T$ (fig. 5). Total rock porosities in the samples studied amount to 10^{-2} to 2×10^{-1} (fig. 6).

Of all the rocks examined during this study (tables 2 and 3), the volcanic rocks have the largest total porosities, from 0.2 to 2×10^{-1}, and ϕ'_D values, from 10^{-2} to 10^{-3} (figs. 4 and 6). Carbonate rocks studied have a fairly narrow range of total porosity values, from about 5×10^{-2} to less than 10^{-2}, whereas the ϕ'_D values range from 10^{-3} to 10^{-4}. The

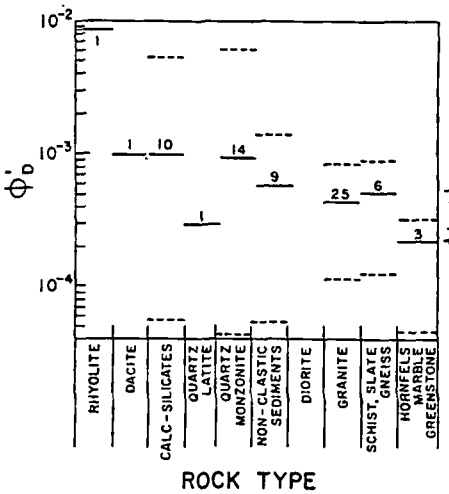

Fig. 4

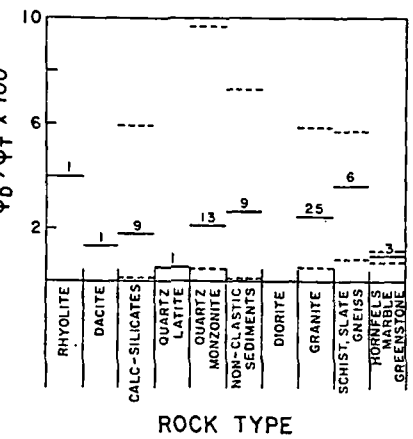

Fig. 5

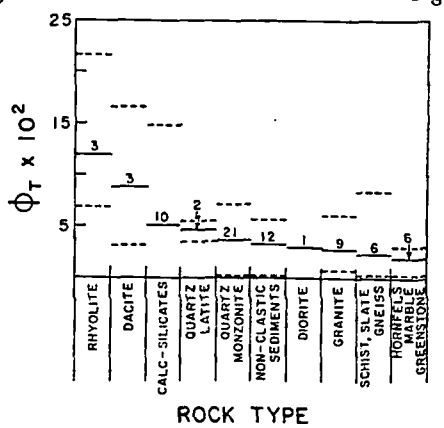

Fig. 6

Fig. 4. Mean values, solid lines, and range of values, dashed lines, of ϕ'_D for the various rock types examined in this study. The numerals denote the number of determinations for each rock type.

Fig. 5. The percentage of the total porosity that is composed of ϕ'_D. The solid lines are mean values, and the dashed lines are the range in values. The numerals denote the number of determinations for each rock type.

Fig. 6. Total porosity values for the various rock types studied. The solid lines are mean values, and the dashed lines the range in values. The numerals denote the number of determinations for each rock type.

TABLE 2

Density and porosity data

Sample no.	Bulk density ρ_B (g/cm³)	Grain density ρ_γ (g/cm³)	Total porosity $\phi_T \times 10^2$	$\phi'_D \times 10^4$	Sample thickness (cm)
Johnson Camp, Ariz.					
BQZ-5	2.61	2.72	4.11	8.1*	1.04
				13.7**	1.04
AL-007	2.68	2.74	2.12	5.5**	0.424
				1.5*	0.988
LA5	2.55	3.00	14.7	10.	0.90
AM-005	2.71	2.79	2.72	14.**	0.843
				2.*	0.800
AU-004	2.62	2.68	2.53		
ML-002	2.78	2.85	2.35		
MM-6	2.55	2.65	3.88		
MU-001	2.55	2.69	5.35		
ESC-3	2.64	2.71	2.62		
BP-4	2.60	2.70	3.85		
PS-1-JC	2.69	2.73	1.54	8.36**	0.925
				4.92*	0.964
Globe-Miami, Ariz.					
PS-1-GM	2.74	2.78	1.30		
Ronda, Spain					
R-71	2.74	2.76	.73	2.4*	0.386
R-80	2.77	2.80	1.07	3.3*	1.224
R-81	2.85	2.89	1.38	59.	1.29
R-125	2.72	2.97	8.42	7.1**	0.673
R-217	2.69	2.77	2.89	3.2	0.880
R-245	3.01	3.03	.660	3.7**	0.831
R-278	2.66	2.73	2.56	2.9	1.14
Chino, N.M.					
CS-1	2.69	2.97	9.43	7.5	1.05
CS-2	2.79	3.01	7.31	3.5	0.942
CS-4	2.75	2.83	2.83		
CS-5	4.25	4.67	8.99	58.	0.881
CS-6	3.01	3.12	3.53	9.7	1.33
CS-7	2.73	2.75	.73		
CS-8	3.18	3.24	1.85	7.0	1.19
CS-9	2.73	2.80	2.50	2.6	1.25
CS-10	2.72	2.73	.366	2.9	0.820
CS-11	2.64	2.71	2.58	4.1	1.02
CS-12	2.62	2.74	4.38	0.53	0.742
CS-13	2.49	2.67	6.74		
Chino pluton	2.62	2.69	2.60	10.	0.839
Silver City, N.M.					
Chino pc	2.97	2.99	.669	0.45	0.979
Cont. pit	2.91	3.03	3.96	0.54	0.949
150 pit	3.62	3.82	5.24	2.0	1.04
Copper Flat Pluton	2.48	2.62	5.34	2.9	0.857
San Manuel, Ariz.					
SM-1	2.71	2.75	1.46	1.1	1.04
SM-2	2.70	2.75	1.82	2.1	0.968
SM-3	2.71	2.87	5.58	4.1	1.02
SM-5	2.63	2.70	2.59	0.42	0.881
SM-7	2.45	2.63	6.84	11.	0.999
SM-8	2.57	2.70	4.82	8.3	0.958
SM-9	2.58	2.73	5.50	5.5	1.05

Sample no.	Bulk density ρ_B (g/cm³)
Butte, Mont.	
8	2.73
9A	3.04
10282-2	2.60
10282-1	2.65
1024-1	2.74
10283-1	2.73
Sierrita-Esperanza, Ariz.	
E-1	2.53
E-2	2.66
E-5	2.44
ST-1	2.57
ST-3	2.79
ST-6	2.64
Schultze Pluton, Globe-Miami, Ari	
SI BB	2.51
SPV	2.61
SD5	
5CM	
3A	
7CM	
2	
3	
4	
Bingham, Utah	
BGP	2.46
BQLP	2.58
BWR	2.44
Miscellaneous	
SG-1	2.52
LG-1	2.65
RM-1	2.16
TC-1	2.56
AG-1	2.60
TR-3	2.62
TR-5	2.46
TR-6	1.68
DAC	2.20

* Oriented perpendicular to foliati
** Oriented parallel to foliation or l

TABLE 2 (continued)

Sample no.	Bulk density ρ_β (g/cm³)	Grain density ρ_γ (g/cm³)	Total porosity $\phi_T \times 10^2$	$\phi'_n \times 10^4$	Sample thickness (cm)
Butte, Mont.					
8	2.73	2.91	6.35	61.	1.03
9A	3.04	3.22	5.41		
10282-2	2.60	2.71	3.77	8.4	1.18
10282-1	2.65	2.66	.0753	8.0	1.52
1024-1	2.74	2.77	1.55		
10283-1	2.73	2.76	1.01	2.4	1.12
Sierrita-Esperanza, Ariz.					
E-1	2.53	2.60	2.96		
E-2	2.66	2.71	1.96		
E-5	2.44	2.63	7.48		
ST-1	2.57	2.64	2.50		
ST-3	2.79	2.86	2.90		
ST-6	2.64	2.70	2.63	3.4	0.807
				1.1	1.27
Schultze Pluton, Globe-Miami, Ariz.					
S1 BB	2.51	2.65	5.35	3.9	0.840
SPV	2.61	2.66	1.77	4.8	1.0
				2.2	1.0
				8.3	0.507
SD5				16.0	0.144
				6.8	0.222
				6.1	0.280
5CM				5.2	0.481
3A				5.4	0.643
7CM				5.1	0.708
2				2.1	0.911
3				6.4	0.987
4				4.6	1.107
Bingham, Utah					
BGP	2.46	2.62	6.11	3.0	1.19
BQLP	2.58	2.65	2.64		
BWR	2.44	2.79	12.5	3.2	1.17
Miscellaneous					
SG-1	2.52	2.62	4.12		
LG-1	2.65	2.68	1.08	3.1	1.0
				2.0	1.0
RM-1	2.16	2.75	21.5	86.	0.888
TC-1	2.56	2.64	2.96		
AG-1	2.60	2.62	.611		
TR-3	2.62	2.65	1.36		
TR-5	2.46	2.66	7.52	9.9	1.09
TR-6	1.68	2.76	3.08		
DAC	2.26	2.61	15.7		

* Oriented perpendicular to foliation or bedding.
** Oriented parallel to foliation or bedding.

TABLE 3
Mineralogy of samples

Sample no.	Rock name	Mineralogy
Johnson Camp, Ariz.		
BQZ-5	Bolsa quartzite	quartz
AL-007	Lower Abrigo shale	clay, calcite
LA5	Lower Abrigo skarn	tremolite, muscovite, quartz, magnetite, hematite
AM-005	Middle Abrigo limestone	calcite, chert
AU-004	Upper Abrigo quartzite	quartz
AU-006	Upper Abrigo limestone	calcite, chert
ML-002	Lower Martin limestone	calcite
MM-6	Middle Martin limestone	calcite
MU-001	Upper Martin quartzite	quartz
ESC-3	Escabrosa marble	calcite
BP-4	Black Prince limestone	calcite
PS-1-JC	Pinal Schist	
Globe-Miami, Ariz.		
PS-1-GM	Pinal Schist	
Ronda, Spain		
R-71	slate	
R-80	biotite-garnet metapelite	andalusite, quartz, sericite, biotite, magnetite
R-81	quartzite	quartz, diopside, biotite, sphene, plagioclase, chlorite
R-125	pelitic schist	muscovite, tourmaline, andalusite, staurolite, quartz, biotite, garnet, plagioclase
R-217	hornfels	quartz, biotite, plagioclase, perthite, cordierite
R-245	granulite-grade gneiss	quartz, garnet, microperthite, plagioclase, sillimanite, biotite
R-278	hornfels	quartz, perthite, cordierite, plagioclase, biotite, sillimanite
Chino, N. Mex.		
CS-1	skarn	quartz, magnetite, pyrite, chalcopyrite
CS-2	skarn	quartz, sericite(?), biotite, magnetite, chlorite, pyrite, chalcopyrite
CS-3	skarn	quartz, andradite, magnetite, calcite, pyrite, chalcopyrite
CS-4	skarn	quartz, tremolite, magnetite, pyrite
CS-5	skarn	magnetite, quartz, pyrite, calcite
CS-6	skarn	amorphous silica, hematite, magnetite, calcite
CS-8	skarn	diopside, quartz, amorphous silica(?), calcite, magnetite
CS-9	skarn	quartz, calcite, diopside(?)
CS-10	Syrena limestone	calcite
CS-11	Upper Oswaldo limestone	calcite, quartz
CS-12	Lower Syrena limestone	calcite, quartz
CS-13	rhyolite subvolcanic	
Chino pluton	altered quartz monzonite porphyry	
Silver City, N. Mex.		
Chino pc	greenstone	
Cont. pit	skarn	quartz, andradite, magnetite, talc, sericite(?), pyrite, chalcopyrite, calcite
150 pit	skarn	andradite, quartz
Copper Flat pluton	quartz latite porphyry	

TABLE 3 (co

Sample no.	Rock name
San Manuel, Ariz.	
SM-1	porphyritic Oracle quartz monzonite, altered
SM-2	porphyritic Oracle quartz monzonite, altered
SM-3	porphyritic Oracle quartz monzonite, altered
SM-5	porphyritic Oracle quartz monzonite, altered
SM-7	quartz monzonite porphyry, altered
SM-8	quartz monzonite porphyry, altered
SM-9	porphyritic Oracle quartz monzonite, altered
Butte, Mont.	
8	sericitized Butte quartz monzonite
9A	sericitized Butte quartz monzonite
10282-2	argillized (white) Butte quartz monzonite
10282-1	argillized (green) Butte quartz monzonite
1024-1	altered Butte quartz monzonite
10283-1	fresh Butte quartz monzonite
Sierrita-Esperanza, Ariz.	
E-1	altered Esperanza quartz monzonite porphyry
E-2	altered Esperanza quartz monzonite porphyry
E-5	altered rhyolite
ST-1	altered quartz monzonite porphyry
ST-3	altered biotite quartz diorite
ST-6	altered Harris Ranch quartz monzonite
Schultze Pluton, Globe-Miami, Ariz.	
SI BB	altered porphyritic Schultze Granite
SPV	equigranular Schultze Granite

TABLE 3 (continued)

Sample no.	Rock name	Mineralogy
San Manuel, Ariz.		
SM-1	porphyritic Oracle quartz monzonite, altered	quartz, microcline, chlorite, biotite, plagioclase, hornblende, montmorillonite, epidote, hematite
SM-2	porphyritic Oracle quartz monzonite, altered	quartz, K-feldspar, plagioclase, chlorite, biotite, kaolinite, montmorillonite
SM-3	porphyritic Oracle quartz monzonite, altered	quartz, K-feldspar, sericite, kaolinite, biotite, plagioclase, pyrite, chlacopyrite, hematite
SM-5	porphyritic Oracle quartz monzonite, altered	quartz, K-feldspar, chlorite, plagioclase, sericite, pyrite, hematite, epidote
SM-7	quartz monzonite porphyry, altered	quartz, K-feldspar, plagioclase, chlorite, biotite, sericite, pyrite
SM-8	quartz monzonite porphyry, altered	quartz, sericite, chlorite, K-feldspar
SM-9	porphyritic Oracle quartz monzonite, altered	quartz, sericite, clay, plagioclase, microcline
Butte, Mont.		
8	sericitized Butte quartz monzonite	
9A	sericitized Butte quartz monzonite	with pyrite, chalcocite, enargite in vein
10282-2	argillized (white) Butte quartz monzonite	
10282-1	argillized (green) Butte quartz monzonite	quartz, potassium feldspar, plagioclase, biotite, hornblende, anhydrite
1024-1	altered Butte quartz monzonite	
10283-1	fresh Butte quartz monzonite	
Sierrita-Esperanza, Ariz.		
E-1	altered Esperanza quartz monzonite porphyry	quartz, plagioclase, K-feldspar, biotite, sericite, rutile, molybdenite, chalcopyrite
E-2	altered Esperanza quartz monzonite porphyry	quartz, plagioclase, K-feldspar, biotite, montmorillonite, pyrite, chalcopyrite, molybdenite
E-5	altered rhyolite	with quartz, hematite, sericite, pyrite
ST-1	altered quartz monzonite porphyry	quartz, K-feldspar, kaolinite, biotite, pyrite, chalcopyrite
ST-3	altered biotite quartz diorite	plagioclase, biotite, montmorillonite(?), chlorite, sericite, epidote, quartz
ST-6	altered Harris Ranch quartz monzonite	quartz, plagioclase, K-feldspar, hornblende, kaolinite, chlorite, biotite, calcite, pyrite, hematite
Schultze Pluton, Globe-Miami, Ariz.		
S1 BB	altered porphyritic Schultze Granite	quartz, K-feldspar, plagioclase, biotite, clays, muscovite, calcite, Cu oxides
SPV	equigranular Schultze Granite	quartz, K-feldspar, plagioclase, biotite, kaolinite, muscovite, clays

TABLE 3 (continued)

Sample no.	Rock name	Mineralogy
Porphyritic Schultze Granite, Globe-Miami, Ariz.		
SD5	porphyritic granite	
SD5	porphyritic granite	
SD5	porphyritic granite	
5CM	porphyritic granite	
3A	porphyritic granite	
7CM	porphyritic granite	
2	porphyritic granite	
3	porphyritic granite	
4	porphyritic granite	
Bingham, Utah		
BGP	Bingham granite porphyry	
BQLP	Bingham quartz latite porphyry	
BWR	Bingham latite dike	
Miscellaneous		
SG-1	Stronghold granite (Cochise's Stronghold, Ariz.)	
LG-1	Sherman granite (Laramie, Wyo.)	
RM-1	altered tuff (Red Mountain, Ariz.)	
TC-1	Texas Canyon granite (Texas Canyon, Ariz.)	quartz, K-feldspar, plagioclase, biotite, muscovite
AG-1	Amole granite (Tucson, Ariz.)	
TR-3	Troy granite (Troy, Ariz.)	
TR-5	rhyodacite dike (Troy, Ariz.)	
TR-6	dacite dike (Troy, Ariz.)	
DAC	dacite flow (Superior, Ariz.)	

plutonic rocks studied have a very uniform total porosity, with all values falling within several units of 4×10^{-2}. But, similar to the carbonate rocks, ϕ'_D varies greatly, between about 5×10^{-3} and 4×10^{-5}. The calc-silicate altered rocks have large values of both total and diffusion porosity, with ϕ_T between 1.5×10^{-1} and 3×10^{-3} and ϕ'_D between about 5×10^{-3} and 5×10^{-5}.

Many of the hydrothermally altered calc-silicate and plutonic rocks have significantly greater values for both total porosity and ϕ'_D than their unaltered equivalents (tables 2 and 3). The mean total porosity for the calc-silicates from Chino, N. M. is 4.6×10^{-2}, compared to 2.4×10^{-2} for their unaltered equivalents, and the mean ϕ'_D for these same rocks is $1.2\ 10^{-3}$ as compared to $2.4\ 10^{-4}$ for the unaltered equivalents. The altered rocks from Butte, Mont. also show this trend; the mean total porosity is 3.2×10^{-2}, compared to 1.1×10^{-2}, respectively, and the mean ϕ'_D is 2.6×10^{-3}, compared to 2.4×10^{-4} for unaltered equivalents.

Comparison of the hydrothe
Manuel and Sierrita-Esperan
Laramie, Wyoming and Tro
although samples SM-5, with
CS-7 (Chino, N.M.), with ϕ_T
this trend. It is interesting to
volume between hydrotherma
alents is due to a markedly
altered rocks (table 2). Since
large, porosity increase due to
residual pores is negligible; t
initial condition or subsequen

Total porosities for the i
from about 3×10^{-2} to less
from about $3.0\ 10^{-4}$ to abou
have a wider range in total
10^{-1} to less than 10^{-2} (table
foliation or bedding is signifi
a factor of about 2 to 7.

A consistent ratio betwee
is also apparent in the data.
estimated from rather simple m

The total diffusion poros
ϕ'_D determined above, eq (22),
steady state in the experiment
SM7, and a metapelite, 80, i
ponent of ϕ_D, that is, $\phi_D = 3\phi$

RES

Residual porosity, ϕ_R, is t
analysis of the flow and diffus
and ϕ_D amounts to a small f
10^{-1}. Therefore, residual poro

NA

Location, relative size dis
be determined by an analysis
(figs. 7 and 8) and direct obse
sive of flow porosity, is obtain

Values for ϕ'_r

Sample
AL007
AM005
PS-1-JC
BQZ

Comparison of the hydrothermally altered plutonic rocks from San Manuel and Sierrita-Esperanza, Ariz. with unaltered rocks from the Laramie, Wyoming and Troy, Ariz. plutons suggests a similar result, although samples SM-5, with $\phi'_D = 4.2 \times 10^{-5}$, (San Manuel, Ariz.), and CS-7 (Chino, N.M.), with $\phi_T = 7.3 \times 10^{-3}$, deviate significantly from this trend. It is interesting to note that the bulk of the difference in pore volume between hydrothermally altered rocks and their unaltered equivalents is due to a markedly larger value of residual porosity in the altered rocks (table 2). Since the mineral surface area:fluid ratio is very large, porosity increase due to irreversible chemical mass transfer in the residual pores is negligible; this larger value must be a result of either initial condition or subsequent modification of the initial porosity.

Total porosities for the isotropic metamorphic rocks studied range from about 3×10^{-2} to less than 10^{-2}; ϕ'_D for these same rocks varies from about $3.0\ 10^{-4}$ to about $4.5\ 10^{-5}$. The anisotropic rocks studied have a wider range in total porosity, with values ranging from about 10^{-1} to less than 10^{-2} (table 4). These values show that ϕ'_D parallel to foliation or bedding is significantly greater than that perpendicular, by a factor of about 2 to 7.

A consistent ratio between ϕ'_D and total porosity, that is, 4×10^{-2}, is also apparent in the data. This consistency suggests that ϕ'_D can be estimated from rather simple measurements of ϕ_T.

The total diffusion porosity, ϕ_D, may be computed from values of ϕ'_D determined above, eq (22), and the transient times required to attain steady state in the experiments. Values for an altered quartz monzonite, SM7, and a metapelite, 80, indicate that ϕ'_D is simply one axial component of ϕ_D, that is, $\phi_D = 3\phi'_D$.

RESIDUAL POROSITY

Residual porosity, ϕ_R, is the bulk of the total rock porosity since the analysis of the flow and diffusion porosity indicates that the sum of ϕ_F and ϕ_D amounts to a small fraction of the total porosity, for example, 10^{-1}. Therefore, residual porosity is $> 0.9\ \phi_T$ in fractured media.

NATURE OF PORES

Location, relative size distribution, and continuity of the pores can be determined by an analysis of porosity and mineral size distributions (figs. 7 and 8) and direct observation. The porosity distribution, exclusive of flow porosity, is obtained by measuring the density as a function

TABLE 4

Values for ϕ'_D by orientation of sample

Sample	Parallel	Perpendicular
AL007	5.40×10^{-4}	1.48×10^{-4}
AM005	13.9	2.01
PS-1-JC	8.86	4.92
BQZ	13.7	8.05

of crushed grain size. Intergranular porosity requires the density of the crushed aggregate and, hence, total measured porosity to increase as the size of the crushed grains decreases. As the crushed-grain size approaches a mineral-grain size a greater increase is expected. The contributions to porosity from pores around grains of various sizes can be calculated by using the density of the smallest grain in the interval as ρ_f in eq 2. Measurements of this type were made on samples of the equigranular and porphyritic Schultze Granite (figs. 7 and 8).

The correlation between mineral grain size and porosity distributions for the porphyritic Schultz Granite (fig. 7) indicates the pores occur between grains and that pore size is bimodally distributed. Mode I is composed almost wholly of pores with a maximum dimension greater than 4 mm, constituting 30 percent of the total pore volume. Mode II is composed of pores that have a maximum dimension less than 1 mm, constituting 70 percent of the pore volume. In mode I there is a large increase in pore volume (30 percent), as the crushed grain size approaches 4 mm. Because this size interval corresponds to the phenocryst size range, it can be concluded that this pore volume is located around the phenocrysts. The imperfect correlation between grain size and porosity in the size interval, 4 to 1 mm, can be interpreted to mean that there is very little pore volume located around the minerals in this size interval. Finally, the porosity distribution volume in mode II roughly mimics

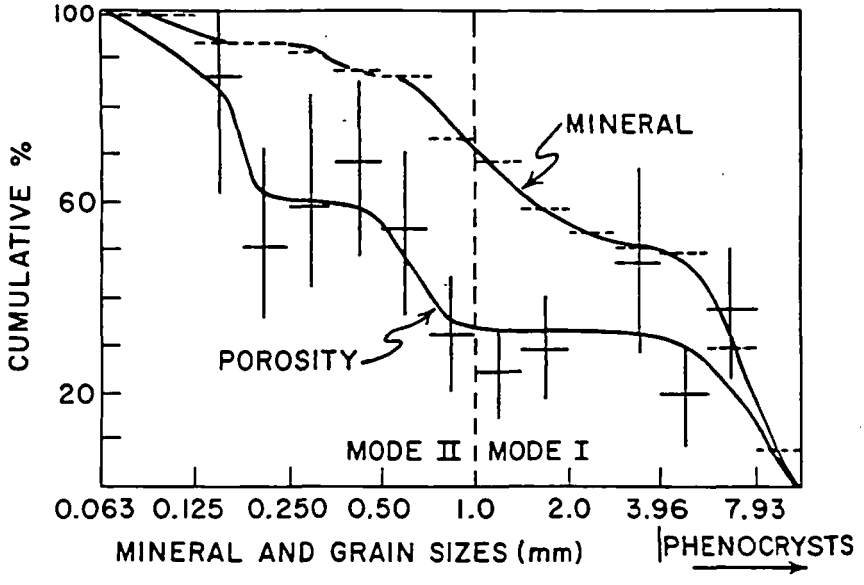

Fig. 7. Measurements of porphyritic Schultze Granite showing cumulative percentage of porosity as a function of crushed grain sizes. Horizontal bars are plotted at actual measured porosity values, with their length representing the precision of the crushed grain size measurement. Vertical bars represent the precision of the porosity measurement, also, cumulative percentage mineral sizes as a function of mineral size. Horizontal dashed lines represent precision for the size ranges.

the mineral distribution, again indic
around these minerals.

The intergranular nature of th
maximum dimension less than or eq
mension; that is, the more continuc
larger mineral sizes. The porosity an
in mode I also indicate that 30 perc
around the larger minerals, which a
the mineral surface area in the rock,
the pore volume is located around 30

The porosity and mineral distrib
Granite also shows there is one don
with mineral distribution (fig. 8). T
however, permits two conclusions ab
The larger pores are either intergran
mineral dimensions or elongate pores

The continuity of intergranular
Granite can be determined from ϕ
thicknesses (fig. 9). Large increases in
pores with a maximum dimension eq
data indicate a discontinuity at abou
correlative changes of porosity and

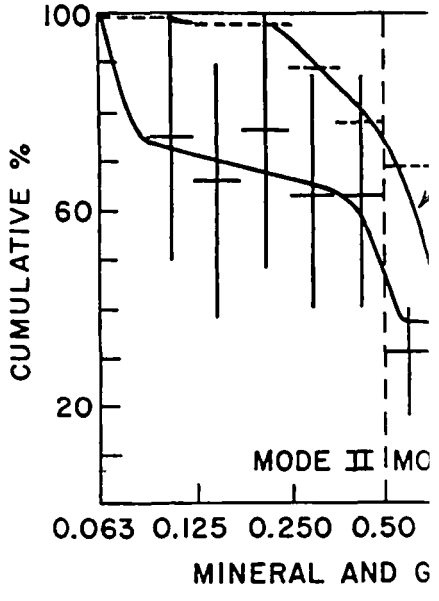

Fig. 8. Measurements on equigranular S
centage of porosity as a function of crushe
at actual measured porosity values, with thei
crushed grain size measurement. Vertical ba
measurement, also, cumulative percentage m
Horizontal dashed lines represent precision fo

the mineral distribution, again indicating that these pores are located around these minerals.

The intergranular nature of the pores implies that they have a maximum dimension less than or equal to their associated mineral dimension; that is, the more continuous pores are located around the larger mineral sizes. The porosity and mineral size distribution curves in mode I also indicate that 30 percent of the pore volume is located around the larger minerals, which at the most comprise 50 percent of the mineral surface area in the rock, whereas in mode II 70 percent of the pore volume is located around 30 percent of the minerals.

The porosity and mineral distribution for the equigranular Schultze Granite also shows there is one domain of porosity closely correlated with mineral distribution (fig. 8). The lack of correlation in mode I, however, permits two conclusions about pore location and continuity. The larger pores are either intergranular and less than or equal to the mineral dimensions or elongate pores that crosscut mineral boundaries.

The continuity of intergranular pores in the porphyritic Schultze Granite can be determined from ϕ'_D values for samples of varying thicknesses (fig. 9). Large increases in ϕ'_D indicate large abundances of pores with a maximum dimension equal to that sample thickness. These data indicate a discontinuity at about 8 mm, which is also suggested by correlative changes of porosity and mineral abundance distribution

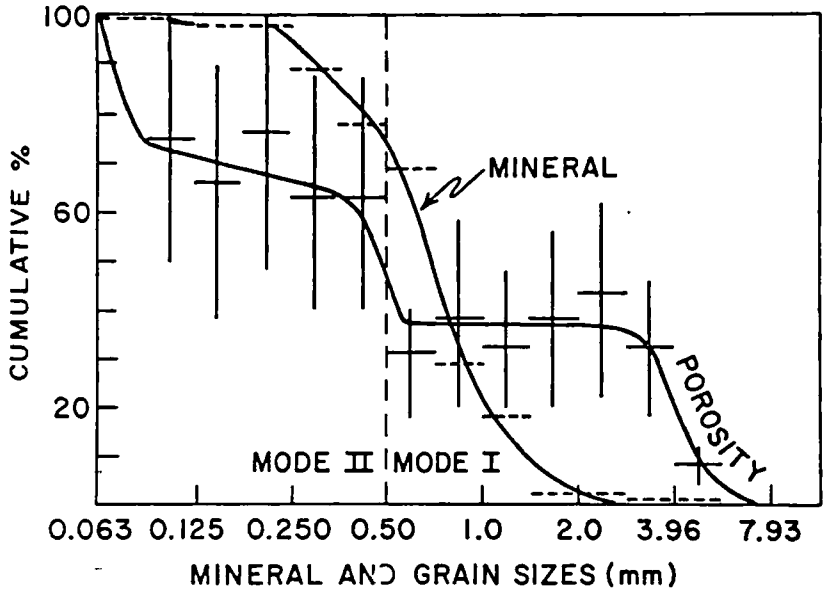

Fig. 8. Measurements on equigranular Schultze Granite showing cumulative percentage of porosity as a function of crushed grain sizes. Horizontal bars are plotted at actual measured porosity values, with their length representing the precision of the crushed grain size measurement. Vertical bars represent the precision of the porosity measurement, also, cumulative percentage mineral sizes as a function of mineral size. Horizontal dashed lines represent precision for the size ranges.

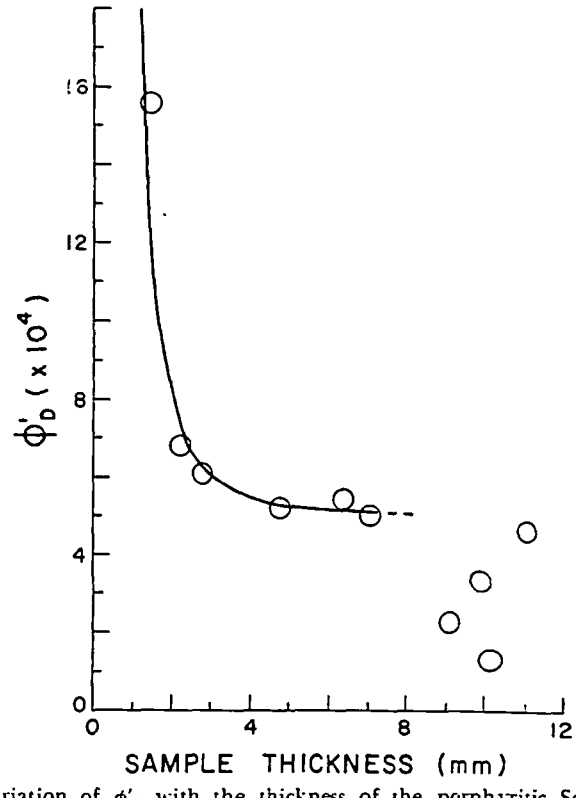

Fig. 9. Variation of ϕ'_D with the thickness of the porphyritic Schultze Granite samples used in diffusion experiment.

curves in mode I (fig. 7). This discontinuity indicates that there is a large abundance of pores with a maximum dimension of about 8 mm and that these more continuous pores are located around the phenocrysts.

The large increase in ϕ'_D at about 2 mm (fig. 9) indicates that the preponderance of pores have a maximum dimension less than this length. This increase of ϕ'_D approaches the value of the total porosity as the sample thickness approaches zero. Previous experiments determined (Garrels, Dreyer, and Howland, 1949) that $\phi'_D/\phi_T = 0.4$ for limestone samples 1 to 2 mm thick. These values are in general agreement with those reported in our study, if one assumes the relationship in figure 9 holds for a variety of rock types.

The geometry of discontinuous pores in fractured media may be classified into two broad categories, equidimensional pores and microcracks. Equidimensional pores vary from less than 1 mm to as great as 5 mm. This upper limit in size for equidimensional pores coincides with the large increase in the porosity distributions (figs. 7 and 8) and serves as partial confirmation of these curves. The pores composing this category have shapes that range from prismatic to highly irregular. Observed apertures of the microcracks range from less than 1 μm to no

PLATE

Scanning electron micrograph of an inter
Granite. This type of pore probably represents
or residual pores. The scale bar is 100 μm.

greater than 40 μm. Clearly, the small
the bulk of the pore volume to be compo
suggested intergranular nature of the
above observations, since the equidimen
around grain boundaries (pl. 2).

In summary, the above data sugg
for fractured igneous rocks consists of
and cylindrical pores, ϕ_D (fig. 10).

ADVECTION–REACTI

Porosity data define the distribu
systems. This information permits forr
differential equations for the advection
cies in a hydrothermal system.

The actual paths described by ci
around cooling intrusive bodies are def

$$\frac{dx}{\bar{v}_x} = \frac{dz}{\bar{v}_z}$$

PLATE 2

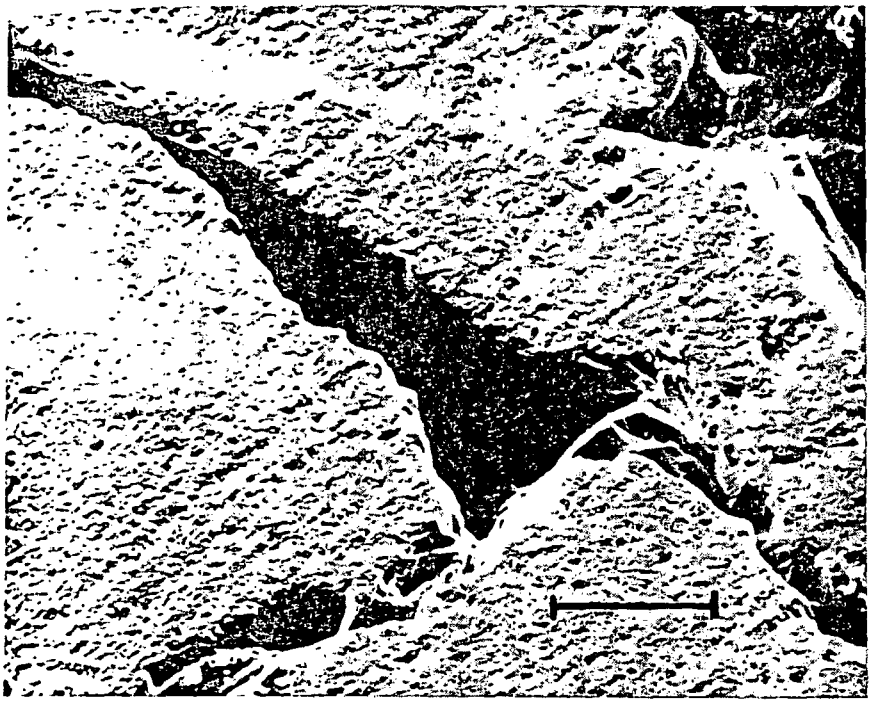

Scanning electron micrograph of an intergranular-prismatic pore in the Sherman Granite. This type of pore probably represents the geometry and size of diffusion and/or residual pores. The scale bar is 100 μm.

greater than 40 μm. Clearly, the small values for the apertures require the bulk of the pore volume to be composed of equidimensional pores. The suggested intergranular nature of the pores is also supported by the above observations, since the equidimensional pores are clearly distributed around grain boundaries (pl. 2).

In summary, the above data suggest that a general porosity model for fractured igneous rocks consists of continuous planar fractures, ϕ_F, and cylindrical pores, ϕ_D (fig. 10).

ADVECTION–REACTION–DIFFUSION

Porosity data define the distribution of fluids in hydrothermal systems. This information permits formulation of the governing partial differential equations for the advection-diffusion-reaction of aqueous species in a hydrothermal system.

The actual paths described by circulating packets of fluid in and around cooling intrusive bodies are defined in two dimensions by

$$\frac{dx}{\bar{v}_x} = \frac{dz}{\bar{v}_z} = dt, \tag{23}$$

where $\bar{v}_x$ and $\bar{v}_z$ are the component velocities. Examples of these pathlines in hydrothermal systems are presented in Norton and Knight, 1977. Fluids circulating along pathlines flow from one chemical environment into another, which results in differences in fluid compositions between those fluids in the flow porosity and those in the diffusion porosity, as well as disequilibrium between fluids and mineral phases. The transfer of heat between circulating fluid and rock may cause further disequilibrium within a rock volume. The mass transfer resulting from this disequilibrium occurs within flow porosity and diffusion porosity.

Advective transport depends directly on the magnitude of the flow velocities in ϕ_F. For flow velocities normally realized in these systems, a parabolic flow profile develops in less than a meter along the fracture and is effective over a thickness equal to half the fracture aperture (fig. 10). The true velocity in the fracture varies from zero at the wall of the fracture to an average value, defined by

$$\bar{v}_t = \frac{\bar{v}_{Darcy}}{\phi_{flow}}. \tag{24}$$

Therefore, the advective flux of the i^{th} ion is

$$\bar{u}_i = \bar{v}_t m_i \phi_F \rho. \tag{25}$$

The diffusional flux within ϕ_F parallel to the flow direction and across a concentration boundary layer, δ_c, follows from eq (17) with the substitution of ϕ_F for ϕ_D.

$$\bar{u}_{iF} = -\phi_F \sum_k D_{ik} \nabla_{xy} m_k. \tag{26}$$

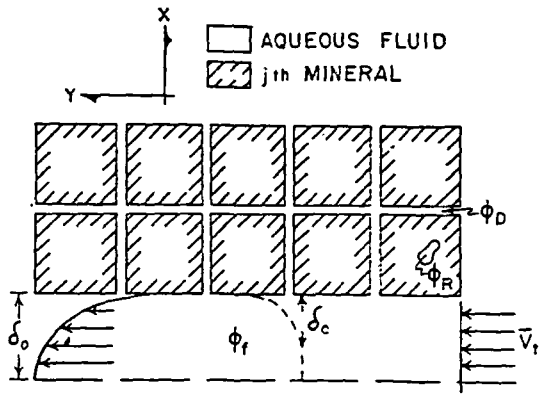

Fig. 10. Schematic two-dimensional porosity model for homogenous and isotropic ϕ_D. The model represents a possible geometric distribution of pores with respect to discrete minerals and is consistent with data collected in this study. In particular, we note that diffusion pores, ϕ_D, occur along each mineral grain boundary and interconnect with continuous fractures, ϕ_F. Although the relative abundance of the porosity types is not represented in this schematic representation, typical values for the porosity parameter are $\phi_D = 2 \times 10^{-4}$, $\phi'_D = 3\phi_D$, $\tau = 1$, diffusion pore radius of 10^{-6} cm and mineral sizes of 0.14 cm. The model and values are a first order approximation of pore geometry in fractured rocks.

in hydrothermal

As discussed previously,
port mechanism within the d

$$\bar{u}_{iD} =$$

The total flux of the i^{th} ion
obtained by summing the ad
porosity domain and the d
domain (eqs 25, 26, and 27).

$$\bar{S}_i$$

An expression for the total
transport can be obtained by

$$M_i = \int_R \rho ($$

The amount of the i^{th} ion los
the divergence of $\bar{S}_i$,

and must be equal to the rat
time derivative of eq (29). In
bining the time derivative of
partial differential equation

$$\rho (\phi_F + \phi_D) (A_i + 1) \frac{\partial m_i}{\partial t} + ($$

Eq (31), together with t
fluid flow in pluton environ
through reactive host rocks.
from previously derived equ
appropriate porosity values i
total rock porosity, which
since we found ϕ_T is as large
$(\phi_D + \phi_F)$.

AC

This research was supp
EAR74-03515-A01 and the U
Timothy Loomis, Mr. Bill E
University of Arizona chapte
donating samples and rock d
of this study. We also wish t
the manuscript.

As discussed previously, aqueous diffusion is the dominant transport mechanism within the diffusion pores and is defined by

$$\bar{u}_{iD} = -\phi'_D \sum_k D_{ik} \nabla_{xy} m_k. \tag{27}$$

The total flux of the i^{th} ion from the representative region, R, can be obtained by summing the advective and diffusive fluxes within the flow porosity domain and the diffusive flux within the diffusion porosity domain (eqs 25, 26, and 27).

$$\bar{S}_i = \bar{u}_i + \bar{u}_{iF} + \bar{u}_{iD}. \tag{28}$$

An expression for the total amount of the i^{th} ion in R available for transport can be obtained by modifying eq (19) to read

$$M_i = \int_R \rho (\phi_F + \phi_D) (m_i + A_i m_i) \, dV. \tag{29}$$

The amount of the i^{th} ion loss from R is equal to the volume integral of the divergence of $\bar{S}_i$,

$$-\int_R \operatorname{div} \bar{S}_i \, dV, \tag{30}$$

and must be equal to the rate of depletion of the ion in R, that is, the time derivative of eq (29). Introducing a conservation of mass and combining the time derivative of eqs (29) and (30) results in the governing partial differential equation for conservation of the i^{th} aqueous species:

$$\rho (\phi_F + \phi_D) (A_i + 1) \frac{\partial m_i}{\partial t} + \rho \bar{v}_t \phi_F \nabla m_i = \nabla D_{ik} \phi_F \nabla m_k + \nabla D_{ik} \phi'_D \nabla m_k. \tag{31}$$

Eq (31), together with the partial differential equations describing fluid flow in pluton environments, accounts for the circulation of fluids through reactive host rocks. This formulation is fundamentally different from previously derived equations in that it explicitly affords for the appropriate porosity values in fractured rocks. Other formulations utilize total rock porosity, which may produce significantly different results since we found ϕ_T is as large as several orders of magnitude greater than $(\phi_D + \phi_F)$.

ACKNOWLEDGMENTS

This research was supported by NSF Grant nos. GA-41136 and EAR74-03515-A01 and the University of Arizona. We wish to thank Dr. Timothy Loomis, Mr. Bill Baltosser, Bear Creek Mining Company, the University of Arizona chapter of SGE, and the Anaconda Company for donating samples and rock descriptions which greatly enhanced the scope of this study. We also wish to thank Lynn McLean for improvements in the manuscript.

REFERENCES

Bianchi, L., and Snow, D. T., 1969, Permeability of crystalline rocks interpreted from measured orientations and apertures of fractures: Jodphur, Rajasthan, Arid Zone Research Assoc. of India, Annals of Arid Zone, v. 8, no. 2, p. 231-245.

Boardman, C. R., and Skrove, J., 1966, Distribution in fracture permeability of a granitic rock mass following a contained nuclear explosion: Jour. Petroleum Technology, v. 18, p. 619-623.

Brace, W. F., Walsh, J. B., and Frangos, W. T., 1968, Permeability of granite under high pressure: Jour. Geophys. Research, v. 73, p. 2225-2236.

Brace, W. F., 1971, Resistivity of saturated crustal rocks to 40 km based on laboratory measurements, *in* Heacock, J. G., ed., The structure and physical properties of the Earth's crust: Am. Geophys. Union, Geophys. Mon. Ser., v. 14, p. 243-255.

Cadek, J., Hazdrova, M., Kacura, G., Krasny, J., and Malkovsky, M., 1968, Hydrogeology of the thermal waters at Teplice and Usti nad Labem: Sbornik Geol. Ved, Hydrogeol., Inzenyrska Geol., rada HIG, sv. 6, p. 1-184.

Davis, S. N., 1969, Porosity and permeability of natural materials. *in* DeWiest, R. J. M., ed., Flow through porous media: New York, Acad. Press, p. 54-90.

DeWiest, R. J. M., 1965, Geohydrology: New York, John Wiley & Sons, Inc., 366 p.

Fatt, I., 1956, The network model of porous media: Am. Inst. Mining Engineers, Petroleum Trans., v. 207, p. 141-181.

Garrels, R. M., Dreyer, Z. M., and Howland, D. L., 1949, Diffusion of ions through intergranular spaces in water saturated rocks: Geol. Soc. America Bull., v. 60, p. 1809-1828.

Grindley, G. W., 1965, The geology, structure, and exploitation of the Wairakei geothermal field: Taupo, New Zealand: Wellington, New Zealand Geol. Survey, 131 p.

Hubbert, M. K., 1940, The theory of ground-water motion: Jour. Geology, v. 48, p. 785-944.

Jackson, D. B., 1966, Deep resistivity probes in the southwestern United States: Geophysics, v. 31, p. 1123-1144.

Keller, G. V., Anderson, L. A., and Pritchard, J. I., 1966, Geological survey investigations of the electrical properties of the crust and upper mantle: Geophysics, v. 31, p. 1078-1087.

Knapp, R. B., ms, 1975, An analysis of the porosities of fractured crystalline rocks: M.S. thesis, Univ. Arizona, 90 p.

Maini, Y. N. T., ms., 1971, In situ hydraulic parameters in jointed rock—their measurement and interpretation: Ph.D. dissert., Univ. London, 312 p.

Marine, I. W., 1966, Hydraulic correlation of fracture zones in buried crystalline rock at the Savannah River plant, near Aiken, South Carolina: U.S. Geol. Survey Prof. Paper 550-D, p. 223-227.

Norton, D. L., and Knight, J. E., 1977, Transport phenomena in hydrothermal systems: cooling plutons: Am. Jour. Sci., v. 277, p. 937-981.

Ohle, E. L., 1951, The influence of permeability on ore distribution in limestone and dolomite: Econ. Geology, v. 46, p. 667-706.

Plauff, D., 1966, Magneto-telluric soundings in the southwestern United States: Geophysics, v. 31, p. 1145-1152.

Pratt, H. R., Black, A. D., Brace, W. F., and Norton, D. L., 1974, In situ joint permeability in a granite: EOS, Am. Geophys. Union Trans., v. 55, p. 433.

Snow, D. T., ms, 1965, A parallel plate model of fractured permeable media: Ph.D. dissert., Univ. California, Berkeley, 331 p.

———— 1970, The frequency and apertures of fractures in rock: Internat. Jour. Rock Mechanics Min. Sci., v. 7, p. 23-40.

Villas, R. N., ms., 1975, Fracture analysis, hydrodynamic properties and mineral abundance in altered igneous wall rocks of the Mayflower mine, Park City district, Utah: Ph.D. dissert., Univ. Utah, Salt Lake City, 253 p.

Winograd, I. J., 1971, Hydrogeology of ash flow tuff: a preliminary statement: Water Resources Research, v. 7, p. 994-1006.

[AMERICAN JOURNAL OF SCIENCE, VOL

TRANSPORT PHENOMEN. SYSTEMS: COOLI

D. NORTON an

Department of Geosciences, University

ABSTRACT. The nature of heat and ma been described by partial differential equatic mations to these equations. A series of heuris equations describes the general features of f trusive igneous body within the upper 10 k

Analysis of these models indicates that quence of the emplacement of magmas in circulation generates convective heat fluxes fluxes when host rock permeabilities exceed pluton are not significantly shortened unless cm^2. The geometries of fluid circulation and tions in pluton size, width, level of emplac distribution of permeable zones in the host r of the fluid properties on heat and mass tra tion is effectively controlled by coincident n of expansion and heat capacity with the vis of the H_2O–system.

Waters in natural pluton systems are pre to positions several kilometers away in a fe bution affects magmatic fluids and fluids in from the pluton. Typically, temperature ar paths produce dramatic changes in solvent actions along the pathlines should generate in isotopic compositions. Average fluid:rock entire permeable portions of the systems.

This analysis reveals the extent of fluid heat flux over broad crustal regions and alo activity is voluminous may be much greater

INTRODU

Heat and mass transport process of magmas into the Earth's crust are in their studies of igneous and volca perature and pressure conditions wi the basis of conductive heat flow, m to modern environments. In particu paths of igneous melt systems are inf experimentally derived phase diagran understanding of the nature of the but they require a considerable ex from a rather complex process.

Magmatic processes may be desc relate all relevant variables in a set tions. Such a description is appealin analysis that is independent of tra sideration of the process at the crust

Emplacement of magma bodies i thermal perturbations which are d conduction and fluid circulation. Ge

[American Journal of Science, Vol. 277, October, 1977, P. 913-936]

American Journal of Science

OCTOBER 1977

TRANSPORT PHENOMENA IN HYDROTHERMAL SYSTEMS: THE NATURE OF POROSITY

D. NORTON and R. KNAPP

Department of Geosciences,
University of Arizona, Tucson, Arizona 85721

ABSTRACT. Porosity of rocks may be described by $\phi_{Total} = \phi_{Flow} + \phi_{Diffusion} + \phi_{Residual}$. Laboratory experiments indicate that total porosities of fractured rocks in hydrothermal systems range from 0.2 to 0.01, and diffusion porosities range from 10^{-3} to 10^{-5}. Synthesis of data from the literature and field observations of fracture characteristics indicate that flow porosities range from 10^{-3} to 10^{-6}. Therefore, the major portion of total porosity in pluton environments is due to residual pores not interconnected to either flow or diffusion porosity.

Permeability may be defined as a function of the abundance and geometry of continuous flow channels. Our observations suggest that a planar fracture model is a reasonable first order approximation for fractures in pluton environments. An analysis of aperture, abundance, and continuity indicates permeabilities on the order of 10^{-14} cm^2 may characterize large regions of the crust.

The proposed porosity model affords for the definition of the interface between circulating hydrothermal fluids and reactant minerals in a manner consistent with the physical phenomena and with the partial differential equations that describe advection-diffusion-reaction processes.

Notation

A — area (cm^2)
A_i — volumetric source of ith component
b — half the fracture aperture (cm)
B — coordinate of fracture aperture (cm)
d — fracture aperture (cm)
D_{ik} — diffusion coefficient of the ith ion due to a concentration gradient of the kth ion (kgH_2O cm^{-1} sec^{-1})
f — fracture frequency (cm fracture^{-1})
F_D — fluid driving force (g cm sec^{-2})
F_r — fluid resistive force (g cm sec^{-2})
k — permeability (cm^2)
l — unit length (cm)
m_i — molality of the ith component (moles kgH_2O^{-1})
M_i — moles of the ith component
n — fracture abundance (fractures cm^{-1})
Q — volumetric flow rate (cm^3 sec^{-1})
S — surface area (cm^2)
$\bar{S}_i$ — summation of component fluxes for the ith ion (mols cm^{-2} sec^{-1})
t — time (sec)
$\hat{u}_i$ — flux of the ith component (moles cm^{-2} sec^{-1})

$\bar{v}$ — fluid velocity (cm sec^{-1})
V — representative elemental volume (cm^3)
δ_c — width of concentration boundary layer (cm)
δ_v — width of laminar flow profile (cm)
η — viscosity (g cm^{-1} sec^{-1})
ν — viscosity (cm^2 sec^{-1})
ρ — fluid density (g cm^{-3})
ρ_β — bulk density (g cm^{-3})
ρ_γ — grain density (g cm^{-3})
σ — shear stress (g cm^{-1} sec^{-2})
τ — tortuosity of pores
ϕ_D — total diffusion porosity
ϕ_F — flow porosity
ϕ_R — residual porosity
ϕ_T — total porosity
ϕ'_D — equal to the directional diffusion porosity divided by τ
$\bar{\phi}$ — equal to ϕ'_D/ϕ_D
Ω — fluid potential (g cm^{-1} sec^{-2})
∇ — operator, $\frac{\partial}{\partial x} + \frac{\partial}{\partial y} + \frac{\partial}{\partial z}$ (cm^{-1})

INTRODUCTION

The interface between circulating aqueous solutions and reactant mineral phases is defined by the relative distribution of solution filled pores and minerals. This interface is a controlling factor in the chemical mass transfer that typically occurs between minerals and solutions in geochemical systems. Conceptual models that have been developed for the sedimentary rock environment (Fatt, 1956) neither adequately describe low total porosity and systematically developed fractures characteristic of igneous rocks nor do they account for the distribution of alteration minerals found in hydrothermal systems. Alteration minerals in hydrothermal systems occur both along and adjacent to continuous fractures. The compositions and assemblages of these minerals do not change over distances of meters to hundreds of meters parallel to the fractures, whereas abrupt changes occur normal to the fracture plane over distances of only millimeters to tens of centimeters. In rocks where the fracture sets are sufficiently close-spaced, the alteration zones may overlap, thereby producing a continuous zone of alteration products normal to the adjacent fractures. These aspects of mineral distributions suggest that the two principal modes of aqueous ion transport are by fluid flow along fractures and by aqueous diffusion away from the fractures.

The reaction between circulating fluids and their host rocks and the diffusion of aqueous ions to and away from flow channels may be described in terms of partial differential equations. Since the distribution of alteration mineral products predicted by the numerical solution to

these equations depends directly on the nature of porosity, the following porosity model was developed.

Porosity model.—The total porosity in fractured media, ϕ_T, may be represented by

$$\phi_T = \phi_F + \phi_D + \phi_R; \tag{1}$$

ϕ_F is the effective flow porosity and represents those pores through which the dominant mode of fluid and aqueous species transport is by fluid flow; ϕ_D is the diffusion porosity and represents those pores through which the dominant mode of transport is by diffusion through the aqueous phase (Garrels, Dreyer, and Howland, 1949); ϕ_R is the residual porosity and represents those pores not connected to ϕ_F or ϕ_D. The geometry and distribution of these pore types is apparent in many outcrops (pl. 1) where one can readily observe continuous fracture sets, ϕ_F, and less continuous sets, ϕ_D. These field observations, together with laboratory measurements that define total diffusion and residual porosity, suggest the porosity distribution in these types of outcrops can be schematically represented by figure 1.

TOTAL POROSITY

The total porosity of a rock is defined by

$$\phi_T = 1 - \frac{\rho_\beta}{\rho_\gamma} \tag{2}$$

where ρ_β is the dry rock bulk density of a representative sample determined by standard immersion techniques, and ρ_γ is the grain density, determined on a finely ground sample with a grain size less than the minimum pore diameter. The porosity determined in this manner is a measure of the total pore volume in rock, if the sample represents all porosity types. Partial or total saturation of the pores with fluid would introduce errors on the order of 2 percent of the total porosity for rocks in the ≤ 0.05 porosity range.

FLOW POROSITY

The flow porosity of fractured rocks is that portion of the total rock that constitutes rock permeability. Continuous pore features in pluton environments include planar features such as faults, joints, cracks, or bedding planes in layered host rocks. A simple flow porosity model based on open-smooth-walled fractures appears to be a reasonable first approximation of permeability.

Fluid flow in natural systems is characterized by laminar flow (fig. 2), which is the basis for development of equations that relate fracture characteristics to rock permeability. Following the formulations of DeWeist (1969), Snow (ms, 1970), and Maini (ms), a representative elemental volume, V, is chosen such that it contains a single fracture parallel to the x-y coordinate axis. A functional expression is derived for one-dimensional fluid velocity at any point in the fracture cross section from

PLATE I

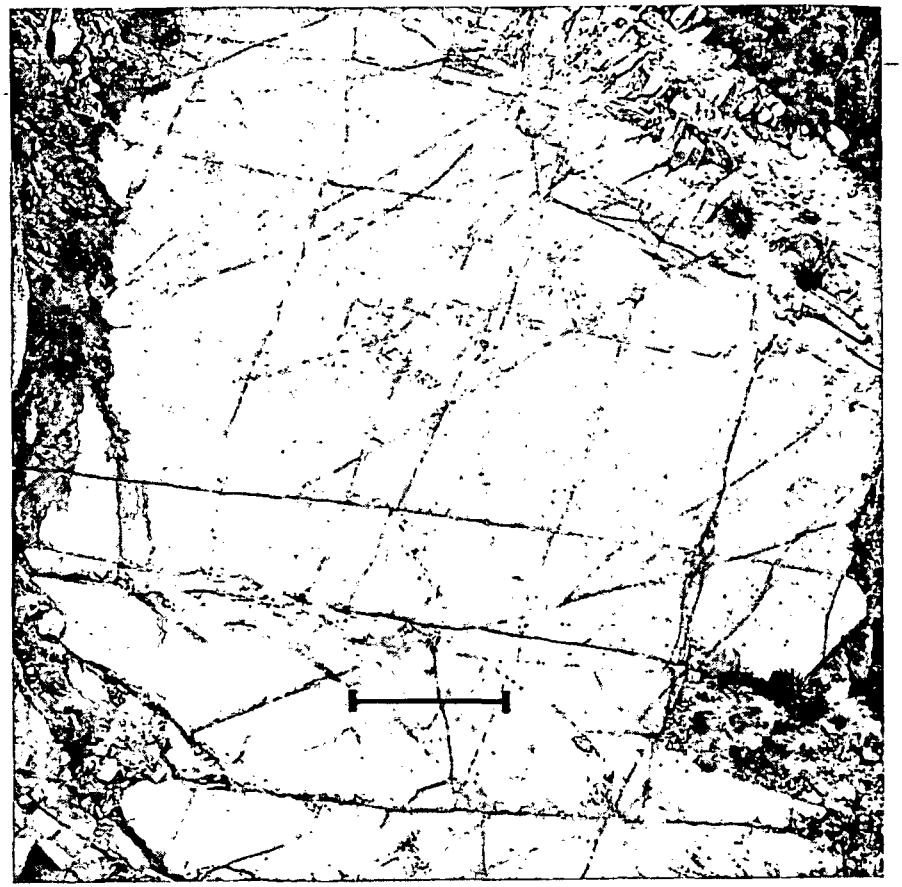

Outcrop of the porphyritic Schultze Granite demonstrating the geometry and distribution of flow and diffusion porosity. Continuous fractures, which cross cut outcrop, represent flow channels, and discontinuous fractures represent diffusion porosity. Scale bar is 5 m.

the differential equation describing the flow. This function is then used to find the mass flow along the fracture by integrating the velocity function over the fracture opening.

Steady state flow conditions require equality between the fluid driving force, F_d, and the resistive viscous force, F_r. The driving force is determined by the gradient in fluid potential and the area on which the force acts:

$$F_d = lA\nabla\Omega. \tag{3}$$

The resistive force is due to shear stress acting on the surface area, S, of the fracture walls:

$$F_r = \sigma S. \tag{4}$$

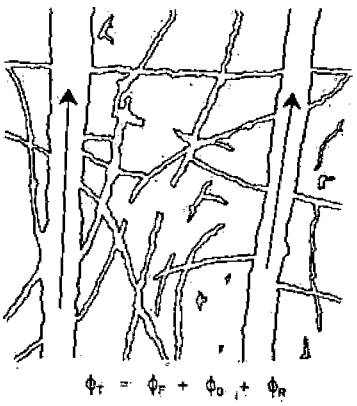

Fig. 1

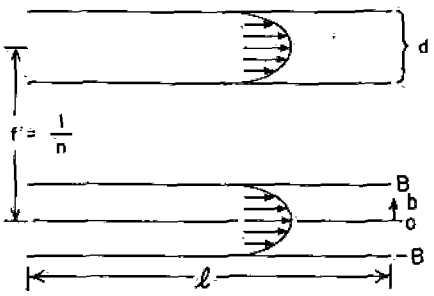

Fig. 2

Fig. 1. Schematic representation of constituent porosities showing the geometric relationships between residual pores, ϕ_R, diffusion pores, ϕ_D, and flow pores, ϕ_F. The arrows denote an arbitrarily chosen direction of fluid flow in ϕ_F. The pores extending from these two flow channels either have apertures that are too small to permit significant fluid flow or are discontinuous; therefore, all these pores are ϕ_D. The relative abundances are not shown.

Fig. 2. The laminar flow profile in planar fractures due to viscous drag forces at the walls. f is the fracture spacing and d the aperture. B and $-B$ represent the limits of integration in eq (9).

where $S = 2l$, and l is the unit length of the representative elemental volume. The shear stress in a viscous fluid is related to the fluid velocity by:

$$\sigma = -\eta \frac{d\bar{v}}{db}, \tag{5}$$

where $b = \frac{1}{2}$ fracture aperture (cm). The area on which the fluid driving force acts is orthogonal to the direction of flow in the fracture:

$$A = 2b \tag{6}$$

Combining eqs (3-6), we have a differential equation in terms of fluid velocity and distance from the fracture wall:

$$d\bar{v} = -b \frac{\nabla\Omega}{\eta} db. \tag{7}$$

Integrating eq (7) and evaluating the integration constant by using $\bar{v} = 0$ when $b = -B$ gives the velocity profile across the aperture of a single fracture:

$$\bar{v} = \frac{\nabla\Omega}{2\eta}(B^2 - b^2). \tag{8}$$

This parabolic flow profile develops in less than 1 m along the fracture for fluid velocities less than 10 cm/sec, and we will, therefore, assume in subsequent discussions that this flow profile is fully developed in geologic systems.

The volumetric flow rate from a single fracture is defined by first considering the flow velocity through an incremental cross-sectional area of the fracture and then integrating this expression over the fracture opening orthogonal to the flow direction (fig. 2).

$$Q = \int_{-B}^{B} \frac{l\nabla\Omega}{2\eta} (B^2 - b^2)\, db. \tag{9}$$

Integrating eq (9) gives the flow rate,

$$Q = \frac{-2B^3\nabla\Omega}{3\eta} \tag{10}$$

per unit length, l, of a single fracture. Substituting the aperture of the fracture into (10) gives the volume flow rate from n such parallel fractures

$$Q = \frac{-nd^3\nabla\Omega}{12\eta}. \tag{11}$$

The general statement of Darcy's Law for flow through porous media is (Hubbert, 1940):

$$Q = \frac{-k\nabla\Omega}{\eta}, \tag{12}$$

and k is a factor describing the shape and length characteristics of the flow passages. By analogy of (12) to (11) we see this intrinsic rock parameter, permeability, for fracture controlled flow is:

$$k = \frac{nd^3}{12}. \tag{13}$$

Fracture sets in natural systems are not precisely represented by this model; however, anisotropic characteristics of the fractures may be formulated into a tensor form:

$$Q = -\frac{k_{ij}}{\eta}\nabla\Omega, \tag{14}$$

where k_{ij} is the permeability tensor in which the subscript i relates to the fluid flow direction, and j relates to the potential gradient direction.

The porosity of the flow channels is also related to the fracture aperture and abundance, where

$$\phi_F = nd \tag{15}$$

for a single parallel fracture set.

Field observations of abundance and aperture on parallel fracture sets, together with eq (13), permit permeability estimates to be made. Abundances of fractures in plutons vary from 0.5 fracture/cm in some ore deposits (Bingham, Utah) to 10^{-3} fractures/cm in unaltered igneous bodies (Villas, ms; Bianchi and Snow, 1969). Aperture variations, which

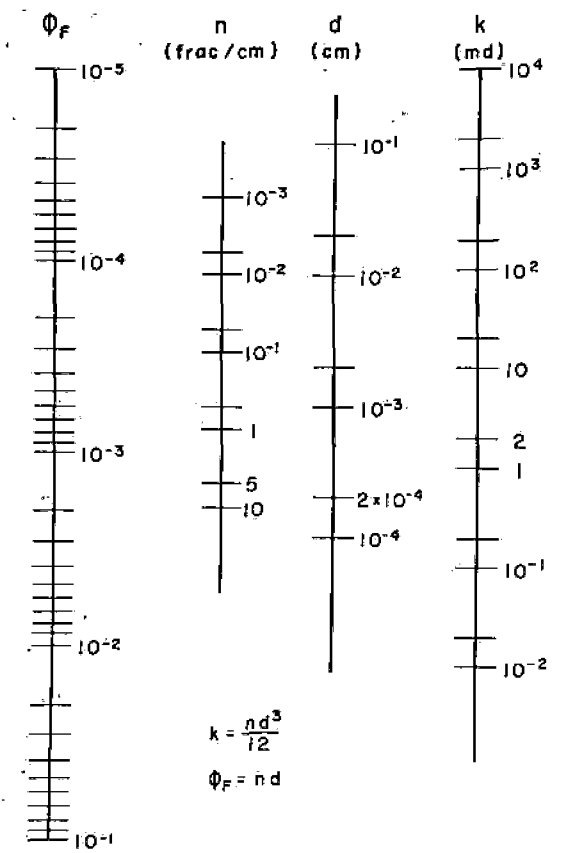

Fig. 3. Graphical solution to eqs (13) and (15). Aperture estimates; d, range from 10^{-6} to 2×10^{-2} cm, whereas fracture abundances, n, range from 5×10^{-1} to ^{1}/cm. With $d \doteq 10^{-4}$ cm and $n = 5 \times 10^{-1}$/cm, $\phi_F = 5 \times 10^{-6}$ and $k = 4 \times$ ^{1} md where 10^{-11} cm^2 = 1 millidarcy.

e the greatest effect on permeability but are the least well known, r range from 5×10^{-5} to 2×10^{-2} cm. Though these ranges in rtures and abundances are large, they place some interesting con- ints on the magnitude of flow porosity when examined with respect single fracture set, compare eqs 13 and 15 and their graphical solu- ı (fig. 3). The maximum range in flow porosity is from 10^{-2} to $5 \times$ ^{8}. Values estimated by Villas (ms) on the Mayflower Pluton range n 2×10^{-3} to 3×10^{-5}. The comparable total porosities for the /flower diorite are in the range of 0.01 to 0.03. Similarly, the flow osity and the total porosity of the Sherman Granite are 5×10^{-6} and ^{2}, respectively (Pratt and others, 1974). We, therefore, conclude that flow porosities are generally a small fraction of the total porosities, ı though precise limits can not be established.

Measurements of permeability by different methods often yield sig- antly different values. In general, in-situ measurements of permea-

bility on large representative blocks of fractured rock indicate values in the range of 10^{-12} to 10^{-8} cm^2 (table 1). An in-situ experiment conducted on the Sherman Granite determined the permeability of this rock to be 10^{-11} cm^2, whereas the permeability determined on intact core samples is about 2 to 3 orders of magnitude lower. Laboratory measurements of intact core samples of limestones, dolomites, and granites (table 1) also indicate very low values of permeability. Clearly, the permeability of rocks in hydrothermal systems is a poorly known quantity.

Estimates of rock permeabilities in the Earth's crust rely on deep drill holes, 10 km in sedimentary basins and 4 to 5 km in crystalline rocks, abundance and aperture of continuous fractures, electrical resistivity profiles, elastic properties of intact rock samples, and seismic data. These various lines of indirect evidence suggest that permeabilities to depths of 10 to 15 km may be significantly greater than 10^{-14} cm^2. Whereas laboratory measurements indicate that a pressure increase from 1 bar to 1 kb produces a $10^{1.5}$ decrease in permeability (Brace, Walsh, and Frangos, 1968), seismic hypocentral data suggest that brittle rock failure and transient fractures occur at depths to at least 15 to 20 km. The persistence of continuous fractures filled with conductive pore fluids at considerable depths is further indicated by relatively high electrical conductivities in the middle to upper crust (Plauff, 1966; Jackson, 1966; Keller, Anderson, and Pritchard, 1966; and Brace, 1971).

The permeability of fractured crystalline rocks is due to continuous fractures, and, even though the rock mass between these channels has a

TABLE 1

Some permeability measurements on crystalline rocks

Rock type	k(cm^2)	ϕ_F	Method	Reference
Hardhat granite	10^{-9}-10^{-12}		pump	Boardman and Skrove, 1966
Sherman granite	10^{-11}	2×10^{-5}	pump	Pratt and others, 1974
Sherman granite	$< 10^{-14}$		core	Pratt and others, 1974
Quartz porphyry	$\sim 10^{-11}$		pump	Cadek and others, 1968
Gneiss schist	5×10^{-11}		pump test in fractured zone	Marine, 1966
Gneiss schist	5×10^{-14}		pump (without fractures)	Marine, 1966
Gneiss schist	10^{-15}		core	Marine, 1966
Metabasalt	2×10^{-8}		pump	Davis, 1969
Schist	1.4×10^{-8}		pump	Davis, 1969
Quartz diorite	10^{-7} to 3×10^{-10}	2×10^{-3} to 3×10^{-5}	planar fracture model	Villas, ms.
Granite	10^{-4} to 10^{-10}	5×10^{-2} to 4×10^{-5}	planar fracture model	Bianchi and Snow, 1969
Welded tuff	$< 2\times10^{-15}$		pump	Winograd, 1971
Bedded tuff	10^{-10}-10^{-12}		pump	Winograd, 1971
Granite	10^{-14}-10^{-17}		core*	Brace, Walsh, and Frangos, 1968
Limestone	2×10^{-15}		disk	Ohle, 1951
Dolomite	10^{-10}		disk	Ohle, 1951
Volcanic (clastics)	10^{-5}-6×10^{-12}		drawn down	Grindley, 1965

* Measured as a function of effective pressure

relatively high total porosity, its effective permeability is nil. This fact is also evidenced by the above observations and the distribution of hydrothermal alteration minerals along the walls of fractures. The fact that alteration minerals occur in veins in ore deposits and active geothermal systems clearly demonstrates the nature of fracture controlled fluid flow. The widespread chemical alteration of rocks in hydrothermal systems further attests to the relatively large permeability of rocks in the Earth's crust.

The importance of deducing broad scale permeabilities of the crust relates directly to studies of the mass movement of aqueous solutions in the crust. Permeabilities greater than 10^{-14} cm^2 are conducive to the circulation of fluids in pluton environments and perhaps over broader regions of the crust (Norton and Knight, 1977). Also, since flow porosity in fractured igneous rocks, and possibly in fractured rocks in general, is apparently a small fraction of the total rock porosity, 10^{-1} to 10^{-5}, the true velocity of particles within a flow fracture, eq (8), will be orders of magnitude greater than the superficial velocity.

$$\bar{v}_{true} = \frac{\bar{v}_{Darcy}}{\phi_F} \tag{16}$$

DIFFUSION POROSITY

The nature of diffusion porosity is apparent, if we consider a typical region, R, within which the transport of aqueous components by fluid flow is insignificant with respect to diffusional transport. These conditions may occur in regions characterized by discontinuous fractures, small aperture fractures, or discontinuous pores. This type of region is typically bounded by continuous sets of fractures which constitute the flow channels in the overall system (fig. 1).

The diffusional flux of the i^{th} ion from the region is defined by the flux vector normal to an incremental area of the region's surface, S,

$$\bar{u}_i = -\phi'_D \sum_k D_{ik} \nabla m_k \tag{17}$$

where ϕ'_D is the ratio of the diffusion porosity coincident with the normal flux vector to the tortuosity, τ, of the pores, m_k is the concentration of the k^{th} ion in molality, and D_{ik} is the diffusion coefficient of the i^{th} ion due to the gradient in concentration of the k^{th} ion. The amount of the i^{th} ion leaving the region, with respect to the volume, is given by the volume integral of the divergence of $\bar{u}_i$,

$$\frac{\partial M_i}{\partial t} = \int_R \text{div } \bar{u}_i dV, \tag{18}$$

whereas the change in the amount of the i^{th} aqueous ion contained within the region as a function of time, is given by,

$$\frac{\partial M_i}{\partial t} = \int_R \rho \phi_D (1 + A_i) \frac{\partial m_i}{\partial t} dV, \tag{19}$$

where ϕ_D is the total diffusion porosity, and A_i is a volumetric source or sink of the i^{th} ion which, in effect, describes the irreversible mass transfer between the aqueous and solid phases. The amount leaving and amount depleted must be equal; therefore, eqs (18) and (19) are equal. Since the integrals hold for any subregion in R, the integrals can be eliminated. Eqs (18) and (19) are combined to describe the conservation of the i^{th} aqueous species in R:

$$\rho\phi_D (1 + A_i) \frac{\partial m_i}{\partial t} = \nabla \cdot \phi'_D \sum_k D_{ik} \nabla m_k. \tag{20}$$

The magnitude and distribution of the directional diffusion porosity, ϕ'_D, as defined by eq (17), have been measured on a variety of rocks. The total diffusion porosity is determined by experiments where $A_i = 0$ and $k = 1$ and are calculated by rearranging (20).

$$\frac{\partial m_i}{\partial t} = \rho D_i \bar{\phi} \nabla^2 m_i, \tag{21}$$

where

$$\bar{\phi} = \frac{\phi'_D}{\phi_D} \tag{22}$$

Eq (21) is then solved numerically to yield $\bar{\phi}$, which substituted in eq (22) gives ϕ_D.

Experimental apparatus modified from Garrels, Dreyer, and Howland (1949) was used to obtain the diffusion porosity data (Knapp, ms). Rock wafers, 1.0 to 2.5 cm in radius and from about 0.2 to 1.0 cm thick, are embedded with epoxy in Plexiglas plugs, so that only the circular surfaces are exposed. The samples are then saturated by drawing 10^{-4} N KCl solution through the wafer for at least 24 hrs. Microscopic examination of the wafers serves to check the epoxy seal for leakage and the rock for any induced fractures.

The plug with the saturated rock is next placed in a Plexiglas diffusion cell; the cell is filled with a measured amount (usually 60 ml) of 10^{-4} N KCl solution, and electrodes are inserted into the cell. The entire assemblage is placed in a thermally insulated, 25°C, tank containing about 10 l of 1 N KCl solution, which sets up an activity gradient across the rock wafer. Care is taken to minimize any fluid potential gradient between the cell and the tank to a negligible value. The concentration change is monitored by conductometric methods.

The experimental error in these measurements is difficult to define precisely. But, based on ϕ'_D measured on adjacent samples of apparently homogeneous and isotropic rocks, the precision is between 4 and 30 percent (Knapp, ms). Though this upper limit is fairly large, it does not seriously affect the conclusions derived from the experimental data.

The results of experiments indicate that the diffusion porosity is on the order of 10^{-3} to 10^{-4} (fig. 4). Furthermore, the diffusion porosity is

a very small fraction of the total rock porosity, since $\phi'_D \simeq 0.04\ \phi_T$ (fig. 5). Total rock porosities in the samples studied amount to 10^{-2} to 2×10^{-1} (fig. 6).

Of all the rocks examined during this study (tables 2 and 3), the volcanic rocks have the largest total porosities, from 0.2 to 2×10^{-1}, and ϕ'_D values, from 10^{-2} to 10^{-3} (figs. 4 and 6). Carbonate rocks studied have a fairly narrow range of total porosity values, from about 5×10^{-2} to less than 10^{-2}, whereas the ϕ'_D values range from 10^{-3} to 10^{-4}. The

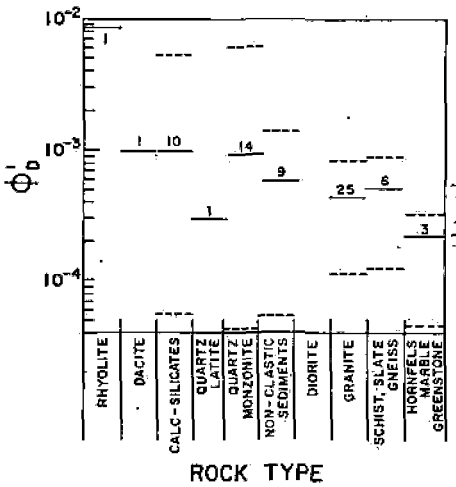

Fig. 4

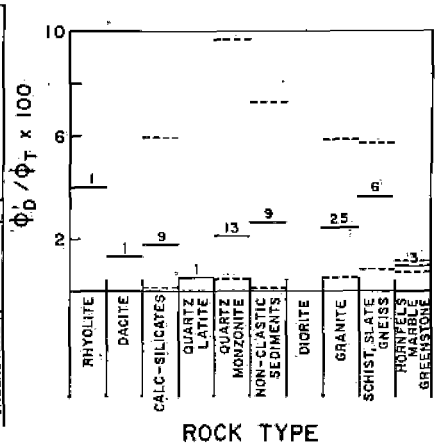

Fig. 5

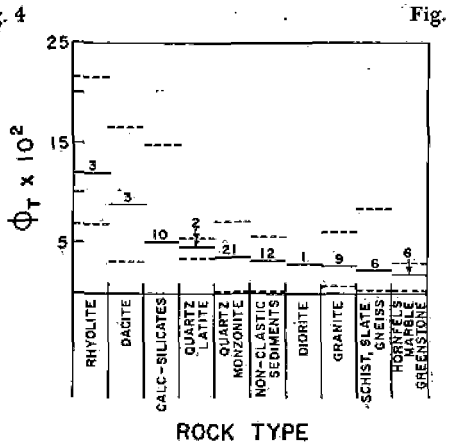

Fig. 6

Fig. 4. Mean values, solid lines, and range of values, dashed lines, of ϕ'_D for the various rock types examined in this study. The numerals denote the number of determinations for each rock type.

Fig. 5. The percentage of the total porosity that is composed of ϕ'_D. The solid lines are mean values, and the dashed lines are the range in values. The numerals denote the number of determinations for each rock type.

Fig. 6. Total porosity values for the various rock types studied. The solid lines are mean values, and the dashed lines the range in values. The numerals denote the number of determinations for each rock type.

TABLE 2

Density and porosity data

Sample no.	Bulk density ρ_B (g/cm^3)	Grain density ρ_Y (g/cm^3)	Total porosity $\phi_T \times 10^2$	$\phi'_D \times 10^4$	Sample thickness (cm)
Johnson Camp, Ariz.					
BQZ-5	2.61	2.72	4.11	8.1*	1.04
				13.7**	1.04
AL-007	2.68	2.74	2.12	5.5**	0.424
				1.5*	0.988
LA5	2.55	3.00	14.7	10.	0.90
AM-005	2.71	2.79	2.72	14.**	0.843
				2.*	0.800
AU-004	2.62	2.68	2.53		
ML-002	2.78	2.85	2.35		
MM-6	2.55	2.65	3.88		
MU-001	2.55	2.69	5.35		
ESC-3	2.64	2.71	2.62		
BP-4	2.60	2.70	3.85		
PS-1-JC	2.69	2.73	1.54	8.86**	0.925
				4.92*	0.964
Globe-Miami, Ariz.					
PS-1-GM	2.74	2.78	1.30		
Ronda, Spain					
R-71	2.74	2.76	.73	2.4*	0.386
R-80	2.77	2.80	1.07	3.3*	1.224
R-81	2.85	2.89	1.38	59.	1.29
R-125	2.72	2.97	8.42	7.1**	0.673
R-217	2.69	2.77	2.89	3.2	0.880
R-245	3.01	3.03	.660	3.7**	0.831
R-278	2.66	2.73	2.56	2.9	1.14
Chino, N.M.					
CS-1	2.69	2.97	9.43	7.5	1.05
CS-2	2.79	3.01	7.31	3.5	0.942
CS-4	2.75	2.83	2.83		
CS-5	4.25	4.67	8.99	53.	0.881
CS-6	3.01	3.12	3.53	9.7	1.33
CS-7	2.73	2.75	.73		
CS-8	3.18	3.24	1.85	7.0	1.19
CS-9	2.73	2.80	2.50	2.6	1.25
CS-10	2.72	2.73	.366	2.9	0.820
CS-11	2.64	2.71	2.58	4.1	1.02
CS-12	2.62	2.74	4.38	0.53	0.742
CS-13	2.49	2.67	6.74		
Chino pluton	2.62	2.69	2.60	10.	0.839
Silver City, N.M.					
Chino pc	2.97	2.99	.669	0.45	0.979
Cont. pit	2.91	3.03	3.96	0.54	0.949
150 pit	3.62	3.82	5.24	2.0	1.04
Copper Flat Pluton	2.48	2.62	5.34	2.9	0.857
San Manuel, Ariz.					
SM-1	2.71	2.75	1.46	1.1	1.04
SM-2	2.70	2.75	1.82	2.1	0.968
SM-3	2.71	2.87	5.58	4.1	1.02
SM-5	2.63	2.70	2.59	0.42	0.881
SM-7	2.45	2.63	6.84	11.	0.999
SM-8	2.57	2.70	4.82	8.8	0.958
SM-9	2.58	2.73	5.50	5.8	1.05

TABLE 2 (continued)

Sample no.	Bulk density ρ_B (g/cm^3)	Grain density ρ_γ (g/cm^3)	Total porosity $\phi_T \times 10^2$	$\phi'_D \times 10^4$	Sample thickness (cm)
Butte, Mont.					
8	2.73	2.91	6.35	61.	1.03
9A	3.04	3.22	5.41		
10282-2	2.60	2.71	3.77	8.4	1.18
10282-1	2.65	2.66	.0753	8.0	1.52
1024-1	2.74	2.77	1.55		
10283-1	2.73	2.76	1.01	2.4	1.12
Sierrita-Esperanza, Ariz.					
E-1	2.53	2.60	2.96		
E-2	2.66	2.71	1.96		
E-5	2.44	2.63	7.48		
ST-1	2.57	2.64	2.50		
ST-3	2.79	2.86	2.90		
ST-6	2.64	2.70	2.63	3.4	0.807
				1.1	1.27
Schultze Pluton, Globe-Miami, Ariz.					
S1 BB	2.51	2.65	5.35	3.9	0.840
SPV	2.61	2.66	1.77	4.8	1.0
				2.2	1.0
				8.3	0.507
SD5				16.0	0.144
				6.8	0.222
				6.1	0.280
5CM				5.2	0.481
3A				5.4	0.643
7CM				5.1	0.708
2				2.1	0.911
3				6.4	0.987
4				4.6	1.107
Bingham, Utah					
BGP	2.46	2.62	6.11	3.0	1.19
BQLP	2.58	2.65	2.64		
BWR	2.44	2.79	12.5	3.2	1.17
Miscellaneous					
SG-1	2.52	2.62	4.12		
LG-1	2.65	2.68	1.08	3.1	1.0
				2.0	1.0
RM-1	2.16	2.75	21.5	86.	0.888
TC-1	2.56	2.64	2.96		
AG-1	2.60	2.62	.611		
TR-3	2.62	2.65	1.36		
TR-5	2.46	2.66	7.52	9.9	1.09
TR-6	1.68	2.76	3.08		
DAC	2.20	2.61	15.7		

* Oriented perpendicular to foliation or bedding.
** Oriented parallel to foliation or bedding.

TABLE 3

Mineralogy of samples

Sample no.	Rock name	Mineralogy
Johnson Camp, Ariz.		
BQZ-5	Bolsa quartzite	quartz
AL-007	Lower Abrigo shale	clay, calcite
LA5	Lower Abrigo skarn	tremolite, muscovite, quartz, magnetite, hematite
AM-005	Middle Abrigo limestone	calcite, chert
AU-004	Upper Abrigo quartzite	quartz
AU-006	Upper Abrigo limestone	calcite, chert
ML-002	Lower Martin limestone	calcite
MM-6	Middle Martin limestone	calcite
MU-001	Upper Martin quartzite	quartz
ESC-3	Escabrosa marble	calcite
BP-4	Black Prince limestone	calcite
PS-1-JC	Pinal Schist	
Globe-Miami, Ariz.		
PS-1-GM	Pinal Schist	
Ronda, Spain		
R-71	slate	
R-80	biotite-garnet metapelite	andalusite, quartz, sericite, biotite, magnetite
R-81	quartzite	quartz, diopside, biotite, sphene, plagioclase, chlorite
R-125	pelitic schist	muscovite, tourmaline, andalusite, staurolite, quartz, biotite, garnet, plagioclase
R-217	hornfels	quartz, biotite, plagioclase, perthite, cordierite
R-245	granulite-grade gneiss	quartz, garnet, microperthite, plagioclase, sillimanite, biotite
R-278	hornfels	quartz, perthite, cordierite, plagioclase, biotite, sillimanite
Chino, N. Mex.		
CS-1	skarn	quartz, magnetite, pyrite, chalcopyrite
CS-2	skarn	quartz, sericite(?), biotite, magnetite, chlorite, pyrite, chalcopyrite
CS-3	skarn	quartz, andradite, magnetite, calcite, pyrite, chalcopyrite
CS-4	skarn	quartz, tremolite, magnetite, pyrite
CS-5	skarn	magnetite, quartz, pyrite, calcite
CS-6	skarn	amorphous silica, hematite, magnetite, calcite
CS-8	skarn	diopside, quartz, amorphous silica(?), calcite, magnetite
CS-9	skarn	quartz, calcite, diopside(?)
CS-10	Syrena limestone	calcite
CS-11	Upper Oswaldo limestone	calcite, quartz
CS-12	Lower Syrena limestone	calcite, quartz
CS-13	rhyolite subvolcanic	
Chino pluton	altered quartz monzonite porphyry	
Silver City, N. Mex.		
Chino pc	greenstone	
Cont. pit	skarn	quartz, andradite, magnetite, talc, sericite(?), pyrite, chalcopyrite, calcite
150 pit	skarn	andradite, quartz
Copper Flat pluton	quartz latite porphyry	

TABLE 3 (continued)

Sample no.	Rock name	Mineralogy
San Manuel, Ariz.		
SM-1	porphyritic Oracle quartz monzonite, altered	quartz, microcline, chlorite, biotite, plagioclase, hornblende, montmorillonite, epidote, hematite
SM-2	porphyritic Oracle quartz monzonite, altered	quartz, K-feldspar, plagioclase, chlorite, biotite, kaolinite, montmorillonite
SM-3	porphyritic Oracle quartz monzonite, altered	quartz, K-feldspar, sericite, kaolinite, biotite, plagioclase, pyrite, chlacopyrite, hematite
SM-5	porphyritic Oracle quartz monzonite, altered	quartz, K-feldspar, chlorite, plagioclase, sericite, pyrite, hematite, epidote
SM-7	quartz monzonite porphyry, altered	quartz, K-feldspar, plagioclase, chlorite, biotite, sericite, pyrite
SM-8	quartz monzonite porphyry, altered	quartz, sericite, chlorite, K-feldspar
SM-9	porphyritic Oracle quartz monzonite, altered	quartz, sericite, clay, plagioclase, microcline
Butte, Mont.		
8	sericitized Butte quartz monzonite	
9A	sericitized Butte quartz monzonite	with pyrite, chalcocite, enargite in vein
10282-2	argillized (white) Butte quartz monzonite	
10282-1	argillized (green) Butte quartz monzonite	quartz, potassium feldspar, plagioclase, biotite, hornblende, anhydrite
1024-1	altered Butte quartz monzonite	
10283-1	fresh Butte quartz monzonite	
Sierrita-Esperanza, Ariz.		
E-1	altered Esperanza quartz monzonite porphyry	quartz, plagioclase, K-feldspar, biotite, sericite, rutile, molybdenite, chalcopyrite
E-2	altered Esperanza quartz monzonite porphyry	quartz, plagioclase, K-feldspar, biotite, montmorillonite, pyrite, chalcopyrite, molybdenite
E-5	altered rhyolite	with quartz, hematite, sericite, pyrite
ST-1	altered quartz monzonite porphyry	quartz, K-feldspar, kaolinite, biotite, pyrite, chalcopyrite
ST-3	altered biotite quartz diorite	plagioclase, biotite, montmorillonite(?), chlorite, sericite, epidote, quartz
ST-6	altered Harris Ranch quartz monzonite	quartz, plagioclase, K-feldspar, hornblende, kaolinite, chlorite, biotite, calcite, pyrite, hematite
Schultze Pluton, Globe-Miami, Ariz.		
SI BB	altered porphyritic Schultze Granite	quartz, K-feldspar, plagioclase, biotite, clays, muscovite, calcite, Cu oxides
SPV	equigranular Schultze Granite	quartz, K-feldspar, plagioclase, biotite, kaolinite, muscovite, clays

TABLE 3 (continued)

Sample no.	Rock name	Mineralogy
Porphyritic Schultze Granite, Globe-Miami, Ariz.		
SD5	porphyritic granite	
SD5	porphyritic granite	
SD5	porphyritic granite	
5CM	porphyritic granite	
3A	porphyritic granite	
7CM	porphyritic granite	
2	porphyritic granite	
3	porphyritic granite	
4	porphyritic granite	
Bingham, Utah		
BGP	Bingham granite porphyry	
BQLP	Bingham quartz latite porphyry	
BWR	Bingham latite dike	
Miscellaneous		
SG-1	Stronghold granite (Cochise's Stronghold, Ariz.)	
LG-1	Sherman granite (Laramie, Wyo.)	
RM-1	altered tuff (Red Mountain, Ariz.)	
TC-1	Texas Canyon granite (Texas Canyon, Ariz.)	quartz, K-feldspar, plagioclase, biotite, muscovite
AG-1	Amole granite (Tucson, Ariz.)	
TR-3	Troy granite (Troy, Ariz.)	
TR-5	rhyodacite dike (Troy, Ariz.)	
TR-6	dacite dike (Troy, Ariz.)	
DAC	dacite flow (Superior, Ariz.)	

plutonic rocks studied have a very uniform total porosity, with all values falling within several units of 4×10^{-2}. But, similar to the carbonate rocks, ϕ'_D varies greatly, between about 5×10^{-3} and 4×10^{-5}. The calc-silicate altered rocks have large values of both total and diffusion porosity, with ϕ_T between 1.5×10^{-1} and 3×10^{-3} and ϕ'_D between about 5×10^{-3} and 5×10^{-5}.

Many of the hydrothermally altered calc-silicate and plutonic rocks have significantly greater values for both total porosity and ϕ'_D than their unaltered equivalents (tables 2 and 3). The mean total porosity for the calc-silicates from Chino, N. M. is 4.6×10^{-2}, compared to 2.4×10^{-2} for their unaltered equivalents, and the mean ϕ'_D for these same rocks is $1.2\ 10^{-3}$ as compared to $2.4\ 10^{-4}$ for the unaltered equivalents. The altered rocks from Butte, Mont. also show this trend; the mean total porosity is 3.2×10^{-2}, compared to 1.1×10^{-2}, respectively, and the mean ϕ'_D is 2.6×10^{-3}, compared to 2.4×10^{-4} for unaltered equivalents.

Comparison of the hydrothermally altered plutonic rocks from San Manuel and Sierrita-Esperanza, Ariz. with unaltered rocks from the Laramie, Wyoming and Troy, Ariz. plutons suggests a similar result, although samples SM-5, with $\phi'_D = 4.2 \times 10^{-5}$, (San Manuel, Ariz.), and CS-7 (Chino, N.M.), with $\phi_T = 7.3 \times 10^{-3}$, deviate significantly from this trend. It is interesting to note that the bulk of the difference in pore volume between hydrothermally altered rocks and their unaltered equivalents is due to a markedly larger value of residual porosity in the altered rocks (table 2). Since the mineral surface area:fluid ratio is very large, porosity increase due to irreversible chemical mass transfer in the residual pores is negligible; this larger value must be a result of either initial condition or subsequent modification of the initial porosity.

Total porosities for the isotropic metamorphic rocks studied range from about 3×10^{-2} to less than 10^{-2}; ϕ'_D for these same rocks varies from about $3.0\ 10^{-4}$ to about $4.5\ 10^{-5}$. The anisotropic rocks studied have a wider range in total porosity, with values ranging from about 10^{-1} to less than 10^{-2} (table 4). These values show that ϕ'_D parallel to foliation or bedding is significantly greater than that perpendicular, by a factor of about 2 to 7.

A consistent ratio between ϕ'_D and total porosity, that is, 4×10^{-2}, is also apparent in the data. This consistency suggests that ϕ'_D can be estimated from rather simple measurements of ϕ_T.

The total diffusion porosity, ϕ_D, may be computed from values of ϕ'_D determined above, eq (22), and the transient times required to attain steady state in the experiments. Values for an altered quartz monzonite, SM7, and a metapelite, 80, indicate that ϕ'_D is simply one axial component of ϕ_D, that is, $\phi_D = 3\phi'_D$.

RESIDUAL POROSITY

Residual porosity, ϕ_R, is the bulk of the total rock porosity since the analysis of the flow and diffusion porosity indicates that the sum of ϕ_F and ϕ_D amounts to a small fraction of the total porosity, for example, 10^{-1}. Therefore, residual porosity is $> 0.9\ \phi_T$ in fractured media.

NATURE OF PORES

Location, relative size distribution, and continuity of the pores can be determined by an analysis of porosity and mineral size distributions (figs. 7 and 8) and direct observation. The porosity distribution, exclusive of flow porosity, is obtained by measuring the density as a function

TABLE 4

Values for ϕ'_D by orientation of sample

Sample	Parallel	Perpendicular
AL007	5.40×10^{-4}	1.48×10^{-4}
AM005	13.9	2.01
PS-1-JC	8.86	4.92
BQZ	13.7	8.05

of crushed grain size. Intergranular porosity requires the density of the crushed aggregate and, hence, total measured porosity to increase as the size of the crushed grains decreases. As the crushed-grain size approaches a mineral-grain size a greater increase is expected. The contributions to porosity from pores around grains of various sizes can be calculated by using the density of the smallest grain in the interval as ρ_γ in eq 2. Measurements of this type were made on samples of the equigranular and porphyritic Schultze Granite (figs. 7 and 8).

The correlation between mineral grain size and porosity distributions for the porphyritic Schultz Granite (fig. 7) indicates the pores occur between grains and that pore size is bimodally distributed. Mode I is composed almost wholly of pores with a maximum dimension greater than 4 mm, constituting 30 percent of the total pore volume. Mode II is composed of pores that have a maximum dimension less than 1 mm, constituting 70 percent of the pore volume. In mode I there is a large increase in pore volume (30 percent), as the crushed grain size approaches 4 mm. Because this size interval corresponds to the phenocryst size range, it can be concluded that this pore volume is located around the phenocrysts. The imperfect correlation between grain size and porosity in the size interval, 4 to 1 mm, can be interpreted to mean that there is very little pore volume located around the minerals in this size interval. Finally, the porosity distribution volume in mode II roughly mimics

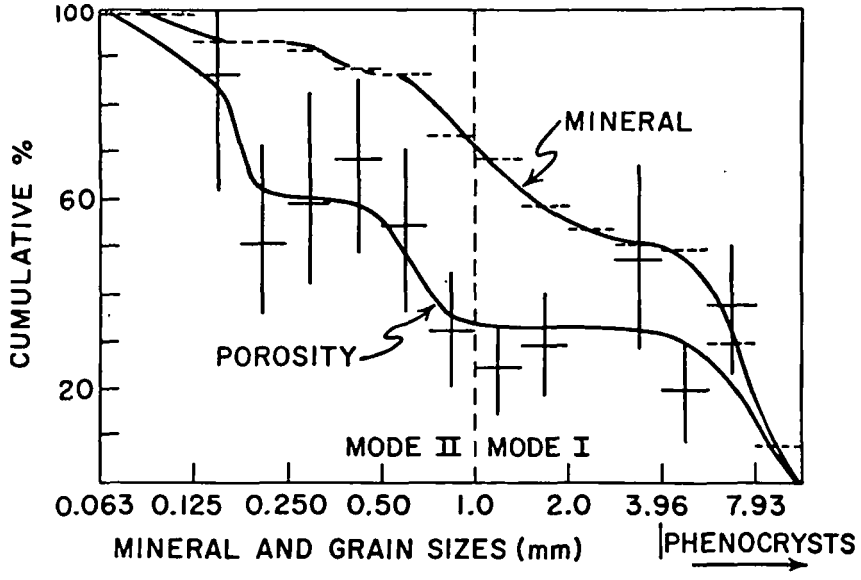

Fig. 7. Measurements of porphyritic Schultze Granite showing cumulative percentage of porosity as a function of crushed grain sizes. Horizontal bars are plotted at actual measured porosity values, with their length representing the precision of the crushed grain size measurement. Vertical bars represent the precision of the porosity measurement, also, cumulative percentage mineral sizes as a function of mineral size. Horizontal dashed lines represent precision for the size ranges.

the mineral distribution, again indicating that these pores are located around these minerals.

The intergranular nature of the pores implies that they have a maximum dimension less than or equal to their associated mineral dimension; that is, the more continuous pores are located around the larger mineral sizes. The porosity and mineral size distribution curves in mode I also indicate that 30 percent of the pore volume is located around the larger minerals, which at the most comprise 50 percent of the mineral surface area in the rock, whereas in mode II 70 percent of the pore volume is located around 30 percent of the minerals.

The porosity and mineral distribution for the equigranular Schultze Granite also shows there is one domain of porosity closely correlated with mineral distribution (fig. 8). The lack of correlation in mode I, however, permits two conclusions about pore location and continuity. The larger pores are either intergranular and less than or equal to the mineral dimensions or elongate pores that crosscut mineral boundaries.

The continuity of intergranular pores in the porphyritic Schultze Granite can be determined from ϕ'_D values for samples of varying thicknesses (fig. 9). Large increases in ϕ'_D indicate large abundances of pores with a maximum dimension equal to that sample thickness. These data indicate a discontinuity at about 8 mm, which is also suggested by correlative changes of porosity and mineral abundance distribution

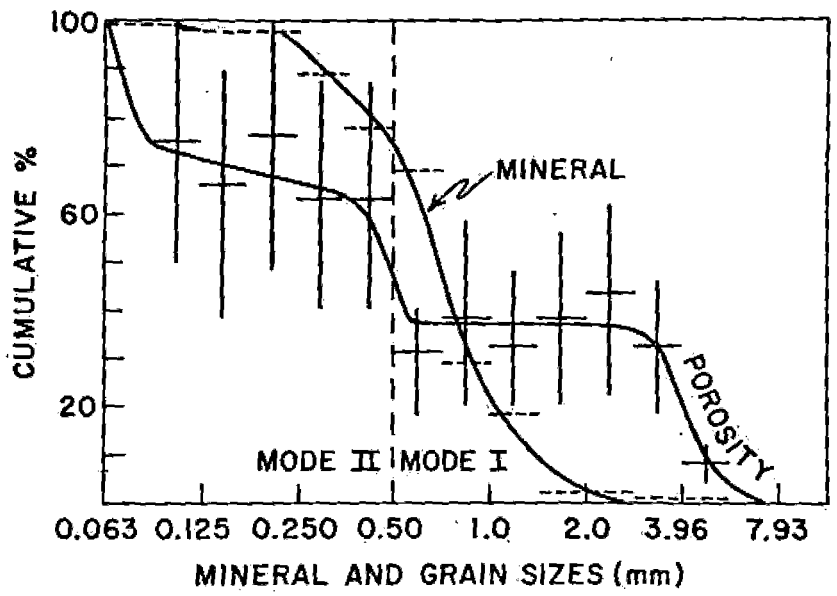

Fig. 8. Measurements on equigranular Schultze Granite showing cumulative percentage of porosity as a function of crushed grain sizes. Horizontal bars are plotted at actual measured porosity values, with their length representing the precision of the crushed grain size measurement. Vertical bars represent the precision of the porosity measurement, also, cumulative percentage mineral sizes as a function of mineral size. Horizontal dashed lines represent precision for the size ranges.

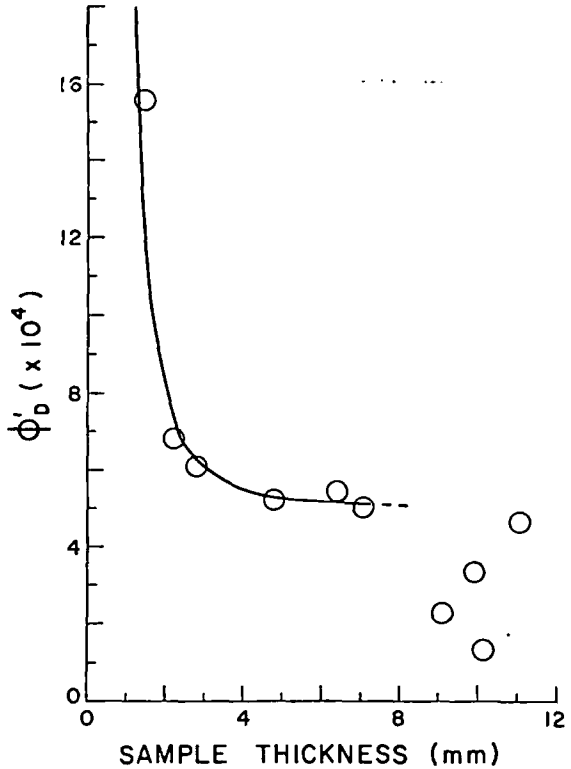

Fig. 9. Variation of ϕ'_D with the thickness of the porphyritic Schultze Granite samples used in diffusion experiment.

curves in mode I (fig. 7). This discontinuity indicates that there is a large abundance of pores with a maximum dimension of about 8 mm and that these more continuous pores are located around the phenocrysts.

The large increase in ϕ'_D at about 2 mm (fig. 9) indicates that the preponderance of pores have a maximum dimension less than this length. This increase of ϕ'_D approaches the value of the total porosity as the sample thickness approaches zero. Previous experiments determined (Garrels, Dreyer, and Howland, 1949) that $\phi'_D/\phi_T = 0.4$ for limestone samples 1 to 2 mm thick. These values are in general agreement with those reported in our study, if one assumes the relationship in figure 9 holds for a variety of rock types.

The geometry of discontinuous pores in fractured media may be classified into two broad categories, equidimensional pores and microcracks. Equidimensional pores vary from less than 1 mm to as great as 5 mm. This upper limit in size for equidimensional pores coincides with the large increase in the porosity distributions (figs. 7 and 8) and serves as partial confirmation of these curves. The pores composing this category have shapes that range from prismatic to highly irregular. Observed apertures of the microcracks range from less than 1 μm to no

PLATE 2

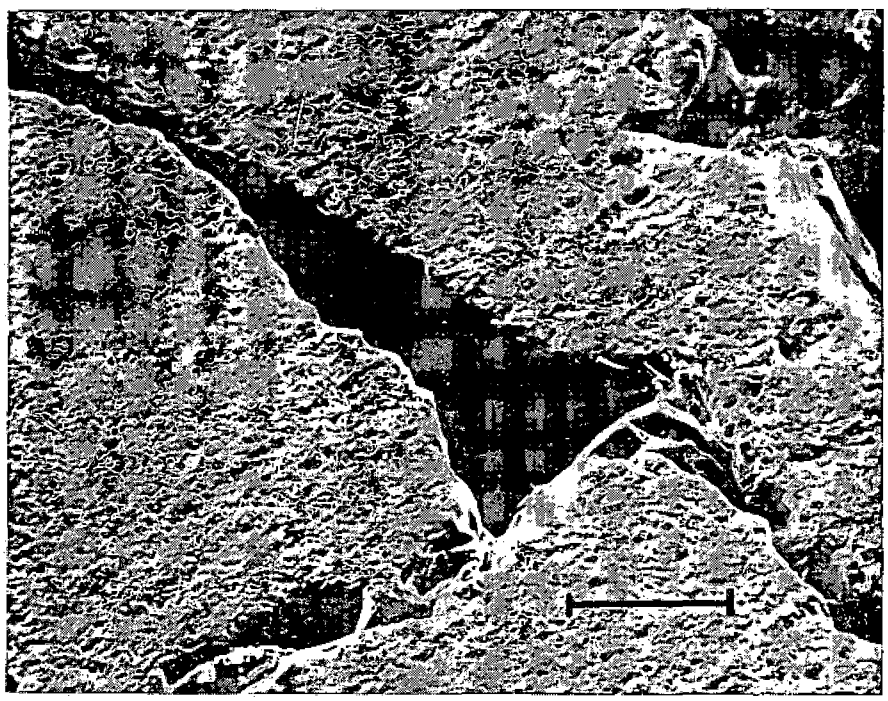

Scanning electron micrograph of an intergranular-prismatic pore in the Sherman Granite. This type of pore probably represents the geometry and size of diffusion and/or residual pores. The scale bar is 100 μm.

greater than 40 μm. Clearly, the small values for the apertures require the bulk of the pore volume to be composed of equidimensional pores. The suggested intergranular nature of the pores is also supported by the above observations, since the equidimensional pores are clearly distributed around grain boundaries (pl. 2).

In summary, the above data suggest that a general porosity model for fractured igneous rocks consists of continuous planar fractures, ϕ_F, and cylindrical pores, ϕ_D (fig. 10).

ADVECTION–REACTION–DIFFUSION

Porosity data define the distribution of fluids in hydrothermal systems. This information permits formulation of the governing partial differential equations for the advection-diffusion-reaction of aqueous species in a hydrothermal system.

The actual paths described by circulating packets of fluid in and around cooling intrusive bodies are defined in two dimensions by

$$\frac{dx}{\bar{v}_x} = \frac{dz}{\bar{v}_z} = dt, \tag{23}$$

where $\bar{v}_x$ and $\bar{v}_z$ are the component velocities. Examples of these pathlines in hydrothermal systems are presented in Norton and Knight, 1977. Fluids circulating along pathlines flow from one chemical environment into another, which results in differences in fluid compositions between those fluids in the flow porosity and those in the diffusion porosity, as well as disequilibrium between fluids and mineral phases. The transfer of heat between circulating fluid and rock may cause further disequilibrium within a rock volume. The mass transfer resulting from this disequilibrium occurs within flow porosity and diffusion porosity.

Advective transport depends directly on the magnitude of the flow velocities in ϕ_F. For flow velocities normally realized in these systems, a parabolic flow profile develops in less than a meter along the fracture and is effective over a thickness equal to half the fracture aperture (fig. 10). The true velocity in the fracture varies from zero at the wall of the fracture to an average value, defined by

$$\bar{v}_t = \frac{\bar{v}_{Darcy}}{\phi_{flow}}. \tag{24}$$

Therefore, the advective flux of the i^{th} ion is

$$\bar{u}_i = \bar{v}_t m_i \phi_F \rho. \tag{25}$$

The diffusional flux within ϕ_F parallel to the flow direction and across a concentration boundary layer, δ_c, follows from eq (17) with the substitution of ϕ_F for ϕ_D.

$$\bar{u}_{iF} = -\phi_F \sum_k D_{ik} \nabla_{xy} m_k. \tag{26}$$

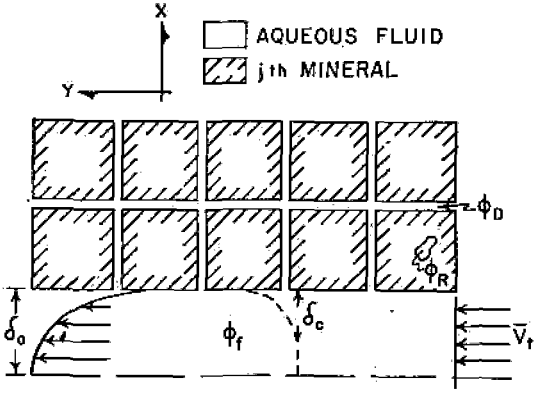

Fig. 10. Schematic two-dimensional porosity model for homogenous and isotropic ϕ_D. The model represents a possible geometric distribution of pores with respect to discrete minerals and is consistent with data collected in this study. In particular, we note that diffusion pores, ϕ_D, occur along each mineral grain boundary and interconnect with continuous fractures, ϕ_F. Although the relative abundance of the porosity types is not represented in this schematic representation, typical values for the porosity parameter are $\phi_D = 2 \times 10^{-4}$, $\phi'_D = 3\phi_D$, $\tau = 1$, diffusion pore radius of 10^{-4} cm and mineral sizes of 0.14 cm. The model and values are a first order approximation of pore geometry in fractured rocks.

As discussed previously, aqueous diffusion is the dominant transport mechanism within the diffusion pores and is defined by

$$\bar{u}_{iD} = -\phi'_D \sum_k D_{ik} \nabla_{xy} m_k. \tag{27}$$

The total flux of the i^{th} ion from the representative region, R, can be obtained by summing the advective and diffusive fluxes within the flow porosity domain and the diffusive flux within the diffusion porosity domain (eqs 25, 26, and 27).

$$\bar{S}_i = \bar{u}_i + \bar{u}_{iF} + \bar{u}_{iD}. \tag{28}$$

An expression for the total amount of the i^{th} ion in R available for transport can be obtained by modifying eq (19) to read

$$M_i = \int_R \rho (\phi_F + \phi_D) (m_i + A_i m_i) \, dV. \tag{29}$$

The amount of the i^{th} ion loss from R is equal to the volume integral of the divergence of $\bar{S}_i$,

$$-\int_R \operatorname{div} \bar{S}_i \, dV, \tag{30}$$

and must be equal to the rate of depletion of the ion in R, that is, the time derivative of eq (29). Introducing a conservation of mass and combining the time derivative of eqs (29) and (30) results in the governing partial differential equation for conservation of the i^{th} aqueous species:

$$\rho (\phi_F + \phi_D) (A_i + 1) \frac{\partial m_i}{\partial t} + \rho \bar{v}_t \phi_F \nabla m_i = \nabla D_{ik} \phi_F \nabla m_k + \nabla D_{ik} \phi'_D \nabla m_k. \tag{31}$$

Eq (31), together with the partial differential equations describing fluid flow in pluton environments, accounts for the circulation of fluids through reactive host rocks. This formulation is fundamentally different from previously derived equations in that it explicitly affords for the appropriate porosity values in fractured rocks. Other formulations utilize total rock porosity, which may produce significantly different results since we found ϕ_T is as large as several orders of magnitude greater than $(\phi_D + \phi_F)$.

ACKNOWLEDGMENTS

This research was supported by NSF Grant nos. GA-41136 and EAR74-03515-A01 and the University of Arizona. We wish to thank Dr. Timothy Loomis, Mr. Bill Baltosser, Bear Creek Mining Company, the University of Arizona chapter of SGE, and the Anaconda Company for donating samples and rock descriptions which greatly enhanced the scope of this study. We also wish to thank Lynn McLean for improvements in the manuscript.

References

Bianchi, L., and Snow, D. T., 1969, Permeability of crystalline rocks interpreted from measured orientations and apertures of fractures: Jodphur, Rajasthan, Arid Zone Research Assoc. of India, Annals of Arid Zone, v. 8, no. 2, p. 231-245.

Boardman, C. R., and Skrove, J., 1966, Distribution in fracture permeability of a granitic rock mass following a contained nuclear explosion: Jour. Petroleum Technology, v. 18, p. 619-623.

Brace, W. F., Walsh, J. B., and Frangos, W. T., 1968, Permeability of granite under high pressure: Jour. Geophys. Research, v. 73, p. 2225-2236.

Brace, W. F., 1971, Resistivity of saturated crustal rocks to 40 km based on laboratory measurements, *in* Heacock, J. G., ed., The structure and physical properties of the Earth's crust: Am. Geophys. Union, Geophys. Mon. Ser., v. 14, p. 243-255.

Cadek, J., Hazdrova, M., Kacura, G., Krasny, J., and Malkovsky, M., 1968, Hydrogeology of the thermal waters at Teplice and Usti nad Labem: Sbornik Geol. Ved, Hydrogeol., Inzenyrska Geol., rada HIG, sv. 6, p. 1-184.

Davis, S. N., 1969, Porosity and permeability of natural materials, *in* DeWiest, R. J. M., ed., Flow through porous media: New York, Acad. Press, p. 54-90.

DeWiest, R. J. M., 1965, Geohydrology: New York, John Wiley & Sons, Inc., 366 p.

Fatt, I., 1956, The network model of porous media: Am. Inst. Mining Engineers, Petroleum Trans., v. 207, p. 141-181.

Garrels, R. M., Dreyer, Z. M., and Howland, D. L., 1949, Diffusion of ions through intergranular spaces in water saturated rocks: Geol. Soc. America Bull., v. 60, p. 1809-1828.

Grindley, G. W., 1965, The geology, structure, and exploitation of the Wairakei geothermal field: Taupo, New Zealand: Wellington, New Zealand Geol. Survey, 131 p.

Hubbert, M. K., 1940, The theory of ground-water motion: Jour. Geology, v. 48, p. 785-944.

Jackson, D. B., 1966, Deep resistivity probes in the southwestern United States: Geophysics, v. 31, p. 1123-1144.

Keller, G. V., Anderson, L. A., and Pritchard, J. I., 1966, Geological survey investigations of the electrical properties of the crust and upper mantle: Geophysics, v. 31, p. 1078-1087.

Knapp, R. B., ms, 1975, An analysis of the porosities of fractured crystalline rocks: M.S. thesis, Univ. Arizona, 90 p.

Maini, Y. N. T., ms., 1971, In situ hydraulic parameters in jointed rock—their measurement and interpretation: Ph.D. dissert., Univ. London, 312 p.

Marine, I. W., 1966, Hydraulic correlation of fracture zones in buried crystalline rock at the Savannah River plant, near Aiken, South Carolina: U.S. Geol. Survey Prof. Paper 550-D, p. 223-227.

Norton, D. L., and Knight, J. E., 1977, Transport phenomena in hydrothermal systems: cooling plutons: Am. Jour. Sci., v. 277, p. 937-981.

Ohle, E. L., 1951, The influence of permeability on ore distribution in limestone and dolomite: Econ. Geology, v. 46, p. 667-706.

Plauff, D., 1966, Magneto-telluric soundings in the southwestern United States: Geophysics, v. 31, p. 1145-1152.

Pratt, H. R., Black, A. D., Brace, W. F., and Norton, D. L., 1974, In situ joint permeability in a granite: EOS, Am. Geophys. Union Trans., v. 55, p. 433.

Snow, D. T., ms, 1965, A parallel plate model of fractured permeable media: Ph.D. dissert., Univ. California, Berkeley, 331 p.

———— 1970, The frequency and apertures of fractures in rock: Internat. Jour. Rock Mechanics Min. Sci., v. 7, p. 23-40.

Villas, R. N., ms., 1975, Fracture analysis, hydrodynamic properties and mineral abundance in altered igneous wall rocks of the Mayflower mine, Park City district, Utah: Ph.D. dissert., Univ. Utah, Salt Lake City, 253 p.

Winograd, I. J., 1971, Hydrogeology of ash flow tuff: a preliminary statement: Water Resources Research, v. 7, p. 994-1006.

GEOTHERMAL PROGRAMS

IDO-10099
Volume I

Idaho Operations Office

SUBJ
GTHM
LTMT

Low-to-Moderate Temperature Hydrothermal Reservoir Engineering Handbook

A Joint-Project Report of
Lawrence Berkeley Laboratory and
The Idaho National Engineering Laboratory

IDO-10099
Volume I
Distribution Category: UC-66a,d,g

LOW-TO-MODERATE TEMPERATURE HYDROTHERMAL RESERVOIR ENGINEERING HANDBOOK

Published June 1982

EG&G Idaho, Inc.
Idaho Falls, Idaho 83415

and

Lawrence Berkeley Laboratory
Berkeley, California 94720

Prepared for the
U.S. Department of Energy
Idaho Operations Office
Under DOE Contract No. DE-AC07-76IDO1570

FOREWORD

Low-to-moderate temperature geothermal energy will augment the future energy needs of industrial process heat, space heating, and district heating systems. As an industry in its infancy, geothermal reservoir engineering is unique and different from the technologies of petroleum and ground water reservoir engineering.

This document which provides guidelines to developers and consultants in evaluating reservoir characteristics contains sections on reservoir classification, conceptual modeling, testing during drilling, current theory of testing, test planning and methodology, instrumentation, and a sample computer program. Although the developer will find the entire document useful and informative, sections on test planning and methodology, geochemistry, reservoir monitoring, and the appendixes, containing technical detail, are designed specifically for the consultant. Sections 2 through 6 provide the developer background information needed to monitor the program of reservoir evaluation. As technology improves, this document will be modified. Future sections will depend upon ongoing and completed research in the low-to-moderate temperature geothermal industry.

Metric units are used whenever possible. However, some equations employ constants in English units and some instrumentation and oil field records (i.e., pressure gauges, rig recorders, and well logs) are calibrated or recorded in English units. Therefore, soft-metric and English units are used wherever logical or appropriate. Appendix A provides the reader with information on conversions.

ACKNOWLEDGMENTS

This document has been jointly prepared by EG&G Idaho, Inc., Geosciences Branch, and Lawrence Berkeley Laboratory, Earth Sciences Division for Dr. Leland L. Mink and Susan M. Prestwich of the Idaho Operations Offfice, U.S. Department of Energy. Robert A. Gray, Charles Bufe, and David Lombard of the Department of Energy, Division of Geothermal Energy provided the funding. Key contributors to this document include Dennis Goldman, Larry Hull, Julie Tullis, Steve Mizell, Brent Russell, and Piotr Skiba, all of EG&G Idaho, Inc.; and Calvin Clyde, appointed to EG&G Idaho, Inc. as a faculty participant through the Associated Western Universities. The EG&G Program management was provided by Max R. Dolenc, Susan Spencer, and Susan Petty. Lawrence Berkeley Laboratory contributors include the program manager, Sally Benson, Raymond Solbau, and Ernie Major, and Micheal Wilt.

Subir Sanyal, a private consultant, discussed the overall scope and direction of the document. A critical review of this document, before release, was also provided by: J. K. Balzhiser, Balzhiser/Hubbard and Associates; Calvin Clyde, Utah Water Research Laboratory; Glenn Coury, Coury and Associates; Gary Harvey, TRC Environmental Consultants, Inc.; Charles Morris, Republic Geothermal Inc.; Paul Lineau, Oregon Institute of Technology; John Lund, Oregon Institute of Technology; Derek Freeston, University of Aukland; Richard Pearl, Colorado Geological Survey; John L. Sondergger, Montana Bureau of Mines; Susan Spencer, Morrison and Knudsen; and P. M. Wright, Earth Science Laboratory, University of Utah Research Institute.

CONTENTS

FIGURES

TABLES

LOW-TO-MODERATE TEMPERATURE HYDROTHERMAL RESERVOIR ENGINEERING HANDBOOK

1. INTRODUCTION

Numerous low- (less than 90°C)-to-moderate temperature (90 to 150°C) geothermal resources occur in many areas of the United States. The number of known geothermal systems increases significantly as the temperature decreases. Geothermal systems occur primarily where the normal geothermal gradient of the earth (30°C/km average) is affected by a positive temperature anomaly. These anomalies are caused by: (a) higher than normal regional heat flow; (b) rocks of low thermal conductivity; (c) higher than normal concentrations of radioactive elements; (d) young magmatic intrusions; and/or (e) hydrothermal circulation.[1]

Low-to-moderate temperature geothermal resources have a wide range of direct-use applications in agriculture and industry. Agricultural uses such as greenhousing, animal husbandry, soil warming, mushroom raising, and biogas generation require the lowest temperature, ranging from 20 to 82°C. Industrial uses such as space heating for homes, offfices, hospitals, and large district heating systems requires temperatures from 45 to 100°C. Industrial processes require temperature up to 150°C with the use of both steam and superheated water. Industrial uses of geothermal fluids also include food processing, crop drying, and multiple use by the forest products industry. Although the unique aspects of each geothermal resource require individual consideration, most development schemes will employ straightforward engineering, using proven technology and existing system components.

The rationale used in developing a low-to-moderate temperature geothermal resource is the same as that used by a hydrologist or petroleum engineer in designing an optimal development scheme for a given water or oil reservoir. Consequently, the geothermal industry depends on two major areas of expertise: hydrology and petroleum engineering.

Hydrologists have applied ground water hydraulics and theory to low-temperature systems (<90°C) that are single phase and liquid and resemble ordinary ground water systems. However, most ground water theory was developed for application to fluids of about 16°C and did not include temperature dependent fluid properties. Problems with ground water theory applications to geothermal systems include those of nonisothermal flow, temperature dependent fluid properties, and proper interpretation of well tests. For well testing, the two most important temperature dependent fluid properties are density and viscosity. Figures 1 and 2 show the value of these parameters from 0 to 150°C.

The petroleum engineering theory was developed for exploitation of hydrocarbon resources. The great depth of some petroleum reserves, gas content of the fluid, and temperature dependent fluid properties make these petroleum reservoirs similar to high-temperature geothermal reservoirs. Because low-to-moderate temperature resources are rarely two-phase steam water mixtures, or have a high gas content, they do not require the sophistication of some of the petroleum techniques developed. Therefore, the reservoir engineering techniques developed for a low-to-moderate temperature geothermal system borrow the most appropriate methods and terminology from hydrology and petroleum engineering. The theories are very similar but the terminology has created a disparity between the petroleum engineering and hydrologic industries when applied to a low-to-moderate temperature resource.

This disparity has created the need for a handbook that will bridge the theories and methodologies of the hydrologic and petroleum engineering fields. This handbook has been prepared for developers with previous experience in one or more of the following: petroleum engineering, ground water hydrology, and/or high-low temperature geothermal systems. In addition, the handbook should provide a useful tool to both consultants and industry personnel. The handbook identifies significant areas of concern, with reference to other

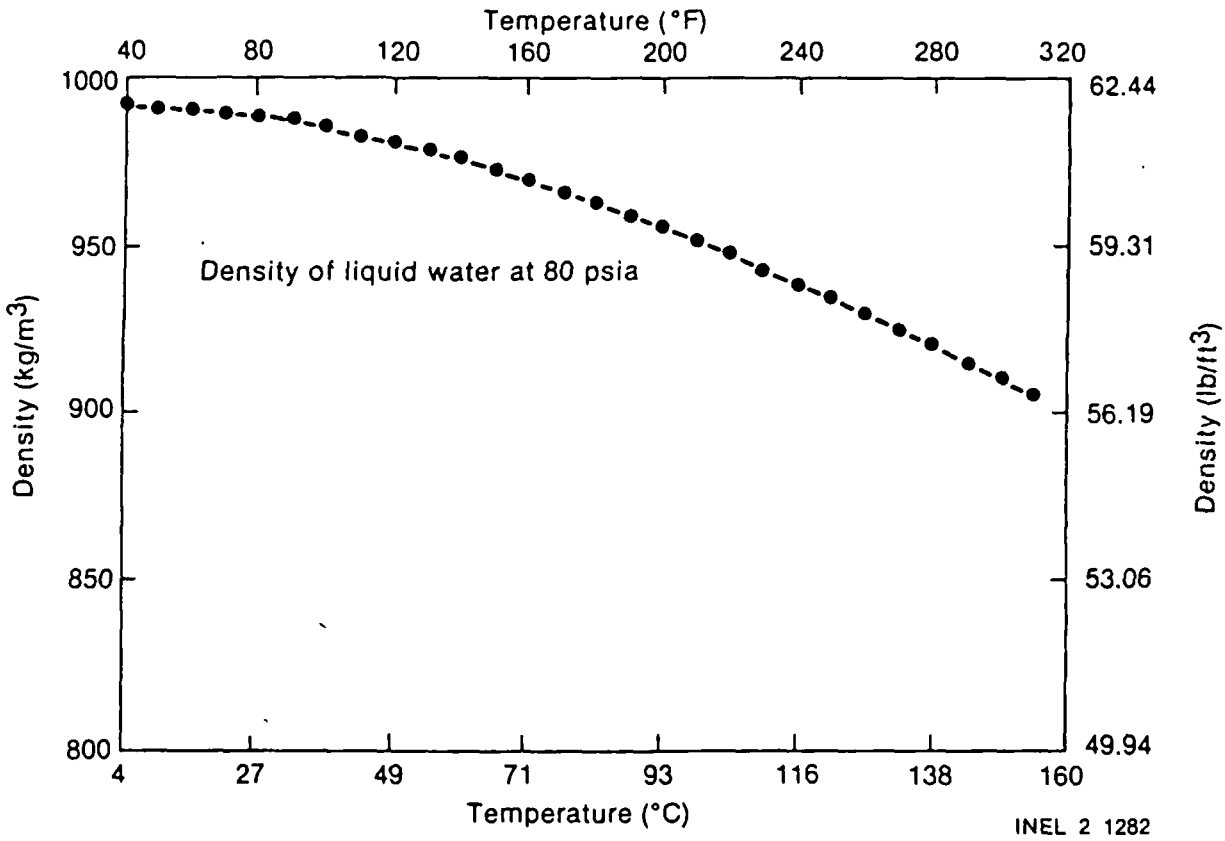

Figure 1. Density of liquid water at 80 psia.

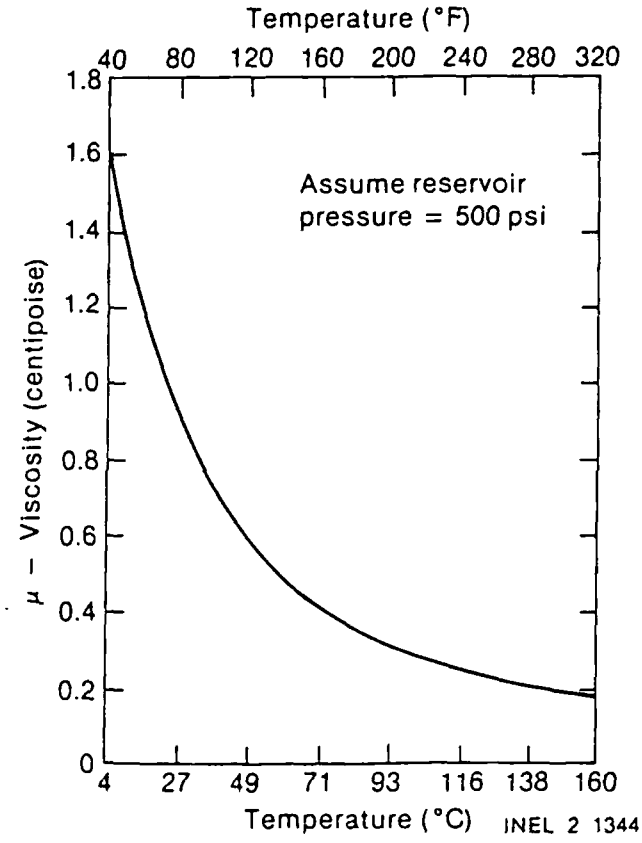

Figure 2. Viscosity of liquid water at 500 psia.

specific documents for in depth "how-to" discussions. The handbook provides an overview of reservoir engineering, basic and applied theory, conceptual modeling, testing during drilling, test planning and methodology, geochemical applications, and reservoir monitoring; it gives the potential developer a firm understanding of the tasks to be performed and the problems that may be anticipated.

2. RESERVOIR CLASSIFICATION

Individual geothermal systems occur in several different geologic environments. These include:

- Areas of recent intrusion and/or extrusion
- Areas where open fractures allow fluid circulation to depth with subsequent heating by the normal geothermal gradient
- Areas where radiogenic heat is trapped in rocks by overlying sediments
- Geopressured areas where hot fluids are confined under high pressures
- Areas where hot rocks exist without adequate natural fluids to transfer the heat (hot dry rock).

Young igneous environments primarily occur in the tectonically active Western United States (Figure 3). These systems provide the majority of known shallow geothermal reservoirs. The Cascade Mountain Range of Washington and Oregon represents a volcanic region caused from heat generated by the converging of plate margins. The Imperial Valley of Southern California is located in a region of crustal extension due to the East Pacific Rise spreading zone. Here the intrusions are emplaced at shallow depth, providing a heat source for the geothermal resource. The Snake River Plain of Idaho and Yellowstone Park represent volcanic areas caused by intraplate melting. Young volcanic regions also occur in some parts of the Basin and Range Province, and in the Rio Grande Rift. The heat source in volcanic belts is provided by the presence of cooling magma.[1]

Deep circulation primarily occurs where the crust of the earth is under tensional stress. The Basin and Range Province and the Rio Grande Rift are extensional environments characterized by active faulting, thick sedimentary basins between young mountain ranges, and occasional sites of active volcanism. The source of heat for this environment comes from higher-than-normal regional heat flow, circulation of fluids to great depths, and igneous intrusions.

Radiogenic heat environments are generally found along the Atlantic Coastal Plain where a thick sedimentary sequence is underlain by granitic rocks. This heat, trapped by rocks with low thermal conductivity, is generated by the decay of U^{238}, Th^{232}, and K^{90} found in high concentrations in granitic intrusions.

Geopressured geothermal reservoirs occur mainly in the Gulf of Mexico where rapid sedimentary loading has trapped the heat under a thick sedimentary blanket. The fluids are under high pressure, usually contain dissolved methane, and are normally 150°C or higher. These reservoirs are not pertinent to a discussion of direct-use application energy resources because of the great diffficulty in developing them; however, waters of low-to-moderate temperatures have been found overlying many geopressured zones.

In this handbook, geothermal systems are classified according to the reservoir characteristics that control fluid flow. These controls are either faults, intergranular permeability, or a combination of both. Fault-controlled systems occur primarily in metamorphic and igneous rocks, but can also occur in sedimentary rocks. Fault control is normally associated with hydrothermal convection systems where cold ground water circulates to depth, heats up, then rises along fractured zones. The heat in these systems is dependent on the regional heat flow, the depth of circulation, and the residence time of water at depth. The permeability of these reservoirs depends on the size and number of fractures in the system, the nature of brecciated material along the fault, and the degree of fracture sealing. Geothermal reservoirs controlled by intergranular permeability normally occur in deep sedimentary basins filled with consolidated or unconsolidated sediments. Ground water from adjacent highlands travels down-dip through the sediments and is heated by the thermal gradient of the earth. Heated water moves upward due to density differences to form geothermal reservoirs within economic exploitation depth. Permeability is controlled by the size and continuity of the pore spaces. Many geothermal reservoirs are controlled by a combination of both faulting and intergranular permeability.

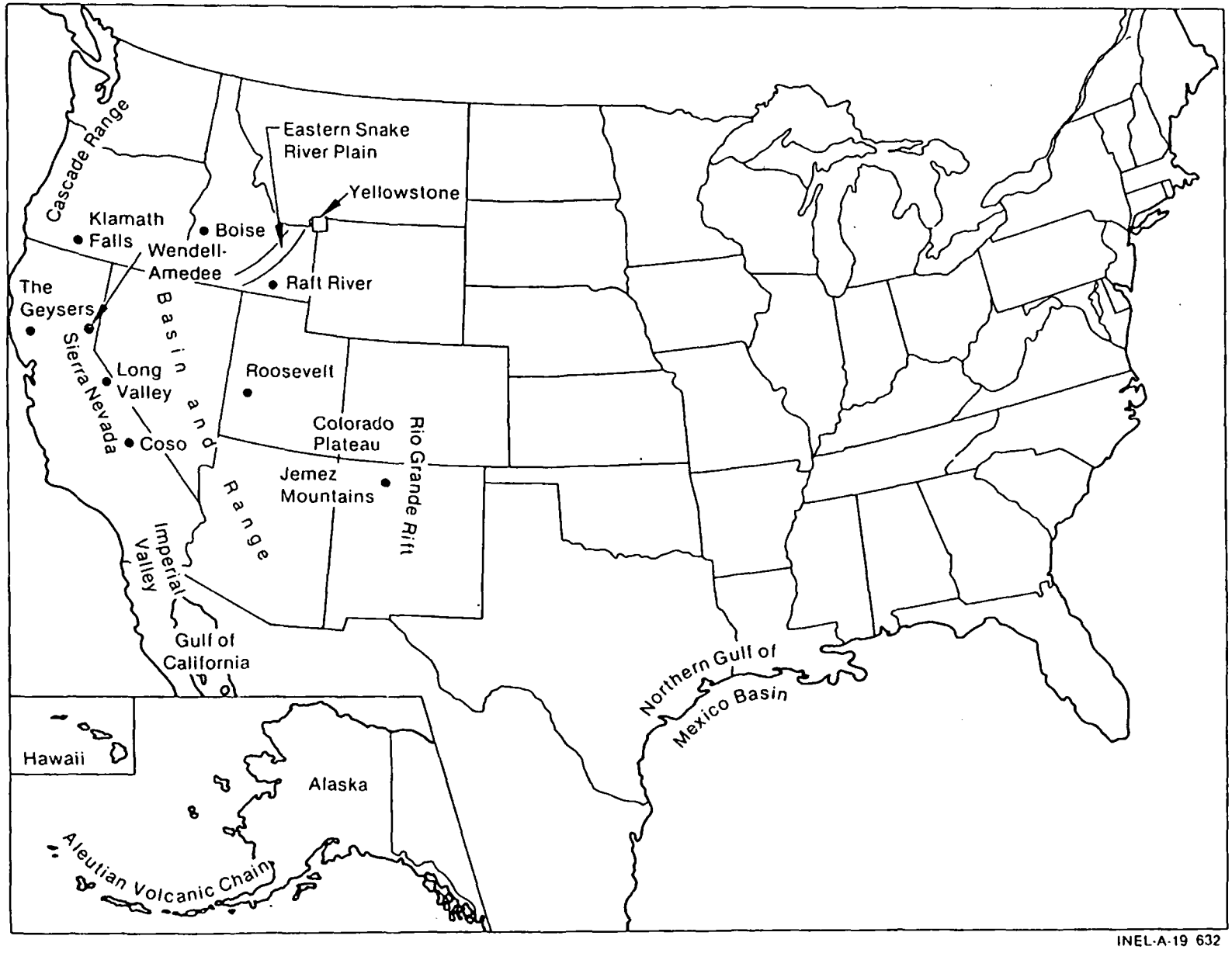

Figure 3. Map of the United States showing geographic features mentioned in the text and selected geothermal installations.

3. RESERVOIR ENGINEERING

Reservoir engineering can be defined "... as the application of scientific principles to the drainage problems arising during the development and production of oil and gas reservoirs. The working tools of the reservoir engineer are subsurface geology, applied mathematics, and the basic laws of physics and chemistry governing the behavior of liquid and vapor phases of crude oil, natural gas, and water."[2]

Reservoir engineering has been developed to a high level of sophistication in both the petroleum and ground water industries. Geothermal reservoir engineering has borrowed heavily from both of these fields. Some features unique to geothermal reservoir engineering include dynamic hydrothermal regimes and non-isothermal temperature distributions.

Reservoir engineering is used to design development strategy, exploitation strategy, and reservoir management programs. The basic problems that should be considered in geothermal reservoir engineering are: pressure, temperature, fracture flow, chemical changes within the thermal reservoir, and hydraulic connection to regional ground water aquifer(s). Specific aspects include: (a) siting production wells and choosing a completion interval; (b) designing well completions; (c) designing and interpreting well tests; (d) selecting the fluid disposal method, i.e., injection or surface disposal; (e) siting injection wells if any; (f) calculating the number of wells needed to supply the required energy; (g) predicting well drawdown; (h) predicting interference effects; (i) predicting the longevity of the resource; and (j) monitoring the exploitation phase.

The reservoir engineer must design a strategy that ensures not only an adequate supply of fluid, but also a fluid temperature that is suffficient for anticipated use. Predicting production temperatures over the life-time of the project is one of the most challenging tasks for the geothermal reservoir engineer.

Reservoir engineering starts during the exploration phase, when geological and geophysical data are collected. A reservoir engineer uses these data to formulate a preliminary conceptual reservoir model by identifying the reservoir type and its approximate size. Drilling data, borehole geophysics, and testing during drilling improve the conceptual model and provide preliminary well and reservoir parameters.

Well testing and test data analysis are important aspects of reservoir engineering that are used to determine the properties of a reservoir system which control the flow of fluids into a well, the migration path of injected fluid, and the natural and induced recharge.

Thus, the reservoir engineer uses all these phases when developing a geothermal resource.

4. CONCEPTUAL MODELING

Conceptual modeling is an important tool at every stage of reservoir evaluation. A conceptual model of the reservoir is envisioned before drilling a well in order to predict what type of rock formations will be penetrated, the expected temperature, and the target depth for the well. After the well has been drilled, a conceptual model is needed to design the well test and interpret well test data. Finally, the conceptual model is used to plan the locations of production and injection wells, optimize production and injection rates, predict the reservoir lifetime, and estimate the total energy available from the hydrothermal system. The conceptual model will evolve and become more refined each time a new piece of information is obtained, analyzed, and integrated into the existing model.

This section describes the types of data required to formulate a working model of a geothermal resource, especially ways of collecting data and integrating them into the model. Examples of different kinds of data gathered in other disciplines are provided for further understanding and conceptualizing the geothermal resource. Since this section is not a definitive work on the subject, references to additional studies are included. The importance of a conceptual model to the design of the well and the interpretation of the well test data are also discussed.

Before drilling any wells the following information can be used to conceptualize the geothermal resource: geothermometry, surface geology, and geophysical surveys. Comparing the geologic setting of the reservoir under investigation to the geology of many known geothermal resource areas can help classify the reservoir. Although every geothermal resource has unique characteristics, the rapid development of many low- and moderate-temperature geothermal resources has provided an adequate data base so that extrapolation of types of phenomena from one system to another is to some extent plausible. The study of similar types of hydrothermal systems should not be overlooked in developing a conceptual model.

Data obtained during drilling provides information on the subsurface characteristics of the hydrothermal system. Drill cuttings and cores can be used to reconstruct the subsurface lithology penetrated by the borehole. Drilling rates provide information on the structural integrity, hardness, and density of the formations penetrated. Loss of circulation fluid while drilling is often a reliable indication of fractures or permeable strata. Drilling mud temperature and mud chemistry are indicators of subsurface temperature and fluid entry into the wellbore.

After drilling a well, a number of borehole geophysical logs are run from which formation porosity and permeability, lithology changes, and formation temperature can be inferred. Well testing is performed to determine the hydrologic and geometric properties of the system. Well tests can also be helpful for inferring subsurface areal temperature distribution.

The effectiveness (i.e., accuracy and refinement) of a conceptual model is dependent on the information that is incorporated into it. The geologic, thermal, geochemical, and structural complexity of the hydrothermal system dictates the amount and type of data required to have a functional and accurate model. For instance, in a system with a near normal geothermal gradient and relatively simple geologic structure, such as the Madison Aquifer, less reconnaissance and exploration effort will be required. On the other hand, in a shallow, highly faulted, complexly fractured volcanic-type system, such as the Klamath Falls known geothermal resource area (KGRA), a substantial amount of exploratory work is necessary to define the hydrothermal system and to predict reservoir performance confidently. The degree of refinement required for an adequate conceptual model depends on the intended use of the resource. If only a small quantity of geothermal fluid is to be extracted from the reservoir compared with the reservoir potential, less exploration and conceptual model development will be required than if the reservoir potential is to be taxed. The model's refinement also depends on the amount of time and effort available to invest in gathering quality data. It should be emphasized that without quality data it is very difficult to predict confidently the reservoir's behavior during exploitation. Sophisticated methods are now being developed to interpret data from complex geothermal systems. Therefore, every effort should be made to obtain quality data. The following subsections describe what data are important to have, how to process them, how to interpret them, and how the conceptual model can be used to the benefit of the resource developer.

Data Base

Surface Geology. Surface maps are the most readily available piece of information used for delineating geologic features. Information obtained from the surface map will be used for preliminary classification of the hydrothermal system. Geologic mapping has been completed for many areas on a regional or site-specific basis. These maps are available through publications from the U.S. Geological Survey, state geological surveys, and universities.

Aerial photography and landsat imagery interpretation can also be useful tools for delineating major geologic features. They are normally used in conjunction with geologic maps to locate fault lineations, fault intersections, and areas of thermal alteration.

Subsurface Geology. The subsurface geology of an area is usually constructed from data obtained from the examination of drill cuttings, cores, geophysical logs, drillers logs, etc. The drilling rate, circulation fluid record, and drilling fluid temperatures provide data on the physical and thermal properties of the penetrated rock unit. Geophysical logs are also useful tools for identifying subsurface lithologic units and the physical properties of the units. The interpretation of geophysical logs is an important technique in evaluating the subsurface lithology when there are no drill cuttings or cores available. Their use and interpretation are, however, limited depending upon the formation encountered, i.e., porosity and permeability values can be determined from logs run in sedimentary units, but may not always be determined in igneous or metamorphic units. Geophysical logs can be a useful tool for correlating rock units, thermal regimes, and hydrothermal mineralization between wells, and in locating fracture zones in wells.

Many of the low-to-moderate temperature hydrothermal reservoirs in areas with above-normal temperature gradients are associated with faults and fractures. These faults and fractured strata contribute significantly to the permeability of the hydrothermal reservoir; therefore, it is essential to detect their presence and estimate their depth. Among the most useful methods for detecting fractures is the examination of a carefully maintained record of the amount of circulation fluid used. Sudden loss of circulation fluid often indicates that fractures have been penetrated. However, the loss of drill cuttings and circulation fluid is not always indicative of fracture zones. Therefore, all of the subsurface data should be correlated to verify the data interpretation.

Temperature Profiles. Temperature profiles are obtained by measuring wellbore temperatures at a number of depths in the well. Temperature profiles are one of the most useful tools for understanding the hydrothermal system being studied. By carefully examining temperature profiles obtained under a variety of wellbore conditions, producing aquifers can be identified, multiple producing aquifers can be identified, hot water recharge detected, conductive versus convective (hydrothermal circulation) thermal regimes identified, the presence of a caprock and basement rock detected, and the thickness of the hydrothermal reservoir penetrated by the wellbore estimated.

Some caution should be taken when interpreting temperature profiles because circulation of fluid in the wellbore can mask the true formation temperature. An example of this can be seen in Figure 4. The only difference, other than the temperature profiles, between the two wells is the casing schedule. Well YMCA No. 1 is cased to 500 ft (152 m) and well YMCA No. 2 is cased to 980 ft (305 m). By comparing the two profiles obtained in wells 500 ft (152 m) apart with identical lithologic columns, it was determined that water was flowing down the wellbore in the well YMCA No. 1. Cold water entering the wellbore in well YMCA No. 1 at 500 ft (102 m), flowed down the wellbore and enters a second reservoir at 1200 ft (366 m). If the data from well YMCA No. 2 had not been available the temperature profile from well YMCA No. 1 may have been misinterpreted to conclude that the isothermal interval from 500 ft (152 m) to 1200 ft (366 m) was the geothermal aquifer. In reality, the main producing aquifer is in a fractured interval between 1200 (366 m) and 1300 ft (396 m).

Geochemistry. Information about geothermal fields which can be deduced from geochemistry includes: estimated subsurface temperature, location of heat source(s), directions of water movement, source of dissolved solids, sources of recharge, age (possibly), and whether hotter water exists nearby. Contouring maps

Thermal methods are among the most direct and commonly used methods for determining the location and size of a geothermal system. Thermal methods include: (a) calculation of the heat flow from the earth using thermal gradient data and thermal conductivity measurements, and (b) evaluation of the measured geothermal gradient. Among other things, these data can indicate the size and shape of the hydrothermal anomaly.

Seismic methods can be passive and active. Passive methods monitor natural earthquake activity to infer anomalous stress states due to possible heat sources, abnormal tectonic activity, and/or abnormal hydrostatic conditions. Detailed microearthquake surveys are also used to delineate active fault zones that may serve as potential ground water conduits. The active methods use the amplitude and velocity variation of seismic waves generated by a controlled source, both compressional (P) and shear (S) waves, to infer the characteristics of the medium in which they are propagated. Active reflection techniques are used to infer the location of discontinuities, layer, thickness, and general structure. Depending upon the size and frequency of the source, reflection techniques can "look" as deep as several kilometers and still define fault boundaries and basement structure. Refraction techniques look at the velocity variation of the P-waves to infer layer thickness, fault location, and structural discontinuities. The refraction techniques are not as detailed as the reflection techniques and require larger "spreads" and more powerful sources to look at comparable depths. The refraction techniques can also miss structure that the reflection surveys will detect if the velocity variations with depth are not continually increasing. However, the refraction techniques are much cheaper and require less sophisticated post processing.

Electrical and electromagnetic methods are used to estimate the electrical resistivity of the earth. Electrical resistivity is a measure of the earth's ability to conduct electrical current and depends upon the porosity, fluid saturation, temperature and clay content of the rock, and the salinity of the pore fluid. In general, the higher these parameters are, the lower the resistivity of the medium. Since geothermal areas are associated with high subsurface temperatures and saline fluids, they are characterized by anomalously low resistivity. Electrical and electromagnetic surveys performed on the surface are therefore very effective methods for locating buried geothermal systems. The most commonly used of these methods is the d.c. resistivity method. Low frequency electrical current is injected into the ground through a portable generator and earth electrodes. The resulting potential at a site of specified distance away is then measured. By varying the spacing between current and potential electrodes, a variation of voltage with separation and/or location is obtained. This may be corrected for a variation of electrical resistivity with depth, depth soundings, spatial variation at resistivity, or a mapping survey. Electromagnetic methods use a time varying signal source and obtain earth resistivity information from variation at electrical fields with frequency.

Gravity and magnetic surveys are structural methods used to estimate: the thickness of sediments, the depth to the basement, the density or density contrasts of basement rocks, and buried volcanic or intrusive rocks. Magnetic surveys detect the magnetic susceptibility of subsurface rocks. Because hydrothermal alteration reduces the magnetic susceptibility of the subsurface rocks, a negative anomaly may be indicative of a hydrothermal resource.

Well Testing. Well testing is the most common and reliable method for determining the parameters which control flow of fluid through the reservoir. The parameters which affect the ease with which water will flow through the reservoir are the rock permeability (k), the viscosity of the reservoir fluid (μ), the porosity (ϕ), the formation compressibility (c), and the production geometry (height, areal extent, layers, etc.). Knowing these parameters or the groups of parameters kh/μ (transmissivity) and ϕch (storativity), well drawdown, well productivity, and interference effects can be calculated.

Well tests are typically conducted by pumping or artesian flowing a well for a period of time at a constant flow rate. The pressure changes in the production well are observed over time. The change of pressure is analyzed to obtain the physical parameters of the reservoir system. If there are other wells in the area, these too can be monitored for pressure (or water level) changes as a function of time. Often the data from interference wells will provide more accurate reservoir information due to instrumentation and logistical constraints at the production well. If an array of observation wells is available, accurate information about the reservoir size and geometry can be obtained.

Data Preparation

Before the data from all of the various disciplines can be synthesized, it is important to prepare them correctly. There are four basic types of displays by which data can be processed to provide a visual respresentation of the various reservoir characteristics: mapping, profiling, contouring, and cross sections. Depending on the amount and quality of data, it may or may not be worthwhile to do all of the types of processing.

Mapping. Mapping is the least sophisticated and most simple display to prepare. It involves locating observed phenomena or physical features on a cartesian coordinate system that overlies the area under study. This type of representation is used when only a two-dimensional representation of the data is required, i.e., when depth is not considered. Temperatures and chemical data from springs are often mapped with this technique. The representation does not account for the fact that the springs may have circulation at different depths, and thus, differing chemical constituents and temperatures.

Mapping is generally used in the early stages of exploration. For example, the relationship between the recent volcanism and the hydrothermal anomaly at Klamath Falls, Oregon, was examined by radiometric dates obtained on rock samples from in and around the Klamath Falls area. A map showing the location and radiometric age of each sample is shown in Figure 5. The concentric pattern of older dates with distance from the Klamath Falls vicinity may suggest that the anomaly is associated with the most recent volcanism in the area.

Profiling. Profiling consists of looking at data from a single penetration through a vertical section. Profiled data are obtained from wellbore surveys. For instance, by plotting the well lithology versus depth a lithologic profile is obtained; by plotting temperature obtained from a temperature survey versus depth, a temperature profile is obtained.

One example of a lithologic column and temperature profile for a well is shown in Figure 6. This type of temperature profile is typical of temperature profiles in shallow fault-charged reservoirs. A comparison of the lithologic column, the drilling circulation record, and the temperature profile shows that a thermal production interval in the well is between 195 ft (59 m) and 240 ft (73 m).

Contouring. Contouring is used to define the shape and extent of the observed physical phenomena. For instance, temperature contours are used to define the areal and vertical extent of a hydrothermal system and can be used to make rough calculations of the amount of hot fluid in place. One of the most common methods of contouring is to plot isotherms, or isobars, at a given depth below the surface. By comparing contours at several elevations, both an areal and vertical description of the phenomena can be obtained.

In Figure 7 the temperatures at three different depths from the Susanville, California wells are contoured. At the shallowest depth, 150 m below surface elevation (1250 m elevation), the hottest part of the anomaly (inside the 60 degree contour) is centered around the Davis well. With increasing depth the shape of the anomaly is asymmetrically elongated around a northwest trending axis. Using these contours and lithologic data, a production well (Susan 1) was sited next to Suzy 9. As predicted from these contours, the new well, Susan 1, was the hottest well drilled thus far.

Concentrations of chemical species may also be contoured at various depths to determine if and how mixing of different fluids is occurring. Static water levels are contoured to determine the extent and direction of regional ground-water flow.

Cross Sections. Cross sections are constructed by correlating or comparing profiles at two or more wells. Multiple cross sections, or cross sections and contours, may be used to get a three-dimensional model of the reservoir. Lithologic data are typically processed this way. Correlations of major geologic features, such as fracture zones, producing aquifers, caprock, and basement rock are obtained by constructing cross sections of the reservoir data. Temperature data are also plotted as cross sections and provide a multidimensional view of the hydrothermal structure. Two cross sections of temperature distribution are shown in Figure 8. This

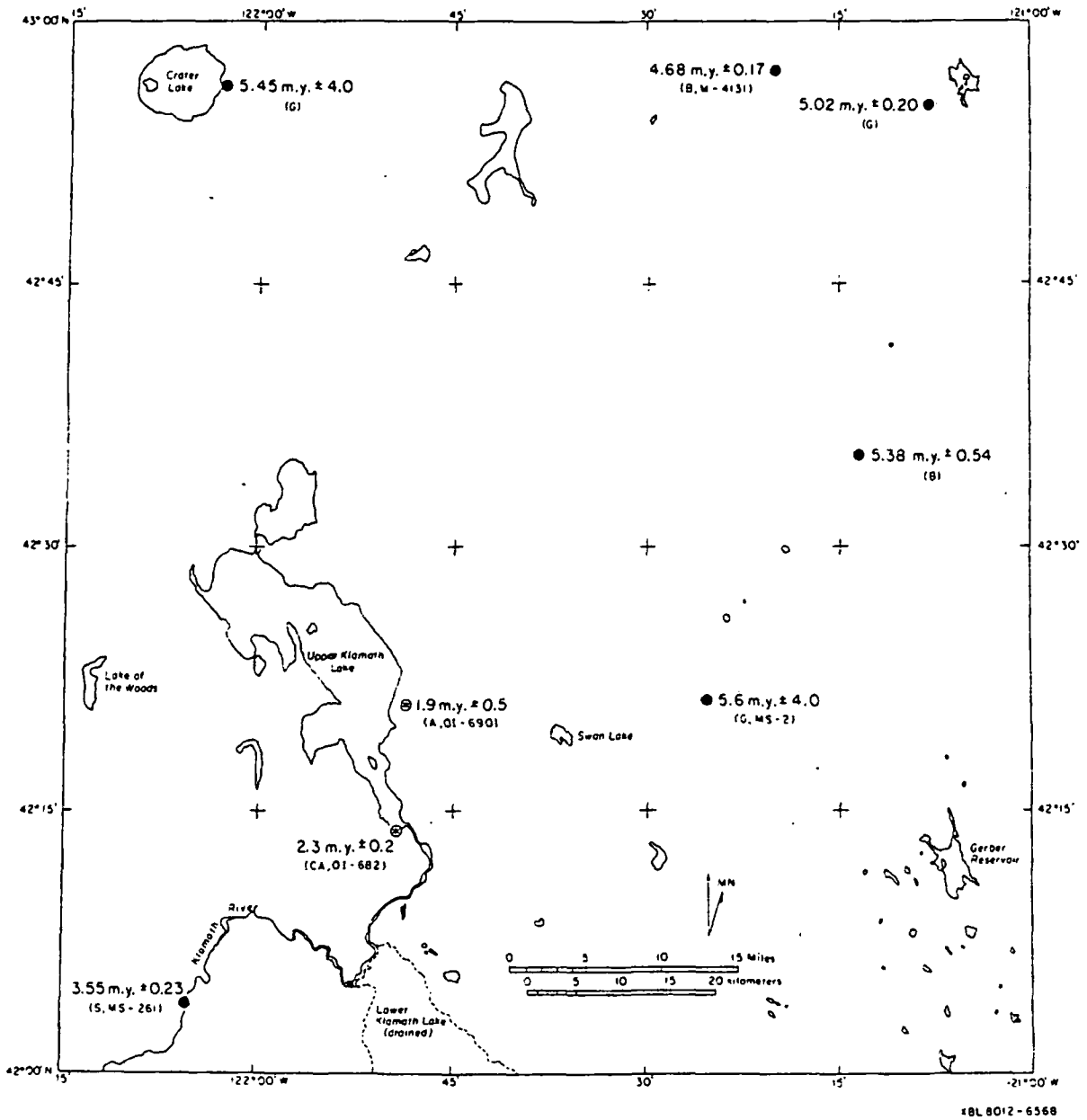

Figure 5. Rock sample locations from Klamath Falls, Oregon.

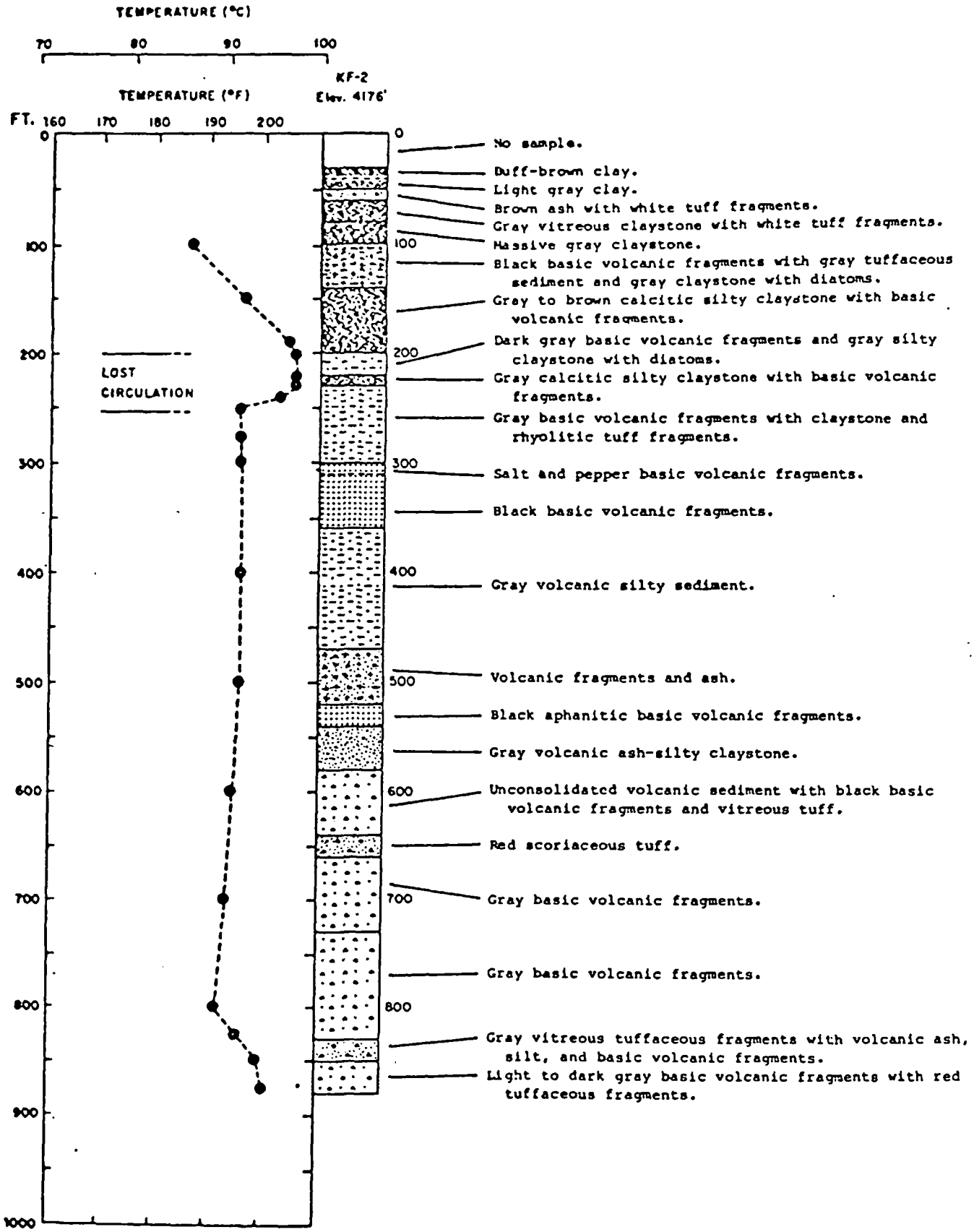

Figure 6. Temperature profile and lithology for Klamath Falls, City Well No. 2.

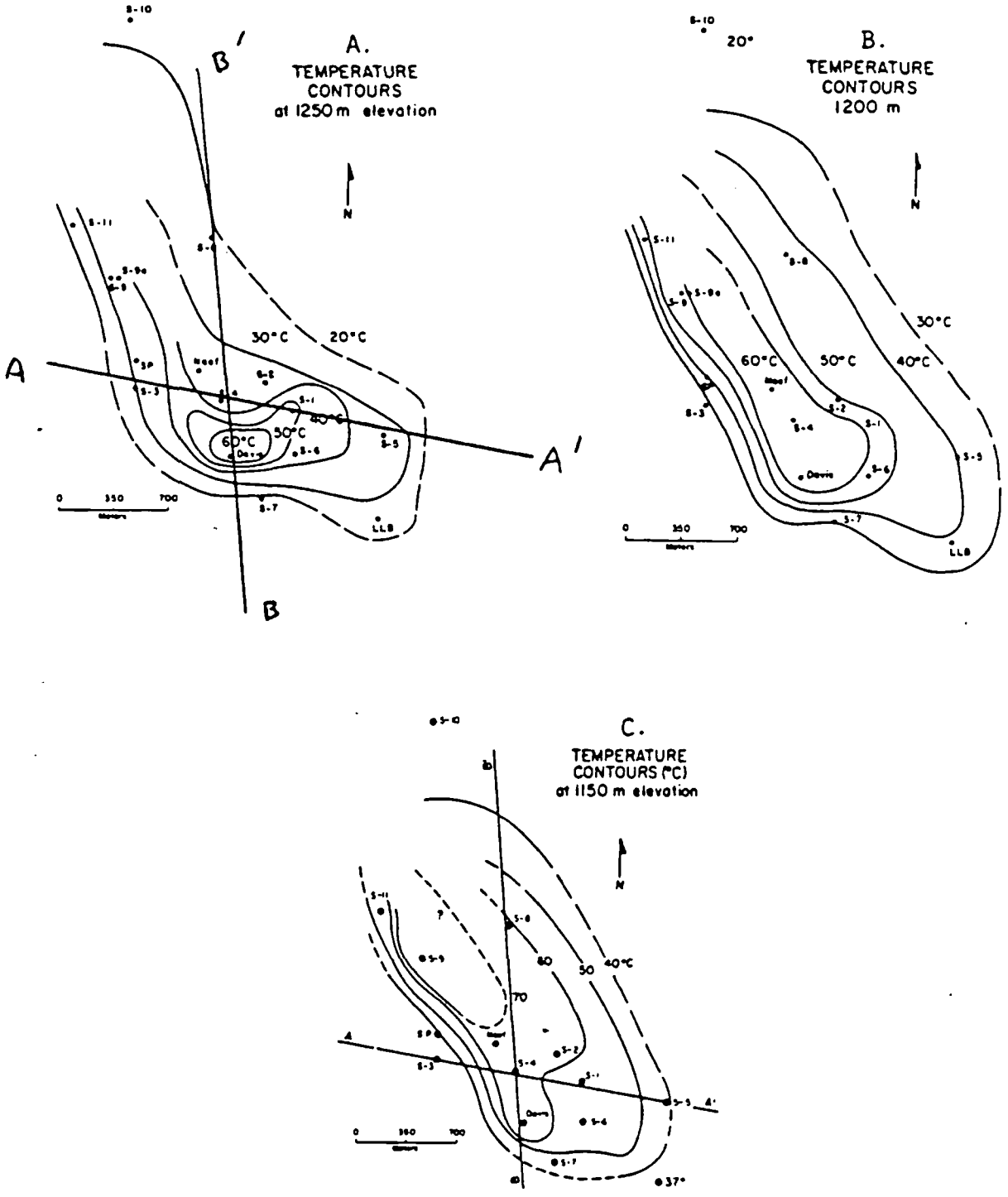

Figure 7. Subsurface temperature contours: (a) at 1250 m elevation, (b) at 1200 m elevation, and (c) at 1150 m elevation.

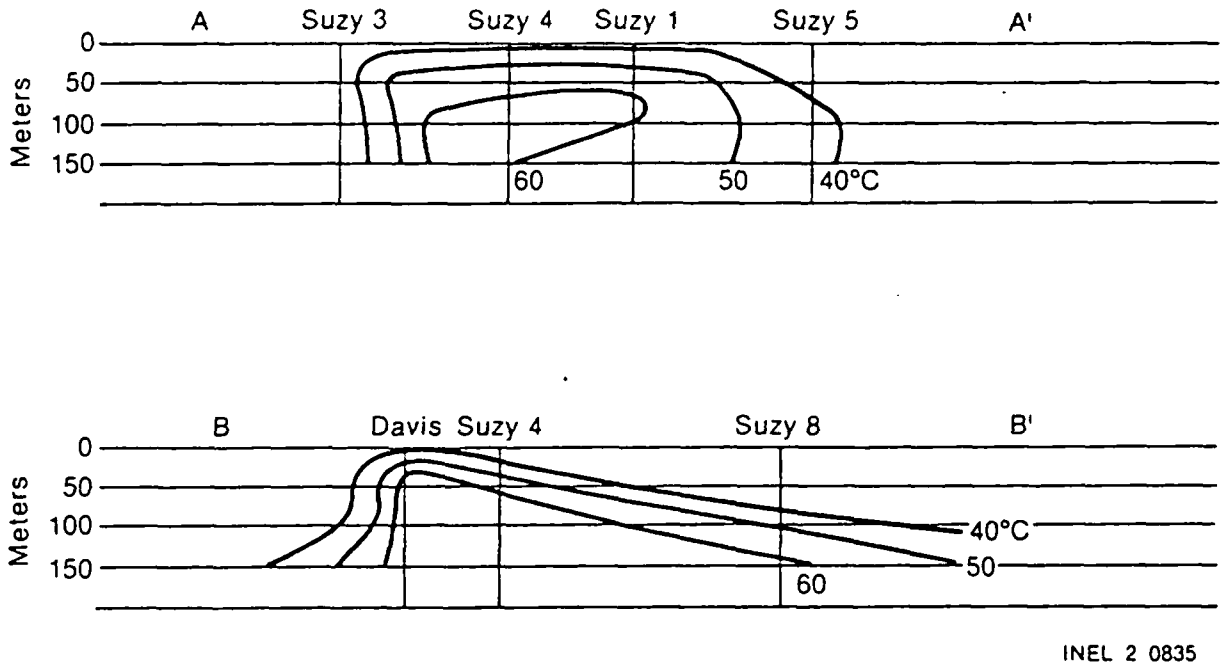

Figure 8. Cross sections of the Susanville hydrothermal anomaly.

type of thermal structure is indicative of upwelling of heated fluids from depth and lateral transport of fluid along permeable beds and fractures. This type of hydrothermal structure is common in shallow geothermal anomalies in the Cascade Range and the Basin and Range Province.

Borehole geophysical logs, such as electrical and nuclear logs, are also correlated on cross sections and are useful indicators of physical properties of the geologic section penetrated by the wellbore.

Graphically representing data in all of the above display forms helps to synthesize subsurface reservoir data with data obtained from surface reconnaissance. The subsurface reconstruction from each discipline should be compared to obtain a coherent conceptual model. Table 1 lists the various ways to process data.

Table 1. Common methods of data preparation

	Map	Profile	Contour	Cross Section
Surface Geological	X	X	—	—
Geochemical	X	X	X	—
Surface Geophysical	—	—	X	X
Hydrologic	X	X	X	—
Lithologic	—	X	—	X
Geophysical Logs	—	X	—	X
Thermal	X	X	X	X

Data Synthesis

The purpose of synthesizing data from each of the disciplines discussed above is to identify the major lithologic, thermal, petrophysical, and structural controls on the hydrothermal system under investigation. The key parameters that govern how a hydrothermal system behaves are: the permeability, storativity, size, and geometry of the production zone(s), the boundary conditions on the producing aquifer such as lateral recharge (hot or cold) caprock and basement rock leakage; regional ground water flow, and thermal distribution in the resource. Hydrothermal reservoirs are often very complex both lithologically and structurally. For this reason it may be diffficult, if not impossible, to identify all of these major features. Nevertheless, an attempt should be made to identify these features because they play a critical role in interpreting well test data, designing the reservoir management program, and providing an overall understanding of the resource.

The first step in synthesizing all of the data is to correlate specific physical, thermal, and lithologic units between wells. If data from only one well are available, correlation between wells will not be possible. However, a thorough evaluation of all of the data from that one well should be performed. The features that identify the production zone, caprock, basement rock, and the physical parameters are discussed below.

Producing Zones. The major production intervals can be identified by numerous features depending on the geologic setting. For instance, in a thick sedimentary sequence, a permeable aquifer will probably occur in a sandstone, and over and underlying impermeable layers will consist of a shale or clay sequence. The temperature profile through such a sequence would consist of several distinct gradients: a convective gradient through the aquifer and a conductive gradient through the underlying boundary layer. An example is shown in Figure 9. In a fractured rock sequence, the production zones (fractures) may be located by fluid entry into the wellbore during drilling, or by loss of circulation fluid into the formation. Production zones in fractured rocks may also be indicated by temperature profiles as was demonstrated in the previous section in Figure 6.

There is no single method of detecting the production zones; however, they can usually be identified by one or more of the following methods:

1. Loss of circulation fluid when drilling through the aquifer
2. A convective thermal gradient as opposed to a conductive gradient
3. Indication of sand zones or high-water-content zones from geophysical logs or cuttings
4. Fluid entry into the wellbore during drilling
5. Fracture zones indicated during drilling
6. Spinner surveys (downhole flow meter).

The properties of the producing aquifer(s) which need to be determined are: transmissivity, storativity, temperature distribution, structure, and geometry.

In general the reservoir transmissivity and storativity can accurately be determined only by well testing. However, before well testing, the type and degree of permeability can be determined by examining items discussed above. The two most common types of permeability are matrix and fracture. Matrix permeability occurs when the fluid flows through porous spaces in the rock. The fluid enters the wellbore from the entire aquifer interval. If the flow in the reservoir is confined mainly to fractures in the rock, then the term fracture permeability is used. In systems with fracture permeability, flow into the well comes only from the fracture, not the matrix of the rock. However, away from the wellbore, fluid may enter the fracture by flowing from the rock matrix into the fracture. The fracture is a conduit for fluid to flow into the wellbore. Many hydrothermal systems are some combination of fracture and matrix permeability and these systems are called dual-porosity systems. In general, hydrothermal systems that occur in volcanic and metamorphic rocks will have a

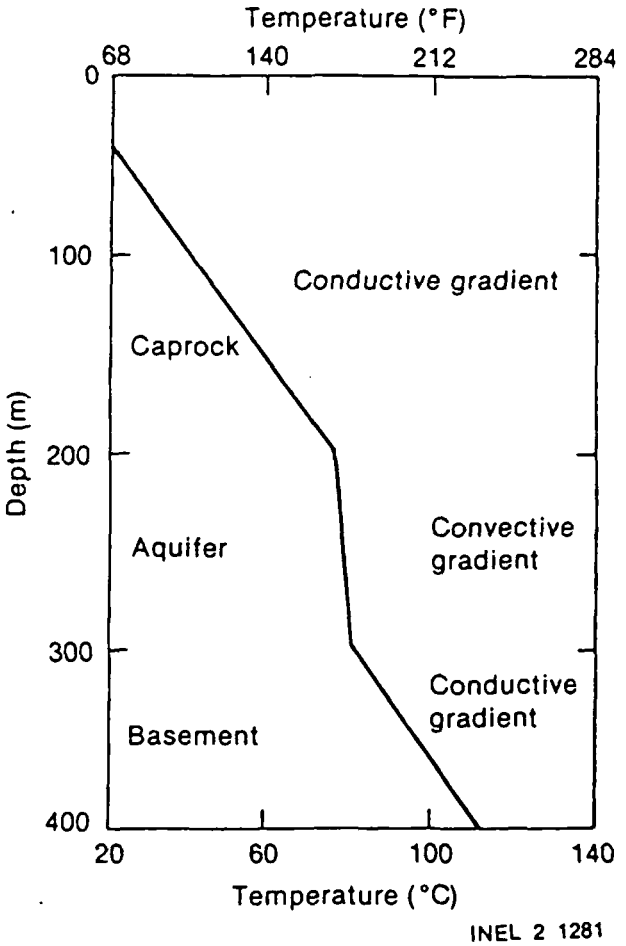

Figure 9. Example of a typical temperature gradient through of sedimentary sequence showing the caprock, aquifer, and basement.

fracture-dominated permeability. Sedimentary formations, except for carbonate systems, will in general have a type of matrix permeability. There are, however, exceptions to this generalization.

The temperature of the producing aquifer may be measured with a downhole temperature probe. It is important to measure the temperature downhole because any measurement taken at the surface may be affected by cooling and mixing as the fluid moves up the wellbore. Except in deep, near-normal geothermal-gradient type reservoirs, the temperature in the producing aquifer will vary spatially. It is important to have measurements of the temperature in the producing aquifer in as many wells as possible because the spatial variation of temperatures in the aquifer is one of the most useful tools for determining where and if hot water recharge is taking place. Temperature contours, at several depths, should be constructed. The interpretation of this is discussed in the previous section.

The important geometric characteristics of a hydrothermal aquifer are the areal extent, height, and shape. The volume of the aquifer (areal extent multiplied by height) is used to make a first-order estimate of the amount of hydrothermal fluids in place. Obviously, data must be available from more than one well to determine the areal extent of the resource. The shape of the hydrothermal aquifer is one of the major clues to understanding the resource. In near-normal geothermal gradient aquifers, it is the size and shape of the permeable (and porous) aquifer that governs the geometry of the hydrothermal system. In Basin and Range and fault-controlled hydrothermal systems it is usually the extent of the thermal anomaly which governs the geometry of the hydrothermal system. It is important to have some idea of the thermal distribution in the producing aquifer because thermal boundaries can be misinterpreted as hydrologic boundaries due to the temperature dependence of fluid viscosity.

Caprock and Basement Properties. The important properties of the confining strata in a hydrothermal system are permeability, continuity, rock type, and temperature. If the caprock or basement rock is permeable, it will supply fluid to the producing aquifer when it is pumped. Even though physical properties of caprock and basement rock are diffficult to determine, proper analysis of well test data can show leakage in caprock or basement rock. This is discussed in the section on well testing. It should be noted that a "true" caprock may not always exist and the resource may be so shallow that the basement characteristics cannot be identified. Caprock and basement rock can be identified by observing one or more of the following items:

1. A conductive thermal gradient as opposed to a convective thermal gradient
2. Delineation of a clay or shale layer from rock cuttings
3. Lack of evidence of fractures during drilling
4. Identification of low water content or shale layers from geophysical logs.

Knowledge of the location and type of confining rock is important because they are used to estimate the thickness of the producing strata and to determine if the wellbore penetrates only part of the hydrothermal aquifer. In this case, partial penetration of the wellbore into the formation, should be considered in the well test analysis.

Boundary Conditions. There are many types of boundary conditions on a hydrothermal aquifer, all of which will affect the results of a well test and reservoir response to sustained production. The aquifer may be infinite, or effectively infinite. The aquifer may be bounded on one side by a linear boundary such as a fault or rapid facies change. The linear boundary may be impermeable to fluid movement, supply a constant flow of hot or cold water into the aquifer, or remain at a constant head. The aquifer may be completely enclosed by impermeable or constant potential boundaries that are square, rectangular, polygonal, or radial. Different types of analysis apply to each of these systems. If the presence of some type of aquifer boundary such as a fault or fracture zone is suspected, the well test should be designed so that it is long enough to determine the hydrologic properties of the boundary. In order to calculate the radius of investigation, the following formula can be used:

$$r = 2\sqrt{\frac{kt}{\phi \mu c}}$$

where

k = permeability (m^2)

t = time (s)

ϕ = porosity

μ = fluid viscosity (Pa·s)

c = total system compressibility $\left(\frac{1}{Pa}\right)$.

In highly fractured and faulted hydrothermal systems, practical experience indicates that it is often difficult to detect the presence and type of reservoir boundaries. This is because the hydrologic systems are so complex that no single phenomena can be isolated and analyzed.

An estimate of the radius of investigation can be obtained even if the parameters are not all precisely known. For example, in a moderately permeable sandstone, the following calculation can be made:

$k = 100 \text{ md} = 1 \times 10^{-13} \text{ m}^2$

$\phi = 20\% \ (.2)$

$C_t = 1 \times 10^{-9} \ \frac{1}{\text{Pa}}$

$\mu = .3 \text{ cp} = 3 \times 10^{-4} \text{Pa•s}$.

The radius of investigation for a 10-hour test will be:

$$r = 2\sqrt{\frac{(1 \times 10^{-13}) \ 3.6 \times 10^{4}}{.2 \times 3 \times 10^{-4} \times 1 \times 10^{-9}}} = 490 \text{ m} .$$

For a one week test, the radius of investigation will be:

$r = 1003 \text{ m}$.

5. TESTING DURING DRILLING

Data collected throughout the drilling operation provide a basis for selecting the well test design and analysis methods to be used in evaluating aquifer characteristics. Mandatory data to be collected during operations include:

- Lithologic logging
- Drilling engineering records
- Geophysical logging
- Transient temperature profiles.

Lithologic Logging

Lithologic logging is an important tool used during drilling and should not be overlooked. Through proper lithologic logging one can identify rock type, formation, and position in the stratigraphic section. If used properly, analysis of the drill cuttings can characterize porosity and hydrothermal alteration, and assist in finding faults and zones of fluid entry. Because of rapid and abrupt changes which occur in faulted and altered rock, composite samples should be taken over no more than 10-foot intervals. Analysis of cuttings should be performed by a qualified geologist familiar with igneous, metamorphic, hydrothermally altered rocks, fault gouge, microbreccia, slickensiding, and mylonite. Unwashed samples should be collected to avoid the loss of fine-grained cuttings.

Drilling Engineering Records

Under ordinary drilling conditions, a number of measurements are made and recorded to assist the drilling engineer in making effective drilling decisions. These drilling parameters include drill rate, rotary speed, pump speed, pump pressure, weight-on-bit, and mud volume totalizers. When parameters are properly employed, decisions can be made on bit changes, borehole deflection, lost circulation, casing sizes and settings, etc.

These data also assist the reservoir engineer in evaluating the subsurface. Although these data are not conclusive, tests during drilling in the typical sense of testing, can assist the reservoir engineer in determining rock strengths and porosity from penetration rate; in identifying hot aquifers from circulation fluid temperature-in, temperature-out; and in assessing fractures and fault zones where lost circulation has occurred. All such information will be of a qualitative nature, to be evaluated further by testing methods of a quantitative nature. Nevertheless, they do identify specific sections in the wellbore that merit further evaluation.

Geophysical Logging

Borehole geophysical logging techniques measure the physical properties of the rock. Coupled with other drilling data, the logging analysis can help in defining porosity, rock type, wellbore size, bulk density, dip of rock strata, fluid temperature, and, to a limited degree, rock fractures.

Commercial logging companies provide the log tool service and deliver a graphical output to the customer. These data should be analyzed with input from other drilling information to provide an interpretation of the wellbore and rock conditions. Conventional analytical techniques for sedimentary rocks cannot be routinely

applied to all geothermal resources because of the nature of the rocks encountered (i.e., igneous and metamorphic). Current research efforts are providing interpretive measures for these geothermal environments. Although, it is a fairly expensive service, geophysical logging is a routine tool that should be used for every geothermal well.

Transient Temperature Profiles

The downhole temperature should be measured routinely during the drilling process. Temperature profiles can be performed by a commercial logging company or by a hydrogeologist. Temperature profiles are inexpensive and do not require a long period of time. They can be used to determine cold- and hot-water production zones and loss-of-circulation zones. Temperature logs can provide useful data for determining the depth for setting casing.

The Horner plot method is used to plot transient downhole temperature. The Horner plot is a graph of temperature build-up versus log $\frac{t_k + \Delta t}{\Delta t}$ where t_k is circulation time before shut-in and Δt is buildup time. The static temperature obtained using the conventional Horner plot is lower than the true reservoir temperature.[4] For example, let us assume that prior to running a log suite to set a string of casing, the well was circulated for four hours. Following this circulation period, a series of logs were run and the following times and temperatures observed:

Time (hr)	Temperature (°F)	$\frac{t_k + \Delta t}{\Delta t}$	
0200	Circulation completed	—	
1215	255	14.25/10.25	= 1.39
1500	255	17/13	= 1.31
1630	257	18.5/14.5	= 1.28
1930	260	21.5/17.5	= 1.23
2400	262	26/22	= 1.18

A plot of this data is shown in Figure 10. The estimated static temperature is obtained by an extrapolation of the straight line to a time ratio of unity, which is equal to 272°F. It can be assumed this is probably a lower limit temperature to the true static temperature.

Optional testing methods include:

- Drill-stem tests
- Coring
- Geochemical logging
- Swab and lift tests
- Downhole flow meter tests.

Drill Stem Tests

Drill stem tests (DSTs) are normally conducted in a zone of undetermined potential.[3] The drill stem tool is attached to the drill string and lowered into the zone to be tested. A packer is set to isolate the zone. Formation fluids from the isolated zone flow into the drill pipe. A continuous pressure record is obtained during the

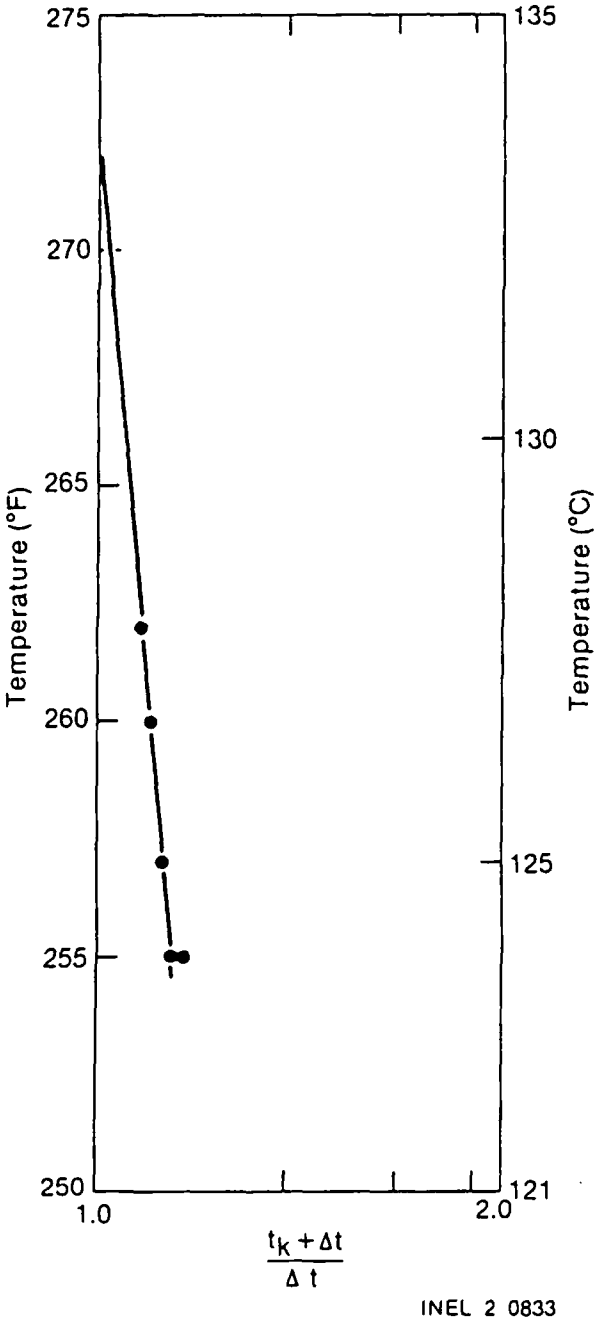

Figure 10. Horner plot of static temperature approximation.

production and shut-in periods. DST data are analyzed to assess preliminary reservoir parameters (i.e., permeability, hydraulic conductivity). At the conclusion of the test, representative fluid samples are collected for further geochemical analysis (refer to Geochemistry Section 8).

An alternative to the drill stem test is a wireline repeat formation test. This test is capable of multiple settings downhole and of retrieving two fluid samples per trip in the hole. The principles governing multiple-level pressure measuring are similar to those of the DST. Wireline testing is attractive because it is fast and less costly than drill stem testing; however, a wireline test is a less accurate method and interpretation of the data is only partially quantitative. Drill stem and wireline formation tests are commonly used in the petroleum industry. Use in geothermal well testing is not expected to be widely applicable due to fractured flow

conditions. In a fractured reservoir environment, the data from these kinds of tests may provide erroneous information due to the short flow durations. However, these types of tests may prove valuable in evaluating the results of well stimulation jobs.

Coring

Core drilling allows for the recovery of whole rock samples from a selected interval. Core samples are used to correlate geophysical logging data with rock properties, to perform laboratory permeability tests, and to delineate stratigraphy and lithology profiles. Core drilling is an important tool used in oil and gas exploratory drilling. The high cost of coring is prohibitive for routine use, but may provide useful information for selected intervals in geothermal wells.

An alternative to core drilling is a technique called sidewall coring. This method uses a wireline for collection of the sample. Sidewall coring is quick and inexpensive; however, core samples are small in size and may have limited laboratory use. Sidewall coring will not provide adequate samples in fracture-dominated geothermal systems due to the limited data regarding fracture density, character, and orientation that can be obtained from the small sample.

Geochemical Logging

Geochemical logging can be useful in identifying geothermal production zones during drilling. Geochemical logging procedures are discussed in detail in Section 8.

Swab and Lift Tests

A swab test is used as a method for withdrawing fluid from a borehole. The procedure employs a swab valve attached to a rig sand line. This method provides limited information on well productivity and allows the collection of representative fluid samples. Swabbing and mechanical surging are commonly used methods for the development of a ground water well but may be of limited use to geothermal resources. This is a hazardous technique because of the possibility of high-pressure vapor and gas blow outs.

Airlifting using compressed air or other gases is another mechanism for withdrawing fluids from the hole. This stimulates the well and yields limited information on well productivity. Approximate flow, water level recovery, and temperature data should be collected. Fluid temperatures are affected by the ambient air temperature. A correction should be made for the estimated cooling effect. The accuracy of reservoir characteristics determined from an airlift test may be questionable, since air or gas may give erroneous flow measurements and water level recovery is diffficult to obtain. Nevertheless, geothermal well drillers may employ swabbing and airlifting methods to both develop wells and perform limited well testing.

Downhole Flow Meter Test

Vertical flow of fluids in the borehole can be measured using a downhole flow meter (spinner device). Downhole flow meter tests may be conducted while producing or injecting fluid into a well. The hole should be relatively clean because the instrumentation can be easily plugged by mud or drilling debris. This method is used to indicate production or high permeability zones. The data can be evaluated to determine the amount of fluid entering the borehole from different zones. Used together with a temperature profile, this test may be useful for casing and screen setting decisions.

6. THEORY OF AQUIFER TESTING

Aquifer testing is the correlation of well production at various rates with temporal pressure or water level changes. Inferences may be drawn from such tests about the size and ability of an aquifer or reservoir to transmit and store fluids. Well testing is the only method that provides in situ information about an aquifer or reservoir on a scale meaningful for long-term exploitation of a resource. Despite the fundamental unity in the principles of well testing, the art of well testing has developed in two parallel fields: hydrogeology, following the lead of C. V. Theis[5] and petroleum engineering, following the early contributions of Hurst.[6] Hydrologists have been concerned with determining aquifer constants (transmissivity and storage coeffficient) and interference-type testing of shallow systems. Petroleum engineers, on the other hand, have been concerned with interpretation of production/injection testing of deep systems. High-temperature geothermal well testing (usually steam flows) has followed the petroleum engineering lead. Low-to-moderate temperature geothermal well testing (usually hot water flows) requires adaptations from both the ground water and petroleum fields.

The equations developed for various aquifer and well conditions provide tools for analyzing data from many different hydrogeologic conditions. However, the simplifying assumptions used to develop the solutions are usually only partially satisfied. In addition, many of the solutions result in curves of similar shape, and thus are not unique to one flow system. Consequently, careful site evaluation and well test design by a qualified petroleum reservoir engineer or hydrogeologist are essential to ensure the success of planned testing.

Essential Elements of Well Tests

Geothermal well testing usually consists of operating the well with a controlled flow rate and measuring three variables (flow rate, water level or pressure, and fluid temperature) as time passes, while other parameters (distance, r, to the observation wells, permeability, reservoir dimensions, and storage capacity) remain constant. The flow rate, water level or pressure, and time are the primary data required for test analysis. Temperature measurements provide data for corrections for temperature effects related to changes in fluid density and viscosity. Fluid chemistry, geology, geophysics, and well construction data are also important parameters in test data interpretation.

Basic Equations

Well testing analysis methods are based on the basic equations of flow through porous media presented below. The symbols used first are those usually found in the water-well literature. The same equations are repeated in the symbols of petroleum engineering references.

Darcy's Law

Darcy[7] observed from experiments on apparatus similar to that illustrated in Figure 11 that the speed of laminar flow of water through sand is proportional to the hydraulic gradient. He expressed this concept by the following equation now known as Darcy's law:

$$q_s = \frac{Q}{A} = -K \frac{\Delta h}{\Delta \ell} = -K \frac{dh}{d\ell}$$

or

$$Q = KiA \qquad (1)$$

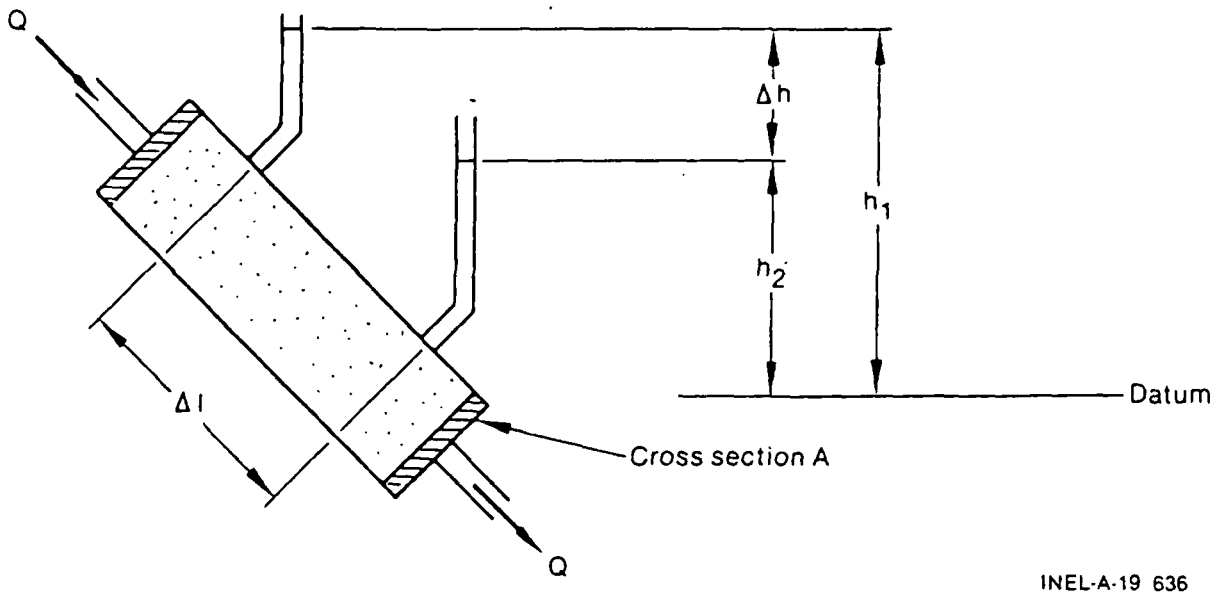

Figure 11. Laminar flow speed measurement apparatus.

where

q_s = specific discharge (L/T)

Q = flow rate (L^3/T)

A = cross-sectional area (L^2)

K = hydraulic conductivity (L/T)

h = hydraulic head (L)

ℓ = length (L)

$i = \frac{dh}{d\ell}$ = *hydraulic gradient (L/L)*

and the minus sign indicates a loss of potential in the direction of flow. If the porosity, ϕ, is known, an estimate of the velocity of flow is given by

$$v = \frac{q_s}{\phi} = \frac{-K}{\phi} \frac{dh}{d\ell} \quad (2)$$

The hydraulic conductivity, K, depends on both the properties of the porous medium and the properties of the fluid. Often it is advantageous to separate these effects and define a permeability that depends only on the medium such that

$$K = \frac{k\rho g}{\mu} \quad (3)$$

where

k = intrinsic permeability (L^2)

ρ = mass density (M/L^3)

g = acceleration of gravity (L/T^2)

$\gamma = \rho g$ = weight density (F/L^3) or (M/L^2T^2)

μ = dynamic viscosity (FT/L^2)

p = pressure (F/L^2)

$\frac{dp}{d\ell}$ = pressure gradient (F/L)

then

$$q_s = \frac{Q}{A} = \frac{-k\gamma}{\mu}\frac{dh}{d\ell}$$

or

$$Q = \frac{-k\gamma A}{\mu}\frac{dh}{d\ell} \qquad (4)$$

and in petroleum symbols

$$q_s = \frac{Q}{A} = \frac{-k}{\mu}\frac{dp}{d\ell}$$

or

$$Q = \frac{-kA}{\mu}\frac{dp}{d\ell}. \qquad (5)$$

Darcy's equation is valid only for laminar flow conditions. Thus, in fractured rock, coarse unconsolidated material, or formations with large solution openings, the equation may not represent the flow.

Steady-State Well Equation. Based on Darcy's work, Thiem[8] developed an equation for steady (equilibrium) flow toward a well as shown in Figure 12. He assumed that:

- The aquifer is horizontal, homogeneous, and isotropic
- The well is fully penetrating
- The steady flow is maintained long enough so that the zone of influence is no longer expanding with time.

The simple continuity concept of equal flow through adjacent concentric cylinders gives the equation

$$Q = 2\pi Kbr\frac{dh}{dr} \qquad (6)$$

where

b = formation (aquifer) thickness (L)

h = height from the botton of the formation to the piezometric surface at the point indicated by the subscript (L)

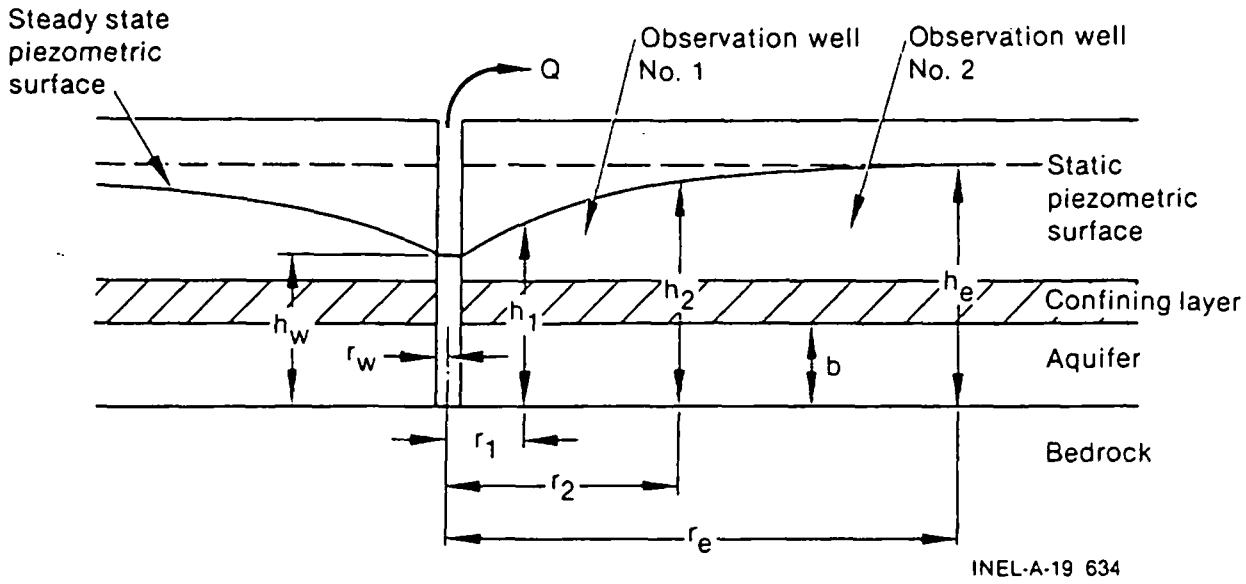

Figure 12. Steady flow toward a well.

r_w = radius of well (L)

r_1, r_2 = radial distance from production well to observation wells 1 and 2 (L)

r_e = radius of influence of the well (L).

When integrated between the two observation wells in an unconfined aquifer

$$Q = \frac{\pi K \left(h_2^2 - h_1^2\right)}{\ell n \left(r_2/r_1\right)}$$

or

$$K = \frac{Q \ \ell n \left(r_2/r_1\right)}{\pi \left(h_2^2 - h_1^2\right)} \tag{7}$$

or in a confined aquifer

$$Q = \frac{2\pi K b \left(h_2 - h_1\right)}{\ell n \left(r_2/r_1\right)}$$

or

$$K = \frac{Q \ \ell n \left(r_2/r_1\right)}{2\pi b \left(h_2 - h_1\right)} \tag{8}$$

When the limits of integration are the production well and the radius of influence, the equation for a confined aquifer is

$$Q = \frac{2\pi Kb\,(h_e - h_w)}{\ell n\,(r_e/r_w)}$$

or

$$K = \frac{Q\ \ell n\,(r_e/r_w)}{2\pi b\,(h_e - h_w)} \qquad (9)$$

In petroleum symbols, Equation (9) is

$$q = \frac{0.00708\ kb\,(p_e - p_w)}{B\mu\ ln\,(r_e/r_w)}$$

$$k = \frac{qB\mu\ \ell n\,(r_e/r_w)}{0.00708\ b\,(p_e - p_w)} \qquad (10)$$

where

q = flow rate (STB/day)

k = intrinsic permeability (md)

p_e = external pressure (psi)

p_w = bottom hole pressure (psi)

B = formation volume factor (RB/STB)

μ = viscosity (cp).

General Differential Equation. Jacob[9] developed a formal, classical development of the general differential equation for transient flow through a saturated, homogeneous, isotropic porous medium. A more complete development is given by Jacob.[10] Freeze and Cherry[11] summarize the development of the equation and the contributions of others to its development. The equation in three dimensions is known as the diffusion equation and is:

$$\frac{\partial^2 h}{\partial x^2} + \frac{\partial^2 h}{\partial y^2} + \frac{\partial^2 h}{\partial z^2} = \frac{S_s}{K}\frac{\partial h}{\partial t} \qquad (11)$$

where

S_s = specific storage (1/L)

and the other symbols are as given earlier.

For flow toward a well in a horizontal aquifer of thickness, b, in cylindrical coordinates, the equation becomes:

$$\frac{\partial^2 h}{\partial r^2} + \frac{1}{r}\frac{\partial h}{\partial r} = \frac{S}{T}\frac{\partial h}{\partial t} \qquad (12)$$

where

$T = Kb$ = transmissivity (L^2/T)

and

$S = S_s b$ = storage coeffficient (dimensionless).

Any compatible system of units can be used in the equation without introduction of constants. For example, if h and r are in meters and t is in days, the transmissivity, T, is in meters squared per day.

In petroleum symbols and units the equation is:

$$\frac{\partial^2 p}{\partial r^2} + \frac{1}{r}\frac{\partial p}{\partial r} = \frac{1}{C}\frac{\phi \mu c_t}{k}\frac{\partial p}{\partial t} \qquad (13)$$

where

C = constant depending on units used

c_t = system total compressibility (L^2/F).

With μ in Centipoise, c_t in 1/psi, k in millidarcy, p in psi, r in feet, and t in hours, then $C = 0.0002637$.

Solution of the General Equation. Theis[5] found a solution of Equation (12) for a steady flow rate, Q, from the well subject to appropriate boundary and initial conditions. The solution, in terms of drawdown, applies to constant discharge from a fully penetrating well in a confined, homogeneous, isotropic aquifer of infinite areal extent with no vertical leakage

$$s = h_o - h(r,t) = \frac{Q}{4\pi T}\int_u^\infty \frac{e^{-u}}{u}\,du = \frac{Q\,W(u)}{4\pi T} \qquad (14)$$

where

$u = \frac{r^2 S}{4Tt}$ = well function argument

s = drawdown at any radius, r, at time, t (L)

h_o = initial height of piezometric surface above the bottom of the formation (L)

h = height of piezometric surface at r and t (L). (15)

The integral term is known as the well function, W(u), and is available in tabular and graphical form in most ground water literature such as Reference 11. It is represented to any desired degree of accuracy by an infinite series as follows

$$W(u) = (-0.5772 - \ln u + u - \frac{u^2}{2\cdot 2!} + \frac{u^3}{3\cdot 3!} - \frac{u^4}{4\cdot 4!} + \ldots) . \qquad (16)$$

Unsteady State Radial Flow in Isotropic Nonleaky Artesian Aquifer with Fully Penetrating Wells and Constant Discharge Conditions

Analysis in Water Well Terms. Consider Equations (14) and (15) and rewrite them as:

$$\ell n\, s = \ell n \left(\frac{Q}{4\pi T}\right) + \ell n\, W(u) \text{ and } \ell n\, t = \ell n \left(\frac{r^2 S}{4T}\right) + \ell n \frac{1}{u} \quad .$$

This suggests a graphical curve matching technique for analyzing pumping test data. If Q is held constant during the test, then $Q/4\pi T$ and $r^2S/4T$ are constants and the relationship between $\ell n\, s$ and $\ell n\, W(u)$ is similar to the relationship between $\ell n\, t$ and $\ell n\, 1/u$. When each pair of variables are plotted on the same scale of two different sheets of log-log paper, the resulting curves are similar and are merely displaced horizontally and/or vertically from each other depending on the values of the two constants.

The method proceeds as follows and is illustrated in Figure 13:

1. A reverse type curve, 1/u (abscissa) versus W(u) (ordinate) is plotted on log-log paper.

2. The pumping test data, t (abscissa) versus s (ordinate) are plotted on another sheet of the same paper.

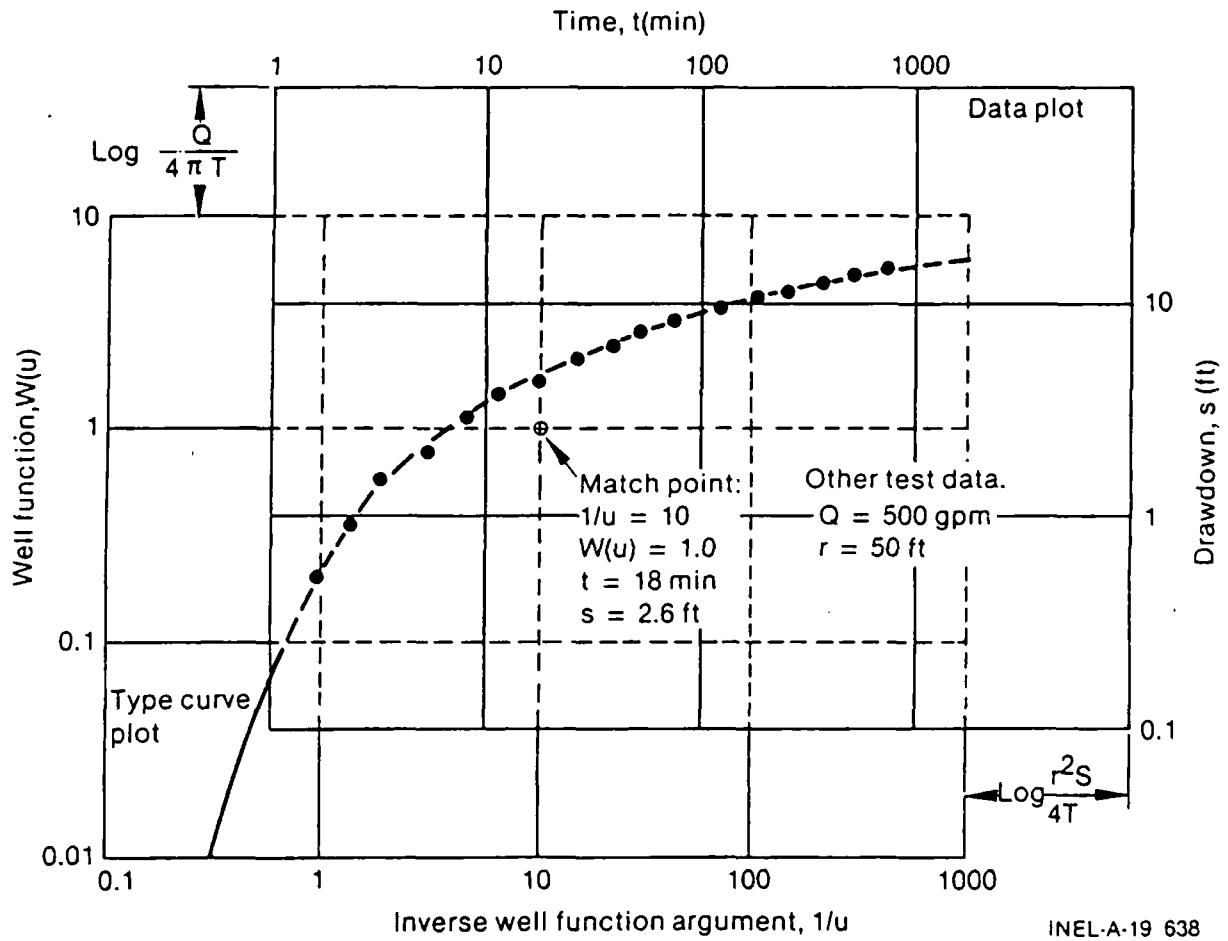

Figure 13. Superimposed curves for aquifer constants.

3. The two plots are superimposed on a light table. The two curves are translated vertically and horizontally, keeping the axes parallel at all times, until the best match of the test data with the type curve is obtained.

4. Then a convenient match point near the type curve is selected and the values of the four variables, t, s, 1/u, W(u) are recorded.

5. Using Equations (14) and (15), the unknown values of the formation coeffficients are calculated from:

$$T = \frac{Q\,W(u)}{4\pi s} \quad \text{and} \quad S = \frac{4tT}{r^2(1/u)} .$$

An alternative is to plot the type curve u versus W(u) and the field data s versus (r^2/t) both on log-log paper. The curves are superimposed, match point coordinates are recorded and the aquifer constants calculated as before.

Analysis in Petroleum Engineering Terms. The petroleum engineering approach has been to plot families of dimensionless curves and to fit the well test data to these. Dimensionless time, radius and pressure are defined as:

$$t_D = \frac{0.0002637\ kt}{\phi\mu c_t\, r_w^2} , \text{ and } r_D = \frac{r}{r_w}$$

then

$$p_D = f(t_D, r_D, C_D, \text{geometry}) \tag{18}$$

where

C_D = dimensionless wellbore storage factor.

If only the effects of dimensionless time and radius are considered, then

$$p_D = f(t_D, r_D) = -1/2\ Ei\left(\frac{-r_D^2}{4t_D}\right) \tag{19}$$

where

$$Ei(-x) = -\int_x^{\infty} \frac{e^{-u}}{u}\, du .$$

The solution of Equation (13) is

$$\Delta p = 141.2\ \frac{qB\mu}{kb}\ f(t_D, r_D) \tag{20}$$

where

$\Delta p = p_i - p(t,r)$

p_i = initial reservoir pressure (psi)

$p(t,r)$ = reservoir pressure at r and t (psi)

B = formation volume factor (RB/STB)

q = flow rate (STB/D).

Expansion of Equations (19) and (20), and rearrangement of terms shows it to be identical to the water well Equations (14) and (15).

The petroleum method is to plot test pressure, Δp, (ordinate) versus test time, Δt, on log-log paper and to superimpose the plot on a type curve for the value of r_D. A match point is chosen and values of $(\Delta p)_m$, $(\Delta t)_m$, $(p_D)_m$, and $(t_D)_m$ and noted.

Then

$$k = 141.2 \frac{qB\mu}{b} \frac{(P_D)_m}{(\Delta p)_m}$$

and

$$\phi c_t = \frac{0.0002637k}{\mu r_w^2} \frac{(\Delta t)_m}{(t_D)_m} \quad (21)$$

Thus, the two methods are seen to be the same in principle.

The petroleum engineers have carried the method further to include other important factors. A more general solutaion of Equation (13) to include the wellbore storage, geometry, and "skin" effects is:

$$\Delta p = 141.2 \frac{qB\mu}{kb} [f(t_D, r_D, C_D, \text{geometry}) + s_s] \quad (22)$$

$$C_D = \frac{5.6146\, C}{2\pi\phi c_t b r_w^2} \quad (23)$$

where

C = wellbore storage constant (bbl/psi)

$$C = \frac{\Delta v}{\Delta p} = V_w c$$

and

Δv = change in volume of fluid in wellbore at wellbore conditions (bbl)

Δp = change in bottom-hole pressure (psi)

V_w = total wellbore volume (bbl)

c = compressibility of the fluid in the wellbore at wellbore conditions (1/psi)

s_s = skin effect, which is a dimensionless pressure drop assumed to occur at the wellbore face (r_D = 1) as a result of wellbore damage or improvement. Positive skin effect is due to damage of the wellbore by the drilling process, plugging by mud, etc. Negative skin effect would be an improvement through development of the well, fracturing, reaming, etc.

A variety of type curves including the effects of wellbore storage, reservoir geometry, and skin effects have been developed and many of these are given in Earlougher.[3] Skilled use of these curves, where appropriate, allows more information to be extracted from the test data than through use of the simple exponential integral type curve alone. The additional data come from the parameters identifying the various type curves and make possible the computation of wellbore storage and skin effect coeffficients, in addition to the permeability and formation storage coeffficients already discussed.

Approximate "Straight-Line" Test Methods

The structure of the infinite series in Equation (16) provides a simple test procedure when the value of u is small. As suggested by Cooper and Jacob,[12] all the terms in the series except the first two can be neglected when $u < 0.01$. Then:

$$s = \frac{Q}{4\pi T}\left(-0.5772 - \ln\frac{r^2S}{4Tt}\right) = \frac{2.3Q}{4\pi T}\log\frac{2.25\,Tt}{r^2S} \quad . \tag{24}$$

For most pumping tests, all parameters except t are constant. Thus s will plot as a straight line with log t. The slope of the straight line is seen to be the drawdown over one log cycle, Δs, or

$$\Delta s = \frac{2.3Q}{4\pi T}$$

and

$$T = \frac{2.3Q}{4\pi\Delta s} \quad . \tag{25}$$

By extrapolating the straight line to the point where $s = 0$, the intercept, t_0, on the time axis can be determined. Then:

$$0 = \frac{2.3Q}{4\pi T}\log\frac{2.25\,Tt_0}{r^2S}$$

or

$$1 = \frac{2.25\,Tt_0}{r^2S}$$

and

$$S = \frac{2.25\,Tt_0}{r^2} \quad . \tag{26}$$

Thus, by plotting s and t on semilog paper, and by noting Δs and t_0, simple calculations give the aquifer constants. If data from more than three observation wells are available at one time, a distance-drawdown plot can be made of s versus log r: Δs and r_0 can be noted. Then:

$$T = \frac{2.3Q}{2\pi\Delta s}$$

and

$$S = \frac{2.25\ Tt}{r_0^2} \quad . \tag{27}$$

Similarly, if drawdowns in several wells are available over a period of time, plot s versus lot (t/r^2). Record the drawdown over one cycle, Δs, and the intercept $(t/r^2)_0$. Then:

$$T = \frac{2.3Q}{4\pi\Delta s}$$

and

$$S = 2.25\ T\ (t/r^2)_0 \quad . \tag{27a}$$

The three straight-line approximate methods are illustrated in Figure 14.

A similar straight-line approximate method is commonly used in petroleum engineering. The flowing bottom hole pressure, pwf, in psi (ordinate) is plotted against log t in hours (abscissa). At early times the wellbore storage makes the plot nonlinear, but this is followed by a straight line portion of the plot. The slope, m, in psi/cycle and the intercept, P/hr (where log t = 0 or t = 1), on the straight line are recorded. Then:

$$k = \frac{-162.6\ qB\mu}{mb}$$

and

$$s_s = 1.1513 \left[\frac{(p_{1hr} - p_i)}{m} - \log\left(\frac{k}{\phi\ uc_t\ r_w^2} \right) + 3.2275 \right].$$

For the observation well the skin effect is zero, then the reservoir porosity-compressibility product may be calculated using the equation:

$$\phi c_t = \frac{k}{r^2\mu}\ \text{antilog}\left(\frac{P_i - P_{1hr}}{m} - 3.2275 \right).$$

Recovery Tests

Analysis in Water-Well Terms. When a pumping test is discontinued after a period of production, data taken during the recovery period can also be used to determine formation constants. Conditions during the recovery period are represented by imagining that production continues from the well while at the same time an injection well at the same location replaces the fluid produced by the well. The net flow rate is zero and the imaginary injection well can be visualized as representing the recharging fluid coming into the cone of depression from the surrounding area. The drawdown at any point and at any time can be computed by adding the effects of the pumping and the injection as shown in Figure 15.

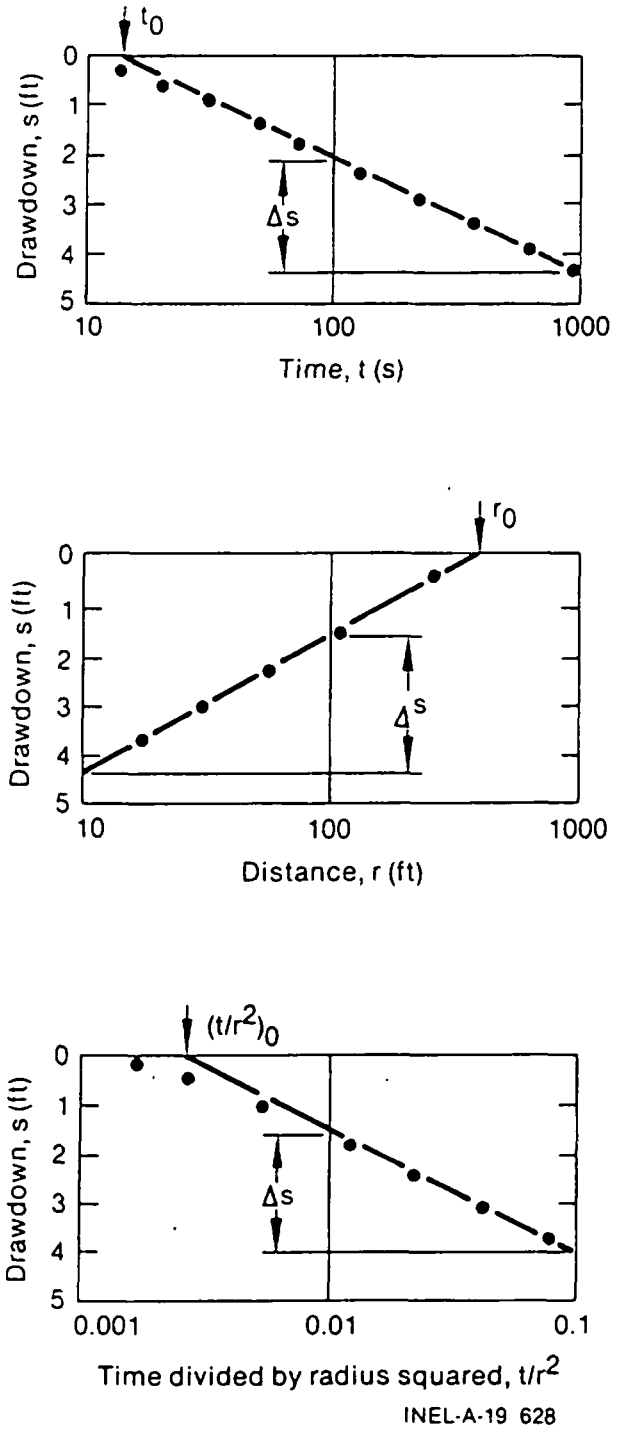

Figure 14. Straight line approximate methods.

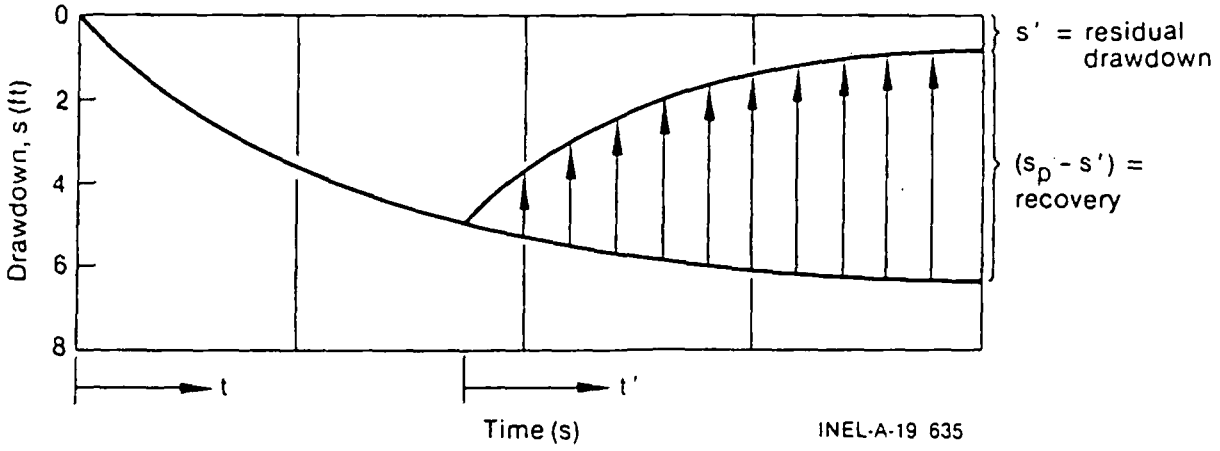

Figure 15. Drawdown computation.

In terms of well functions, the residual or remaining drawdown

$$s' = \frac{Q}{4\pi T} \int_{u}^{\infty} \frac{e^{-u}}{u}\, du - \int_{u'}^{\infty} \frac{e^{-u'}}{u'}\, du' \tag{28}$$

where

$$u = \frac{r^2 S}{4Tt}$$

$$u' = \frac{r^2 S}{4Tt'}$$

and

t = time since pumping began

t' = time since shutoff.

Once t' becomes large, $u' < 0.01$ and the well function can be represented by the first two terms of the infinite series

$$s' = \frac{2.3Q}{4\pi T} \log \frac{t}{t'} \tag{29}$$

and a plot of s' versus $\log t/t'$ is a straight line. If $\Delta s'$ is the drawdown over log cycle, then

$$T = \frac{2.3Q}{4\pi \Delta s'} \tag{30}$$

When concurrent data from one or more observation wells are available, the storativity, S, can be estimated from

$$S = \frac{2.25\, T\, t'/r^2}{\log^{-1}\left[(s_p - s')/\Delta(s_p - s')\right]} \tag{31}$$

where

s_p = pumping period drawdown projected to t'

s' = residual drawdown at t'

$\Delta(s_p - s')$ = change in recovery over one log cycle

$(s_p - s')$ = recovery at t'.

Horner Method

Analysis in Petroleum Engineering Terms. The Horner method is used to analyze pressure buildup data. The method has been used extensively in both the geothermal and petroleum industries. The technique is based on superposition of the exponential integral solution. The derivation is as follows:

$\Delta P_{\text{well shut in}} = \Delta P_{\text{due to the well flowing for a time } \Delta t + t \text{ at a rate of } +q}$

$+ \Delta P$ due to a well flowing at a rate of $-q$ for a period of time Δt.

By adding the flow rates at any time the appropriate conditions are modeled:

time $< t$ flow rate $= +q$

time $> t$ flow rate $= +q - q = 0.$

The pressure drop due to a well flowing at $+q$ for a time of $t + \Delta t$ can be expressed:

$$\Delta P_{(t+\Delta t)} = \frac{\mu q}{4\pi kh} \ln\left(\frac{\gamma\phi\mu\, cr_w^2}{4k(t+\Delta t)}\right)$$

and similarly,

$$\Delta P(\Delta t) = \frac{-\mu q}{4\pi kh} \ln\left(\frac{\gamma\phi\mu\, cr_w^2}{4k\Delta t}\right).$$

Adding these together:

$$P_i - P_{\text{well shutin}} = \frac{q\mu}{4\pi kh} \ln\left(\frac{t+\Delta t}{\Delta t}\right).$$

In standard petroleum engineering units

$$P_i - P_{\text{well shutin}} = 162.6\, q \frac{\mu B}{kh} \log \frac{t+\Delta t}{\Delta t}.$$

This equation forms the basis for the Horner method. As can be seen from the equation, when $(t + \Delta t/\Delta t)$ and $P_{\text{well shutin}}$ are plotted on semilog paper, the data should plot as a straight line with the slope $= \frac{162.6\, q\mu\, B}{kh}$.

Therefore:

$$\frac{kh}{\mu} = \frac{162.6\ q\ B}{\text{slope}}$$

The skin value can be calculated as discussed in the previous section:

$$S = 1.151\left[\frac{P_{1\ hour} - P_{flowing}}{\text{slope}} - \log\frac{k}{\phi\ \mu\ c\ r_w^2} + 3.23\right] .$$

In order to estimate the skin value an independent estimate of ϕch must be available. In the petroleum industry, this is usually obtained by testing cores in the laboratory. For geothermal reservoirs this is best estimated from the analysis of interference test data.

Analysis of Unsteady State Radial Flow in Isotropic Nonleaky Artesian Aquifer with Fully Penetrating Wells and Constant Drawdown Conditions

Analysis in Water-Well Terms — Curve Matching Techniques. For a flowing artesian well, it may be simpler to test the well with a constant drawdown and a varying flow rate than with the methods, already discussed, that require a constant discharge and variable drawdown. Under geothermal conditions, the well would need to be preheated by flowing at a low rate before the test so that thermal effects on pressure at the well will be largely eliminated. Jacob and Lohman[13] found the solution to the general equation for these conditions as follows:

$$Q = 2\pi T s_w\ G(\alpha)$$

where

$$\alpha = \frac{Tt}{Sr_w^2}$$

and

$$G(\alpha) = \frac{4\alpha}{\pi}\int_0^\infty xe^{-\alpha x^2}\left[\frac{\pi}{2} + \tan^{-1}\left(\frac{Y_0(x)}{J_0(x)}\right)\right]dx \qquad (32)$$

where

$J_0(x)$ = zero order Bessel function of the first kind

$Y_0(x)$ = zero order Bessel function of the second kind.

The function $G(\alpha)$ is available in Jacob and Lohman[13] or Walton.[14]

A curve matching technique is used for the well test. Values of Q/s_w (ordinate) are plotted against t/r_w^2 (abscissa) on log paper (or plot Q versus t). This well test plot is superimposed over the type curve $G(\alpha)$ (ordinate) versus α (abscissa). A match point is chosen and the aquifer constants determined from

$$T = \frac{Q}{2\pi s_w G(\alpha)}$$

and

$$S = \frac{Tt}{\alpha r_w^2} \quad . \tag{33}$$

Analysis in Water-Well Terms — Straight Line Approximations. Jacob and Lohman[13] observed that the function $G(\alpha)$ can be approximated closely by $2/W(u)$ for all except very small values of t. The approximation of $W(u)$ by the first two terms of the infinite series in Equation (16) has already been noted. Thus, it can be expected that (s_w/Q) versus log (t/r_w^2) will plot as a straight line since by substitution in Equation (32),

$$Q = \frac{4\pi T s_w}{2.3 \log \left(\frac{2.25\ Tt}{r_w^2 S}\right)}$$

or

$$\frac{s_w}{Q} = \frac{2.3}{4\pi T} \log \left(\frac{2.25\ Tt}{r_w^2 S}\right) \quad . \tag{34}$$

The test data are plotted as (s_w/Q) (ordinate) against log (t/r_w^2) (abscissa), where Q is the average discharge during a timed interval in the test (L^3/T). A straight line is fitted to the data and the slope (the change in $\Delta(s_w/Q)$ over log cycle) and the intercept (the value of t/r_w^2 at $s_w/Q = 0$) are noted. Then

$$T = \frac{2.3}{4\pi \Delta(s_w/Q)}$$

and

$$S = 2.25\ T \left(t/r_w^2\right)_0 \tag{35}$$

$$S = \frac{2.25\ Tt/r_w^2}{\log^{-1}\left[\frac{(s_w/Q)}{\Delta(s_w/Q)}\right]} \quad . \tag{36}$$

If the intercept is diffficult to obtain because of the distant extrapolation required, the S may be determined from Equation 36

where

s_w/Q = value taken near the middle of the straight line plot

and

$\Delta(s_w/Q)$ = change in the value over one log cycle.

Analysis in Petroleum Engineering Terms. The constant-pressure flow testing has been described by Earlougher[3] in petroleum terminology. For the curve matching technique, the test data are plotted as flow rate (q) in STB/D (ordinate) against time (t) in hours (abscissa) on log-log paper. The data are superimposed over the type curve, q_D (t_D), on the same type of log-log paper as given by Earlougher.[3] Once the best superposition has been found, the coordinates of a match point are recorded. Then:

$$k = \frac{141.2\ B\mu}{(p_i - p_{wf})^b} \left(\frac{q_m}{(q_D)_m}\right)$$

and

$$(\phi\ c_t b) = 0.0002637 \left(\frac{kb}{\mu r_w^2}\right) \left[\frac{t_m}{(t_D)_m}\right]. \qquad (37)$$

A zero skin factor is assumed in the type curve, and P_{wf} = flowing bottom hole pressure (psi).

A straight-line method has also been developed which is within 2% when $t_D \geq 5000$. A skin factor is included in the formulation. In the method 1/q is plotted versus log t and a straight line is fitted to the data. The straight line slope, m_q, and the intercept at t = 1 hour, $(1/q)_{1\ hr}$ are recorded. Then:

$$k = \frac{162.6\ B\mu}{m_q (p_i - p_{wf})^b}$$

and

$$S_s = 1.1513 \left[\frac{(1/q)_{1\ hr}}{m_q} - \log\left(\frac{k}{\phi\mu c_t r_w^2}\right) + 3.2275\right]. \qquad (38)$$

Well Losses

The total drawdown, s, during a test of a production well is made up of some or all of the following parts:

s_f = formation loss due to the laminar flow through the aquifer towards the well

s_w = well loss due to turbulent or near turbulent flow through the developed zone and/or the gravel pack and the well screen

s_p = additional formation loss due to the effects of partial penetration of the well into the aquifer

s_d = additional drawdown in cases of dewatering a portion of the aquifer

s_b = drawdown due to barrier boundaries of the aquifer

s_r = buildup due to recharge boundaries of the aquifer

s_T = apparent drawdown or buildup due to temperature effects.

Stated as an equation

$$s = s_f + s_w + s_p + s_d + s_b + s_r \pm s_T\ . \qquad (39)$$

Step Drawdown Tests for Well Losses

In many wells where there are no effects due to partial penetration or dewatering, the test may not go on long enough to be affected by boundaries and temperature effects may be negligible due to preheating. Thus, only the first two terms of the equation remain.

In laminar flow the drawdown is related linearly to the flow rate, Q, while in turbulent flow it is related to some power of Q near 2 as suggested by Cooper and Jacob:[12]

$$s = s_f + s_w = C_f Q + C_w Q^n \quad . \tag{40}$$

Rorabaugh[15] developed a graphical procedure whereby C_f, C_w, and n are evaluated from a step drawdown test. The procedure is to pump the well at a selected Q until s changes little with time; then Q is immediately increased and s is measured after the same time interval as used for the first step; and the process is repeated for four or five values. No recovery of the well is allowed between different pumping rates. Equation (40) can be rewritten as:

$$\frac{s}{Q} - C_f = C_w Q^{n-1}$$

or

$$\log \left(\frac{s}{Q} - C_f \right) = \log C_w + (n - 1) \log Q \quad . \tag{41}$$

Thus $(s/Q - C_f)$ versus Q on log-log paper will plot as a straight line with a slope of $(n - 1)$ and an intercept C_w where $(s/Q - C_f) = 1$. Such a plot cannot be constructed, however, since C_f is not known. The procedure is to assume different values of C_f and plot a series of lines until a value of C_f is formed that makes the plot a straight line, as illustrated in Figure 16 which is taken from Bouwer.[16]

In the example, $C_f = 0.004$ gives a straight line whose slope is $n - 1 = 1.3$ and thus $n = 2.3$. In actual tests n may be as high as 3.5 but is usually near 2. The value of C_w can be determined by extrapolating the straight line to where $(s/Q - C_f) = 1$ or, alternatively, known values of C_f, n, s, and Q can be substituted into Equation (41).

Once the constants in Equation (41) are known, estimates can be made of the drawdown, s, for different (increased) values of flow rate, Q.

In petroleum parlance, the step drawdown test is called the "flow after flow" test.

Pulse Tests

If the well is allowed to recover for a time between increasing flow rate steps, the procedure is known as a pulse test. In petroleum terms, this test is called the "modified isochronal flow test." A "pulse test" in petroleum engineering is a multiple well test in which flow rate pulses of constant rate with equal shut-in periods in between are produced and the resulting pressure changes are recorded in a nearby observation well.[3]

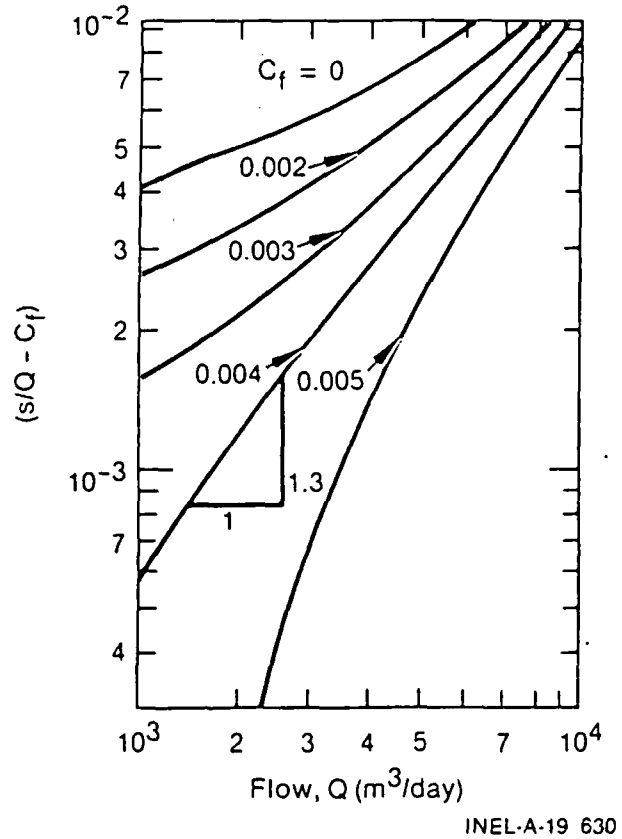

Figure 16. A plot to determine C_f.

Superposition of Solutions Applied to Multiple Wells and Multiple Rates

The drawdown at any point in a confined aquifer with more than one well is the sum of the drawdowns that would occur from each well individually. This is so because Equation (12) is linear (that is, there are no cross terms of the form $(\partial h/\partial r)(\partial h/\partial t)$. Thus, in terms of well functions, one can write for a system of n wells, each with different flow rates:

$$s = \frac{1}{4\pi T} \sum_{i=1}^{n} Q_i W\left(\frac{r_i^2 S}{4Tt_i}\right)$$

$$i = 1, 2, 3, \ldots n \qquad (42)$$

where

s = drawdown at a selected location

r_i = distance from the selected location to the i^{th} well

and

t_i = time since pumping began at the well whose flow rate is Q_i.

A negative flow rate can be used to represent injection of fluid at a well. The equation also defines the interference of wells with each other.

This principle can also be applied to multiple flow rates at one well as given by Bear[17] and illustrated in Figure 17. For these conditions

$$s = \frac{1}{4\pi T} \sum_{j=1}^{m} (Q_j - Q_{j-1})\, W\left[\frac{r^2 S}{4T(t - t_{j-1})}\right] \qquad j = 1, 2, 3, \ldots, m \qquad (43)$$

where

$Q_0 = 0$ at $t \leq 0$

s = drawdown at a given point a distance r from the well at time t

t_j = time since pumping began at rate Q_j

and

index j identifies the pumping period.

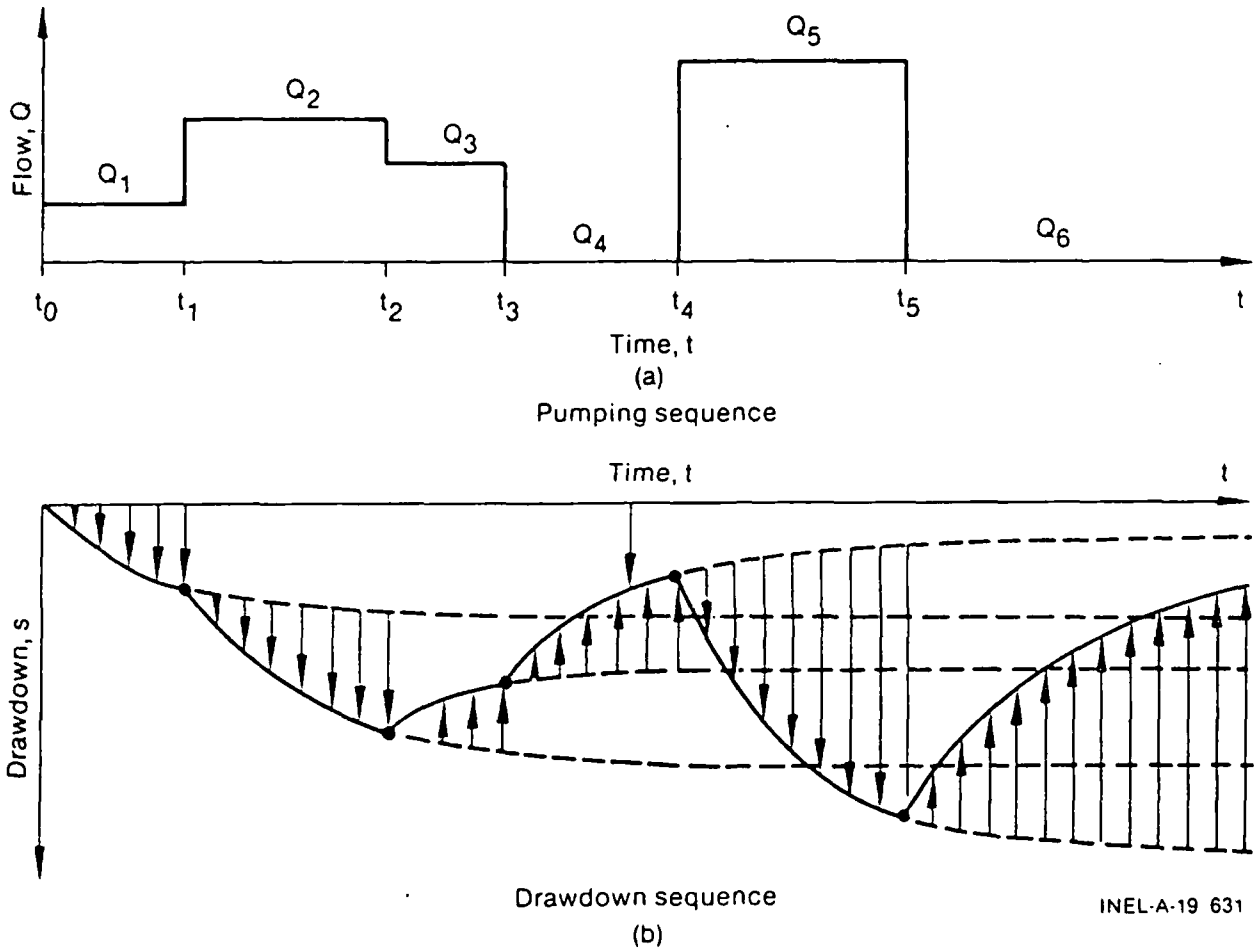

Figure 17. Multiple pumping rates.

The Effect of Fluid Density on Water Level and Wellhead Pressure Measurements

If it is not possible to obtain downhole pressure transient data, the free water level in a well (or the wellhead pressure) must be used for all pressure transient measurements. When the static level or wellhead pressure is used for pressure transient calculations, it is important to understand the effects of changes in density of the fluid filling the wellbore. The density of the fluid in the wellbore is dependent on the temperature and salinity of the fluid. Since the salinity will probably remain relatively constant throughout the test, only the change in density due to temperature will be considered. The density of water as a function of temperature is plotted in Figure 1.

If static water level (SWL) is the water level in the wellbore, the reservoir pressure can be calculated as follows:

$$P_{res} = \int_0^{H-SWL} \rho g \, dz + P_{wellhead}$$

where

SWL = static water level (m)

ρ = fluid density (kg/m^3)

g = gravitational constant (m/s^2)

z = depth (z = 0 reservoir)

H = length of the wellbore (m)

P_{res} = reservoir pressure (Pa).

If the density of the fluid along the entire length of the wellbore is known, then the integral can be evaluated and the reservoir pressure determined. Several examples are given below.

Example 1

What will the SWL be if the temperature of the wellbore changes from a 50°C isothermal profile to a 100°C isothermal profile?

$$P_{res} = \int_0^{H-SWL(50°C)} \rho g \, dz = \int_0^{H-SWL(100°C)} \rho g \, dz \; .$$

If ρ is only a function of temperature, and the temperature is constant, then it is trivial to evaluate the integral

$$P_{res} = \rho(50°C)g\,(H - SWL_{50°C}) = \rho(100°C)g\,(H - SWL_{100°C}) \; .$$

To convert P_{res} from psi to Pa, multiply by 6895 Pa/psi.

The difference in static water level can be calculated for several well depths (h).

P_{res} (psia)	H (m)	$SWL_{50°C}$ (m)	$SWL_{100°C}$ (m)
120	100	13.82	10.73
600	500	69.14	53.65
1200	1000	138.3	107.3
2400	2000	276.6	214.6

Example 2

What will the approximate SWL be in a well with a linear temperature gradient (with 50°C at the SWL and 150°C at the reservoir) compared with a hot wellbore at 150°?

$$P_{res} = \int_0^{H - SWL} \rho g \, dz$$

$$\rho(T) \approx 980 - 0.75 \, (T - 50°C)$$

$$T(z) \approx 150 - 100\frac{z}{H}$$

so: $$\rho(z) \approx 980 - 75 \left(1 - \frac{z}{H}\right)$$

$$P_{res} = \int_0^{H - SWL} \left[980 - 75 \left(1 - \frac{z}{H}\right) g dz\right]$$

P_{res} (psia)	H (m)	$SWL_{Linear\ Gradient}$ (m)	$SWL_{150°C}$ (m)
120	100	9.75	6.7
600	500	50.3	33.4
1200	1000	100.6	66.8
2400	2000	201.2	133.7

As can be seen from the two examples presented above, the temperature of the fluid has a large effect on the SWL. When the temperature changes as a function of depth in the wellbore, it is diffficult to separate this phenomena from true pressure changes in the reservoir. This phenomena is particularly important to understand in the interpretation of pressure build-up data because the wellbore quickly starts to cool when the well is shut-in. The effects of the density changes in the wellbore fluid on the measured pressure response can be eliminated in two ways: by using downhole pressure instrumentation, or by using a wellbore code to calculate the temperature of the fluid in the wellbore.

As can be seen from the two examples, the density changes of the fluid will have the most pronounced effect on deep wellbores. For a wellbore length of less than than 100 m, these changes may not be significant. However, for a deep well (500 to 2000 m), even small temperature changes will dramatically affect the SWL or wellhead pressure.

7. TEST PLANNING AND METHODOLOGY

Preliminary Test Preparation and Design

Before planning a test the developer and his hydrogeologic/reservoir engineering consultant should review the local, state, and federal regulations for fluid production and disposal. These regulations are available through individual state geothermal resource teams, the state water resource or oil and gas department, the U.S. Geological Survey, or the Environmental Protection Agency. Special permits to produce and dispose geothermal fluids may be required. Therefore, any limitations or restrictions must be considered before designing the test. Certain restrictions (i.e., discharge of geothermal fluids to lined ponds only) will raise the cost of testing and limit test duration and/or test discharge rates which could result in inappropriate or inadequate data. The restrictions will probably depend on the water quality, the temperature of the thermal fluid, and/or the compatibility with local water resources. Some eastern states, such as New Jersey, require all geothermal fluid, including any testing fluid, to be discharged into an injection well. Thus, testing of any production or test well will require the additional cost of an injection well.

After the developer or consultant has evaluated and made allowances for testing regulations they need to determine the end use of the well, i.e., whether it will be a production or a test/monitor well. They then need to determine whether the reservoir is intergranular permeable, fracture-controlled, or has dual porosity. If the type of reservoir is unknown, it should be treated as a fracture flow case.

The first design decision to be made is whether to test produce the well using a pump or by natural artesian flow. This decision will be clear cut if artesian conditions are not present. An air lift or nitrogen lift test is not recommended for geothermal resources because flow rate control is at best diffficult. For a production well test, the anticipated end-use method of producing the geothermal fluid should be used. However, for test wells, the less expensive method of artesian flow testing is recommended. If a moderate temperature resource is being tested, the additional factor of flashing (boiling) at the wellhead or orifice must be considered. At temperatures greater than approximately 100°F, suffficient pressure must be maintained across a fluid discharge measuring device to prevent flashing, otherwise expensive two-phase measurement equipment will be necessary. If the well is to be artesian flow tested, an additional possibility must be considered, i.e., can the well be completely shut-in? If the well cannot be shut-in, the capability of flow rate regulation is necessary. In all cases the consultant should determine the testing parameters and be sure that all relevant data can be obtained and pertinent variables controlled.

Test Pump. If a pump is required, the consultant must select the pump, determine the pump elevation setting, and evaluate the pump limitations. A combustion-engine-driven pump is recommended for testing as this will allow for a wide range of discharge rates. An additional reason for using a test pump rather than the intended production pump is the potential damage to the pump by the corrosive nature of early postdevelopment discharge fluids. The estimated pump setting depth should be developed from the data collected during the drilling and development process. It is better to set the pump deep rather than run a test at too low a flow rate or for too short a time, or to be forced to pull the pump out and set it deeper.

There are technical problems with off-the-shelf, water well type pumps even at low temperatures. The main problems are in lubrication of moving parts, cooling of motors and moving parts, and differential expansion. Information from several brand name pump distributors suggests that warranties on submersible pump motors will not be honored at temperatures above 37.8°C. Vertical turbine pumps can be used for extended periods of time in geothermal fluids if care is taken to account for differential thermal expansion and lubrication. In addition, the corrosive nature of the geothermal fluid must be considered in selecting pump materials.

Test Instrumentation. After anticipated drawdown, temperature, and flow rates have been estimated, instrumentation suitable to measure those parameters should be chosen. The recommended accuracy and resolution of the data limits or restricts the instruments that should be used. Most off-the-shelf, low-cost

pressure gauges are not suffficiently accurate or do not have sufficient resolution. On the other hand, it may be uneconomical for the developer of a low-temperature resource to use the sophisticated and expensive surface or downhole instrumentation used in moderate- to high-temperature geothermal developments. One alternative for low-temperature resources is that the producing well be supplied with a continuous bubbler tube in conjunction with moderate-cost surface gauges that at least meet the resolution requirements. This will reduce early-time thermal effects and result in accurate relative change of pressure or water level. It is also recommended that fluid discharge temperature data be obtained continuously or at least on the same measurement schedule as pressure and discharge rate. It is also necessary to consider the thermal effects on the instrument operation. Economical instrumentation, due to the required accuracy and resolution and due to thermal problems, is currently a problem in low-temperature geothermal development. Additional cost-effective instrumentation needs to be developed.

Appendix C lists a variety of instruments employed in low-to-moderate temperature systems. A brief discussion of accuracy and resolution is also available for reference.

Test Parameters. General statements on test parameters are diffficult to make, because the test design depends on the information needed. The general recommendations provided here should be applied with extreme caution, and used only after the end use of the well and the purpose of the test has been determined.

The test parameters that need to be addressed at this time are a function of the test type, discharge rate, the duration of the test, and fluid temperature. The "test type" refers to the standard procedural well tests in the petroleum and ground water industries, i.e., step test, pulse test, constant-discharge variable-head test, etc. The recommended method and limits will depend not only on the decision path taken during test preparation and test design, but also on the dollar investment of the project. It is assumed for this document that the testing of moderate-temperature resources will be expensive.

Recommendations of test parameters for low-temperature cases are presented in Table 2.

Recommendations of test parameters for moderate-temperature cases are presented in Table 3. There is less divergence from standard ground water or petroleum testing procedures, because downhole instrumentation is subjected to minimal temperature change and eliminates the problems created by borehole density effects. Moderate-temperature cases that do not use downhole pressure/temperature instrumentation should follow the recommendations for low-temperature resources.

Testing Methods. Testing methods may be categorized according to the following:

1. Discharge or injection rate:
    a. Constant rate flow tests (variable drawdown)
    b. Multiple flow rate tests
    c. Variable flow rate tests (constant drawdown).
2. Flow duration:
    a. Step tests
    b. Pulse tests
    c. Short-term tests
    d. Long-term tests

Table 2. Recommended test parameters for low-temperature hydrothermal systems

Test Parameters	Test Well								Production Well							
	Intergranular Permeable				Fractured or Unknown				Intergranular Permeable				Fractured or Unknown			
		Flow				Flow				Flow				Flow		
	Pump	Shut-In	Rate Control	No Rate Control	Pump	Shut-In	Rate Control	No Rate Control	Pump	Shut-In	Rate Control	No Rate Control	Pump	Shut-In	Rate Control	No Rate Control
Type Test(s)	B	B	B	B	B	B	B	B	B	B	B	B	B	B	B	B
	CD	CD	CD	—	CD	CD	CD	—	Pr	Pr	Pr	—	Pr	Pr	Pr	—
	R	R	R	—	R	R	R	—	CD	CD	CD	—	CD	CD	CD	—
	—	—	—	—	—	—	—	—	R	R	R	—	R	R	R	—
	—	—	—	CH	—	—	—	CH	—	—	—	CH	—	—	—	CH
Flow Rate	RD	RD	RD	—	MP	MP	MP	—	RD	RD	RD	—	E	E	E	—
Minimum duration (days)	2-4	2-4	2-4	30+	3-7	3-7	3-7	30+	5-10	5-10	5-10	30+	10-20	10-20	10-20	30+

Legend
- B = Borehole temperature log (if possible)
- CD = Constant-discharge variable-head
- PR = Pulse and recovery
- R = Recovery
- E = End-use requirements
- MP = Maximum practical
- RD = Reduced discharge rate
- CH = Constant head, variable discharge

Data Requirements[a]

	Resolution	Accuracy
Pressure	1.0 psi	±1% F.S.
Temperature	±0.5°C	±1°C
Flow	±0.5% F.S.	±1% F.S.

a. See Reference 18.

Table 3. Recommended test parameters for moderate-temperature hydrothermal resources

	Test Well		Production Well	
Test Parameter	Intergranular Permeable	Fracture Control	Intergranular Permeable	Fracture Control
Type test(s)	StD R —	StD R —	S or P StD R	S or P StD R
Flow rate	RD	MP	RD	E
Minimum duration (days)	0.3-3	3-7	3-7	10-20

Assumes use of downhole instrumentation in production zone

Legend
- S or P = Step test or pulse test
- StD = Acceptable standard for testing groundwater or petroleum resources
- R = Recovery
- RD = Reduced discharge rate
- MP = Maximum practical discharge rate
- E = End use requirements discharge rate

Data Requirements (Lamers, 1974)

	Resolution	Accuracy
Pressure	1.0 psi	±1% F.S.
Temperature	±0.5°C	±1°C
Flow	±0.5% F.S.	±1% F.S.

3. Test geometry:
   a. Single well test
   b. Multiple-well production
4. Well tests with observation wells
5. Injection testing
6. Recovery tests.

Constant Rate Flow Tests — Constant rate flow tests are commonly used in both ground water and petroleum industries and are highly recommended for low-to-moderate temperature geothermal well testing. In the constant rate flow test, the desired pumping rate has to be obtained as fast as possible and maintained throughout the test duration. The flow rate is carefully monitored and adjusted if changes are observed. Pumping rates for a constant rate flow test should be carefully designed to provide enough flexibility for these adjustments. Drawdown and temperature data are collected according to a time schedule designed specifically for each test. An advantage to the constant rate flow test method is that analysis techniques are well developed.

Multiple-Flow Rate Tests — Multiple-flow rate tests are used to estimate well losses, specific capacity, well productivity, skin effects, and reservoir parameters. This type of test is commonly conducted before testing at constant rates to aid in subsequent test planning.

Variable Flow Rate Tests — The hydraulic properties of a reservoir can be determined from a well test in which the discharge rate varies with time and the drawdown remains constant.[19] The change in discharge rate is plotted against the logarithm of time. This type of test is most effective for an artesian flowing well. Thermal changes may cause problems in maintaining a constant head. This type of test is not normally used for testing geothermal wells.

Step Tests — A step test consists of an abrupt increase or decrease in the fluid discharge rate with no recovery allowed between steps. Each pumping rate is continued at a constant flow until the well approaches a steady flow condition, after which the discharge rate is abruptly increased or decreased to the next level. Each step interval may last from 30 minutes to four hours. This procedure is continued for several discharge rates. This type of testing is most useful in geothermal wells in which downhole instrumentation, i.e., downhole pressure bombs and temperature probes are used to collect data. This is because some time is required after each discharge change before the surface temperature becomes stable and temperature effects can be neglected.

Pulse Tests — Pulse tests are conducted at increasing or decreasing discharge rates with recovery allowed between each pulse interval. Data are collected for the pumping and recovery portions of each rate. Each pulse interval may last from one hour to several days. In geothermal well testing, longer pulses are recommended to provide enough time so that early recovery data with thermal effects will not have to be used. Pulse testing is not commonly used in the ground water industry. The petroleum industry uses this type of test to determine reservoir anisotropy.

Short- and Long-Term Tests — Duration of a test in terms of "long or short" is a relative measure; however, these terms are commonly used in practice. A test conducted for less than three days should be considered short-term. A long-term test is commonly conducted for more than three days with no defined maximum time limit. Tests of long duration are recommended more often in geothermal aquifer testing than in ground water or petroleum well testing. This recommendation is based on the following factors: the hydrogeology and geologic structure of a geothermal reservoir is often complex; reservoir volumes are so large that long production periods are needed to produce significant pressure responses; and there is no alternative method to predict resource temperature changes.

Single- and Multiple-Well Tests — Classification of tests by geometry includes single well tests and multiple-well tests. The multiple-well production test is more complex, and more diffficult to evaluate than single-well production tests. A single-well production test may be needed prior to the multiple well test to provide a basis for comparison. The multiple-well production test should provide information about both interference effects between wells and aquifer properties. In general, less precise reservoir data are obtained from multiple-production well tests due to reservoir heterogeneity.

Well Tests with Observation Wells — Generally, there is little difference between test procedures with or without observation wells. Tests with observation wells provide a more complete data base for evaluating aquifers. These data are average values for a large area of the reservoir. Whenever practical, the use of observation wells is recommended.

Injection Testing — Injection testing may be accomplished by injecting fluids from a body of surface water or a production well. The following factors should be considered when choosing the injection interval:

1. Interference and cooling effect on a production zone
2. Environmental impact of the injected fluid on a potable ground water aquifer
3. Cost of the injection well.

Skin Factor and Wellbore Storage — The skin factor is a petroleum term which is represented by a steady-state pressure drop of the well face in addition to the normal transient pressure drop in the reservoir.[3] The skin factor increases or decreases the pressure change of the well, depending on the flow rate of the well. Wellbore storage affects the short-time transient pressure behavior in the test well. The skin factor and wellbore storage both affect the early-time portion of the data. These effects can be accounted for in test analysis.

Well-Loss Constant — The well-loss constant characterizes the losses due to the well screen plus the gravel pack or developed area near the well and can be evaluated from a step test or several pulse tests. A properly developed well has a well-loss constant less than 5 sec^2/ft^5.[20]

Aquifer Permeability, Thickness-Permeability Product and Porosity-Compressibility Thickness Product — Aquifer permeability (k) or the absolute permeability of the rock,[2] is a property of the rock and not of the fluid which flows through it. The unit of permeability used in the petroleum industry is the Darcy unit. A rock of one Darcy permeability will allow a fluid of one centipoise viscosity to move at a velocity of one centimeter per second under a pressure gradient of one atmosphere per centimeter.[2]

The thickness-permeability product (kh) is a term characterizing the fluid transmitting ability of the aquifer. The thickness-permeability product is a petroleum industry term which is somewhat similar to the term transmissivity used in the ground water industry. The difference is that the transmissivity characterizes fluid transmitting aquifer properties for a fluid, and thickness-permeability product is independent of the fluid.

The porosity-compressibility-thickness product ($\phi c_t h$) is a term used in the petroleum industry that is equivalent to the term storativity used in the ground water industry. The unit used for the porosity-compressibility-thickness product is in ft/psi.

Analyzing Test Data.

Evaluating Early-Time Data — Data which are not thermally affected are evaluated according to standard petroleum and ground water techniques.[3,14] However, all of the techniques are not applicable. The methods recommended in Table 4 are general categories of techniques which should be applied. The specific techniques applicable to each category will depend on the quantity and quality of the reservoir test data plus other geologic and hydrologic inferences gathered during the exploration and drilling phases. These specific techniques are described by Walton,[14] Earlougher[3] and others conversant in the ground water and petroleum fields.

Early-time data emphasized in the ground water and petroleum industries are often not as useful in analyzing low-temperature geothermal production wells due to thermal and density changes effecting surface data. These problems can be eliminated by collecting downhole data.

The recovery data may also be affected by time-dependent thermal changes if downhole data is not used. The thermal effect increases with time from the start of recovery. This means that early-time recovery data is important and late-time data becomes hard to analyze.

Analyzing Fracture Flow — Fracture flow analysis has been discussed by numerous authors, i.e., Warren and Root, Papadopulos, Rofail, Gringarten, Streltsova, Dugiud, and Aquilera.[21-28] Most analytical methods assume either a single fracture for production or a block response. The solutions are for the most part not analytical or field oriented, but computer model comparisons. Field analyses of fractured systems have conventionally relied on anisotropic analysis of intergranular permeable systems. The assumption that fracture flow averaged over a large enough area, acts like an intergranular permeable system, is not unreasonable.[29] However, this approach suggests that early-time data may not be useful.

Evaluating Reservoir Parameters — A critical part of well test analysis is evaluation of reservoir parameters. The theoretical background and essential elements of well test analysis were presented in Section 6. This section presents several methods developed by the ground water and petroleum industries that are commonly used in the geothermal industry as well.

Skin Factor and Wellbore Storage — The skin factor is a petroleum term which is represented by a steady-state pressure drop of the well face in addition to the normal transient pressure drop in the reservoir.[3] The skin factor increases or decreases the pressure change of the well, depending on the flow rate of the well. Wellbore storage affects the short-time transient pressure behavior in the test well. The skin factor and wellbore storage both affect the early-time portion of the data. These effects can be accounted for in test analysis.

Well-Loss Constant — The well-loss constant characterizes the losses due to the well screen plus the gravel pack or developed area near the well and can be evaluated from a step test or several pulse tests. A properly developed well has a well-loss constant less than 5 sec^2/ft^5.[20]

Aquifer Permeability, Thickness-Permeability Product and Porosity-Compressibility Thickness Product — Aquifer permeability (k) or the absolute permeability of the rock,[2] is a property of the rock and not of the fluid which flows through it. The unit of permeability used in the petroleum industry is the Darcy unit. A rock of one Darcy permeability will allow a fluid of one centipoise viscosity to move at a velocity of one centimeter per second under a pressure gradient of one atmosphere per centimeter.[2]

The thickness-permeability product (kh) is a term characterizing the fluid transmitting ability of the aquifer. The thickness-permeability product is a petroleum industry term which is somewhat similar to the term transmissivity used in the ground water industry. The difference is that the transmissivity characterizes fluid transmitting aquifer properties for a fluid, and thickness-permeability product is independent of the fluid.

The porosity-compressibility-thickness product ($\phi c_t h$) is a term used in the petroleum industry that is equivalent to the term storativity used in the ground water industry. The unit used for the porosity-compressibility-thickness product is in ft/psi.

Analyzing Test Data.

Evaluating Early-Time Data — Data which are not thermally affected are evaluated according to standard petroleum and ground water techniques.[3,14] However, all of the techniques are not applicable. The methods recommended in Table 4 are general categories of techniques which should be applied. The specific techniques applicable to each category will depend on the quantity and quality of the reservoir test data plus other geologic and hydrologic inferences gathered during the exploration and drilling phases. These specific techniques are described by Walton,[14] Earlougher[3] and others conversant in the ground water and petroleum fields.

Early-time data emphasized in the ground water and petroleum industries are often not as useful in analyzing low-temperature geothermal production wells due to thermal and density changes effecting surface data. These problems can be eliminated by collecting downhole data.

The recovery data may also be affected by time-dependent thermal changes if downhole data is not used. The thermal effect increases with time from the start of recovery. This means that early-time recovery data is important and late-time data becomes hard to analyze.

Analyzing Fracture Flow — Fracture flow analysis has been discussed by numerous authors, i.e., Warren and Root, Papadopulos, Rofail, Gringarten, Streltsova, Dugiud, and Aquilera.[21-28] Most analytical methods assume either a single fracture for production or a block response. The solutions are for the most part not analytical or field oriented, but computer model comparisons. Field analyses of fractured systems have conventionally relied on anisotropic analysis of intergranular permeable systems. The assumption that fracture flow averaged over a large enough area, acts like an intergranular permeable system, is not unreasonable.[29] However, this approach suggests that early-time data may not be useful.

Evaluating Reservoir Parameters — A critical part of well test analysis is evaluation of reservoir parameters. The theoretical background and essential elements of well test analysis were presented in Section 6. This section presents several methods developed by the ground water and petroleum industries that are commonly used in the geothermal industry as well.

Table 4. Recommended test analysis methods for low-temperature hydrothermal development

Type Well	Test Type	Considerations	Recommended Methods: Intergranular Permeability	Recommended Methods: Fracture Controlled
Production	Pulse	Transient density skin effects or well loss wellbore storage boundaries	Graphical[a] (straight line)	Graphical[a] (straight line)
	Drawdown	Transient density	Graphical[a] (type curve or straight line)	Graphical[a] (type curve or straight line)
	Recovery	Same		
		Same	Transient and semisteady state (straight line)	Graphical[a] (straight line)
Observation	Drawdown and recovery	Anisotropy, boundaries	Transient and semisteady state (type curve)	Anisotropic and fracture methods (type curve)

a. Use of Q/s_{10} technique.

Evaluating Graphical Methods of Test Data — Graphical methods are commonly used in the water well and petroleum industries. One such method is the type-curve matching method.

Type Curves — The graphical methods of superposition provide one way of evaluating reservoir parameters. The type-curve matching analysis method may be used for drawdown, buildup, interference, and constant pressure testing. The method should be applied where downhole data are being obtained since early-time thermal effects will impact surface readings. Type curves are obtained by plotting selected values of W(u) versus u on a logarithmic graph paper.[5] For constant flow during a test W(u) is related to u in the same manner as drawdown is related to the r^2/t or $1/t$. Therefore, if the recorded values of drawdown are plotted on a logarithmic scale against r^2/t or $1/t$ on a similar logarithmic scale, the raw data curve should be similar in shape to the type curve. However, the two curves may be displaced both vertically and horizontally.

The type-curve-matching method used in the petroleum industry is similar to that used in the water well industry. Data are typically plotted in terms of logarithm pressure change versus logarithm test time. The type curve is in units of dimensionless pressure versus dimensionless time.

Standard type curves are developed for various aquifer geometries and conditions such as wellbore storage and skin effects. The type curve evaluation technique is widely used in water well industry and to some extent the petroleum industry. Use of type curves for geothermal well testing analysis is limited when using uphole data because of time-dependent thermal effects.

Straight-Line Solutions — The straight-line solution is another graphical method for aquifer test analysis when considering semisteady-state conditions. Typically, time is plotted on the logarithmic scale versus drawdown, which is plotted on a linear scale. The data points should ideally form a straight line.[12] The slope of water level change over one log cycle of time is needed to calculate reservoir parameters.

Recovery data should be analyzed using the ratio of time from start of pumping and time from start of recovery plotted on the logarithmic scales. Reservoir parameters are calculated using the same equation as for a drawdown plot.

If more than one observation well is used for data collection, a distance-drawdown plot may be used for test analysis.[8] Distance is plotted in the logarithmic scale and drawdown on the linear scale.

The straight-line plot is recommended for geothermal well testing. However, it must be remembered that time-dependent thermal effects on the water level data may significantly influence the plot. For example, an increase in water temperature may have an effect similar to a recharge boundary and a decrease in temperature during shut-in may appear similar to a barrier boundary.

Monitoring Observation Wells (Interference Tests)

Any well or spring within a 1 to 5 km radius of the producing well that is potentially connected hydraulically with the geothermal reservoir should be monitored during testing. The geology and construction of any observation wells should be evaluated. It will be necessary to determine the elevation of a measuring point relative to the producing well, and the use schedule of the observation well, if appropriate. Pressure measurement and the instrumentation for the observation wells should follow water well standards and practices.

There should be no diffficulties with thermal conditions at observation wells, unless the well is flowing and cannot be shut-in. If a well or spring is flowing, discharge, temperature and water quality measurements should be obtained.

If there are any wells or springs within a 1 to 5 km radius of the production well which cannot be shut-in for the test duration, it will be necessary to determine if there will be any potential hydraulic interference problems. If there are, discharge should be regulated during and after the test. If this is not possible, then at least a record of production from the observation well should be kept.

Fluid Disposal

The technical aspects of fluid disposal must be considered. This may mean calculating the fill rate of a pond to determine if the test can run for the projected duration at the desired discharge rate. It may mean determining the anticipated thermal or water quality change in a stream at the desired discharge rate. The disposal must consider the waste heat in addition to the water quality.

Because elevated temperatures increase solution kinetics and mineral solubility, geothermal waters tend to be higher in dissolved solids than surrounding ground waters. Thermal waters can also have high concentrations of particular dissolved species that may cause special disposal problems, such as arsenic, mercury, boron, or fluoride. Environmental regulations generally prohibit the disposal of effffluents into surface streams where the effffluent will degrade the quality. Table 5 lists the dissolved species most likely to be present in troublesome quantities in geothermal fluids. Water samples should be collected and analyzed for these species to evaluate the potential for disposal problems. In addition to chemical aspects, thermal pollution from disposing fluids also must be controlled.

Test Procedures

Before beginning the actual reservoir test, it is necessary to meet all the facility requirements. This may mean installing power for a pump, instruments, or lighting. It would also mean obtaining permission to monitor a well on private land or constructing access roads. The pump, production well instrumentation, and the observation well instrumentation should be installed at this time. Any technicians or professionals who will be involved with the test should be trained in the operation of the pump and testing instrumentation. In addition, the field staff should understand the anticipated data responses during the test.

Table 5. Dissolved species found in geothermal waters

Total dissolved solids	Boron
Chloride	Arsenic
Sulfate	Sulfide
pH	Carbon dioxide
Fluoride	Mercury

The reservoir test begins with obtaining background data on all the wells and springs to be monitored (historic water levels, temperature, chemistry data). These data will be used to determine short- and long-term trends in order to correct the test data for these trends. The required duration of background monitoring will vary according to the site. It is recommended that the minimum duration be at least equal to the duration of the intended reservoir test.

The next step is to determine if suffficient field support has been employed for the reservoir test. The required number of people will depend on the disposal method, the number of monitor wells and springs, the distance or travel time between monitor wells and springs, and the type of instrumentation at each monitoring site. It will be desirable to have more assistance during the early-time rapid measurements of the production and recovery portion of any test. If there is insuffficient field assistance, then additional help should be employed and properly trained.

A static or nonproducing borehole temperature log of the production well should be run at or before this time. It may be preferable for technical and economic reasons to run this log before setting a pump. The log should be recorded while entering the well (logging down) to minimize any thermal disturbance (mixing) within the well. Finally, the data will be used for calculating time-dependent changes in fluid density and early-time thermal borehole storage effects in the producing well. A temperature log obtained after drilling was completed may be used, if the time between drilling and testing was less than three to five days. Otherwise, a new temperature log is recommended.

Preheating of the wellbore should be considered before the start of testing if pressure or water-level information during the test is to be obtained in any portion of the well that sees a temperature change. The well or spring should be preheated by producing at 10 to 20% of the intended testing discharge rate. The preheating lessens the time-dependent density changes during the test, and usually does not cause problems with the latter analysis.[30] The preheat procedure should continue until the discharge temperature is constant.

A step rate or pulse test should be run in order to determine the optimal flow rate for a long-term test and the productivity index. A standard water well step test and analysis may be run if the pressure or water level data do not have time-dependent density changes (downhole data). A step test is not recommended if downhole data are not available due to probable thermal changes at the differing discharge rates. The variable thermal conditions and the short duration of most step tests make comparison and analysis impractical. At least two pulse steps are recommended, one at a higher rate and one at a lower rate than the intended end-use production rate. The highest rate should be run first to aid in preheating the borehole. The duration of each pulse and recovery will depend on the time required to reach thermal equilibrium at the wellhead and obtain suffficient analyzable pressure or water level data. This may be on the order of four to eight hours per pulse. If a step test is run, one to four hours may be required, since the wellbore should be stabilized by the inital high rate step test.

The discharge rate for the long-duration test will depend on the well type, reservoir type, drilling data, etc. and the pulse test data. The end-use required rate be used for all fracture-controlled type springs or wells. The end-use rate is recommended due to the low reliability of standard extrapolation techniques in fractured rock reservoirs.[31] A higher than end-use rate is not recommended, as extrapolation of temperature for the lower rate is not reliable. If there is no specified end use requirement, the test should be conducted at the maximum possible rate. A reduced discharge rate (less than the end-use production rate) can be used for intergranular permeable reservoirs.

The recommended test duration for low-to-moderate temperature geothermal resources is somewhat longer than a standard cold-water aquifer or petroleum test to allow for stabilization of early-time thermal effects. Also, the test duration for fracture flow cases should be somewhat longer than intergranular permeable cases due to problems in the analysis and projection of reservoir longevity. In general, the longer the test, the more reliable the data.

After concluding the production phase of a test, it is important to obtain recovery data level/pressure at the production well and at all monitor wells and discharge rates at all springs. The duration of the recovery portion of a test will depend on the type of instruments used and/or the rate of cooling in the production well. In the water well and petroleum fields, one would expect the recovery portion of a test to run approximately the same duration as the production portion. In low-to-moderate temperature geothermal systems, the recovery portion of a test (considering the production well only) will be of shorter duration. This is a result of thermal effects. The recovery data at a production well is especially useful if the discharge rate during the test was somewhat erratic or had several step changes. The evaluation technique assumes a constant discharge rate by averaging the discharge during the production. Recovery data are also useful for a monitor well to confirm that a water level/pressure response was due solely to the test and not part of a short- or long-duration background trend.

8. GEOCHEMISTRY

Geochemical information on geothermal fields both supplements hydrologic information and provides additional data. For instance, chemical logging during drilling can indicate the presence of cold and hot aquifers and aids in the placement of casing. Subsurface temperature can be estimated with chemical geothermometers. Isotopic composition variations in water can be used to determine sources of water, the occurrence of boiling in the reservoir, or the amount of interaction between water and wall-rock. The chemical composition of the water may foretell of problems with corrosion or scaling, or may indicate environmental problems from specific dissolved species. The scope of this section is to provide information available from geochemical studies and to briefly describe the geochemical methods involved.

Chemical geothermometers may be used to estimate aquifer temperatures in wells weeks or months before underground temperatures return to normal after drilling. Flow testing may speed the temperature recovery in the production zone, but interferes with obtaining information about predrilling temperatures elsewhere in the well. Also, extensive flow testing immediately after the termination of drilling is not always possible because of fluid disposal problems or delayed delivery of test equipment. Production and collection of a small amount of fluid at the wellhead or from a downhole water sampler, however, may be all that is necessary to provide a good indication of the aquifer temperature.

Where well design requires interruption of production of a geothermal well to run a temperature log, geochemical temperatures may be monitored. Logging wells is also a relatively slow process, and a temperature survey of a field with several production wells could take many days or weeks. Monitoring temperatures of waters supplying drillholes can be accomplished using the silica content of water where calculated temperatures and downhole measured temperatures are in close agreement. Water samples can be collected without interrupting production. Mahon[32] has shown that the silica concentration in the water entering wells decreases at Wairakei, New Zealand, in response to decreasing temperatures in the aquifer.

By producing a well at various flow rates, the contribution to total discharge from multiple aquifers may vary. If different aquifers have different chemical compositions, and different pressures or transmissivities, the chemical composition of the discharge fluid would change as the production rate was varied. Collection of water samples during a step drawdown tests could be analyzed to detect production from different aquifers.

The following subsections present a brief overview of some of the geochemical methods that can be used in low-to-moderate temperature geothermal reservoirs.

Chemical Logging

The growth of the geothermal industry has created a need for techniques that can be used during drilling operations to determine the depth at which to complete a well, depth for casing placement, and the best method for well development. Techniques developed by the petroleum industry, such as geophysical logging, lithologic logging, and core drilling, can be useful. However, little development has been oriented toward the specific conditions encountered during geothermal exploration and well drilling. Chemical logging[33] is one of the methods developed at the Raft River KGRA for geothermal applications.

Chemical logging can indicate the depth and relative flow of geothermal aquifers penetrated during drilling. The method involves periodic collection of drilling fluid for chemical analysis while drilling is in progress. A chemical log is prepared by plotting the concentrations of the analyzed chemical species, or their ratios, versus drill string depth. The resulting log is a profile of chemical changes taking place in the drill fluid during the drilling operation. Changes in the chemical composition of drilling fluids indicate the entrance of formation waters into the wellbore. Changes in particular species indicate the presence of geothermal water.

Changes in the chemical composition of the drilling fluid result from mixing the fluid with water from aquifers penetrated by the drill string. Figure 18 is a cross-sectional view of a drill string that has penetrated several water-bearing strata. Drilling fluid is pumped through the drill stem and bit and returns to the surface between the drill stem and the wall of the borehole carrying the drill cuttings with it. When a water-bearing stratum is penetrated, it contributes water to the drilling fluid, diluting the fluid and causing variations in its chemical composition. Generally, after the drill string passes through the water-bearing stratum, the drilling mud or sediments in the drill water form a mud cake on the walls of the borehole, sealing off the aquifer. If the flow from the stratum is too great and the stratum is not sealed by the mud cake, the incoming water will produce a permanent change in the background chemical composition of the drilling fluid. The chemical log determines the change in chemical composition of the drilling fluid as each aquifer is penetrated; it also determines the separation of this change from the chemical background contributed by the drilling fluid.

Interpretation of chemical logs is complicated by a number of factors, the most important of which are the effects of drilling mud on the composition of drilling fluids. Drilling muds absorb much of the free hydrogen ion in the solution raising the pH, and consequently the alkalinity. Other cations will also be affected by ion exchange reactions, but anions will be relatively unaffected. Problems arising from this will not seriously interfere with the chemical logging technique because the plot with depth will show changes relative to the background, which are more important than the absolute values of species. Instances when the drilling fluid is changed, for example when drilling mud is replaced by mud-free water, will make comparisons between different parts of the hole difficult, if not impossible.

Sampling Procedure

The procedure is to collect samples of the drill return fluid at specified depth intervals. Drill fluid is pumped from the mud pit, through the drill string, and returns up the borehole between the borehole walls and the drill stem. Drilling fluid samples are collected where the drill-return fluid enters the mud pit. Samples of 4 to 5 L should be collected to ensure an adequate sample size when drilling mud is being used. Frequently, water is used as a drilling fluid in geothermal wells, in which case only 1-L samples need be collected.

Sampling frequency depends on the detail desired in the chemical log, and the proximity of the hole to the geothermal resource. Also, changes in drilling rate or other changes in drilling indicate that a sample should be collected. Sample frequency may vary from once every 100 m in the upper portion of the hole, to as often as every 5 to 10 m when proximity to the geothermal resource is anticipated. Sampling depths must be corrected for lag time or travel time in the wellbore. This information can usually be supplied by personnel compiling the mud log.

Drilling mud, cuttings, and other residues are separated from the water sample by centrifuging or filtering. In many cases, centrifuging will not settle gelatinous suspensions of drilling mud. Filtering with a coarse filter in a funnel, and a flask with side tube connected to a hand-operated vacuum pump is readily adapted to field filtration of samples.

Chemical species that will provide the most information when drilling in an area must be determined by comparing chemical analyses of cold-water aquifers, drilling fluid make-up water, and the geothermal resource. Those constituents that show the greatest differences in concentration among these water sources would be the best species to use in constructing the chemical log. Constituents that might commonly be expected to show large differences between geothermal and other waters are silica, fluoride, magnesium, chloride, specific conductance, and alkalinity. Also useful are ratios of constituents. Ratios may produce an even more sensitive log if the two species in the ratio show opposite behavior in the background water and in geothermal water.

By compiling the chemical log in the field, during drilling, the chemical log will have its greatest utility in locating geothermal zones as they are penetrated. During development at Raft River, the most useful log was

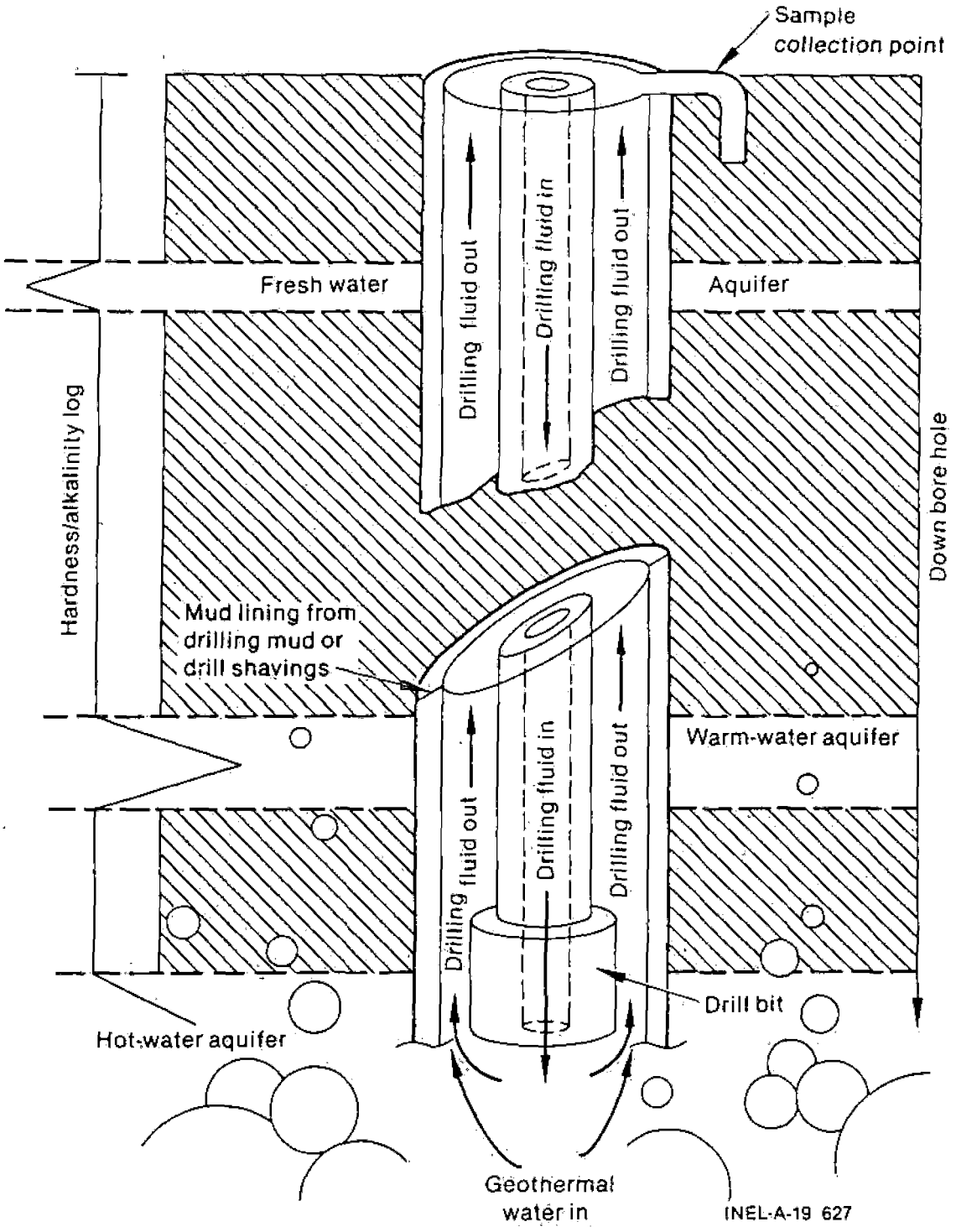

Figure 18. Changes in drilling fluid composition by fluid from a geothermal aquifer.

found to be the hardness-alkalinity ratio log. Both hardness and alkalinity can be measured very easily in the field by colorometric titration. Thus, information gained from this chemical log will be immediately available for decision-making during drilling.

Raft River Example. The concept of chemical logging originated during drilling of exploratory well RRGE-3 at the Raft River KGRA, and was developed and refined during drilling of production wells RRGP-4 and RRGP-5 and injection well RRGI-6. At Raft River, shallow drilling used mud as a drilling fluid. Once casing was set, further drilling used geothermal water as the drilling fluid to prevent possible damage to the formation from the mud. Because geothermal water was used as the drilling fluid, only small chemical differences were anticipated between drilling fluid and any geothermal aquifers that were penetrated. Chemical constituents that would best differentiate between geothermal waters and cold waters, at Raft River, are hardness, alkalinity, fluoride, chloride, and total dissolved solids.

Figure 19 shows the chemical log collected during the drilling of well RRGP-5. The log shows sharp changes in the chemical composition of the drill fluid at 488 m. At this depth, the alkalinity and hardness increase and fluoride and silica concentrations decrease. This would be a typical change in chemical composition when fresh water dilutes the drilling water. The relative constancy in chloride ion concentration and conductivity indicate, however, that the fresh-water aquifer had fairly high dissolved solids, probably from intrusion of geothermal water. The production zone of a geothermal aquifer was penetrated at 1280 m. Because the drill fluid was geothermal water similar to that in the aquifer, only small changes were observed in the drill fluid chemical composition. There was a small increase in SiO_2 concentration and a small decrease in conductivity. The decrease in alkalinity was the only large change detected at this depth.

The hardness/alkalinity log is shown in Figure 20. Evaluation of the hardness/alkalinity log reveals a sharp change in the ratio at a depth of 1220 m. This increase in the hardness/alkalinity ratio was observed until the drill string reached a depth of 1280 m, where a flow of hot water with an estimated rate of 68 L/s was observed. Geothermal water from the 1280 m depth washed away the chemical profile of the well for the remainder of drilling. The lower part of this borehole was lost when a concrete plug was set at 1051 m depth to install the well casing. After the well was cased and reentry was made with the drill string, the concrete plug could not be drilled through. Sidetrack drilling was initiated at the top of the plug, but the second leg either did not penetrate the high-flow zone penetrated in the first leg or the fractures were sealed with concrete. The second leg is shown as Leg B in Figure 20, and indicates the penetration of a narrow, hot-water-bearing aquifer, which flowed at about 13 L/s with a maximum temperature of 123°C.

The hardness/alkalinity ratio log (Figure 20) also showed that as the drill approached a geothermal zone, the ratio increased before the zone was reached, with the resulting chemical log displaced uphole relative to the temperature log. The uphole displacement varied between 16 and 120 m for the wells tested, and appears to be a function of the permeability or fracturing of material above the geothermal aquifer. Additional confirmation of the value of chemical logging was demonstrated during the drilling of RRGI-6. Comparison of the hardness/alkalinity ratio to the temperature log for RRGI-6 revealed similarities as shown in Figure 21 . The hardness/alkalinity log is displaced about 60 m uphole relative to the temperature log. This characteristic of the hardness/alkalinity ratio, of anticipating geothermal aquifers, combined with the information on the permeability of stratum already penetrated, furnished by the mud logger, could be used to determine the depth at which to set the well casing.

Figure 22 shows the hardness/alkalinity chemical log collected during the redrilling of well RRGP-4 with the object of converting an injection well into a production well. Sidetrack drilling started at 565 m to a total depth of 1650 m for Leg A. To improve resolution, samples were taken at 15 m intervals with additional samples collected at 8 m intervals where the driller detected structural changes. To make the chemical log more useful as a predictive tool, the hardness/alkalinity chemical log was kept current with the drilling progress. The object was to anticipate any significant temperature changes before the drill string reached a production zone.

An upper geothermal zone was penetrated by the drill between 700 and 870 m, with the hardness/alkalinity ratio increasing sharply through this area. In this upper portion of the hole, drilling mud was being

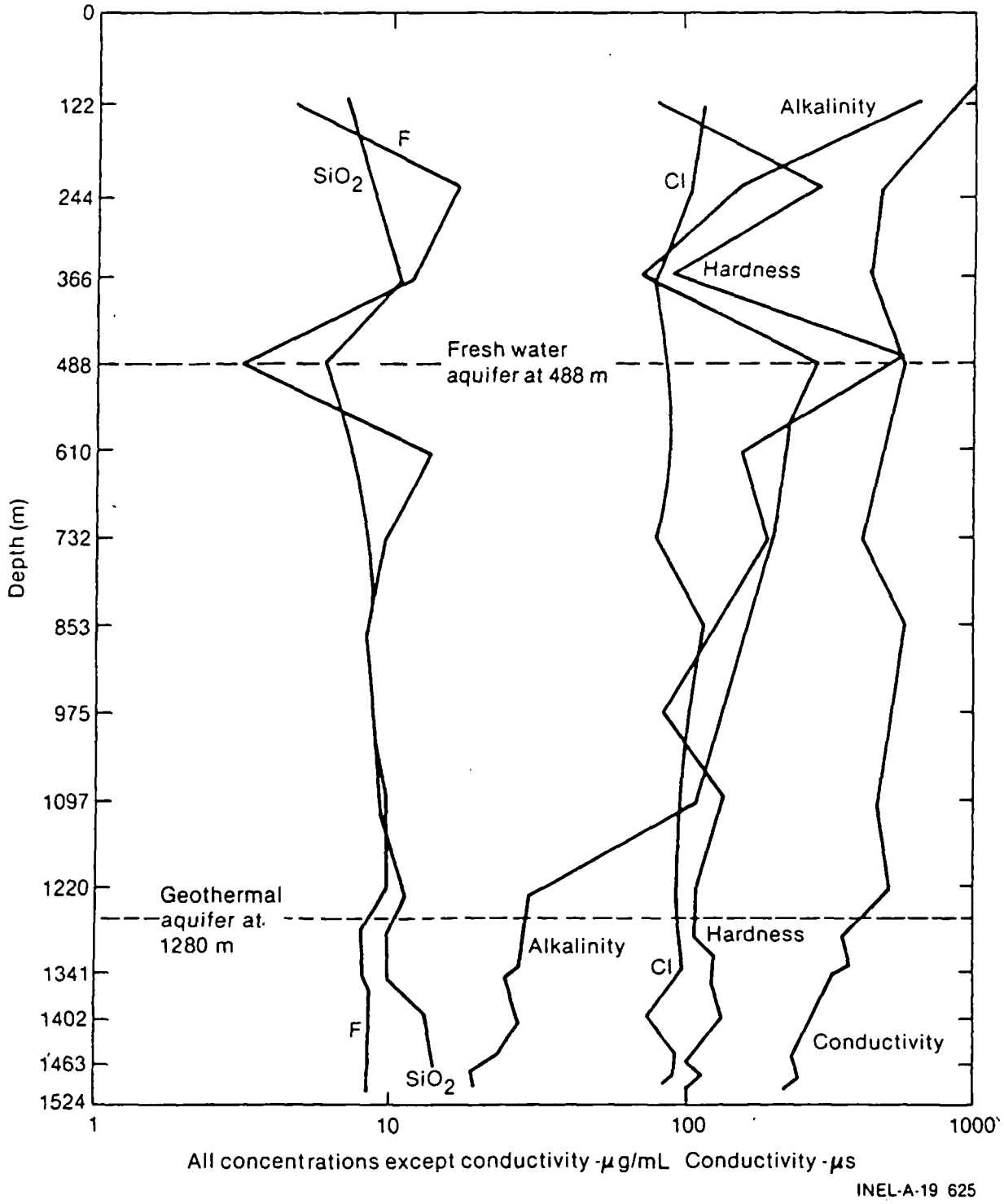

Figure 19. Chemical log of all analyzed chemical species for Well RRGP-5.

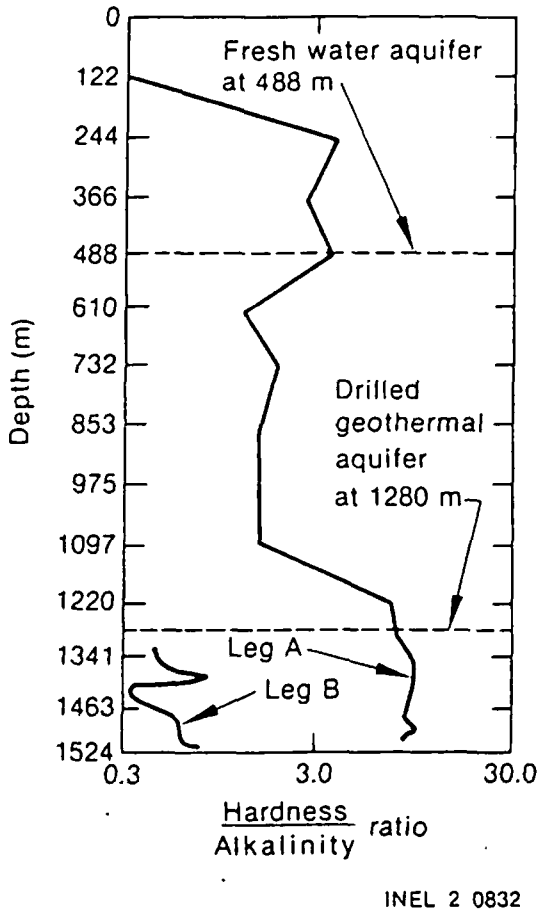

Figure 20. Hardness/alkalinity chemical log for Well RRGP-5.

used in the drilling fluid. Although the background chemical composition of the fluid was much different because of the presence of the drilling mud, the change in the ratio is still quite apparent. After casing the upper hole to a depth of 1070 m, the background hardness/alkalinity ratio changed significantly. Comparison of the chemical and lithologic logs of the upper portion of the wellbore shows that the section having high hardness/alkalinity ratios corresponds to a sandstone layer. Geophysical logging confirmed that this sandstone layer is an aquifer. At a depth of 1520 m, the driller noticed a decrease in drilling rate when the drill bit encountered a hard stratum about 10 m before penetration of a narrow, low-producing, hot-water zone. The hardness/alkalinity ratio began to increase about the time the drill reached the hard stratum, and continued to increase as the zone was penetrated. The ratio decreased after the drill passed through the producing zone. This same sequence was repeated at 1580 m. The combined flow of the two producing zones was about 2.25 L/s, with water temperatures above the boiling point.

Corrosion and Scale-Forming Species in Moderate Temperature Geothermal Brines

Geothermal brines, in general, represent an environment that is very corrosive and contains high concentrations of scale-forming species. This subsection provides general guidelines for proper selection of material and scale control techniques to nontechnical individuals that are involved in geothermal applications. Additional information can be obtained from Casper and Pinchback.[34] These guidelines presented here will apply to any geothermal area but should not be used in lieu of professional advice.

Corrosion. The predominate factors affecting corrosion in moderate temperature brines are temperature, brine chemistry, fluid velocity, and the specific material in contact with the brine. Specific chemical species associated with corrosion are:

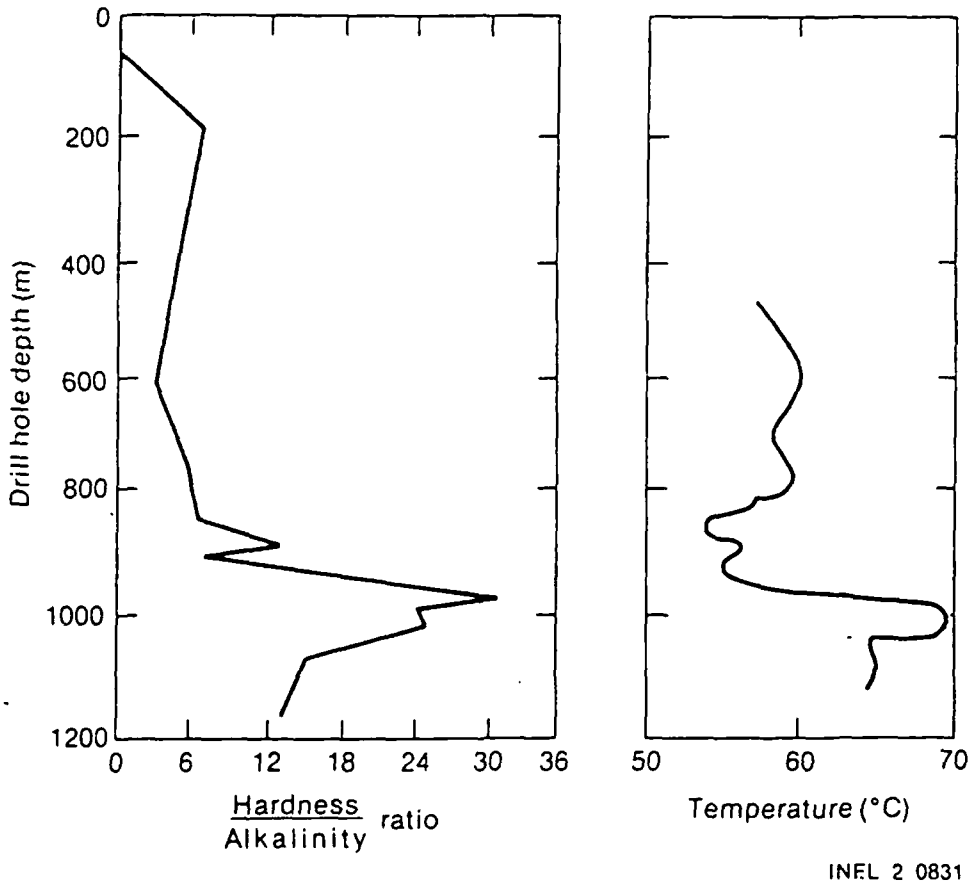

Figure 21. Hardness/alkalinity chemical log and temperature log for Well RRGI-6.

- Oxygen
- Hydrogen ion (pH)
- Chloride ion
- Hydrogen sulfide
- Carbon dioxide
- Ammonia
- Sulfate ion.

The presence of boron and heavy metals such as copper, mercury, tin, etc., will also affect the corrosion rates of different materials. The specific corrosive effect of each of the materials listed above will vary with the material selected. When two or more of the above species are present, the corrosion rate may be significantly greater than the additive corrosion rates associated with the individual species.

Scaling. The predominant factors affecting scale deposition in pipes are brine chemistry, change in temperature, change in pressure, fluid velocity, and the material in contract with the brine. The specific chemical species associated with scale deposition are:

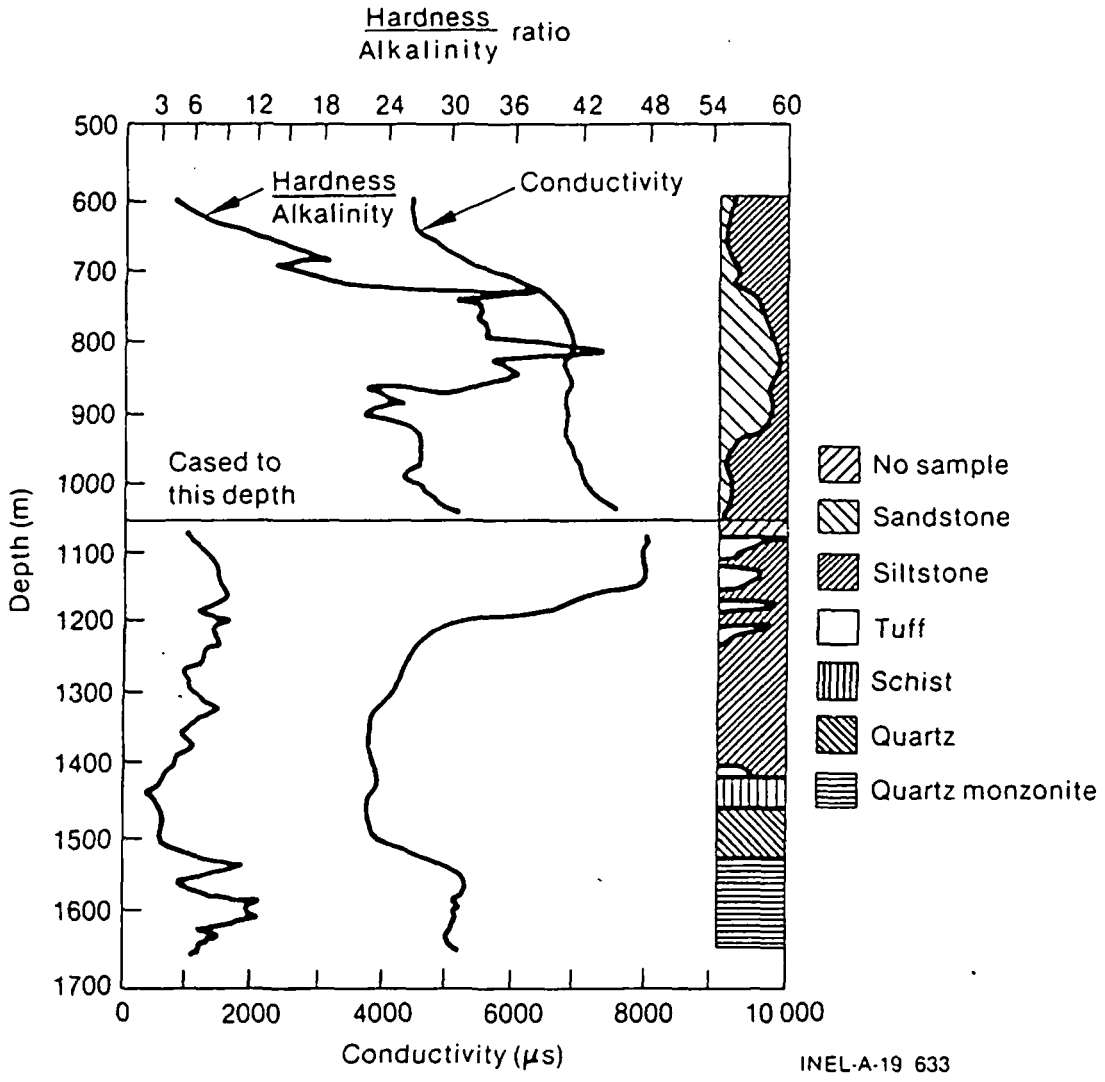

Figure 22. Hardness/alkalinity chemical log for Well RRGP-4A.

- Silica
- Hardness—recorded as calcium hardness and magnesium hardness
- Hydrogen ion (pH)
- Alkalinity—recorded as total and methyl orange alkalinity
- Sulfate ion
- Fluoride ion.

Corrosion products will also affect scale deposition.

Material Selection. Since scale and corrosion are not mutually exclusive, material should be selected with both in mind. There are a large number of materials to select from, ranging from plastics to carbon steels to exotic alloys.

Plastics — Plastic pipes are relatively free from both scaling and corrosion problems. They may be excellent for transporting fluids from wellhead to process areas, but may not be used where transfer of heat is required. Plastic pipes are available in many different forms and price ranges. Restrictions on their use are those of operating temperature and pressure. The higher the temperature, the lower the operating pressure must be.

Carbon Steel — Carbon steels are readily available and are the most inexpensive kind of metal piping. Carbon steel can be used both as transportation and heat transfer material provided adequate corrosion allowance is made. It may not be used if oxygen is present in the brine or if the pH is below six, as this will result in greatly increased corrosion rates and iron scale deposition.

Copper and Copper Alloys — The use of copper and its alloys represents an approximately three-fold increase in material cost and may be required when oxygen is present. Copper has excellent heat transfer properties but should not be used if the pH is below six, as corrosion rates significantly increase with lowering pH, i.e., more acidic water. Copper may not be used if ammonia or sulfide is present.

Stainless Steels — Stainless steels should not be used in brines as the high chloride concentration may result in early failure of components.

Other Materials — There are many other alloys on the market, such as nickel alloys, chrome-moly alloys, titanium, cobalt, etc. The use of these materials should be made after consultation with a corrosion expert, as they are very expensive.

The following are basic guidelines for selecting materials for a geothermal application.

1. Obtain a water sample of the brine and analyze it for the species listed in the Corrosion and Scaling subsections above. The sample should be unflashed and taken by a reputable firm. If the sample is flashed, the noncondensable gasses such as oxygen, carbon dioxide, hydrogen sulfide, and ammonia will flash, resulting in an inaccurate analysis.

2. Select, tentatively, a material based on the analysis. This selection should be confirmed with a professional corrosion engineer.

3. Determine optimum velocity for the given material. As velocity increases, erosion-corrosion increases dramatically while scale deposition decreases; hence the optimum for the given material.

4. Review the system with a water treatment specialist after the material has been selected. The primary considerations are the analysis at the wellhead and the temperature and pressure drops across the system. Temperature is the largest single factor in the solubility of many chemical species. If a large temperature drop occurs across a system, many chemical species may become supersaturated and deposit a scale. Also if pressure drops occur across the system, i.e., across valves, elbows, carbon dioxide may flash, resulting in calcite deposition. This may be eliminated by maintaining pressure across the entire system.

Chemical Geothermometers

Chemical geothermometers are probably the most recognized contribution of geochemistry to the development of geothermal fields. Application to low- and moderate-temperature reservoirs requires careful assessment of the techniques, as many of the assumptions involved in development of geothermometers are based on high-temperature reservoirs. Geothermometers do not stand alone and must be viewed in the geologic and hydrologic context of the field.

There are five basic assumptions that must be met for the geothermometry techniques to be valid. These are:[35]

1. Chemical concentrations are determined by water-rock interactions
2. There is an excess of all reactants
3. Water and rock are in equilibrium at reservoir temperature
4. After leaving the reservoir, water does not reequilibrate with rocks
5. Either no mixing occurs with cooler, shallower water, or the mixing can be quantified.

The geochemist must test the validity of these assumptions after he has considered the hydrology, geology, and mineralogy of the reservoir. Water produced from deep wells offers advantages for sampling in that flow up the wellbore can limit external alterations of water chemistry.

Geothermometers most applicable to low- and moderate-temperature reservoirs are the silica and sodium-potassium-calcium (Na-K-Ca) geothermometers. The Na/K geothermometer is generally limited to reservoirs with temperatures over 180°C. Even with the other two geothermometers, however, results at temperatures below 150°C tend to be less consistent than at higher temperatures. This problem is due in part to kinetic effects and the broad range of mineralogic compositions found in lower-temperature reservoirs.

Silica Geothermometer. The silica geothermometer is based on the theoretical solubility curves of various silica phases, and is applicable to the temperature range from 0 to 250°C.[36,37] The range of temperatures over which the technique works best is from 150 to 225°C. The first consideration in applying this geothermometer is to collect and preserve the sample properly. As waters cool, silica polymerizes and may precipitate. Polymerization can interfere with analysis when colorimetric techniques are used. Water samples, especially if water temperatures are over 140°C, should be diluted as much as 5 to 10 times to prevent polymerization and precipitation.

Silica solubility can be controlled by a number of silica phases, including quartz, chalcedony, and amorphous silica. Equations for calculating estimated reservoir temperatures assuming control of SiO_2 concentrations by these silica phases are:

$$\text{Quartz } t(°C) = \frac{1309}{5.19 - \log C} - 273.15$$

$$\text{Chalcedony } t(°C) = \frac{1032}{4.69 - \log C} - 273.15$$

$$\text{Amorphous silica } t(°C) = \frac{731}{4.52 - \log C} - 273.15$$

Silica concentration, C, is in mg/kg as SiO_2, and the calculated temperature is in degrees centigrade.

In freshly drilled boreholes, in basaltic terrains, or in areas with chert in sediments, quartz may not be the phase controlling silica solubility. If the assumptions of geothermometers are valid for a site, and the proper controlling phase can be determined, the silica geothermometer seems to give the best reservoir temperature estimates.

Na-K-Ca Geothermometer. This geothermometer is based on an ion exchange equilibrium among feldspars controlling the concentrations of sodium, potassium, and calcium.[38] The following equation for calculating temperature is empirical, but feldspar control is assumed.

$$t(°C) = \frac{1647}{\log (Na/k) + \beta [\log (Ca/Na) + 2.06] + 2.47} - 273.15$$

$t < 100°C, \beta = 4/3$

$t \geq 100°C, \beta = 1/3$

Na, K, Ca concentrations in mg/kg.

In geothermal systems where calcium concentrations are significantly affected by gypsum or calcite solubility, calculated temperatures may not be valid. Loss of calcium by mineral precipitation will produce anomalously high temperatures. For waters that are fairly high in magnesium, an empirical correction to the Na-K-Ca geothermometer has been proposed by Fournier and Potter.[39]

Glenwood Springs Example. The situation at Glenwood Springs, Colorado is an example of the equivocality of geothermometers in low-temperature reservoirs. At Glenwood Springs, the temperatures of seven springs, which range in discharge from a fraction of a liter per second to over 125 L/s, are remarkably similar and suggest a fairly uniform reservoir at about 50°C (mean = 48.9°C, standard deviation = 2.7°C).[40] Quartz geothermometer calculations give closely grouped, although much higher temperatures for the springs, averaging 79.7°C with a standard deviation of 2.2°C. Estimates using the Na-K-Ca (Mg corrected) geothermometer give a much broader range of temperatures, averaging 85.1°C with a standard deviation of 15.5°C. An analysis of the mineralogy of the geothermal reservoir, however, indicates that these geothermometers may not be valid in this case.

There is extensive evidence of the presence of evaporites in the limestone reservoir, mainly gypsum or anhydrite. Thermodynamic calculations show the springs to be supersaturated with calcite, which may, therefore, be precipitating in the subsurface. Lowering of calcium concentrations by calcite precipitation would raise the temperature predicted by Na-K-Ca geothermometer. The wide range in geothermometer temperatures would reflect the variability in calcite precipitation.

Sediments in the reservoir contain chert, which is much more soluble than quartz. Calculations of reservoir temperature using the chalcedony geothermometer give temperature estimates that average 48.6°C with a standard deviation of 2.4°C.

The potential questionability of the quartz and Na-K-Ca geothermometers, and evaluation of mineralogy, spring discharge, measured temperatures, and chalcedony geothermometer suggests that the reservoir temperature is closer to 50°C than 80°C. This difference can mean the success or failure of a low-temperature project. Drilling in the Glenwood Springs area during the fall of 1981 found 52°C water in the Leadville Limestone at a depth of 174 m.[41]

Isotopic Composition of Water

Oxygen and hydrogen isotopes in water can be used to indicate sources of geothermal fluids, as evidence for mixing of thermal waters with shallow, cool waters, and to give qualitative estimates of the extent of reaction between water and rock. The most significant contribution of isotopes to the hydrology of geothermal systems was demonstrating that significant quantities of geothermal waters are derived from meteoric sources. Truesdell and Hulston[42] present an in-depth analysis of isotope methods in geothermal systems, from which this section is excerpted.

Stable Isotopes. During the evaporation of sea water, lighter isotopes of water (oxygen-16, hydrogen) can escape into the vapor phase more readily than the heavier oxygen-18 and deuterium. As this water vapor forms precipitation, the heavier isotopes condense first, resulting in progressively lighter precipitation during movement toward the poles, inland over land masses, and to higher elevations. The average annual precipitation at any location will have a fairly constant isotopic composition reflecting its elevation, latitude, and distance from the ocean.

Oxygen and hydrogen isotopic compositions of precipitation are related by the equation:

$$18\,\delta D = 8\,\delta\,^{18}0 + 10$$

where δ is the difference in parts per thousand ($^{0}/_{00}$) between a water sample and a standard water known as "standard mean ocean water" (SMOW). Ground waters in an area frequently display the same relation between oxygen and hydrogen isotopes as precipitation. Surface and ground waters that have undergone evaporation fall to the right of the meteoric water line (Figure 22) along lines with slopes of about five. The deuterium isotopic composition can be used as a label reflecting the recharge area and history of a water sample.

The isotopic composition of many high-temperature geothermal waters is related to that of local meteoric water, but indicates a change in oxygen isotopic composition (Figure 23) from exchange between reservoir rocks and hot waters. Because few rock-forming minerals contain very much hydrogen, a concurrent change in hydrogen does not occur. The magnitude of the oxygen isotope shift depends on the original isotopic compositions of water and rock, mineralogy and texture of rocks, temperature, water/rock ratio, and time of contact. Systems with maximum temperatures below 150°C, moderate water/rock ratios, and igneous rocks with original δ^{18} 0 values near +50/00 may show little or no isotopic shift. Most low- and moderate-temperature reservoirs would, therefore, be expected to show little or no isotope shift.

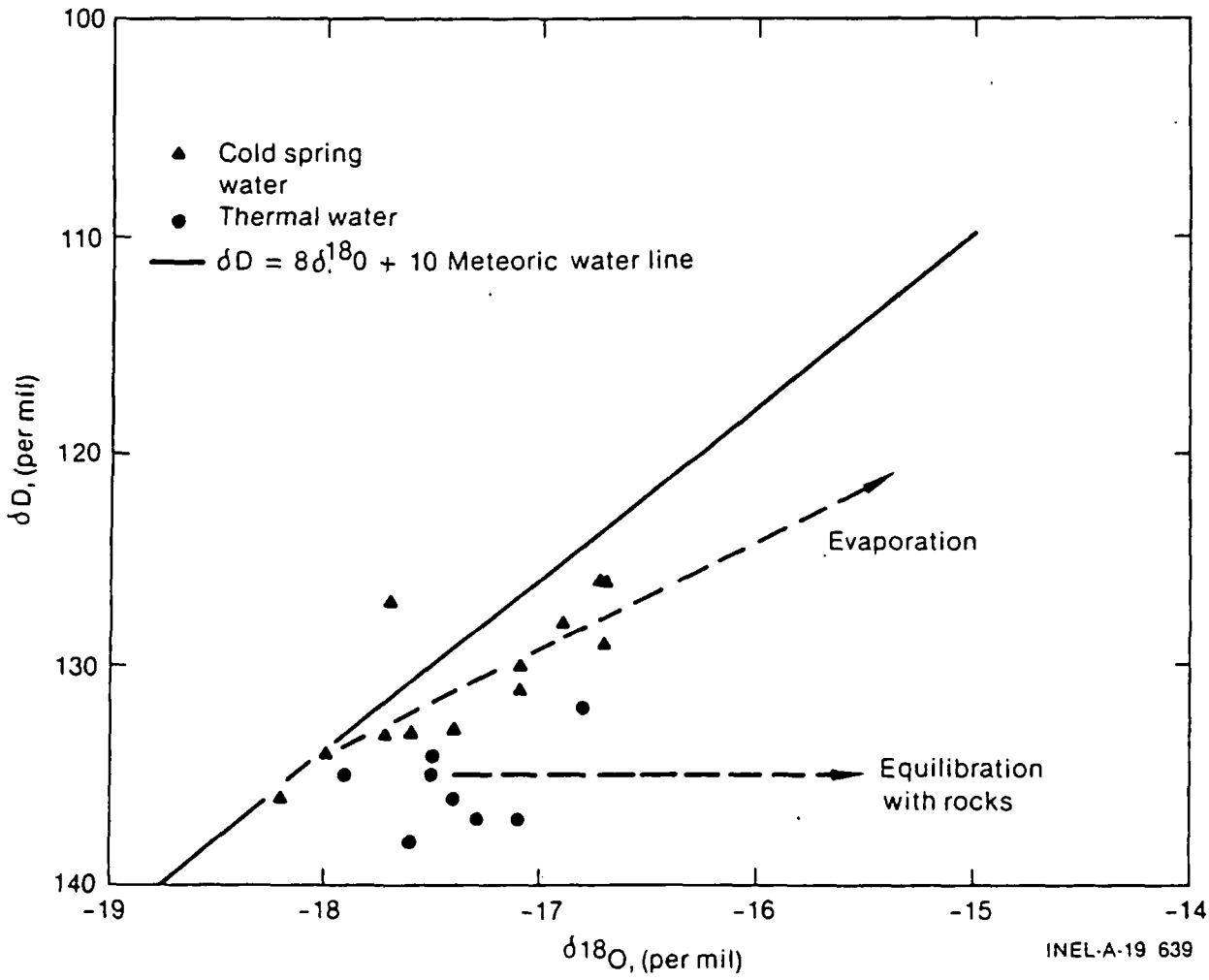

Figure 23. Oxygen-18 and deuterium compositions of hot and cold ground waters from the Raft River KGRA.

Mixing with shallow, cooler ground waters commonly occurs in the upper portions of geothermal systems, which may be feeding thermal springs. Isotopic compositions combined with dissolved salt contents may be used to demonstrate this mixing. Correlations between the isotopes of oxygen or hydrogen and dissolved salts would be expected where shallow waters were lower in salt content and isotopically different than thermal waters.

Tritium. Tritium is a radioactive isotope of hydrogen with a half life of 12.3 years, and is produced naturally by cosmic rays. Atmospheric testing of nuclear weapons between 1954 and 1965 produced a 100-fold increase in peak tritium levels in the northern hemisphere. The current detection level for tritium allows dating of waters up to 60 years old. Most measurements of deep thermal waters show no significant tritium, indicating that waters are greater than 60 years old. Measurable tritium in thermal wells and springs probably indicates the mixing of deep thermal waters with recent, shallow ground water.

9. RESERVOIR MONITORING

Reservoir analysis is not complete when the end-use production of a thermal well or well field begins. It is necessary to monitor the hydrologic system(s) to confirm initial predictions; to anticipate and plan for any geochemical changes in pressure and temperature of the resource; and to obtain a larger data base for confirming the reservoir conceptual model. Confirmation of the conceptual model can be used to evaluate reservoir capacity, recharge, and the potential for future expansion.

Monitoring of a well or well field includes pressure monitoring, temperature monitoring, and geochemical sampling of production/injection wells, observation wells, and springs. Observation wells may include fully or partially penetrating wells designed to monitor reservoir response and any deep or shallow existing irrigation or domestic wells. Monitoring also includes discharge/recharge rates for all wells and springs, and geochemical sampling and temperature changes in a disposal stream or pond.

It is essential that monitoring be accomplished throughout the life of any development to ensure economical use and predict potential environmental hazards.

Pressure Monitoring

The completion of a geothermal well and the start of production from the reservoir should signal the beginning of a regularly scheduled, permanent program of pressure monitoring of the following:

1. The producing aquifer or reservoir formation
2. The confining strata above the reservoir
3. The unconfined aquifer above the confining layer (springs)
4. The production and injection wells.

The pressure measurements will usually be done with surface instruments, i.e., pressure gauges installed at the well head. If the well is not under pressure, a bubbler tube must be installed so that the depth to the water level in the well can be conveniently determined. In a few wells on some occasions, downhole pressure may be needed.

The Producing Aquifer or Reservoir Formation. The pressure in all available observation wells open to the geothermal reservoir should be recorded each month. A few important observation wells may be read weekly if there is a need to indicate shorter-term fluctuations of pressure.

The Confining Strata Above the Aquifer. Some observation wells may have been completed in the confining layers above the reservoir. The water level in these also should be observed at least monthly to show the pressure conditions in the confining layer and to give indications of interference problems.

The Unconfined Aquifer Above the Confining Layer(s). Some observation wells (and local water wells) may be open to the unconfined aquifer near the surface. The water level in these wells and also any nearby springs gives a measure of the water table elevation and should be recorded at least monthly. These data, along with the pressure measurements described above, can give an indication of the gradient causing vertical leakage through the confining layer(s) as well as evidence of well interference problems.

Production and Injection Wells. These wells are the most important in the field and should be monitored most often. In fact, a continuous watch of pressure in production and injection wells is probably needed for the operational control of reservoir production. A permanent daily record should be kept of the pressure, temperature, production and injection rates.

Temperature Monitoring

Temperature monitoring should include discharge/recharge measurements at the surface and where feasible, downhole measurements. Surface measurements are inexpensive and easy to obtain. It is recommended that surface temperatures be obtained whenever a pressure measurement is obtained at a production/injection well. At nearby observation wells, springs, or discharge rivers or ponds, it may be sufficient to obtain surface discharge temperature (where appropriate) on a weekly schedule. Downhole temperature data are usually more expensive and may be impractical if a pump is in a well. If downhole data can be collected, it is recommended that measurements be taken at a minimum of every ten feet to total well depth at least biannually.

Confirmation of Reservoir Conceptual Model

As data are gathered from reservoir monitoring, it is necessary to assimilate them into initial projections and note any deviations from these projections. This assimilation is critical for verifying the conceptual model of the reservoir system, which logically ties into not only reservoir longevity, capacity and recharge, but also chemical changes, water level changes, and a group of potential environmental impacts.

Verification of the conceptual model would provide an early-warning system to a developer to modify or correct potential problems before they are encountered. In addition, reservoir monitoring allows the system to be expanded based upon a confirmed conceptual model, provides confidence to investors in reservoir development, and enhances further development of this technology.

REFERENCES

1. L. J. P. Muffler et al., "Nature and Distribution of Geothermal Energy," *Geothermal Resources Council Special Report No. 7, Direct Utilization of Geothermal Energy: A Technical Handbook*, 1979.

2. B. C. Craft and M. F. Hawkins, *Applied Petroleum Reservoir Engineering*, Englewood Cliffs, New Jersey: Prentice-Hall, Inc., 1959.

3. R. C. Earlougher, Jr., "Advances in Well Test Analysis," *Society of Petroleum Engineers, AIME, Monograph*, 5, 1977.

4. B. Renx et al., "An Improved Approach to Estimating True Reservoir Temperature from Transient Temperature Data," *50th California Regional Meeting of the Society of Petroleum Engineers of AIME, Los Angeles, California*, April 9-11, 1980, SPE 8888.

5. C. V. Theis, "The Relation Between the Lowering of the Piezometric Surface and the Rate and Duration of Discharge at a Well Using Ground Water Storage," *American Geophysical Union Transactions, 16*, 1935, pp. 519-524.

6. W. Hurst, "Unsteady Flow of Fluids in Oil Reservoirs," *Physics*, January 1934.

7. H. Darcy, *Les Foutaines Publiques de la Ville de Dijon*, Paris: Victor Dalmont, 1856, p. 647.

8. G. Thiem, *Hydrologische Methoden*, Leipzig: J. M. Gebhart, 1906, p. 56.

9. C. E. Jacob, "On the Flow of Water in an Elastic Artesian Aquifer," American Geophysical Union Transactions, 1940, part 2, pp. 574-586.

10. C. E. Jacob, "Flow of Groundwater," in *Engineering Hydraulics*, New York: John Wiley & Sons, 1950, pp. 321-386.

11. R. A. Freeze and J. A. Cherry, *Groundwater*, Englewood Cliffs, New Jersey: Prentice-Hall Inc., 1979.

12. H. H. Cooper and C. E. Jacob, "A Generalized Graphical Method for Evaluating Formation Constants and Summarizing Wellfield History," *American Geophysical Union Transactions, 27*, 4, 1946, pp. 526-534.

13. C. E. Jacob and S. W. Lohman, "Nonsteady Flow to a Well of Constant Drawdown in an Extensive Aquifer," *American Geophysical Union Transactions, 33*, 1952, pp. 559-569.

14. W. C. Walton, *Groundwater Resource Evaluation*, New York: McGraw-Hill, 1970.

15. M. I. Rorabaugh, "Graphical and Theoretical Analysis of Step-Drawdown Test of Artesian Well," *Proceedings of the American Society of Civil Engineers, 79*, 362, 1953.

16. H. Bouwer, *Groundwater Hydrology*, New York: McGraw-Hill, 1978, p. 84.

17. J. Bear, *Hydraulics of Groundwater*, Israel: McGraw-Hill, 1979.

18. M. D. Lamers, *Measurement Requirements and Methods for Geothermal Reservoir System Parameters (An Appraisal)*, LBL-9090, GREMP-6, 1979.

19. M. S. Hantush, "Nonsteady Flow to Flowing Wells in Leaky Aquifers," *Journal of Geophysical Research, 64*, 8, 1959.

20. W. C. Walton, *Selected Analytical Methods for Well and Aquifer Evaluation*, Urbana: Illinois State Water Survey, 1962.

21. D. C. Mangold, C. F. Tsang, M. J. Lippmann, and P. A. Witherspoon, "A Study of Thermal Effects in Well Test Analysis," *54th Annual Fall Technical Conference and Exhibitions, Las Vegas, Nevada, September 23-26, 1979.*

22. J. E. Warren and P. J. Root, "The Behavior of Naturally Fractured Reservoirs," *Society of Petroleum Engineers Journal*, 1963, pp. 245-255.

23. I. S. Papadopulos, "Nonsteady Flow to a Well in an Infinite Anistropic Aquifer," *Proceedings Dubrovnik Symposium on Hydrology of Fractured Rocks*, 1965, p. 21.

24. N. Rofail, "Analysis of Pumping Test in Fractured Rocks," *Proceedings: Dubrovnik Symposium on Hydrology of Fractured Rocks*, 1965, p. 81.

25. A. C. Gringarten, H. J. Ramey, and R. Raghovan, "Applied Pressure Analysis for Fractured Wells," *Journal of Petroleum Technology, 27*, July 1975, pp. 887-892.

26. T. D. Streltsova, "Hydrodynamics of Ground-Water Flow in a Fractured Formation," *Water Resources Research, 12*, 3, 1976, pp. 405-414.

27. J. O. Duguid and P. G. Y. Lee, "Flow in Fractured Porous Media," *Water Resources Research, 13*, 3, 1977.

28. R. Aguilera, *Naturally Fractured Reservoirs*, Tulsa, Oklahoma: Petroleum Publishing Company, 1980.

29. R. W. Parsons, "Permeability of Idealized Fractured Rock," *Proceedings of 1965 Fall Society of Petroleum Engineers Meeting, Denver, Colorado, 6, 1966.*

30. D. Goldman and S. Petty, "Testing and Analysis of Low-Temperature Hydrothermal Reservoirs," *National Conference on Renewable Energies, Honolulu, Hawaii, December 1980.*

31. D. W. Allman, D. Goldman, and W. L. Niemi, "Evaluation of Testing and Reservoir Parameters in Geothermal Wells at Raft River and Boise, Idaho," *Ninth Annual Rocky Mountain Ground-Water Conference, Reno, Nevada, October 1979.*

32. W. A. J. Mahon, "Silica in Hot Water Discharged from Drillholes at Wairakei, New Zealand," *New Zealand Journal of Science, 9*, 1966, pp. 135-144.

33. R. E. McAtee and C. A. Allen, "Chemical Logging, A Geothermal Technique," *Geothermal Resources Council, Trans., 3*, 1979, pp. 423-426.

34. L. Casper and T. Pinchback, eds., *Geothermal Scaling and Corrosion*, Special Technical Publication 717, ASTM, 1981.

35. R. O. Fournier, D. E. White, and A. H. Truesdell, "Geochemical Indicators of Subsurface Temperature, 1. Basic Assumptions," *U.S. Geological Survey Journal of Research, 2*, 1974, pp. 259-262.

36. R. O. Fournier and J. J. Rowe, "Estimation of Underground Temperatures from the Silica Content of Water from Hot Springs and Wet-Steam Wells," *American Journal of Science, 264*, 1966, pp. 685-697.

37. R. O. Fournier, "Chemical Geothermometers and Mixing Models for Geothermal Systems," *Geothermics, 5*, 1977, pp. 41-50.

38. R. O. Fournier and A. H. Truesdell, "An Empirical Na-K-Ca Geothermometer for Natural Waters," *Geochemica Cosmochima Acta*, 37, 1973, pp. 1259-1275.

39. R. O. Fournier and R. W. Potter, III, "Magnesium Correction to the Na-K-Ca Chemical Geothermometer," *Geochemica Cosmochima Acta*, 43, 1979, pp. 1543-1550.

40. Denver Research Institute, *Municipal Geothermal Heat Utilization Plan for Glenwood Springs, Colorado*, DOE/ID/12049-3, 1980.

41. R. Pearl, private communication, Colorado Geological Survey, 1982.

42. A. H. Truesdell and J. R. Hulston, "Isotopic Evidence on Environments of Geothermal Systems, in: *Handbook of Environmental Isotope Geochemistry*, Peter Fritz and J. Ch. Fontes, editors, New York: Elsevier Scientific Publishing Co., 1980, pp. 179-226.

IDO-10099
Volume I

GEOTHERMAL PROGRAMS

Idaho Operations Office

SubJ
GTHM
LTMT

Low-to-Moderate Temperature Hydrothermal Reservoir Engineering Handbook

A Joint-Project Report of Lawrence Berkeley Laboratory and The Idaho National Engineering Laboratory

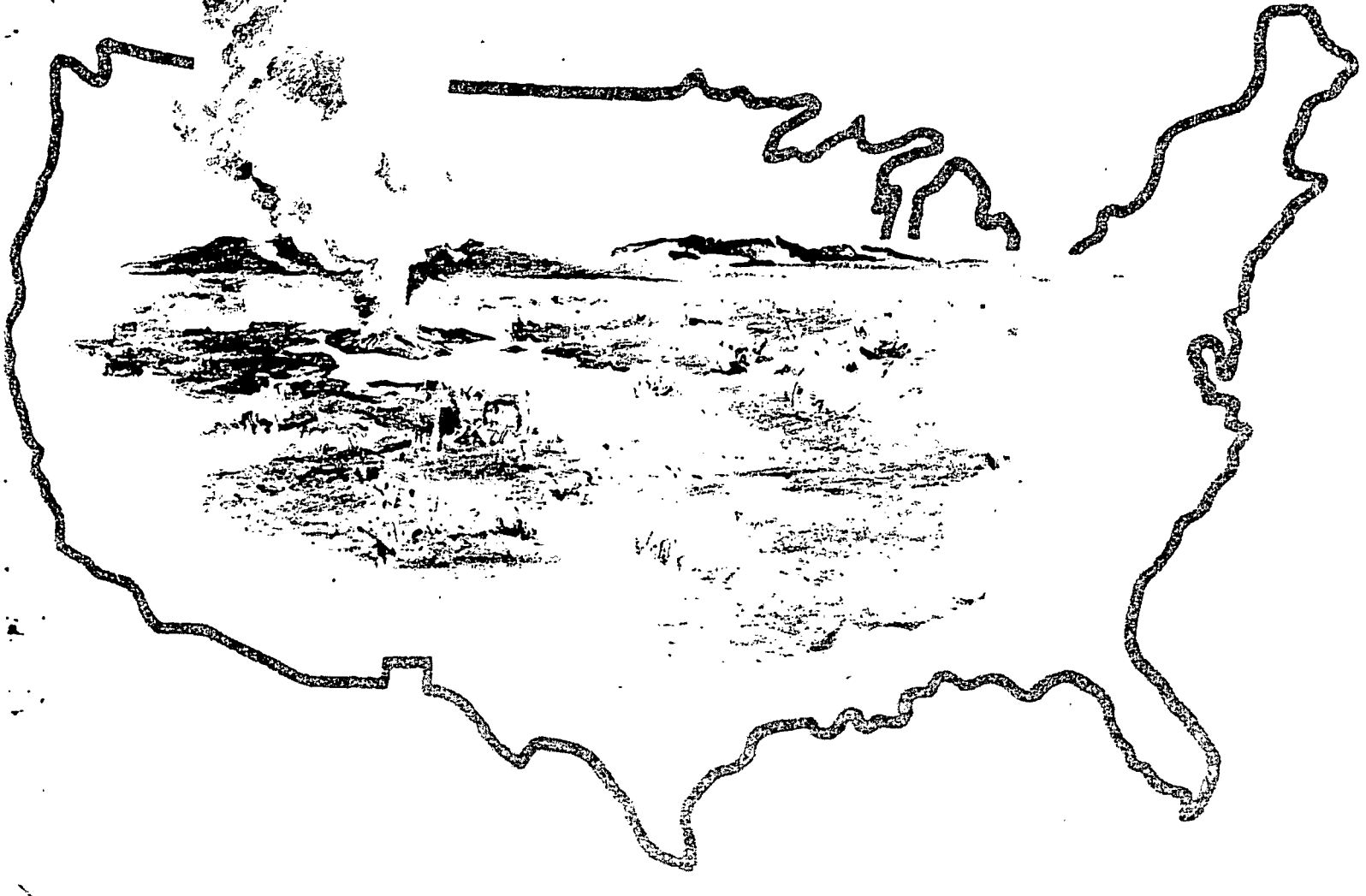

IDO-10099
Volume I
Distribution Category: UC-66a,d,g

LOW-TO-MODERATE TEMPERATURE HYDROTHERMAL RESERVOIR ENGINEERING HANDBOOK

Published June 1982

EG&G Idaho, Inc.
Idaho Falls, Idaho 83415

and

Lawrence Berkeley Laboratory
Berkeley, California 94720

Prepared for the
U.S. Department of Energy
Idaho Operations Office
Under DOE Contract No. DE-AC07-76IDO1570

FOREWORD

Low-to-moderate temperature geothermal energy will augment the future energy needs of industrial process heat, space heating, and district heating systems. As an industry in its infancy, geothermal reservoir engineering is unique and different from the technologies of petroleum and ground water reservoir engineering.

This document which provides guidelines to developers and consultants in evaluating reservoir characteristics contains sections on reservoir classification, conceptual modeling, testing during drilling, current theory of testing, test planning and methodology, instrumentation, and a sample computer program. Although the developer will find the entire document useful and informative, sections on test planning and methodology, geochemistry, reservoir monitoring, and the appendixes, containing technical detail, are designed specifically for the consultant. Sections 2 through 6 provide the developer background information needed to monitor the program of reservoir evaluation. As technology improves, this document will be modified. Future sections will depend upon ongoing and completed research in the low-to-moderate temperature geothermal industry.

Metric units are used whenever possible. However, some equations employ constants in English units and some instrumentation and oil field records (i.e., pressure gauges, rig recorders, and well logs) are calibrated or recorded in English units. Therefore, soft-metric and English units are used wherever logical or appropriate. Appendix A provides the reader with information on conversions.

ACKNOWLEDGMENTS

This document has been jointly prepared by EG&G Idaho, Inc., Geosciences Branch, and Lawrence Berkeley Laboratory, Earth Sciences Division for Dr. Leland L. Mink and Susan M. Prestwich of the Idaho Operations Offfice, U.S. Department of Energy. Robert A. Gray, Charles Bufe, and David Lombard of the Department of Energy, Division of Geothermal Energy provided the funding. Key contributors to this document include Dennis Goldman, Larry Hull, Julie Tullis, Steve Mizell, Brent Russell, and Piotr Skiba, all of EG&G Idaho, Inc.; and Calvin Clyde, appointed to EG&G Idaho, Inc. as a faculty participant through the Associated Western Universities. The EG&G Program management was provided by Max R. Dolenc, Susan Spencer, and Susan Petty. Lawrence Berkeley Laboratory contributors include the program manager, Sally Benson, Raymond Solbau, and Ernie Major, and Micheal Wilt.

Subir Sanyal, a private consultant, discussed the overall scope and direction of the document. A critical review of this document, before release, was also provided by: J. K. Balzhiser, Balzhiser/Hubbard and Associates; Calvin Clyde, Utah Water Research Laboratory; Glenn Coury, Coury and Associates; Gary Harvey, TRC Environmental Consultants, Inc.; Charles Morris, Republic Geothermal Inc.; Paul Lineau, Oregon Institute of Technology; John Lund, Oregon Institute of Technology; Derek Freeston, University of Aukland; Richard Pearl, Colorado Geological Survey; John L. Sondergger, Montana Bureau of Mines; Susan Spencer, Morrison and Knudsen; and P. M. Wright, Earth Science Laboratory, University of Utah Research Institute.

CONTENTS

FIGURES

TABLES

LOW-TO-MODERATE TEMPERATURE HYDROTHERMAL RESERVOIR ENGINEERING HANDBOOK

1. INTRODUCTION

Numerous low- (less than 90°C)-to-moderate temperature (90 to 150°C) geothermal resources occur in many areas of the United States. The number of known geothermal systems increases significantly as the temperature decreases. Geothermal systems occur primarily where the normal geothermal gradient of the earth (30°C/km average) is affected by a positive temperature anomaly. These anomalies are caused by: (a) higher than normal regional heat flow; (b) rocks of low thermal conductivity; (c) higher than normal concentrations of radioactive elements; (d) young magmatic intrusions; and/or (e) hydrothermal circulation.[1]

Low-to-moderate temperature geothermal resources have a wide range of direct-use applications in agriculture and industry. Agricultural uses such as greenhousing, animal husbandry, soil warming, mushroom raising, and biogas generation require the lowest temperature, ranging from 20 to 82°C. Industrial uses such as space heating for homes, offfices, hospitals, and large district heating systems requires temperatures from 45 to 100°C. Industrial processes require temperature up to 150°C with the use of both steam and superheated water. Industrial uses of geothermal fluids also include food processing, crop drying, and multiple use by the forest products industry. Although the unique aspects of each geothermal resource require individual consideration, most development schemes will employ straightforward engineering, using proven technology and existing system components.

The rationale used in developing a low-to-moderate temperature geothermal resource is the same as that used by a hydrologist or petroleum engineer in designing an optimal development scheme for a given water or oil reservoir. Consequently, the geothermal industry depends on two major areas of expertise: hydrology and petroleum engineering.

Hydrologists have applied ground water hydraulics and theory to low-temperature systems (<90°C) that are single phase and liquid and resemble ordinary ground water systems. However, most ground water theory was developed for application to fluids of about 16°C and did not include temperature dependent fluid properties. Problems with ground water theory applications to geothermal systems include those of nonisothermal flow, temperature dependent fluid properties, and proper interpretation of well tests. For well testing, the two most important temperature dependent fluid properties are density and viscosity. Figures 1 and 2 show the value of these parameters from 0 to 150°C.

The petroleum engineering theory was developed for exploitation of hydrocarbon resources. The great depth of some petroleum reserves, gas content of the fluid, and temperature dependent fluid properties make these petroleum reservoirs similar to high-temperature geothermal reservoirs. Because low-to-moderate temperature resources are rarely two-phase steam water mixtures, or have a high gas content, they do not require the sophistication of some of the petroleum techniques developed. Therefore, the reservoir engineering techniques developed for a low-to-moderate temperature geothermal system borrow the most appropriate methods and terminology from hydrology and petroleum engineering. The theories are very similar but the terminology has created a disparity between the petroleum engineering and hydrologic industries when applied to a low-to-moderate temperature resource.

This disparity has created the need for a handbook that will bridge the theories and methodologies of the hydrologic and petroleum engineering fields. This handbook has been prepared for developers with previous experience in one or more of the following: petroleum engineering, ground water hydrology, and/or high-low temperature geothermal systems. In addition, the handbook should provide a useful tool to both consultants and industry personnel. The handbook identifies significant areas of concern, with reference to other

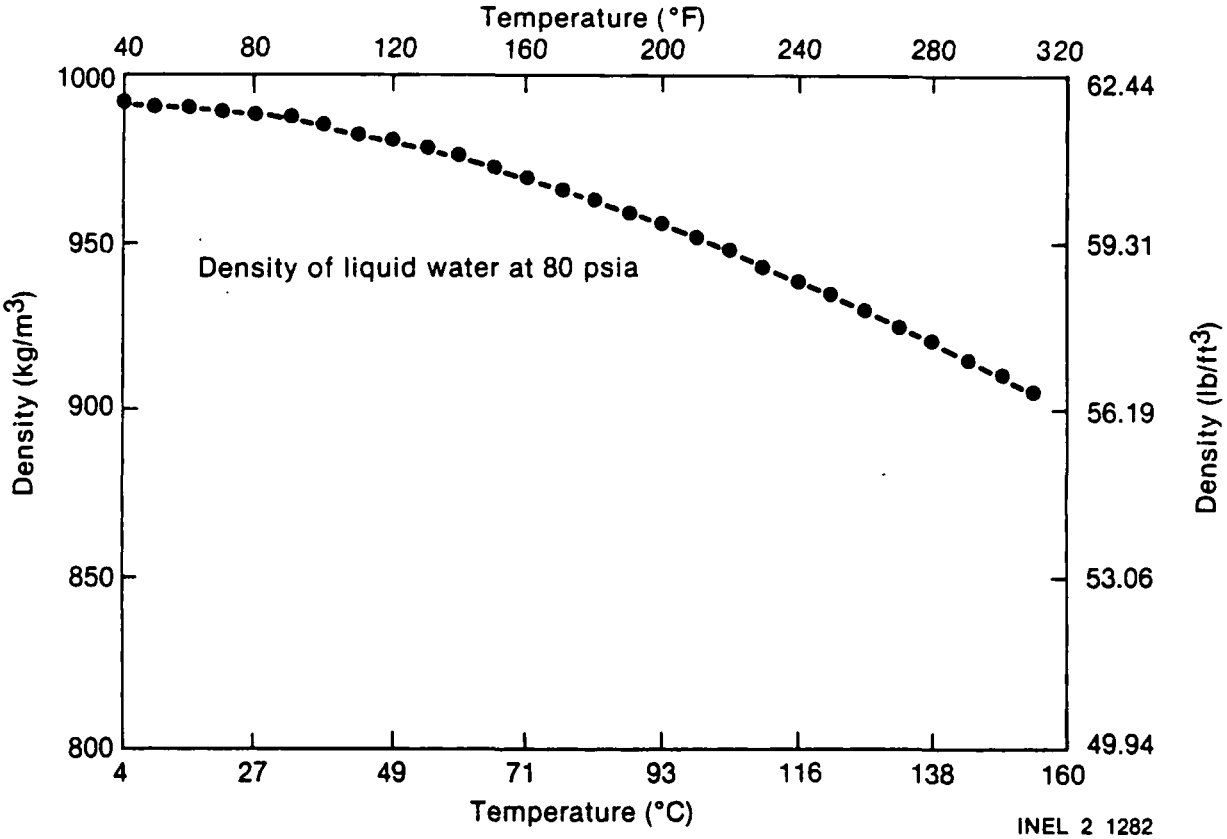

Figure 1. Density of liquid water at 80 psia.

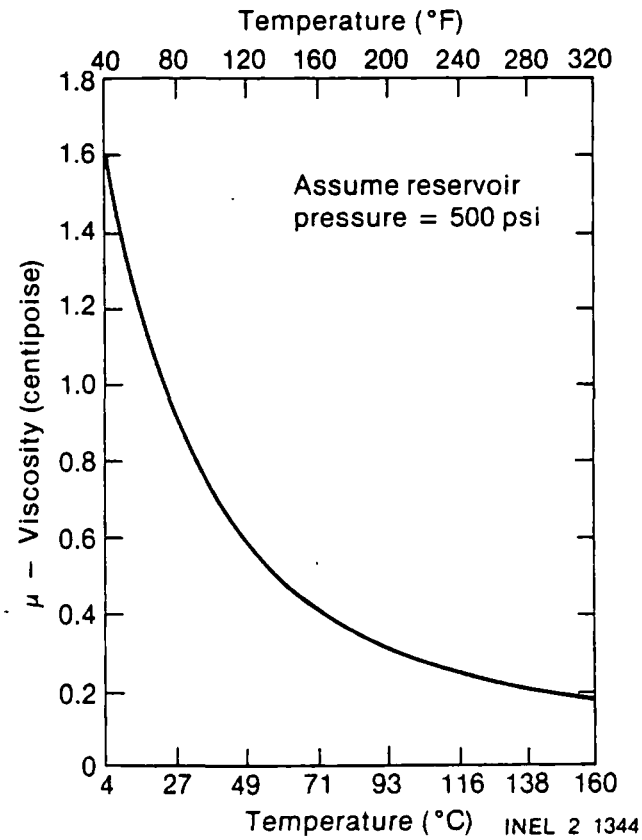

Figure 2. Viscosity of liquid water at 500 psia.

specific documents for in depth "how-to" discussions. The handbook provides an overview of reservoir engineering, basic and applied theory, conceptual modeling, testing during drilling, test planning and methodology, geochemical applications, and reservoir monitoring; it gives the potential developer a firm understanding of the tasks to be performed and the problems that may be anticipated.

2. RESERVOIR CLASSIFICATION

Individual geothermal systems occur in several different geologic environments. These include:

- Areas of recent intrusion and/or extrusion
- Areas where open fractures allow fluid circulation to depth with subsequent heating by the normal geothermal gradient
- Areas where radiogenic heat is trapped in rocks by overlying sediments
- Geopressured areas where hot fluids are confined under high pressures
- Areas where hot rocks exist without adequate natural fluids to transfer the heat (hot dry rock).

Young igneous environments primarily occur in the tectonically active Western United States (Figure 3). These systems provide the majority of known shallow geothermal reservoirs. The Cascade Mountain Range of Washington and Oregon represents a volcanic region caused from heat generated by the converging of plate margins. The Imperial Valley of Southern California is located in a region of crustal extension due to the East Pacific Rise spreading zone. Here the intrusions are emplaced at shallow depth, providing a heat source for the geothermal resource. The Snake River Plain of Idaho and Yellowstone Park represent volcanic areas caused by intraplate melting. Young volcanic regions also occur in some parts of the Basin and Range Province, and in the Rio Grande Rift. The heat source in volcanic belts is provided by the presence of cooling magma.[1]

Deep circulation primarily occurs where the crust of the earth is under tensional stress. The Basin and Range Province and the Rio Grande Rift are extensional environments characterized by active faulting, thick sedimentary basins between young mountain ranges, and occasional sites of active volcanism. The source of heat for this environment comes from higher-than-normal regional heat flow, circulation of fluids to great depths, and igneous intrusions.

Radiogenic heat environments are generally found along the Atlantic Coastal Plain where a thick sedimentary sequence is underlain by granitic rocks. This heat, trapped by rocks with low thermal conductivity, is generated by the decay of U^{238}, Th^{232}, and K^{90} found in high concentrations in granitic intrusions.

Geopressured geothermal reservoirs occur mainly in the Gulf of Mexico where rapid sedimentary loading has trapped the heat under a thick sedimentary blanket. The fluids are under high pressure, usually contain dissolved methane, and are normally 150°C or higher. These reservoirs are not pertinent to a discussion of direct-use application energy resources because of the great diffficulty in developing them; however, waters of low-to-moderate temperatures have been found overlying many geopressured zones.

In this handbook, geothermal systems are classified according to the reservoir characteristics that control fluid flow. These controls are either faults, intergranular permeability, or a combination of both. Fault-controlled systems occur primarily in metamorphic and igneous rocks, but can also occur in sedimentary rocks. Fault control is normally associated with hydrothermal convection systems where cold ground water circulates to depth, heats up, then rises along fractured zones. The heat in these systems is dependent on the regional heat flow, the depth of circulation, and the residence time of water at depth. The permeability of these reservoirs depends on the size and number of fractures in the system, the nature of brecciated material along the fault, and the degree of fracture sealing. Geothermal reservoirs controlled by intergranular permeability normally occur in deep sedimentary basins filled with consolidated or unconsolidated sediments. Ground water from adjacent highlands travels down-dip through the sediments and is heated by the thermal gradient of the earth. Heated water moves upward due to density differences to form geothermal reservoirs within economic exploitation depth. Permeability is controlled by the size and continuity of the pore spaces. Many geothermal reservoirs are controlled by a combination of both faulting and intergranular permeability.

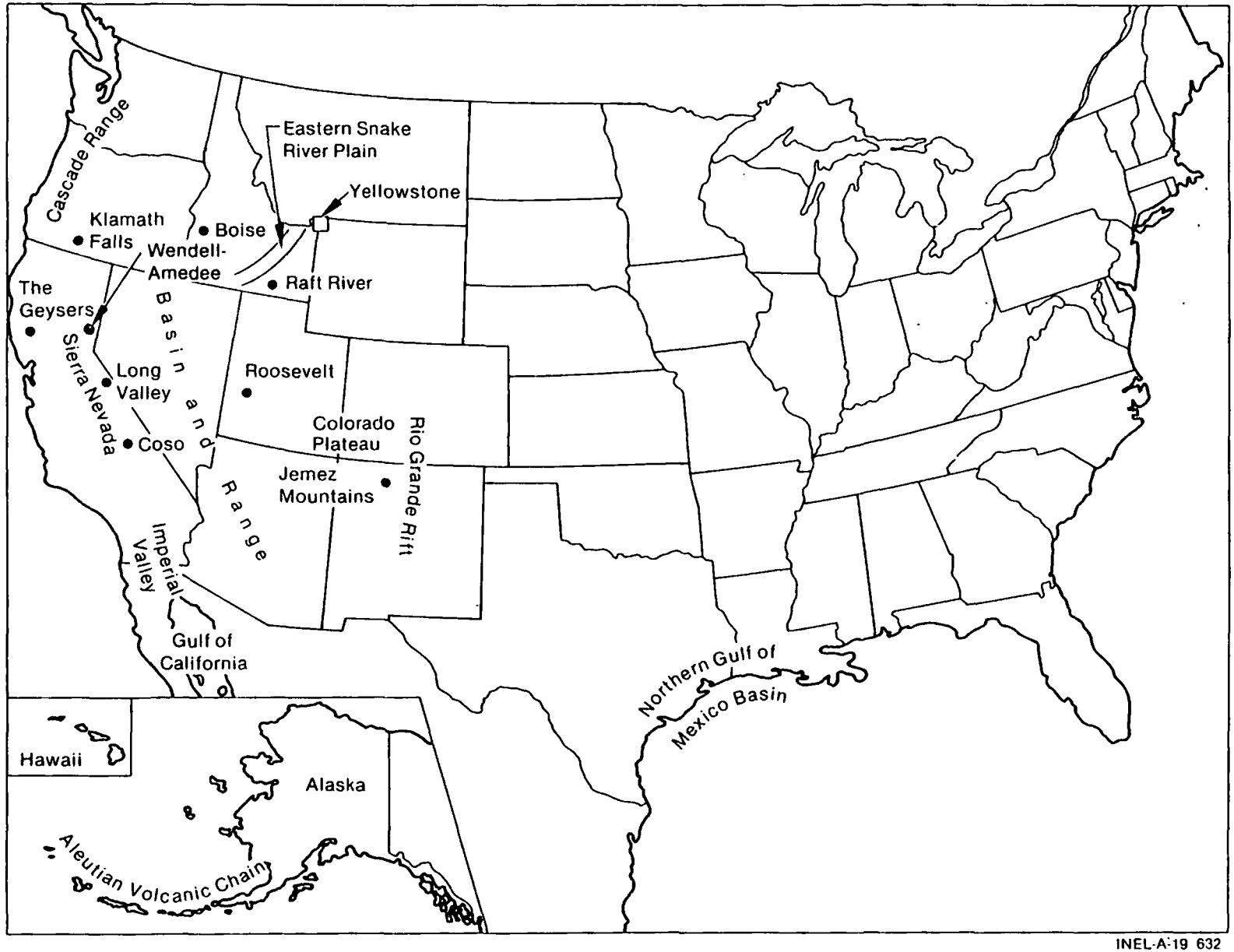

Figure 3. Map of the United States showing geographic features mentioned in the text and selected geothermal installations.

3. RESERVOIR ENGINEERING

Reservoir engineering can be defined ". . . as the application of scientific principles to the drainage problems arising during the development and production of oil and gas reservoirs. The working tools of the reservoir engineer are subsurface geology, applied mathematics, and the basic laws of physics and chemistry governing the behavior of liquid and vapor phases of crude oil, natural gas, and water."[2]

Reservoir engineering has been developed to a high level of sophistication in both the petroleum and ground water industries. Geothermal reservoir engineering has borrowed heavily from both of these fields. Some features unique to geothermal reservoir engineering include dynamic hydrothermal regimes and non-isothermal temperature distributions.

Reservoir engineering is used to design development strategy, exploitation strategy, and reservoir management programs. The basic problems that should be considered in geothermal reservoir engineering are: pressure, temperature, fracture flow, chemical changes within the thermal reservoir, and hydraulic connection to regional ground water aquifer(s). Specific aspects include: (a) siting production wells and choosing a completion interval; (b) designing well completions; (c) designing and interpreting well tests; (d) selecting the fluid disposal method, i.e., injection or surface disposal; (e) siting injection wells if any; (f) calculating the number of wells needed to supply the required energy; (g) predicting well drawdown; (h) predicting interference effects; (i) predicting the longevity of the resource; and (j) monitoring the exploitation phase.

The reservoir engineer must design a strategy that ensures not only an adequate supply of fluid, but also a fluid temperature that is suffficient for anticipated use. Predicting production temperatures over the life-time of the project is one of the most challenging tasks for the geothermal reservoir engineer.

Reservoir engineering starts during the exploration phase, when geological and geophysical data are collected. A reservoir engineer uses these data to formulate a preliminary conceptual reservoir model by identifying the reservoir type and its approximate size. Drilling data, borehole geophysics, and testing during drilling improve the conceptual model and provide preliminary well and reservoir parameters.

Well testing and test data analysis are important aspects of reservoir engineering that are used to determine the properties of a reservoir system which control the flow of fluids into a well, the migration path of injected fluid, and the natural and induced recharge.

Thus, the reservoir engineer uses all these phases when developing a geothermal resource.

4. CONCEPTUAL MODELING

Conceptual modeling is an important tool at every stage of reservoir evaluation. A conceptual model of the reservoir is envisioned before drilling a well in order to predict what type of rock formations will be penetrated, the expected temperature, and the target depth for the well. After the well has been drilled, a conceptual model is needed to design the well test and interpret well test data. Finally, the conceptual model is used to plan the locations of production and injection wells, optimize production and injection rates, predict the reservoir lifetime, and estimate the total energy available from the hydrothermal system. The conceptual model will evolve and become more refined each time a new piece of information is obtained, analyzed, and integrated into the existing model.

This section describes the types of data required to formulate a working model of a geothermal resource, especially ways of collecting data and integrating them into the model. Examples of different kinds of data gathered in other disciplines are provided for further understanding and conceptualizing the geothermal resource. Since this section is not a definitive work on the subject, references to additional studies are included. The importance of a conceptual model to the design of the well and the interpretation of the well test data are also discussed.

Before drilling any wells the following information can be used to conceptualize the geothermal resource: geothermometry, surface geology, and geophysical surveys. Comparing the geologic setting of the reservoir under investigation to the geology of many known geothermal resource areas can help classify the reservoir. Although every geothermal resource has unique characteristics, the rapid development of many low- and moderate-temperature geothermal resources has provided an adequate data base so that extrapolation of types of phenomena from one system to another is to some extent plausible. The study of similar types of hydrothermal systems should not be overlooked in developing a conceptual model.

Data obtained during drilling provides information on the subsurface characteristics of the hydrothermal system. Drill cuttings and cores can be used to reconstruct the subsurface lithology penetrated by the borehole. Drilling rates provide information on the structural integrity, hardness, and density of the formations penetrated. Loss of circulation fluid while drilling is often a reliable indication of fractures or permeable strata. Drilling mud temperature and mud chemistry are indicators of subsurface temperature and fluid entry into the wellbore.

After drilling a well, a number of borehole geophysical logs are run from which formation porosity and permeability, lithology changes, and formation temperature can be inferred. Well testing is performed to determine the hydrologic and geometric properties of the system. Well tests can also be helpful for inferring subsurface areal temperature distribution.

The effectiveness (i.e., accuracy and refinement) of a conceptual model is dependent on the information that is incorporated into it. The geologic, thermal, geochemical, and structural complexity of the hydrothermal system dictates the amount and type of data required to have a functional and accurate model. For instance, in a system with a near normal geothermal gradient and relatively simple geologic structure, such as the Madison Aquifer, less reconnaissance and exploration effort will be required. On the other hand, in a shallow, highly faulted, complexly fractured volcanic-type system, such as the Klamath Falls known geothermal resource area (KGRA), a substantial amount of exploratory work is necessary to define the hydrothermal system and to predict reservoir performance confidently. The degree of refinement required for an adequate conceptual model depends on the intended use of the resource. If only a small quantity of geothermal fluid is to be extracted from the reservoir compared with the reservoir potential, less exploration and conceptual model development will be required than if the reservoir potential is to be taxed. The model's refinement also depends on the amount of time and effort available to invest in gathering quality data. It should be emphasized that without quality data it is very diffficult to predict confidently the reservoir's behavior during exploitation. Sophisticated methods are now being developed to interpret data from complex geothermal systems. Therefore, every effort should be made to obtain quality data. The following subsections describe what data are important to have, how to process them, how to interpret them, and how the conceptual model can be used to the benefit of the resource developer.

Data Base

Surface Geology. Surface maps are the most readily available piece of information used for delineating geologic features. Information obtained from the surface map will be used for preliminary classification of the hydrothermal system. Geologic mapping has been completed for many areas on a regional or site-specific basis. These maps are available through publications from the U.S. Geological Survey, state geological surveys, and universities.

Aerial photography and landsat imagery interpretation can also be useful tools for delineating major geologic features. They are normally used in conjunction with geologic maps to locate fault lineations, fault intersections, and areas of thermal alteration.

Subsurface Geology. The subsurface geology of an area is usually constructed from data obtained from the examination of drill cuttings, cores, geophysical logs, drillers logs, etc. The drilling rate, circulation fluid record, and drilling fluid temperatures provide data on the physical and thermal properties of the penetrated rock unit. Geophysical logs are also useful tools for identifying subsurface lithologic units and the physical properties of the units. The interpretation of geophysical logs is an important technique in evaluating the subsurface lithology when there are no drill cuttings or cores available. Their use and interpretation are, however, limited depending upon the formation encountered, i.e., porosity and permeability values can be determined from logs run in sedimentary units, but may not always be determined in igneous or metamorphic units. Geophysical logs can be a useful tool for correlating rock units, thermal regimes, and hydrothermal mineralization between wells, and in locating fracture zones in wells.

Many of the low-to-moderate temperature hydrothermal reservoirs in areas with above-normal temperature gradients are associated with faults and fractures. These faults and fractured strata contribute significantly to the permeability of the hydrothermal reservoir; therefore, it is essential to detect their presence and estimate their depth. Among the most useful methods for detecting fractures is the examination of a carefully maintained record of the amount of circulation fluid used. Sudden loss of circulation fluid often indicates that fractures have been penetrated. However, the loss of drill cuttings and circulation fluid is not always indicative of fracture zones. Therefore, all of the subsurface data should be correlated to verify the data interpretation.

Temperature Profiles. Temperature profiles are obtained by measuring wellbore temperatures at a number of depths in the well. Temperature profiles are one of the most useful tools for understanding the hydrothermal system being studied. By carefully examining temperature profiles obtained under a variety of wellbore conditions, producing aquifers can be identified, multiple producing aquifers can be identified, hot water recharge detected, conductive versus convective (hydrothermal circulation) thermal regimes identified, the presence of a caprock and basement rock detected, and the thickness of the hydrothermal reservoir penetrated by the wellbore estimated.

Some caution should be taken when interpreting temperature profiles because circulation of fluid in the wellbore can mask the true formation temperature. An example of this can be seen in Figure 4. The only difference, other than the temperature profiles, between the two wells is the casing schedule. Well YMCA No. 1 is cased to 500 ft (152 m) and well YMCA No. 2 is cased to 980 ft (305 m). By comparing the two profiles obtained in wells 500 ft (152 m) apart with identical lithologic columns, it was determined that water was flowing down the wellbore in the well YMCA No. 1. Cold water entering the wellbore in well YMCA No. 1 at 500 ft (102 m), flowed down the wellbore and enters a second reservoir at 1200 ft (366 m). If the data from well YMCA No. 2 had not been available the temperature profile from well YMCA No. 1 may have been misinterpreted to conclude that the isothermal interval from 500 ft (152 m) to 1200 ft (366 m) was the geothermal aquifer. In reality, the main producing aquifer is in a fractured interval between 1200 (366 m) and 1300 ft (396 m).

Geochemistry. Information about geothermal fields which can be deduced from geochemistry includes: estimated subsurface temperature, location of heat source(s), directions of water movement, source of dissolved solids, sources of recharge, age (possibly), and whether hotter water exists nearby. Contouring maps

Thermal methods are among the most direct and commonly used methods for determining the location and size of a geothermal system. Thermal methods include: (a) calculation of the heat flow from the earth using thermal gradient data and thermal conductivity measurements, and (b) evaluation of the measured geothermal gradient. Among other things, these data can indicate the size and shape of the hydrothermal anomaly.

Seismic methods can be passive and active. Passive methods monitor natural earthquake activity to infer anomalous stress states due to possible heat sources, abnormal tectonic activity, and/or abnormal hydrostatic conditions. Detailed microearthquake surveys are also used to delineate active fault zones that may serve as potential ground water conduits. The active methods use the amplitude and velocity variation of seismic waves generated by a controlled source, both compressional (P) and shear (S) waves, to infer the characteristics of the medium in which they are propagated. Active reflection techniques are used to infer the location of discontinuities, layer, thickness, and general structure. Depending upon the size and frequency of the source, reflection techniques can "look" as deep as several kilometers and still define fault boundaries and basement structure. Refraction techniques look at the velocity variation of the P-waves to infer layer thickness, fault location, and structural discontinuities. The refraction techniques are not as detailed as the reflection techniques and require larger "spreads" and more powerful sources to look at comparable depths. The refraction techniques can also miss structure that the reflection surveys will detect if the velocity variations with depth are not continually increasing. However, the refraction techniques are much cheaper and require less sophisticated post processing.

Electrical and electromagnetic methods are used to estimate the electrical resistivity of the earth. Electrical resistivity is a measure of the earth's ability to conduct electrical current and depends upon the porosity, fluid saturation, temperature and clay content of the rock, and the salinity of the pore fluid. In general, the higher these parameters are, the lower the resistivity of the medium. Since geothermal areas are associated with high subsurface temperatures and saline fluids, they are characterized by anomalously low resistivity. Electrical and electromagnetic surveys performed on the surface are therefore very effective methods for locating buried geothermal systems. The most commonly used of these methods is the d.c. resistivity method. Low frequency electrical current is injected into the ground through a portable generator and earth electrodes. The resulting potential at a site of specified distance away is then measured. By varying the spacing between current and potential electrodes, a variation of voltage with separation and/or location is obtained. This may be corrected for a variation of electrical resistivity with depth, depth soundings, spatial variation at resistivity, or a mapping survey. Electromagnetic methods use a time varying signal source and obtain earth resistivity information from variation at electrical fields with frequency.

Gravity and magnetic surveys are structural methods used to estimate: the thickness of sediments, the depth to the basement, the density or density contrasts of basement rocks, and buried volcanic or intrusive rocks. Magnetic surveys detect the magnetic susceptibility of subsurface rocks. Because hydrothermal alteration reduces the magnetic susceptibility of the subsurface rocks, a negative anomaly may be indicative of a hydrothermal resource.

Well Testing. Well testing is the most common and reliable method for determining the parameters which control flow of fluid through the reservoir. The parameters which affect the ease with which water will flow through the reservoir are the rock permeability (k), the viscosity of the reservoir fluid (μ), the porosity (ϕ), the formation compressibility (c), and the production geometry (height, areal extent, layers, etc.). Knowing these parameters or the groups of parameters kh/μ (transmissivity) and ϕch (storativity), well drawdown, well productivity, and interference effects can be calculated.

Well tests are typically conducted by pumping or artesian flowing a well for a period of time at a constant flow rate. The pressure changes in the production well are observed over time. The change of pressure is analyzed to obtain the physical parameters of the reservoir system. If there are other wells in the area, these too can be monitored for pressure (or water level) changes as a function of time. Often the data from interference wells will provide more accurate reservoir information due to instrumentation and logistical constraints at the production well. If an array of observation wells is available, accurate information about the reservoir size and geometry can be obtained.

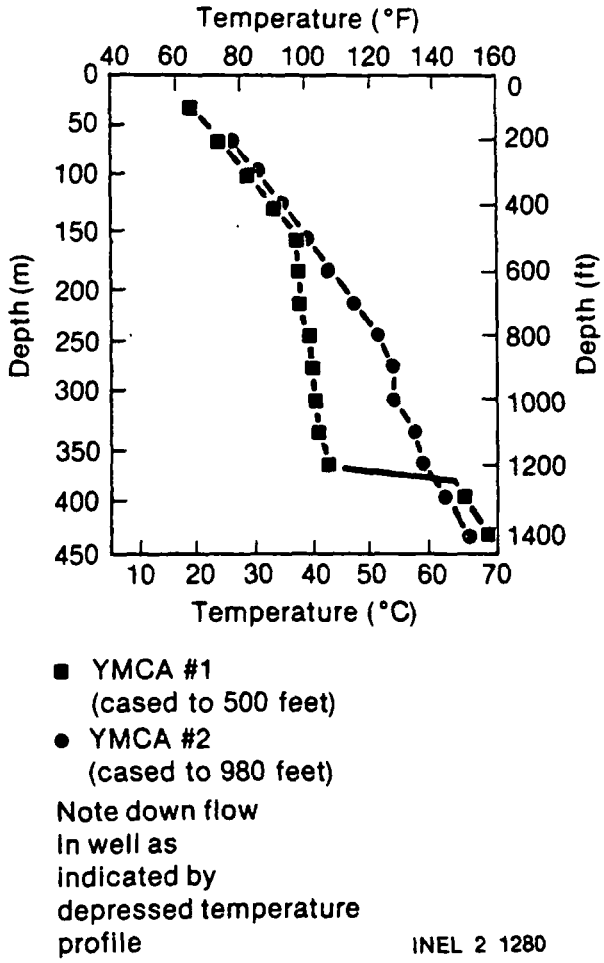

Figure 4. Downflow in well as indicated by depressed temperature profile.

or cross-sectional views of chemical concentrations in a geothermal area can provide insight into water movement and the sources of dissolved salts, heat, and water. Care must be taken, however, to ensure that the data being contoured are from the same hydrogeologic unit. For example, in a geothermal area containing shallow domestic and irrigation wells, intermediate depth wells, and deep geothermal production wells, each depth level must be treated separately. Patterns of contours can indicate directions of water movement. A comparison of contour maps or cross-sections for species whose concentrations are related to temperature (SiO_2) and conservative species (Cl^-) can indicate differences between locations of heat sources and high dissolved solids waters. Spatial variations in water chemistry can be due to mixing of waters from different sources, evaporation, steam loss, precipitation of solid phase, or reactions with aquifer materials. Simple mixing calculations can be used to determine if mixing is responsible for spatial variations.

Stable isotopes in water (hydrogen and oxygen) can be used to determine the source of water. Studies have shown that many geothermal waters are comprised of local meteoric water heated by circulation to depth. Variations in the isotopic composition of recharge water can occur by evaporation before recharge, or by recharge occurring at different elevations. If these variations can be traced through the geothermal system, detailed information on sources of water can be obtained.

Geophysics. Geophysical methods used in the exploration for hydrothermal resources can be categorized in five groups: thermal, seismic, electrical, magnetic, and gravity. These methods can provide valuable exploration data, insofar as they are used to delineate the hydrothermal resource. However, because of the ambiguity inherent in their interpretation, these may or may not be the type of data needed for a conceptual model of the resource.

Data Preparation

Before the data from all of the various disciplines can be synthesized, it is important to prepare them correctly. There are four basic types of displays by which data can be processed to provide a visual respresentation of the various reservoir characteristics: mapping, profiling, contouring, and cross sections. Depending on the amount and quality of data, it may or may not be worthwhile to do all of the types of processing.

Mapping. Mapping is the least sophisticated and most simple display to prepare. It involves locating observed phenomena or physical features on a cartesian coordinate system that overlies the area under study. This type of representation is used when only a two-dimensional representation of the data is required, i.e., when depth is not considered. Temperatures and chemical data from springs are often mapped with this technique. The representation does not account for the fact that the springs may have circulation at different depths, and thus, differing chemical constituents and temperatures.

Mapping is generally used in the early stages of exploration. For example, the relationship between the recent volcanism and the hydrothermal anomaly at Klamath Falls, Oregon, was examined by radiometric dates obtained on rock samples from in and around the Klamath Falls area. A map showing the location and radiometric age of each sample is shown in Figure 5. The concentric pattern of older dates with distance from the Klamath Falls vicinity may suggest that the anomaly is associated with the most recent volcanism in the area.

Profiling. Profiling consists of looking at data from a single penetration through a vertical section. Profiled data are obtained from wellbore surveys. For instance, by plotting the well lithology versus depth a lithologic profile is obtained; by plotting temperature obtained from a temperature survey versus depth, a temperature profile is obtained.

One example of a lithologic column and temperature profile for a well is shown in Figure 6. This type of temperature profile is typical of temperature profiles in shallow fault-charged reservoirs. A comparison of the lithologic column, the drilling circulation record, and the temperature profile shows that a thermal production interval in the well is between 195 ft (59 m) and 240 ft (73 m).

Contouring. Contouring is used to define the shape and extent of the observed physical phenomena. For instance, temperature contours are used to define the areal and vertical extent of a hydrothermal system and can be used to make rough calculations of the amount of hot fluid in place. One of the most common methods of contouring is to plot isotherms, or isobars, at a given depth below the surface. By comparing contours at several elevations, both an areal and vertical description of the phenomena can be obtained.

In Figure 7 the temperatures at three different depths from the Susanville, California wells are contoured. At the shallowest depth, 150 m below surface elevation (1250 m elevation), the hottest part of the anomaly (inside the 60 degree contour) is centered around the Davis well. With increasing depth the shape of the anomaly is asymmetrically elongated around a northwest trending axis. Using these contours and lithologic data, a production well (Susan 1) was sited next to Suzy 9. As predicted from these contours, the new well, Susan 1, was the hottest well drilled thus far.

Concentrations of chemical species may also be contoured at various depths to determine if and how mixing of different fluids is occurring. Static water levels are contoured to determine the extent and direction of regional ground water flow.

Cross Sections. Cross sections are constructed by correlating or comparing profiles at two or more wells. Multiple cross sections, or cross sections and contours, may be used to get a three-dimensional model of the reservoir. Lithologic data are typically processed this way. Correlations of major geologic features, such as fracture zones, producing aquifers, caprock, and basement rock are obtained by constructing cross sections of the reservoir data. Temperature data are also plotted as cross sections and provide a multidimensional view of the hydrothermal structure. Two cross sections of temperature distribution are shown in Figure 8. This

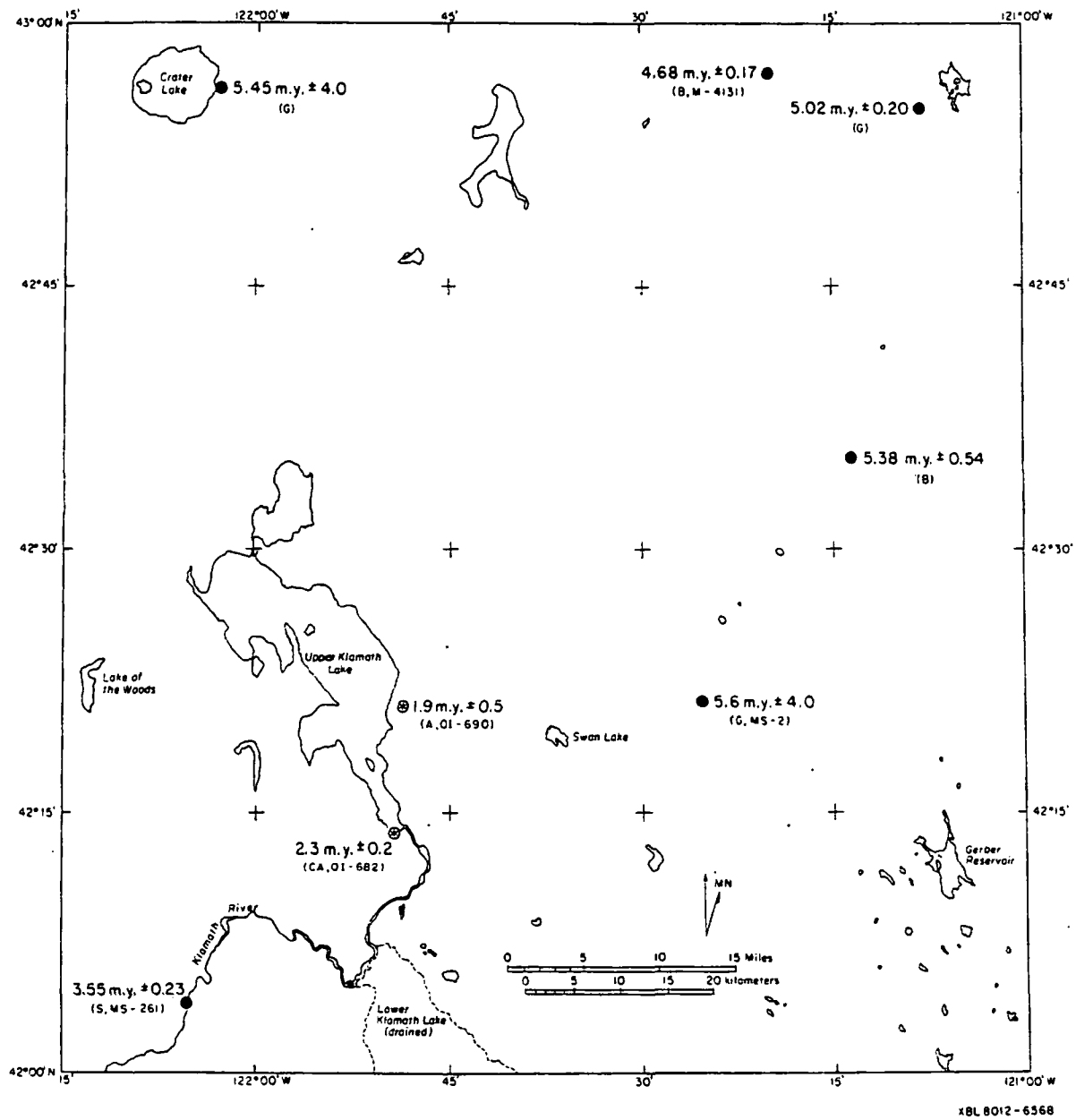

Figure 5. Rock sample locations from Klamath Falls, Oregon.

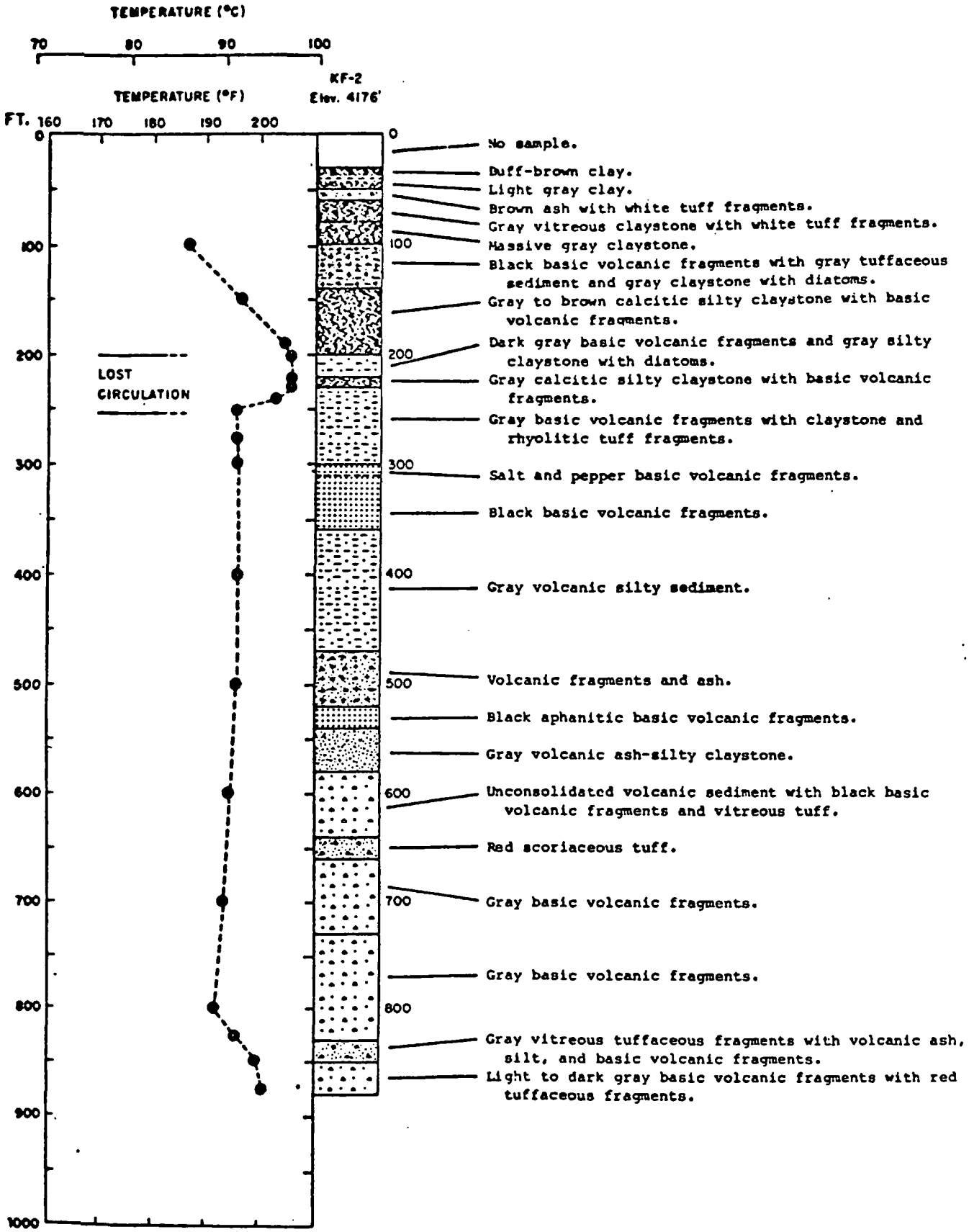

Figure 6. Temperature profile and lithology for Klamath Falls, City Well No. 2.

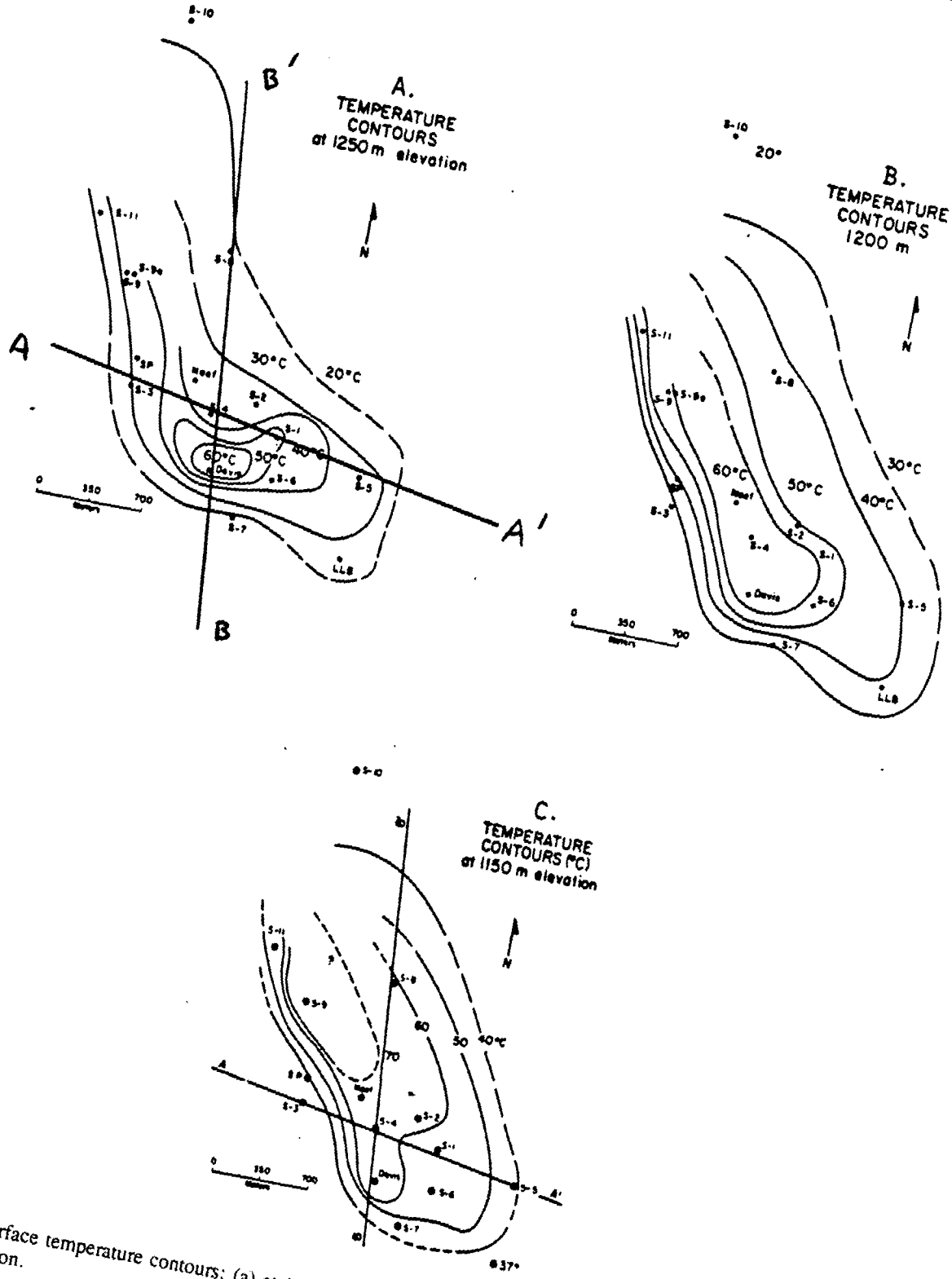

Figure 7. Subsurface temperature contours: (a) at 1250 m elevation, (b) at 1200 m elevation, and (c) at 1150 m elevation.

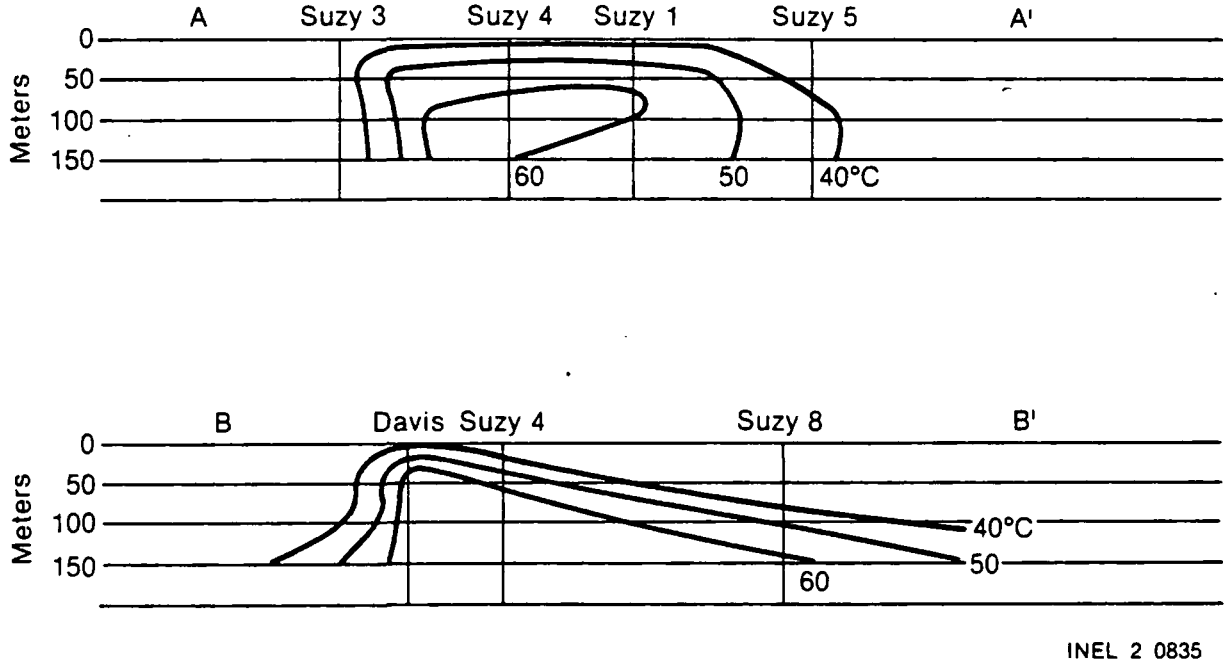

Figure 8. Cross sections of the Susanville hydrothermal anomaly.

type of thermal structure is indicative of upwelling of heated fluids from depth and lateral transport of fluid along permeable beds and fractures. This type of hydrothermal structure is common in shallow geothermal anomalies in the Cascade Range and the Basin and Range Province.

Borehole geophysical logs, such as electrical and nuclear logs, are also correlated on cross sections and are useful indicators of physical properties of the geologic section penetrated by the wellbore.

Graphically representing data in all of the above display forms helps to synthesize subsurface reservoir data with data obtained from surface reconnaissance. The subsurface reconstruction from each discipline should be compared to obtain a coherent conceptual model. Table 1 lists the various ways to process data.

Table 1. Common methods of data preparation

	Map	Profile	Contour	Cross Section
Surface Geological	X	X	—	—
Geochemical	X	X	X	—
Surface Geophysical	—	—	X	X
Hydrologic	X	X	X	—
Lithologic	—	X	—	X
Geophysical Logs	—	X	—	X
Thermal	X	X	X	X

Data Synthesis

The purpose of synthesizing data from each of the disciplines discussed above is to identify the major lithologic, thermal, petrophysical, and structural controls on the hydrothermal system under investigation. The key parameters that govern how a hydrothermal system behaves are: the permeability, storativity, size, and geometry of the production zone(s), the boundary conditions on the producing aquifer such as lateral recharge (hot or cold) caprock and basement rock leakage; regional ground water flow, and thermal distribution in the resource. Hydrothermal reservoirs are often very complex both lithologically and structurally. For this reason it may be diffficult, if not impossible, to identify all of these major features. Nevertheless, an attempt should be made to identify these features because they play a critical role in interpreting well test data, designing the reservoir management program, and providing an overall understanding of the resource.

The first step in synthesizing all of the data is to correlate specific physical, thermal, and lithologic units between wells. If data from only one well are available, correlation between wells will not be possible. However, a thorough evaluation of all of the data from that one well should be performed. The features that identify the production zone, caprock, basement rock, and the physical parameters are discussed below.

Producing Zones. The major production intervals can be identified by numerous features depending on the geologic setting. For instance, in a thick sedimentary sequence, a permeable aquifer will probably occur in a sandstone, and over and underlying impermeable layers will consist of a shale or clay sequence. The temperature profile through such a sequence would consist of several distinct gradients: a convective gradient through the aquifer and a conductive gradient through the underlying boundary layer. An example is shown in Figure 9. In a fractured rock sequence, the production zones (fractures) may be located by fluid entry into the wellbore during drilling, or by loss of circulation fluid into the formation. Production zones in fractured rocks may also be indicated by temperature profiles as was demonstrated in the previous section in Figure 6.

There is no single method of detecting the production zones; however, they can usually be identified by one or more of the following methods:

1. Loss of circulation fluid when drilling through the aquifer
2. A convective thermal gradient as opposed to a conductive gradient
3. Indication of sand zones or high-water-content zones from geophysical logs or cuttings
4. Fluid entry into the wellbore during drilling
5. Fracture zones indicated during drilling
6. Spinner surveys (downhole flow meter).

The properties of the producing aquifer(s) which need to be determined are: transmissivity, storativity, temperature distribution, structure, and geometry.

In general the reservoir transmissivity and storativity can accurately be determined only by well testing. However, before well testing, the type and degree of permeability can be determined by examining items discussed above. The two most common types of permeability are matrix and fracture. Matrix permeability occurs when the fluid flows through porous spaces in the rock. The fluid enters the wellbore from the entire aquifer interval. If the flow in the reservoir is confined mainly to fractures in the rock, then the term fracture permeability is used. In systems with fracture permeability, flow into the well comes only from the fracture, not the matrix of the rock. However, away from the wellbore, fluid may enter the fracture by flowing from the rock matrix into the fracture. The fracture is a conduit for fluid to flow into the wellbore. Many hydrothermal systems are some combination of fracture and matrix permeability and these systems are called dual-porosity systems. In general, hydrothermal systems that occur in volcanic and metamorphic rocks will have a

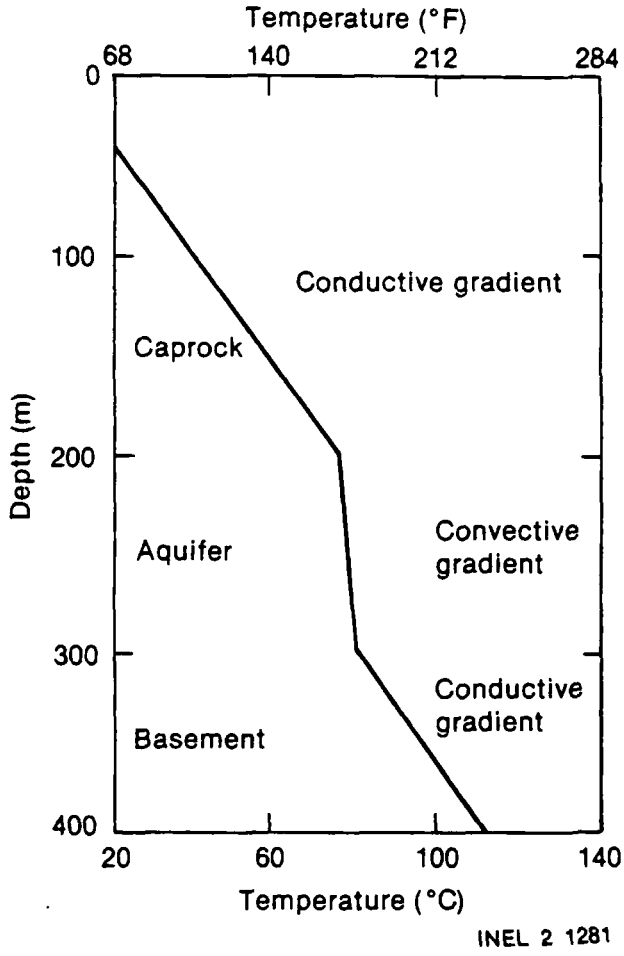

Figure 9. Example of a typical temperature gradient through of sedimentary sequence showing the caprock, aquifer, and basement.

fracture-dominated permeability. Sedimentary formations, except for carbonate systems, will in general have a type of matrix permeability. There are, however, exceptions to this generalization.

The temperature of the producing aquifer may be measured with a downhole temperature probe. It is important to measure the temperature downhole because any measurement taken at the surface may be affected by cooling and mixing as the fluid moves up the wellbore. Except in deep, near-normal geothermal-gradient type reservoirs, the temperature in the producing aquifer will vary spatially. It is important to have measurements of the temperature in the producing aquifer in as many wells as possible because the spatial variation of temperatures in the aquifer is one of the most useful tools for determining where and if hot water recharge is taking place. Temperature contours, at several depths, should be constructed. The interpretation of this is discussed in the previous section.

The important geometric characteristics of a hydrothermal aquifer are the areal extent, height, and shape. The volume of the aquifer (areal extent multiplied by height) is used to make a first-order estimate of the amount of hydrothermal fluids in place. Obviously, data must be available from more than one well to determine the areal extent of the resource. The shape of the hydrothermal aquifer is one of the major clues to understanding the resource. In near-normal geothermal gradient aquifers, it is the size and shape of the permeable (and porous) aquifer that governs the geometry of the hydrothermal system. In Basin and Range and fault-controlled hydrothermal systems it is usually the extent of the thermal anomaly which governs the geometry of the hydrothermal system. It is important to have some idea of the thermal distribution in the producing aquifer because thermal boundaries can be misinterpreted as hydrologic boundaries due to the temperature dependence of fluid viscosity.

Caprock and Basement Properties. The important properties of the confining strata in a hydrothermal system are permeability, continuity, rock type, and temperature. If the caprock or basement rock is permeable, it will supply fluid to the producing aquifer when it is pumped. Even though physical properties of caprock and basement rock are diffficult to determine, proper analysis of well test data can show leakage in caprock or basement rock. This is discussed in the section on well testing. It should be noted that a "true" caprock may not always exist and the resource may be so shallow that the basement characteristics cannot be identified. Caprock and basement rock can be identified by observing one or more of the following items:

1. A conductive thermal gradient as opposed to a convective thermal gradient
2. Delineation of a clay or shale layer from rock cuttings
3. Lack of evidence of fractures during drilling
4. Identification of low water content or shale layers from geophysical logs.

Knowledge of the location and type of confining rock is important because they are used to estimate the thickness of the producing strata and to determine if the wellbore penetrates only part of the hydrothermal aquifer. In this case, partial penetration of the wellbore into the formation, should be considered in the well test analysis.

Boundary Conditions. There are many types of boundary conditions on a hydrothermal aquifer, all of which will affect the results of a well test and reservoir response to sustained production. The aquifer may be infinite, or effectively infinite. The aquifer may be bounded on one side by a linear boundary such as a fault or rapid facies change. The linear boundary may be impermeable to fluid movement, supply a constant flow of hot or cold water into the aquifer, or remain at a constant head. The aquifer may be completely enclosed by impermeable or constant potential boundaries that are square, rectangular, polygonal, or radial. Different types of analysis apply to each of these systems. If the presence of some type of aquifer boundary such as a fault or fracture zone is suspected, the well test should be designed so that it is long enough to determine the hydrologic properties of the boundary. In order to calculate the radius of investigation, the following formula can be used:

$$r = 2\sqrt{\frac{kt}{\phi\mu c}}$$

where

k = permeability (m^2)

t = time (s)

ϕ = porosity

μ = fluid viscosity (Pa•s)

c = total system compressibility $\left(\frac{1}{Pa}\right)$.

In highly fractured and faulted hydrothermal systems, practical experience indicates that it is often difficult to detect the presence and type of reservoir boundaries. This is because the hydrologic systems are so complex that no single phenomena can be isolated and analyzed.

An estimate of the radius of investigation can be obtained even if the parameters are not all precisely known. For example, in a moderately permeable sandstone, the following calculation can be made:

$k = 100 \text{ md} = 1 \times 10^{-13} \text{ m}^2$

$\phi = 20\% \ (.2)$

$C_t = 1 \times 10^{-9} \ \frac{1}{\text{Pa}}$

$\mu = .3 \text{ cp} = 3 \times 10^{-4} \text{Pa•s}$.

The radius of investigation for a 10-hour test will be:

$$r = 2\sqrt{\frac{(1 \times 10^{-13}) \ 3.6 \times 10^{4}}{.2 \times 3 \times 10^{-4} \times 1 \times 10^{-9}}} = 490 \text{ m} .$$

For a one week test, the radius of investigation will be:

$r = 1003 \text{ m}$.

5. TESTING DURING DRILLING

Data collected throughout the drilling operation provide a basis for selecting the well test design and analysis methods to be used in evaluating aquifer characteristics. Mandatory data to be collected during operations include:

- Lithologic logging
- Drilling engineering records
- Geophysical logging
- Transient temperature profiles.

Lithologic Logging

Lithologic logging is an important tool used during drilling and should not be overlooked. Through proper lithologic logging one can identify rock type, formation, and position in the stratigraphic section. If used properly, analysis of the drill cuttings can characterize porosity and hydrothermal alteration, and assist in finding faults and zones of fluid entry. Because of rapid and abrupt changes which occur in faulted and altered rock, composite samples should be taken over no more than 10-foot intervals. Analysis of cuttings should be performed by a qualified geologist familiar with igneous, metamorphic, hydrothermally altered rocks, fault gouge, microbreccia, slickensiding, and mylonite. Unwashed samples should be collected to avoid the loss of fine-grained cuttings.

Drilling Engineering Records

Under ordinary drilling conditions, a number of measurements are made and recorded to assist the drilling engineer in making effective drilling decisions. These drilling parameters include drill rate, rotary speed, pump speed, pump pressure, weight-on-bit, and mud volume totalizers. When parameters are properly employed, decisions can be made on bit changes, borehole deflection, lost circulation, casing sizes and settings, etc.

These data also assist the reservoir engineer in evaluating the subsurface. Although these data are not conclusive, tests during drilling in the typical sense of testing, can assist the reservoir engineer in determining rock strengths and porosity from penetration rate; in identifying hot aquifers from circulation fluid temperature-in, temperature-out; and in assessing fractures and fault zones where lost circulation has occurred. All such information will be of a qualitative nature, to be evaluated further by testing methods of a quantitative nature. Nevertheless, they do identify specific sections in the wellbore that merit further evaluation.

Geophysical Logging

Borehole geophysical logging techniques measure the physical properties of the rock. Coupled with other drilling data, the logging analysis can help in defining porosity, rock type, wellbore size, bulk density, dip of rock strata, fluid temperature, and, to a limited degree, rock fractures.

Commercial logging companies provide the log tool service and deliver a graphical output to the customer. These data should be analyzed with input from other drilling information to provide an interpretation of the wellbore and rock conditions. Conventional analytical techniques for sedimentary rocks cannot be routinely

applied to all geothermal resources because of the nature of the rocks encountered (i.e., igneous and metamorphic). Current research efforts are providing interpretive measures for these geothermal environments. Although, it is a fairly expensive service, geophysical logging is a routine tool that should be used for every geothermal well.

Transient Temperature Profiles

The downhole temperature should be measured routinely during the drilling process. Temperature profiles can be performed by a commercial logging company or by a hydrogeologist. Temperature profiles are inexpensive and do not require a long period of time. They can be used to determine cold- and hot-water production zones and loss-of-circulation zones. Temperature logs can provide useful data for determining the depth for setting casing.

The Horner plot method is used to plot transient downhole temperature. The Horner plot is a graph of temperature build-up versus log $\frac{t_k + \Delta t}{\Delta t}$ where t_k is circulation time before shut-in and Δt is buildup time. The static temperature obtained using the conventional Horner plot is lower than the true reservoir temperature.[4] For example, let us assume that prior to running a log suite to set a string of casing, the well was circulated for four hours. Following this circulation period, a series of logs were run and the following times and temperatures observed:

Time (hr)	Temperature (°F)	$\frac{t_k + \Delta t}{\Delta t}$	
0200	Circulation completed	—	
1215	255	14.25/10.25	= 1.39
1500	255	17/13	= 1.31
1630	257	18.5/14.5	= 1.28
1930	260	21.5/17.5	= 1.23
2400	262	26/22	= 1.18

A plot of this data is shown in Figure 10. The estimated static temperature is obtained by an extrapolation of the straight line to a time ratio of unity, which is equal to 272°F. It can be assumed this is probably a lower limit temperature to the true static temperature.

Optional testing methods include:

- Drill-stem tests
- Coring
- Geochemical logging
- Swab and lift tests
- Downhole flow meter tests.

Drill Stem Tests

Drill stem tests (DSTs) are normally conducted in a zone of undetermined potential.[3] The drill stem tool is attached to the drill string and lowered into the zone to be tested. A packer is set to isolate the zone. Formation fluids from the isolated zone flow into the drill pipe. A continuous pressure record is obtained during the

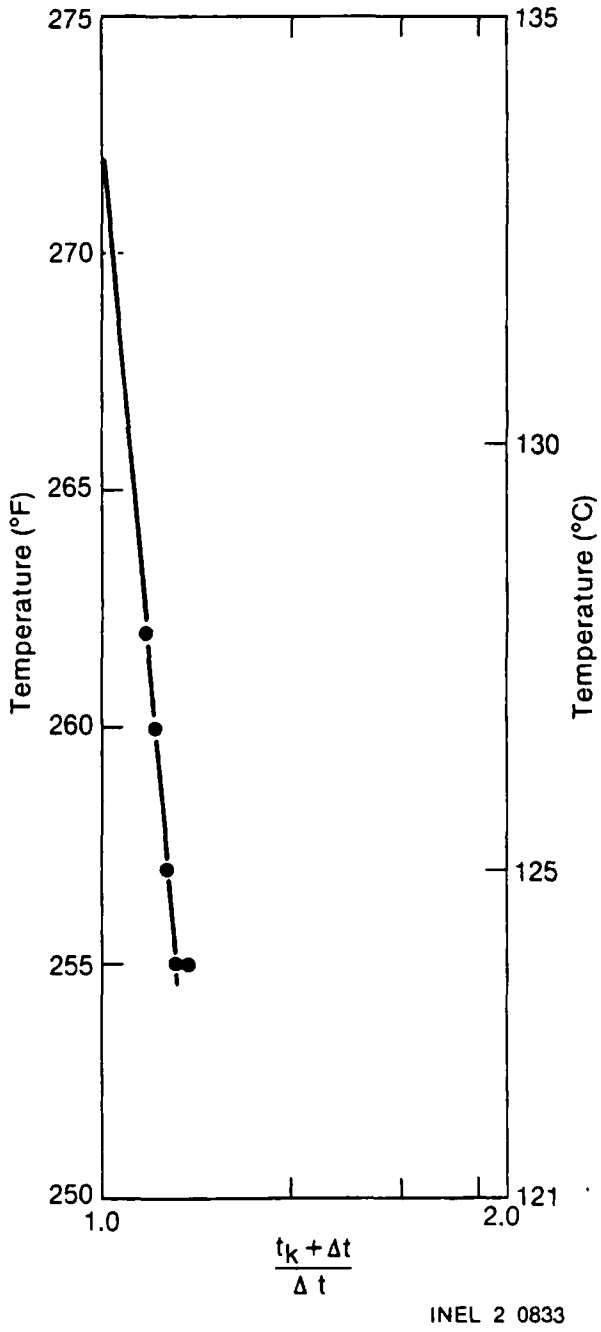

Figure 10. Horner plot of static temperature approximation.

production and shut-in periods. DST data are analyzed to assess preliminary reservoir parameters (i.e., permeability, hydraulic conductivity). At the conclusion of the test, representative fluid samples are collected for further geochemical analysis (refer to Geochemistry Section 8).

An alternative to the drill stem test is a wireline repeat formation test. This test is capable of multiple settings downhole and of retrieving two fluid samples per trip in the hole. The principles governing multiple-level pressure measuring are similar to those of the DST. Wireline testing is attractive because it is fast and less costly than drill stem testing; however, a wireline test is a less accurate method and interpretation of the data is only partially quantitative. Drill stem and wireline formation tests are commonly used in the petroleum industry. Use in geothermal well testing is not expected to be widely applicable due to fractured flow

conditions. In a fractured reservoir environment, the data from these kinds of tests may provide erroneous information due to the short flow durations. However, these types of tests may prove valuable in evaluating the results of well stimulation jobs.

Coring

Core drilling allows for the recovery of whole rock samples from a selected interval. Core samples are used to correlate geophysical logging data with rock properties, to perform laboratory permeability tests, and to delineate stratigraphy and lithology profiles. Core drilling is an important tool used in oil and gas exploratory drilling. The high cost of coring is prohibitive for routine use, but may provide useful information for selected intervals in geothermal wells.

An alternative to core drilling is a technique called sidewall coring. This method uses a wireline for collection of the sample. Sidewall coring is quick and inexpensive; however, core samples are small in size and may have limited laboratory use. Sidewall coring will not provide adequate samples in fracture-dominated geothermal systems due to the limited data regarding fracture density, character, and orientation that can be obtained from the small sample.

Geochemical Logging

Geochemical logging can be useful in identifying geothermal production zones during drilling. Geochemical logging procedures are discussed in detail in Section 8.

Swab and Lift Tests

A swab test is used as a method for withdrawing fluid from a borehole. The procedure employs a swab valve attached to a rig sand line. This method provides limited information on well productivity and allows the collection of representative fluid samples. Swabbing and mechanical surging are commonly used methods for the development of a ground water well but may be of limited use to geothermal resources. This is a hazardous technique because of the possibility of high-pressure vapor and gas blow outs.

Airlifting using compressed air or other gases is another mechanism for withdrawing fluids from the hole. This stimulates the well and yields limited information on well productivity. Approximate flow, water level recovery, and temperature data should be collected. Fluid temperatures are affected by the ambient air temperature. A correction should be made for the estimated cooling effect. The accuracy of reservoir characteristics determined from an airlift test may be questionable, since air or gas may give erroneous flow measurements and water level recovery is diffficult to obtain. Nevertheless, geothermal well drillers may employ swabbing and airlifting methods to both develop wells and perform limited well testing.

Downhole Flow Meter Test

Vertical flow of fluids in the borehole can be measured using a downhole flow meter (spinner device). Downhole flow meter tests may be conducted while producing or injecting fluid into a well. The hole should be relatively clean because the instrumentation can be easily plugged by mud or drilling debris. This method is used to indicate production or high permeability zones. The data can be evaluated to determine the amount of fluid entering the borehole from different zones. Used together with a temperature profile, this test may be useful for casing and screen setting decisions.

6. THEORY OF AQUIFER TESTING

Aquifer testing is the correlation of well production at various rates with temporal pressure or water level changes. Inferences may be drawn from such tests about the size and ability of an aquifer or reservoir to transmit and store fluids. Well testing is the only method that provides in situ information about an aquifer or reservoir on a scale meaningful for long-term exploitation of a resource. Despite the fundamental unity in the principles of well testing, the art of well testing has developed in two parallel fields: hydrogeology, following the lead of C. V. Theis[5] and petroleum engineering, following the early contributions of Hurst.[6] Hydrologists have been concerned with determining aquifer constants (transmissivity and storage coeffficient) and interference-type testing of shallow systems. Petroleum engineers, on the other hand, have been concerned with interpretation of production/injection testing of deep systems. High-temperature geothermal well testing (usually steam flows) has followed the petroleum engineering lead. Low-to-moderate temperature geothermal well testing (usually hot water flows) requires adaptations from both the ground water and petroleum fields.

The equations developed for various aquifer and well conditions provide tools for analyzing data from many different hydrogeologic conditions. However, the simplifying assumptions used to develop the solutions are usually only partially satisfied. In addition, many of the solutions result in curves of similar shape, and thus are not unique to one flow system. Consequently, careful site evaluation and well test design by a qualified petroleum reservoir engineer or hydrogeologist are essential to ensure the success of planned testing.

Essential Elements of Well Tests

Geothermal well testing usually consists of operating the well with a controlled flow rate and measuring three variables (flow rate, water level or pressure, and fluid temperature) as time passes, while other parameters (distance, r, to the observation wells, permeability, reservoir dimensions, and storage capacity) remain constant. The flow rate, water level or pressure, and time are the primary data required for test analysis. Temperature measurements provide data for corrections for temperature effects related to changes in fluid density and viscosity. Fluid chemistry, geology, geophysics, and well construction data are also important parameters in test data interpretation.

Basic Equations

Well testing analysis methods are based on the basic equations of flow through porous media presented below. The symbols used first are those usually found in the water-well literature. The same equations are repeated in the symbols of petroleum engineering references.

Darcy's Law

Darcy[7] observed from experiments on apparatus similar to that illustrated in Figure 11 that the speed of laminar flow of water through sand is proportional to the hydraulic gradient. He expressed this concept by the following equation now known as Darcy's law:

$$q_s = \frac{Q}{A} = -K \frac{\Delta h}{\Delta \ell} = -K \frac{dh}{d\ell}$$

or

$$Q = KiA \qquad (1)$$

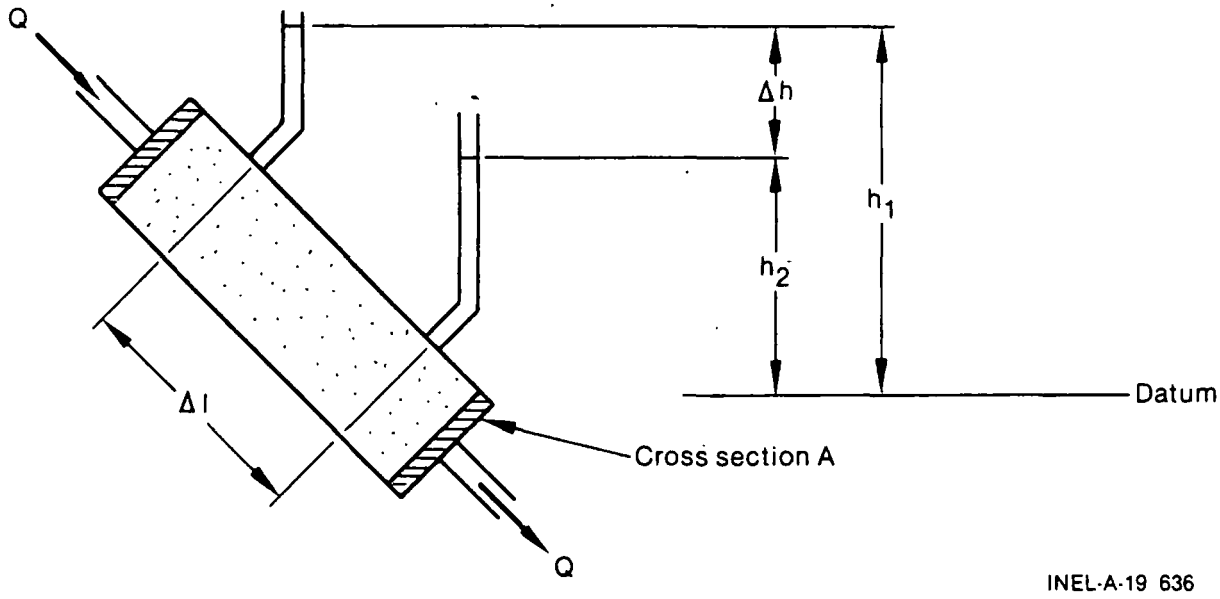

Figure 11. Laminar flow speed measurement apparatus.

where

q_s = specific discharge (L/T)

Q = flow rate (L^3/T)

A = cross-sectional area (L^2)

K = hydraulic conductivity (L/T)

h = hydraulic head (L)

ℓ = length (L)

$i = \frac{dh}{d\ell}$ = hydraulic gradient (L/L)

and the minus sign indicates a loss of potential in the direction of flow. If the porosity, ϕ, is known, an estimate of the velocity of flow is given by

$$v = \frac{q_s}{\phi} = \frac{-K}{\phi} \frac{dh}{d\ell} \quad (2)$$

The hydraulic conductivity, K, depends on both the properties of the porous medium and the properties of the fluid. Often it is advantageous to separate these effects and define a permeability that depends only on the medium such that

$$K = \frac{k\rho g}{\mu} \quad (3)$$

where

k = intrinsic permeability (L^2)

ρ = mass density (M/L^3)

g = acceleration of gravity (L/T^2)

γ = ρg = weight density (F/L^3) or (M/L^2T^2)

μ = dynamic viscosity (FT/L^2)

p = pressure (F/L^2)

$\frac{dp}{d\ell}$ = pressure gradient (F/L)

then

$$q_s = \frac{Q}{A} = \frac{-k\gamma}{\mu}\frac{dh}{d\ell}$$

or

$$Q = \frac{-k\gamma A}{\mu}\frac{dh}{d\ell} \qquad (4)$$

and in petroleum symbols

$$q_s = \frac{Q}{A} = \frac{-k}{\mu}\frac{dp}{d\ell}$$

or

$$Q = \frac{-kA}{\mu}\frac{dp}{d\ell}. \qquad (5)$$

Darcy's equation is valid only for laminar flow conditions. Thus, in fractured rock, coarse unconsolidated material, or formations with large solution openings, the equation may not represent the flow.

Steady-State Well Equation. Based on Darcy's work, Thiem[8] developed an equation for steady (equilibrium) flow toward a well as shown in Figure 12. He assumed that:

- The aquifer is horizontal, homogeneous, and isotropic
- The well is fully penetrating
- The steady flow is maintained long enough so that the zone of influence is no longer expanding with time.

The simple continuity concept of equal flow through adjacent concentric cylinders gives the equation

$$Q = 2\pi Kbr\frac{dh}{dr} \qquad (6)$$

where

b = formation (aquifer) thickness (L)

h = height from the botton of the formation to the piezometric surface at the point indicated by the subscript (L)

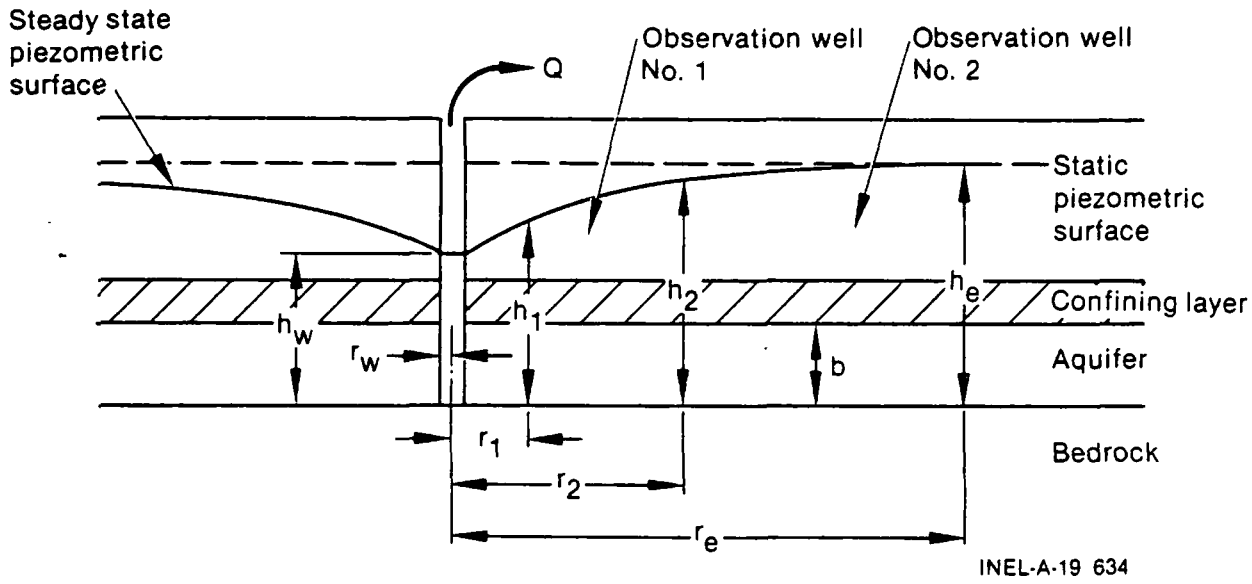

Figure 12. Steady flow toward a well.

r_w = radius of well (L)

r_1, r_2 = radial distance from production well to observation wells 1 and 2 (L)

r_e = radius of influence of the well (L).

When integrated between the two observation wells in an unconfined aquifer

$$Q = \frac{\pi K \left(h_2^2 - h_1^2\right)}{\ell n \, (r_2/r_1)}$$

or

$$K = \frac{Q \ \ell n \ (r_2/r_1)}{\pi \left(h_2^2 - h_1^2\right)} \tag{7}$$

or in a confined aquifer

$$Q = \frac{2\pi K b \, (h_2 - h_1)}{\ell n \, (r_2/r_1)}$$

or

$$K = \frac{Q \, \ell n \, (r_2/r_1)}{2\pi b \, (h_2 - h_1)} \tag{8}$$

When the limits of integration are the production well and the radius of influence, the equation for a confined aquifer is

$$Q = \frac{2\pi Kb\,(h_e - h_w)}{\ell n\,(r_e/r_w)}$$

or

$$K = \frac{Q\ \ell n\,(r_e/r_w)}{2\pi b\,(h_e - h_w)} \qquad (9)$$

In petroleum symbols, Equation (9) is

$$q = \frac{0.00708\ kb\,(p_e - p_w)}{B\mu\ ln\,(r_e/r_w)}$$

$$k = \frac{qB\mu\ \ell n\,(r_e/r_w)}{0.00708\ b\,(p_e - p_w)} \qquad (10)$$

where

q = flow rate (STB/day)

k = intrinsic permeability (md)

p_e = external pressure (psi)

p_w = bottom hole pressure (psi)

B = formation volume factor (RB/STB)

μ = viscosity (cp).

General Differential Equation. Jacob[9] developed a formal, classical development of the general differential equation for transient flow through a saturated, homogeneous, isotropic porous medium. A more complete development is given by Jacob.[10] Freeze and Cherry[11] summarize the development of the equation and the contributions of others to its development. The equation in three dimensions is known as the diffusion equation and is:

$$\frac{\partial^2 h}{\partial x^2} + \frac{\partial^2 h}{\partial y^2} + \frac{\partial^2 h}{\partial z^2} = \frac{S_s}{K}\frac{\partial h}{\partial t} \qquad (11)$$

where

S_s = specific storage (1/L)

and the other symbols are as given earlier.

For flow toward a well in a horizontal aquifer of thickness, b, in cylindrical coordinates, the equation becomes:

$$\frac{\partial^2 h}{\partial r^2} + \frac{1}{r}\frac{\partial h}{\partial r} = \frac{S}{T}\frac{\partial h}{\partial t} \tag{12}$$

where

$T = Kb$ = transmissivity (L^2/T)

and

$S = S_s b$ = storage coeffficient (dimensionless).

Any compatible system of units can be used in the equation without introduction of constants. For example, if h and r are in meters and t is in days, the transmissivity, T, is in meters squared per day.

In petroleum symbols and units the equation is:

$$\frac{\partial^2 p}{\partial r^2} + \frac{1}{r}\frac{\partial p}{\partial r} = \frac{1}{C}\frac{\phi \mu c_t}{k}\frac{\partial p}{\partial t} \tag{13}$$

where

C = constant depending on units used

c_t = system total compressibility (L^2/F).

With μ in Centipoise, c_t in 1/psi, k in millidarcy, p in psi, r in feet, and t in hours, then $C = 0.0002637$.

Solution of the General Equation. Theis[5] found a solution of Equation (12) for a steady flow rate, Q, from the well subject to appropriate boundary and initial conditions. The solution, in terms of drawdown, applies to constant discharge from a fully penetrating well in a confined, homogeneous, isotropic aquifer of infinite areal extent with no vertical leakage

$$s = h_o - h(r,t) = \frac{Q}{4\pi T}\int_u^\infty \frac{e^{-u}}{u}\,du = \frac{Q\,W(u)}{4\pi T} \tag{14}$$

where

$u = \frac{r^2 S}{4Tt}$ = well function argument

s = drawdown at any radius, r, at time, t (L)

h_o = initial height of piezometric surface above the bottom of the formation (L)

h = height of piezometric surface at r and t (L). (15)

The integral term is known as the well function, W(u), and is available in tabular and graphical form in most ground water literature such as Reference 11. It is represented to any desired degree of accuracy by an infinite series as follows

$$W(u) = (-0.5772 - \ell n\, u + u - \frac{u^2}{2\cdot 2!} + \frac{u^3}{3\cdot 3!} - \frac{u^4}{4\cdot 4!} + \ldots .) . \tag{16}$$

Unsteady State Radial Flow in Isotropic Nonleaky Artesian Aquifer with Fully Penetrating Wells and Constant Discharge Conditions

Analysis in Water Well Terms. Consider Equations (14) and (15) and rewrite them as:

$$\ell n\, s = \ell n \left(\frac{Q}{4\pi T}\right) + \ell n\, W(u) \text{ and } \ell n\, t = \ell n \left(\frac{r^2 S}{4T}\right) + \ell n \frac{1}{u} \quad .$$

This suggests a graphical curve matching technique for analyzing pumping test data. If Q is held constant during the test, then $Q/4\pi T$ and $r^2S/4T$ are constants and the relationship between $\ell n\, s$ and $\ell n\, W(u)$ is similar to the relationship between $\ell n\, t$ and $\ell n\, 1/u$. When each pair of variables are plotted on the same scale of two different sheets of log-log paper, the resulting curves are similar and are merely displaced horizontally and/or vertically from each other depending on the values of the two constants.

The method proceeds as follows and is illustrated in Figure 13:

1. A reverse type curve, 1/u (abscissa) versus W(u) (ordinate) is plotted on log-log paper.

2. The pumping test data, t (abscissa) versus s (ordinate) are plotted on another sheet of the same paper.

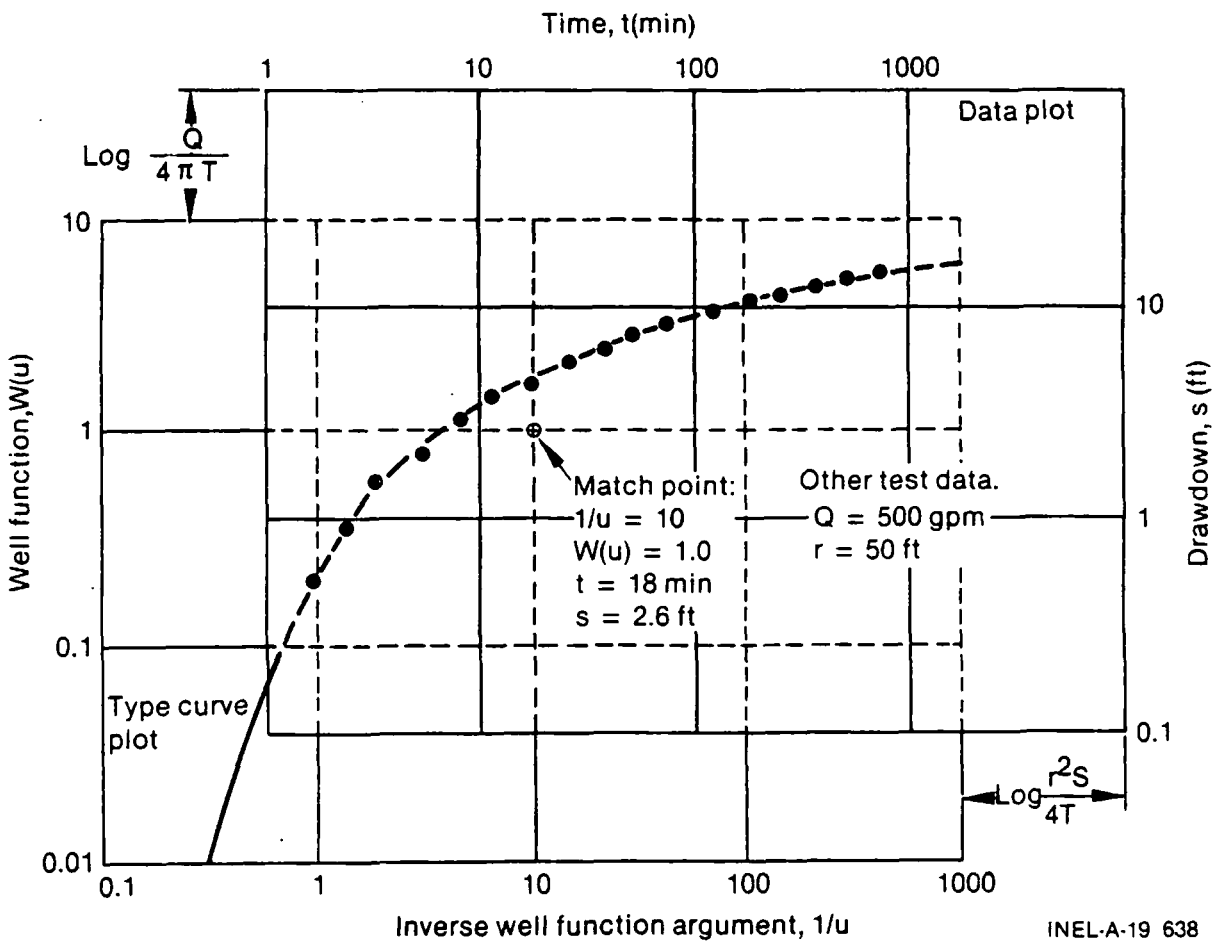

Figure 13. Superimposed curves for aquifer constants.

3. The two plots are superimposed on a light table. The two curves are translated vertically and horizontally, keeping the axes parallel at all times, until the best match of the test data with the type curve is obtained.

4. Then a convenient match point near the type curve is selected and the values of the four variables, t, s, 1/u, W(u) are recorded.

5. Using Equations (14) and (15), the unknown values of the formation coeffficients are calculated from:

$$T = \frac{Q\,W(u)}{4\pi s} \quad \text{and} \quad S = \frac{4tT}{r^2(1/u)} .$$

An alternative is to plot the type curve u versus W(u) and the field data s versus (r^2/t) both on log-log paper. The curves are superimposed, match point coordinates are recorded and the aquifer constants calculated as before.

Analysis in Petroleum Engineering Terms. The petroleum engineering approach has been to plot families of dimensionless curves and to fit the well test data to these. Dimensionless time, radius and pressure are defined as:

$$t_D = \frac{0.0002637\,kt}{\phi\mu c_t r_w^2} , \text{ and } r_D = \frac{r}{r_w}$$

then

$$p_D = f(t_D, r_D, C_D, \text{geometry}) \tag{18}$$

where

C_D = dimensionless wellbore storage factor.

If only the effects of dimensionless time and radius are considered, then

$$p_D = f(t_D, r_D) = -1/2\ Ei\left(\frac{-r_D^2}{4t_D}\right) \tag{19}$$

where

$$Ei(-x) = -\int_x^{\infty} \frac{e^{-u}}{u}\,du .$$

The solution of Equation (13) is

$$\Delta p = 141.2\ \frac{qB\mu}{kb}\ f(t_D, r_D) \tag{20}$$

where

$\Delta p = p_i - p(t,r)$

p_i = initial reservoir pressure (psi)

$p(t,r)$ = reservoir pressure at r and t (psi)

B = formation volume factor (RB/STB)

q = flow rate (STB/D).

Expansion of Equations (19) and (20), and rearrangement of terms shows it to be identical to the water well Equations (14) and (15).

The petroleum method is to plot test pressure, Δp, (ordinate) versus test time, Δt, on log-log paper and to superimpose the plot on a type curve for the value of r_D. A match point is chosen and values of $(\Delta p)_m$, $(\Delta t)_m$, $(p_D)_m$, and $(t_D)_m$ and noted.

Then

$$k = 141.2 \frac{qB\mu}{b} \frac{(P_D)_m}{(\Delta p)_m}$$

and

$$\phi c_t = \frac{0.0002637k}{\mu r_w^2} \frac{(\Delta t)_m}{(t_D)_m} \quad (21)$$

Thus, the two methods are seen to be the same in principle.

The petroleum engineers have carried the method further to include other important factors. A more general solutaion of Equation (13) to include the wellbore storage, geometry, and "skin" effects is:

$$\Delta p = 141.2 \frac{qB\mu}{kb} [f(t_D, r_D, C_D, \text{geometry}) + s_s] \quad (22)$$

$$C_D = \frac{5.6146\, C}{2\pi\phi c_t b r_w^2} \quad (23)$$

where

C = wellbore storage constant (bbl/psi)

$$C = \frac{\Delta v}{\Delta p} = V_w c$$

and

Δv = change in volume of fluid in wellbore at wellbore conditions (bbℓ)

Δp = change in bottom-hole pressure (psi)

V_w = total wellbore volume (bbℓ)

c = compressibility of the fluid in the wellbore at wellbore conditions (1/psi)

s_s = skin effect, which is a dimensionless pressure drop assumed to occur at the wellbore face (r_D = 1) as a result of wellbore damage or improvement. Positive skin effect is due to damage of the wellbore by the drilling process, plugging by mud, etc. Negative skin effect would be an improvement through development of the well, fracturing, reaming, etc.

A variety of type curves including the effects of wellbore storage, reservoir geometry, and skin effects have been developed and many of these are given in Earlougher.[3] Skilled use of these curves, where appropriate, allows more information to be extracted from the test data than through use of the simple exponential integral type curve alone. The additional data come from the parameters identifying the various type curves and make possible the computation of wellbore storage and skin effect coeffficients, in addition to the permeability and formation storage coeffficients already discussed.

Approximate "Straight-Line" Test Methods

The structure of the infinite series in Equation (16) provides a simple test procedure when the value of u is small. As suggested by Cooper and Jacob,[12] all the terms in the series except the first two can be neglected when $u < 0.01$. Then:

$$s = \frac{Q}{4\pi T}\left(-0.5772 - \ln\frac{r^2S}{4Tt}\right) = \frac{2.3Q}{4\pi T}\log\frac{2.25\,Tt}{r^2S} \quad . \tag{24}$$

For most pumping tests, all parameters except t are constant. Thus s will plot as a straight line with log t. The slope of the straight line is seen to be the drawdown over one log cycle, Δs, or

$$\Delta s = \frac{2.3Q}{4\pi T}$$

and

$$T = \frac{2.3Q}{4\pi\Delta s} \quad . \tag{25}$$

By extrapolating the straight line to the point where $s = 0$, the intercept, t_0, on the time axis can be determined. Then:

$$0 = \frac{2.3Q}{4\pi T}\log\frac{2.25\,Tt_0}{r^2S}$$

or

$$1 = \frac{2.25\,Tt_0}{r^2S}$$

and

$$S = \frac{2.25\,Tt_0}{r^2} \quad . \tag{26}$$

Thus, by plotting s and t on semilog paper, and by noting Δs and t_0, simple calculations give the aquifer constants. If data from more than three observation wells are available at one time, a distance-drawdown plot can be made of s versus log r; Δs and r_0 can be noted. Then:

$$T = \frac{2.3Q}{2\pi\Delta s}$$

and

$$S = \frac{2.25\ Tt}{r_0^2} \quad . \tag{27}$$

Similarly, if drawdowns in several wells are available over a period of time, plot s versus lot (t/r^2). Record the drawdown over one cycle, Δs, and the intercept $(t/r^2)_0$. Then:

$$T = \frac{2.3Q}{4\pi\Delta s}$$

and

$$S = 2.25\ T\ (t/r^2)_0 \quad . \tag{27a}$$

The three straight-line approximate methods are illustrated in Figure 14.

A similar straight-line approximate method is commonly used in petroleum engineering. The flowing bottom hole pressure, pwf, in psi (ordinate) is plotted against log t in hours (abscissa). At early times the wellbore storage makes the plot nonlinear, but this is followed by a straight line portion of the plot. The slope, m, in psi/cycle and the intercept, P/hr (where log t = 0 or t = 1), on the straight line are recorded. Then:

$$k = \frac{-162.6\ qB\mu}{mb}$$

and

$$s_s = 1.1513 \left[\frac{(p_{1hr} - p_i)}{m} - \log\left(\frac{k}{\phi\ uc_t\ r_w^2} \right) + 3.2275 \right].$$

For the observation well the skin effect is zero, then the reservoir porosity-compressibility product may be calculated using the equation:

$$\phi c_t = \frac{k}{r^2\mu}\ \text{antilog}\left(\frac{P_i - P_{1hr}}{m} - 3.2275 \right).$$

Recovery Tests

Analysis in Water-Well Terms. When a pumping test is discontinued after a period of production, data taken during the recovery period can also be used to determine formation constants. Conditions during the recovery period are represented by imagining that production continues from the well while at the same time an injection well at the same location replaces the fluid produced by the well. The net flow rate is zero and the imaginary injection well can be visualized as representing the recharging fluid coming into the cone of depression from the surrounding area. The drawdown at any point and at any time can be computed by adding the effects of the pumping and the injection as shown in Figure 15.

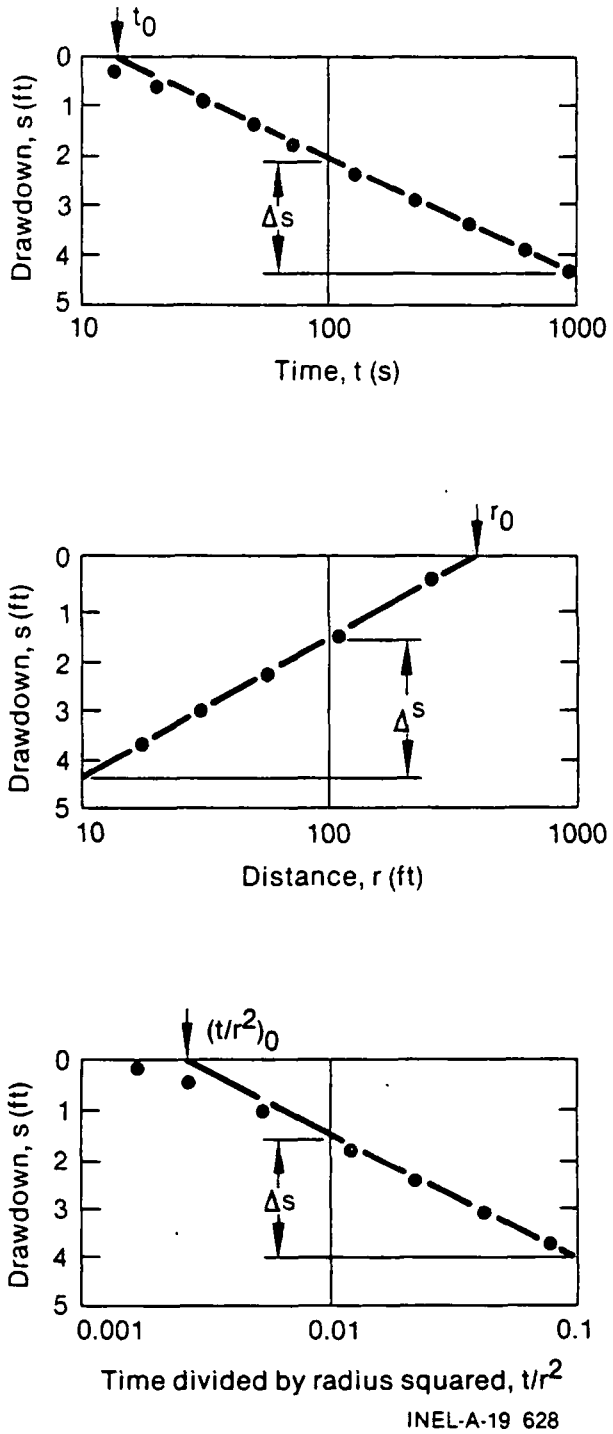

Figure 14. Straight line approximate methods.

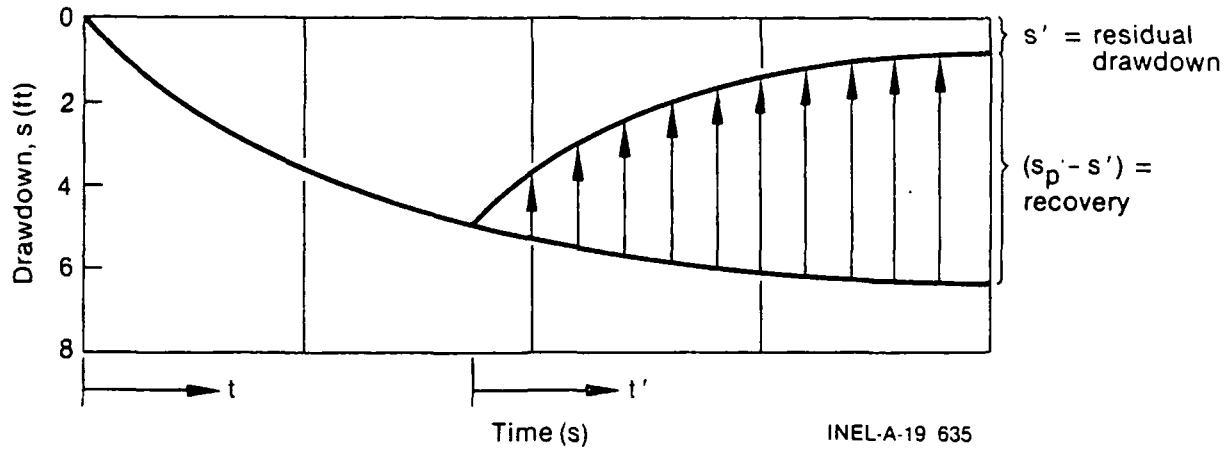

Figure 15. Drawdown computation.

In terms of well functions, the residual or remaining drawdown

$$s' = \frac{Q}{4\pi T} \int_{u}^{\infty} \frac{e^{-u}}{u}\, du - \int_{u'}^{\infty} \frac{e^{-u'}}{u'}\, du' \qquad (28)$$

where

$$u = \frac{r^2 S}{4Tt}$$

$$u' = \frac{r^2 S}{4Tt'}$$

and

t = time since pumping began

t' = time since shutoff.

Once t' becomes large, $u' < 0.01$ and the well function can be represented by the first two terms of the infinite series

$$s' = \frac{2.3Q}{4\pi T} \log \frac{t}{t'} \qquad (29)$$

and a plot of s' versus log t/t' is a straight line. If $\Delta s'$ is the drawdown over log cycle, then

$$T = \frac{2.3Q}{4\pi \Delta s'} \qquad (30)$$

When concurrent data from one or more observation wells are available, the storativity, S, can be estimated from

$$S = \frac{2.25\, T\, t'/r^2}{\log^{-1}[(s_p - s')/\Delta(s_p - s')]} \qquad (31)$$

where

s_p = pumping period drawdown projected to t'

s' = residual drawdown at t'

$\Delta(s_p - s')$ = change in recovery over one log cycle

$(s_p - s')$ = recovery at t'.

Horner Method

Analysis in Petroleum Engineering Terms. The Horner method is used to analyze pressure buildup data. The method has been used extensively in both the geothermal and petroleum industries. The technique is based on superposition of the exponential integral solution. The derivation is as follows:

$\Delta P_{\text{well shut in}} = \Delta P_{\text{due to the well flowing for a time } \Delta t + t \text{ at a rate of } +q}$

$+ \Delta P$ due to a well flowing at a rate of $-q$ for a period of time Δt.

By adding the flow rates at any time the appropriate conditions are modeled:

time $< t$ flow rate $= +q$

time $> t$ flow rate $= +q - q = 0$.

The pressure drop due to a well flowing at $+q$ for a time of $t + \Delta t$ can be expressed:

$$\Delta P_{(t+\Delta t)} = \frac{\mu q}{4\pi kh} \ln\left(\frac{\gamma\phi\mu\, cr_w^2}{4k(t+\Delta t)}\right)$$

and similarly,

$$\Delta P(\Delta t) = \frac{-\mu q}{4\pi kh} \ln\left(\frac{\gamma\phi\mu\, cr_w^2}{4k\Delta t}\right).$$

Adding these together:

$$P_i - P_{\text{well shutin}} = \frac{q\mu}{4\pi kh} \ln\left(\frac{t+\Delta t}{\Delta t}\right).$$

In standard petroleum engineering units

$$P_i - P_{\text{well shutin}} = 162.6\, q \frac{\mu B}{kh} \log \frac{t + \Delta t}{\Delta t}.$$

This equation forms the basis for the Horner method. As can be seen from the equation, when $(t + \Delta t/\Delta t)$ and $P_{\text{well shutin}}$ are plotted on semilog paper, the data should plot as a straight line with the slope $= \frac{162.6\, q\mu\, B}{kh}$.

Therefore:

$$\frac{kh}{\mu} = \frac{162.6\ q\ B}{\text{slope}}$$

The skin value can be calculated as discussed in the previous section:

$$S = 1.151\left[\frac{P_{1\ hour} - P_{flowing}}{\text{slope}} - \log\frac{k}{\phi\ \mu\ c\ r_w^2} + 3.23\right] .$$

In order to estimate the skin value an independent estimate of ϕch must be available. In the petroleum industry, this is usually obtained by testing cores in the laboratory. For geothermal reservoirs this is best estimated from the analysis of interference test data.

Analysis of Unsteady State Radial Flow in Isotropic Nonleaky Artesian Aquifer with Fully Penetrating Wells and Constant Drawdown Conditions

Analysis in Water-Well Terms — Curve Matching Techniques. For a flowing artesian well, it may be simpler to test the well with a constant drawdown and a varying flow rate than with the methods, already discussed, that require a constant discharge and variable drawdown. Under geothermal conditions, the well would need to be preheated by flowing at a low rate before the test so that thermal effects on pressure at the well will be largely eliminated. Jacob and Lohman[13] found the solution to the general equation for these conditions as follows:

$$Q = 2\pi T s_w\ G(\alpha)$$

where

$$\alpha = \frac{Tt}{Sr_w^2}$$

and

$$G(\alpha) = \frac{4\alpha}{\pi}\int_0^\infty xe^{-\alpha x^2}\left[\frac{\pi}{2} + \tan^{-1}\left(\frac{Y_0(x)}{J_0(x)}\right)\right] dx \qquad (32)$$

where

$J_0(x)$ = zero order Bessel function of the first kind

$Y_0(x)$ = zero order Bessel function of the second kind.

The function $G(\alpha)$ is available in Jacob and Lohman[13] or Walton.[14]

A curve matching technique is used for the well test. Values of Q/s_w (ordinate) are plotted against t/r_w^2 (abscissa) on log paper (or plot Q versus t). This well test plot is superimposed over the type curve $G(\alpha)$ (ordinate) versus α (abscissa). A match point is chosen and the aquifer constants determined from

$$T = \frac{Q}{2\pi s_w G(\alpha)}$$

and

$$S = \frac{Tt}{\alpha r_w^2} \quad . \tag{33}$$

Analysis in Water-Well Terms — Straight Line Approximations. Jacob and Lohman[13] observed that the function $G(\alpha)$ can be approximated closely by $2/W(u)$ for all except very small values of t. The approximation of W(u) by the first two terms of the infinite series in Equation (16) has already been noted. Thus, it can be expected that (s_w/Q) versus log (t/r_w^2) will plot as a straight line since by substitution in Equation (32),

$$Q = \frac{4\pi T s_w}{2.3 \log \left(\frac{2.25\ Tt}{r_w^2 S}\right)}$$

or

$$\frac{s_w}{Q} = \frac{2.3 \log}{4\pi T} \left(\frac{2.25\ Tt}{r_w^2 S}\right) \quad . \tag{34}$$

The test data are plotted as (s_w/Q) (ordinate) against log (t/r_w^2) (abscissa), where Q is the average discharge during a timed interval in the test (L^3/T). A straight line is fitted to the data and the slope (the change in $\Delta(s_w/Q)$ over log cycle) and the intercept (the value of t/r_w^2 at $s_w/Q = 0$) are noted. Then

$$T = \frac{2.3}{4\pi\Delta(s_w/Q)}$$

and

$$S = 2.25\ T \left(t/r_w^2\right)_0 \tag{35}$$

$$S = \frac{2.25\ Tt/r_w^2}{\log^{-1}\left[\frac{(s_w/Q)}{\Delta(s_w/Q)}\right]} \quad . \tag{36}$$

If the intercept is diffficult to obtain because of the distant extrapolation required, the S may be determined from Equation 36

where

s_w/Q = value taken near the middle of the straight line plot

and

$\Delta(s_w/Q)$ = change in the value over one log cycle.

Analysis in Petroleum Engineering Terms. The constant-pressure flow testing has been described by Earlougher[3] in petroleum terminology. For the curve matching technique, the test data are plotted as flow rate (q) in STB/D (ordinate) against time (t) in hours (abscissa) on log-log paper. The data are superimposed over the type curve, q_D (t_D), on the same type of log-log paper as given by Earlougher.[3] Once the best superposition has been found, the coordinates of a match point are recorded. Then:

$$k = \frac{141.2\ B\mu}{(p_i - p_{wf})^b} \left(\frac{q_m}{(q_D)_m}\right)$$

and

$$(\phi\ c_t b) = 0.0002637 \frac{kb}{\mu r_w^2} \left[\frac{t_m}{(t_D)_m}\right]. \quad (37)$$

A zero skin factor is assumed in the type curve, and P_{wf} = flowing bottom hole pressure (psi).

A straight-line method has also been developed which is within 2% when $t_D \geq 5000$. A skin factor is included in the formulation. In the method l/q is plotted versus log t and a straight line is fitted to the data. The straight line slope, m_q, and the intercept at t = 1 hour, $(l/q)_{1\ hr}$ are recorded. Then:

$$k = \frac{162.6\ B\mu}{m_q (p_i - p_{wf})^b}$$

and

$$S_s = 1.1513 \left[\frac{(l/q)_{1\ hr}}{m_q} - \log\left(\frac{k}{\phi\mu c_t r_w^2}\right) + 3.2275\right]. \quad (38)$$

Well Losses

The total drawdown, s, during a test of a production well is made up of some or all of the following parts:

s_f = formation loss due to the laminar flow through the aquifer towards the well

s_w = well loss due to turbulent or near turbulent flow through the developed zone and/or the gravel pack and the well screen

s_p = additional formation loss due to the effects of partial penetration of the well into the aquifer

s_d = additional drawdown in cases of dewatering a portion of the aquifer

s_b = drawdown due to barrier boundaries of the aquifer

s_r = buildup due to recharge boundaries of the aquifer

s_T = apparent drawdown or buildup due to temperature effects.

Stated as an equation

$$s = s_f + s_w + s_p + s_d + s_b + s_r \pm s_T. \quad (39)$$

Step Drawdown Tests for Well Losses

In many wells where there are no effects due to partial penetration or dewatering, the test may not go on long enough to be affected by boundaries and temperature effects may be negligible due to preheating. Thus, only the first two terms of the equation remain.

In laminar flow the drawdown is related linearly to the flow rate, Q, while in turbulent flow it is related to some power of Q near 2 as suggested by Cooper and Jacob:[12]

$$s = s_f + s_w = C_f Q + C_w Q^n \quad . \tag{40}$$

Rorabaugh[15] developed a graphical procedure whereby C_f, C_w, and n are evaluated from a step drawdown test. The procedure is to pump the well at a selected Q until s changes little with time; then Q is immediately increased and s is measured after the same time interval as used for the first step; and the process is repeated for four or five values. No recovery of the well is allowed between different pumping rates. Equation (40) can be rewritten as:

$$\frac{s}{Q} - C_f = C_w Q^{n-1}$$

or

$$\log \left(\frac{s}{Q} - C_f \right) = \log C_w + (n - 1) \log Q \quad . \tag{41}$$

Thus $(s/Q - C_f)$ versus Q on log-log paper will plot as a straight line with a slope of $(n - 1)$ and an intercept C_w where $(s/Q - C_f) = 1$. Such a plot cannot be constructed, however, since C_f is not known. The procedure is to assume different values of C_f and plot a series of lines until a value of C_f is formed that makes the plot a straight line, as illustrated in Figure 16 which is taken from Bouwer.[16]

In the example, $C_f = 0.004$ gives a straight line whose slope is $n - 1 = 1.3$ and thus $n = 2.3$. In actual tests n may be as high as 3.5 but is usually near 2. The value of C_w can be determined by extrapolating the straight line to where $(s/Q - C_f) = 1$ or, alternatively, known values of C_f, n, s, and Q can be substituted into Equation (41).

Once the constants in Equation (41) are known, estimates can be made of the drawdown, s, for different (increased) values of flow rate, Q.

In petroleum parlance, the step drawdown test is called the "flow after flow" test.

Pulse Tests

If the well is allowed to recover for a time between increasing flow rate steps, the procedure is known as a pulse test. In petroleum terms, this test is called the "modified isochronal flow test." A "pulse test" in petroleum engineering is a multiple well test in which flow rate pulses of constant rate with equal shut-in periods in between are produced and the resulting pressure changes are recorded in a nearby observation well.[3]

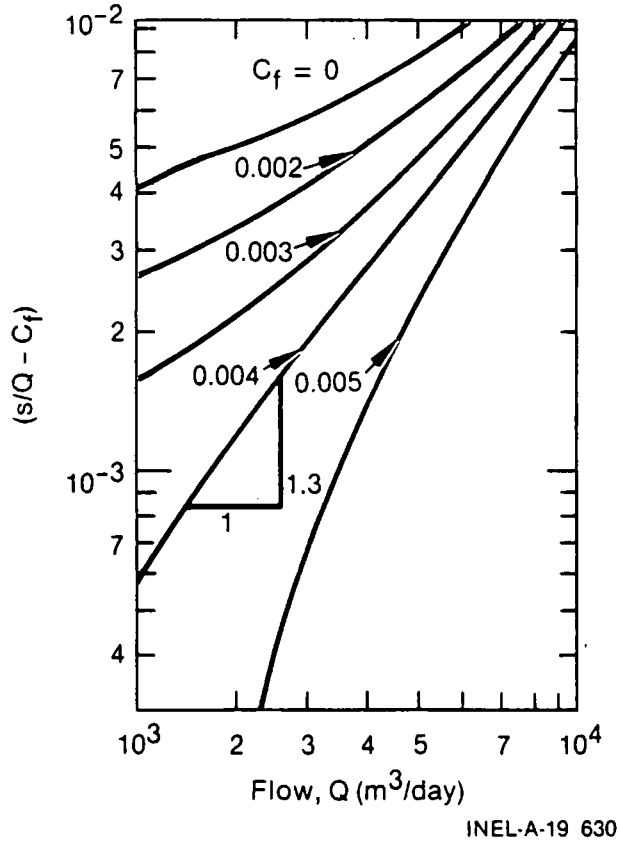

Figure 16. A plot to determine C_f.

Superposition of Solutions Applied to Multiple Wells and Multiple Rates

The drawdown at any point in a confined aquifer with more than one well is the sum of the drawdowns that would occur from each well individually. This is so because Equation (12) is linear (that is, there are no cross terms of the form $(\partial h/\partial r)(\partial h/\partial t)$. Thus, in terms of well functions, one can write for a system of n wells, each with different flow rates:

$$s = \frac{1}{4\pi T} \sum_{i=1}^{n} Q_i W\left(\frac{r_i^2 S}{4Tt_i}\right)$$

$$i = 1, 2, 3, \ldots n \qquad (42)$$

where

s = drawdown at a selected location

r_i = distance from the selected location to the i^{th} well

and

t_i = time since pumping began at the well whose flow rate is Q_i.

A negative flow rate can be used to represent injection of fluid at a well. The equation also defines the interference of wells with each other.

This principle can also be applied to multiple flow rates at one well as given by Bear[17] and illustrated in Figure 17. For these conditions

$$s = \frac{1}{4\pi T} \sum_{j=1}^{m} (Q_j - Q_{j-1})\, W\left[\frac{r^2 S}{4T(t - t_{j-1})}\right] \qquad j = 1, 2, 3, \ldots, m \qquad (43)$$

where

$Q_0 = 0$ at $t \leq 0$

s = drawdown at a given point a distance r from the well at time t

t_j = time since pumping began at rate Q_j

and

index j identifies the pumping period.

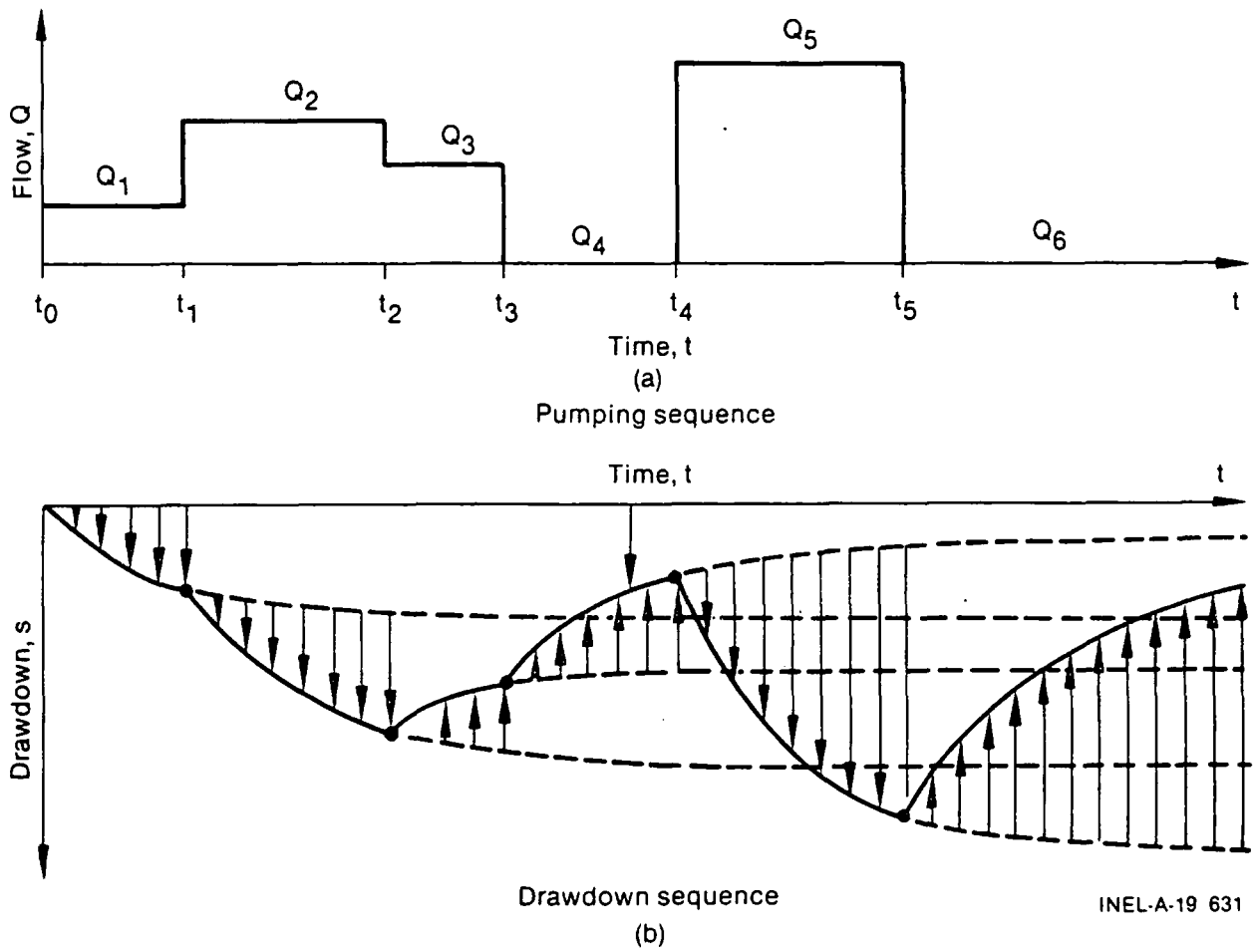

Figure 17. Multiple pumping rates.

The Effect of Fluid Density on Water Level and Wellhead Pressure Measurements

If it is not possible to obtain downhole pressure transient data, the free water level in a well (or the wellhead pressure) must be used for all pressure transient measurements. When the static level or wellhead pressure is used for pressure transient calculations, it is important to understand the effects of changes in density of the fluid filling the wellbore. The density of the fluid in the wellbore is dependent on the temperature and salinity of the fluid. Since the salinity will probably remain relatively constant throughout the test, only the change in density due to temperature will be considered. The density of water as a function of temperature is plotted in Figure 1.

If static water level (SWL) is the water level in the wellbore, the reservoir pressure can be calculated as follows:

$$P_{res} = \int_0^{H-SWL} \rho g \, dz + P_{wellhead}$$

where

SWL = static water level (m)

ρ = fluid density (kg/m^3)

g = gravitational constant (m/s^2)

z = depth (z = 0 reservoir)

H = length of the wellbore (m)

P_{res} = reservoir pressure (Pa).

If the density of the fluid along the entire length of the wellbore is known, then the integral can be evaluated and the reservoir pressure determined. Several examples are given below.

Example 1

What will the SWL be if the temperature of the wellbore changes from a 50°C isothermal profile to a 100°C isothermal profile?

$$P_{res} = \int_0^{H-SWL(50°C)} \rho g \, dz = \int_0^{H-SWL(100°C)} \rho g \, dz \; .$$

If ρ is only a function of temperature, and the temperature is constant, then it is trivial to evaluate the integral

$$P_{res} = \rho(50°C)g\,(H - SWL_{50°C}) = \rho(100°C)g\,(H - SWL_{100°C}) \; .$$

To convert P_{res} from psi to Pa, multiply by 6895 Pa/psi.

The difference in static water level can be calculated for several well depths (h).

P_{res} (psia)	H (m)	$SWL_{50°C}$ (m)	$SWL_{100°C}$ (m)
120	100	13.82	10.73
600	500	69.14	53.65
1200	1000	138.3	107.3
2400	2000	276.6	214.6

Example 2

What will the approximate SWL be in a well with a linear temperature gradient (with 50°C at the SWL and 150°C at the reservoir) compared with a hot wellbore at 150°?

$$P_{res} = \int_0^{H - SWL} \rho g \, dz$$

$$\rho(T) \approx 980 - 0.75 \, (T - 50°C)$$

$$T(z) \approx 150 - 100\frac{z}{H}$$

so: $$\rho(z) \approx 980 - 75 \quad 1 - \frac{z}{H}$$

$$P_{res} = \int_0^{H - SWL} \left[980 - 75 \left(1 - \frac{z}{H}\right) \, gdz\right]$$

P_{res} (psia)	H (m)	$SWL_{Linear\ Gradient}$ (m)	$SWL_{150°C}$ (m)
120	100	9.75	6.7
600	500	50.3	33.4
1200	1000	100.6	66.8
2400	2000	201.2	133.7

As can be seen from the two examples presented above, the temperature of the fluid has a large effect on the SWL. When the temperature changes as a function of depth in the wellbore. it is diffficult to separate this phenomena from true pressure changes in the reservoir. This phenomena is particularly important to understand in the interpretation of pressure build-up data because the wellbore quickly starts to cool when the well is shut-in. The effects of the density changes in the wellbore fluid on the measured pressure response can be eliminated in two ways: by using downhole pressure instrumentation, or by using a wellbore code to calculate the temperature of the fluid in the wellbore.

As can be seen from the two examples, the density changes of the fluid will have the most pronounced effect on deep wellbores. For a wellbore length of less than than 100 m, these changes may not be significant. However, for a deep well (500 to 2000 m). even small temperature changes will dramatically affect the SWL or wellhead pressure.

7. TEST PLANNING AND METHODOLOGY

Preliminary Test Preparation and Design

Before planning a test the developer and his hydrogeologic/reservoir engineering consultant should review the local, state, and federal regulations for fluid production and disposal. These regulations are available through individual state geothermal resource teams, the state water resource or oil and gas department, the U.S. Geological Survey, or the Environmental Protection Agency. Special permits to produce and dispose geothermal fluids may be required. Therefore, any limitations or restrictions must be considered before designing the test. Certain restrictions (i.e., discharge of geothermal fluids to lined ponds only) will raise the cost of testing and limit test duration and/or test discharge rates which could result in inappropriate or inadequate data. The restrictions will probably depend on the water quality, the temperature of the thermal fluid, and/or the compatibility with local water resources. Some eastern states, such as New Jersey, require all geothermal fluid, including any testing fluid, to be discharged into an injection well. Thus, testing of any production or test well will require the additional cost of an injection well.

After the developer or consultant has evaluated and made allowances for testing regulations they need to determine the end use of the well, i.e., whether it will be a production or a test/monitor well. They then need to determine whether the reservoir is intergranular permeable, fracture-controlled, or has dual porosity. If the type of reservoir is unknown, it should be treated as a fracture flow case.

The first design decision to be made is whether to test produce the well using a pump or by natural artesian flow. This decision will be clear cut if artesian conditions are not present. An air lift or nitrogen lift test is not recommended for geothermal resources because flow rate control is at best diffficult. For a production well test, the anticipated end-use method of producing the geothermal fluid should be used. However, for test wells, the less expensive method of artesian flow testing is recommended. If a moderate temperature resource is being tested, the additional factor of flashing (boiling) at the wellhead or orifice must be considered. At temperatures greater than approximately 100°F, suffficient pressure must be maintained across a fluid discharge measuring device to prevent flashing, otherwise expensive two-phase measurement equipment will be necessary. If the well is to be artesian flow tested, an additional possibility must be considered, i.e., can the well be completely shut-in? If the well cannot be shut-in, the capability of flow rate regulation is necessary. In all cases the consultant should determine the testing parameters and be sure that all relevant data can be obtained and pertinent variables controlled.

Test Pump. If a pump is required, the consultant must select the pump, determine the pump elevation setting, and evaluate the pump limitations. A combustion-engine-driven pump is recommended for testing as this will allow for a wide range of discharge rates. An additional reason for using a test pump rather than the intended production pump is the potential damage to the pump by the corrosive nature of early postdevelopment discharge fluids. The estimated pump setting depth should be developed from the data collected during the drilling and development process. It is better to set the pump deep rather than run a test at too low a flow rate or for too short a time, or to be forced to pull the pump out and set it deeper.

There are technical problems with off-the-shelf, water well type pumps even at low temperatures. The main problems are in lubrication of moving parts, cooling of motors and moving parts, and differential expansion. Information from several brand name pump distributors suggests that warranties on submersible pump motors will not be honored at temperatures above 37.8°C. Vertical turbine pumps can be used for extended periods of time in geothermal fluids if care is taken to account for differential thermal expansion and lubrication. In addition, the corrosive nature of the geothermal fluid must be considered in selecting pump materials.

Test Instrumentation. After anticipated drawdown, temperature, and flow rates have been estimated, instrumentation suitable to measure those parameters should be chosen. The recommended accuracy and resolution of the data limits or restricts the instruments that should be used. Most off-the-shelf, low-cost

pressure gauges are not suffficiently accurate or do not have suffficient resolution. On the other hand, it may be uneconomical for the developer of a low-temperature resource to use the sophisticated and expensive surface or downhole instrumentation used in moderate- to high-temperature geothermal developments. One alternative for low-temperature resources is that the producing well be supplied with a continuous bubbler tube in conjunction with moderate-cost surface gauges that at least meet the resolution requirements. This will reduce early-time thermal effects and result in accurate relative change of pressure or water level. It is also recommended that fluid discharge temperature data be obtained continuously or at least on the same measurement schedule as pressure and discharge rate. It is also necessary to consider the thermal effects on the instrument operation. Economical instrumentation, due to the required accuracy and resolution and due to thermal problems, is currently a problem in low-temperature geothermal development. Additional cost-effective instrumentation needs to be developed.

Appendix C lists a variety of instruments employed in low-to-moderate temperature systems. A brief discussion of accuracy and resolution is also available for reference.

Test Parameters. General statements on test parameters are diffficult to make, because the test design depends on the information needed. The general recommendations provided here should be applied with extreme caution, and used only after the end use of the well and the purpose of the test has been determined.

The test parameters that need to be addressed at this time are a function of the test type, discharge rate, the duration of the test, and fluid temperature. The "test type" refers to the standard procedural well tests in the petroleum and ground water industries, i.e., step test, pulse test, constant-discharge variable-head test, etc. The recommended method and limits will depend not only on the decision path taken during test preparation and test design, but also on the dollar investment of the project. It is assumed for this document that the testing of moderate-temperature resources will be expensive.

Recommendations of test parameters for low-temperature cases are presented in Table 2.

Recommendations of test parameters for moderate-temperature cases are presented in Table 3. There is less divergence from standard ground water or petroleum testing procedures, because downhole instrumentation is subjected to minimal temperature change and eliminates the problems created by borehole density effects. Moderate-temperature cases that do not use downhole pressure/temperature instrumentation should follow the recommendations for low-temperature resources.

Testing Methods. Testing methods may be categorized according to the following:

1. Discharge or injection rate:
    a. Constant rate flow tests (variable drawdown)
    b. Multiple flow rate tests
    c. Variable flow rate tests (constant drawdown).
2. Flow duration:
    a. Step tests
    b. Pulse tests
    c. Short-term tests
    d. Long-term tests

Table 2. Recommended test parameters for low-temperature hydrothermal systems

Test Parameters	Test Well								Production Well							
	Intergranular Permeable				Fractured or Unknown				Intergranular Permeable				Fractured or Unknown			
		Flow				Flow				Flow				Flow		
	Pump	Shut-In	Rate Control	No Rate Control	Pump	Shut-In	Rate Control	No Rate Control	Pump	Shut-In	Rate Control	No Rate Control	Pump	Shut-In	Rate Control	No Rate Control
Type Test(s)	B	B	B	B	B	B	B	B	B	B	B	B	B	B	B	B
	CD	CD	CD	—	CD	CD	CD	—	Pr	Pr	Pr	—	Pr	Pr	Pr	—
	R	R	R	—	R	R	R	—	CD	CD	CD	—	CD	CD	CD	—
	—	—	—	—	—	—	—	—	R	R	R	—	R	R	R	—
	—	—	—	CH	—	—	—	CH	—	—	—	CH	—	—	—	CH
Flow Rate	RD	RD	RD	—	MP	MP	MP	—	RD	RD	RD	—	E	E	E	—
Minimum duration (days)	2-4	2-4	2-4	30+	3-7	3-7	3-7	30+	5-10	5-10	5-10	30+	10-20	10-20	10-20	30+

Legend
- B = Borehole temperature log (if possible)
- CD = Constant-discharge variable-head
- PR = Pulse and recovery
- R = Recovery
- E = End-use requirements
- MP = Maximum practical
- RD = Reduced discharge rate
- CH = Constant head, variable discharge

Data Requirements[a]

	Resolution	Accuracy
Pressure	1.0 psi	±1% F.S.
Temperature	±0.5°C	±1°C
Flow	±0.5% F.S.	±1% F.S.

a. See Reference 18.

Table 3. Recommended test parameters for moderate-temperature hydrothermal resources

	Test Well		Production Well	
Test Parameter	Intergranular Permeable	Fracture Control	Intergranular Permeable	Fracture Control
Type test(s)	StD R —	StD R —	S or P StD R	S or P StD R
Flow rate	RD	MP	RD	E
Minimum duration (days)	0.3-3	3-7	3-7	10-20

Assumes use of downhole instrumentation in production zone

Legend
- S or P = Step test or pulse test
- StD = Acceptable standard for testing groundwater or petroleum resources
- R = Recovery
- RD = Reduced discharge rate
- MP = Maximum practical discharge rate
- E = End use requirements discharge rate

Data Requirements (Lamers, 1974)		
	Resolution	Accuracy
Pressure	1.0 psi	±1% F.S.
Temperature	±0.5°C	±1°C
Flow	±0.5% F.S.	±1% F.S.

3. Test geometry:
   a. Single well test
   b. Multiple-well production
4. Well tests with observation wells
5. Injection testing
6. Recovery tests.

Constant Rate Flow Tests — Constant rate flow tests are commonly used in both ground water and petroleum industries and are highly recommended for low-to-moderate temperature geothermal well testing. In the constant rate flow test, the desired pumping rate has to be obtained as fast as possible and maintained throughout the test duration. The flow rate is carefully monitored and adjusted if changes are observed. Pumping rates for a constant rate flow test should be carefully designed to provide enough flexibility for these adjustments. Drawdown and temperature data are collected according to a time schedule designed specifically for each test. An advantage to the constant rate flow test method is that analysis techniques are well developed.

Multiple-Flow Rate Tests — Multiple-flow rate tests are used to estimate well losses, specific capacity, well productivity, skin effects, and reservoir parameters. This type of test is commonly conducted before testing at constant rates to aid in subsequent test planning.

Variable Flow Rate Tests — The hydraulic properties of a reservoir can be determined from a well test in which the discharge rate varies with time and the drawdown remains constant.[19] The change in discharge rate is plotted against the logarithm of time. This type of test is most effective for an artesian flowing well. Thermal changes may cause problems in maintaining a constant head. This type of test is not normally used for testing geothermal wells.

Step Tests — A step test consists of an abrupt increase or decrease in the fluid discharge rate with no recovery allowed between steps. Each pumping rate is continued at a constant flow until the well approaches a steady flow condition, after which the discharge rate is abruptly increased or decreased to the next level. Each step interval may last from 30 minutes to four hours. This procedure is continued for several discharge rates. This type of testing is most useful in geothermal wells in which downhole instrumentation, i.e., downhole pressure bombs and temperature probes are used to collect data. This is because some time is required after each discharge change before the surface temperature becomes stable and temperature effects can be neglected.

Pulse Tests — Pulse tests are conducted at increasing or decreasing discharge rates with recovery allowed between each pulse interval. Data are collected for the pumping and recovery portions of each rate. Each pulse interval may last from one hour to several days. In geothermal well testing, longer pulses are recommended to provide enough time so that early recovery data with thermal effects will not have to be used. Pulse testing is not commonly used in the ground water industry. The petroleum industry uses this type of test to determine reservoir anisotropy.

Short- and Long-Term Tests — Duration of a test in terms of "long or short" is a relative measure; however, these terms are commonly used in practice. A test conducted for less than three days should be considered short-term. A long-term test is commonly conducted for more than three days with no defined maximum time limit. Tests of long duration are recommended more often in geothermal aquifer testing than in ground water or petroleum well testing. This recommendation is based on the following factors: the hydrogeology and geologic structure of a geothermal reservoir is often complex; reservoir volumes are so large that long production periods are needed to produce significant pressure responses; and there is no alternative method to predict resource temperature changes.

Single- and Multiple-Well Tests — Classification of tests by geometry includes single well tests and multiple-well tests. The multiple-well production test is more complex, and more diffficult to evaluate than single-well production tests. A single-well production test may be needed prior to the multiple well test to provide a basis for comparison. The multiple-well production test should provide information about both interference effects between wells and aquifer properties. In general, less precise reservoir data are obtained from multiple-production well tests due to reservoir heterogeneity.

Well Tests with Observation Wells — Generally, there is little difference between test procedures with or without observation wells. Tests with observation wells provide a more complete data base for evaluating aquifers. These data are average values for a large area of the reservoir. Whenever practical, the use of observation wells is recommended.

Injection Testing — Injection testing may be accomplished by injecting fluids from a body of surface water or a production well. The following factors should be considered when choosing the injection interval:

1. Interference and cooling effect on a production zone
2. Environmental impact of the injected fluid on a potable ground water aquifer
3. Cost of the injection well.

Skin Factor and Wellbore Storage — The skin factor is a petroleum term which is represented by a steady-state pressure drop of the well face in addition to the normal transient pressure drop in the reservoir.[3] The skin factor increases or decreases the pressure change of the well, depending on the flow rate of the well. Wellbore storage affects the short-time transient pressure behavior in the test well. The skin factor and wellbore storage both affect the early-time portion of the data. These effects can be accounted for in test analysis.

Well-Loss Constant — The well-loss constant characterizes the losses due to the well screen plus the gravel pack or developed area near the well and can be evaluated from a step test or several pulse tests. A properly developed well has a well-loss constant less than 5 sec^2/ft^5.[20]

Aquifer Permeability, Thickness-Permeability Product and Porosity-Compressibility Thickness Product — Aquifer permeability (k) or the absolute permeability of the rock,[2] is a property of the rock and not of the fluid which flows through it. The unit of permeability used in the petroleum industry is the Darcy unit. A rock of one Darcy permeability will allow a fluid of one centipoise viscosity to move at a velocity of one centimeter per second under a pressure gradient of one atmosphere per centimeter.[2]

The thickness-permeability product (kh) is a term characterizing the fluid transmitting ability of the aquifer. The thickness-permeability product is a petroleum industry term which is somewhat similar to the term transmissivity used in the ground water industry. The difference is that the transmissivity characterizes fluid transmitting aquifer properties for a fluid, and thickness-permeability product is independent of the fluid.

The porosity-compressibility-thickness product ($\phi c_t h$) is a term used in the petroleum industry that is equivalent to the term storativity used in the ground water industry. The unit used for the porosity-compressibility-thickness product is in ft/psi.

Analyzing Test Data.

Evaluating Early-Time Data — Data which are not thermally affected are evaluated according to standard petroleum and ground water techniques.[3,14] However, all of the techniques are not applicable. The methods recommended in Table 4 are general categories of techniques which should be applied. The specific techniques applicable to each category will depend on the quantity and quality of the reservoir test data plus other geologic and hydrologic inferences gathered during the exploration and drilling phases. These specific techniques are described by Walton,[14] Earlougher[3] and others conversant in the ground water and petroleum fields.

Early-time data emphasized in the ground water and petroleum industries are often not as useful in analyzing low-temperature geothermal production wells due to thermal and density changes effecting surface data. These problems can be eliminated by collecting downhole data.

The recovery data may also be affected by time-dependent thermal changes if downhole data is not used. The thermal effect increases with time from the start of recovery. This means that early-time recovery data is important and late-time data becomes hard to analyze.

Analyzing Fracture Flow — Fracture flow analysis has been discussed by numerous authors, i.e., Warren and Root, Papadopulos, Rofail, Gringarten, Streltsova, Dugiud, and Aquilera.[21-28] Most analytical methods assume either a single fracture for production or a block response. The solutions are for the most part not analytical or field oriented, but computer model comparisons. Field analyses of fractured systems have conventionally relied on anisotropic analysis of intergranular permeable systems. The assumption that fracture flow averaged over a large enough area, acts like an intergranular permeable system, is not unreasonable.[29] However, this approach suggests that early-time data may not be useful.

Evaluating Reservoir Parameters — A critical part of well test analysis is evaluation of reservoir parameters. The theoretical background and essential elements of well test analysis were presented in Section 6. This section presents several methods developed by the ground water and petroleum industries that are commonly used in the geothermal industry as well.

Data on injection rate, wellhead temperature, and wellhead or downhole pressure are collected from the injection well. Injection test data are analyzed by the same methods as the previously discussed test data. Because disposal of the geothermal fluid by injection is often necessary, injection testing may be used frequently in geothermal fields. However, care should be taken to prevent damage to the formation due to clay swelling or fluid incompatibility. Injection testing, as a means of determining reservoir parameters, is not recommended in sedimentary formations.

Recovery or Fall-Off Testing — A recovery or fall-off test should follow all production or injection tests. Measurements of pressure or head recovery begin immediately after pumping or injection is stopped. Theoretically, the recovery phase should last as long as the production/injection phase. If surface instrumentation is used for a geothermal well, time-dependent fluid-density effects will limit the usefulness of early-time data. An advantage in analyzing recovery data is that major fluctuations in discharge have minimal effect. It should be stressed that recovery data are as important as production data and often are of better quality. This is one of the most common test methods used by the oil and gas industry.

Reservoir Parameters

The following well and reservoir parameters, determined by analyzing test data, are given in order of increasing complexity:

1. Specific capacity and well effficiency
2. Aquifer transmissivity (T) and storativity (S)
3. Skin factor and wellbore storage
4. Well-loss constant
5. Aquifer permeability (k), or thickness-permeability product (kh) and porosity-compressibility-thickness product (ϕcth).

Definitions of Key Parameters.

Specific Capacity and Well Efficiency — The specific capacity (productivity index) of a well is its yield per unit of drawdown at a specific time and is a practical number characterizing a given well. Generally, high specific capacity indicates high aquifer transmissivity. Correlation between specific capacity and transmissivity can be made;[20] however, it is not recommended for final aquifer evaluations. The higher the specific capacity, the better the well. A good geothermal well may have a productivity index as high as 50 gpm/psi drawdown.

Well effficiency is the ratio of the theoretical drawdown in the formation to the actual drawdown measured in a pumped well including well losses. Specific capacity and well effficiency are well parameters widely used in ground water well-testing methods.

The ratio of the rate of production to the pressure drawdown at midpoint of the producing interval is called the productivity index. The productivity index is a term used in the petroleum industry and is equivalent to the term specific capacity used in the water well industry. The index measures the well's potential to produce.

Aquifer Transmissivity (T) and Storativity (S) — Transmissivity is a term used in the ground water industry to characterize the ability of the aquifer to transmit a fluid. The transmissivity (T) is a number indicating the rate at which fluid flows through a unit width of the aquifer under a unit hydraulic gradient. Although, transmissivity characterizes a property of the aquifer, it is also a property of the transmissivity fluid.

Storativity is the ground water term used to express the storage capacity of an aquifer. The storativity (S) is a number indicating the volume of water released from or taken into storage per unit surface area of the aquifer per unit change in head. Storativity (S) is dimensionless.

Table 4. Recommended test analysis methods for low-temperature hydrothermal development

Type Well	Test Type	Considerations	Recommended Methods: Intergranular Permeability	Recommended Methods: Fracture Controlled
Production	Pulse	Transient density skin effects or well loss wellbore storage boundaries	Graphical[a] (straight line)	Graphical[a] (straight line)
	Drawdown	Transient density	Graphical[a] (type curve or straight line)	Graphical[a] (type curve or straight line)
	Recovery	Same		
		Same	Transient and semisteady state (straight line)	Graphical[a] (straight line)
Observation	Drawdown and recovery	Anisotropy, boundaries	Transient and semisteady state (type curve)	Anisotropic and fracture methods (type curve)

a. Use of Q/s_{10} technique.

Evaluating Graphical Methods of Test Data — Graphical methods are commonly used in the water well and petroleum industries. One such method is the type-curve matching method.

Type Curves — The graphical methods of superposition provide one way of evaluating reservoir parameters. The type-curve matching analysis method may be used for drawdown, buildup, interference, and constant pressure testing. The method should be applied where downhole data are being obtained since early-time thermal effects will impact surface readings. Type curves are obtained by plotting selected values of W(u) versus u on a logarithmic graph paper.[5] For constant flow during a test W(u) is related to u in the same manner as drawdown is related to the r^2/t or $1/t$. Therefore, if the recorded values of drawdown are plotted on a logarithmic scale against r^2/t or $1/t$ on a similar logarithmic scale, the raw data curve should be similar in shape to the type curve. However, the two curves may be displaced both vertically and horizontally.

The type-curve-matching method used in the petroleum industry is similar to that used in the water well industry. Data are typically plotted in terms of logarithm pressure change versus logarithm test time. The type curve is in units of dimensionless pressure versus dimensionless time.

Standard type curves are developed for various aquifer geometries and conditions such as wellbore storage and skin effects. The type curve evaluation technique is widely used in water well industry and to some extent the petroleum industry. Use of type curves for geothermal well testing analysis is limited when using uphole data because of time-dependent thermal effects.

Straight-Line Solutions — The straight-line solution is another graphical method for aquifer test analysis when considering semisteady-state conditions. Typically, time is plotted on the logarithmic scale versus drawdown, which is plotted on a linear scale. The data points should ideally form a straight line.[12] The slope of water level change over one log cycle of time is needed to calculate reservoir parameters.

Recovery data should be analyzed using the ratio of time from start of pumping and time from start of recovery plotted on the logarithmic scales. Reservoir parameters are calculated using the same equation as for a drawdown plot.

If more than one observation well is used for data collection, a distance-drawdown plot may be used for test analysis.[8] Distance is plotted in the logarithmic scale and drawdown on the linear scale.

The straight-line plot is recommended for geothermal well testing. However, it must be remembered that time-dependent thermal effects on the water level data may significantly influence the plot. For example, an increase in water temperature may have an effect similar to a recharge boundary and a decrease in temperature during shut-in may appear similar to a barrier boundary.

Monitoring Observation Wells (Interference Tests)

Any well or spring within a 1 to 5 km radius of the producing well that is potentially connected hydraulically with the geothermal reservoir should be monitored during testing. The geology and construction of any observation wells should be evaluated. It will be necessary to determine the elevation of a measuring point relative to the producing well, and the use schedule of the observation well, if appropriate. Pressure measurement and the instrumentation for the observation wells should follow water well standards and practices.

There should be no diffficulties with thermal conditions at observation wells, unless the well is flowing and cannot be shut-in. If a well or spring is flowing, discharge, temperature and water quality measurements should be obtained.

If there are any wells or springs within a 1 to 5 km radius of the production well which cannot be shut-in for the test duration, it will be necessary to determine if there will be any potential hydraulic interference problems. If there are, discharge should be regulated during and after the test. If this is not possible, then at least a record of production from the observation well should be kept.

Fluid Disposal

The technical aspects of fluid disposal must be considered. This may mean calculating the fill rate of a pond to determine if the test can run for the projected duration at the desired discharge rate. It may mean determining the anticipated thermal or water quality change in a stream at the desired discharge rate. The disposal must consider the waste heat in addition to the water quality.

Because elevated temperatures increase solution kinetics and mineral solubility, geothermal waters tend to be higher in dissolved solids than surrounding ground waters. Thermal waters can also have high concentrations of particular dissolved species that may cause special disposal problems, such as arsenic, mercury, boron, or fluoride. Environmental regulations generally prohibit the disposal of effffluents into surface streams where the effffluent will degrade the quality. Table 5 lists the dissolved species most likely to be present in troublesome quantities in geothermal fluids. Water samples should be collected and analyzed for these species to evaluate the potential for disposal problems. In addition to chemical aspects, thermal pollution from disposing fluids also must be controlled.

Test Procedures

Before beginning the actual reservoir test, it is necessary to meet all the facility requirements. This may mean installing power for a pump, instruments, or lighting. It would also mean obtaining permission to monitor a well on private land or constructing access roads. The pump, production well instrumentation, and the observation well instrumentation should be installed at this time. Any technicians or professionals who will be involved with the test should be trained in the operation of the pump and testing instrumentation. In addition, the field staff should understand the anticipated data responses during the test.

Table 5. Dissolved species found in geothermal waters

Total dissolved solids	Boron
Chloride	Arsenic
Sulfate	Sulfide
pH	Carbon dioxide
Fluoride	Mercury

The reservoir test begins with obtaining background data on all the wells and springs to be monitored (historic water levels, temperature, chemistry data). These data will be used to determine short- and long-term trends in order to correct the test data for these trends. The required duration of background monitoring will vary according to the site. It is recommended that the minimum duration be at least equal to the duration of the intended reservoir test.

The next step is to determine if suffficient field support has been employed for the reservoir test. The required number of people will depend on the disposal method, the number of monitor wells and springs, the distance or travel time between monitor wells and springs, and the type of instrumentation at each monitoring site. It will be desirable to have more assistance during the early-time rapid measurements of the production and recovery portion of any test. If there is insuffficient field assistance, then additional help should be employed and properly trained.

A static or nonproducing borehole temperature log of the production well should be run at or before this time. It may be preferable for technical and economic reasons to run this log before setting a pump. The log should be recorded while entering the well (logging down) to minimize any thermal disturbance (mixing) within the well. Finally, the data will be used for calculating time-dependent changes in fluid density and early-time thermal borehole storage effects in the producing well. A temperature log obtained after drilling was completed may be used, if the time between drilling and testing was less than three to five days. Otherwise, a new temperature log is recommended.

Preheating of the wellbore should be considered before the start of testing if pressure or water-level information during the test is to be obtained in any portion of the well that sees a temperature change. The well or spring should be preheated by producing at 10 to 20% of the intended testing discharge rate. The preheating lessens the time-dependent density changes during the test, and usually does not cause problems with the latter analysis.[30] The preheat procedure should continue until the discharge temperature is constant.

A step rate or pulse test should be run in order to determine the optimal flow rate for a long-term test and the productivity index. A standard water well step test and analysis may be run if the pressure or water level data do not have time-dependent density changes (downhole data). A step test is not recommended if downhole data are not available due to probable thermal changes at the differing discharge rates. The variable thermal conditions and the short duration of most step tests make comparison and analysis impractical. At least two pulse steps are recommended, one at a higher rate and one at a lower rate than the intended end-use production rate. The highest rate should be run first to aid in preheating the borehole. The duration of each pulse and recovery will depend on the time required to reach thermal equilibrium at the wellhead and obtain suffficient analyzable pressure or water level data. This may be on the order of four to eight hours per pulse. If a step test is run, one to four hours may be required, since the wellbore should be stabilized by the inital high rate step test.

The discharge rate for the long-duration test will depend on the well type, reservoir type, drilling data, etc. and the pulse test data. The end-use required rate be used for all fracture-controlled type springs or wells. The end-use rate is recommended due to the low reliability of standard extrapolation techniques in fractured rock reservoirs.[31] A higher than end-use rate is not recommended, as extrapolation of temperature for the lower rate is not reliable. If there is no specified end use requirement, the test should be conducted at the maximum possible rate. A reduced discharge rate (less than the end-use production rate) can be used for intergranular permeable reservoirs.

The recommended test duration for low-to-moderate temperature geothermal resources is somewhat longer than a standard cold-water aquifer or petroleum test to allow for stabilization of early-time thermal effects. Also, the test duration for fracture flow cases should be somewhat longer than intergranular permeable cases due to problems in the analysis and projection of reservoir longevity. In general, the longer the test, the more reliable the data.

After concluding the production phase of a test, it is important to obtain recovery data level/pressure at the production well and at all monitor wells and discharge rates at all springs. The duration of the recovery portion of a test will depend on the type of instruments used and/or the rate of cooling in the production well. In the water well and petroleum fields, one would expect the recovery portion of a test to run approximately the same duration as the production portion. In low-to-moderate temperature geothermal systems, the recovery portion of a test (considering the production well only) will be of shorter duration. This is a result of thermal effects. The recovery data at a production well is especially useful if the discharge rate during the test was somewhat erratic or had several step changes. The evaluation technique assumes a constant discharge rate by averaging the discharge during the production. Recovery data are also useful for a monitor well to confirm that a water level/pressure response was due solely to the test and not part of a short- or long-duration background trend.

8. GEOCHEMISTRY

Geochemical information on geothermal fields both supplements hydrologic information and provides additional data. For instance, chemical logging during drilling can indicate the presence of cold and hot aquifers and aids in the placement of casing. Subsurface temperature can be estimated with chemical geothermometers. Isotopic composition variations in water can be used to determine sources of water, the occurrence of boiling in the reservoir, or the amount of interaction between water and wall-rock. The chemical composition of the water may foretell of problems with corrosion or scaling, or may indicate environmental problems from specific dissolved species. The scope of this section is to provide information available from geochemical studies and to briefly describe the geochemical methods involved.

Chemical geothermometers may be used to estimate aquifer temperatures in wells weeks or months before underground temperatures return to normal after drilling. Flow testing may speed the temperature recovery in the production zone, but interferes with obtaining information about predrilling temperatures elsewhere in the well. Also, extensive flow testing immediately after the termination of drilling is not always possible because of fluid disposal problems or delayed delivery of test equipment. Production and collection of a small amount of fluid at the wellhead or from a downhole water sampler, however, may be all that is necessary to provide a good indication of the aquifer temperature.

Where well design requires interruption of production of a geothermal well to run a temperature log, geochemical temperatures may be monitored. Logging wells is also a relatively slow process, and a temperature survey of a field with several production wells could take many days or weeks. Monitoring temperatures of waters supplying drillholes can be accomplished using the silica content of water where calculated temperatures and downhole measured temperatures are in close agreement. Water samples can be collected without interrupting production. Mahon[32] has shown that the silica concentration in the water entering wells decreases at Wairakei, New Zealand, in response to decreasing temperatures in the aquifer.

By producing a well at various flow rates, the contribution to total discharge from multiple aquifers may vary. If different aquifers have different chemical compositions, and different pressures or transmissivities, the chemical composition of the discharge fluid would change as the production rate was varied. Collection of water samples during a step drawdown tests could be analyzed to detect production from different aquifers.

The following subsections present a brief overview of some of the geochemical methods that can be used in low-to-moderate temperature geothermal reservoirs.

Chemical Logging

The growth of the geothermal industry has created a need for techniques that can be used during drilling operations to determine the depth at which to complete a well, depth for casing placement, and the best method for well development. Techniques developed by the petroleum industry, such as geophysical logging, lithologic logging, and core drilling, can be useful. However, little development has been oriented toward the specific conditions encountered during geothermal exploration and well drilling. Chemical logging[33] is one of the methods developed at the Raft River KGRA for geothermal applications.

Chemical logging can indicate the depth and relative flow of geothermal aquifers penetrated during drilling. The method involves periodic collection of drilling fluid for chemical analysis while drilling is in progress. A chemical log is prepared by plotting the concentrations of the analyzed chemical species, or their ratios, versus drill string depth. The resulting log is a profile of chemical changes taking place in the drill fluid during the drilling operation. Changes in the chemical composition of drilling fluids indicate the entrance of formation waters into the wellbore. Changes in particular species indicate the presence of geothermal water.

Changes in the chemical composition of the drilling fluid result from mixing the fluid with water from aquifers penetrated by the drill string. Figure 18 is a cross-sectional view of a drill string that has penetrated several water-bearing strata. Drilling fluid is pumped through the drill stem and bit and returns to the surface between the drill stem and the wall of the borehole carrying the drill cuttings with it. When a water-bearing stratum is penetrated, it contributes water to the drilling fluid, diluting the fluid and causing variations in its chemical composition. Generally, after the drill string passes through the water-bearing stratum, the drilling mud or sediments in the drill water form a mud cake on the walls of the borehole, sealing off the aquifer. If the flow from the stratum is too great and the stratum is not sealed by the mud cake, the incoming water will produce a permanent change in the background chemical composition of the drilling fluid. The chemical log determines the change in chemical composition of the drilling fluid as each aquifer is penetrated; it also determines the separation of this change from the chemical background contributed by the drilling fluid.

Interpretation of chemical logs is complicated by a number of factors, the most important of which are the effects of drilling mud on the composition of drilling fluids. Drilling muds absorb much of the free hydrogen ion in the solution raising the pH, and consequently the alkalinity. Other cations will also be affected by ion exchange reactions, but anions will be relatively unaffected. Problems arising from this will not seriously interfere with the chemical logging technique because the plot with depth will show changes relative to the background, which are more important than the absolute values of species. Instances when the drilling fluid is changed, for example when drilling mud is replaced by mud-free water, will make comparisons between different parts of the hole diffficult, if not impossible.

Sampling Procedure

The procedure is to collect samples of the drill return fluid at specified depth intervals. Drill fluid is pumped from the mud pit, through the drill string, and returns up the borehole between the borehole walls and the drill stem. Drilling fluid samples are collected where the drill-return fluid enters the mud pit. Samples of 4 to 5 L should be collected to ensure an adequate sample size when drilling mud is being used. Frequently, water is used as a drilling fluid in geothermal wells, in which case only 1-L samples need be collected.

Sampling frequency depends on the detail desired in the chemical log, and the proximity of the hole to the geothermal resource. Also, changes in drilling rate or other changes in drilling indicate that a sample should be collected. Sample frequency may vary from once every 100 m in the upper portion of the hole, to as often as every 5 to 10 m when proximity to the geothermal resource is anticipated. Sampling depths must be corrected for lag time or travel time in the wellbore. This information can usually be supplied by personnel compiling the mud log.

Drilling mud, cuttings, and other residues are separated from the water sample by centrifuging or filtering. In many cases, centrifuging will not settle gelatinous suspensions of drilling mud. Filtering with a coarse filter in a funnel, and a flask with side tube connected to a hand-operated vacuum pump is readily adapted to field filtration of samples.

Chemical species that will provide the most information when drilling in an area must be determined by comparing chemical analyses of cold-water aquifers, drilling fluid make-up water, and the geothermal resource. Those constituents that show the greatest differences in concentration among these water sources would be the best species to use in constructing the chemical log. Constituents that might commonly be expected to show large differences between geothermal and other waters are silica, fluoride, magnesium, chloride, specific conductance, and alkalinity. Also useful are ratios of constituents. Ratios may produce an even more sensitive log if the two species in the ratio show opposite behavior in the background water and in geothermal water.

By compiling the chemical log in the field, during drilling, the chemical log will have its greatest utility in locating geothermal zones as they are penetrated. During development at Raft River, the most useful log was

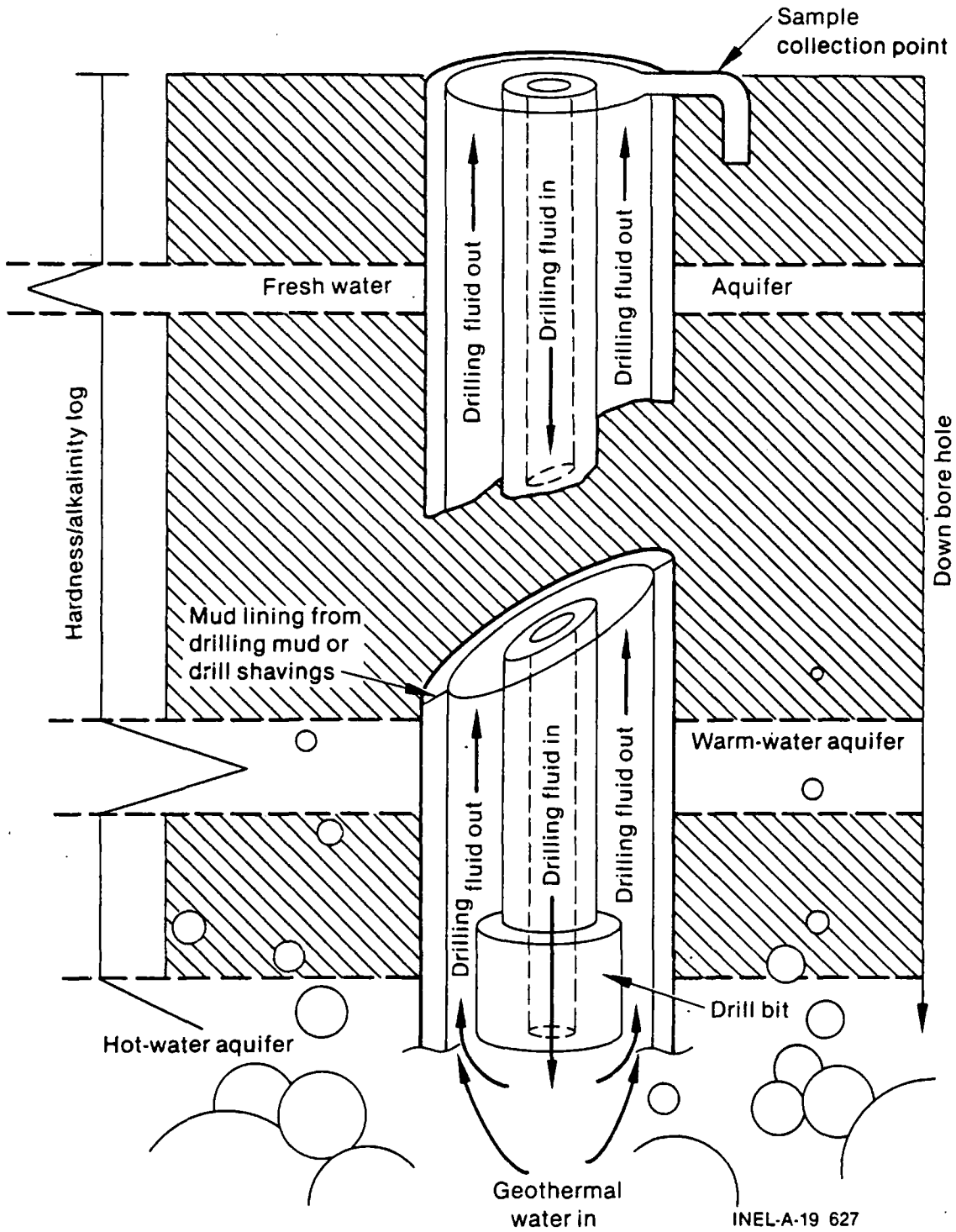

Figure 18. Changes in drilling fluid composition by fluid from a geothermal aquifer.

found to be the hardness-alkalinity ratio log. Both hardness and alkalinity can be measured very easily in the field by colorometric titration. Thus, information gained from this chemical log will be immediately available for decision-making during drilling.

Raft River Example. The concept of chemical logging originated during drilling of exploratory well RRGE-3 at the Raft River KGRA, and was developed and refined during drilling of production wells RRGP-4 and RRGP-5 and injection well RRGI-6. At Raft River, shallow drilling used mud as a drilling fluid. Once casing was set, further drilling used geothermal water as the drilling fluid to prevent possible damage to the formation from the mud. Because geothermal water was used as the drilling fluid, only small chemical differences were anticipated between drilling fluid and any geothermal aquifers that were penetrated. Chemical constituents that would best differentiate between geothermal waters and cold waters, at Raft River, are hardness, alkalinity, fluoride, chloride, and total dissolved solids.

Figure 19 shows the chemical log collected during the drilling of well RRGP-5. The log shows sharp changes in the chemical composition of the drill fluid at 488 m. At this depth, the alkalinity and hardness increase and fluoride and silica concentrations decrease. This would be a typical change in chemical composition when fresh water dilutes the drilling water. The relative constancy in chloride ion concentration and conductivity indicate, however, that the fresh-water aquifer had fairly high dissolved solids, probably from intrusion of geothermal water. The production zone of a geothermal aquifer was penetrated at 1280 m. Because the drill fluid was geothermal water similar to that in the aquifer, only small changes were observed in the drill fluid chemical composition. There was a small increase in SiO_2 concentration and a small decrease in conductivity. The decrease in alkalinity was the only large change detected at this depth.

The hardness/alkalinity log is shown in Figure 20. Evaluation of the hardness/alkalinity log reveals a sharp change in the ratio at a depth of 1220 m. This increase in the hardness/alkalinity ratio was observed until the drill string reached a depth of 1280 m, where a flow of hot water with an estimated rate of 68 L/s was observed. Geothermal water from the 1280 m depth washed away the chemical profile of the well for the remainder of drilling. The lower part of this borehole was lost when a concrete plug was set at 1051 m depth to install the well casing. After the well was cased and reentry was made with the drill string, the concrete plug could not be drilled through. Sidetrack drilling was initiated at the top of the plug, but the second leg either did not penetrate the high-flow zone penetrated in the first leg or the fractures were sealed with concrete. The second leg is shown as Leg B in Figure 20. and indicates the penetration of a narrow, hot-water-bearing aquifer, which flowed at about 13 L/s with a maximum temperature of 123°C.

The hardness/alkalinity ratio log (Figure 20) also showed that as the drill approached a geothermal zone, the ratio increased before the zone was reached, with the resulting chemical log displaced uphole relative to the temperature log. The uphole displacement varied between 16 and 120 m for the wells tested, and appears to be a function of the permeability or fracturing of material above the geothermal aquifer. Additional confirmation of the value of chemical logging was demonstrated during the drilling of RRGI-6. Comparison of the hardness/alkalinity ratio to the temperature log for RRGI-6 revealed similarities as shown in Figure 21 . The hardness/alkalinity log is displaced about 60 m uphole relative to the temperature log. This characteristic of the hardness/alkalinity ratio, of anticipating geothermal aquifers, combined with the information on the permeability of stratum already penetrated, furnished by the mud logger, could be used to determine the depth at which to set the well casing.

Figure 22 shows the hardness/alkalinity chemical log collected during the redrilling of well RRGP-4 with the object of converting an injection well into a production well. Sidetrack drilling started at 565 m to a total depth of 1650 m for Leg A. To improve resolution, samples were taken at 15 m intervals with additional samples collected at 8 m intervals where the driller detected structural changes. To make the chemical log more useful as a predictive tool, the hardness/alkalinity chemical log was kept current with the drilling progress. The object was to anticipate any significant temperature changes before the drill string reached a production zone.

An upper geothermal zone was penetrated by the drill between 700 and 870 m, with the hardness/alkalinity ratio increasing sharply through this area. In this upper portion of the hole, drilling mud was being

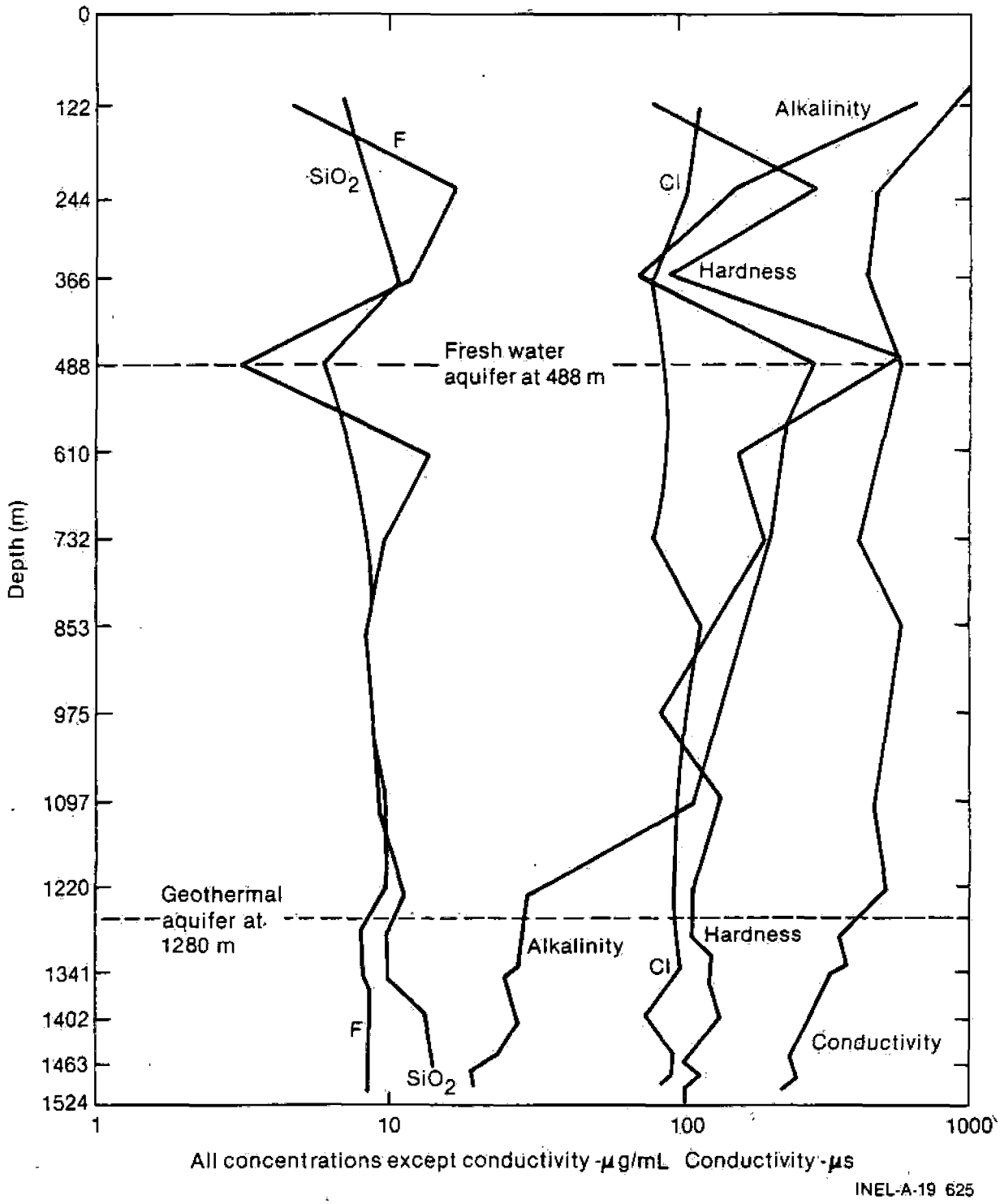

Figure 19. Chemical log of all analyzed chemical species for Well RRGP-5.

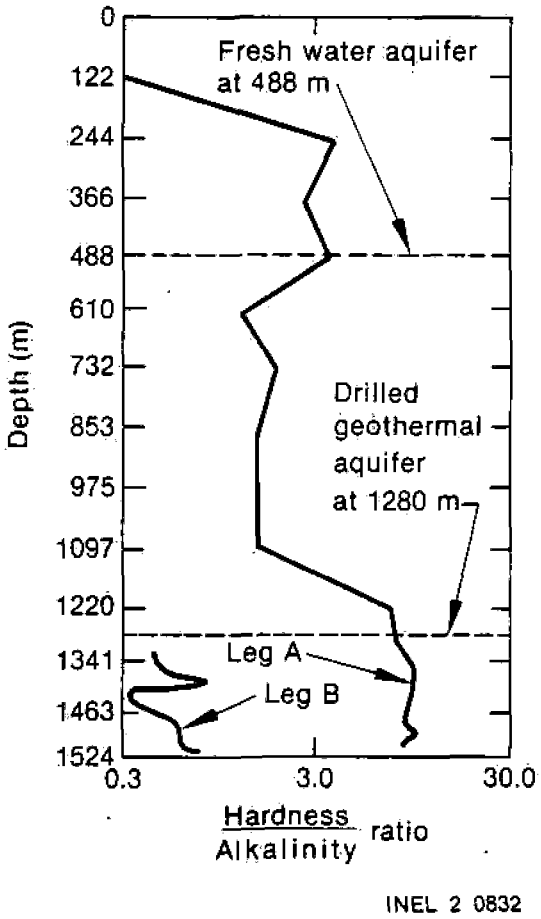

Figure 20. Hardness/alkalinity chemical log for Well RRGP-5.

used in the drilling fluid. Although the background chemical composition of the fluid was much different because of the presence of the drilling mud, the change in the ratio is still quite apparent. After casing the upper hole to a depth of 1070 m, the background hardness/alkalinity ratio changed significantly. Comparison of the chemical and lithologic logs of the upper portion of the wellbore shows that the section having high hardness/alkalinity ratios corresponds to a sandstone layer. Geophysical logging confirmed that this sandstone layer is an aquifer. At a depth of 1520 m, the driller noticed a decrease in drilling rate when the drill bit encountered a hard stratum about 10 m before penetration of a narrow, low-producing, hot-water zone. The hardness/alkalinity ratio began to increase about the time the drill reached the hard stratum, and continued to increase as the zone was penetrated. The ratio decreased after the drill passed through the producing zone. This same sequence was repeated at 1580 m. The combined flow of the two producing zones was about 2.25 L/s, with water temperatures above the boiling point.

Corrosion and Scale-Forming Species in Moderate Temperature Geothermal Brines

Geothermal brines, in general, represent an environment that is very corrosive and contains high concentrations of scale-forming species. This subsection provides general guidelines for proper selection of material and scale control techniques to nontechnical individuals that are involved in geothermal applications. Additional information can be obtained from Casper and Pinchback.[34] These guidelines presented here will apply to any geothermal area but should not be used in lieu of professional advice.

Corrosion. The predominate factors affecting corrosion in moderate temperature brines are temperature, brine chemistry, fluid velocity, and the specific material in contact with the brine. Specific chemical species associated with corrosion are:

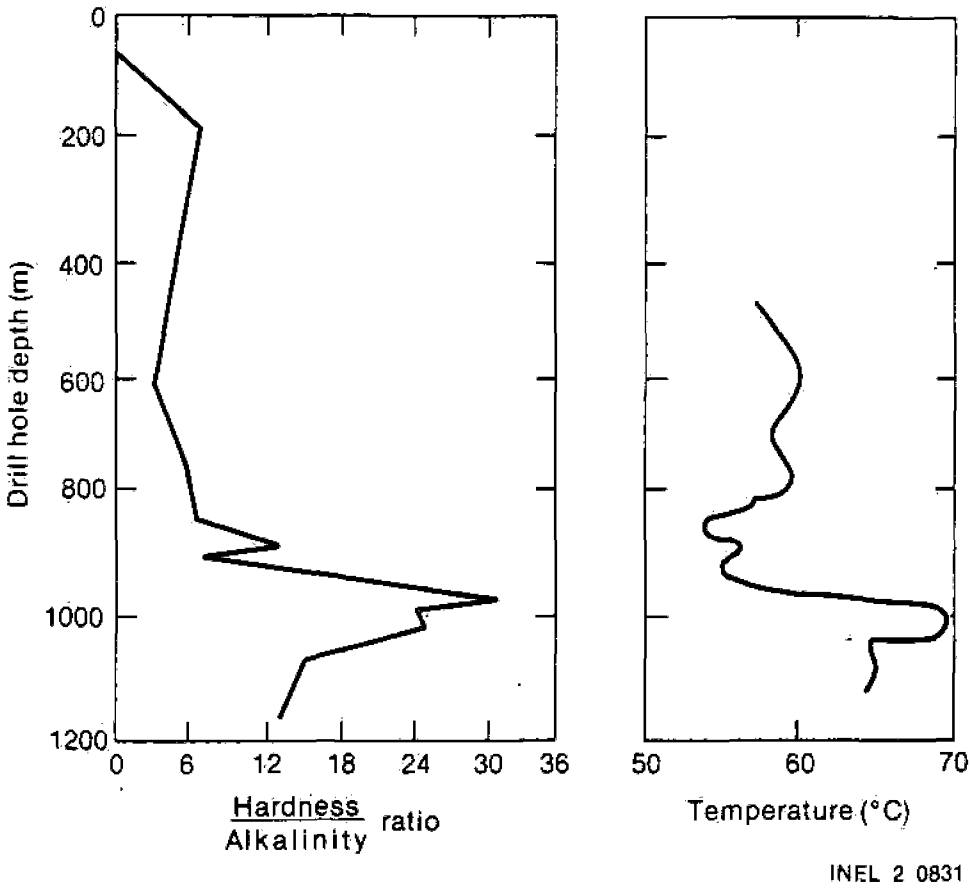

Figure 21. Hardness/alkalinity chemical log and temperature log for Well RRGI-6.

- Oxygen
- Hydrogen ion (pH)
- Chloride ion
- Hydrogen sulfide
- Carbon dioxide
- Ammonia
- Sulfate ion.

The presence of boron and heavy metals such as copper, mercury, tin, etc., will also affect the corrosion rates of different materials. The specific corrosive effect of each of the materials listed above will vary with the material selected. When two or more of the above species are present, the corrosion rate may be significantly greater than the additive corrosion rates associated with the individual species.

Scaling. The predominant factors affecting scale deposition in pipes are brine chemistry, change in temperature, change in pressure, fluid velocity, and the material in contract with the brine. The specific chemical species associated with scale deposition are:

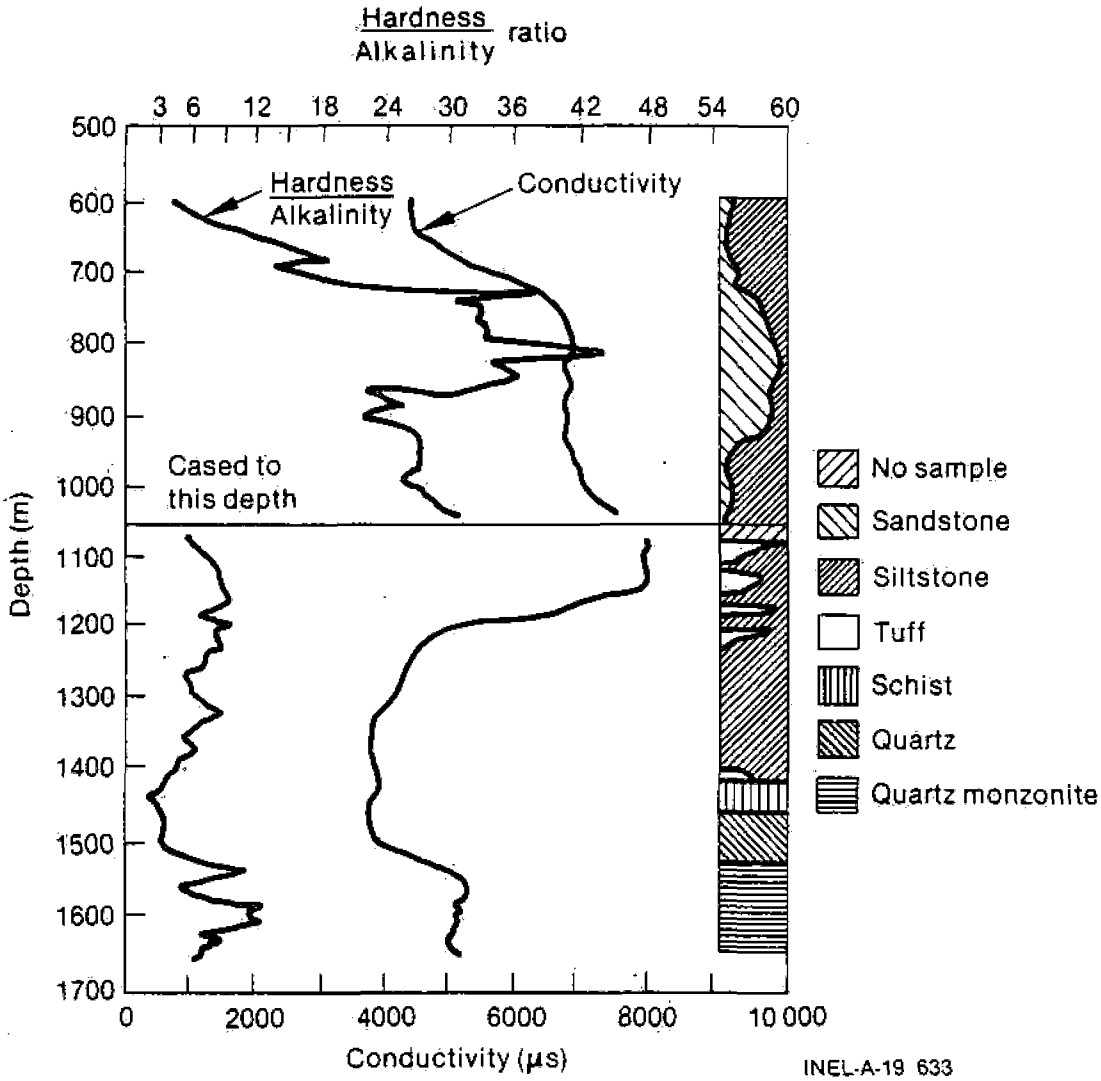

Figure 22. Hardness/alkalinity chemical log for Well RRGP-4A.

- Silica
- Hardness—recorded as calcium hardness and magnesium hardness
- Hydrogen ion (pH)
- Alkalinity—recorded as total and methyl orange alkalinity
- Sulfate ion
- Fluoride ion.

Corrosion products will also affect scale deposition.

Material Selection. Since scale and corrosion are not mutually exclusive, material should be selected with both in mind. There are a large number of materials to select from, ranging from plastics to carbon steels to exotic alloys.

Plastics — Plastic pipes are relatively free from both scaling and corrosion problems. They may be excellent for transporting fluids from wellhead to process areas, but may not be used where transfer of heat is required. Plastic pipes are available in many different forms and price ranges. Restrictions on their use are those of operating temperature and pressure. The higher the temperature, the lower the operating pressure must be.

Carbon Steel — Carbon steels are readily available and are the most inexpensive kind of metal piping. Carbon steel can be used both as transportation and heat transfer material provided adequate corrosion allowance is made. It may not be used if oxygen is present in the brine or if the pH is below six, as this will result in greatly increased corrosion rates and iron scale deposition.

Copper and Copper Alloys — The use of copper and its alloys represents an approximately three-fold increase in material cost and may be required when oxygen is present. Copper has excellent heat transfer properties but should not be used if the pH is below six, as corrosion rates significantly increase with lowering pH, i.e., more acidic water. Copper may not be used if ammonia or sulfide is present.

Stainless Steels — Stainless steels should not be used in brines as the high chloride concentration may result in early failure of components.

Other Materials — There are many other alloys on the market, such as nickel alloys, chrome-moly alloys, titanium, cobalt, etc. The use of these materials should be made after consultation with a corrosion expert, as they are very expensive.

The following are basic guidelines for selecting materials for a geothermal application.

1. Obtain a water sample of the brine and analyze it for the species listed in the Corrosion and Scaling subsections above. The sample should be unflashed and taken by a reputable firm. If the sample is flashed, the noncondensable gasses such as oxygen, carbon dioxide, hydrogen sulfide, and ammonia will flash, resulting in an inaccurate analysis.

2. Select, tentatively, a material based on the analysis. This selection should be confirmed with a professional corrosion engineer.

3. Determine optimum velocity for the given material. As velocity increases, erosion-corrosion increases dramatically while scale deposition decreases; hence the optimum for the given material.

4. Review the system with a water treatment specialist after the material has been selected. The primary considerations are the analysis at the wellhead and the temperature and pressure drops across the system. Temperature is the largest single factor in the solubility of many chemical species. If a large temperature drop occurs across a system, many chemical species may become supersaturated and deposit a scale. Also if pressure drops occur across the system, i.e., across valves, elbows, carbon dioxide may flash, resulting in calcite deposition. This may be eliminated by maintaining pressure across the entire system.

Chemical Geothermometers

Chemical geothermometers are probably the most recognized contribution of geochemistry to the development of geothermal fields. Application to low- and moderate-temperature reservoirs requires careful assessment of the techniques, as many of the assumptions involved in development of geothermometers are based on high-temperature reservoirs. Geothermometers do not stand alone and must be viewed in the geologic and hydrologic context of the field.

There are five basic assumptions that must be met for the geothermometry techniques to be valid. These are:[35]

1. Chemical concentrations are determined by water-rock interactions
2. There is an excess of all reactants
3. Water and rock are in equilibrium at reservoir temperature
4. After leaving the reservoir, water does not reequilibrate with rocks
5. Either no mixing occurs with cooler, shallower water, or the mixing can be quantified.

The geochemist must test the validity of these assumptions after he has considered the hydrology, geology, and mineralogy of the reservoir. Water produced from deep wells offers advantages for sampling in that flow up the wellbore can limit external alterations of water chemistry.

Geothermometers most applicable to low- and moderate-temperature reservoirs are the silica and sodium-potassium-calcium (Na-K-Ca) geothermometers. The Na/K geothermometer is generally limited to reservoirs with temperatures over 180°C. Even with the other two geothermometers, however, results at temperatures below 150°C tend to be less consistent than at higher temperatures. This problem is due in part to kinetic effects and the broad range of mineralogic compositions found in lower-temperature reservoirs.

Silica Geothermometer. The silica geothermometer is based on the theoretical solubility curves of various silica phases, and is applicable to the temperature range from 0 to 250°C.[36,37] The range of temperatures over which the technique works best is from 150 to 225°C. The first consideration in applying this geothermometer is to collect and preserve the sample properly. As waters cool, silica polymerizes and may precipitate. Polymerization can interfere with analysis when colorimetric techniques are used. Water samples, especially if water temperatures are over 140°C, should be diluted as much as 5 to 10 times to prevent polymerization and precipitation.

Silica solubility can be controlled by a number of silica phases, including quartz, chalcedony, and amorphous silica. Equations for calculating estimated reservoir temperatures assuming control of SiO_2 concentrations by these silica phases are:

$$\text{Quartz } t(°C) = \frac{1309}{5.19 - \log C} - 273.15$$

$$\text{Chalcedony } t(°C) = \frac{1032}{4.69 - \log C} - 273.15$$

$$\text{Amorphous silica } t(°C) = \frac{731}{4.52 - \log C} - 273.15$$

Silica concentration, C, is in mg/kg as SiO_2, and the calculated temperature is in degrees centigrade.

In freshly drilled boreholes, in basaltic terrains, or in areas with chert in sediments, quartz may not be the phase controlling silica solubility. If the assumptions of geothermometers are valid for a site, and the proper controlling phase can be determined, the silica geothermometer seems to give the best reservoir temperature estimates.

Na-K-Ca Geothermometer. This geothermometer is based on an ion exchange equilibrium among feldspars controlling the concentrations of sodium, potassium, and calcium.[38] The following equation for calculating temperature is empirical, but feldspar control is assumed.

$$t(°C) = \frac{1647}{\log (Na/k) + \beta [\log (Ca/Na) + 2.06] + 2.47} - 273.15$$

$t < 100°C, \beta = 4/3$

$t \geq 100°C, \beta = 1/3$

Na, K, Ca concentrations in mg/kg.

In geothermal systems where calcium concentrations are significantly affected by gypsum or calcite solubility, calculated temperatures may not be valid. Loss of calcium by mineral precipitation will produce anomalously high temperatures. For waters that are fairly high in magnesium, an empirical correction to the Na-K-Ca geothermometer has been proposed by Fournier and Potter.[39]

Glenwood Springs Example. The situation at Glenwood Springs, Colorado is an example of the equivocality of geothermometers in low-temperature reservoirs. At Glenwood Springs, the temperatures of seven springs, which range in discharge from a fraction of a liter per second to over 125 L/s, are remarkably similar and suggest a fairly uniform reservoir at about 50°C (mean = 48.9°C, standard deviation = 2.7°C).[40] Quartz geothermometer calculations give closely grouped, although much higher temperatures for the springs, averaging 79.7°C with a standard deviation of 2.2°C. Estimates using the Na-K-Ca (Mg corrected) geothermometer give a much broader range of temperatures, averaging 85.1°C with a standard deviation of 15.5°C. An analysis of the mineralogy of the geothermal reservoir, however, indicates that these geothermometers may not be valid in this case.

There is extensive evidence of the presence of evaporites in the limestone reservoir, mainly gypsum or anhydrite. Thermodynamic calculations show the springs to be supersaturated with calcite, which may, therefore, be precipitating in the subsurface. Lowering of calcium concentrations by calcite precipitation would raise the temperature predicted by Na-K-Ca geothermometer. The wide range in geothermometer temperatures would reflect the variability in calcite precipitation.

Sediments in the reservoir contain chert, which is much more soluble than quartz. Calculations of reservoir temperature using the chalcedony geothermometer give temperature estimates that average 48.6°C with a standard deviation of 2.4°C.

The potential questionability of the quartz and Na-K-Ca geothermometers, and evaluation of mineralogy, spring discharge, measured temperatures, and chalcedony geothermometer suggests that the reservoir temperature is closer to 50°C than 80°C. This difference can mean the success or failure of a low-temperature project. Drilling in the Glenwood Springs area during the fall of 1981 found 52°C water in the Leadville Limestone at a depth of 174 m.[41]

Isotopic Composition of Water

Oxygen and hydrogen isotopes in water can be used to indicate sources of geothermal fluids, as evidence for mixing of thermal waters with shallow, cool waters, and to give qualitative estimates of the extent of reaction between water and rock. The most significant contribution of isotopes to the hydrology of geothermal systems was demonstrating that significant quantities of geothermal waters are derived from meteoric sources. Truesdell and Hulston[42] present an in-depth analysis of isotope methods in geothermal systems, from which this section is excerpted.

Stable Isotopes. During the evaporation of sea water, lighter isotopes of water (oxygen-16, hydrogen) can escape into the vapor phase more readily than the heavier oxygen-18 and deuterium. As this water vapor forms precipitation, the heavier isotopes condense first, resulting in progressively lighter precipitation during movement toward the poles, inland over land masses, and to higher elevations. The average annual precipitation at any location will have a fairly constant isotopic composition reflecting its elevation, latitude, and distance from the ocean.

Oxygen and hydrogen isotopic compositions of precipitation are related by the equation:

$$18\,\delta D = 8\,\delta\,^{18}0 + 10$$

where δ is the difference in parts per thousand ($^{0}/_{00}$) between a water sample and a standard water known as "standard mean ocean water" (SMOW). Ground waters in an area frequently display the same relation between oxygen and hydrogen isotopes as precipitation. Surface and ground waters that have undergone evaporation fall to the right of the meteoric water line (Figure 22) along lines with slopes of about five. The deuterium isotopic composition can be used as a label reflecting the recharge area and history of a water sample.

The isotopic composition of many high-temperature geothermal waters is related to that of local meteoric water, but indicates a change in oxygen isotopic composition (Figure 23) from exchange between reservoir rocks and hot waters. Because few rock-forming minerals contain very much hydrogen, a concurrent change in hydrogen does not occur. The magnitude of the oxygen isotope shift depends on the original isotopic compositions of water and rock, mineralogy and texture of rocks, temperature, water/rock ratio, and time of contact. Systems with maximum temperatures below 150°C, moderate water/rock ratios, and igneous rocks with original $\delta^{18}0$ values near $+5^{0}/_{00}$ may show little or no isotopic shift. Most low- and moderate-temperature reservoirs would, therefore, be expected to show little or no isotope shift.

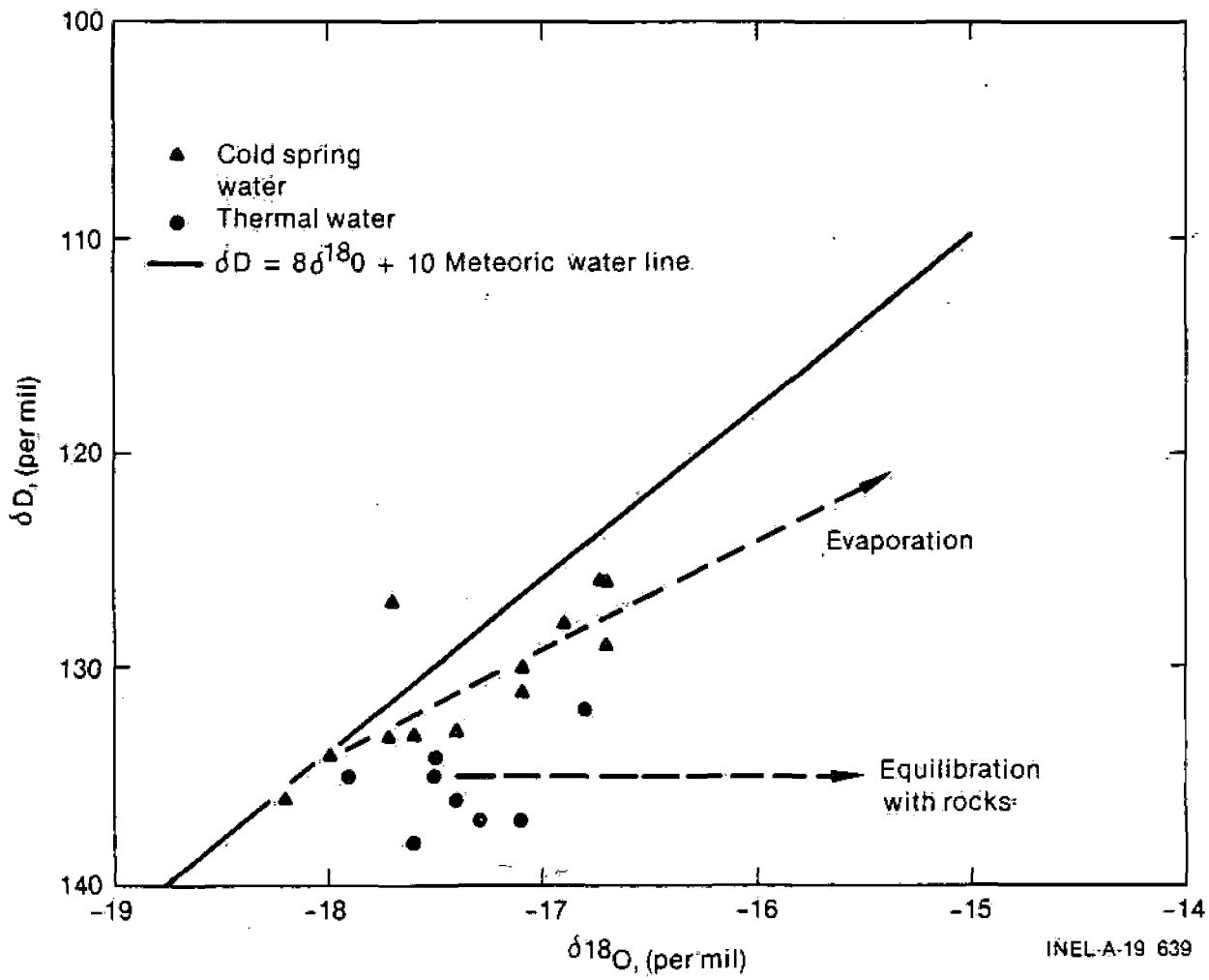

Figure 23. Oxygen-18 and deuterium compositions of hot and cold ground waters from the Raft River KGRA.

Mixing with shallow, cooler ground waters commonly occurs in the upper portions of geothermal systems, which may be feeding thermal springs. Isotopic compositions combined with dissolved salt contents may be used to demonstrate this mixing. Correlations between the isotopes of oxygen or hydrogen and dissolved salts would be expected where shallow waters were lower in salt content and isotopically different than thermal waters.

Tritium. Tritium is a radioactive isotope of hydrogen with a half life of 12.3 years, and is produced naturally by cosmic rays. Atmospheric testing of nuclear weapons between 1954 and 1965 produced a 100-fold increase in peak tritium levels in the northern hemisphere. The current detection level for tritium allows dating of waters up to 60 years old. Most measurements of deep thermal waters show no significant tritium, indicating that waters are greater than 60 years old. Measurable tritium in thermal wells and springs probably indicates the mixing of deep thermal waters with recent, shallow ground water.

9. RESERVOIR MONITORING

Reservoir analysis is not complete when the end-use production of a thermal well or well field begins. It is necessary to monitor the hydrologic system(s) to confirm initial predictions; to anticipate and plan for any geochemical changes in pressure and temperature of the resource; and to obtain a larger data base for confirming the reservoir conceptual model. Confirmation of the conceptual model can be used to evaluate reservoir capacity, recharge, and the potential for future expansion.

Monitoring of a well or well field includes pressure monitoring, temperature monitoring, and geochemical sampling of production/injection wells, observation wells, and springs. Observation wells may include fully or partially penetrating wells designed to monitor reservoir response and any deep or shallow existing irrigation or domestic wells. Monitoring also includes discharge/recharge rates for all wells and springs, and geochemical sampling and temperature changes in a disposal stream or pond.

It is essential that monitoring be accomplished throughout the life of any development to ensure economical use and predict potential environmental hazards.

Pressure Monitoring

The completion of a geothermal well and the start of production from the reservoir should signal the beginning of a regularly scheduled, permanent program of pressure monitoring of the following:

1. The producing aquifer or reservoir formation
2. The confining strata above the reservoir
3. The unconfined aquifer above the confining layer (springs)
4. The production and injection wells.

The pressure measurements will usually be done with surface instruments, i.e., pressure gauges installed at the well head. If the well is not under pressure, a bubbler tube must be installed so that the depth to the water level in the well can be conveniently determined. In a few wells on some occasions, downhole pressure may be needed.

The Producing Aquifer or Reservoir Formation. The pressure in all available observation wells open to the geothermal reservoir should be recorded each month. A few important observation wells may be read weekly if there is a need to indicate shorter-term fluctuations of pressure.

The Confining Strata Above the Aquifer. Some observation wells may have been completed in the confining layers above the reservoir. The water level in these also should be observed at least monthly to show the pressure conditions in the confining layer and to give indications of interference problems.

The Unconfined Aquifer Above the Confining Layer(s). Some observation wells (and local water wells) may be open to the unconfined aquifer near the surface. The water level in these wells and also any nearby springs gives a measure of the water table elevation and should be recorded at least monthly. These data, along with the pressure measurements described above, can give an indication of the gradient causing vertical leakage through the confining layer(s) as well as evidence of well interference problems.

Production and Injection Wells. These wells are the most important in the field and should be monitored most often. In fact, a continuous watch of pressure in production and injection wells is probably needed for the operational control of reservoir production. A permanent daily record should be kept of the pressure, temperature, production and injection rates.

Temperature Monitoring

Temperature monitoring should include discharge/recharge measurements at the surface and where feasible, downhole measurements. Surface measurements are inexpensive and easy to obtain. It is recommended that surface temperatures be obtained whenever a pressure measurement is obtained at a production/injection well. At nearby observation wells, springs, or discharge rivers or ponds, it may be sufficient to obtain surface discharge temperature (where appropriate) on a weekly schedule. Downhole temperature data are usually more expensive and may be impractical if a pump is in a well. If downhole data can be collected, it is recommended that measurements be taken at a minimum of every ten feet to total well depth at least biannually.

Confirmation of Reservoir Conceptual Model

As data are gathered from reservoir monitoring, it is necessary to assimilate them into initial projections and note any deviations from these projections. This assimilation is critical for verifying the conceptual model of the reservoir system, which logically ties into not only reservoir longevity, capacity and recharge, but also chemical changes, water level changes, and a group of potential environmental impacts.

Verification of the conceptual model would provide an early-warning system to a developer to modify or correct potential problems before they are encountered. In addition, reservoir monitoring allows the system to be expanded based upon a confirmed conceptual model, provides confidence to investors in reservoir development, and enhances further development of this technology.

REFERENCES

1. L. J. P. Muffler et al., "Nature and Distribution of Geothermal Energy," *Geothermal Resources Council Special Report No. 7, Direct Utilization of Geothermal Energy: A Technical Handbook*, 1979.

2. B. C. Craft and M. F. Hawkins, *Applied Petroleum Reservoir Engineering*, Englewood Cliffs, New Jersey: Prentice-Hall, Inc., 1959.

3. R. C. Earlougher, Jr., "Advances in Well Test Analysis," *Society of Petroleum Engineers, AIME, Monograph, 5*, 1977.

4. B. Renx et al., "An Improved Approach to Estimating True Reservoir Temperature from Transient Temperature Data," *50th California Regional Meeting of the Society of Petroleum Engineers of AIME, Los Angeles, California*, April 9-11, 1980, SPE 8888.

5. C. V. Theis, "The Relation Between the Lowering of the Piezometric Surface and the Rate and Duration of Discharge at a Well Using Ground Water Storage," *American Geophysical Union Transactions, 16*, 1935, pp. 519-524.

6. W. Hurst, "Unsteady Flow of Fluids in Oil Reservoirs," *Physics*, January 1934.

7. H. Darcy, *Les Foutaines Publiques de la Ville de Dijon*, Paris: Victor Dalmont, 1856, p. 647.

8. G. Thiem, *Hydrologische Methoden*, Leipzig: J. M. Gebhart, 1906, p. 56.

9. C. E. Jacob, "On the Flow of Water in an Elastic Artesian Aquifer," American Geophysical Union Transactions, 1940, part 2, pp. 574-586.

10. C. E. Jacob, "Flow of Groundwater," in *Engineering Hydraulics*, New York: John Wiley & Sons, 1950, pp. 321-386.

11. R. A. Freeze and J. A. Cherry, *Groundwater*, Englewood Cliffs, New Jersey: Prentice-Hall Inc., 1979.

12. H. H. Cooper and C. E. Jacob, "A Generalized Graphical Method for Evaluating Formation Constants and Summarizing Wellfield History," *American Geophysical Union Transactions, 27*, 4, 1946, pp. 526-534.

13. C. E. Jacob and S. W. Lohman, "Nonsteady Flow to a Well of Constant Drawdown in an Extensive Aquifer," *American Geophysical Union Transactions, 33*, 1952, pp. 559-569.

14. W. C. Walton, *Groundwater Resource Evaluation*, New York: McGraw-Hill, 1970.

15. M. I. Rorabaugh, "Graphical and Theoretical Analysis of Step-Drawdown Test of Artesian Well," *Proceedings of the American Society of Civil Engineers, 79*, 362, 1953.

16. H. Bouwer, *Groundwater Hydrology*, New York: McGraw-Hill, 1978, p. 84.

17. J. Bear, *Hydraulics of Groundwater*, Israel: McGraw-Hill, 1979.

18. M. D. Lamers, *Measurement Requirements and Methods for Geothermal Reservoir System Parameters (An Appraisal)*, LBL-9090, GREMP-6, 1979.

19. M. S. Hantush, "Nonsteady Flow to Flowing Wells in Leaky Aquifers," *Journal of Geophysical Research, 64*, 8, 1959.

20. W. C. Walton, *Selected Analytical Methods for Well and Aquifer Evaluation*, Urbana: Illinois State Water Survey, 1962.

21. D. C. Mangold, C. F. Tsang, M. J. Lippmann, and P. A. Witherspoon, "A Study of Thermal Effects in Well Test Analysis," *54th Annual Fall Technical Conference and Exhibitions, Las Vegas, Nevada, September 23-26, 1979.*

22. J. E. Warren and P. J. Root, "The Behavior of Naturally Fractured Reservoirs," *Society of Petroleum Engineers Journal*, 1963, pp. 245-255.

23. I. S. Papadopulos, "Nonsteady Flow to a Well in an Infinite Anistropic Aquifer," *Proceedings Dubrovnik Symposium on Hydrology of Fractured Rocks*, 1965, p. 21.

24. N. Rofail, "Analysis of Pumping Test in Fractured Rocks," *Proceedings: Dubrovnik Symposium on Hydrology of Fractured Rocks*, 1965, p. 81.

25. A. C. Gringarten, H. J. Ramey, and R. Raghovan, "Applied Pressure Analysis for Fractured Wells," *Journal of Petroleum Technology, 27*, July 1975, pp. 887-892.

26. T. D. Streltsova, "Hydrodynamics of Ground-Water Flow in a Fractured Formation," *Water Resources Research, 12*, 3, 1976, pp. 405-414.

27. J. O. Duguid and P. G. Y. Lee, "Flow in Fractured Porous Media," *Water Resources Research, 13*, 3, 1977.

28. R. Aguilera, *Naturally Fractured Reservoirs*, Tulsa, Oklahoma: Petroleum Publishing Company, 1980.

29. R. W. Parsons, "Permeability of Idealized Fractured Rock," *Proceedings of 1965 Fall Society of Petroleum Engineers Meeting, Denver, Colorado, 6, 1966.*

30. D. Goldman and S. Petty, "Testing and Analysis of Low-Temperature Hydrothermal Reservoirs," *National Conference on Renewable Energies, Honolulu, Hawaii, December 1980.*

31. D. W. Allman, D. Goldman, and W. L. Niemi, "Evaluation of Testing and Reservoir Parameters in Geothermal Wells at Raft River and Boise, Idaho," *Ninth Annual Rocky Mountain Ground-Water Conference, Reno, Nevada, October 1979.*

32. W. A. J. Mahon, "Silica in Hot Water Discharged from Drillholes at Wairakei, New Zealand," *New Zealand Journal of Science, 9*, 1966, pp. 135-144.

33. R. E. McAtee and C. A. Allen, "Chemical Logging, A Geothermal Technique," *Geothermal Resources Council, Trans., 3*, 1979, pp. 423-426.

34. L. Casper and T. Pinchback, eds., *Geothermal Scaling and Corrosion*, Special Technical Publication 717, ASTM, 1981.

35. R. O. Fournier, D. E. White, and A. H. Truesdell, "Geochemical Indicators of Subsurface Temperature, 1. Basic Assumptions," *U.S. Geological Survey Journal of Research, 2*, 1974, pp. 259-262.

36. R. O. Fournier and J. J. Rowe, "Estimation of Underground Temperatures from the Silica Content of Water from Hot Springs and Wet-Steam Wells," *American Journal of Science, 264*, 1966, pp. 685-697.

37. R. O. Fournier, "Chemical Geothermometers and Mixing Models for Geothermal Systems," *Geothermics, 5*, 1977, pp. 41-50.

38. R. O. Fournier and A. H. Truesdell, "An Empirical Na-K-Ca Geothermometer for Natural Waters," *Geochemica Cosmochima Acta*, *37*, 1973, pp. 1259-1275.

39. R. O. Fournier and R. W. Potter, III, "Magnesium Correction to the Na-K-Ca Chemical Geothermometer," *Geochemica Cosmochima Acta*, *43*, 1979, pp. 1543-1550.

40. Denver Research Institute, *Municipal Geothermal Heat Utilization Plan for Glenwood Springs, Colorado*, DOE/ID/12049-3, 1980.

41. R. Pearl, private communication, Colorado Geological Survey, 1982.

42. A. H. Truesdell and J. R. Hulston, "Isotopic Evidence on Environments of Geothermal Systems, in: *Handbook of Environmental Isotope Geochemistry*, Peter Fritz and J. Ch. Fontes, editors, New York: Elsevier Scientific Publishing Co., 1980, pp. 179-226.

SubJ
GTHM
LTMT

GEOTHERMAL PROGRAMS

IDO-10099
Volume II

Idaho Operations Office

Low-to-Moderate Temperature Hydrothermal Reservoir Engineering Handbook

A Joint-Project Report
of Lawrence Berkeley Laboratory and
The Idaho National Engineering Laboratory

IDO-10090
Volume II
Distribution Category: UC-66a,d,g

LOW-TO-MODERATE TEMPERATURE HYDROTHERMAL RESERVOIR ENGINEERING HANDBOOK

Published June 1982

EG&G Idaho, Inc.
Idaho Falls, Idaho 83415

and

Lawrence Berkeley Laboratory
Berkeley, California 94720

Prepared for the
U.S. Department of Energy
Idaho Operations Office
Under DOE Contract No. DE-AC07-76ID01570

CONTENTS

FIGURES

TABLES

APPENDIX A
UNITS AND CONVERSIONS

APPENDIX A

UNITS AND CONVERSIONS[a]

Units

	Metric	English
Pressure	Pa	psia
Temperature	°C	°F
Flow	m^3/s or l/s	gpm
Compressibility	l/Pa	l/psi
Length	m (Meter)	ft
Permeability	m^2	mD
Static water level	m	ft
Viscosity	Pa·sec	cP

a. Abstracted from the Invitational Well Testing Symposium, Berkeley, California, 1977.

TABLE A-1. Permeability

ρ_w = 1 viscosity = 1 centipoise

	cm^2	m^2	ft^2	Darcy	cm/s	ft/s	ft/year	$L/s \cdot m^2$	gpd(U.S.)/ ft^2 (Heinzer)	Ebhlm
cm^2	1	10^{-4}	1.076×10^{-3}	1.014×10^{8}	9.804×10^{4}	3.216×10^{3}	1.015×10^{11}	8.698×10^{5}	1.845×10^{9}	0.9
m^2	10^{4}	1	1.076×10^{1}	1.014×10^{12}	9.804×10^{8}	3.216×10^{7}	1.015×10^{15}	8.697×10^{9}	1.845×10^{13}	0.8
ft^2	9.294×10^{2}	9.294×10^{-2}	1	9.417×10^{10}	9.109×10^{7}	2.988×10^{6}	9.430×10^{13}	8.080×10^{8}	1.714×10^{12}	0.7
Darcy	9.862×10^{-9}	9.862×10^{-13}	1.062×10^{-11}	1	9.66×10^{-4}	3.173×10^{-5}	1.001×10^{3}	8.58×10^{-3}	1.82×10^{1}	0.6
cm/s	1.020×10^{-5}	1.020×10^{-9}	1.097×10^{-8}	1.035×10^{3}	1	3.281×10^{-2}	1.035×10^{6}	9.985×10^{0}	2.118×10^{4}	0.5
ft/s	3.109×10^{-4}	3.109×10^{-8}	3.347×10^{-7}	3.152×10^{4}	3.048×10^{1}	1	3.156×10^{7}	2.704×10^{2}	5.736×10^{5}	0.4
ft/year	9.852×10^{-12}	9.852×10^{-16}	1.060×10^{-14}	9.990×10^{-4}	9.662×10^{-7}	3.169×10^{-8}	1	8.570×10^{-6}	1.818×10^{-2}	0.3
$L/s \cdot m^2$	1.150×10^{-6}	1.150×10^{-10}	1.238×10^{-9}	1.166×10^{2}	1.001×10^{-1}	3.698×10^{-3}	1.167×10^{5}	1	2.121×10^{3}	0.2
gpd(U.S.)/ ft^2 (Heinzer)	5.420×10^{-10}	5.420×10^{-14}	5.834×10^{-13}	5.494×10^{-2}	4.721×10^{-5}	1.743×10^{-6}	5.500×10^{1}	4.714×10^{-4}	1	0.1
Ebhlm	0.9	0.8	0.7	0.6	0.5	0.4	0.3	0.2	0.1	1

TABLE A-2. Compressibility (Lt^2/M)

	m^2/N $(Pa)^{-1}$	m^2/kgf	$in.^2$ lbf $(psi)^{-1}$	$Bars^{-1}$	Atm^{-1}	$(ft\ of\ water)^{-1}$ at 68°F	$(m\ of\ water)^{-1}$ at 68°F
m^2/N $(Pa)^{-1}$	1	9.807	6.897×10^{3}	10^{5}	1.0133×10^{5}	2.984×10^{3}	9.794×10^{3}
m^2/kgf	1.020×10^{-1}	1	7.031×10^{2}	1.0197×10^{4}	1.0332×10^{4}	3.042×10^{7}	9.980×10^{2}
$in.^2/lbf$ $(psi)^{-1}$	1.450×10^{-4}	1.4223×10^{-3}	1	14.504	14.696	0.4327	1.419
$Bars^{-1}$	10^{-5}	9.8068×10^{-5}	6.895×10^{-2}	1	1.01325	2.984×10^{-2}	9.790×10^{-2}
Atm^{-1}	9.8692×10^{-6}	9.6787×10^{-5}	6.805×10^{-2}	0.98692	1	2.945×10^{-2}	9.662×10^{-2}
$(ft\ of\ water)^{-1}$ at 68°F	3.351×10^{-4}	3.287×10^{-3}	2.311	33.512	33.956	1	3.281
$(m\ of\ water)^{-1}$ at 68°F	1.021×10^{-4}	1.002×10^{-3}	0.7044	10.214	10.349	0.3048	1

Table A-3. Temperature °C to °F

°C	°F	°C	°F	°C	°F	°C	°F	°C	°F
0	32	100	212	200	392	300	572	400	752
5	41	105	221	205	401	305	581	405	761
10	50	110	230	210	410	310	590	410	770
15	59	115	239	215	419	315	599	415	779
20	68	120	248	220	428	320	608	420	788
25	77	125	257	225	437	325	617	425	797
30	86	130	266	230	446	330	626	430	806
35	95	135	275	235	455	335	635	435	815
40	104	140	284	240	464	340	644	440	824
45	113	145	293	245	473	345	653	445	833
50	122	150	302	250	482	350	662	450	842
55	131	155	311	255	491	355	671	455	851
60	140	160	320	260	500	360	680	460	860
65	149	165	329	265	509	365	689	465	869
70	158	170	338	270	518	370	698	470	878
75	167	175	347	275	527	375	707	475	887
80	176	180	356	280	536	380	716	480	896
85	185	185	365	285	545	385	725	485	905
90	194	190	374	290	554	390	734	490	914
95	203	195	383	295	563	395	743	495	923

Table A-4. Volume (L^3)

	m^3	L	bbl	gal (U.S.)	gal (Imp.)	ft^3
m^3	1	10^3	6.289	2.642×10^2	2.20×10^2	35.315
L	10^{-3}	1	6.289×10^{-3}	0.2642	0.220	3.5315×10^{-2}
bbl	0.1590	1.590×10^2	1	42.0	34.97	5.6146
gal (U.S.)	3.7854×10^{-3}	3.7854	2.381×10^{-2}	1	0.8327	0.13368
gal (Imp.)	4.546×10^{-3}	4.546	2.860×10^{-2}	1.2009	1	0.16054
ft^3	2.832×10^{-2}	28.32	0.178	7.481	6.229	1

TABLE A-5. Flow rate
(L^3/t or M/t)

	m^3/s	L/min	bbl/day	gal/min (U.S.)	gal/min (Imp.)	ft^3/s	klb/h ($\rho_w = 1.0$)	klb/h ($\rho_w = 0.9$)
m^3/s	1	6×10^4	5.434×10^5	1.585×10^4	1.320×10^4	35.315	7.94×10^3	7.15×10^3
L/min	1.667×10^{-5}	1	9.058	0.2642	0.220	5.885×10^{-4}	1.32×10^{-1}	1.19×10^{-1}
bbl/day 6.498×10^5		1.840×10^{-6} 1.46×10^{-2}	1.31×10^{-2}	1.10×10^{-1}	1	2.917×10^{-2}	2.428×10^{-2}	
gal/min (U.S.)	6.31×10^{-5}	3.785	34.28	1	0.8327	2.2280×10^{-3}	0.50	0.45
gal/min (Imp.)	7.58×10^{-5}	4.546	41.19	1.2009	1	2.676×10^{-3}	0.601	0.541
ft^3/s	2.8317×10^{-2}	1.699×10^3	1.539×10^4	4.488×10^2	3.737×10^2	1	2.25×10^2	2.03×10^2
klb/h $\rho_w = 1.0$	1.26×10^{-4}	7.56	68.5	2.00	1.66	4.45×10^{-3}	1	0.900
klb/h $\rho_w = 0.9$	1.40×10^{-4}	8.42	76.2	2.22	1.85	4.93×10^{-3}	1.11	1

TABLE A-6. Pressure (M/Lt^2)

	N/m^2 (Pa)	kgf/m^2	lbf/in^2 (psi)	Bars	Atm	ft of water (at 68°F)	m of water (at 68°F)
N/m^2 (Pa)	1	1.020×10^{-1}	1.450×10^{-4}	10^{-5}	9.8692×10^{-6}	3.351×10^{-4}	1.021×10^{-4}
kgf/m^2	9.804	1	1.4223×10^{-3}	9.806×10^{-5}	9.6787×10^{-5}	3.287×10^{-3}	1.002×10^{-3}
$lbf/in.^2$ (psi)	6.895×10^{3}	7.031×10^{2}	1	6.895×10^{-2}	6.805×10^{-2}	2.311	0.7042
Bars	10^{5}	1.0197×10^{4}	14.504	1	0.98692	35.512	10.214
Atm	1.0133×10^{5}	1.0332×10^{4}	14.696	1.01325	1	33.956	10.349
ft of water (at 68°F)	2.984×10^{3}	3.042×10^{2}	0.4328	2.984×10^{-2}	2.945×10^{-2}	1	0.3048
m of water (at 68°F)	9.794×10^{3}	9.980×10^{2}	1.419	9.790×10^{-2}	9.662×10^{-2}	3.281	1

TABLE A-7. Viscosity (Dynamic)

Pa•s	$lbf•s/in.^2$	$lbf•s/ft^2$	$kgf•s/m^2$	lbm/ft•s	$dyne•s/cm^2$	cP	lbm/ft•h
Pa•s	6.894 757 E+03	4.788 026 E+01	9.806 650 E+00	1.488 164 E+00	1.0 E-01	1.0 E-03	4.133 789 E-04

TABLE A-8. Viscosity (Kinematic)

m^2/s	ft^2/s	$in.^2/s$	m^2/h	cm^2/s	ft^2/h	cSt
m^2/s	9.290 304 E+04	6.451 6 E+02	2.777 778 E+02	1.0 E+02	2.580 64 E+01	1

TABLE A-9. Diffusivity

m^2/s	ft^2/s	cm^2/s	ft^2/h
m^2/s	9.290 304 E+04	1.0 E+02	2.580 64 E+01

TABLE A-10. Thermal Conductivity

W/m·K	cal/s·cm^2·°C/cm	Btu/h·ft^2·°F/ft	kcal/h·m^2·°C/m	Btu/h·ft^2·°F/in.	cal/h·cm^2·°C/cm
W/m·K	4.184 E+02	1.730 735 E+00	1.162 222 E+00	1.442 279 E-01	1.162 222 E-01

TABLE A-11. Density (Liquids)

kg/m	lbm/gal (U.K.)	lbm/gal (Imp.)	lbm/ft	g/cm
kg/m^3	1.198 264 E+02	9.977 633 E+01	1.601 846 E+01	1.0 E+03
	1.198 264 E-01	9.977 633 E-02	1.601 846 E-02	1

TABLE A-12. Specific heat capacity (Mass basis)

J/kg·K	kW·h/kg·°C	Btu/lbm·°F	kcal/kg·°C
J/Kg·K	3.6 E+03	4.186 8 E+00	4.184 E+00

TABLE A-13. Enthalpy calorific value (Mass basis)

J/kg	Btu/lbm	cal/g	cal/lbm
J/kg	2.326 000 E-03	4.184 E+00	9.224 141 E+00
	2.325 000 E+00		
	6.461 112 E-04		

APPENDIX B
GLOSSARY OF TERMS

APPENDIX B

GLOSSARY OF TERMS[a]

ANISOTROPY: Term used to denote the dependence of properties such as permeability on spacial orientation. Anisotropy is usually expressed as a tensor. When the principal axes are perpendicular to each other, the material is said to be orthotropic.

AQUICLUDE (GW)[b]: A body of saturated but relatively impermeable material that does not yield appreciable amounts of water to wells. Characterized by very low "leakance" (the ratio of vertical hydraulic conductivity to thickness) and very low rates of yield from compressible storage.

AQUIFER SYSTEM (GW): A heterogeneous body consisting of two or more permeable beds separated at least locally by aquitards that impede groundwater movement but do not greatly affect the regional hydraulic continuity of the system.

AQUITARD (GW): A bed with low permeability that impedes groundwater movement and does not yield water freely to wells, but which may transmit water between aquifers and may constitute an important storage unit. Leakance values vary over a wide range. When low, an aquitard may function as a boundary to an aquifer flow system.

AREA OF INFLUENCE (GW): Defined by Meinzer to be the land area of the same horizontal extent as the portion of the potentiometric surface that is perceptibly lowered due to withdrawal of water by a production well.

---

a. Adapted from the Invitational Well Testing Symposium, Berkeley, California, 1977.

b. Terms commonly used in hydrogeology.

BANK STORAGE (GW): The change in storage in an aquifer resulting from a change in stage of an adjacent surface water body especially in alluvial deposits adjacent to surface streams.

BAROMETRIC EFFICIENCY OF A WELL: The ratio of water-level changes in the well to the water-level changes in a water barometer.

BOUNDARY PRESSURE (PE)[c]: Pressure at boundary of drainage area.

CAPILLARY FRINGE (GW): A zone whose lower part is completely saturated, but with water under less than atmospheric pressure. May range in thickness from a small fraction of an inch in gravel to more than 5 ft in silt.

COEFFICIENT OF PERMEABILITY (GW): See "Hydraulic Conductivity."

COEFFICIENT OF SPECIFIC STORAGE (GW): See "Specific Storage."

COEFFICIENT OF STORAGE (GW): See "Storage Coefficient."

COEFFICIENT OF TRANSMISSIBILITY (GW): See "Transmissivity."

COMMINGLED SYSTEMS (PE): Two-layered or multiple layer reservoirs with communication taking place between layers, either through the wellbore alone or directly across the layer interface.
(cf: multiaquifer well)

COMPACTION (GW): Decrease in volume of sediments, as a result of compressive stress, usually resulting from continued deposition. Also called "one-dimensional consolidation."

---

c. Terms commonly used in petroleum engineering.

COMPACTION, RESIDUAL (GW): The difference between (a) the amount of compaction that will occur ultimately for a given increase in applied stress, once steady-state pore pressures are achieved, and (b) that which has occurred as of a specified time.

COMPRESSIBILITY, TOTAL SYSTEM (PE): A term representing the combined compressibility of all the elements in an aquifer system. Accounts for the compressibilities of the oil phase, water phase, gas phase, and of the rock formation itself, according to the relative fraction of the total system volume occupied by each.

CONDITION RATIO (PE): Also called flow efficiency, indicates approximate fraction of a well's undamaged producing capacity. Ratio of actual productivity index to the productivity index if there were no skin (ideal conditions).

CONFINING BED (GW): A body of relatively impermeable material stratigraphically adjacent to one or more aquifers. Can be either an "aquitard" or an "aquiclude."

CONSOLIDATION (GW): See "Compaction."

CONSTANT DRAWDOWN TEST (GW): also known as constant pressure test in petroleum engineering. A test in which flow rate is gradually varied in time to maintain a constant drawdown (or constant pressure) in the producing well.

CONSTANT PRESSURE TESTING (PE): Also known as constant drawdown test in groundwater hydrology. Involves recording change in flow rate with time while bottom-hole pressure is held constant.

CRITICAL FLOW (PE): occurs in high-permeability zones; the rate of flow into the drill pipe is independent of drawdown during a drill-stem test.

CRITICAL FLOW PROVER (PE): Device that measures flow rate of a gas through an orifice under critical conditions (velocity is constant at a maximum value despite downstream pressure variations).

DAMAGE FACTOR: A measure of wellbore damage obtained by subtracting the condition ratio from 1.

DAMAGE RATIO (PE): Inverse of condition ratio. Indicates wellbore condition.

DELAYED DRAINAGE (GW): Term used to identify the slow release of water from the unsaturated zone in an unconfined aquifer.

DELIVERABILITY TESTING OF OIL WELLS (PE): Determines capability of a well to deliver against a specific flow bottom-hole pressure. Two main types: (a) flow-after-flow test; flowing pressure is recorded for three or more successive flow rates. Each flow rate is held constant until pressure has stabilized. (b) modified isochronal flow test; used for systems where stabilization time is too long for flow-after-flow test. For each flow rate, the well is shut-in after pressure transience is recorded, but before stabilization occurs. At each step the final flowing pressure and then the final shut-in pressure are observed. At the final flow rate, the well is allowed to produce until the pressure stabilizes, and this pressure is recorded.

DIMENSIONLESS PRESSURE (PE): A dimensionless solution to the diffusivity equation. Directly proportional to physical pressure, where the scaling factor is dependent on flow rate and reservoir properties. Usually denoted by $P_D = \frac{2\pi kH\Delta P}{q\mu}$.

DIMENSIONLESS TIME (PE): A scaled version of real time. Scaling factor depends on reservoir properties and distance to point of observation $t = \frac{kt}{\phi\mu c r^2}$, where k is intrinsic permeability; t is time; ϕ is porosity; μ is viscosity; c is total compressibility; r is distance to point of observation.

DRAWDOWN (GW): Difference in water level (or pressure) between the static condition and that at any given instant during discharge.

DRAWDOWN TESTING (PE): Involves recording the drop in bottom-hole pressure when a shut-in production well is switched to production at constant flow rate.

DRILL STEM TESTING--DST (PE): Used in testing uncompleted wells. An arrangement of packers seals off the interval to be tested, allowing a pressure to be built up as formation fluid flows into the drill stem and surface-actuated valves are closed. Pressure changes are observed by a pressure gauge located in the test interval. See "Single Packer Test," "Straddle Packer Test."

DYNAMIC PRESSURE (PE): The pressure at a given time and location in a reservoir during a period of transient pressure distribution, such as during a build-up or drawdown test.

EFFECTIVE WELL RADIUS (GW): The radius of an imaginary cylinder centered at the wellbore in which the permeability is much higher than in the reservoir. In a gravel-packed well it often denotes the probable radius of the gravel pack.

EQUIVALENT INJECTION TIME (PE): In a fall-off test on an injection well where the injection rate before shut-in varies, the equivalent injection time is the length of time it would have taken to inject the same volume of fluid at a constant flow rate as was injected at a variable flow rate since the last pressure equalization.

EXCESS PORE PRESSURE (GW): Transient pore pressure at any point in an aquitard or aquiclude in excess of the pressure that would exist under steady-flow condition.

EXPANSION, SPECIFIC (GW): The increase in thickness of deposits per unit decrease in applied stress.

EXPANSION, SPECIFIC UNIT: The expansion (increase in volume) of deposits, per unit thickness, per unit decrease in applied stress.

EXPONENTIAL INTEGRAL (PE): See "Theis Solution."

FALLOFF TESTING (PE): Involves shutting in an injection well and observing the decrease in bottom-hole pressure with time.

FALSE PRESSURE (PE): Obtained by extrapolating the straight-line section of a Horner plot of pressure build-up data to infinite shut-in time. Approximates average reservoir pressure in an infinite system and can be used to estimate average drainage region pressure in a bounded system.

FIVE-SPOT PATTERN (PE): An arrangement of production and injection wells with four production wells at the corners of a square and one injection well in the center.

FLOW-AFTER-FLOW TESTING (PE): See "Deliverability Testing of Oil Wells."

FLOW EFFICIENCY (PE): See "Condition Ratio."

FLUID POTENTIAL (GW): The mechanical energy per unit mass of a fluid at any given point in space and time with respect to an arbitrary state and datum.

FORMATION VOLUME FACTOR (PE): A factor to account for changes in volume in each phase upon transition from reservoir to standard surface conditions. The ratio of the volume at reservoir conditions to the volume at standard surface conditions.

GROUND WATER, PERCHED (GW): Confined ground water separated from an underlying body of ground water by an unsaturated zone. It is held up by a "perching bed" of low permeability, and its water table is a "perched water table."

HEAD, STATIC (GW): The height (above a datum) of a column of water that can be supported by the static pressure at a given point. The sum of the "elevation head" and the "pressure head." See "Head, Total."

HEAD, TOTAL (GW): The sum of three components: (a) "elevation head," which is the elevation of the point above a datum; (b) "pressure head," the height of a column of static water that can be supported by the static pressure at the point; (c) "velocity head," the height the kinetic energy of the liquid is capable of lifting the liquid.

HORNER PLOT (PE): A plot of pressure build-up versus log $\frac{t + \Delta t}{t}$ where t is time since production and Δt is time since shut-in. A similar plot was proposed in ground water hydrology by Theis to analyze recovery data.

HYDRAULIC CONDUCTIVITY (K) (GW): Has dimensions of length per unit time. A medium has a hydraulic conductivity of unit length per unit time if it will transmit in unit time a unit volume of groundwater at the prevailing viscosity through a cross section of unit area, measured at right angles to the direction of flow, under a hydraulic gradient of unit change in head through unit length of flow. Replaces the term "coefficient of permeability."

HYDRAULIC CONDUCTIVITY, EFFECTIVE (GW): The rate of flow of water through a porous medium that contains more than one fluid.

HYDRAULIC DIFFUSIVITY (GW): The ratio between hydraulic conductivity and specific storage.

HYDRAULIC GRADIENT (GW): The change in static head per unit of distance in a given direction.

HYDROCOMPACTION (GW): The process of volume decrease and density increase that occurs when moisture-deficient deposits are wetted for the first time.

IMAGE METHOD (METHOD OF IMAGES) (PE): The technique of using image wells to generate no-flow and constant pressure boundaries in an infinite system.

IMAGE WELL (GW): An imaginary well which effectively produces the same drawdown (or recovery) as a linear boundary limiting the aquifer. See "Image Method."

INFLOW PERFORMANCE RELATIONSHIP (PE): Used to predict a well's deliverability when deliverability test data are not available. A relationship between flow rate, bottom-hole pressure, average reservoir pressure, and a productivity index.

INFLUENCE REGION (PE): The region surrounding a well or wells whose properties influence transient tests performed on those wells. (Not to be confused with Meinzer's "area of influence.")

INJECTIVITY TESTING OR INJECTION WELL TESTING (PE): Pressure transient testing during injection into a well. Bottom-hole pressure is recorded while injection rate is held constant.

INTERFERENCE TESTING (PE): A multiple-well transient test which involves the production of an active well (injection) and observing the resulting pressure changes in an observation well.

INTERPOROSITY FLOW PARAMETER (PE): A dimensionless property of a fractured system. Dependent on the well radius, a matrix-to-fracture geometric factor, and the ratio of the formation matrix permeability to the effective fracture permeability.

ISOCHRONAL TESTING (PE): See "Deliverability Testing of Oil Wells."

JACOB'S METHOD (GW): Also known as asymptotic solution. Involves a semi-logarithmic plot of drawdown as a function of the log of time.

LEAKANCE (GW): The ratio of vertical hydraulic conductivity to thickness of the aquiclude.

LEAKY AQUIFER (GW): An aquifer into which overlying and/or underlying aquitards discharge water as the potentiometric head in the aquifer is lowered.

MEINZER UNIT (GW): A unit of hydraulic conductivity defined as the flow of water in gallons per day through a cross-sectional area of 1 ft^2 under a hydraulic gradient of 1 at a temperature of 60°F.

MOBILITY (PE): The ratio of absolute permeability to viscosity.

MOBILITY RATIO: The ratio of the mobility of the injected fluid to that of the in situ fluid.

MULTI-AQUIFER WELL (GW): A well which is screened to produce fluids from multiple aquifers which are separated by zones of low permeability. (cf: "commingled systems")

MULTIFLOW EVALUATOR (PE): A tool used in drill stem testing which allows unlimited sequences of production and shut-in. Includes a fluid chamber to recover an uncontaminated formation-fluid sample under pressure at the end of the flow period.

MULTIPLE RATE TESTING (PE): Tests involving a variable flow-rate. Testing at a series of constant flow rates, or testing at constant bottom-hole pressure with continuously changing flow rate.

ORTHOTROPY (GW): See "anisotropy."

PERMEABILITY, EFFECTIVE (GW): See "Hydraulic Conductivity, Effective."

PERMEABILITY, INTRINSIC: Same as "Permeability." Term adopted by U.S. Geological Survey to indicate a property of the medium alone, independent of the fluid properties. Has dimensions of L^2. Also called "Absolute Permeability."

PIEZOMETRIC SURFACE (GW): See "Potentiometric Surface."

POROSITY (GW): The property of a rock or soil of containing interstices. Expressed as the ratio of the volume of interstices to the total volume.

POROSITY, DUAL: The porosity of the rock having substantial primary and secondary porosity.

POROSITY, EFFECTIVE (GW): Refers to the amount of interconnected pore space available for fluid transmission. Expressed as the percentage of total volume occupied by interconnecting interstices.

POROSITY, PRIMARY (GW): Refers to the original interstices created when a rock or soil was formed in its present state.

POROSITY, SECONDARY (GW): Refers to the porosity created by fractures, openings along planes of bedding and solution cavities. Occur mostly in consolidated rocks having low primary porosity.

POTENTIOMETRIC SURFACE: A surface which represents the static head. An imaginary surface connecting points to which water would rise in tightly cased wells from a specified surface or stratum in the aquifer.

PRESSURE, AVERAGE RESERVOIR: The pressure a reservoir would attain if all wells were shut in for infinite time, assuming no natural influx of fluid.

PRESSURE BUILDUP TESTING (PE): Involves shutting in a producing well and analyzing the resultant pressure buildup curve for reservoir properties and wellbore condition

PRESSURE, INITIAL RESERVOIR (PE): Stabilized pressure of a shut-in well.

PRESSURE, INTERWELL (PE): The pressure halfway between an injection well and a production well. Sometimes used to approximate average reservoir pressure.

PRODUCTIVITY INDEX (PE): Also known as the specific capacity of a well. Denotes the productivity of a well per unit drawdown.

PSEUDO SKIN FACTOR (PE): The apparent skin factor in a well which has no true physical damage (or improvement) but is not drilled completely through the formation thickness or is only partially completed, thus appearing damaged.

PSEUDO STEADY STATE (PE): A transient flow regime in which the rate of pressure change with time is constant at all points in the reservoir.

PULSE TESTING (PE): A multiple-well transient test, in which flow rate pulses are produced in an active well and the resulting pressure changes are recorded in an observation well. Provides reservoir information for the region around and between the two wells. (Because of the shorter time intervals, the influence region for a pulse test is less than that for an interference test, and thus information is gained about a smaller portion of the reservoir.)

RADIUS OF DRAINAGE (PE): Defines a circular system around a well in which a pseudo steady state pressure distribution exists.

RECOVERY TEST (GW): Also known as build-up test in petroleum engineering. Denotes a test which involves the measurement of recovery in a well after the well is shut in following a known period of production.

RELATIVE PERMEABILITY (PE): Also called effective permeability in ground water hydrology. Denotes the permeability of the porous medium to a particular fluid when more than one fluid is present.

RESIDUAL DRAWDOWN (GW): During recovery, the difference between the static water level and the water level at any instant during recovery.

SAFE YIELD (GW): Given a variety of meanings, but originally defined (by Meinzer) as the rate at which ground water can be withdrawn year after year from a given aquifer system without depleting the supply to the point where withdrawal at this rate is no longer economically feasible.

SEEPAGE FACE (GW): For a well piercing an unconfined aquifer, seepage face denotes that segment of the well screen over which the total head equals elevation above datum and water flows from the aquifer into the well.

SEEPAGE FORCE: See "Stress, Seepage."

SHAPE FACTOR (PE): A geometric factor, characteristic of the reservoir shape and well location.

SLUG METHOD (GW): Used to determine transmissivity of an aquifer. A known volume or "slug" of water is suddenly injected into or removed from a well and the decline or recovery of the water level is measured at closely spaced time intervals during the ensuing minute or two.

SINGLE-PACKER TEST (PE): A drill stem test utilizing one packer in which fluid flows through the perforated anchor pipe into the drill string.

SKIN (PE): A zone of decreased permeability near the wellbore created by drilling and completion practices.

SKIN FACTOR (PE): A constant which relates the pressure drop across the skin to the dimensionless rate of flow. A measure of wellbore damage.

SPECIFIC CAPACITY (GW): The rate of discharge of water from a well divided by the drawdown of water level within the well. Varies slowly with duration of discharge. Also called productivity index in petroleum engineering.

SPECIFIC DISCHARGE or SPECIFIC FLUX (GW): The rate of discharge of ground water per unit area measured at right angles to the direction of flow.

SPECIFIC RETENTION (GW): The ratio of the volume of water a saturated rock or soil will retain against the pull of gravity to its own volume.

SPECIFIC STORAGE (GW): The volume of water released from or taken into storage per unit volume of the porous medium per unit change in head.

SPECIFIC YIELD (GW): The water yielded by water-bearing material by gravity drainage, as occurs when the water table declines. The ratio of the volume of water a saturated rock or soil will yield by gravity to its own volume.

STABILIZATION TIME (PE): The time corresponding to the start of the pseudo steady state period.

STATIC WATER LEVEL (GW): The static position of the potentiometric surface in a well prior to the commencement of discharge. (See also initial reservoir pressure in petroleum engineering.)

STEADY STATE: Pressure is constant at all points in the reservoir.

STEP DRAWDOWN TEST (GW): Also known as productivity index test or step-rate test in petroleum engineering. Involves producing a well at different rates for predetermined periods of time and monitoring drawdown.

STEP-RATE TESTING (PE): A multiple-rate injection well test in which fluid is injected at a series of increasing rates, each rate lasting an equal amount of time. Injection pressure at the end of each rate is plotted versus injection rate.

STORAGE COEFFICIENT: The volume of water an aquifer releases from or takes into storage per unit surface area of the aquifer per unit change in head.

STRADDLE-PACKER TEST (PE): A drill stem test in which the tested interval lies between two packers.

STRESS: APPLIED: The downward stress imposed at the aquifer boundary by (a) the weight (per unit area) of sediments and moisture above the water table, (b) the submerged weight of the saturated sediments overlying the boundary, and (c) the net seepage stress due to flow within the saturated sediments above the boundary.

STRESS, EFFECTIVE: Stress that is borne by and transmitted through the grain to grain contacts of a deposit. The effective stress at a point in an aquifer differs from the applied stress at the aquifer boundary by the submerged weight (per unit area) of the intervening sediments and the net seepage stress due to flow within the intervening sediments.

STRESS, SEEPAGE: Stress created by the seepage force, which is transferred from the water to the porous medium by viscous friction. Seepage force is exerted in direction of flow.

SUBSIDENCE: Sinking or settlement of the land surfaces, due to any of several processes, but most importantly due to artificial withdrawal of subsurface fluids.

TEMPERATURE, PSEUDOCRITICAL (PE): For a mixture of gases, calculated from the relative amounts and critical temperatures of the components.

TEMPERATURE, PSEUDOREDUCED (PE): The ratio of the temperature of interest to the pseudocritical temperature.

THEIM EQUATION (GW): Represents steady-state radial flow solution to a well in the center of a circular, homogeneous, horizontal aquifer with prescribed potential at the circular boundary.

THEIS SOLUTION (GW): Represents the solution to a continuous line source in a homogeneous, horizontal, infinite, isotropic aquifer. (Also known as exponential intergral in petroleum engineering.)

TIDAL EFFICIENCY: A measure of the response of the water level in a well to changes in ocean level. Equal to the barometric efficiency subtracted from 1.

TRANSIENT TESTING: The study of pressure variation with time in an active well (production or injection) under a variety of conditions and possible operating procedures.

TRANSMISSIVITY (T), (GW): The rate at which water of the prevailing kinematic viscosity is transmitted through a unit width of the aquifer under a unit hydraulic grandient.

TWO-RATE TESTING (PE): A multiple-rate test on a production well using only two different flow rates.

TWO-ZONE SYSTEMS: See "Composite Systems."

u (GW): Dimensionless quantity related to the reciprocal of dimensionless time, t_D, used in petroleum engineering.

$$u = \frac{r^2 s}{4Tt} = \frac{1}{4t_D}$$

UNCONFINED AQUIFER (GW): Also called water table aquifer. An aquifer which contains a water table, at which it is in direct contact with the atmosphere.

UNIFORM-FLUX FRACTURE (PE): One in which fluid enters at a uniform flow rate per unit area. A first approximation to the behavior of a vertically fractured well.

VERTICAL PULSE TESTING (PE): Used to determine vertical permeability of a formation. Fluid is injected in pulses above a packer, escapes the wellbore through flow perforations and reenters below the packer through observation perforations where pressure changes are observed with a pressure gauge.

VOID RATIO (GW): The ratio of the volume of the interstices in a rock or soil to the volume of its mineral particles.

WATER DRIVE RESERVOIRS (PE): Reservoirs in direct communication with an active aquifer.

WELLBORE STORAGE (PE): Fluid stored in the wellbore above reservoir level. Usually occurs when a production well is shut-in without packers used to maintain fluid level. Affects pressure build-up data at early time as fluid continues to flow into the wellbore after shut-in.

WELL FUNCTION OF u (GW): Equal to twice the value of P_D, dimensionless pressure, which denotes the value of the exponential integral.

WELL LOSSES (GW): Denotes drawdowns at the well in excess of the theoretical capability of the reservoir. Such well losses may be due to poor development of the well, excessive entrance velocities and casing damages due to skin, scaling, or corrosion.

WIRELINE FORMATION TESTING (PE): A tool is lowered into the well on a logging cable. The mechanism establishes communication with formation fluid and measures pressure response. Slightly more qualitative than a DST.

APPENDIX C
INSTRUMENTATION

APPENDIX C

INSTRUMENTATION

Requirements

Before the appropriate type of instrument can be selected, the developer or consultant must calculate the anticipated pressure changes, flow rates, temperatures, and time resolution requirements. Methods for doing this have been discussed in Volume I. The importance of correctly anticipating these parameters is that the instrument chosen must have accuracy and precision far greater than the expected changes. For instance, when measuring pressure changes in an observation well with an expected 1 psi maximum of pressure change, then the instrument should have a resolution of at least 0.1 psi. On the other hand, in a production well there will be a relatively large pressure change and therefore only require 1 psi resolution. Instruments with a wide range of precision and accuracy are available. In general, the finer the resolution and greater the accuracy, the more expensive the instrument. However, advances in the development and availability of these instruments is lowering the cost of the high precision gauges.

An often overlooked area in test planning is the time element. If pressure changes take place very rapidily the recording equipment and/or personnel may not be suitable to record the data at a sufficiently small time interval. In general, in fractured or highly permeable aquifers the pressure changes will take place very quickly and be of a smaller magnitude than in a moderate or low intergranular permeability system. In almost every case it is valuable to have continuous recording devices with accurately synchronized clocks for measuring and recording each parameter of the test. This minimizes operator error, missed events, ambiguity in the data, and simplifies data analysis and interpretation.

Before any meaningful analysis of the data can be obtained, data of good quality is essential; it can be obtained from careful test planning, control, execution, and adequate instrumentation. Knowing how to use downhole pressure transducers to obtain pressure transient data is important. In principle, downhole data will always provide more reliable data insofar as the effects of temperature changes in the wellbore become unimportant. However, the use of downhole instrumentation may not always be possible or cost effective. For instance, if the production well is being pumped, it may not be possible to use a downhole tool because of the difficulty in setting the tools and the pump. Alternatively, the budget allocation for testing may prohibit the use of downhole tools. In general, the deeper the well or the hotter the well, the more important it is to use downhole instrumentation. If the well is over 100°C and sufficient wellhead pressure cannot be maintained, the water will start to flash (boil) in the wellbore. In this event, wellhead data or water level data will be useless for pressure transient testing and productivity calculations. For this case, downhole data is essential. If good quality production well data cannot be obtained, it is recommended that every effort be made to conduct a simultaneous production and interference test. Instrumentation for interference testing is readily available and, in general, easy to install and maintain.

In the following sections, subdivided by the test parameter to be measured, a variety of instruments will be discussed. Relevant to the discussion is the definition of accuracy and resolution. Accuracy is a measure of how closely a measured parameter compares to the correct value, as determined by the Bureau of Standards. The accuracy of an instrument is a function of its calibration, hysteresis, drift, repeatability and resolution. The resolution of an instrument is a function of sensitivity of the transducer to the parameter being measured, and the smallest quantity that can be observed and measured when using the instrument. For instance, a thermistor may have infinite resolution to temperature changes, but the ohm-meter being used to read the resistance may only have a resolution of five ohms; thus, the meter, not the probe controls the resolution of the instrument. The resolution or accuracy of a measured system is only as good as the worst component. For geothermal applications, the resolution of a pressure

gauge is often the more significant measure of the quality (or suitability) of a gauge. However, for temperature and flow rate measurements, accuracy is a more important requirement.

The following pages list some of the instruments currently available, their assets and drawbacks, and the types of instruments most suitable for a variety of applications. In addition to the detailed discussions, Tables C-1 through C-3 at the end of this subsection, summarize many of the performance characteristics of temperature and pressure sensors as defined in Reference C-1.

Flow Measurement

1. Weirs and flumes

   Accuracy: ±10%

   Range: 1 gpm to any maximum.

   Advantages: Very inexpensive, can be home-built. Construction details and formulas are contained in several engineering handbooks.

   Disadvantages: Cannot be used if the temperature is greater than 100°C. Also, cannot be installed in a pressurized pipeline and cannot be connected to a continuous recording device very easily.

   Suppliers: F. B. Leopold Company and BIF Industries.

2. Known-Volume container or weighing tank and stopwatch

   Accuracy: ±20%.

   Range: Limited only by the scales, container or tank, and the flow control apparatus.

Advantages: Very inexpensive.

Disadvantages: Cannot be connected to a continuous recorder. The person measuring the flow can get burned.

3. Differential pressure meters (orifice meters, nozzles, Pitot tubes, Venturi tubes, and low-pressure loss tubes)

Accuracy: ±10%.

Range: Pitot tubes--<1 to >30 ft/sec. Others--0.1 to 30 ft/sec. Depends on orifice and pipeline size.

Advantages: Most pump companies and drillers use these methods and are comfortable and familiar with them. They are most easily connected to continuous recording devices; therefore, these methods are very suitable for most applications.

Disadvantages: Scaling or flashing across the orifice can create undetected inaccuracy in the measurements.

Cost: Costs vary widely with the type of element and also with line size and pressure rating; less than $100 for an orifice plate to several thousand dollars for a venturi or one of the patented flow tubes. Installed cost also varies greatly with line size and pressure rating except for the pitot tube which is installed in a boss on the pipe wall.

Readout and Recording Equipment: A method must be provided to measure the pressure difference, and if desired, convert that to flow rate. In some cases, ΔP can be measured with a homemade manometer made from clear plastic tubing and a yard

stick, or a commercial manometer. At high line pressures, a ΔP gauge or transmitter with output indicator may be required. In either case the measured ΔP is then used to calculate flow rate. If direct flow reading is required, a pressure gauge scale (nonlinear) can be calibrated in flow units or a transmitter output can be converted electronically to a direct flow indication or output proportional to flow for recording or display. Cost of equipment to provide transmitting, recording, and indication could range from $2,000 to $3,000 or more, depending on the grade or quality of equipment.

Partial List of Suppliers: Pitot Tubes--Foxboro Corp., Meriam Instrument Co., Rosemount Engineering, Deitrich Standard, Taylor Instrument Co. Orifice Plates, Venturi tubes and nozzles--Daniel Industries, Inc., Badger Meter, Meriam Instrument Co., Fischer & Porter Co., Foxboro Corp., Tech Tube Corp.

4. Turbine Flow Meters

Accuracy: $\pm$5%.

Range: Depends on impeller and pipe diameter 0.1 to 50 ft/s.

Cost: Relatively expensive; several hundred dollars to several thousand depending on size and features.

Output: Output signal of most transmitters is a frequency proportional to volumetric flow rate that can be fed directly to a compatible flow rate indicator meter.

Advantages: Good accuracy, repeatability, and linearity. Wide ranges. Can be installed in-line or on a probe through the pipe wall.

Disadvantages: Can be degraded by other than clean fluids. Relatively high cost.

Partial List of Suppliers: Daniel Industries, Flow Technology, Inc., Foxboro Corp., Brooks Instruments, Fischer & Porter, and Electronic Flow-Meters.

5. Others

There are many other types of meters available that could be investigated if those listed above are not suitable. The following types would be in that category:

Acoustic/ultrasonic--no obstruction, thus no pressure loss. The clamp-on Doppler eliminates scaling and corrosion problems.

Magnetic--No obstruction in the line thus no pressure loss. Somewhat pressure and temperature limited by liner material. Relatively insensitive to dirty fluids.

Vortex--Good accuracy--subject to scaling.

Wellhead and Differential Pressure Measurement

1. In addition to the transducers in the preceding table, the following instruments are available:

a. Manometers: Measure pressure or differential pressure.

Accuracy: ±1% of span for most. ±0.1% for precision types.

Range: Minimum span is 0.15" H_2O, maximum span 60 psig.

Design pressure:	Up to 6,000 psig.
Design temperature:	Function of seal fluid, usually ambient.
Advantages:	Relatively low cost. Availability.
Disadvantages:	Difficulty connecting to a recording device, not sufficiently rugged for field testing.
Cost:	Ranges from a few dollars for the simple units to approximately $1,000 for the more sophisticated and precise.
Partial List of Suppliers:	Meriam Instrument Co., Bailey Meter Co., and Foxboro Corp.

b. Mechanical pressure gauges bourdon tube

Accuracy:	Between ±0.1% and ±5% of span.
Range:	From 10 in. H_2O to 100,000 psig.
Advantages:	Readily available and replaceable. Most drillers and pump operators have them.
Disadvantages:	Difficult to connect to recording devices.
Cost:	From $20 to thousands depending on dial size and accuracy.
Partial List of Suppliers:	Ashcroft, Foxboro Corp., Robert Shaw Controls, Heise (Dresser) Wallace and Tiernan Inc., ITT Barton.

c. Electronic pressure and differential pressure transmitters, capacitors, strain gauges, piezoelectric semiconductors (piezoresistive), potentiometers. (Process grade field instrumentation.)

Accuracy:	0.1% to 1% of calibrated span.
Range:	A few inches of water to several thousand psig.
Advantages:	Easily connected to continuous recording devices. Usually these devices are fairly reliable.
Disadvantages:	High cost and lead time for replacement.
Cost:	$750 to $2,000 depending on accuracy and pressure.
Partial List of Suppliers:	ITT Barton, Fisher Controls, Foxboro Corp., Honeywell, Taylor Instrument Co., Rosemount, Bailey Meter Co.

Temperature

Temperature gauges should be placed in thermal wells near the wellhead on the discharge line.

1. Mercury Thermometer

Accuracy: Depends on range 0.1 to 1°C.

Advantages: Readily available. Very accurate if small enough range.

Disadvantages: Cannot be connected to a recording device.

2. Electronic gauges

There are a wide variety of electronic gauges available. Tables C-1 and C-2 summarize the many varieties and manufacturers. Most of the available transducers are suitable for wellhead temperature measurements. One advantage of electronic gauges is that they can be easily connected to readout and recording devices. Calibration and recalibration of these gauges will ensure their repeated accuracy.

Downhole Instrumentation

Downhole Temperature Measurement

Tables C-1 through C-3 compare the performance of various sensors. For simple downhole temperature measurement a max-reading thermometer can be lowered into the well on a line. If more than maximum temperature is required, i.e., temperature versus depth or a continuous indication, a thermocouple, RTD or thermistor can be lowered into the well on a conductor line and temperature measured on the surface with a portable bridge, potentiometer or the temperature can be recorded if desired. Small reels or winches with conductor lines are available at reasonable cost. For more precise and detailed temperature logs, it may be more suitable to rent the equipment or hire a well logging service. Downhole tools can be purchased outright but the cost is usually prohibitive. The "Kuster" temperature tool incorporates a downhole recorder and can be run on a wire line. A logging service's charge will include costs/foot of depth, a flat service charge, and other charges depending on well condition, location, etc. The charges to log a 5,000-ft. deep cased hole could be several thousand dollars.

The following companies rent equipment or provide service as noted:

Schlumberger Well Services--Service

Dresser Atlas--Service

Birdwell--Service

Kuster Company--Tool Rental and Sale

Gearhart Owen Industries--Tool rental, sales, and service

Halliburton Services--Service

Sperry-Sun--Tool rental, sales, and service

Downhole Pressure Measurement

1. Bubbler Tube. Perhaps the simplest and least expensive method to measure downhole pressure and water level is the bubbler tube. A crude but sometimes appropriate arrangement consists of a tire pump and a gauge connected to a small pipe or tube suspended in the well. Accuracy of the bubbler tube in well measurement applications can vary widely depending on the equipment, temperature effects, and operating techniques. In ordinary tank level measurement accuracies of ±1% can be achieved.

2. Downhole Capillary Tube. This consists of a small tube suspended in the well with a pressure coupling chamber at the bottom and a precision pressure transducer on the surface. The tube is filled with inert gas or a synthetic fluid. Sperry-Sun Inc., supplies such a system.

3. Electronic Pressure Transducers. Table C-3 compares the performance of several transducers suitable for downhole measurements. As in the case of downhole temperature measurements, the tools can be rented, purchased, or the services can be hired. The table lists suppliers, some of which will rent tools. The same companies listed as renting temperature tools or providing logging service will also provide pressure tools and service at similar costs. In the following section, an instrument incorporating a Paro-scientific digiquartz transducer is discussed.

Downhole Flow Measurement

Most of the downhole flow meters use a variation of the turbine discussed previously. As with downhole pressure and temperature measurement the tools and/or service are available for rent or hire. Most of the companies listed above will provide flow measurement tools or service.

Water Level Measurement

1. Bubbler Tube. The bubbler is usable in subsurface water level or artesian wells. Several companies supply systems and equipment for ordinary tank level measurements which may be suitable for well measurements. Cost would be on the order of several hundred dollars. Some of the companies are: Fisher Governor Co., Meriam Instrument Co., Petrometer Corp., and Uehling Instrument Co.

2. Tape and Float. This method can be used on wells with water levels below the surface. They can be suspended by hand and the distance measured, or wound on a drum with provisions for continuous recording of level. Several companies make the latter unit which is well suited for monitoring well water level at depths up to 30(ft. Cost is approximately $1,000. Partial list of suppliers: Leopold & Stevens and Keck Instrument Inc.

3. Others. This would include the conductivity probes, which can be fouled by oil, etc., the chalked tape, and other float and changing resistance type systems.

Approximate Cost: $50 to $100 for 100 ft of chalk tape.
$300 to $800 for an electric tape.
$500 for a conductivity probe and meter.

Partial List of Suppliers:

Lufkin and Roe Instrument: chalk tape.
Sepa-Air Inc.: electric tape.
Springs Instruments: conductivity probe.

TABLE C-1. Manufacturers of temperature sensors reviewed

Manufacturer/Supplier	Electrical Sensing			Passive Indicating	
	Resistance Temperature Detectors (RTDs)	Thermistors	Thermocouples	Maximum Indicating Sensors	Bi-Metallic Stem Thermometers
ARi Industries	X	--	X	--	--
Barber-Coleman Co.	X	X	X	--	--
Big Three Industries	--	--	--	X thermochemical	--
Brooklin Thermometer	--	--	--	X glass/bi-metallic	--
Celesco Transducer Products	X	X	X	--	--
C. S. Gordon Co.	--	--	X	--	--
Fenwal Electronics	--	X	--	--	--
Fischer & Porter Co.	X	--	X	--	--
Foxboro Co.	X	--	X	--	--
Hi-Cal Engineering	X	--	X	--	--
ITT-Barton	X	--	--	--	--
Markal Co.	--	--	--	X thermochemical	--
Matthey Bishop, Inc.	X	--	--	--	--
Minco Products, Inc.	X	--	X	--	--
Rosemont, Inc.	X	--	--	--	--
Semco, Inc.	X	--	X	--	--
Spectro Systems, Inc.	--	--	--	X metal pellets	--
Sybron-Taylor Corp.	X	--	X	X glass	X
Thermometrics, Inc.	--	X	--	--	--
Victory Engineering	--	X	--	--	--
W. Wahl Corp.	X	X	X	X thermochemical and bi-metallic dial	X
Weed Instrument Co.	X	--	--	--	--
W. H. Keseler Co., Inc.	--	--	--	X glass	--
Weston Instruments	--	--	--	--	X
Yellow Springs Instruments	X	X	--	--	--
Omega Engineering	X	X	X	--	--

TABLE C-2.[a] Performance comparison of some commercial pressure transducers

No.	Manufacturer and (Model)	Sensor Technique	Accuracy (overall) (% FS)	Resolution (% FS)	Stability and Drift	Max °F	Coefficient	Maximum Pressure Range(s) (psia)	Size	Comments
1.	Hewlett Packard, (2811B)	Diaphragm with oscillating quartz crystal	0.025%	Infinite (0.01 psi typ)	0.01%/yr	300	?	11,000	1-7/16" dia. by 40" long	Accepted standard for precision downhole oil/gas well testing. Temp correction to ±1°C recorded.
2.	Mensor, (Digital Quartz manometer)	Fused quartz helical bourdon tube w/optical sensor and electronic nulling	<0.2%	0.0005%	0 @ 3 mos (0.01%/yr)	122	0.0004%/°C	1,000	11" by 10" by 8-1/2"	System temp control/ compensation to ±2°C to achieve performance quoted. Also makes unit like #3 below.
3.	Heise (Dresser), (Digiquartz)	C bourdon tube and servo force balance	0.05%	0.005%	NA	125	Very small, 0.1% FS over range	10,000	4-3/8" by 6" by 16"	Sperry-Sun sells for use with their 'tube' pressure transmission system.
4.	Paroscientific, (Digiquartz)	Bellows linked to vibrating quartz bar	0.1%	<0.1%	0.1%/yr	225	0.004%/°F	5,000	1.15" dia. by 3-1/4"	Hi temp @ pressure (530°F @ 10,000 psi) unit currently under joint development with Sandia Labs--will have high temp electronics.
5.	Sundstrand Data Controls, Inc., (Developmental)	Bellow linked via quartz structure w/force-balance and capacitor feedback	0.11%	0.004%	0.1%/yr ?	176	NA	500	1-5/8" dia. by 2"	Mfg claims higher pressure (5K-10K) unit is developable, basic sensor capable of higher temperature
6.	Setra Systems, (204/205)	Diaphragm w/capacitor plate displacement	0.11%	<0.01%	0.05%/yr ?	250	0.004%/°F	10,000	1-3/4" dia.	Basic sensor w/o integral electronics capable of much higher temperature.
7A.	Heise (Dresser), (#CMM16)	C bourdon tube linked to dial and potentiometer	0.1%	0.01%	0.02%/yr	125	0	10,000	17-3/8" dia. by 3-1/4"	16" by 660 dial readout, electrical output also provided.
7B.	Mensor, (2792)			0.01%	0.02%/yr	125	0	10,000	17-3/8" dia. by 3-1/4"	Can operate up to 250°F w/external compensation.
8.	Robinson-Halpern, (144)	Helical bourdon tube linked to differential transformer	0.1%	<0.01%	NA	165	0.1%/°F	10,000	6" by 6" by 4-1/4"	--

TABLE C-2.[a] (continued)

No.	Manufacturer and (Model)	Sensor Technique	Accuracy (overall) (% FS)	Resolution (% FS)	Stability and Drift	Max °F	Coefficient	Maximum Pressure Range(s) (psia)	Size	Comments
9.	Bell & Howell, (CEC-1000)	Diaphragm w/thin film strain gage (sputtered)	0.15%	<0.01%	0.1%/yr	600+	0.005%/°F	10,000	1" dia. by 2-/2"	Mfgr claims higher accuracy and temp performance available
10.	Bell & Howell, (CEC-4-361)	Diaphragm w/unbonded wire strain gage	<0.2%	<0.05%	0.5%/yr	700	0.1%/°F	5,000	1-1/4" dia. by 2-1/2"	Fragile and slow temp response time (mfgr feels thin film will replace).
11.	Kaman Sciences, (KP-1911)	Diaphragm with eddy current variable impedance coil	0.25%	0.1%	NA	1000	0.1%/°F	5,000	5/8" dia. by 1-1/2"	--
12.	Sparton South-west, (890 HT)	C bourdon tube with wire potentiometer	1%	0.3%	NA	600+	0.1%/°F	10,000	1" dia. by 2-1/2"	--
13.	Celesco, (P2)	Diaphragm w/variable reluctance transducer	1%	0.1%	0.5%/yr	250	0.2%/°F	10,000	1-1/4" dia.	Mgfr has built high temp (600°F) unit w/derated accuracy (~1-1/4%).
14.	Data Instruments, (MPA 1000)	Diaphragm w/bonded semiconductor strain gage	0.25%	<0.05%	0.5%/yr	250	0.001%/°F	5,000	1-1/4" dia. by 2-1/2"	--
15.	Vernitech	C bourdon tube with film potentiometer	0.7%	<0.05%	0.5%/yr	185	0.01%/°F	10,000	2-1/2" dia. by 2"	--

a. See Reference C-1.

TABLE C-3. Performance comparison of geothermal process temperature sensors

Performance Parameter	Resistance Temperature Detectors (RTDs)	Thermistors	Thermocouples	Bi-Metallic Thermometer	Thermochemical and Physical Melt Indicators	Bulb-Bourdon Tube (thermal fluid filled)
Temperature range	-260 to 900°C	-100 to 400°C	-270 to 2000°C	-60 to 450°C	38 to 1649°C labels (38 to 600°C)	0 to 340°C
Accuracy	0.01% (<0.1°C)	1%	0.1%	1% (0.5% available)	1% (0.3% available)	1%
Sensitivity (signal level)	Good: +0.5%/°C (<0.1V/°C with bridge)	High: -5%/°C -0.5% linearized (<0.5 V/°C with bridge)	Very low, 1%/°C	Depends on dial size, etc.	NA	0.5% of F.S.
Linearity	Excellent: 1%	Poor: 10-20% Linearized: 2%	Poor: 10-25%	1%	NA	1%
Stability	Excellent	Poor	Excellent	Good	NA	Fair
Interchangeability	Excellent	Good	Poor	NA	NA	NA
Size	Medium: >1/8" diam. by >1/4" long	Very small	Small	1" to 5" dial, stem dia. >1/8"	Typically >1/8"	Very large
Time constant	0.2 to 10 s	0.05 to 10 s	0.1 to 4 s	10 to 30 s	1 s	Long
Cost	$25 to $1000	$2 to $300	$1 to $50		$0.50 to $7	High
Comments	Best overall	Narrow span (typically <105°C)	Requires reference temp. junction	Can be configured w/maximum registering dial. Used in Kuster 'bomb' type high temp		Used in GRC 'bomb' type high temp logging tool (span limited ~150°C). Kuster also makes system rated for 260°C.

REFERENCE

C-1. M. D. Lamers, Measurement Requirements and Methods for Geothermal Reservoir System Parameters (An Appraisal), LBL-9090, GREMP-6, 1979.

APPENDIX D
FABRICATION OF INSTRUMENTS

APPENDIX D

FABRICATION OF INSTRUMENTS

The cost of commercially available downhole instrumentation is often prohibitive. For this reason, and to obtain the highest quality data possible, the Earth Sciences group at Lawrence Berkeley Laboratory has developed a suite of downhole instruments for low-to-moderate temperature geothermal well testing. Three components of a downhole instrument package are described here: a downhole pressure temperature tool, a multiconductor cablehead, and a line driver for transmitting the pressure tool signal. A fourth instrument, a float type water level detector is also discussed. The complete engineering drawings for these instruments are available in Reference D-1.

Downhole Pressure and Temperature Instrument

The Paroscientific 400 psi and 900 psi digiquartz pressure transducers have been used for many years in measuring precise changes in wellhead pressures, pressure differentials across orifice plates and also in conjunction with "Perk" tubes and Sperry Sun downhole pressure chambers. In order to obtain precise pressure data during interference testing and accurate downhole pressure data, the Lawrence Berkeley Laboratory Reservoir Engineering group decided to incorporated the digiquartz pressure transducer in a downhole pressure temperature package which can be used in artesian and non-artesian wells. The maximum operating temperature of the tool is 107°C.

The downhole instrument package incorporates the Paroscientific 400 psi model 2400-A or 900 psi model 2900-A digiquartz pressure transducer (Figures D-1, D-2, and D-3). The transducer is shock-mounted inside the instrument package and connected to the pressure port with a stainless steel capillary tubing filled with Dow Corning f.s. 1265 fluid. The pressure device, when interfaced with the Paroscientific model 600 digiquartz computer and the Hewlett Packard 5150A thermal printer, can record pressure data at intervals of 1 second to 2 hours. The combination pressure-temperature housing is constructed from 316 stainless steel and has an outside diameter of 2.75 in. and a length of 9.5 in.

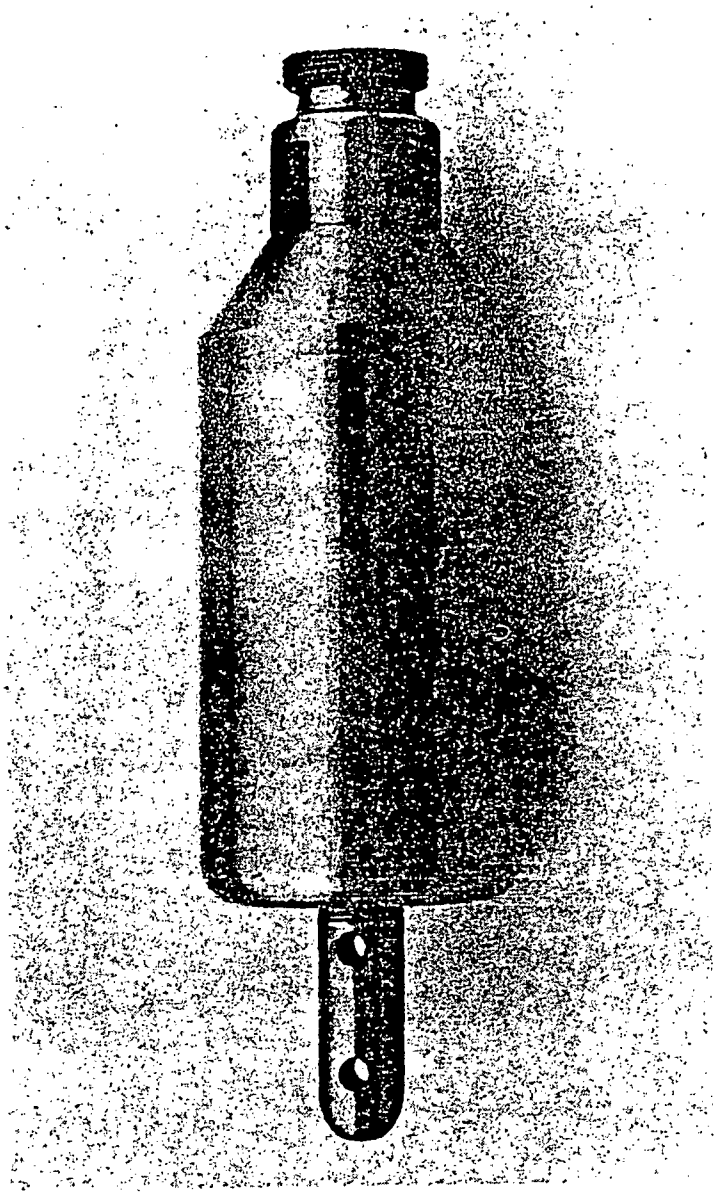

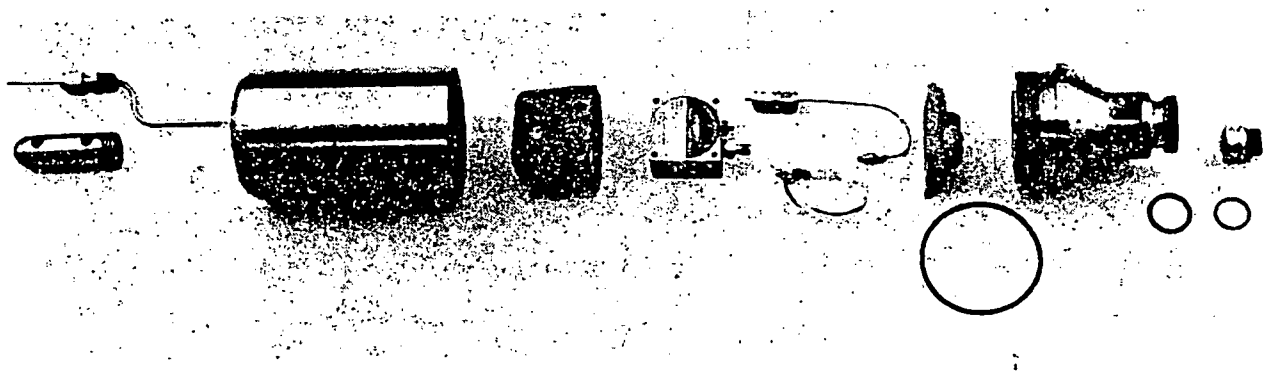

Figure D-1. Downhole instrument package.

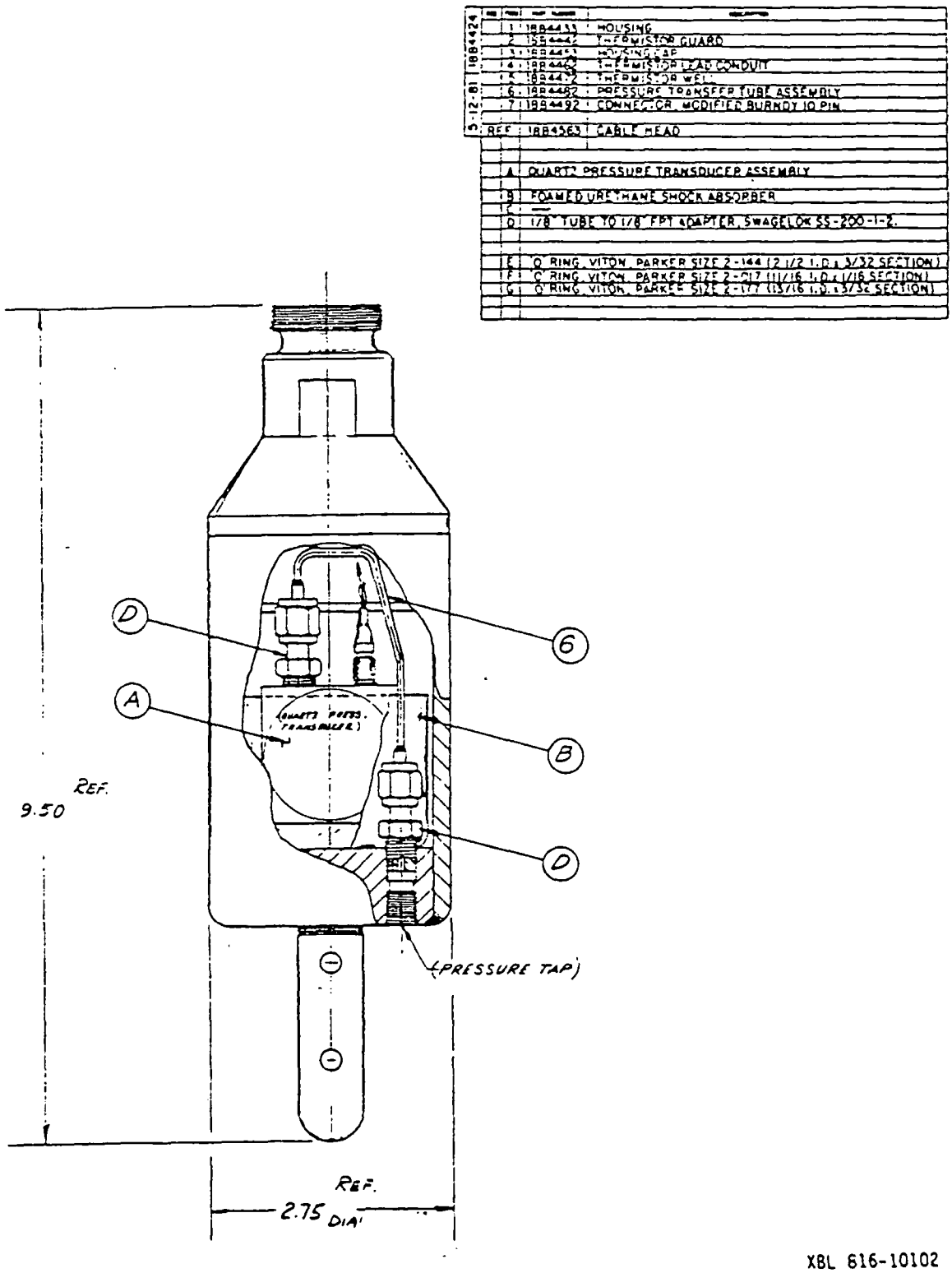

Figure D-2. Downhole pressure and temperature instrument.

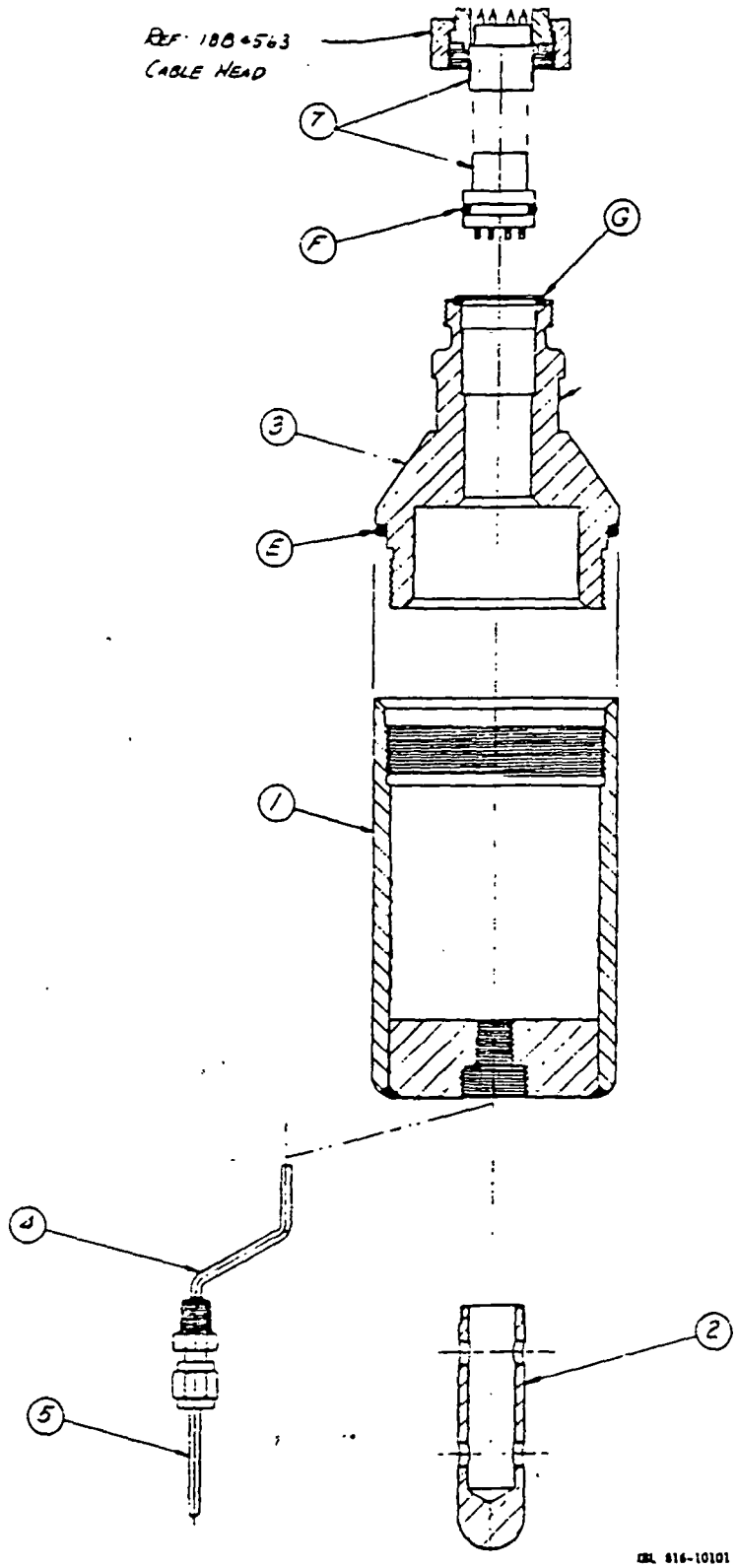

Figure D-3. Downhole pressure and temperature instrument continued.

The combination pressure-temperature chambers are lowered into the well on armored four-conductor cable. The cable is connected to the tool by a designed cablehead, but can also be run with a conventional multiconductor cablehead. The temperature sensing element is a YSI 44011 100,000 ohm at 25°C thermistor, isolated from the well fluid by 1/8 in. outside diameter stainless steel tubing with a 0.010 in. wall thickness. The thermistor has a resolution of ±.2°C (including thermistor interchangeability) and a response time of approximately 1 second in liquids. The resistance of the thermistor, which is temperature dependent, is read at the surface and converted to temperature.

The system has been field tested at Klamath Falls, Oregon; Susanville, California; and Cerro Prieto, Mexico.

Geothermal Multiconductor Cablehead

A cablehead is a connector used to mechanically and electrically attach the armored logging cable to a downhole instrumentation package. Commercially available cableheads perform properly in noncorrosive environments, but when subjected to the corrosive brines and the elevated temperatures found in geothermal wells, the corrosive brine will eventually enter the cablehead. This will short the electrical connectors and cause the armored steel strands to corrode. Loss of data and eventual loss of instrument package downhole can result.

The geothermal group at the Lawrence Berkeley Laboratory has designed an inexpensive multiconductor cablehead (Figure D-4). The body is machined from stainless steel with a length of 9 in. and a 1.5 in. diameter. It has an overshoot provision for retrieval should the instrument package be lost downhole. The cable is mechanically attached within the cablehead by letting a brass cone force the unbraided cable strands against the walls of an internally tapered sleeve. The cablehead incorporates an epoxy pressure seal. The high temperature epoxy used has excellent corrosion, chemical and solvent resistant properties. The epoxy is rated for continuous operation at temperatures up to 600°F. The epoxy seal is formed by pouring the epoxy mix around the electrical conductors inside the specially machined

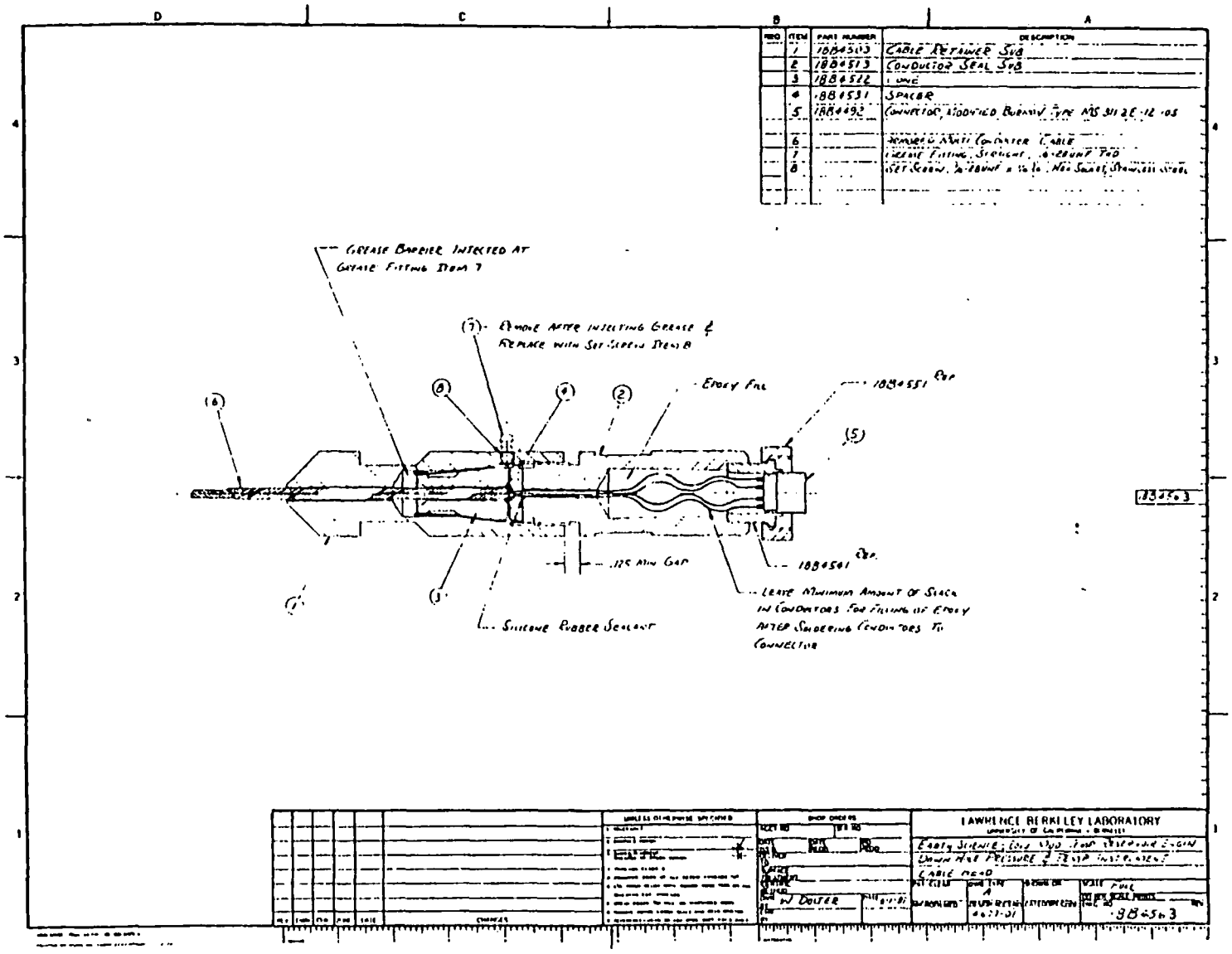

Figure D-4. Multiconductor cablehead.

tapered cablehead cavity. The insulation on the conductors has been previously etched to ensure maximum adhesion of the epoxy. Should it become necessary, the epoxy seal can be easily removed with the aid of an electric drill. The cable can then be reheaded and a new seal poured in place. This can be carried out even under field conditions.

The cablehead also incorporates a grease barrier. A high temperature grease is pumped through a removable zerk fitting and fills void spaces within the cablehead assembly. This procedure keeps the often very corrosive, well bore fluid from entering the cablehead assembly. This eliminates the frequent reheading of the cable due to strand corrosion. The connection of cablehead to instrument package is made with a threaded fastener incorporating an "O" ring seal, and multi-conductor electrical connector.

Line Drivers

When using a Paroscientific pressure transducer it is often desirable to transmit the signal from the measurement location to a central data acquisition location. This allows for accurate clock synchronization and continuous observation of the instrument function. Because the transducer has a limited range in transmitting its frequency output, it is necessary to amplify the signal before it is relayed to the central data acquisition location.

The Field Systems Group at Lawrence Berkeley Laboratory designed an inexpensive line driver that detects, amplifies, and transmits the frequency signal from the transducer. The line driver provides power to the transducer from a 12 V automatic battery and transmits the output signal to a central location on an inexpensive twisted two-conductor wire.

The line driver is housed in a small instrument enclosure. The electronic circuit uses inexpensive commercially available components. A schematic of how the line driver is used in conjunction with the pressure tool is shown in Figure D-5.

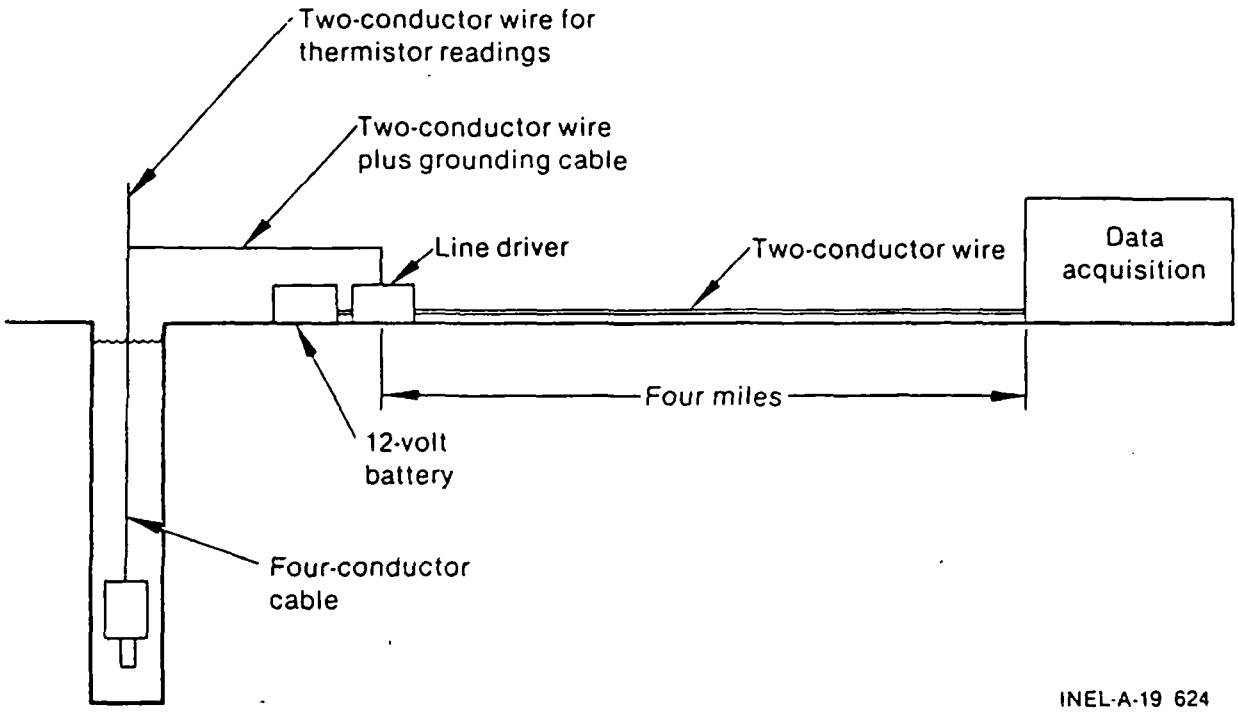

Figure D-5. Schematic of a line driver used in conjunction with the pressure tool.

Water Level Indicator

Description

Fluid level indicators, as used in well testing, are portable instruments used to detect the water level in the wellbore. The most commonly used type of probe is a conductivity-type gauge. The weighted probe attached to a two conductor cable is run down a well. When the probe contacts the water an electrical circuit is completed and the current flow is measured at the surface. When used in cold water wells, such a probe performs adequately; but for hot wells it is often unreliable. Because a conductivity-type gauge relies solely on the conductivity of the downhole fluid to complete the electrical circuit, erroneous readings may result due to heavy steam layers, spill over from pumps, and casing leaks. Non-conductive fluids floating on the water surface, such as liquid paraffin or oil, can also cause erroneous readings.

By replacing a conventional conductivity-type probe with a GEMS model LS-1700 liquid-level switch, these problems can be avoided. In the GEMS unit a magnet-equipped float rises with the fluid level and closes a reed switch encased in the unit's central stem. An electrical circuit is completed and the current is detected at the surface. The assembly drawing for this unit is shown in Figure D-6. It is easily fabricated and the instructions to do so follow.

Fabrication

The assembly and fabrication drawings are as shown. The GEMS liquid-level switch (model LS-1700) is inexpensive and readily available. The parts surrounding the unit, Parts 3 and 4 (see assembly drawing) should be made of a nonmagnetic material to avoid interference with the operation of the probe.

1. Insert the GEMS liquid level switch into the fabricated housing (Items 3 and 4) letting the leads and threaded portion of the GEMS unit protrude through the hole (Item 4). Slip the hose fitting (Item 2) over the leads.

2. Fill the hose fitting with silicon rubber sealant and screw it securely to the GEMS unit.

3. Insert the two-conductor cable with the conductivity type probe removed through a one-foot section of appropriately-sized heat shrink tubing.

4. Solder the leads from the GEMS Unit to the leads of the two-conductor cable approximately two inches beyond the end of the hose fitting. Cover the solder joint, the cable, and the end of the hose fitting with silicon rubber sealant.

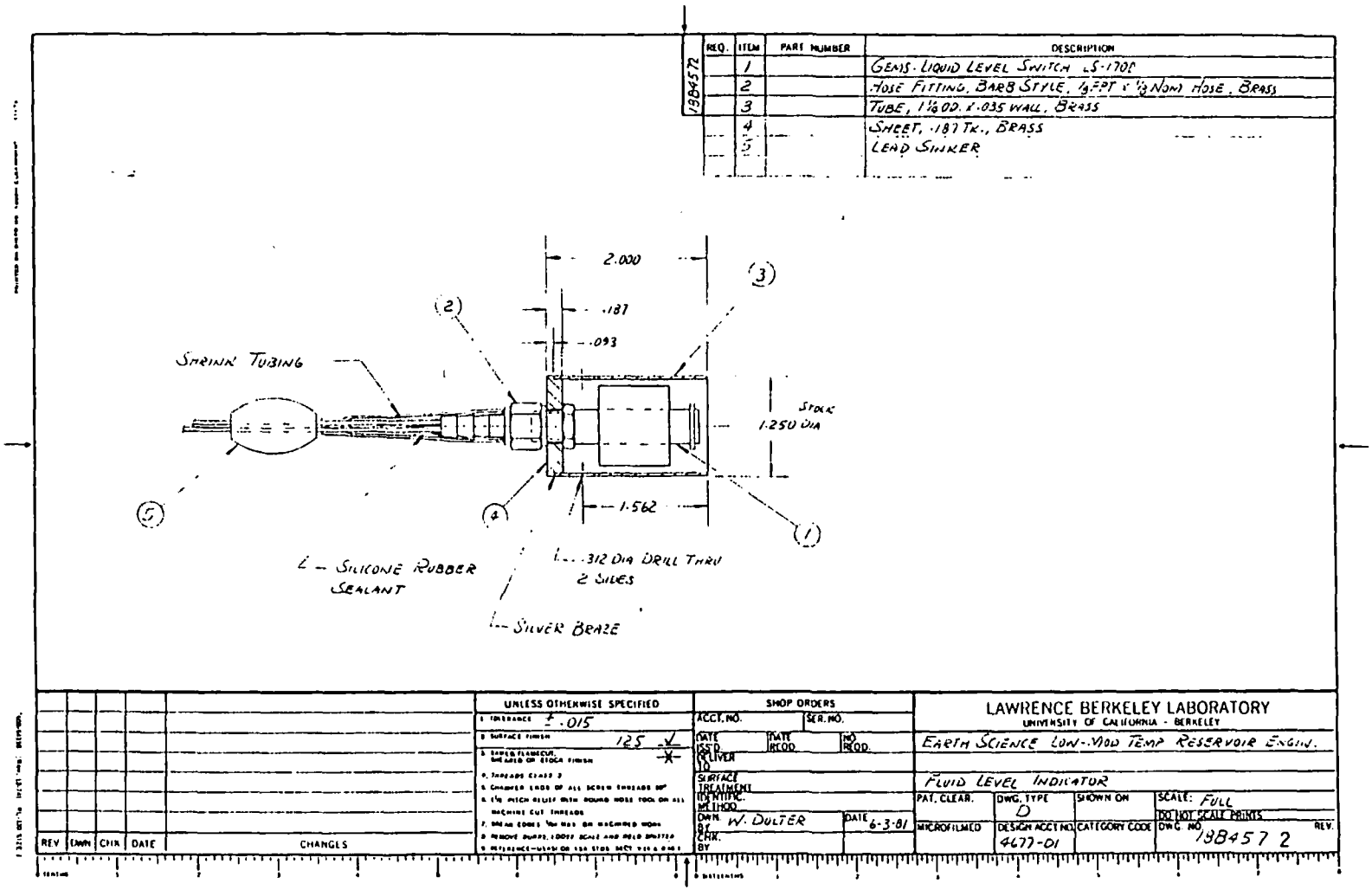

XBL 816-10189

Figure D-6. Fluid level indicator.

5. Slip the shrink tubing over the cable solder joint and hose fitting. Heat the shrink tubing until it fits snugly on the cable. Do not use the probe until the silicon rubber sealant has set.

6. Add split-type lead weights to the cable to facilitate running the probe down a well.

Use

The unit described here can be substituted on the end of a conventional conductivity-type water-level indicator. When the fluid level is reached, a current will be detected on the current-detecting instrument at the surface. If an entire water level detector is to be constructed, a suitable substitute for the surface readout is an ohmmeter. When the fluid level is reached by the probe, the ohmmeter will indicate that a circuit has been closed.

REFERENCE

D-1. Recently Developed Well Test Instrumentation for Low-to-Moderate Temperature Hydrothermal Reservoirs, LBL-13260.

APPENDIX E
VARFLOW PROGRAM USER'S GUIDE

APPENDIX F

VARFLOW PROGRAM USER'S GUIDE

Before a well test is conducted, you should calculate the anicipated drawdown at each of the wells to be monitored during the test. If a single well is being flowed at a constant rate, the drawdown can easily be calculated from the equations in Section 6 of Volume I. However, if two or more wells are flowing and/or you are also reinjecting the produced brine, the calculations are more complicated. Also, if the flow rate from the well is not held at a constant rate, the calculations are more complex. The following computer program can be used to calculate the anticipated pressure response at up to 10 wells, due to the flow rate of up to 10 production and/or injection wells.

Program Description

VARFLOW calculates pressure changes in response to fluid production/injection from/into an idealized reservoir system. The program is set up to calculate pressure changes at up to ten observation wells. These observation wells may be interference monitoring wells or production wells. The reservoir description is as follows:

1. The reservoir is of infinite areal extent, or bounded on one side by a linear constant potential or barrier boundary.

2. The reservoir is completely saturated with a slightly compressible single phase fluid.

3. The reservoir is isothermal.

4. The reservoir is horizontal and has a constant thickness, H.

5. The flow of fluid in the reservoir is described by Darcy's law.

6. The reservoir is homogeneous and bounded above and below by imper meable layers.

7. The reservoir permeability can be anisotropic in a horizontal plane (x-y anisotropy) or isotropic.

The flow into or from a fully penetrating well is uniformly distributed over the length of the well. The well is modeled as a line source. However, a skin effect, indicative of wellbore condition can be included in the analysis.

Flow rates from up to ten wells can vary arbitrarily. Flow rates are modeled by superposition of consecutive "production pulses." Within any "production pulse" the flow rate may be constant or vary linearly. Figure E-1 demonstrates the construction and definition of a "production pulse." With this scheme for modeling flow rates, any variable flow rate history can be represented to the desired accuracy by a series of sequential straight-line segments, each of the appropriate duration and inclination.

Basic Equations

Variable Flow Rate

In an isotropic reservoir, which complies with the description discussed above, pressure changes caused by production/injection from a single well with a variable flow rate can be calculated from Equation (E-1).

$$\Delta P(t) = \frac{\mu}{4\pi kH} \int_{\tau_n}^{\tau_{n+1}} \frac{q(\tau)}{t - \tau} \exp\left[\frac{-r^2}{4\eta(t - \tau)}\right] d\tau \qquad \text{(E-1)}$$

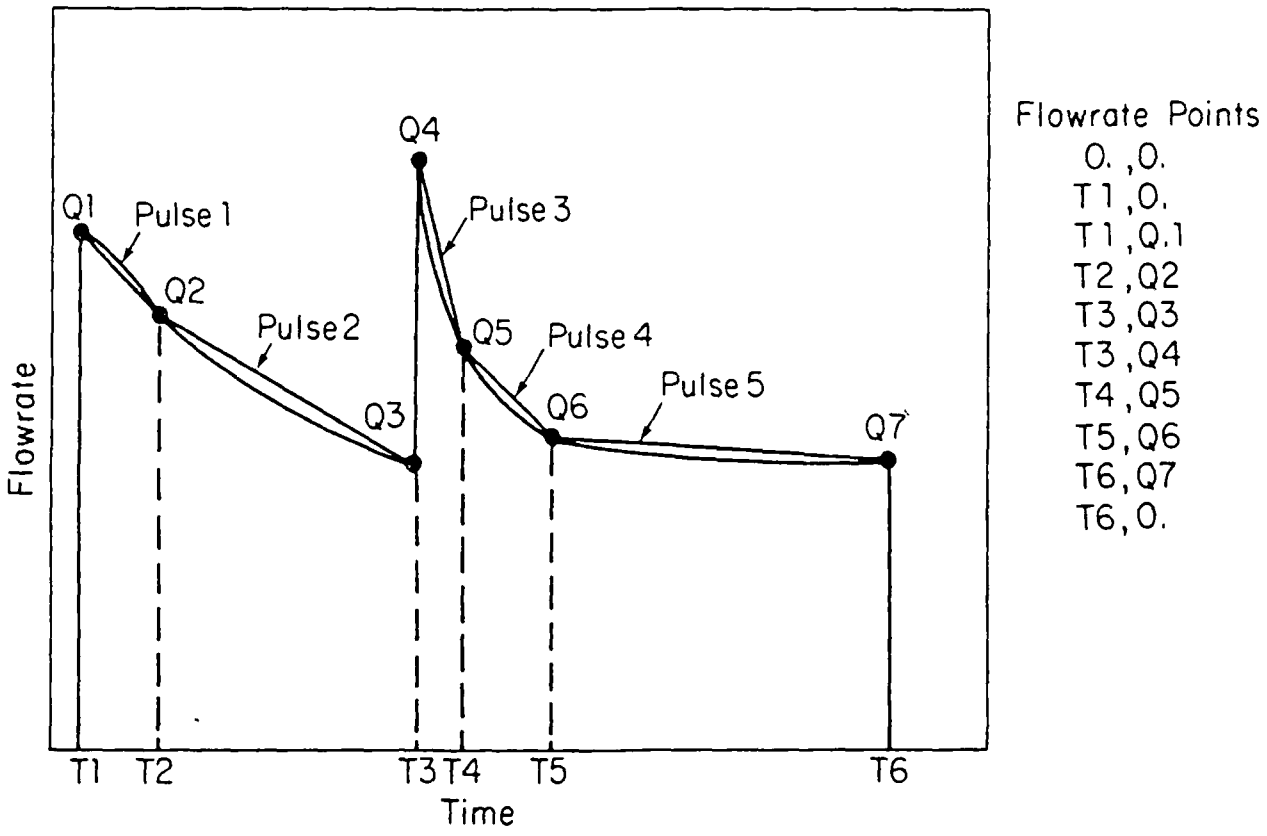

Figure E-1. Representation of a production pulse.

where

$\Delta P(t)$ = pressure change at time t due to the flow rate $q(\tau)$ for $\tau_n < t < \tau_n + 1$

μ = dynamic viscosity of the fluid

k = permeability

H = reservoir thickness

τ_n = time at which the flow starts

τ_{n+1} = time at which the flow stops

$q(\tau)$ = volumetric flow rate at time τ

r = distance between the observation well and the production/injection well

η = the hydraulic diffusivity ($k/\phi\mu c$)

ϕ = storage coefficient = $c_r (1 - \phi) + c_f \phi$.

Then, if $q(\tau)$ expressed as

$$q_n(\tau) = A_n + B (\tau - \tau_n) \qquad \text{(E-2)}$$

where

$q_n(\tau)$ = the flow rate at time τ which is within production pulse n

A_n = the flow rate at the beginning of production pulse k

B = the slope of the production pulse

$= (A_{n+1} - A_n) / (\tau_{n+1} - \tau_n)$

τ_n = the time at which production pulse n begins

and it:

$$u_n = \frac{\mu\phi c r^2}{4k(t - \tau_n)}$$

$$u_{n+1} = \frac{\mu\phi c r^2}{4k(t - \tau_{n+1})}$$

$$w(u) = \int_u^\infty \frac{\exp(-y)}{y}\, dy$$

N = the total number of production pulses which begin prior to time τ,

then, the pressure response is calculated by Equation (E-3).[E-2, E-3]

$$\Delta P(t) = \frac{\mu}{4\pi kH} \sum_{n=1}^{N} \Big\{ [A_n + B_n (t - \tau_n)(1 + u_n)] [w(u_n) - w(u_{n+1})] - B_n [(t - \tau_n) \exp(-u_n) - (t - \tau_{n+1}) \exp(-u_{n+1})] \Big\} . \quad (F-3)$$

The pressure response, caused by production/injection from more than one well is calculated by summing the response due to each production/injection well.

Anisotropy. If the reservoir is anisotropic then the equations are modified in the following manner. If that the principal axes of anisotropy are at 90 degrees to each other and that the x and y axes are chosen to be the principal axes (see Figure E-2) the Equation (E-1) is rewritten as Equation (E-4).[E-4]

$$\Delta P(t) = \frac{1}{4\pi} \left(\frac{\mu}{kH}\right)_e \int_{\tau_n}^{\tau_{n+1}} \frac{q(\tau)}{t - \tau} \exp\left(\frac{-r^2}{4\eta_\theta (t - \tau)}\right) d\tau \quad (E-4)$$

where

$(kH/\mu)_e$ = effective transmissivity

$$= \sqrt{(kH/\mu)_x \cdot (kH/\mu)_y}$$

and

$$\eta_\theta = \frac{(kH/\mu)}{\phi c H} \theta$$

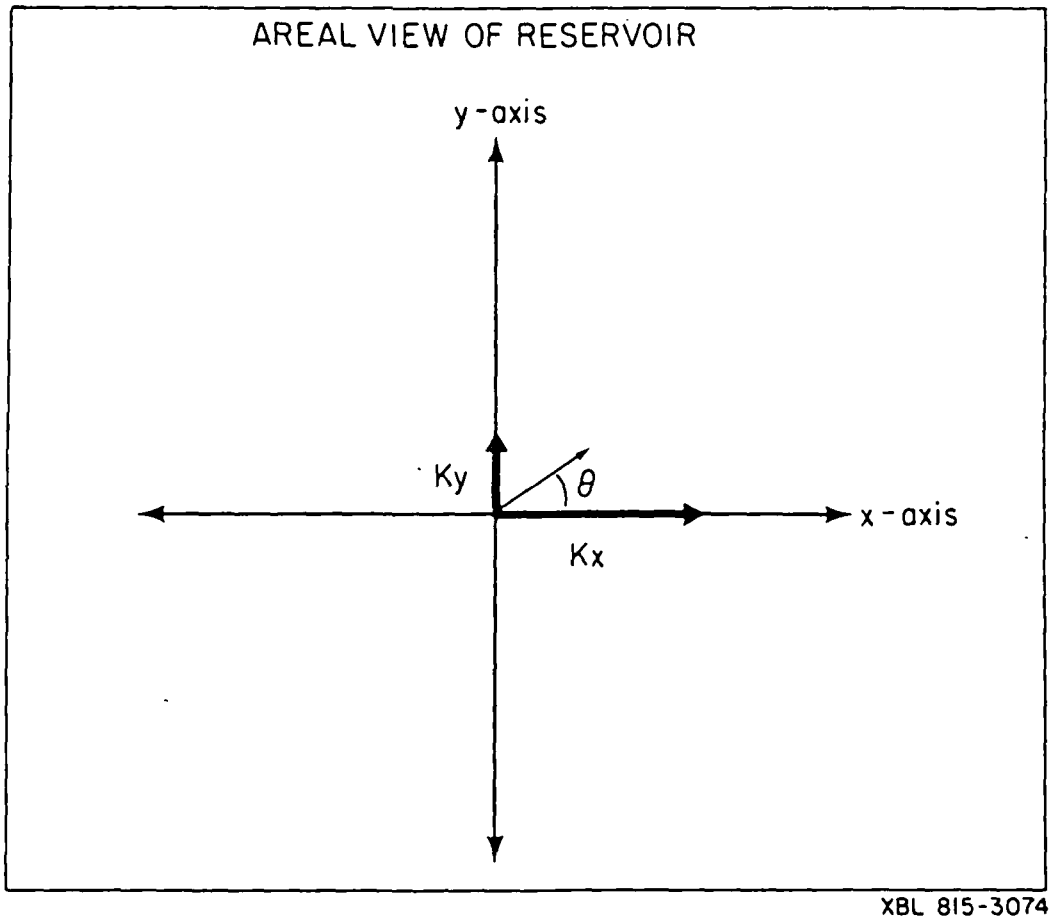

Figure E-2. Anisotropy representation.

$$(kH/\mu)_\theta = \frac{(kH/\mu)_x}{\cos^2\theta + \frac{(kH/\mu)_x}{(kH/\mu)_y}\sin^2\theta}$$

Theta is defined as the angle between the line adjoining the observation well and the production/injection well as measured counter-clockwise from a line parallel to the x-axis. (See Figure E-2). Since both $(kH/\mu)_e$ and η_θ are constants for any single production-observation well pair, the integral in Equation (E-4) may be evaluated analogously to the integral in Equation (E-1). In addition, because the reservoir is still homogeneous, regardless of the anisotropy, superposition of pressure responses, from each production well, is allowable.

Hydrologic Boundaries

A single fully penetrating linear hydrologic boundary can be modeled using the method of images.[E-5] Briefly stated, a boundary may be modeled as a line of bilateral symmetry about which image wells are arrayed in one-to-one symmetric correspondence with the real production/injection wells. Figure E-3 shows the image well locations for a case with two production wells and a barrier boundary. A barrier boundary is modeled by using image wells which have flow rates which are identical to the production/injection well counterparts. A constant potential boundary (leaky boundary) is modeled using image wells which have flow rates that are identical in magnitude but opposite in sign to the production/injection well counterparts. The image wells contribute an additional pressure response at each observation well.

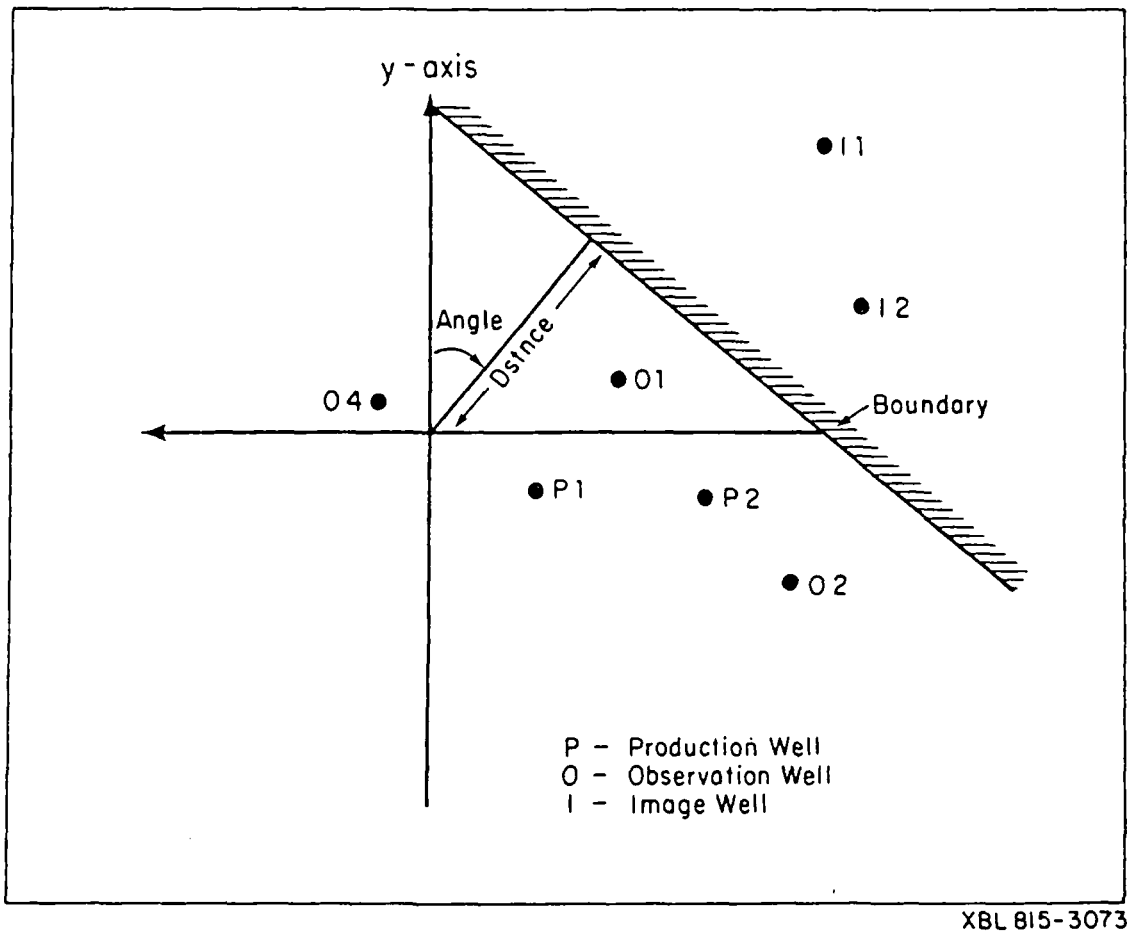

Figure E-3. Boundary location scheme.

Skin Effect

The calculated pressure response at a production well may also include the effects of a zone of enhancement or damage around a wellbore. The pressure change is calculated using the steady-state pressure change as defined below in Equation (E-5).[E-6]

$$\Delta P_{skin}(t) = s \frac{q(t)\mu}{2\pi kH} \qquad \text{(E-5)}$$

where

$q(t)$ = the instantaneous value of the flowrate at time t

s = the skin value

$\Delta P(t)_{skin}$ = the pressure change due to the skin at time t.

A damaged wellbore is indicated by a positive skin value and an enhanced wellbore is indicated by a negative skin value. When the reservoir is anisotropic, kH/μ is replaced by $(kH/\mu)_e$.

Program Input

Input Data Categories

Run Parameters and Problem Description. To run the program, the following information must be specified:

Variable name	Description
IHH	The number of observation wells in this run. (default 0) (maximum 10)

Variable name	Description
JJ	The number of production wells in this run. (default 0) (maximum 10)
IDIMEN	A flag to indicate that the data are not being input in S.I. units. (0 default--data are input in S.I. units) (1 set flag--data are not in S.I. units) See the following section for a description of the conversion factors.
NTIMES	The number of times at which pressure changes will be calculated. (default 0) (maximum 100)
RKHUX	The transmissivity $(kh/\mu)_x$ in the x-direction.
NOTE:	The x-axis is always a principal direction of anisotropy, and the second axis is at 90 degree to it, in the y direction. (default value 0.0) (default units $m^3/Pa \cdot s$)
RKHUY	The transmissivity $(kh/\mu)_y$ in the y-direction. (default value 0.0) (default units $m^3/Pa \cdot s$)
PCH	The storativity (ϕch). (default value 0.0) (default units m/Pa)

Variable name	Description
ANGLE	The azimuth to the boundary (see Figure E-3) measured clockwise from the positive y-axis.
DSTNCE	The perpendicular distance to the boundary from the origin of the coordinate system. (default value 0.0) (default units m)
BOUND	If the effects of a boundary are to be included, then the type of boundary, either barrier or constant potential, is input as an alphanumeric variable; either IOHBARRIER, or or IOHLEAKY,. which must be specified

Unit Conversion Factors. All parameter inputs are converted to S.I. units for internal calculation. At the termination of the calculation they are all converted back to the original input units. The conversion factor data required are listed below.

If IDIMEN was set to 1, the following information must be supplied. If IDIMEN is equal to 0, this data card is eliminated altogether.

Variable name	Description
PAPRESS	Number of pascals per pressure input unit.
CMSFLOW	Number of m^3/s per flow rate input unit.
SECTIME	Number of seconds per time input unit.

Variable name	Description
MLENGTH	Number of meters per length unit.
PASVISC	Number of pascal·seconds (Pa·s) per viscosity input unit.
SMPERM	Number of m^2 per permeability input unit.

Observation Well Locations and Specifications. The observation wells may be located at any position as specified by a set of x-y coordinates in a cartesian coordinate system. The following is a list of the specifications required for each observation well(I):

Variable	Description
NAME(I)	An alphanumeric name for the well. (default--blank)
OX(I)	The x-coordinate of the well. (default 0.) (default units m)
OY(I)	The y-coordinate of the well. (default 0.) (default units m)
YSTART(I)	The initial pressure at the well prior to any production or injection. (default units Pa)
LOBS(I)	A number (as read) that indicates that this observation well(I) is also production well LOBS(I). (Default 0 indicates the well is an interference monitoring well.)

Variable	Description
SKIN(I)	If the well(I) is also production well LOBS(I) the well may be assigned a non-zero skin value. (default 0. no skin)

Production Well Specifications and Flow Rate. To input a flow rate schedule, the data must be put in the format of pairs of flow rate points such that the flow rate is specified at the beginning and the end of a production pulse. Then, the flow rate, at all times, between the beginning and end of a production pulse, is known from Equation (E-3). The flow rate record will then consist of consecutive production pulses arranged in chronological order. If there is a step change from one flow rate to another, this is represented by two sequential production pulses, and must be input as such (see Sample Problem 1).

The following is a list of the specifications for each production well(J):

Variable	Description
PNAME(J)	An alphanumeric name for production well (J). (default value--BLANK)
PX(J)	The x-coordinate, in cartesian coordinates of production well(J). (default value 0.0) (default units m)
PY(J)	The y-coordinate, in cartesian coordinates, of production well(J). (default value 0.0) (default units m)

Variable	Description
KKJ(J)	The number of flow rate points for production well (J). (default value 0)
[TQ(K,J), AQ(K,J)]	The flow rate data points for well(J) which are of the form (time, flow rate). Up to 100 points per well are allowed. (default [0.0, 0.0]) (default units [s, m^3/s]) (K = 1, KKJ(J))

Times at Which Pressures Are To Be Calculated. Up to 100 different times can be specified at which pressure changes will be calculated:

Variable	Description
TIMES (L)	The times at which pressure calculations will be made up to 100 points. (default value 0.0) (default units, s)

INPUT DATA FORMAT

PROBLEM DESCRIPTION AND UNIT CONVERSION FACTORS

---

1 CARD	-	Title card alphanumeric to 80 characters	(8A10)
1 CARD	-	IHH, II, IDIMEN, NTIMES	(4I10)

If IDIMEN Is set equal to 1 on CARD 2

THEN INCLUDE

1 CARD - PAPRESS, CMSFLOW, SECTIME, RLENGTH, PASVISC, SMPERM (6E10.4)

OTHERWISE

1 CARD - RKHUX, RKHUY, PCH, ANGLE, DSTNCE, BOUND (5E10.4, A10)

OBSERVATION WELL DATA

IIH CARDS - NAME(I), OX(I), OY(I), YSTART(I),
LOBS(I), SKIN(I), etc.
(I = 1, IIH) (A10, 2F10.2, E10.4, I10, F10.2)

Repeat for each observation well.

PRODUCTION WELL DATA

JJ SETS OF CARDS - PNAME(J), PX(J), PY(J), KKJ(J) (A10, 2F10.2, I10)

TQ (1, J)	, AQ (1, J)	(2E10.4)
•	•	
•	•	
•	•	
•	•	
TQ (KKJ(J),J)	AQ (KKJ(J), J)	

Repeat this set of cards for each production well.

TIMES FOR CALCULATIONS OF PRESSURE CHANGES

TIMES(1), TIMES(2), TIMES(3),.....TIMES(8) (8E10.4)

Put eight per card - repeat until amount specified by NTIMES on CARD 2.

Sample Problems

Four sample problems are discussed in which the various capabilities of the program are demonstrated. Data decks and outputs are provided for each problem.

Sample Problem

No Anisotropy--Variable Flow Rate (Step-Wise)

In this problem a single production well is produced at a step wise variable flow rate and four observation wells monitor the pressure response. The observation wells are located symmetrically around the observation well (Figure E-4). Since there is no x-y reservoir anisotropy, the pressure drop at each of the observation wells should be identical. The flow rate from the production well is shown in Figure E-5. As is shown, there are three consecutive "production" pulses, the first two lasting 1000 minutes each, and the third lasting 2000 minutes.

The data deck for Sample 1 is shown in Figure E-6. The first card (card 1) gives the title information for the problem. The second card indicates that there are four observation wells (column 10, 1 production well (column 20), the IDIMEN flag is set (column 30) and the pressure changes will be calculated at 56 times (columns 30-40). On card three, the unit conversion factors are shown. The following table shows the units used for each quantity and the conversion factor to S.I. units.

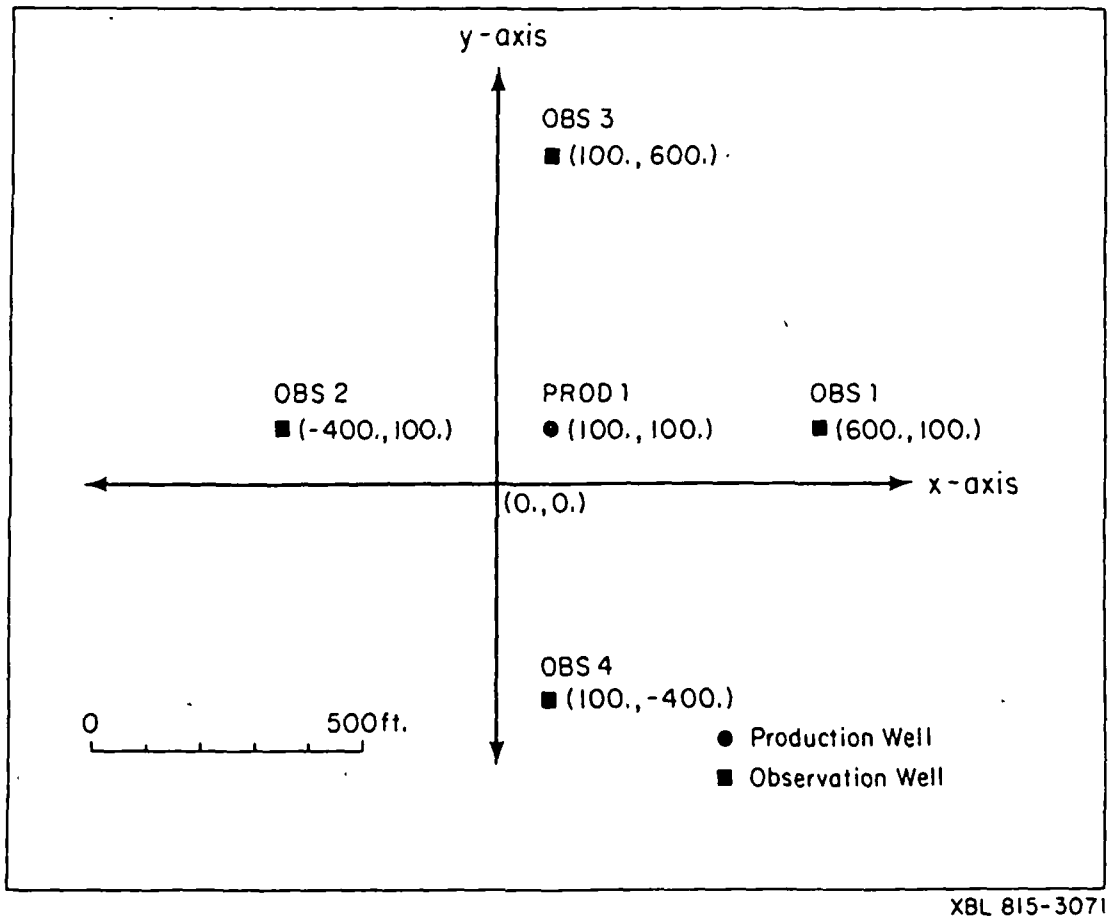

Figure E-4. Location scheme, in cartesian coordinates, for the production well and observation wells for Sample Problem 1.

Quantity	Unit	Conversion factor
Pressure	Psia	6895
Flow rate	Gal/min	6.31×10^{-5}
Time	Hours	3600
Length	Feet	0.3048
Viscosity	Centipoise	1×10^{-3}
Permeability	Millidarcies	9.862 x 10-16

It is important to note that once a time or distance unit is chosen, it must be used consistently throughout the input deck. For instance, when the flow rate is input, the time units must be the same as the time units used for the specification of times at which pressure calculations will be made.

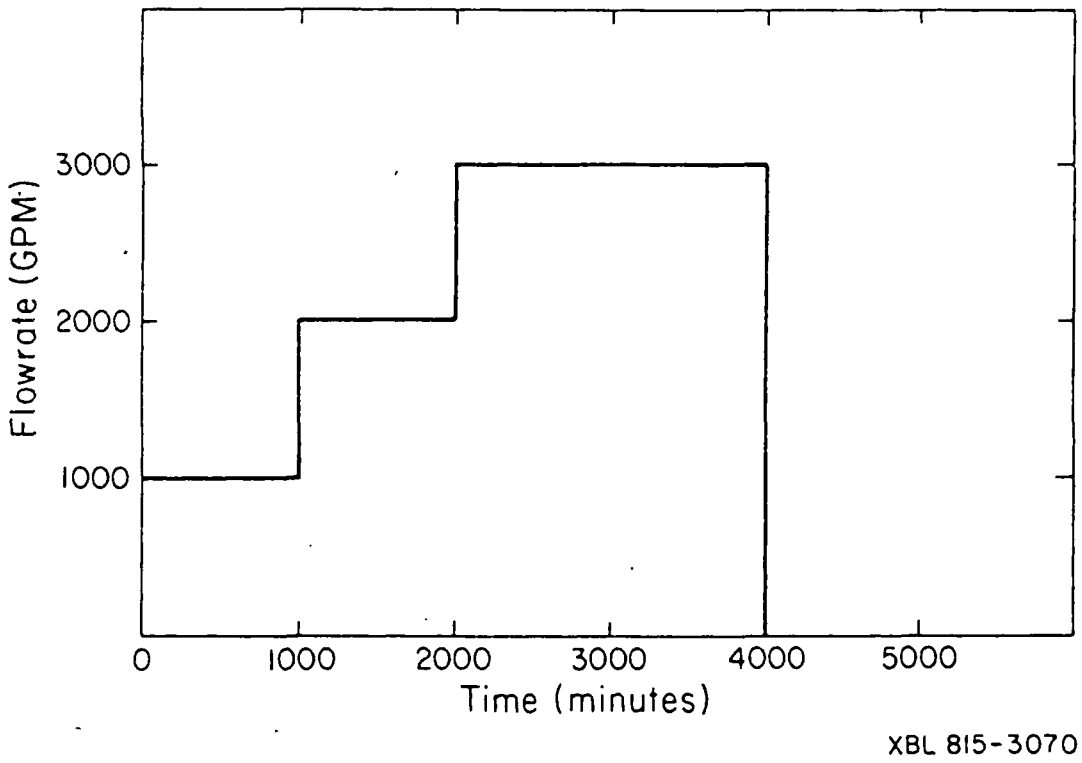

Figure E-5. Variable flow rate schedule for the production well in Sample Problem 1.

Card 4 lists the information about the x and y direction transmissivity and the reservoir storativity. For this problem, since there is no anisotropy, both the x-direction and y-direction transmissivity are equal and set to 150,000 md-ft/cp. The storativity for this problem is set equal to 2×10^{-3} ft/psi.

Cards 5 through 8 list the alphanumeric names for each observation well (columns 1-10), the (x,y) coordinates of each well (columns 11-20 and 21-30 respectively) and the initial reservoir pressure for each well (columns 31-40). The coordinates of each well are shown in Figure E-4.

Cards 9 through 15 contain all of the relevant information about the production well. On card 9, the alphanumeric name of the production well (column 1-10), the coordinates of the production well (columns 11-20, 21-30) and the number of flow rate points (columns 31-40, format I10) are input. For this problem six flow rate points are used to model the stepwise variable flow rate shown in Figure E-5. Note the construction of three "production pulses" to represent the flow rate.

CODED BY NOW NAME GEOTHERMAL PROGRAM VARFLOW DATE NOW

PROBLEM SAMPLE PROBLEM 1

DATA ENTRY FORMS

PAGE 1

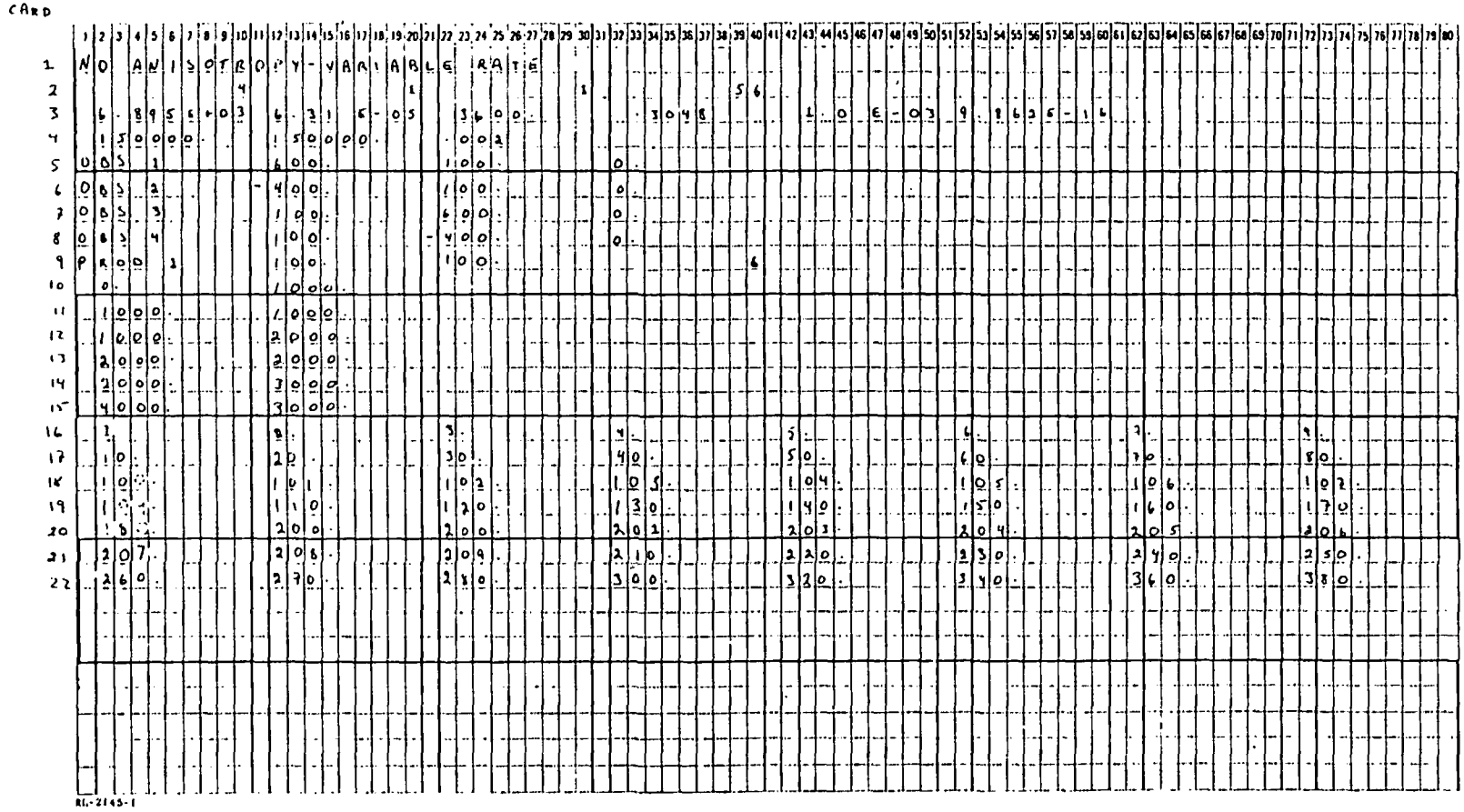

Figure E-6. Input deck for Sample Problem 1.

Cards 16 through 22 specify times at which pressure calculations, at each of the four observation wells, will be calculated. For this problem, pressures will be calculated at 1 hour, 2 hours, 3 hours, etc. to 380 hours. The units for the times specified here are input on card 3. If 3.6×10^3 s had not been specified, the default units would have been used, implying that pressures would be calculated at 1 s, 2 s, 3 s, etc., to 380 s.

The output for this problem is shown in Figure E-7. As can be seen, the pressure drop at each well is identical, because each well is equidistant from the production well (500 ft). The next sample problem will show a similar problem but one in which there is extreme x-y anisotropy.

```
 NO ANISOTROPY-VARIABLE FLOWRATE

NUMBER OF OBSERVATION WELLS          4
NUMBER OF PRODUCTION WELLS           1
NUMBER OF TIMES AT WHICH PRESSURES WILL BE CALCULATED        56

                  CONVERSION FACTORS
                  ==================

        PRESSURE UNIT PER PASCAL                          .6895E+04
        FLOWRATE UNIT PER CUBIC METER PER SECOND          .6310E-04
        TIME UNIT PER SECOND                               3600.00
        LENGTH PER METER                                       .30
        VISCOSITY PER PASCAL-SECOND                       .100E-02
        PERMEABILITY PER SQUARE METER                     .9862E-15

   PARAMETER VALUES
   ================
   X-AXIS TRANSIMISSIVITY = .1500E+06
   Y-AXIS TRANSMISSIVITY = .1500E+06
   STORATIVITY = .2000E-02


OBSERVATION WELL NUMBER      1
   WELL OBS   1     COORDINATES (     600.00,     100.00)
   INITIAL PRESSURE=0.


OBSERVATION WELL NUMBER      2
   WELL OBS 2       COORDINATES (    -400.00,     100.00)
   INITIAL PRESSURE=0.
```

Figure E-7. Output for Sample Problem 1.

```
OBSERVATION WELL NUMBER      3
   WELL OBS 3       COORDINATES (     100.00,     600.00)
   INITIAL PRESSURE=-.0

OBSERVATION WELL NUMBER      4
   WELL OBS 4       COORDINATES (     100.00,    -400.00)
   INITIAL PRESSURE=-.0

PRODUCTION WELL NUMBER            1
   PROD 1        COORDINATES (     100.00,     100.00)
   NUMBER OF FLOWRATE POINTS=     6

                      TIME          FLOWRATE

                    0.              .1000E+04
                     .1000E+03      .1000E+04
                     .1000E+03      .2000E+04
                     .2000E+03      .2000E+04
                     .2000E+03      .3000E+04
                     .4000E+03      .3000E+04

DISTANCES BETWEEN OBSERVATION WELLS AND PRODUCTION WELLS

          OBS   1      OBS 2        OBS 3        OBS 4
PROD 1         500.00       500.00       500.00       500.00

         TIME   OBS   1      OBS 2        OBS 3        OBS 4
          1.00  -.1715E+00  -.1715E+00  -.1715E+00  -.1715E+00
          2.00  -.1433E+01  -.1433E+01  -.1433E+01  -.1433E+01
          3.00  -.3238E+01  -.3238E+01  -.3238E+01  -.3238E+01
          4.00  -.5102E+01  -.5102E+01  -.5102E+01  -.5102E+01
          5.00  -.6878E+01  -.6878E+01  -.6878E+01  -.6878E+01

          6.00  -.8531E+01  -.8531E+01  -.8531E+01  -.8531E+01
          7.00  -.1006E+02  -.1006E+02  -.1006E+02  -.1006E+02
          9.00  -.1278E+02  -.1278E+02  -.1278E+02  -.1278E+02
         10.00  -.1400E+02  -.1400E+02  -.1400E+02  -.1400E+02
         20.00  -.2292E+02  -.2292E+02  -.2292E+02  -.2292E+02

         30.00  -.2867E+02  -.2867E+02  -.2867E+02  -.2867E+02
         40.00  -.3291E+02  -.3291E+02  -.3291E+02  -.3291E+02
         50.00  -.3627E+02  -.3627E+02  -.3627E+02  -.3627E+02
         60.00  -.3905E+02  -.3905E+02  -.3905E+02  -.3905E+02
         70.00  -.4142E+02  -.4142E+02  -.4142E+02  -.4142E+02
```

Figure E-7. (continued).

TIME	OBS 1	OBS 2	OBS 3	OBS 4
90.00	-.4349E+02	-.4349E+02	-.4349E+02	-.4349E+02
100.00	-.4697E+02	-.4697E+02	-.4697E+02	-.4697E+02
101.00	-.4729E+02	-.4729E+02	-.4729E+02	-.4729E+02
102.00	-.4871E+02	-.4871E+02	-.4871E+02	-.4871E+02
103.00	-.5067E+02	-.5067E+02	-.5067E+02	-.5067E+02
104.00	-.5268E+02	-.5268E+02	-.5268E+02	-.5268E+02
105.00	-.5461E+02	-.5461E+02	-.5461E+02	-.5461E+02
106.00	-.5641E+02	-.5641E+02	-.5641E+02	-.5641E+02
107.00	-.5809E+02	-.5809E+02	-.5809E+02	-.5809E+02
109.00	-.6110E+02	-.6110E+02	-.6110E+02	-.6110E+02
110.00	-.6246E+02	-.6246E+02	-.6246E+02	-.6246E+02
120.00	-.7275E+02	-.7275E+02	-.7275E+02	-.7275E+02
130.00	-.7976E+02	-.7976E+02	-.7976E+02	-.7976E+02
140.00	-.8517E+02	-.8517E+02	-.8517E+02	-.8517E+02
150.00	-.8962E+02	-.8962E+02	-.8962E+02	-.8962E+02
160.00	-.9342E+02	-.9342E+02	-.9342E+02	-.9342E+02
170.00	-.9675E+02	-.9675E+02	-.9675E+02	-.9675E+02
180.00	-.9973E+02	-.9973E+02	-.9973E+02	-.9973E+02
200.00	-.1049E+03	-.1049E+03	-.1049E+03	-.1049E+03
201.00	-.1053E+03	-.1053E+03	-.1053E+03	-.1053E+03
202.00	-.1068E+03	-.1068E+03	-.1068E+03	-.1068E+03
203.00	-.1088E+03	-.1088E+03	-.1088E+03	-.1088E+03
204.00	-.1109E+03	-.1109E+03	-.1109E+03	-.1109E+03
205.00	-.1129E+03	-.1129E+03	-.1129E+03	-.1129E+03
206.00	-.1148E+03	-.1148E+03	-.1148E+03	-.1148E+03
207.00	-.1165E+03	-.1165E+03	-.1165E+03	-.1165E+03
208.00	-.1182E+03	-.1182E+03	-.1182E+03	-.1182E+03
209.00	-.1197E+03	-.1197E+03	-.1197E+03	-.1197E+03
210.00	-.1211E+03	-.1211E+03	-.1211E+03	-.1211E+03
220.00	-.1322E+03	-.1322E+03	-.1322E+03	-.1322E+03
230.00	-.1399E+03	-.1399E+03	-.1399E+03	-.1399E+03
240.00	-.1460E+03	-.1460E+03	-.1460E+03	-.1460E+03
250.00	-.1511E+03	-.1511E+03	-.1511E+03	-.1511E+03
260.00	-.1555E+03	-.1555E+03	-.1555E+03	-.1555E+03
270.00	-.1594E+03	-.1594E+03	-.1594E+03	-.1594E+03
280.00	-.1630E+03	-.1630E+03	-.1630E+03	-.1630E+03
300.00	-.1693E+03	-.1693E+03	-.1693E+03	-.1693E+03
320.00	-.1747E+03	-.1747E+03	-.1747E+03	-.1747E+03
340.00	-.1794E+03	-.1794E+03	-.1794E+03	-.1794E+03
360.00	-.1838E+03	-.1838E+03	-.1838E+03	-.1838E+03
380.00	-.1877E+03	-.1877E+03	-.1877E+03	-.1877E+03

Figure E-7. (continued).

Sample Problem 2

Verification of Anisotropy. In Sample Problem 2 a well in an anisotropic reservoir is produced at a constant flow rate of 1000 GPM for a period of 5000 hours. Four observation wells, located symmetrically about the production well, along the major axes of anisotropy, are used to observe the pressure changes. For this problem, the x-axis permeability was chosen to be 150 times larger than the permeability in the y-direction. Thus, transmissivity values of 150,000 md*ft/cp and 1000 md*ft/cp were used. Figure E-8 shows the well location scheme and the representation of the reservoir anisotropy.

The data deck for Sample Problem 2 is shown in Figure E-9. The first three cards are the same as they are in Sample Problem 1. On card 4 the x-direction transmissivity (column 1-10) is set to 150,000 md*ft/cp, and

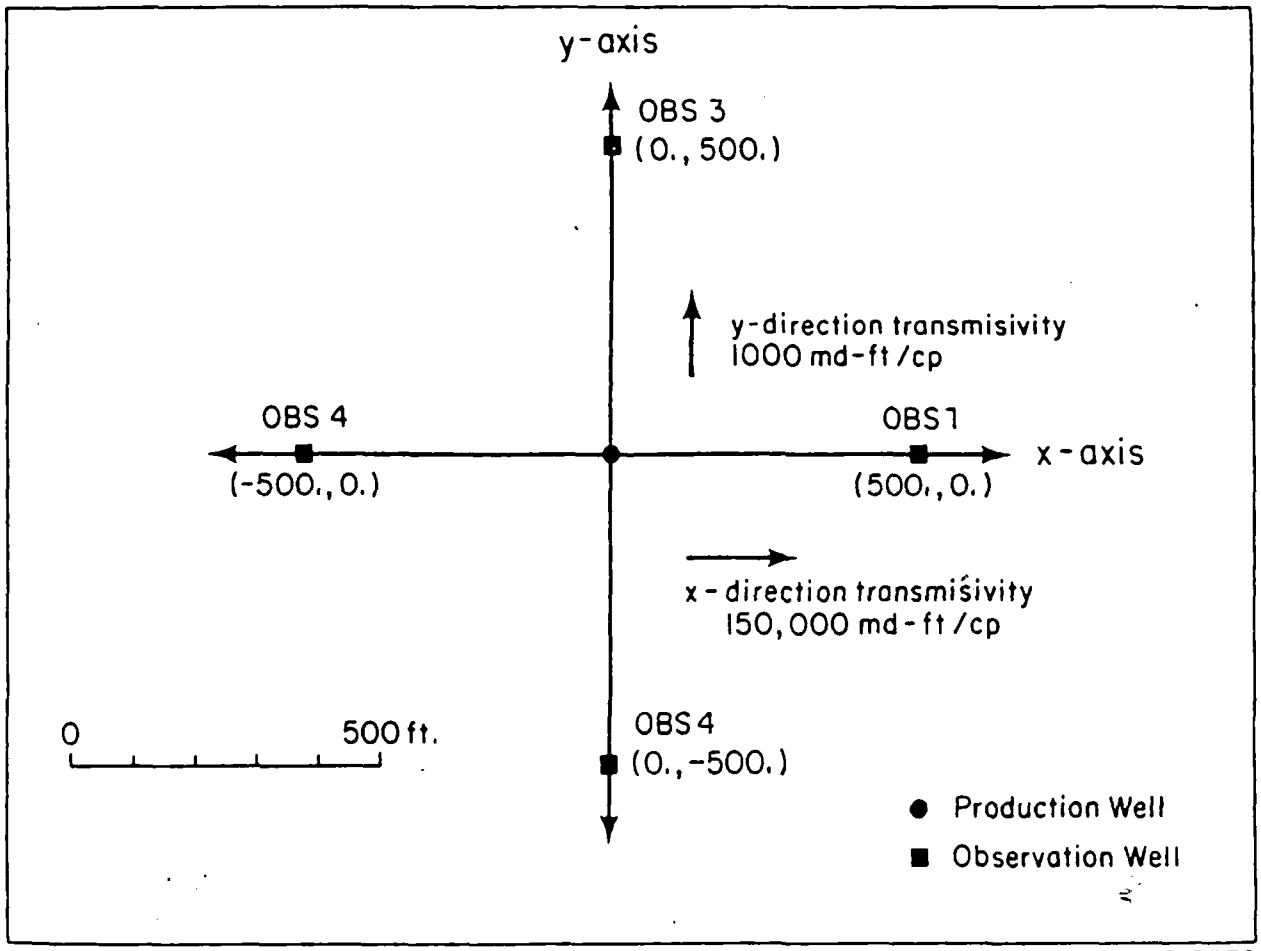

Figure E-8. Well location scheme for Sample Problems 2 and 3.

```
VERIFICATION OF ANISOTROPY
      04          1          1          56
6.895 E+03 5.310E-05   3.5E+03  .3048     1.0  E-03 9.862E-16
150000.    1000.      .002       00.        0000.
OBS   1      500.      0.          0.                0        0.
OBS 2       -500.      0.          0.
OBS 3        000.        500.
OBS 4        000.        -500.
PROD 1         0.         0.                  2
0.          1000.
5000.       1000.
1.          2.         3.         4.         5.         6.         7.         9.
10.         20.        30.        40.        50.        60.        70.        80.
100.        101.       102.       103.       104.       105.       106.       107.
109.        110.       120.       130.       140.       150.       160.       170.
180.        200.       201.       202.       203.       204.       205.       206.
207.        208.       209.       210.       220.       230.       240.       250.
260.        270.       280.       300.       320.       340.       360.       380.
```

Figure E-9. Input deck for Sample Problem 2.

the y-direction transmissivity is set to 1000 md*ft/cp. As in Problem 1, the storativity, ϕch, is set to 0.002 ft/psi. The remaining part of the data deck is similar to that in Problem 1, except that only one production pulse or two flow rate points are required to model the flow rate.

The output for Sample Problem 2 is shown in Figure E-10. Note the effect of the extreme anisotropy on the reservoir pressure response.

Sample Problem 3

Verification of Anisotropy--Boundary Problem. Sample Problem 3 is identical to Problem 2 except that there is a barrier boundary in the reservoir 1000 ft from the production well, in a direction perpendicular to the x-axis. Figure E-11 shows the well locations and the boundary location scheme. Note that the alpha is measured clockwise from the positive y-axis.

The data deck (Figure E-12) for this problem is identical to the data deck in Problem 2 except for card 4. Columns 1-10 and 11-20 contain the reservoir transmissivity information and columns 21-30 contain the storativity data. Alpha, the angle seen in Figure E-11, is input in columns 31-40 and DSTNCE, the distance from the origin to the perpendicular of the boundary, is input in columns 41-50. The type of boundary is indicated alphanumerically in columns 51-60. Note that the type, either BARRIER or LEAKY must begin in column 51.

```
VERIFICATION OF ANISOTROPY

NUMBER OF OBSERVATION WELLS          4
NUMBER OF PRODUCTION WELLS           1
NUMBER OF TIMES AT WHICH PRESSURES WILL BE CALCULATED        56

                CONVERSION FACTORS
                ==================

        PRESSURE UNIT PER PASCAL                          .6895E+04
        FLOWRATE UNIT PER CUBIC METER PER SECOND          .6310E-04
        TIME UNIT PER SECOND                               3600.00
        LENGTH PER METER                                       .30
        VISCOSITY PER PASCAL-SECOND                       .100E-02
        PERMEABILITY PER SQUARE METER                     .9862E-15

    PARAMETER VALUES
    ================
    X-AXIS TRANSIMISSIVITY = .1500E+06
    Y-AXIS TRANSMISSIVITY = .1000E+04
    STORATIVITY = .2000E-02

 OBSERVATION WELL NUMBER    1
    WELL OBS   1    COORDINATES (     500.00,       0.   )
    INITIAL PRESSURE=0.

 OBSERVATION WELL NUMBER     2
    WELL OBS 2      COORDINATES (    -500.00,       0.   )
    INITIAL PRESSURE=0.

 OBSERVATION WELL NUMBER     3
    WELL OBS 3      COORDINATES (       0.   ,     500.00)
    INITIAL PRESSURE=-.0

 OBSERVATION WELL NUMBER     4
    WELL OBS 4      COORDINATES (       0.   ,    -500.00)
    INITIAL PRESSURE=-.0

  PRODUCTION WELL NUMBER          1
     PROD 1      COORDINATES (       0.   ,       0.   )
     NUMBER OF FLOWRATE POINTS=     2

                    TIME          FLOWRATE

                    0.            .1000E+04
                   .5000E+04      .1000E+04

   DISTANCES BETWEEN OBSERVATION WELLS AND PRODUCTION WELLS

            OBS   1      OBS 2        OBS 3        OBS 4
  PROD 1      500.00       500.00       500.00       500.00
```

Figure E-10. Output for Sample Problem 2.

TIME	OBS 1	OBS 2	OBS 3	OBS 4
1.00	-.2131E+01	-.2101E+01	-.3917-206	-.3917-206
2.00	-.1755E+02	-.1755E+02	-.8058-103	-.8058-103
3.00	-.3966E+02	-.3966E+02	-.2625E-63	-.2625E-68
4.00	-.6251E+02	-.6249E+02	-.5152E-51	-.5152E-51
5.00	-.8436E+02	-.8424E+02	-.1286E-40	-.1286E-40
6.00	-.1045E+03	-.1045E+03	-.1136E-33	-.1136E-33
7.00	-.1239E+03	-.1232E+03	-.1064E-28	-.1064E-28
8.00	-.1397E+03	-.1356E+03	-.4742E-22	-.4742E-22
10.00	-.1746E+03	-.1715E+03	-.1025E-19	-.1025E-19
20.00	-.3029E+03	-.2815E+03	-.4294E-09	-.4294E-09
30.00	-.3936E+03	-.3553E+03	-.1870E-05	-.1870E-05
40.00	-.4754E+03	-.4131E+03	-.1373E-03	-.1373E-03
50.00	-.5399E+03	-.4618E+03	-.1916E-02	-.1916E-02
60.00	-.5954E+03	-.5043E+03	-.1151E-01	-.1151E-01
70.00	-.6441E+03	-.5424E+03	-.4241E-01	-.4241E-01
80.00	-.6875E+03	-.5769E+03	-.1147E+00	-.1147E+00
100.00	-.7522E+03	-.6377E+03	-.4767E+00	-.4767E+00
101.00	-.7555E+03	-.6405E+03	-.5048E+00	-.5048E+00
102.00	-.7588E+03	-.6432E+03	-.5341E+00	-.5341E+00
103.00	-.7722E+03	-.6561E+03	-.5644E+00	-.5644E+00
104.00	-.7755E+03	-.6589E+03	-.5959E+00	-.5959E+00
105.00	-.7788E+03	-.6617E+03	-.6286E+00	-.6286E+00
106.00	-.7821E+03	-.6642E+03	-.6624E+00	-.6624E+00
107.00	-.7853E+03	-.6669E+03	-.6975E+00	-.6975E+00
109.00	-.7917E+03	-.6723E+03	-.7712E+00	-.7712E+00
110.00	-.7946E+03	-.6749E+03	-.8098E+00	-.8098E+00
120.00	-.8250E+03	-.6703E+03	-.1267E+01	-.1267E+01
130.00	-.8530E+03	-.7141E+03	-.1861E+01	-.1861E+01
140.00	-.8792E+03	-.7365E+03	-.2597E+01	-.2597E+01
150.00	-.9038E+03	-.7579E+03	-.3480E+01	-.3480E+01
160.00	-.9269E+03	-.7780E+03	-.4509E+01	-.4509E+01
170.00	-.9493E+03	-.7972E+03	-.5683E+01	-.5683E+01
180.00	-.9696E+03	-.8156E+03	-.6997E+01	-.6997E+01
200.00	-.1009E+04	-.8498E+03	-.1002E+02	-.1002E+02
201.00	-.1013E+04	-.8514E+03	-.1019E+02	-.1019E+02
202.00	-.1012E+04	-.8530E+03	-.1035E+02	-.1035E+02
203.00	-.1013E+04	-.8546E+03	-.1052E+02	-.1052E+02
204.00	-.1015E+04	-.8563E+03	-.1069E+02	-.1069E+02
205.00	-.1017E+04	-.8579E+03	-.1086E+02	-.1086E+02
206.00	-.1019E+04	-.8596E+03	-.1103E+02	-.1103E+02

Figure E-10. (continued)..

TIME	OBS 1	OBS 2	OBS 3	OBS 4
207.00	-.7160E+03	-.7160E+03	-.6501E+01	-.6501E+01
208.00	-.7169E+03	-.7169E+03	-.6598E+01	-.6598E+01
209.00	-.7178E+03	-.7178E+03	-.6695E+01	-.6695E+01
210.00	-.7188E+03	-.7188E+03	-.6793E+01	-.6793E+01
220.00	-.7278E+03	-.7278E+03	-.7806E+01	-.7806E+01
230.00	-.7365E+03	-.7365E+03	-.8874E+01	-.8874E+01
240.00	-.7448E+03	-.7448E+03	-.9992E+01	-.9992E+01
250.00	-.7528E+03	-.7528E+03	-.1116E+02	-.1116E+02
260.00	-.7604E+03	-.7604E+03	-.1236E+02	-.1236E+02
270.00	-.7678E+03	-.7678E+03	-.1361E+02	-.1361E+02
280.00	-.7749E+03	-.7749E+03	-.1489E+02	-.1489E+02
300.00	-.7884E+03	-.7884E+03	-.1755E+02	-.1755E+02
320.00	-.8011E+03	-.8011E+03	-.2031E+02	-.2031E+02
340.00	-.8129E+03	-.8129E+03	-.2316E+02	-.2316E+02
360.00	-.8241E+03	-.8241E+03	-.2607E+02	-.2607E+02
380.00	-.8348E+03	-.8348E+03	-.2904E+02	-.2904E+02

Figure E-10. (continued).

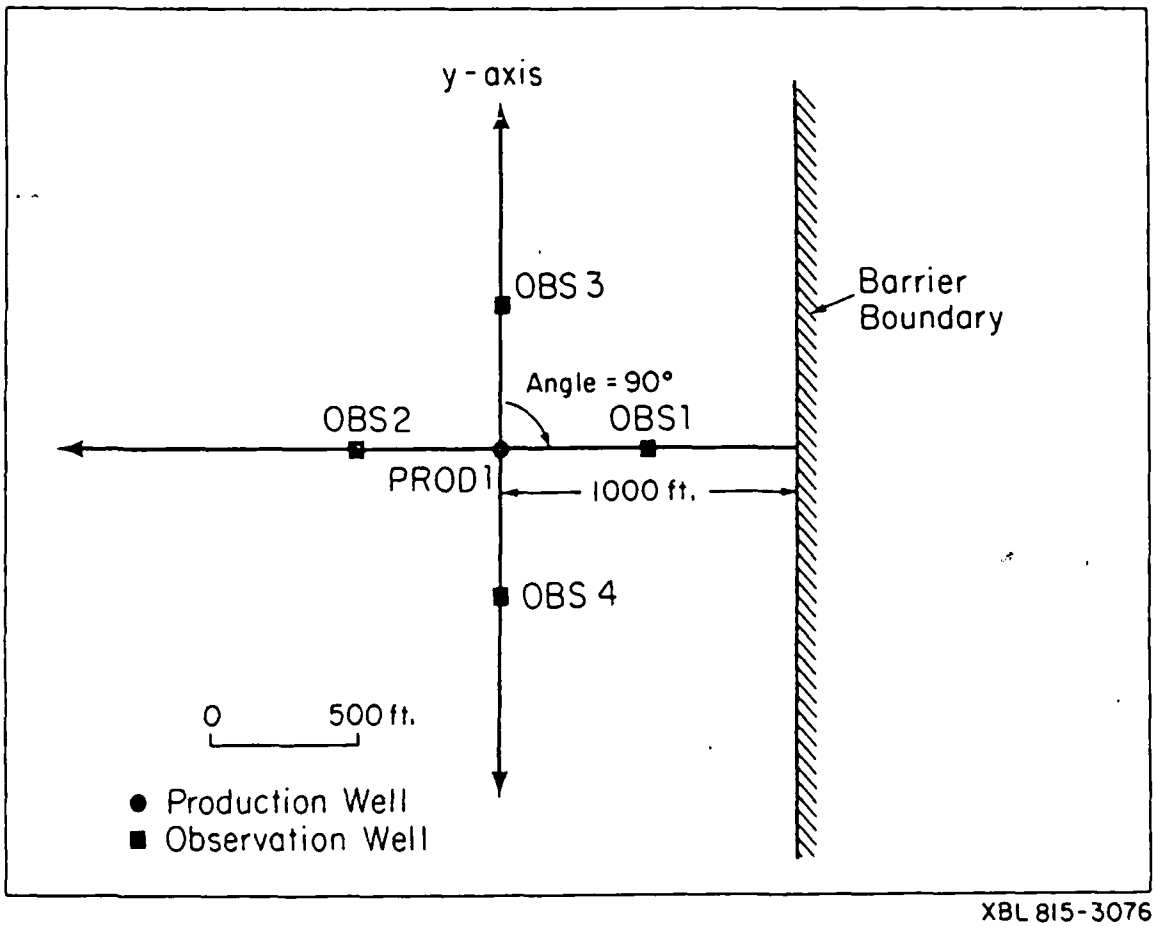

Figure E-11. Boundary location scheme for Sample Problem 3.

```
VERIFICATION OF ANISOTROPY-RUN TO COMPARE WITH BOUNDARY
        04          1          1          56
6.895 E+03 6.310E-05   3.6E+03   .3048     1.0  E-03 9.862E-16
150000.    1000.      .002       90.       1000.      BARRIER
OBS  1      500.       0.         0.                 0          0.
OBS 2      -500.       0.         0.
OBS 3       000.      500.
OBS 4       000.     -500.
PROD 1        0.        0.                   2
0.         1000.
5000.      1000.
1.         2.         3.         4.         5.         6.         7.         9.
10.        20.        30.        40.        50.        60.        70.        80.
100.       101.       102.       103.       104.       105.       106.       107.
109.       110.       120.       130.       140.       150.       160.       170.
180.       200.       201.       202.       203.       204.       205.       206.
207.       208.       209.       210.       220.       230.       240.       250.
260.       270.       280.       300.       320.       340.       360.       380.
```

Figure E-12. Input deck for Sample Problem 3.

The output for the Sample Problem 3 is shown in Figure E-13.

Sample Problem 4

Verification of Anisotropy--Run to Compare with Boundary. Sample Problem 4 demonstrates how the algorithm in VARFLOW accounts for the effects of a barrier or constant potential boundary in the pressure calculations. In this calculation the existence of a boundary is not specified, however, a well which would be the image well for the calculation in Sample Problem 3 is explicitly included in the calculation. The well locations for the observation wells, the production well and the "image" production well are shown in Figure E-14.

The input deck (Figure E-15) for the problem is similar to the data decks in problems 2 and 3. Note that on Card 2, Column 20, it is specified that there are two production wells for this problem. The production data and production well specifications for the second production well, PROD2, are on Cards 12-14. Note that the production rate for PROD2 is identical to that of PROD1.

The output for this problem is shown in Figure E-16. Note that the pressure response is identical to the pressure response in Problem 3.

```
VERIFICATION OF ANISOTROPY-RUN TO COMPARE WITH BOUNDARY

NUMBER OF OBSERVATION WELLS          4
NUMBER OF PRODUCTION WELLS           1
NUMBER OF TIMES AT WHICH PRESSURES WILL BE CALCULATED        56

                CONVERSION FACTORS
                ******************

        PRESSURE UNIT PER PASCAL                        .6895E+04
        FLOWRATE UNIT PER CUBIC METER PER SECOND        .6310E-04
        TIME UNIT PER SECOND                             3600.00
        LENGTH PER METER                                     .30
        VISCOSITY PER PASCAL-SECOND                      .100E-02
        PERMEABILITY PER SQUARE METER                   .9862E-15

    PARAMETER VALUES
    ****************
    X-AXIS TRANSMISSIVITY = .1500E+06
    Y-AXIS TRANSMISSIVITY = .1000E+04
    STORATIVITY = .2000E-02

THERE IS A BARRIER  BOUNDARY AT AN ANGLE OF      90.00 DEGREES AND A DISTANCE OF    1000.00

OBSERVATION WELL NUMBER     1
   WELL OBS  1    COORDINATES (     500.00,       0.  )
   INITIAL PRESSURE=0.

OBSERVATION WELL NUMBER     2
   WELL OBS 2     COORDINATES (    -500.00,       0.  )
   INITIAL PRESSURE=0.

OBSERVATION WELL NUMBER     3
   WELL OBS 3     COORDINATES (       0.  ,     500.00)
   INITIAL PRESSURE=-.0

OBSERVATION WELL NUMBER     4
   WELL OBS 4     COORDINATES (       0.  ,    -500.00)
   INITIAL PRESSURE=-.0

PRODUCTION WELL NUMBER          1
   PROD 1      COORDINATES (       0.  ,       0.  )
   NUMBER OF FLOWRATE POINTS=    2

                    TIME          FLOWRATE

                   0.              .1000E+04
                   .5000E+04       .1000E+04

DISTANCES BETWEEN OBSERVATION WELLS AND PRODUCTION WELLS

          OBS  1     OBS 2      OBS 3      OBS 4
PROD 1      500.00     500.00     500.00     500.00
```

Figure E-13. Output for Sample Problem 3.

TIME	OBS 1	OBS 2	OBS 3	OBS 4
1.00	-.2101E+01	-.2101E+01	-.3917-206	-.3917-206
2.00	-.1755E+02	-.1755E+02	-.8058-103	-.8058-103
3.00	-.3766E+02	-.3766E+02	-.2625E-68	-.2625E-68
4.00	-.6251E+02	-.6249E+02	-.5152E-51	-.5152E-51
5.00	-.9435E+02	-.9424E+02	-.1286E-40	-.1286E-40
6.00	-.1045E+03	-.1045E+03	-.1136E-33	-.1136E-33
7.00	-.1239E+03	-.1232E+03	-.1064E-28	-.1064E-28
9.00	-.1587E+03	-.1566E+03	-.4742E-22	-.4742E-22
10.00	-.1746E+03	-.1715E+03	-.1025E-19	-.1025E-19
20.00	-.3027E+03	-.2815E+03	-.4294E-09	-.4294E-09
30.00	-.3955E+03	-.3553E+03	-.1870E-05	-.1870E-05
40.00	-.4754E+03	-.4131E+03	-.1373E-03	-.1373E-03
50.00	-.5399E+03	-.4616E+03	-.1916E-02	-.1916E-02
60.00	-.5954E+03	-.5043E+03	-.1151E-01	-.1151E-01
70.00	-.6441E+03	-.5424E+03	-.4241E-01	-.4241E-01
80.00	-.6875E+03	-.5769E+03	-.1147E+00	-.1147E+00
100.00	-.7522E+03	-.6377E+03	-.4767E+00	-.4767E+00
101.00	-.7556E+03	-.6405E+03	-.5048E+00	-.5048E+00
102.00	-.7589E+03	-.6433E+03	-.5341E+00	-.5341E+00
103.00	-.7622E+03	-.6461E+03	-.5644E+00	-.5644E+00
104.00	-.7655E+03	-.6488E+03	-.5959E+00	-.5959E+00
105.00	-.7688E+03	-.6515E+03	-.6286E+00	-.6286E+00
106.00	-.7721E+03	-.6542E+03	-.6624E+00	-.6624E+00
107.00	-.7753E+03	-.6569E+03	-.6975E+00	-.6975E+00
109.00	-.7817E+03	-.6623E+03	-.7712E+00	-.7712E+00
110.00	-.7948E+03	-.6649E+03	-.8098E+00	-.8098E+00
120.00	-.8250E+03	-.6903E+03	-.1267E+01	-.1267E+01
130.00	-.8530E+03	-.7141E+03	-.1861E+01	-.1861E+01
140.00	-.8792E+03	-.7365E+03	-.2597E+01	-.2597E+01
150.00	-.9038E+03	-.7579E+03	-.3480E+01	-.3480E+01
160.00	-.9269E+03	-.7780E+03	-.4509E+01	-.4509E+01
170.00	-.9488E+03	-.7972E+03	-.5683E+01	-.5683E+01
180.00	-.9695E+03	-.8155E+03	-.6997E+01	-.6997E+01
200.00	-.1008E+04	-.8496E+03	-.1002E+02	-.1002E+02
201.00	-.1013E+04	-.8514E+03	-.1019E+02	-.1019E+02
202.00	-.1012E+04	-.8530E+03	-.1036E+02	-.1035E+02
203.00	-.1013E+04	-.8546E+03	-.1052E+02	-.1052E+02
204.00	-.1015E+04	-.8563E+03	-.1069E+02	-.1069E+02
205.00	-.1017E+04	-.8579E+03	-.1086E+02	-.1086E+02
206.00	-.1019E+04	-.8595E+03	-.1103E+02	-.1103E+02

Figure E-13. (continued).

TIME	OBS 1	OBS 2	OBS 3	OBS 4
207.00	-.1021E+04	-.9511E+03	-.1120E+02	-.1120E+02
208.00	-.1022E+04	-.8627E+03	-.1137E+02	-.1137E+02
209.00	-.1024E+04	-.8642E+03	-.1155E+02	-.1155E+02
210.00	-.1026E+04	-.8659E+03	-.1172E+02	-.1172E+02
220.00	-.1043E+04	-.8813E+03	-.1354E+02	-.1354E+02
230.00	-.1059E+04	-.8961E+03	-.1546E+02	-.1546E+02
240.00	-.1075E+04	-.9104E+03	-.1747E+02	-.1747E+02
250.00	-.1090E+04	-.9243E+03	-.1959E+02	-.1959E+02
260.00	-.1105E+04	-.9376E+03	-.2178E+02	-.2178E+02
270.00	-.1119E+04	-.9505E+03	-.2406E+02	-.2406E+02
280.00	-.1133E+04	-.9630E+03	-.2641E+02	-.2641E+02
300.00	-.1158E+04	-.9869E+03	-.3129E+02	-.3129E+02
320.00	-.1183E+04	-.1009E+04	-.3640E+02	-.3640E+02
340.00	-.1206E+04	-.1031E+04	-.4169E+02	-.4169E+02
360.00	-.1227E+04	-.1051E+04	-.4712E+02	-.4712E+02
380.00	-.1248E+04	-.1070E+04	-.5268E+02	-.5268E+02

Figure E-13. (continued).

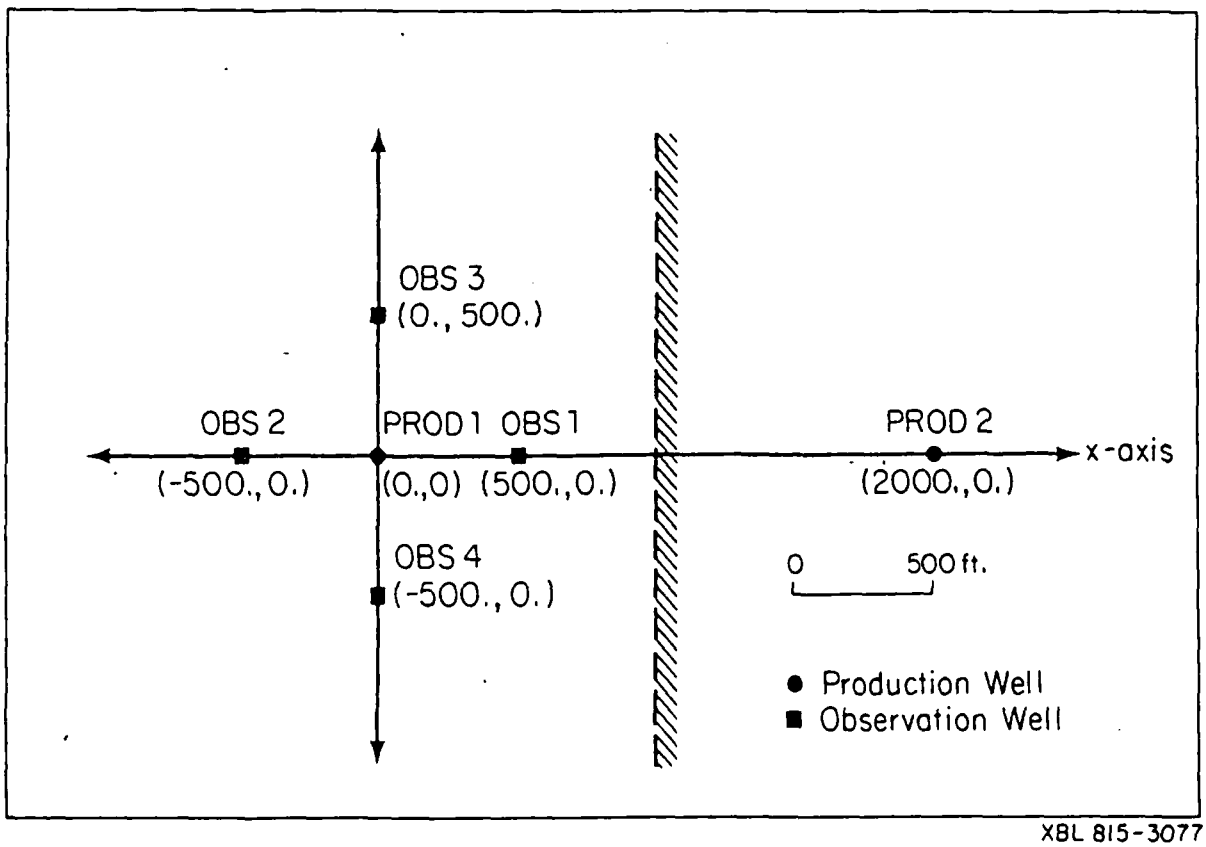

Figure E-14. Observation well locations, production well location, and "image" well location for Sample Problem 4.

```
VERIFICATION OF ANISOTROPY-RUN TO COMPARE WITH BOUNDARY
 04          2          1          56
6.895 E+03 6.310E-05   3.6E+03  .3048    1.0  E-03 9.862E-16
150000.    1000.      .002        0.          0.
OBS  1      500.       0.          0.              0        0.
OBS 2      -500.       0.          0.
OBS 3       000.       500.
OBS 4       000.      -500.
PROD 1        0.        0.              2
0.          1000.
5000.       1000.
PROD 2      2000.       0.              2
0.          1000.
5000.       1000.
 1.          2.          3.          4.          5.          6.          7.          9.
 10.         20.         30.         40.         50.         60.         70.         80.
 100.        101.        102.        103.        104.        105.        106.        107.
 109.        110.        120.        130.        140.        150.        160.        170.
 180.        200.        201.        202.        203.        204.        205.        206.
 207.        208.        209.        210.        220.        230.        240.        250.
 260.        270.        280.        300.        320.        340.        360.        380.
```

Figure E-15. Input deck for Sample Problem 4.

```
VERIFICATION OF ANISOTROPY-RUN TO COMPARE WITH BOUNDARY

NUMBER OF OBSERVATION WELLS                              4
NUMBER OF PRODUCTION WELLS                               2
NUMBER OF TIMES AT WHICH PRESSURES WILL BE CALCULATED                56

                    CONVERSION FACTORS
                    ==================

          PRESSURE UNIT PER PASCAL                          .6895E+04
          FLOWRATE UNIT PER CUBIC METER PER SECOND          .6310E-04
          TIME UNIT PER SECOND                               3600.00
          LENGTH PER METER                                       .30
          VISCOSITY PER PASCAL-SECOND                        .100E-02
          PERMEABILITY PER SQUARE METER                      .9862E-15


     PARAMETER VALUES
     ================
     X-AXIS TRANSMISSIVITY = .1500E+06
     Y-AXIS TRANSMISSIVITY = .1000E+04
     STORATIVITY = .2000E-02


OBSERVATION WELL NUMBER      1
     WELL OBS   1    COORDINATES (      500.00,        0.   )
     INITIAL PRESSURE=0.
```

Figure E-16. Output for Sample Problem 4.

```
OBSERVATION WELL NUMBER      2
   WELL OBS 2       COORDINATES (    -500.00,       0.   )
   INITIAL PRESSURE=0.


OBSERVATION WELL NUMBER      3
   WELL OBS 3       COORDINATES (       0.   ,     500.00)
   INITIAL PRESSURE=-.0


OBSERVATION WELL NUMBER      4
   WELL OBS 4       COORDINATES (       0.   ,    -500.00)
   INITIAL PRESSURE=-.0


  PRODUCTION WELL NUMBER           1
     PROD 1        COORDINATES (       0.   ,       0.   )
     NUMBER OF FLOWRATE POINTS=     2

                       TIME           FLOWRATE


                     0.                .1000E+04
                      .5000E+04        .1000E+04


  PRODUCTION WELL NUMBER           2
     PROD 2        COORDINATES (    2000.00,       0.   )
     NUMBER OF FLOWRATE POINTS=     2

                       TIME           FLOWRATE


                     0.                .1000E+04
                      .5000E+04        .1000E+04


  DISTANCES BETWEEN OBSERVATION WELLS AND PRODUCTION WELLS

            OBS   1      OBS 2        OBS 3        OBS 4
  PROD 1        500.00       500.00       500.00       500.00
  PROD 2       1500.00      2500.00      2061.55      2061.55
```

Figure E-16. (continued).

TIME	OBS 1	OBS 2	OBS 3	OBS 4
1.00	-.2101E+01	-.2101E+01	-.3917-206	-.3917-206
2.00	-.1755E+02	-.1755E+02	-.8058-103	-.8058-103
3.00	-.3966E+02	-.3966E+02	-.2625E-68	-.2625E-68
4.00	-.6249E+02	-.6249E+02	-.5152E-51	-.5152E-51
5.00	-.8424E+02	-.8424E+02	-.1286E-40	-.1286E-40
6.00	-.1045E+03	-.1045E+03	-.1135E-33	-.1135E-33
7.00	-.1232E+03	-.1232E+03	-.1063E-28	-.1063E-28
9.00	-.1566E+03	-.1566E+03	-.4727E-22	-.4727E-22
10.00	-.1715E+03	-.1715E+03	-.1020E-19	-.1020E-19
20.00	-.2807E+03	-.2807E+03	-.4004E-09	-.4004E-09
30.00	-.3512E+03	-.3512E+03	-.1601E-05	-.1601E-05
40.00	-.4031E+03	-.4031E+03	-.1092E-03	-.1092E-03
50.00	-.4442E+03	-.4442E+03	-.1440E-02	-.1440E-02
60.00	-.4783E+03	-.4783E+03	-.8268E-02	-.8268E-02
70.00	-.5073E+03	-.5073E+03	-.2939E-01	-.2939E-01
80.00	-.5326E+03	-.5326E+03	-.7720E-01	-.7720E-01
100.00	-.5752E+03	-.5752E+03	-.3071E+00	-.3071E+00
101.00	-.5771E+03	-.5771E+03	-.3246E+00	-.3246E+00
102.00	-.5790E+03	-.5790E+03	-.3428E+00	-.3428E+00
103.00	-.5809E+03	-.5809E+03	-.3617E+00	-.3617E+00
104.00	-.5828E+03	-.5828E+03	-.3812E+00	-.3812E+00
105.00	-.5846E+03	-.5846E+03	-.4014E+00	-.4014E+00
106.00	-.5864E+03	-.5864E+03	-.4223E+00	-.4223E+00
107.00	-.5882E+03	-.5882E+03	-.4439E+00	-.4439E+00
109.00	-.5918E+03	-.5918E+03	-.4893E+00	-.4893E+00
110.00	-.5935E+03	-.5935E+03	-.5130E+00	-.5130E+00
120.00	-.6103E+03	-.6103E+03	-.7912E+00	-.7912E+00
130.00	-.6257E+03	-.6257E+03	-.1147E+01	-.1147E+01
140.00	-.6400E+03	-.6400E+03	-.1583E+01	-.1583E+01
150.00	-.6534E+03	-.6534E+03	-.2101E+01	-.2101E+01
160.00	-.6659E+03	-.6659E+03	-.2699E+01	-.2699E+01
170.00	-.6777E+03	-.6777E+03	-.3375E+01	-.3375E+01
180.00	-.6888E+03	-.6888E+03	-.4126E+01	-.4126E+01
200.00	-.7093E+03	-.7093E+03	-.5840E+01	-.5840E+01
201.00	-.7102E+03	-.7102E+03	-.5932E+01	-.5932E+01
202.00	-.7112E+03	-.7112E+03	-.6026E+01	-.6026E+01
203.00	-.7122E+03	-.7122E+03	-.6119E+01	-.6119E+01
204.00	-.7131E+03	-.7131E+03	-.6214E+01	-.6214E+01
205.00	-.7141E+03	-.7141E+03	-.6309E+01	-.6309E+01
206.00	-.7150E+03	-.7150E+03	-.6405E+01	-.6405E+01

Figure E-16. (continued).

TIME	OBS 1	OBS 2	OBS 3	OBS 4
207.00	-.1021E+04	-.8611E+03	-.1120E+02	-.1120E+02
208.00	-.1022E+04	-.8627E+03	-.1137E+02	-.1137E+02
209.00	-.1024E+04	-.8642E+03	-.1155E+02	-.1155E+02
210.00	-.1026E+04	-.8658E+03	-.1172E+02	-.1172E+02
220.00	-.1043E+04	-.8813E+03	-.1354E+02	-.1354E+02
230.00	-.1059E+04	-.8961E+03	-.1546E+02	-.1546E+02
240.00	-.1075E+04	-.9104E+03	-.1747E+02	-.1747E+02
250.00	-.1090E+04	-.9243E+03	-.1959E+02	-.1959E+02
260.00	-.1105E+04	-.9376E+03	-.2178E+02	-.2178E+02
270.00	-.1119E+04	-.9505E+03	-.2406E+02	-.2406E+02
280.00	-.1133E+04	-.9630E+03	-.2641E+02	-.2641E+02
300.00	-.1158E+04	-.9869E+03	-.3129E+02	-.3129E+02
320.00	-.1183E+04	-.1009E+04	-.3640E+02	-.3640E+02
340.00	-.1206E+04	-.1031E+04	-.4169E+02	-.4169E+02
350.00	-.1227E+04	-.1051E+04	-.4712E+02	-.4712E+02
380.00	-.1248E+04	-.1070E+04	-.5268E+02	-.5268E+02

Figure E-16. (continued).

```
                        **PROGRAM VARFLOW(INPUT,OUTPUT,TAPE1,TAPE2)**

  1.   0000008          PROGRAM VARFLOW(INPUT,OUTPUT,TAPE1,TAPE2)
                  C
                  CCCCCCCCCCCCCCCCCCCCCCCCCCCCCCCCCCCCCCCCCCCCCCCCCCCCCCCCCCCCCCCCCCC
                  C
                  C     THIS PROGRAM CALCULTES DRAWDOWN IN AN ANISOTROPIC,HOMOGENEOUS,
                  C     CONSTANT THICKNESS POROUS MEDIUM. THERE CAN BE UP TO 10
                  C     PRODUCTION WELLS AND TEN OBSERVATION WELLS. FLOWRATES
                  C     CAN BE VARIABLE. THE PROGRAM CAN ALSO INCLUDE DRAWDOWN DUE TO
                  C     SKIN EFFECTS AND A SINGLE LINEAR RESERVOIR BOUNDARY (BARRIER
                  C     OR CONSTANT POTENTIAL).
                  C
  2.   0022058          DIMENSION X(3),TITLE(8),YSTART(10),LOBS(10),KKJ(10),ROY(10),
                       $SKIN(10),R(10,10),TIMES(100),RI2(10,10),OX(10),OY(10),ROX(10),
                       $PX(10),PY(10),AQ(100,10),TQ(100,10),BQ(100,10),YCALC(100,10)
                       $,NAME(10),PNAME(10),RPX(10),RPY(10),RIPX(10),RIPY(10)
  3.   0022058          COMMON /SUB/ PI
  4.   0022058          DATA ((KKJ(J),J=1,10),L)/11*0/
  5.   0022058          DATA (PI,PAPRESS,CMSFLOW,SECTIME,RLENGTH,SMPERM,PASVISC)
                       &/3.14159265,6*1.0/
                  CCCCCCCCCCCCCCCCCCCCCCCCCCCCCCCCCCCCCCCCCCCCCCCCCCCCCCCCCCCCCCCCCCCC
                  C           READ IN ALL OF THE PROBLEM PARAMETERS AND FLOW RATE DATA
                  C           PRINT OUT ALL OF THE ABOVE
  6.   0022058
  7.   0022058          READ 100,(TITLE(I),I=1,8)
  8.   0130128   100    FORMAT(8A10)
  9.   0130128          PRINT 200, (TITLE(I),I=1,8)
 10.   0130218   200    FORMAT(1H1,2X,8A10)
 11.   0130218          READ 101,IHH,JJ,IDIMEN,NTIMES
 12.   0130308   101    FORMAT(4I10)
 13.   0130308          PRINT 201,IHH,JJ,NTIMES
 14.   0130368   201    FORMAT(//,*  NUMBER OF OBSERVATION WELLS*,I10,
                       $/,*  NUMBER OF PRODUCTION WELLS *,I10,
                       $/,*  NUMBER OF TIMES AT WHICH PRESSURES WILL BE CALCULATED*,I10)
 15.   0130368          IF(IDIMEN  .EQ.    0)GO TO 10
 16.   0130378          READ 102,PAPRESS,CMSFLOW,SECTIME,RLENGTH,PASVISC,SMPERM
 17.   0130508   102    FORMAT(6E10.4)
 18.   0130508   10     PRINT 202,PAPRESS,CMSFLOW,SECTIME,RLENGTH,PASVISC,SMPERM
 19.   0130618   202    FORMAT(//,20X,*CONVERSION FACTORS*,/,20X,18(1H=),/,
                       $/,10X,*PRESSURE UNIT PER PASCAL*,21X,E10.4,/,10X,
                       $*FLOWRATE UNIT PER CUBIC METER PER SECOND*,5XE10.4,/,10X,
                       $*TIME UNIT PER SECOND*,25XF10.2,/,10X,*LENGTH PER METER*,29XF10.2,
                       $/,10X,*VISCOSITY PER PASCAL-SECOND*,18XE10.3,/,10X,
                       $*PERMEABILITY PER SQUARE METER*,16XE10.4)
```

Figure E-17. VARFLOW Program sample.

```
0130618        READ 103,RKHUX,RKHUY,PCH,ANGLE,DSTNCE,BOUND
0130728  103   FORMAT(5E10.4,A10)
0130728        PRINT 203,RKHUX,RKHUY,PCH
0131008  203   FORMAT(//,5X,*PARAMETER VALUES*,/,5X,16(1H=),/,
              $5X,*X-AXIS TRANSIMISSIVITY =*,E10.4,/,5X,
              $*Y-AXIS TRANSMISSIVITY =*,E10.4,/,5X,*STORATIVITY =*,E10.4)
0131008        IF(BOUND  .NE.  10H          )PRINT 204,BOUND,ANGLE,DSTNCE
0131108  204   FORMAT(/,2X,*THERE IS A *,A10,*BOUNDARY AT AN ANGLE OF *,F10.2,
              $* DEGREES AND A DISTANCE OF *,F10.2)
0131108        DO 1000 I=1,IHH
0131128        READ 105, NAME(I),OX(I),OY(I),YSTART(I),LOBS(I),SKIN(I)
0131328        PRINT 205,I,NAME(I),OX(I),OY(I),YSTART(I)
0131468  1000  IF(LOBS(I)  .GT.  0)PRINT 206,LOBS(I),SKIN(I)
0131618  205   FORMAT(//,*  OBSERVATION WELL NUMBER *,I5,/,5X,*WELL *,A10,
              $* COORDINATES (*F10.2,*,*F10.2,*)*,/,5X,*INITIAL PRESSURE=*,E10.4)
0131618  206   FORMAT(5X,*THIS OBSERVATION WELL IS ALSO PRODUCTION WELL NUMBER*
              $,I10,/,5X,*IT HAS A SKIN VALUE OF*,F10.2)
0131618  105   FORMAT(A10,2F10.2,E10.4,I10,F10.2)
0131618        DO 1020 J=1,JJ
0131638        READ 106, PNAME(J),PX(J),PY(J),KKJ(J)
0131778        PRINT 207,J,PNAME(J),PX(J),PY(J),KKJ(J)
0132138        DO 1020 IJ=1,KKJ(J)
0132168        READ 107, TQ(IJ,J),AQ(IJ,J)
0132318  1020  PRINT 208,TQ(IJ,J),AQ(IJ,J)
0132458  207   FORMAT(//,*  PRODUCTION WELL NUMBER *,I10,/,5X,A10,
              $2X,*COORDINATES (*,F10.2,*,*,F10.2,*)*,2X,/,5X,
              $*NUMBER OF FLOWRATE POINTS=*,I5,//,23X,*TIME*,9X,*FLOWRATE*,//)
0132458  106   FORMAT(A10,2F10.2,I10)
0132458  107   FORMAT(2E10.4)
0132458  208   FORMAT(20X,E10.4,5X,E10.4)
0132458  108   FORMAT(8E10.4)
0132458        DO 1030 I=1,NTIMES,8
0132478  1030  READ 108, (TIMES(K),K=I,I+7)
         C
         CCCCCCCCCCCCCCCCCCCCCCCCCCCCCCCCCCCCCCCCCCCCCCCCCCCCCCCCCCCCCCCCCCCC
         C     SET UP THE PROBLEM
         C
         C     CALCULATE THE GRADIENTS FOR THE FLOW RATE DATA
0132628        DO 1050 I=1,JJ
0132648        DO 1050 IJ=1,KKJ(I)-1
0132708        IF( ABS(TQ(IJ+1,I)-TQ(IJ,I)) .EQ. 0. ) GO TO 1050
0132778        BQ(IJ,I)=(AQ(IJ+1,I)-AQ(IJ,I))/(TQ(IJ+1,I)-TQ(IJ,I))
0133078  1050  CONTINUE
         C
         C     CALCULATE RADIAL DISTANCES BETWEEN THE OBSERVATION WELLS
         C     AND THE PRODUCTION WELLS
0133148        DO 1070 IH=1,IHH
0133168        DO 1070 J=1,JJ
0133218  1070  R(IH,J)=SQRT((PX(J)-OX(IH))**2. + (PY(J)-OY(IH))**2.)
0133438        PRINT 211,(NAME(I),I=1,IHH)
0133538  211   FORMAT(//,*  DISTANCES BETWEEN OBSERVATION WELLS AND PRODUCTION*
              $,* WELLS*,//,12X,10(A10,2X),//)
0133538        DO 1080 I=1,JJ
0133558  1080  PRINT 210, PNAME(I),(R(IH,I),IH=1,IHH)
0133748  210   FORMAT(2X,A10,10(F10.2,2X))
         C
         CCCCCCCCCCCCCCCCCCCCCCCCCCCCCCCCCCCCCCCCCCCCCCCCCCCCCCCCCCCCCCCCCCC
         C      CALCULATE THE PARAMETERS
0133748         RKHUE=SQRT(RKHUX*RKHUY)
0134008        X(1)=CMSFLOW*PASVISC/4./PI/RKHUE/SMPERM/RLENGTH/PAPRESS
0134068        ALPHA=ANGLE*PI/180.
0134108        IF(BOUND    .EQ. 10H                  )GO TO 40
         CCCCCCCCCCCCCCCCCCCCCCCCCCCCCCCCCCCCCCCCCCCCCCCCCCCCCCCCCCCCCCCCCCC
         C     CALCULATE THE COORDINATES OF THE IMAGE WELLS
0134128        DO 1090 IH=1,IHH
0134148        ROX(IH)=OX(IH)*SIN(ALPHA)+OY(IH)*COS(ALPHA)
0134248        ROY(IH)=OY(IH)*SIN(ALPHA)-OX(IH)*COS(ALPHA)
0134348  1090  IF(BOUND  .EQ.10HLEAKY           )L=1
0134438  40    DO 2001 IH=1,IHH
0134468        DO 2002 N=1,NTIMES
0134518        YCALC(N,IH)=YSTART(IH)
0134548        DO 2000 J=1,JJ
```

Figure E-17. (continued).

```
0134608         CALL RKHUNF(RKHUX,RKHUY,OX(IH),OY(IH),PX(J),PY(J),RKHUN)
0134678         RKHUN=X(1)*RKHUE/RKHUN
0134718         X(2)=R(IH,J)*R(IH,J)*(RLENGTH**3.)*PI*PCH*RKHUN/CMSFLOW/SECTIME
0135028         IF( BOUND .EQ. 10H          )GO TO 50
0135058         RPX(J)=PX(J)*SIN(ALPHA)+PY(J)*COS(ALPHA)
0135158         RPY(J)=PY(J)*SIN(ALPHA)-PX(J)*COS(ALPHA)
0135258         RIPY(J)=RPY(J)
0135268         RIPX(J)=2.*DSTNCE-RPX(J)
          CCCCCCCCCCCCCCCCCCCCCCCCCCCCCCCCCCCCCCCCCCCCCCCCCCCCCCCCCCCCCCCCCCCCCC
          C     CALCULATE THE DISTANCE BETWEEN THE IMAGE WELLS AND THE OBSERVATION
          C     WELLS
0135308         RI2(IH,J)=(ROX(IH)-RIPX(J))**2.  + (ROY(IH)-RIPY(J))**2.
0135368         CALL COORD(RIPX(J),RIPY(J),XI,YI,ANGLE)
0135448         CALL RKHUNF(RKHUX,RKHUY,OX(IH),OY(IH),XI,YI,RKHUN)
0135508         RKHUN=X(1)*RKHUE/RKHUN
0135528         X(3)=RI2(IH,J)*(RLENGTH**3.)*PI*PCH*RKHUN/CMSFLOW/SECTIME
0135618         NNW=3
0135628   50    IF(BOUND  .EQ. 10H                 )NNW=2
          C
          CCCCCCCCCCCCCCCCCCCCCCCCCCCCCCCCCCCCCCCCCCCCCCCCCCCCCCCCCCCCCCCCCCCCCC
          C     MAIN CALCULATION LOOP
0135668         TR=TIMES(N)
0135678         FII=0.
0135708         DO 1100 I=2,NNW
0135728         FI=0.0
0135728         DO 1110 KJ=1,KKJ(J)-1
0135778         IF(ABS(TO(KJ+1,J)-TO(KJ,J)).LT.1.E-5) GO TO 1110
0136068         TN=TR-TO(KJ,J)
0136138         TN1=TR-TO(KJ+1,J)
0136168         IF(TN.LE.0.) GO TO 1100
0136218         IF(TN1.LE.0.0) GO TO 80
0136238         FI=(AO(KJ,J)+BO(KJ,J)*(TN+X(I)))*(EI(-X(I),TN1)-EI(-X(I),TN))
                S=BO(KJ,J)*(TN*EXP(-X(I)/TN)-TN1*EXP(-X(I)/TN1))+FI
0136648 1110    CONTINUE
0136678         GO TO 90
0136708   80    FI=-(AO(KJ,J)+BO(KJ,J)*(TN+X(I)))*EI(-X(I),TN)
                A=BO(KJ,J)*TN*EXP(-X(I)/TN)+FI
0137148   90    IF(L.EQ.1.AND.I.GT.2)FI=-FI
0137238 1100    FII=FII+FI
0137278         IF(LOBS(IH).NE.J) GO TO 70
0137318         FII=(FII+2.*SKIN(IH)*(AO(KJ,J)+BO(KJ,J)*TN))
0137428   70    F=FII*X(1)
0137448 2000    YCALC(N,IH)=YCALC(N,IH)+F
0137528 2002    CONTINUE
0137548 2001    CONTINUE
          C
          CCCCCCCCCCCCCCCCCCCCCCCCCCCCCCCCCCCCCCCCCCCCCCCCCCCCCCCCCCCCCCCCCCCCCC
          C
          C     PRINT OUT RESULTS OF THE CALCULATION
0137578         PRINT 118,(NAME(I),I=1,IHH)
0137708         N=0
0137708         IN=0
0137708         DO 1120 I=1,NTIMES
0137738         PRINT 119,TIMES(I),(YCALC(I,IH),IH=1,IHH)
0140128         N=N+1
0140138         IF(N  .NE.  5)GO TO 1120
0140148         PRINT 120
0140208         IN=IN+1
0140218         N=0
0140218         IF(IN  .NE.  8)GO TO 1120
0140238         PRINT 118,(NAME(M),M=1,IHH)
0140348         IN=0
0140348 1120    CONTINUE
0140378  118    FORMAT(1H1,//,5X,*   TIME    *,10(A10,2X),/,5X,130(1H=),//)
0140378  119    FORMAT(3X,F10.2,2X,10(E10.4,2X))
0140378  120    FORMAT(/)
0140378         STOP
0140408         END
```

EI **FUNCTION EI(X,T)**

```
0000008         FUNCTION EI(X,T)
0000008         A=-X/T
```

```
VARFLOW                 **PROGRAM VARFLOW(INPUT,OUTPUT,TAPE1,TAPE2)**

    3.  0000028         IF(A.GT.10.0) GO TO 20
    4.  0000058         ET=-ALOG(A)-.5772156649
    5.  0000108         TERM=1.0
    6.  0000118         DO 10 J=1,100
    7.  0000148         TERM=-TERM*A/J
    8.  0000168         ET=ET-TERM/J
    9.  0000218         IF(ABS(TERM/J/ET).LT.1.E-8) GO TO 12
   10.  0000218      10 CONTINUE
   11.  0000308      12 ET=-ET
   12.  0000328         RETURN
   13.  0000348      20 ET=-EXP(-A)/A*(1.0-1.0/A+2.0/A**2-6.0/A**3)
   14.  0000468         RETURN
   15.  0000518         END


RKHUNF                  **SUBROUTINE RKHUNF(RKHUX,RKHUY,OXD,OYD,PXD,PYD,RKHUN)**

    1.  0000008         SUBROUTINE RKHUNF(RKHUX,RKHUY,OXD,OYD,PXD,PYD,RKHUN)
    2.  0000008         COMMON /SUB/ PI
    3.  0000008         YD=OYD-PYD
    4.  0000018         XD=OXD-PXD
    5.  0000038         THETA=ATAN2(YD,XD)
    6.  0000068         PRINT 99,THETA
    7.  0000138      99 FORMAT(5X,*THETA=*,F10.2)
    8.  0000138         RKHUN=RKHUX/((COS(THETA)**2.) + RKHUX*(SIN(THETA)**2.)/RKHUY)
    9.  0000248         PRINT 100,RKHUN
   10.  0000318     100 FORMAT(5X,*RKHUN=*,F10.2)
   11.  0000318         RETURN
   12.  0000338         END


COOR                    **SUBROUTINE COOR(RIPXD,RIPYD,XI,YI,ANGLE)**

    1.  0000008         SUBROUTINE COOR(RIPXD,RIPYD,XI,YI,ANGLE)
    2.  0000008         COMMON /SUB/ PI
    3.  0000008         ANG=90.-ANGLE
    4.  0000018         ANG=ANG*PI/180.
    5.  0000038         XI=RIPXD*COS(ANG)+RIPYD*SIN(ANG)
    6.  0000128         YI=RIPYD*COS(ANG)-RIPXD*SIN(ANG)
    7.  0000218         RETURN
    8.  0000248         END
```

Figure E-17. (continued).

Acknowledgments

S. M. Benson acknowledges Dr. Chin Fu Tsang and Dr. Donald McEdwards for their contribution to this work, insofar as the original variable flow rate algorithm was developed by them.

REFERENCES

E-1. H. S. Carslaw, and J. C. Jaeger, Conduction of Heat in Solids, Oxford: Clarendon Press, pp. 258-262, 1959.

E-2. D. G. McEdwards, Variable Rate Well Test Analysis (Ph.D Dissertation) Berkeley: University of California, 1979.

E-3. D. G. McEdwards, and C. F. Tsang, "Variable Rate Well Testing Analysis," in Proceedings of the Invitational Well-Testing Symposium, LBL-7027, 1977.

E-4. G. P. Kruseman and N. A. De Ridder, Analysis and Evaluation of Pumping Test Data, Ulageningen, The Netherlands: International Institute for Land Reclamation and Improvement, 1976.

E-5. M. S. Hantush, "Drawdown Around Wells of Variable Discharge" Journal of Geophysical Research, 69, 29, 1964, pp. 4221-4235.

E-6. R. C. Earlougher, Advances in Well Test Analysis, Society of Petroleum Engineers Monographs, 1977.

APPENDIX F
REFERENCE BIBLIOGRAPHY

APPENDIX F

REFERENCE BIBLIOGRAPHY

D. W. Allman, D. Goldman, and W. L. Niemi, "Evaluation of Testing and Reservoir Parameters in Geothermal Wells at Raft River and Boise, Idaho," Geothermal Resources Council Annual Meeting, Reno, NV, September 24, 1979, p. 4.

C. B. Ammann, "Case Histories of Analysis of Characteristics of Reservoir Rock from Drill-Stem Tests," Journal of Petroleum Technology, 12, 5, 1960, p. 27.

K. E. Anderson, Water Well Handbook, St. Louis: Scholin Brothers Printing Corp., 1967.

J. K. Applegate, P. R. Donaldson, D. L. Hinkley, and T. L. Wallace, "Borehole Geophysics Evaluation of the Raft River Geothermal Reservoir, Idaho," Geophysics, 42, 1, 1977, pp. 138-139.

S. Arnorsson, "Application of the Silica Geothermometer in Low Temperature Hydrothermal Areas in Iceland," American Journal of Science 275, 1975, pp. 763-784.

S. R. Aydelotte, Transient Well Testing in Two-Phase Geothermal Reservoirs, LBL NTIS PCA07/MFA01, March 1980, p. 148.

R. Bentall, "Methods of Collecting and Interpreting Ground-Water Data," U.S. Geologic Survey Water Supply Paper, 1544-H, 1963, pp. 1-97.

R. Bentall, "Shortcuts and Special Problems in Aquifer Tests," U.S. Geological Survey Water-Supply Paper 1545-C, 1963, p. C1-C117.

H. C. Bixel, B. K. Larkin, and H. K. Van Poollen, "Effect of Linear Discontinuities, or Pressure Build-up and Drawdown Behavior," Journal of Petroleum Technolgoy, August 1963, pp. 885-895.

G. Bodvarsson, "Capacitative Perturbations in Well Interference Testing," Proceedings of the Fifth Workshop on Geothermal Reservoir Engineering, Stanford, California, December 12, 1979, pp. 85-90.

G. Bodvarsson, "Mechanism of Reservoir Testing," Proceedings Fourth Workshop Geothermal Reservoir Engineering, Stanford, California, December 13, 1978, pp. 146-152.

N. S. Boulton, "Analysis Data from Non-Equilibrium Pumping Tests Allowing for Delayed Yield from Storage," Proceedings of the Institution of Civil Engineers, London, Paper No. 6693, 26, 1963, pp. 469-178.

C. A. Brook et al., "Hydrothermal Convection Systems with Reservoir Temperatures 90°C," U.S. Geological Survey Circular 790, 1978, pp. 18-85.

D. H. Brownell et al., "Governing Equation for Geothermal Reservoirs," Water Resources, 13, 6, 1977, pp. 929-934.

D. A. Campbell, "Hot Water vs. Dry Steam Reservoir Assessment," Geothermal Environment Seminar, 1978, Sacramento, California, May 9, 1978, pp. 118-138.

H. S. Carslaw and J. C. Jaeger, Conduction of Heat in Solids, Oxford: Oxford at the Claredon Press, 1959.

B. Chen, Geothermal Reservoir and Well Test Analysis: A Literature Survey, University of Hawaii, NTIS PCA031 MFA01, 1974, p. 38.

P. Cheng and K. H. Lau, The Effects of Steady State Withdrawal of Fluid in Geothermal Reservoirs, University of Hawaii, NTIS PCA03/MFA01, 1975, p. 31.

C. Y. Chiang and C. R. Y. Chang, "Application of the Horner Method to the Estimation of Static Reservoir Temperature During Drilling Operations," Proceedings of Fifth Workshop on Geothermal Reservoir Engineering, Stanford, CA, December 12, 1979, pp. 367-372.

R. N. Clayton and A. Steiner, "Oxygen Isotope Studies of the Geothermal System at Wairakei, New Zealand," Geochemica Cosmochimica Acta, 39, 1975, pp. 1179-1186.

G. Cortecci, "Oxygen Isotropic Ratios of Sulfate Ions-Water Pairs as a Possible Geothermometer," Geothermics 3, 1974, pp. 60-64.

A. Desplan, J. Deschamps and M. Leleu, "Chemical Reactions Occurring During the Exploitation of Geothermal Well Doublet: Thermodynamic and Experimental Approach for the Case of the Dogger Reservoir in the Pairs Basin," First Seminar on Geothermal Energy, Brussels, Belgium, December 6, 1977, pp. 529-547.

R. J. M. De Wiest, "On the Storage Coefficient and the Equations of Ground-Water Flow," Journal of Geophysical Research, 71, 4, 1966.

A. Domenico, Concepts and Models in Groundwater Hydrology, New York: McGraw-Hill Book Company, Inc., 1972, p. 405.

I. G. Donaldson, "Geothermal Reservoir Engineering Research in New Zealand," Proceedings Fourth Workshop Geothermal Reservoir Engineering, Stanford, California, December 13, 1978, pp. 36-41.

M. H. Dorfman and R. W. Deller, "Well Design and Reservoir Research and Technology," Proceedings of Second Geopressured Geothermal Energy Conference, Volume I, Austin, Texas, February 23, 1976, pp. 19-23.

R. C. Earlougher, Jr., K. M. Kersch, and H. J. Ramey, "Wellbore Effects in Injection Well Testing," Journal of Petroleum Technology, November 1973, pp. 1244-1250.

R. C. Earlougher, Jr. and K. M. Kersch, "Analysis of Short-time Transient Test Data by Type Curve Matching," Journal of Petroleum Technology, July 1974, pp. 793-800, Transactions, AIME, p. 257.

R. C. Earlougher, "Advances in Well Test Analysis," SPE Monograph Series, 5, 1977.

C. Economides, "Recent Development in Well Test Analysis in the Stanford Geothermal Program," Proceedings Fourth Workshop Geothermal Reservoir Engineering, Standford, California, December 18, 1978, pp. 188-200.

M. J. Economides, "Shut-in and Flowing Button Hole Pressure Calculation for Geothermal Steam Wells," Proceedings of the Fifth Workshop on Geothermal Reservoir Engineering, Stanford, California, December 12, 1979, pp. 139-151.

R. O. Elemo, "Estimation of Stress-Sensitive Reservoirs' Initial Parameters by Use of the Conventional Well Test Methods," Fourth United States Gulf Coast Geopressured-Geothermal Energy Conference: Research and Development, Austin, Texas, October 29, 1979, pp. 960-971.

A. J. Ellis and N. A. J. Mahon, "National Hydrothermal Systems and Experimental Hot-Water/Rock Interactions," Geochemica et Cosmochimica Acta, 28, 1964, pp. 1323-1357.

G. Endo, "Numerical Model for Steam-Dominated Type Geothermal Reservoir," Third Meeting of the Japan Geothermal Energy Association, Tokyo, Japan, December 9, 1976, p. 2

Energy Research and Development Administration, "Geothermal Resource Assessment and Reservoir Engineering," DOE Workshop on Geothermal Resources Assessment and Reservoir Engineering, Larderello, Italy, September 12, 1977, p. 442.

J. G. Ferris, D. B. Knowles, R. H. Brown, and R. H. Stallman, "Theory of Aquifer Tests," U.S. Geological Survey Water-Supply Paper 1536-E, 1962, pp. 69-174.

R. O. Fournier, D. E. White, and A. H. Truesdell, "Geochemical Indicators of Subsurface Temperature-1, Basic Assumptions," U.S. Geological Survey Journal of Research, 2, 1974, pp. 259-262.

R. O. Fournier and A. H. Truesdell, "Geochemical Indicators of Subsurface Temperature-2. Estimation of Temperature and Fraction of Hot Water Mixed with Cold Water," U.S. Geological Survey Journal of Research, 2, 1974, pp. 263-269.

R. O. Fournier and A. H. Truesdell, Geochemical Indicators of Subsurface Temperature Applied to Hot Spring Waters of Yellowstone National Park, Wyoming, U.S.A.," Geothermics 2, 1970, pp. 529-535.

R. O. Fournier and R. W. Potter II, "Magnesium Correction to the Na-K-Ca Chemical Geothermometer," Geochemica Cosmochimica Acta, 43, pp. 1543-1550.

R. O. Fournier and J. J. Rowe, "Estimation of Underground Temperatures from the Silica Content of Water from Hot Springs and Wet-Steam Wells," American Journal of Science, 264, 1966, pp. 685-697.

R. O. Fournier and A. H. Truesdell, "An Empirical Na-K-Ca Geothermometer for Natural Waters," Geochemica et Cosmochimica Acta, 37, 1973, pp. 1255-1275.

R. O. Fournier, "Chemical Geothermometers and Mixing Models for Geothermal Systems," Geothermics, 5, 1977, pp. 41-50.

S. K. Garg, "Pressure Transient Analysis for Two-Phase Geothermal Reservoirs," Geothermal Resources Council Meeting, Hilo, Hawaii, July 25, 1978, pp. 203-206.

R. E. Glover, "Studies of Ground Water Movement," Bureau of Reclamation Technical Memorandum 657, Bureau of Reclamation, Denver, 1960.

C. B. Goranson and R. C. Schroeder, "Site-Specific Geothermal Reservoir Engineering Activities," LBL Earth Sciences Division Annual Report 1978, NTIS PCAS12/MFA01, pp. 97-106.

K. P. Goyal and D. R. Kassdy, "Fault Zone Controlled Charging of a Liquid-Dominated Geothermal Reservoir," Journal of Geophysics, 85, 84, pp. 1867-1875.

"Geophysics and Ground Water, An Introduction--Part I; Applied Use of Geophysics--Part II," Water Well Journal, 25, 7,; 25, 8, 1971.

K. E. Gray, "Approximating Well to Fault Distance From Pressure Build-up Tests," Journal of Petroleum Technology, July 1965, pp. 761-767.

B. D. Gunter and B. C. Musgrave, "New Evidence on the Origin of Methane in Hydrothermal Gases," Geochemica Cosmochimica Acta, 35, 1971, pp. 113-118.

M. S. Hantush, "Analysis of Data from Pumping Tests in Anisotropic Aquifers," Journal of Geophysical Research, 71, 2, January 15, 1966, pp. 421-425.

M. S. Hantush, "Analysis of Data from Pumping Tests in Leaky Aquifers," Transactions of the American Geophysical Union, 37, December 1956, pp. 702-714.

M. S. Hantush, "Hydraulics of Wells," Advances in Hydroscience, 1, 1964.

S. Hirakawa, Y. Mizuishi, Y. Fujinaga, and K. Hida, "Geothermal Reservoir Modeling," Meeting of the Mining and Metallurgical Institute, Tokyo, Japan, March 30, 1976, p. 2.

S. Hirakawa, "System Approach to Geothermal Field Development," Proceedings Fourth Workshop Geothermal Reservoir Engineering, Stanford, California, December 13, 1978, pp. 234-238.

J. R. Hoagland, "Applications of Solute Equilibrium Models to the Study of Geothermal Reservoirs," Geothermal Resources Council, San Diego, California, May 9, 1977, pp. 143-145.

W. A. Hobba, D. W. Fisher, F. J. Pearson Jr. and J. C. Chemerys, "Hydrology and Geochemistry of Thermal Springs of the Appalachians, II. Geochemistry," U.S. Geological Survey Paper, 1044-E, 1978.

R. N. Horne, D. O. Ogbe, K. Temeng and H. J. Ramey Jr., Geothermal Reservoir Engineering Computer Code Comparison and Validation Using the GEONZ Simulator Program, NTIS PCA04/MF A01, November 1980, p. 67.

D. R. Horner, "Pressure Build-up in Wells," Proceedings of the Third World Petroleum Congress, Leiden: E. J. Brill, 1951.

J. H. Howard, Geothermal Reservoir Engineering Management Program: Developmental in Fiscal 1979, NTIS PCA07/MFA01, August 1980, pp. 66-69.

M. K. Hubbert, The Theory of Ground-Water Motion and Related Papers, Hafner Publishing Co., 1969.

A. Hunsbedt, et al., "Laboratory Studies of Non-Isothermal Fluid Production from Fractured Geothermal Reservoirs," American Society Mechanical Engineering Paper No. 77-HT-53, 1977, pp. 1-8.

C. E. Jacob, "Drawdown Test to Determine the Effective Radius of an Artesian Well," Transactions of the ASCE, 112, 1947, pp. 1047-1070.

C. E. Jacob, "Flow of Groundwater: Engineering Hydraulics, New York: John Wiley and Sons, 1950, pp. 321-386.

C. E. Jacob, "Full Utilization of Groundwater Reservoirs," Transactions of the American Geophysical Union, 38, June 1957, p. 417.

C. E. Jacob and S. W. Lohman, "Nonsteady Flow to a Well of Constant Drawdown in an Extensive Aquifer," Transactions of the American Geophysical Union, 33, 4, August 1952, pp. 559-569.

C. E. Jacob, "On the Flow of Water in an Elastic Artesian Aquifer," Transactions of the American Geophysical Union, 21, part II, pp. 574-596.

W. C. Kettenacker, Two-Dimensional Simulation of the Raft River Geothermal Reservoir and Wells, INEL, NTIS PCA06/MFA01, 1977, p. 107.

W. S. Keys and L. M. MacCary, "Application of Borehole Geophysics to Water-Resources Investigations," U.S. Geological Survey Technical Water Resources Investigations, Book 2, Chapt. E1, 1971.

L. E. Klyen, "A Vessel for Collecting Subsurface Water Samples from Geothermal Drillholes," Geothermics, 2, 1973, pp. 57-60.

P. Kruger and H. J. Ramey, Jr., Geothermal Reservoir Engineering, Second Workshop Summaries, December 1-3, 1976, Stanford University, NTIS PCA16/MFA01, 1976, p. 352.

P. Kruger and H. J. Ramey, Jr. (eds), Proceedings Fourth Workshop Geothermal Reservoir Engineering, NTIS PCA15/MFA01, December 1978, p. 336.

P. Kruger and H. J. Ramey, Jr., Stimulation and Reservoir Engineering of Geothermal Resources First Annual Report, June 1, 1977-March 31, 1978, Stanford University, NTIS PCA04/MFA01, April 1978, p. 68.

J. F. Kunze and P. A. Witherspoon, "Energy Extraction and Reservoir Management of a Moderate Temperature Hydrothermal System," American Nuclear Society Topical Meeting on Energy and Mineral Recovery Research, Golden, CO, April 12, 1977, pp. 68-76.

R. B. Leonard, T. M. Brosten, and N. A. Midtlyng, "Selected Data from Thermal Springs Areas, Southwestern Montana," U.S. Geological Survey Open-File Report 78-438, 1978.

W. H. Li, "Interaction Between Well and Aquifer," Proceedings of the ASCE, 80, Separate No. 578, December 1954.

T. M. C. Li, J. W. Mercer, C. R. Faust, and R. J. Greenfield, "Simulation of Geothermal Reservoirs Including Changes in Porosity and Permeability Due to Silica-Water Reactions," Proceedings Fourth Workshop Geothermal Reservoir Engineering, Stanford, December 13, 1978, pp. 275-279.

M. J. Lippmann, C. F. Tsang, and P. A. Witherspoon, "Analysis of the Response of Geothermal Reservoirs Under Injection and Production Procedures," 47 Annual California Regional Meeting of the Society of Petroleum Engineers of AIME, Bakersfield, CA, April 13, 1977, p. 15.

R. M. Lloyd, "Oxygen Isotope Behavior in the Sulfate-Water System," Journal of Geophysical Research, 73, 1968, pp. 6099-6110.

R. Marconcini et al, "Modeling Vapor Dominated Geothermal Reservoirs," DOE Workshop on Geothermal Resources Assessment and Reservoir Engineering, Larderello, Italy, September 12, 1977, pp. 256-298.

R. H. Mariner, T. S. Presser, and W. C. Evans, "Chemical Characteristics of the Major Thermal Springs of Montana," U.S. Geological Survey Open-File Report 76-480, 1976, 31 pp.

R. H. Mariner and L. M. Willey, "Geochemistry of Thermal Waters in [illegible] Valley, Mono County, California," Journal of Geophysical Research, [illegible] 1976, pp. 792-800.

R. H. Mariner, C. A. Brook, J. R. Swanson, and D. R. Mabey, "Selected Data for Hydrothermal Convection Systems in the United States with Estimated Temperatures 90°C," U.S. Geological Survey Open File Report 78-858, 1978.

C. S. Matthews and D. G. Russell, "Pressure Buildup and Flow Test in Wells," SPE Monograph Series, 1, 1967.

W. F. McKenzie and A. H. Truesdell, "Geothermal Reservoir Temperatures Estimated from the Oxygen Isotope Compositions of Dissolved Sulfate and Water from Hot Springs and Shallow Drillholes," Geothermics, 5, 1977, pp. 51-62.

T. Meider, "Geophysical Methods in Reservoir Engineering and Reservoir Management," Proceedings of the Third Annual Geothermal Conference and Workshop, Monterey, California, June 26, 1979, pp. 2.31-2.37.

D. E. Meinzer, "Large Springs in the United States," U.S. Geological Survey Water Supply Paper 557, 1927.

D. E. Meinzer, "Outline of Groundwater Hydrology," U.S. Geological Survey Water Supply Paper 494, 1923.

S. Mercado, "High Activity Hydrothermal Zones Detected by Nalk, Cerro Prieto, Mexico, Geothermics 2, 1970, pp. 1367-1376.

J. W. Mercer and C. R. Faust, Reservoir Engineering and Evaluation, USGS, NTIS PCA06/MFA01, April 1979, pp. 37-42.

"Methods and Techniques of Ground Water Investigations and Developments," UNESCO Water Resources Series, 33, 1967.

C. C. Miller, A. B. Dyes, and C. A. Hutchison, "The Estimation of Permeability and Reservoir Pressure from Bottomhole Pressure Build-up Characteristics," Transactions, AIME, 1950 pp. 91-105, 189.

F. G. Miller, H. Cinco, H. J. Ramey, Jr., F. Kucuk, "Reservoir Engineering Aspects of Fluid Recharge and Heat Transfer in Geothermal Reservoirs," Geothermal Resources Council Meeting, Hilo, Hawaii, July 25, 1978, pp. 449-452.

A. F. Moench, "Effect of Thermal Conduction Upon Pressure Drawdown and Buildup in Fissured, Vapor Dominated Geothermal Reservoirs," Proceedings Fourth Workshop Geothermal Reservoir Engineering, Stanford, December 13, 1978, pp. 112-117.

A. F. Moench and P. G. Atkinson, "Transient-Pressure Analysis in Geothermal Steam Reservoirs with an Immobile Vaporizing Liquid Phase," Geothermics, 7, 2-4, pp. 253-264.

W. G. Mook, J. C. Bommerson, and W. H. Staverman, "Carbon Isotope Fractionation Between Dissolved Bicarbonate and Gaseous Carbon Dioxide," Earth Planetary Science Letter, 22, 1974, pp. 169-176.

J. G. Morse, "Reservoir Engineering Study of a Portion of the Salton Sea Geothermal Field," Geothermal Resources Council Meeting, Hilo, Hawaii, July 25, 1978, pp. 471-474.

T. D. Mueller and P. A. Witherspoon, "Pressure Interference Effects Within Reservoirs and Aquifers," Journal of Petroleum Technology, April 1975, pp. 471-474, AIME p. 234.

M. Muskat, The Flow of Homogeneous Fluids Through Porous Media, New York: McGraw-Hill Book Company, 1937.

M. Muskat, "Use of Data on the Build-up of Bottomhole Pressures," Transactions of AIME, 1937, pp. 123, 44-88.

T. N. Narasimhan and P. A. Witherspoon, Reservoir Evaluation Tests on RRGE1 and RRGE2, Raft River Geothermal Project, Idaho, LBL NTIS PCA04/MFA01, 1977, p. 53.

M. Nathenson, T. C. Urban, and W. H. Diment, "Approximate Solution for the Temperature Distribution Caused by Flow up a Fault and its Application to Temperatures Measured in a Drillhole at Raft River Geothermal Area, Cassia County, Idaho," Geothermal Resources Council Transactions, V. 3, 1979, pp. 477-480.

M. Nathenson, " Summary of Section VII: Production Technology, Reservoir Engineering, and Field Management," Proceedings of the Second United Nations Symposium the Development and Use of Geothermal Resources, San Francisco, May 20, 1975, pp. XCVII-CI.

A. S. Odeh and L. G. Jones, "Pressure Drawdown Analysis Variable Rate Case," Journal of Petroleum Technology, August 1965, pp. 960-964.

T. Paces, "A Systematic Deviation from Na-K-Ca Geothermometer Below 75°C and above 10^{-4} ATM P_{CO_2}," Geochemica et Cosmchimica Acta 39, 1975.

F. J. Pearson Jr. and A. H. Truesdell, "Tritium in the Waters of Yellowstone National Park (Wyoming)," Short Papers of the Fourth International Conference of Geochronology, Cosmochronology, and Isotope Geology, Open-File Report 78-701, 1978, pp. 327-329.

J. D. Pendergrass and V. J. Berry, Jr., "Pressure Transient Performance in a Multi-layered Reservoir with Cross-flow," Society of Petroleum Engineers Journal, December 1962, pp. 347-354.

G. F. Pinder, State-of-the-Art Review of Geothermal Reservoir Modelling, LBL, NTIS, PCA08/MFA01, March 1979, p. 151.

P. Polubarinova-Kochina, Theory of Groundwater Movement, Princeton: Princeton University Press, 1972.

T. A. Prickett and C. G. Lonnquist, "Selected Digital Computer Techniques for Groundwater Resource Evaluation," Illinois State Water Survey, Urbana, Bulletin 55, 1971, p. 62.

K. Pruess and R. C. Schroeder, "Basic Theory and Equations Used in the Two Phase Multi-Dimensional Geothermal Reservoir Simulator, Geothermal Resources Council Annual Meeting, Reno, Nevada, September 24, 1979, p. 5.

R. Raghavan, G. V. Cady, and H. J. Ramey, Jr., "Well Test Analysis for Vertically Fractured Wells," Journal of Petroleum Technology, August 1972, pp. 1014-1020; Transactions, AIME, p. 253.

H. J. Ramey, Jr., Interference Analysis for Anisotopic Formations--A Case History" Journal of Petroleum Technology, October 1975, pp. 1290-1298, Transactions AIME, p. 259.

H. J. Ramey, Jr., "Short-Time Well Test Data Interpretation in Presence of Skin Effect and Wellbore Storage" Journal of Petroleum Technology, January 1970, Transactions AIME, p. 249.

H. J. Ramey, Jr., "Commercialization of Geothermal Resources," Conference on Commercialization of Geothermal Resources, San Diego, California, November 28, 1978, pp. 15-17.

H. J. Ramey Jr. and P. Kruger (eds), Proceedings of Fifth Workshop on Geothermal Reservoir Engineering, December 12-14, 1979, NTIS PCA17/MFA01, December 1979, pp. 261-267.

H. J. Ramey Jr., and A. L. London, Stimulation and Reservoir Engineering of Geothermal Resources, Stanford University Geothermal Program Report No. 4, NTIS PCA05/MFA01, August 1975, p. 78.

G. S. Randall and R. F. Harrison, "Annotated Research Bibliography for Geothermal Reservoir Engineering," Proceedings Fourth Workshop Geothermal Reservoir Engineering, Stanford, California, December 13, 1978, pp. 272-274.

R. C. Reda, "Influence of Steam/Water Relative Permeability Models on Predicted Geothermal Reservoir Performance: A Sensitivity Study," Sixth Annual Workshop on Geothermal Reservoir Engineering, Stanford, California December 16, 1980, p. 7.

Republic Geothermal et al., Raft River Well Stimulation Experiments: Geothermal Reservoir Well Stimulation Program, NTIS PCA08/MFA01, August 1980, p. 158.

L. F. Rice, Pressure Drawdown and Buildup Analyses in Geothermal Reservoirs, Science and Software Systems, 1976, p. 24.

C. T. Rightmire, H. W. Young, and R. L. Whitehead, "Geothermal Investigations in Idaho, IV. Isotropic and Geochemical Analyses of Water from the Bruneau-Grand View and Weiser Areas, Southwest Idaho," Idaho Dep. Water Admin., Water Information Bulletin, 30, 1976.

R. J. Rivera, "Decline Curve Analysis--A Useful Reservoir Engineering Tool for Predicting the Performance of Geothermal Wells," Geothermal Resources Council, San Diego, California, May 9, 1977, pp. 257-259.

M. I. Rorabaugh, "Graphic and Theoretical Analysis of Step-Drawdown Tests of Artesian Wells," Proceedings of the ASCE, 79, 362, September 1953.

D. G. Russell and N. E. Truitt, "Transient Pressure Behavior in Vertically Fractured Reservoirs," Journal of Petroleum Technology, October 1964, pp. 1159-1170.

H. Sakai, "Sulfate-Water Isotope Thermometry Applied to Geothermal Systems," Geothermics, 5, 1977, pp. 67-74.

M. Saltuklaroglu, "Interference Effect of Producting Wells on Observation Wells in a Geothermal Field," Proceedings of the Fifth Workshop on Geothermal Reservoir Engineering Stanford, California, December 12, 1979, pp. 49-59.

G. Sandquist, S. Swanson, R. Stoker, and J. Kunze, "Evaluating the Energy Capacity and Lifetime of Fracture Dominated Geothermal Reservoirs," 12th Intersociety Energy Conversion Engineering Conference, Washington, D.C., August 28, 1977, pp. 804-809.

S. K. Sanyal, H. J. Ramey Jr., and H. T. Meidav, "Geothermal Reservoir Assessment Techniques Manual," EPRI Annual Geothermal Program, January 1978, pp. 2.85-2.90.

C. R. Scherer, Geothermal Reservoir Management, University of California, Berkeley, NTIS PCA10/MFA01, 1978, p. 203.

R. Schneider, "An Application of Thermometry to the Study of Ground Water," U.S. Geological Survey Water Supply Paper 1544-B, 1962.

R. J. Schicht, "Selected Methods of Aquifer Test Analysis," Water Resources Bulletin, 8, 1, February 1972, pp. 175-187.

C. S. Slichter, "Field Measurements of Rate of Movement of Underground Water," U.S. Geological Survey Water Supply Paper 140, 1905.

C. S. Slichter, "Theoretical Investigation of the Motion of Ground Waters: Washington, D.C.," U.S. Geological Survey Nineteenth Annual Report, Part 2, 1899, pp. 295-384.

G. A. Sudol, R. F. Harrison, and H. J. Ramey Jr., "Annotated Research Bibliography for Geothermal Reservoir Engineering," NTIS PCA08/MFA01, August 1979, p. 155.

W. K. Summers, The Annotated Indexed Bibliography of Geothermal Phenomena, Socorro: New Mexico Institute of Mining and Technology, 1971.

P. K. Takahashi, B. H. Chen, K. I. Mashima, and A. S. Seki, "State-of-the-Art of Geothermal Reservoir Engineering," Proceedings of American Society of Civil Engineers, 101, 1, July 1975, pp. 11-126.

C. V. Theis, "Relation Between the Lowering of the Piezometer Surface on the Rate and Duration of Discharge of a Well Using Ground Water Storage," Transactions of the American Geophysical Union, 16, 1935, pp. 519-524.

D. K. Todd, Ground Water Hydrology, New York: John Wiley and Sons, 1960.

C. F. Tolman, Ground Water, New York: McGraw-Hill Book Company, Inc., 1957 pp. 341-346.

C. F. Tsang, M. J. Lippman and P. A. Witherspoon, "Production and Reinjection in Geothermal Reservoirs," Geothermal: State of the Art, 1977, pp. 301-303.

F. VanderLeeden, Ground Water, A Selected Bibliography, New York: Water Information Center, 1971.

A. F. van Everdingen, "The Skin Effect and its Influence on the Productive Capacity of a Well," Transactions of AIME, 1953.

A. F. van Everdingen and W. Hurst, "The Application of the Laplace Transformation to Flow Problems in Reservoirs," Transactions of AIME, 1949, pp. 186, 305-324.

D. J. Vetter, "Tritium Tracer as a Means for Reservoir Verification in Geothermal Reservoirs," EPRI Annual Geothermal Program, California, January 1978, pp. 4.17-4.23.

W. C. Walton, Groundwater Resource Evaluation, New York: McGraw-Hill Book Company, Inc., 1970, p. 194.

W. C. Walton, "Selected Analytical Methods for Well and Aquifer Evaluation," Illinois State Water Survey, Department of Regulation and Education Bulletin No. 49, Urbana, 1962.

S. H. Ward, Program Review: Resource Evaluation, Reservoir Confirmation, and Exploration Technology, NTIS PCA09/MFA01, May 1978, p. 182.

J. E. Warren and P. J. Root, "The Behavior of Naturally Fractured Reservoirs" Society of Petroleum Engineers Journal, September 1963, pp. 245-255.

"Well Logging in Ground Water Hydrology," Ground Water, 6, 1, 1968, pp. 10-18.

D. Weres, "Dynamics of Steam Producing Geothermal Reservoirs," Geothermal Environmental Seminar, 1978, Sacramento, California, May 9, 1978, pp. 189-195.

P. W. Werner, "Notes on Flow-Time Effects in the Great Artesian Aquifers of the Earth; Transactions of the American Geophysical Union, 27, October 1946.

N. D. White, "Annual Report on Ground Water in Arizona," Water Resources Report, 24, 1964-1965.

P. A. Witherspoon, T. N. Narasimhan, and D. G. McEdwards, "Results of Interference Tests from Two Geothermal Reservoirs," Journal of Petroleum Engineering, 30, January 1978, pp. 10-16.

SubJ
GTHM
LTMT

GEOTHERMAL PROGRAMS

IDO-10099
Volume II

Idaho Operations Office

Low-to-Moderate Temperature Hydrothermal Reservoir Engineering Handbook

A Joint-Project Report
of Lawrence Berkeley Laboratory and
The Idaho National Engineering Laboratory

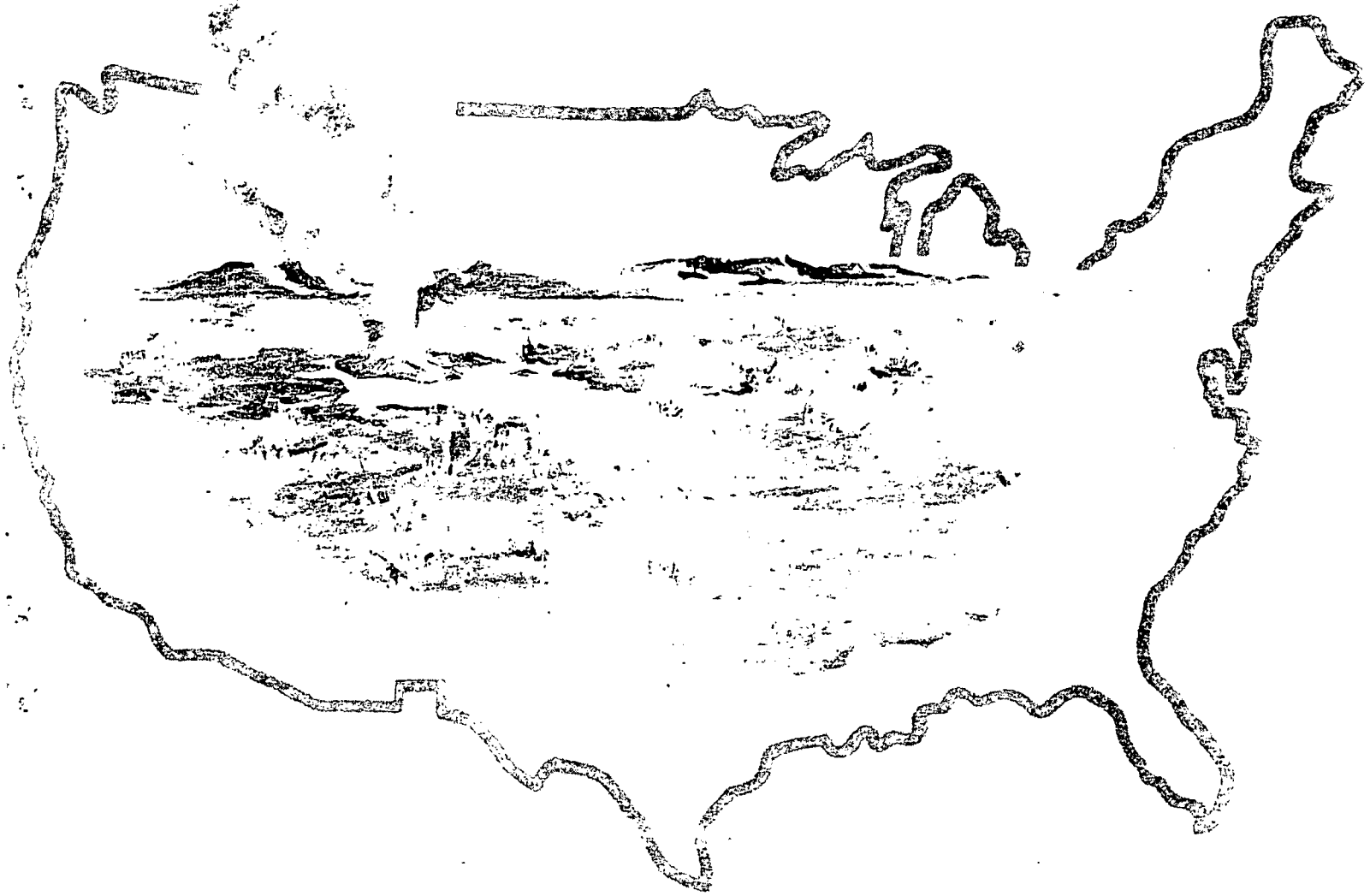

IDO-10099
Volume II
Distribution Category: UC-66a,d,g

LOW-TO-MODERATE TEMPERATURE HYDROTHERMAL RESERVOIR ENGINEERING HANDBOOK

Published June 1982

EG&G Idaho, Inc.
Idaho Falls, Idaho 83415

and

Lawrence Berkeley Laboratory
Berkeley, California 94720

Prepared for the
U.S. Department of Energy
Idaho Operations Office
Under DOE Contract No. DE-AC07-76ID01570

CONTENTS

FIGURES

TABLES

APPENDIX A
UNITS AND CONVERSIONS

APPENDIX A

UNITS AND CONVERSIONS[a]

Units

	Metric	English
Pressure	Pa	psia
Temperature	°C	°F
Flow	m^3/s or l/s	gpm
Compressibility	1/Pa	1/psi
Length	m (Meter)	ft
Permeability	m^2	mD
Static water level	m	ft
Viscosity	Pa•sec	cP

a. Abstracted from the Invitational Well Testing Symposium, Berkeley, California, 1977.

TABLE A-1. Permeability

ρ_w = 1 viscosity = 1 centipoise

	cm^2	m^2	ft^2	Darcy	cm/s	ft/s	ft/year	$L/s \cdot m^2$	gpd(U.S.)/ ft^2 (Meinzer)	Ebhlm
cm^2	1	10^{-4}	1.076×10^{-3}	1.014×10^{8}	9.804×10^{4}	3.216×10^{3}	1.015×10^{11}	8.698×10^{5}	1.845×10^{9}	0.9
m^2	10^{4}	1	1.076×10^{1}	1.014×10^{12}	9.804×10^{8}	3.216×10^{7}	1.015×10^{15}	8.697×10^{9}	1.845×10^{13}	0.8
ft^2	9.294×10^{2}	9.294×10^{-2}	1	9.417×10^{10}	9.109×10^{7}	2.988×10^{6}	9.430×10^{13}	8.080×10^{8}	1.714×10^{12}	0.7
Darcy	9.862×10^{-9}	9.862×10^{-13}	1.062×10^{-11}	1	9.66×10^{-4}	3.173×10^{-5}	1.001×10^{3}	8.58×10^{-3}	1.82×10^{1}	0.6
cm/s	1.020×10^{-5}	1.020×10^{-9}	1.097×10^{-8}	1.035×10^{3}	1	3.281×10^{-2}	1.035×10^{6}	9.985×10^{0}	2.118×10^{4}	0.5
ft/s	3.109×10^{-4}	3.109×10^{-8}	3.347×10^{-7}	3.152×10^{4}	3.048×10^{1}	1	3.156×10^{7}	2.704×10^{2}	5.736×10^{5}	0.4
ft/year	9.852×10^{-12}	9.852×10^{-16}	1.060×10^{-14}	9.990×10^{-4}	9.662×10^{-7}	3.169×10^{-8}	1	8.570×10^{-6}	1.818×10^{-2}	0.3
$L/s \cdot m^2$	1.150×10^{-6}	1.150×10^{-10}	1.238×10^{-9}	1.166×10^{2}	1.001×10^{-1}	3.698×10^{-3}	1.167×10^{5}	1	2.121×10^{3}	0.2
gpd(U.S.)/ ft^2 (Meinzer)	5.420×10^{-10}	5.420×10^{-14}	5.834×10^{-13}	5.494×10^{-2}	4.721×10^{-5}	1.743×10^{-6}	5.500×10^{1}	4.714×10^{-4}	1	0.1
Ebhlm	0.9	0.8	0.7	0.6	0.5	0.4	0.3	0.2	0.1	1

TABLE A-2. Compressibility (Lt^2/M)

	m^2/N $(Pa)^{-1}$	m^2/kgf	$in.^2\ lbf$ $(psi)^{-1}$	$Bars^{-1}$	Atm^{-1}	$(ft\ of\ water)^{-1}$ at 68°F	$(m\ of\ water)^{-1}$ at 68°F
m^2/N $(Pa)^{-1}$	1	9.807	6.897×10^{3}	10^{5}	1.0133×10^{5}	2.984×10^{3}	9.794×10^{3}
m^2/kgf	1.020×10^{-1}	1	7.031×10^{2}	1.0197×10^{4}	1.0332×10^{4}	3.042×10^{2}	9.980×10^{2}
$in.^2/lbf$ $(psi)^{-1}$	1.450×10^{-4}	1.4223×10^{-3}	1	14.504	14.696	0.4327	1.419
$Bars^{-1}$	10^{-5}	9.8068×10^{-5}	6.895×10^{-2}	1	1.01325	2.984×10^{-2}	9.790×10^{-2}
Atm^{-1}	9.8692×10^{-6}	9.6787×10^{-5}	6.805×10^{-2}	0.98692	1	2.945×10^{-2}	9.662×10^{-2}
$(ft\ of\ water)^{-1}$ at 68°F	3.351×10^{-4}	3.287×10^{-3}	2.311	33.512	33.956	1	3.281
$(m\ of\ water)^{-1}$ at 68°F	1.021×10^{-4}	1.002×10^{-3}	0.7044	10.214	10.349	0.3048	1

Table A-3. Temperature °C to °F

°C	°F	°C	°F	°C	°F	°C	°F	°C	°F
0	32	100	212	200	392	300	572	400	752
5	41	105	221	205	401	305	581	405	761
10	50	110	230	210	410	310	590	410	770
15	59	115	239	215	419	315	599	415	779
20	68	120	248	220	428	320	608	420	788
25	77	125	257	225	437	325	617	425	797
30	86	130	266	230	446	330	626	430	806
35	95	135	275	235	455	335	635	435	815
40	104	140	284	240	464	340	644	440	824
45	113	145	293	245	473	345	653	445	833
50	122	150	302	250	482	350	662	450	842
55	131	155	311	255	491	355	671	455	851
60	140	160	320	260	500	360	680	460	860
65	149	165	329	265	509	365	689	465	869
70	158	170	338	270	518	370	698	470	878
75	167	175	347	275	527	375	707	475	887
80	176	180	356	280	536	380	716	480	896
85	185	185	365	285	545	385	725	485	905
90	194	190	374	290	554	390	734	490	914
95	203	195	383	295	563	395	743	495	923

Table A-4. Volume (L^3)

	m^3	L	bbl	gal (U.S.)	gal (Imp.)	ft^3
m^3	1	10^3	6.289	2.642×10^2	2.20×10^2	35.315
L	10^{-3}	1	6.289×10^{-3}	0.2642	0.220	3.5315×10^{-2}
bbl	0.1590	1.590×10^2	1	42.0	34.97	5.6146
gal (U.S.)	3.7854×10^{-3}	3.7854	2.381×10^{-2}	1	0.8327	0.13368
gal (Imp.)	4.546×10^{-3}	4.546	2.860×10^{-2}	1.2009	1	0.16054
ft^3	2.832×10^{-2}	28.32	0.178	7.481	6.229	1

TABLE A-5. Flow rate
(L^3/t or M/t)

	m^3/s	L/min	bbl/day	gal/min (U.S.)	gal/min (Imp.)	ft^3/s	klb/h ($\rho_w = 1.0$)	klb/h ($\rho_w = 0.9$)
m^3/s	1	6×10^4	5.434×10^5	1.585×10^4	1.320×10^4	35.315	7.94×10^3	7.15×10^3
L/min	1.667×10^{-5}	1	9.058	0.2642	0.220	5.885×10^{-4}	1.32×10^{-1}	1.19×10^{-1}
bbl/day	6.498×10^5	1.840×10^{-6} 1.46×10^{-2}	1.31×10^{-2}	1.10×10^{-1}	1	2.917×10^{-2}	2.428×10^{-2}	
gal/min (U.S.)	6.31×10^{-5}	3.785	34.28	1	0.8327	2.2280×10^{-3}	0.50	0.45
gal/min (Imp.)	7.58×10^{-5}	4.546	41.19	1.2009	1	2.676×10^{-3}	0.601	0.541
ft^3/s	2.8317×10^{-2}	1.699×10^3	1.539×10^4	4.488×10^2	3.737×10^2	1	2.25×10^2	2.03×10^2
klb/h $\rho_w = 1.0$	1.26×10^{-4}	7.56	68.5	2.00	1.66	4.45×10^{-3}	1	0.900
klb/h $\rho_w = 0.9$	1.40×10^{-4}	8.42	76.2	2.22	1.85	4.93×10^{-3}	1.11	1

TABLE A-6. Pressure
(M/Lt^2)

	N/m^2 (Pa)	kgf/m^2	lbf/in^2 (psi)	Bars	Atm	ft of water (at 68°F)	m of water (at 68°F)
N/m^2 (Pa)	1	1.020×10^{-1}	1.450×10^{-4}	10^{-5}	9.8692×10^{-6}	3.351×10^{-4}	1.021×10^{-4}
kgf/m^2	9.804	1	1.4223×10^{-3}	9.806×10^{-5}	9.6787×10^{-5}	3.287×10^{-3}	1.002×10^{-3}
$lbf/in.^2$ (psi)	6.895×10^{3}	7.031×10^{2}	1	6.895×10^{-2}	6.805×10^{-2}	2.311	0.7042
Bars	10^{5}	1.0197×10^{4}	14.504	1	0.98692	35.512	10.214
Atm	1.0133×10^{5}	1.0332×10^{4}	14.696	1.01325	1	33.956	10.349
ft of water (at 68°F)	2.984×10^{3}	3.042×10^{2}	0.4328	2.984×10^{-2}	2.945×10^{-2}	1	0.3048
m of water (at 68°F)	9.794×10^{3}	9.980×10^{2}	1.419	9.790×10^{-2}	9.662×10^{-2}	3.281	1

TABLE A-7. Viscosity (Dynamic)

Pa•s	$lbf•s/in.^2$	$lbf•s/ft^2$	$kgf•s/m^2$	lbm/ft•s	$dyne•s/cm^2$	cP	lbm/ft•h
Pa•s	6.894 757 E+03	4.788 026 E+01	9.806 650 E+00	1.488 164 E+00	1.0 E-01	1.0 E-03	4.133 789 E-04

TABLE A-8. Viscosity (Kinematic)

m^2/s	ft^2/s	$in.^2/s$	m^2/h	cm^2/s	ft^2/h	cSt
m^2/s	9.290 304 E+04	6.451 6 E+02	2.777 778 E+02	1.0 E+02	2.580 64 E+01	1

TABLE A-9. Diffusivity

m^2/s	ft^2/s	cm^2/s	ft^2/h
m^2/s	9.290 304 E+04	1.0 E+02	2.580 64 E+01

TABLE A-10. Thermal Conductivity

W/m°K	$cal/s \cdot cm^2 \cdot °C/cm$	$Btu/h \cdot ft^2 \cdot °F/ft$	$kcal/h \cdot m^2 \cdot °C/m$	$Btu/h \cdot ft^2 \cdot °F/in.$	$cal/h \cdot cm^2 \cdot °C/cm$
W/m°K	4.184 E+02	1.730 735 E+00	1.162 222 E+00	1.442 279 E-01	1.162 222 E-01

TABLE A-11. Density (Liquids)

kg/m	lbm/gal (U.K.)	lbm/gal (Imp.)	lbm/ft	g/cm
kg/m^3	1.198 264 E+02	9.977 633 E+01	1.601 846 E+01	1.0 E+03
	1.198 264 E-01	9.977 633 E-02	1.601 846 E-02	1

TABLE A-12. Specific heat capacity (Mass basis)

J/kg°K	kW·h/kg·°C	Btu/lbm·°F	kcal/kg·°C
J/Kg°K	3.6 E+03	4.186 8 E+00	4.184 E+00

TABLE A-13. Enthalpy calorific value (Mass basis)

J/kg	Btu/lbm	cal/g	cal/lbm
J/kg	2.326 000 E-03	4.184 E+00	9.224 141 E+00
	2.325 000 E+00		
	6.461 112 E-04		

APPENDIX B
GLOSSARY OF TERMS

APPENDIX B

GLOSSARY OF TERMS[a]

ANISOTROPY: Term used to denote the dependence of properties such as permeability on spacial orientation. Anisotropy is usually expressed as a tensor. When the principal axes are perpendicular to each other, the material is said to be orthotropic.

AQUICLUDE (GW)[b]: A body of saturated but relatively impermeable material that does not yield appreciable amounts of water to wells. Characterized by very low "leakance" (the ratio of vertical hydraulic conductivity to thickness) and very low rates of yield from compressible storage.

AQUIFER SYSTEM (GW): A heterogeneous body consisting of two or more permeable beds separated at least locally by aquitards that impede groundwater movement but do not greatly affect the regional hydraulic continuity of the system.

AQUITARD (GW): A bed with low permeability that impedes groundwater movement and does not yield water freely to wells, but which may transmit water between aquifers and may constitute an important storage unit. Leakance values vary over a wide range. When low, an aquitard may function as a boundary to an aquifer flow system.

AREA OF INFLUENCE (GW): Defined by Meinzer to be the land area of the same horizontal extent as the portion of the potentiometric surface that is perceptibly lowered due to withdrawal of water by a production well.

---

a. Adapted from the Invitational Well Testing Symposium, Berkeley, California, 1977.

b. Terms commonly used in hydrogeology.

BANK STORAGE (GW): The change in storage in an aquifer resulting from a change in stage of an adjacent surface water body especially in alluvial deposits adjacent to surface streams.

BAROMETRIC EFFICIENCY OF A WELL: The ratio of water-level changes in the well to the water-level changes in a water barometer.

BOUNDARY PRESSURE (PE)[c]: Pressure at boundary of drainage area.

CAPILLARY FRINGE (GW): A zone whose lower part is completely saturated, but with water under less than atmospheric pressure. May range in thickness from a small fraction of an inch in gravel to more than 5 ft in silt.

COEFFICIENT OF PERMEABILITY (GW): See "Hydraulic Conductivity."

COEFFICIENT OF SPECIFIC STORAGE (GW): See "Specific Storage."

COEFFICIENT OF STORAGE (GW): See "Storage Coefficient."

COEFFICIENT OF TRANSMISSIBILITY (GW): See "Transmissivity."

COMMINGLED SYSTEMS (PE): Two-layered or multiple layer reservoirs with communication taking place between layers, either through the wellbore alone or directly across the layer interface.
(cf: multiaquifer well)

COMPACTION (GW): Decrease in volume of sediments, as a result of compressive stress, usually resulting from continued deposition. Also called "one-dimensional consolidation."

---

c. Terms commonly used in petroleum engineering.

COMPACTION, RESIDUAL (GW): The difference between (a) the amount of compaction that will occur ultimately for a given increase in applied stress, once steady-state pore pressures are achieved, and (b) that which has occurred as of a specified time.

COMPRESSIBILITY, TOTAL SYSTEM (PE): A term representing the combined compressibility of all the elements in an aquifer system. Accounts for the compressibilities of the oil phase, water phase, gas phase, and of the rock formation itself, according to the relative fraction of the total system volume occupied by each.

CONDITION RATIO (PE): Also called flow efficiency, indicates approximate fraction of a well's undamaged producing capacity. Ratio of actual productivity index to the productivity index if there were no skin (ideal conditions).

CONFINING BED (GW): A body of relatively impermeable material stratigraphically adjacent to one or more aquifers. Can be either an "aquitard" or an "aquiclude."

CONSOLIDATION (GW): See "Compaction."

CONSTANT DRAWDOWN TEST (GW): also known as constant pressure test in petroleum engineering. A test in which flow rate is gradually varied in time to maintain a constant drawdown (or constant pressure) in the producing well.

CONSTANT PRESSURE TESTING (PE): Also known as constant drawdown test in groundwater hydrology. Involves recording change in flow rate with time while bottom-hole pressure is held constant.

CRITICAL FLOW (PE): occurs in high-permeability zones; the rate of flow into the drill pipe is independent of drawdown during a drill-stem test.

CRITICAL FLOW PROVER (PE): Device that measures flow rate of a gas through an orifice under critical conditions (velocity is constant at a maximum value despite downstream pressure variations).

DAMAGE FACTOR: A measure of wellbore damage obtained by subtracting the condition ratio from 1.

DAMAGE RATIO (PE): Inverse of condition ratio. Indicates wellbore condition.

DELAYED DRAINAGE (GW): Term used to identify the slow release of water from the unsaturated zone in an unconfined aquifer.

DELIVERABILITY TESTING OF OIL WELLS (PE): Determines capability of a well to deliver against a specific flow bottom-hole pressure. Two main types: (a) flow-after-flow test; flowing pressure is recorded for three or more successive flow rates. Each flow rate is held constant until pressure has stabilized. (b) modified isochronal flow test; used for systems where stabilization time is too long for flow-after-flow test. For each flow rate, the well is shut-in after pressure transience is recorded, but before stabilization occurs. At each step the final flowing pressure and then the final shut-in pressure are observed. At the final flow rate, the well is allowed to produce until the pressure stabilizes, and this pressure is recorded.

DIMENSIONLESS PRESSURE (PE): A dimensionless solution to the diffusivity equation. Directly proportional to physical pressure, where the scaling factor is dependent on flow rate and reservoir properties. Usually denoted by $P_D = \frac{2\pi kH\Delta P}{q\mu}$.

DIMENSIONLESS TIME (PE): A scaled version of real time. Scaling factor depends on reservoir properties and distance to point of observation $t = \frac{kt}{\phi\mu c r^2}$, where k is intrinsic permeability; t is time; ϕ is porosity; μ is viscosity; c is total compressibility; r is distance to point of observation.

DRAWDOWN (GW): Difference in water level (or pressure) between the static condition and that at any given instant during discharge.

DRAWDOWN TESTING (PE): Involves recording the drop in bottom-hole pressure when a shut-in production well is switched to production at constant flow rate.

DRILL STEM TESTING--DST (PE): Used in testing uncompleted wells. An arrangement of packers seals off the interval to be tested, allowing a pressure to be built up as formation fluid flows into the drill stem and surface-actuated valves are closed. Pressure changes are observed by a pressure gauge located in the test interval. See "Single Packer Test," "Straddle Packer Test."

DYNAMIC PRESSURE (PE): The pressure at a given time and location in a reservoir during a period of transient pressure distribution, such as during a build-up or drawdown test.

EFFECTIVE WELL RADIUS (GW): The radius of an imaginary cylinder centered at the wellbore in which the permeability is much higher than in the reservoir. In a gravel-packed well it often denotes the probable radius of the gravel pack.

EQUIVALENT INJECTION TIME (PE): In a fall-off test on an injection well where the injection rate before shut-in varies, the equivalent injection time is the length of time it would have taken to inject the same volume of fluid at a constant flow rate as was injected at a variable flow rate since the last pressure equalization.

EXCESS PORE PRESSURE (GW): Transient pore pressure at any point in an aquitard or aquiclude in excess of the pressure that would exist under steady-flow condition.

EXPANSION, SPECIFIC (GW): The increase in thickness of deposits per unit decrease in applied stress.

EXPANSION, SPECIFIC UNIT: The expansion (increase in volume) of deposits, per unit thickness, per unit decrease in applied stress.

EXPONENTIAL INTEGRAL (PE): See "Theis Solution."

FALLOFF TESTING (PE): Involves shutting in an injection well and observing the decrease in bottom-hole pressure with time.

FALSE PRESSURE (PE): Obtained by extrapolating the straight-line section of a Horner plot of pressure build-up data to infinite shut-in time. Approximates average reservoir pressure in an infinite system and can be used to estimate average drainage region pressure in a bounded system.

FIVE-SPOT PATTERN (PE): An arrangement of production and injection wells with four production wells at the corners of a square and one injection well in the center.

FLOW-AFTER-FLOW TESTING (PE): See "Deliverability Testing of Oil Wells."

FLOW EFFICIENCY (PE): See "Condition Ratio."

FLUID POTENTIAL (GW): The mechanical energy per unit mass of a fluid at any given point in space and time with respect to an arbitrary state and datum.

FORMATION VOLUME FACTOR (PE): A factor to account for changes in volume in each phase upon transition from reservoir to standard surface conditions. The ratio of the volume at reservoir conditions to the volume at standard surface conditions.

GROUND WATER, PERCHED (GW): Confined ground water separated from an underlying body of ground water by an unsaturated zone. It is held up by a "perching bed" of low permeability, and its water table is a "perched water table."

HEAD, STATIC (GW): The height (above a datum) of a column of water that can be supported by the static pressure at a given point. The sum of the "elevation head" and the "pressure head." See "Head, Total."

HEAD, TOTAL (GW): The sum of three components: (a) "elevation head," which is the elevation of the point above a datum; (b) "pressure head," the height of a column of static water that can be supported by the static pressure at the point; (c) "velocity head," the height the kinetic energy of the liquid is capable of lifting the liquid.

HORNER PLOT (PE): A plot of pressure build-up versus $\log \frac{t + \Delta t}{t}$ where t is time since production and Δt is time since shut-in. A similar plot was proposed in ground water hydrology by Theis to analyze recovery data.

HYDRAULIC CONDUCTIVITY (K) (GW): Has dimensions of length per unit time. A medium has a hydraulic conductivity of unit length per unit time if it will transmit in unit time a unit volume of groundwater at the prevailing viscosity through a cross section of unit area, measured at right angles to the direction of flow, under a hydraulic gradient of unit change in head through unit length of flow. Replaces the term "coefficient of permeability."

HYDRAULIC CONDUCTIVITY, EFFECTIVE (GW): The rate of flow of water through a porous medium that contains more than one fluid.

HYDRAULIC DIFFUSIVITY (GW): The ratio between hydraulic conductivity and specific storage.

HYDRAULIC GRADIENT (GW): The change in static head per unit of distance in a given direction.

HYDROCOMPACTION (GW): The process of volume decrease and density increase that occurs when moisture-deficient deposits are wetted for the first time.

IMAGE METHOD (METHOD OF IMAGES) (PE): The technique of using image wells to generate no-flow and constant pressure boundaries in an infinite system.

IMAGE WELL (GW): An imaginary well which effectively produces the same drawdown (or recovery) as a linear boundary limiting the aquifer. See "Image Method."

INFLOW PERFORMANCE RELATIONSHIP (PE): Used to predict a well's deliverability when deliverability test data are not available. A relationship between flow rate, bottom-hole pressure, average reservoir pressure, and a productivity index.

INFLUENCE REGION (PE): The region surrounding a well or wells whose properties influence transient tests performed on those wells. (Not to be confused with Meinzer's "area of influence.")

INJECTIVITY TESTING OR INJECTION WELL TESTING (PE): Pressure transient testing during injection into a well. Bottom-hole pressure is recorded while injection rate is held constant.

INTERFERENCE TESTING (PE): A multiple-well transient test which involves the production of an active well (injection) and observing the resulting pressure changes in an observation well.

INTERPOROSITY FLOW PARAMETER (PE): A dimensionless property of a fractured system. Dependent on the well radius, a matrix-to-fracture geometric factor, and the ratio of the formation matrix permeability to the effective fracture permeability.

ISOCHRONAL TESTING (PE): See "Deliverability Testing of Oil Wells."

JACOB'S METHOD (GW): Also known as asymptotic solution. Involves a semi-logarithmic plot of drawdown as a function of the log of time.

LEAKANCE (GW): The ratio of vertical hydraulic conductivity to thickness of the aquiclude.

LEAKY AQUIFER (GW): An aquifer into which overlying and/or underlying aquitards discharge water as the potentiometric head in the aquifer is lowered.

MEINZER UNIT (GW): A unit of hydraulic conductivity defined as the flow of water in gallons per day through a cross-sectional area of 1 ft^2 under a hydraulic gradient of 1 at a temperature of 60°F.

MOBILITY (PE): The ratio of absolute permeability to viscosity.

MOBILITY RATIO: The ratio of the mobility of the injected fluid to that of the in situ fluid.

MULTI-AQUIFER WELL (GW): A well which is screened to produce fluids from multiple aquifers which are separated by zones of low permeability. (cf: "commingled systems")

MULTIFLOW EVALUATOR (PE): A tool used in drill stem testing which allows unlimited sequences of production and shut-in. Includes a fluid chamber to recover an uncontaminated formation-fluid sample under pressure at the end of the flow period.

MULTIPLE RATE TESTING (PE): Tests involving a variable flow-rate. Testing at a series of constant flow rates, or testing at constant bottom-hole pressure with continuously changing flow rate.

ORTHOTROPY (GW): See "anisotropy."

PERMEABILITY, EFFECTIVE (GW): See "Hydraulic Conductivity, Effective."

PERMEABILITY, INTRINSIC: Same as "Permeability." Term adopted by U.S. Geological Survey to indicate a property of the medium alone, independent of the fluid properties. Has dimensions of L^2. Also called "Absolute Permeability."

PIEZOMETRIC SURFACE (GW): See "Potentiometric Surface."

POROSITY (GW): The property of a rock or soil of containing interstices. Expressed as the ratio of the volume of interstices to the total volume.

POROSITY, DUAL: The porosity of the rock having substantial primary and secondary porosity.

POROSITY, EFFECTIVE (GW): Refers to the amount of interconnected pore space available for fluid transmission. Expressed as the percentage of total volume occupied by interconnecting interstices.

POROSITY, PRIMARY (GW): Refers to the original interstices created when a rock or soil was formed in its present state.

POROSITY, SECONDARY (GW): Refers to the porosity created by fractures, openings along planes of bedding and solution cavities. Occur mostly in consolidated rocks having low primary porosity.

POTENTIOMETRIC SURFACE: A surface which represents the static head. An imaginary surface connecting points to which water would rise in tightly cased wells from a specified surface or stratum in the aquifer.

PRESSURE, AVERAGE RESERVOIR: The pressure a reservoir would attain if all wells were shut in for infinite time, assuming no natural influx of fluid.

PRESSURE BUILDUP TESTING (PE): Involves shutting in a producing well and analyzing the resultant pressure buildup curve for reservoir properties and wellbore condition

PRESSURE, INITIAL RESERVOIR (PE): Stabilized pressure of a shut-in well.

PRESSURE, INTERWELL (PE): The pressure halfway between an injection well and a production well. Sometimes used to approximate average reservoir pressure.

PRODUCTIVITY INDEX (PE): Also known as the specific capacity of a well. Denotes the productivity of a well per unit drawdown.

PSEUDO SKIN FACTOR (PE): The apparent skin factor in a well which has no true physical damage (or improvement) but is not drilled completely through the formation thickness or is only partially completed, thus appearing damaged.

PSEUDO STEADY STATE (PE): A transient flow regime in which the rate of pressure change with time is constant at all points in the reservoir.

PULSE TESTING (PE): A multiple-well transient test, in which flow rate pulses are produced in an active well and the resulting pressure changes are recorded in an observation well. Provides reservoir information for the region around and between the two wells. (Because of the shorter time intervals, the influence region for a pulse test is less than that for an interference test, and thus information is gained about a smaller portion of the reservoir.)

RADIUS OF DRAINAGE (PE): Defines a circular system around a well in which a pseudo steady state pressure distribution exists.

RECOVERY TEST (GW): Also known as build-up test in petroleum engineering. Denotes a test which involves the measurement of recovery in a well after the well is shut in following a known period of production.

RELATIVE PERMEABILITY (PE): Also called effective permeability in ground water hydrology. Denotes the permeability of the porous medium to a particular fluid when more than one fluid is present.

RESIDUAL DRAWDOWN (GW): During recovery, the difference between the static water level and the water level at any instant during recovery.

SAFE YIELD (GW): Given a variety of meanings, but originally defined (by Meinzer) as the rate at which ground water can be withdrawn year after year from a given aquifer system without depleting the supply to the point where withdrawal at this rate is no longer economically feasible.

SEEPAGE FACE (GW): For a well piercing an unconfined aquifer, seepage face denotes that segment of the well screen over which the total head equals elevation above datum and water flows from the aquifer into the well.

SEEPAGE FORCE: See "Stress, Seepage."

SHAPE FACTOR (PE): A geometric factor, characteristic of the reservoir shape and well location.

SLUG METHOD (GW): Used to determine transmissivity of an aquifer. A known volume or "slug" of water is suddenly injected into or removed from a well and the decline or recovery of the water level is measured at closely spaced time intervals during the ensuing minute or two.

SINGLE-PACKER TEST (PE): A drill stem test utilizing one packer in which fluid flows through the perforated anchor pipe into the drill string.

SKIN (PE): A zone of decreased permeability near the wellbore created by drilling and completion practices.

SKIN FACTOR (PE): A constant which relates the pressure drop across the skin to the dimensionless rate of flow. A measure of wellbore damage.

SPECIFIC CAPACITY (GW): The rate of discharge of water from a well divided by the drawdown of water level within the well. Varies slowly with duration of discharge. Also called productivity index in petroleum engineering.

SPECIFIC DISCHARGE or SPECIFIC FLUX (GW): The rate of discharge of ground water per unit area measured at right angles to the direction of flow.

SPECIFIC RETENTION (GW): The ratio of the volume of water a saturated rock or soil will retain against the pull of gravity to its own volume.

SPECIFIC STORAGE (GW): The volume of water released from or taken into storage per unit volume of the porous medium per unit change in head.

SPECIFIC YIELD (GW): The water yielded by water-bearing material by gravity drainage, as occurs when the water table declines. The ratio of the volume of water a saturated rock or soil will yield by gravity to its own volume.

STABILIZATION TIME (PE): The time corresponding to the start of the pseudo steady state period.

STATIC WATER LEVEL (GW): The static position of the potentiometric surface in a well prior to the commencement of discharge. (See also initial reservoir pressure in petroleum engineering.)

STEADY STATE: Pressure is constant at all points in the reservoir.

STEP DRAWDOWN TEST (GW): Also known as productivity index test or step-rate test in petroleum engineering. Involves producing a well at different rates for predetermined periods of time and monitoring drawdown.

STEP-RATE TESTING (PE): A multiple-rate injection well test in which fluid is injected at a series of increasing rates, each rate lasting an equal amount of time. Injection pressure at the end of each rate is plotted versus injection rate.

STORAGE COEFFICIENT: The volume of water an aquifer releases from or takes into storage per unit surface area of the aquifer per unit change in head.

STRADDLE-PACKER TEST (PE): A drill stem test in which the tested interval lies between two packers.

STRESS: APPLIED: The downward stress imposed at the aquifer boundary by (a) the weight (per unit area) of sediments and moisture above the water table, (b) the submerged weight of the saturated sediments overlying the boundary, and (c) the net seepage stress due to flow within the saturated sediments above the boundary.

STRESS, EFFECTIVE: Stress that is borne by and transmitted through the grain to grain contacts of a deposit. The effective stress at a point in an aquifer differs from the applied stress at the aquifer boundary by the submerged weight (per unit area) of the intervening sediments and the net seepage stress due to flow within the intervening sediments.

STRESS, SEEPAGE: Stress created by the seepage force, which is transferred from the water to the porous medium by viscous friction. Seepage force is exerted in direction of flow.

SUBSIDENCE: Sinking or settlement of the land surfaces, due to any of several processes, but most importantly due to artificial withdrawal of subsurface fluids.

TEMPERATURE, PSEUDOCRITICAL (PE): For a mixture of gases, calculated from the relative amounts and critical temperatures of the components.

TEMPERATURE, PSEUDOREDUCED (PE): The ratio of the temperature of interest to the pseudocritical temperature.

THEIM EQUATION (GW): Represents steady-state radial flow solution to a well in the center of a circular, homogeneous, horizontal aquifer with prescribed potential at the circular boundary.

THEIS SOLUTION (GW): Represents the solution to a continuous line source in a homogeneous, horizontal, infinite, isotropic aquifer. (Also known as exponential intergral in petroleum engineering.)

TIDAL EFFICIENCY: A measure of the response of the water level in a well to changes in ocean level. Equal to the barometric efficiency subtracted from 1.

TRANSIENT TESTING: The study of pressure variation with time in an active well (production or injection) under a variety of conditions and possible operating procedures.

TRANSMISSIVITY (T), (GW): The rate at which water of the prevailing kinematic viscosity is transmitted through a unit width of the aquifer under a unit hydraulic grandient.

TWO-RATE TESTING (PE): A multiple-rate test on a production well using only two different flow rates.

TWO-ZONE SYSTEMS: See "Composite Systems."

u (GW): Dimensionless quantity related to the reciprocal of dimensionless time, t_D, used in petroleum engineering.

$$u = \frac{r^2 s}{4Tt} = \frac{1}{4t_D}$$

UNCONFINED AQUIFER (GW): Also called water table aquifer. An aquifer which contains a water table, at which it is in direct contact with the atmosphere.

UNIFORM-FLUX FRACTURE (PE): One in which fluid enters at a uniform flow rate per unit area. A first approximation to the behavior of a vertically fractured well.

VERTICAL PULSE TESTING (PE): Used to determine vertical permeability of a formation. Fluid is injected in pulses above a packer, escapes the wellbore through flow perforations and reenters below the packer through observation perforations where pressure changes are observed with a pressure gauge.

VOID RATIO (GW): The ratio of the volume of the interstices in a rock or soil to the volume of its mineral particles.

WATER DRIVE RESERVOIRS (PE): Reservoirs in direct communication with an active aquifer.

WELLBORE STORAGE (PE): Fluid stored in the wellbore above reservoir level. Usually occurs when a production well is shut-in without packers used to maintain fluid level. Affects pressure build-up data at early time as fluid continues to flow into the wellbore after shut-in.

WELL FUNCTION OF u (GW): Equal to twice the value of P_D, dimensionless pressure, which denotes the value of the exponential integral.

WELL LOSSES (GW): Denotes drawdowns at the well in excess of the theoretical capability of the reservoir. Such well losses may be due to poor development of the well, excessive entrance velocities and casing damages due to skin, scaling, or corrosion.

WIRELINE FORMATION TESTING (PE): A tool is lowered into the well on a logging cable. The mechanism establishes communication with formation fluid and measures pressure response. Slightly more qualitative than a DST.

APPENDIX C
INSTRUMENTATION

Before any meaningful analysis of the data can be obtained, data of good quality is essential; it can be obtained from careful test planning, control, execution, and adequate instrumentation. Knowing how to use downhole pressure transducers to obtain pressure transient data is important. In principle, downhole data will always provide more reliable data insofar as the effects of temperature changes in the wellbore become unimportant. However, the use of downhole instrumentation may not always be possible or cost effective. For instance, if the production well is being pumped, it may not be possible to use a downhole tool because of the difficulty in setting the tools and the pump. Alternatively, the budget allocation for testing may prohibit the use of downhole tools. In general, the deeper the well or the hotter the well, the more important it is to use downhole instrumentation. If the well is over 100°C and sufficient wellhead pressure cannot be maintained, the water will start to flash (boil) in the wellbore. In this event, wellhead data or water level data will be useless for pressure transient testing and productivity calculations. For this case, downhole data is essential. If good quality production well data cannot be obtained, it is recommended that every effort be made to conduct a simultaneous production and interference test. Instrumentation for interference testing is readily available and, in general, easy to install and maintain.

In the following sections, subdivided by the test parameter to be measured, a variety of instruments will be discussed. Relevant to the discussion is the definition of accuracy and resolution. Accuracy is a measure of how closely a measured parameter compares to the correct value, as determined by the Bureau of Standards. The accuracy of an instrument is a function of its calibration, hysteresis, drift, repeatability and resolution. The resolution of an instrument is a function of sensitivity of the transducer to the parameter being measured, and the smallest quantity that can be observed and measured when using the instrument. For instance, a thermistor may have infinite resolution to temperature changes, but the ohm-meter being used to read the resistance may only have a resolution of five ohms; thus, the meter, not the probe controls the resolution of the instrument. The resolution or accuracy of a measured system is only as good as the worst component. For geothermal applications, the resolution of a pressure

APPENDIX C
INSTRUMENTATION

Requirements

Before the appropriate type of instrument can be selected, the developer or consultant must calculate the anticipated pressure changes, flow rates, temperatures, and time resolution requirements. Methods for doing this have been discussed in Volume I. The importance of correctly anticipating these parameters is that the instrument chosen must have accuracy and precision far greater than the expected changes. For instance, when measuring pressure changes in an observation well with an expected 1 psi maximum of pressure change, then the instrument should have a resolution of at least 0.1 psi. On the other hand, in a production well there will be a relatively large pressure change and therefore only require 1 psi resolution. Instruments with a wide range of precision and accuracy are available. In general, the finer the resolution and greater the accuracy, the more expensive the instrument. However, advances in the development and availability of these instruments is lowering the cost of the high precision gauges.

An often overlooked area in test planning is the time element. If pressure changes take place very rapidily the recording equipment and/or personnel may not be suitable to record the data at a sufficiently small time interval. In general, in fractured or highly permeable aquifers the pressure changes will take place very quickly and be of a smaller magnitude than in a moderate or low intergranular permeability system. In almost every case it is valuable to have continuous recording devices with accurately synchronized clocks for measuring and recording each parameter of the test. This minimizes operator error, missed events, ambiguity in the data, and simplifies data analysis and interpretation.

gauge is often the more significant measure of the quality (or suitability) of a gauge. However, for temperature and flow rate measurements, accuracy is a more important requirement.

The following pages list some of the instruments currently available, their assets and drawbacks, and the types of instruments most suitable for a variety of applications. In addition to the detailed discussions, Tables C-1 through C-3 at the end of this subsection, summarize many of the performance characteristics of temperature and pressure sensors as defined in Reference C-1.

Flow Measurement

1. Weirs and flumes

   Accuracy: ±10%

   Range: 1 gpm to any maximum.

   Advantages: Very inexpensive, can be home-built. Construction details and formulas are contained in several engineering handbooks.

   Disadvantages: Cannot be used if the temperature is greater than 100°C. Also, cannot be installed in a pressurized pipeline and cannot be connected to a continuous recording device very easily.

   Suppliers: F. B. Leopold Company and BIF Industries.

2. Known-Volume container or weighing tank and stopwatch

   Accuracy: ±20%.

   Range: Limited only by the scales, container or tank, and the flow control apparatus.

Advantages: Very inexpensive.

Disadvantages: Cannot be connected to a continuous recorder. The person measuring the flow can get burned.

3. Differential pressure meters (orifice meters, nozzles, Pitot tubes, Venturi tubes, and low-pressure loss tubes)

Accuracy: ±10%.

Range: Pitot tubes--<1 to >30 ft/sec. Others--0.1 to 30 ft/sec. Depends on orifice and pipeline size.

Advantages: Most pump companies and drillers use these methods and are comfortable and familiar with them. They are most easily connected to continuous recording devices; therefore, these methods are very suitable for most applications.

Disadvantages: Scaling or flashing across the orifice can create undetected inaccuracy in the measurements.

Cost: Costs vary widely with the type of element and also with line size and pressure rating; less than $100 for an orifice plate to several thousand dollars for a venturi or one of the patented flow tubes. Installed cost also varies greatly with line size and pressure rating except for the pitot tube which is installed in a boss on the pipe wall.

Readout and Recording Equipment: A method must be provided to measure the pressure difference, and if desired, convert that to flow rate. In some cases, ΔP can be measured with a homemade manometer made from clear plastic tubing and a yard

stick, or a commercial manometer. At high line pressures, a ΔP gauge or transmitter with output indicator may be required. In either case the measured ΔP is then used to calculate flow rate. If direct flow reading is required, a pressure gauge scale (nonlinear) can be calibrated in flow units or a transmitter output can be converted electronically to a direct flow indication or output proportional to flow for recording or display. Cost of equipment to provide transmitting, recording, and indication could range from $2,000 to $3,000 or more, depending on the grade or quality of equipment.

Partial List of Suppliers: Pitot Tubes--Foxboro Corp., Meriam Instrument Co., Rosemount Engineering, Deitrich Standard, Taylor Instrument Co. Orifice Plates, Venturi tubes and nozzles--Daniel Industries, Inc., Badger Meter, Meriam Instrument Co., Fischer & Porter Co., Foxboro Corp., Tech Tube Corp.

4. Turbine Flow Meters

Accuracy: $\pm$5%.

Range: Depends on impeller and pipe diameter 0.1 to 50 ft/s.

Cost: Relatively expensive; several hundred dollars to several thousand depending on size and features.

Output: Output signal of most transmitters is a frequency proportional to volumetric flow rate that can be fed directly to a compatible flow rate indicator meter.

Advantages: Good accuracy, repeatability, and linearity. Wide ranges. Can be installed in-line or on a probe through the pipe wall.

Disadvantages: Can be degraded by other than clean fluids. Relatively high cost.

Partial List of Suppliers: Daniel Industries, Flow Technology, Inc., Foxboro Corp., Brooks Instruments, Fischer & Porter, and Electronic Flow-Meters.

5. Others

There are many other types of meters available that could be investigated if those listed above are not suitable. The following types would be in that category:

Acoustic/ultrasonic--no obstruction, thus no pressure loss. The clamp-on Doppler eliminates scaling and corrosion problems.

Magnetic--No obstruction in the line thus no pressure loss. Somewhat pressure and temperature limited by liner material. Relatively insensitive to dirty fluids.

Vortex--Good accuracy--subject to scaling.

Wellhead and Differential Pressure Measurement

1. In addition to the transducers in the preceding table, the following instruments are available:

a. Manometers: Measure pressure or differential pressure.

Accuracy: ±1% of span for most. ±0.1% for precision types.

Range: Minimum span is 0.15" H_2O, maximum span 60 psig.

Design pressure:	Up to 6,000 psig.
Design temperature:	Function of seal fluid, usually ambient.
Advantages:	Relatively low cost. Availability.
Disadvantages:	Difficulty connecting to a recording device, not sufficiently rugged for field testing.
Cost:	Ranges from a few dollars for the simple units to approximately $1,000 for the more sophisticated and precise.
Partial List of Suppliers:	Meriam Instrument Co., Bailey Meter Co., and Foxboro Corp.

b. Mechanical pressure gauges bourdon tube

Accuracy:	Between ±0.1% and ±5% of span.
Range:	From 10 in. H_2O to 100,000 psig.
Advantages:	Readily available and replaceable. Most drillers and pump operators have them.
Disadvantages:	Difficult to connect to recording devices.
Cost:	From $20 to thousands depending on dial size and accuracy.
Partial List of Suppliers:	Ashcroft, Foxboro Corp., Robert Shaw Controls, Heise (Dresser) Wallace and Tiernan Inc., ITT Barton.

c. Electronic pressure and differential pressure transmitters, capacitors, strain gauges, piezoelectric semiconductors (piezoresistive), potentiometers. (Process grade field instrumentation.)

Accuracy:	0.1% to 1% of calibrated span.
Range:	A few inches of water to several thousand psig.
Advantages:	Easily connected to continuous recording devices. Usually these devices are fairly reliable.
Disadvantages:	High cost and lead time for replacement.
Cost:	$750 to $2,000 depending on accuracy and pressure.
Partial List of Suppliers:	ITT Barton, Fisher Controls, Foxboro Corp., Honeywell, Taylor Instrument Co., Rosemount, Bailey Meter Co.

Temperature

Temperature gauges should be placed in thermal wells near the wellhead on the discharge line.

1. Mercury Thermometer

Accuracy: Depends on range 0.1 to 1°C.

Advantages: Readily available. Very accurate if small enough range.

Disadvantages: Cannot be connected to a recording device.

2. Electronic gauges

There are a wide variety of electronic gauges available. Tables C-1 and C-2 summarize the many varieties and manufacturers. Most of the available transducers are suitable for wellhead temperature measurements. One advantage of electronic gauges is that they can be easily connected to readout and recording devices. Calibration and recalibration of these gauges will ensure their repeated accuracy.

Downhole Instrumentation

Downhole Temperature Measurement

Tables C-1 through C-3 compare the performance of various sensors. For simple downhole temperature measurement a max-reading thermometer can be lowered into the well on a line. If more than maximum temperature is required, i.e., temperature versus depth or a continuous indication, a thermocouple, RTD or thermistor can be lowered into the well on a conductor line and temperature measured on the surface with a portable bridge, potentiometer or the temperature can be recorded if desired. Small reels or winches with conductor lines are available at reasonable cost. For more precise and detailed temperature logs, it may be more suitable to rent the equipment or hire a well logging service. Downhole tools can be purchased outright but the cost is usually prohibitive. The "Kuster" temperature tool incorporates a downhole recorder and can be run on a wire line. A logging service's charge will include costs/foot of depth, a flat service charge, and other charges depending on well condition, location, etc. The charges to log a 5,000-ft. deep cased hole could be several thousand dollars.

The following companies rent equipment or provide service as noted:

Schlumberger Well Services--Service

Dresser Atlas--Service

Birdwell--Service

Kuster Company--Tool Rental and Sale

Gearhart Owen Industries--Tool rental, sales, and service

Halliburton Services--Service

Sperry-Sun--Tool rental, sales, and service

Downhole Pressure Measurement

1. Bubbler Tube. Perhaps the simplest and least expensive method to measure downhole pressure and water level is the bubbler tube. A crude but sometimes appropriate arrangement consists of a tire pump and a gauge connected to a small pipe or tube suspended in the well. Accuracy of the bubbler tube in well measurement applications can vary widely depending on the equipment, temperature effects, and operating techniques. In ordinary tank level measurement accuracies of ±1% can be achieved.

2. Downhole Capillary Tube. This consists of a small tube suspended in the well with a pressure coupling chamber at the bottom and a precision pressure transducer on the surface. The tube is filled with inert gas or a synthetic fluid. Sperry-Sun Inc., supplies such a system.

3. Electronic Pressure Transducers. Table C-3 compares the performance of several transducers suitable for downhole measurements. As in the case of downhole temperature measurements, the tools can be rented, purchased, or the services can be hired. The table lists suppliers, some of which will rent tools. The same companies listed as renting temperature tools or providing logging service will also provide pressure tools and service at similar costs. In the following section, an instrument incorporating a Paro-scientific digiquartz transducer is discussed.

Downhole Flow Measurement

Most of the downhole flow meters use a variation of the turbine discussed previously. As with downhole pressure and temperature measurement the tools and/or service are available for rent or hire. Most of the companies listed above will provide flow measurement tools or service.

Water Level Measurement

1. Bubbler Tube. The bubbler is usable in subsurface water level or artesian wells. Several companies supply systems and equipment for ordinary tank level measurements which may be suitable for well measurements. Cost would be on the order of several hundred dollars. Some of the companies are: Fisher Governor Co., Meriam Instrument Co., Petrometer Corp., and Uehling Instrument Co.

2. Tape and Float. This method can be used on wells with water levels below the surface. They can be suspended by hand and the distance measured, or wound on a drum with provisions for continuous recording of level. Several companies make the latter unit which is well suited for monitoring well water level at depths up to 30(ft. Cost is approximately $1,000. Partial list of suppliers: Leopold & Stevens and Keck Instrument Inc.

3. Others. This would include the conductivity probes, which can be fouled by oil, etc., the chalked tape, and other float and changing resistance type systems.

Approximate Cost: $50 to $100 for 100 ft of chalk tape.
$300 to $800 for an electric tape.
$500 for a conductivity probe and meter.

Partial List of Suppliers:

Lufkin and Roe Instrument: chalk tape.
Sepa-Air Inc.: electric tape.
Springs Instruments: conductivity probe.

TABLE C-1. Manufacturers of temperature sensors reviewed

Manufacturer/Supplier	Electrical Sensing			Passive Indicating	
	Resistance Temperature Detectors (RTDs)	Thermistors	Thermocouples	Maximum Indicating Sensors	Bi-Metallic Stem Thermometers
ARi Industries	X	--	X	--	--
Barber-Coleman Co.	X	X	X	--	--
Big Three Industries	--	--	--	X thermochemical	--
Brooklin Thermometer	--	--	--	X glass/bi-metallic	--
Celesco Transducer Products	X	X	X	--	--
C. S. Gordon Co.	--	--	X	--	--
Fenwal Electronics	--	X	--	--	--
Fischer & Porter Co.	X	--	X	--	--
Foxboro Co.	X	--	X	--	--
Hi-Cal Engineering	X	--	X	--	--
ITT-Barton	X	--	--	--	--
Markal Co.	--	--	--	X thermochemical	--
Matthey Bishop, Inc.	X	--	--	--	--
Minco Products, Inc.	X	--	X	--	--
Rosemont, Inc.	X	--	--	--	--
Semco, Inc.	X	--	X	--	--
Spectro Systems, Inc.	--	--	--	X metal pellets	--
Sybron-Taylor Corp.	X	--	X	X glass	X
Thermometrics, Inc.	--	X	--	--	--
Victory Engineering	--	X	--	--	--
W. Wahl Corp.	X	X	X	X thermochemical and bi-metallic dial	X
Weed Instrument Co.	X	--	--	--	--
W. H. Keseler Co., Inc.	--	--	--	X glass	--
Weston Instruments	--	--	--	--	X
Yellow Springs Instruments	X	X	--	--	--
Omega Engineering	X	X	X	--	--

TABLE C-2.[a] Performance comparison of some commercial pressure transducers

No.	Manufacturer and (Model)	Sensor Technique	Accuracy (overall) (% FS)	Resolution (% FS)	Stability and Drift	Max °F	Coefficient	Maximum Pressure Range(s) (psia)	Size	Comments
1.	Hewlett Packard, (2811B)	Diaphragm with oscillating quartz crystal	0.025%	Infinite (0.01 psi typ)	0.01%/yr	300	?	11,000	1-7/16" dia. by 40" long	Accepted standard for precision downhole oil/gas well testing. Temp correction to ±1°C recorded.
2.	Mensor, (Digital Quartz manometer)	Fused quartz helical bourdon tube w/optical sensor and electronic nulling	<0.2%	0.0005%	0 @ 3 mos (0.01%/yr)	122	0.0004%/°C	1,000	11" by 10" by 8-1/2"	System temp control/ compensation to ±2°C to achieve performance quoted. Also makes unit like #3 below.
3.	Heise (Dresser), (Digiquartz)	C bourdon tube and servo force balance	0.05%	0.005%	NA	125	Very small, 0.1% FS over range	10,000	4-3/8" by 6" by 16"	Sperry-Sun sells for use with their 'tube' pressure transmission system.
4.	Paroscientific, (Digiquartz)	Bellows linked to vibrating quartz bar	0.1%	<0.1%	0.1%/yr	225	0.004%/°F	5,000	1.15" dia. by 3-1/4"	Hi temp @ pressure (530°F @ 10,000 psi) unit currently under joint development with Sandia Labs-- will have high temp electronics.
5.	Sundstrand Data Controls, Inc., (Developmental)	Bellow linked via quartz structure w/force-balance and capacitor feedback	0.11%	0.004%	0.1%/yr ?	176	NA	500	1-5/8" dia. by 2"	Mfg claims higher pressure (5K-10K) unit is developable, basic sensor capable of higher temperature
6.	Setra Systems, (204/205)	Diaphragm w/capacitor plate displacement	0.11%	<0.01%	0.05%/yr ?	250	0.004%/°F	10,000	1-3/4" dia.	Basic sensor w/o integral electronics capable of much higher temperature.
7A.	Heise (Dresser), (#CMM16)	C bourdon tube linked to dial and potentiometer	0.1%	0.01%	0.02%/yr	125	0	10,000	17-3/8" dia. by 3-1/4"	16" by 660 dial readout, electrical output also provided.
7B.	Mensor, (2792)			0.01%	0.02%/yr	125	0	10,000	17-3/8" dia. by 3-1/4"	Can operate up to 250°F w/external compensation.
8.	Robinson-Halpern, (144)	Helical bourdon tube linked to differential transformer	0.1%	<0.01%	NA	165	0.1%/°F	10,000	6" by 6" by 4-1/4"	--

TABLE C-2.[a] (continued)

No.	Manufacturer and (Model)	Sensor Technique	Accuracy (overall) (% FS)	Resolution (% FS)	Stability and Drift	Max °F	Coefficient	Maximum Pressure Range(s) (psia)	Size	Comments
9.	Bell & Howell, (CEC-1000)	Diaphragm w/thin film strain gage (sputtered)	0.15%	<0.01%	0.1%/yr	600+	0.005%/°F	10,000	1" dia. by 2-/2"	Mfgr claims higher accuracy and temp performance available
10.	Bell & Howell, (CEC-4-361)	Diaphragm w/unbonded wire strain gage	<0.2%	<0.05%	0.5%/yr	700	0.1%/°F	5,000	1-1/4" dia. by 2-1/2"	Fragile and slow temp response time (mfgr feels thin film will replace).
11.	Kaman Sciences, (KP-1911)	Diaphragm with eddy current variable impedance coil	0.25%	0.1%	NA	1000	0.1%/°F	5,000	5/8" dia. by 1-1/2"	--
12.	Sparton South-west, (890 HT)	C bourdon tube with wire potentiometer	1%	0.3%	NA	600+	0.1%/°F	10,000	1" dia. by 2-1/2"	--
13.	Celesco, (P2)	Diaphragm w/variable reluctance transducer	1%	0.1%	0.5%/yr	250	0.2%/°F	10,000	1-1/4" dia.	Mgfr has built high temp (600°F) unit w/derated accuracy (~1-1/4%).
14.	Data Instruments, (MPA 1000)	Diaphragm w/bonded semiconductor strain gage	0.25%	<0.05%	0.5%/yr	250	0.001%/°F	5,000	1-1/4" dia. by 2-1/2"	--
15.	Vernitech	C bourdon tube with film potentiometer	0.7%	<0.05%	0.5%/yr	185	0.01%/°F	10,000	2-1/2" dia. by 2"	--

a. See Reference C-1.

TABLE C-3. Performance comparison of geothermal process temperature sensors

Performance Parameter	Resistance Temperature Detectors (RTDs)	Thermistors	Thermocouples	Bi-Metallic Thermometer	Thermochemical and Physical Melt Indicators	Bulb-Bourdon Tube (thermal fluid filled)
Temperature range	-260 to 900°C	-100 to 400°C	-270 to 2000°C	-60 to 450°C	38 to 1649°C labels (38 to 600°C)	0 to 340°C
Accuracy	0.01% (<0.1°C)	1%	0.1%	1% (0.5% available)	1% (0.3% available)	1%
Sensitivity (signal level)	Good: +0.5%/°C (<0.1V/°C with bridge)	High: -5%/°C -0.5% linearized (<0.5 V/°C with bridge)	Very low, 1%/°C	Depends on dial size, etc.	NA	0.5% of F.S.
Linearity	Excellent: 1%	Poor: 10-20% Linearized: 2%	Poor: 10-25%	1%	NA	1%
Stability	Excellent	Poor	Excellent	Good	NA	Fair
Interchangeability	Excellent	Good	Poor	NA	NA	NA
Size	Medium: >1/8" diam. by >1/4" long	Very small	Small	1" to 5" dial. stem dia. >1/8"	Typically >1/8"	Very large
Time constant	0.2 to 10 s	0.05 to 10 s	0.1 to 4 s	10 to 30 s	1 s	Long
Cost	$25 to $1000	$2 to $300	$1 to $50		$0.50 to $7	High
Comments	Best overall	Narrow span (typically <105°C)	Requires reference temp. junction	Can be configured w/maximum registering dial. Used in Kuster 'bomb' type high temp		Used in GRC 'bomb' type high temp logging tool (span limited ~150°C). Kuster also makes system rated for 260°C.

REFERENCE

C-1. M. D. Lamers, Measurement Requirements and Methods for Geothermal Reservoir System Parameters (An Appraisal), LBL-9090, GREMP-6, 1979.

APPENDIX D
FABRICATION OF INSTRUMENTS

APPENDIX D

FABRICATION OF INSTRUMENTS

The cost of commercially available downhole instrumentation is often prohibitive. For this reason, and to obtain the highest quality data possible, the Earth Sciences group at Lawrence Berkeley Laboratory has developed a suite of downhole instruments for low-to-moderate temperature geothermal well testing. Three components of a downhole instrument package are described here: a downhole pressure temperature tool, a multiconductor cablehead, and a line driver for transmitting the pressure tool signal. A fourth instrument, a float type water level detector is also discussed. The complete engineering drawings for these instruments are available in Reference D-1.

Downhole Pressure and Temperature Instrument

The Paroscientific 400 psi and 900 psi digiquartz pressure transducers have been used for many years in measuring precise changes in wellhead pressures, pressure differentials across orifice plates and also in conjunction with "Perk" tubes and Sperry Sun downhole pressure chambers. In order to obtain precise pressure data during interference testing and accurate downhole pressure data, the Lawrence Berkeley Laboratory Reservoir Engineering group decided to incorporated the digiquartz pressure transducer in a downhole pressure temperature package which can be used in artesian and non-artesian wells. The maximum operating temperature of the tool is 107°C.

The downhole instrument package incorporates the Paroscientific 400 psi model 2400-A or 900 psi model 2900-A digiquartz pressure transducer (Figures D-1, D-2, and D-3). The transducer is shock-mounted inside the instrument package and connected to the pressure port with a stainless steel capillary tubing filled with Dow Corning f.s. 1265 fluid. The pressure device, when interfaced with the Paroscientific model 600 digiquartz computer and the Hewlett Packard 5150A thermal printer, can record pressure data at intervals of 1 second to 2 hours. The combination pressure-temperature housing is constructed from 316 stainless steel and has an outside diameter of 2.75 in. and a length of 9.5 in.

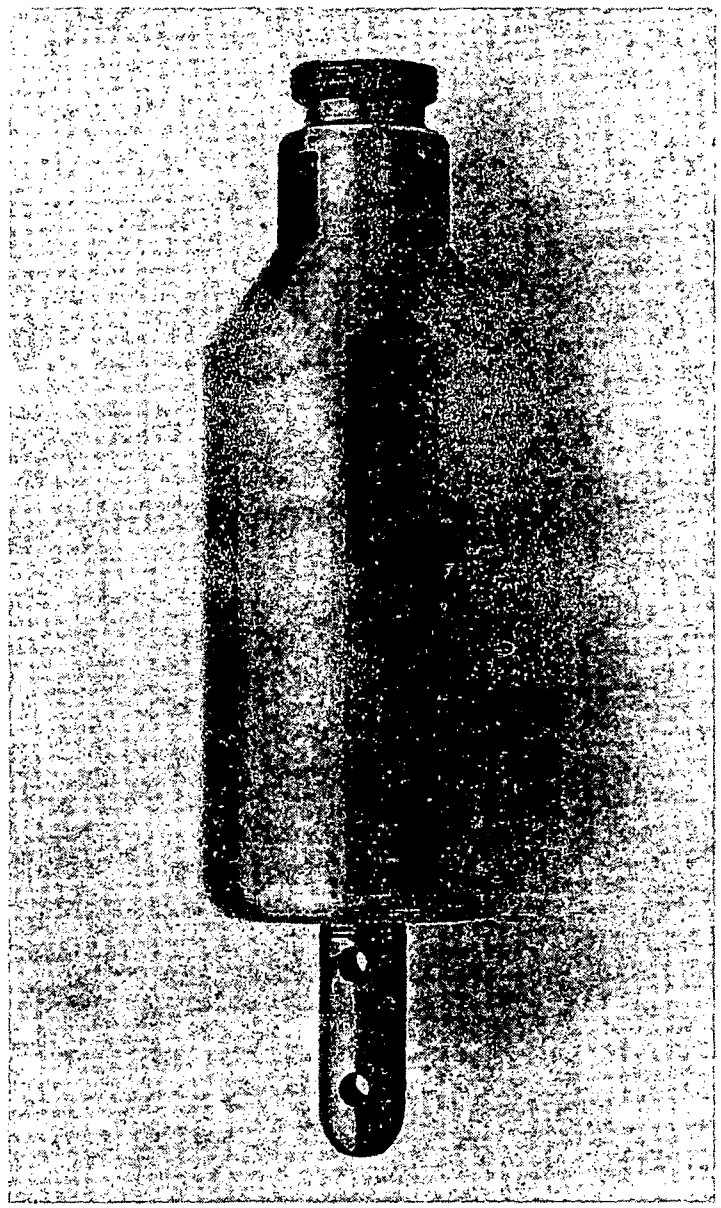

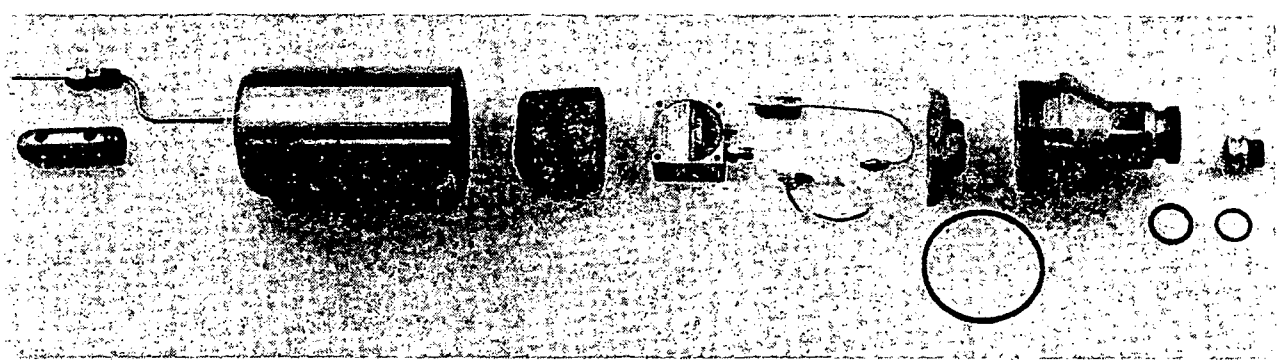

Figure D-1. Downhole instrument package.

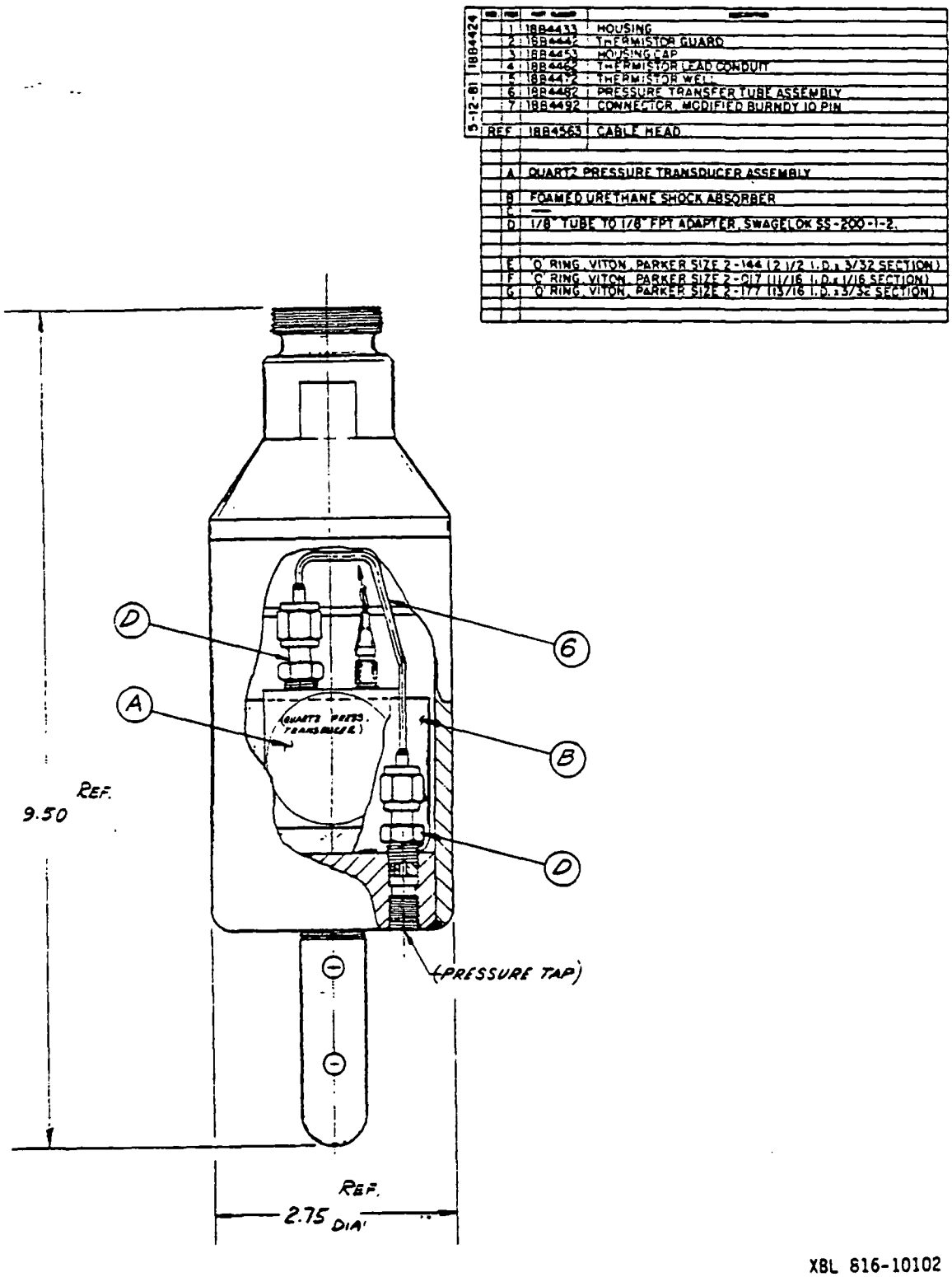

Figure D-2. Downhole pressure and temperature instrument.

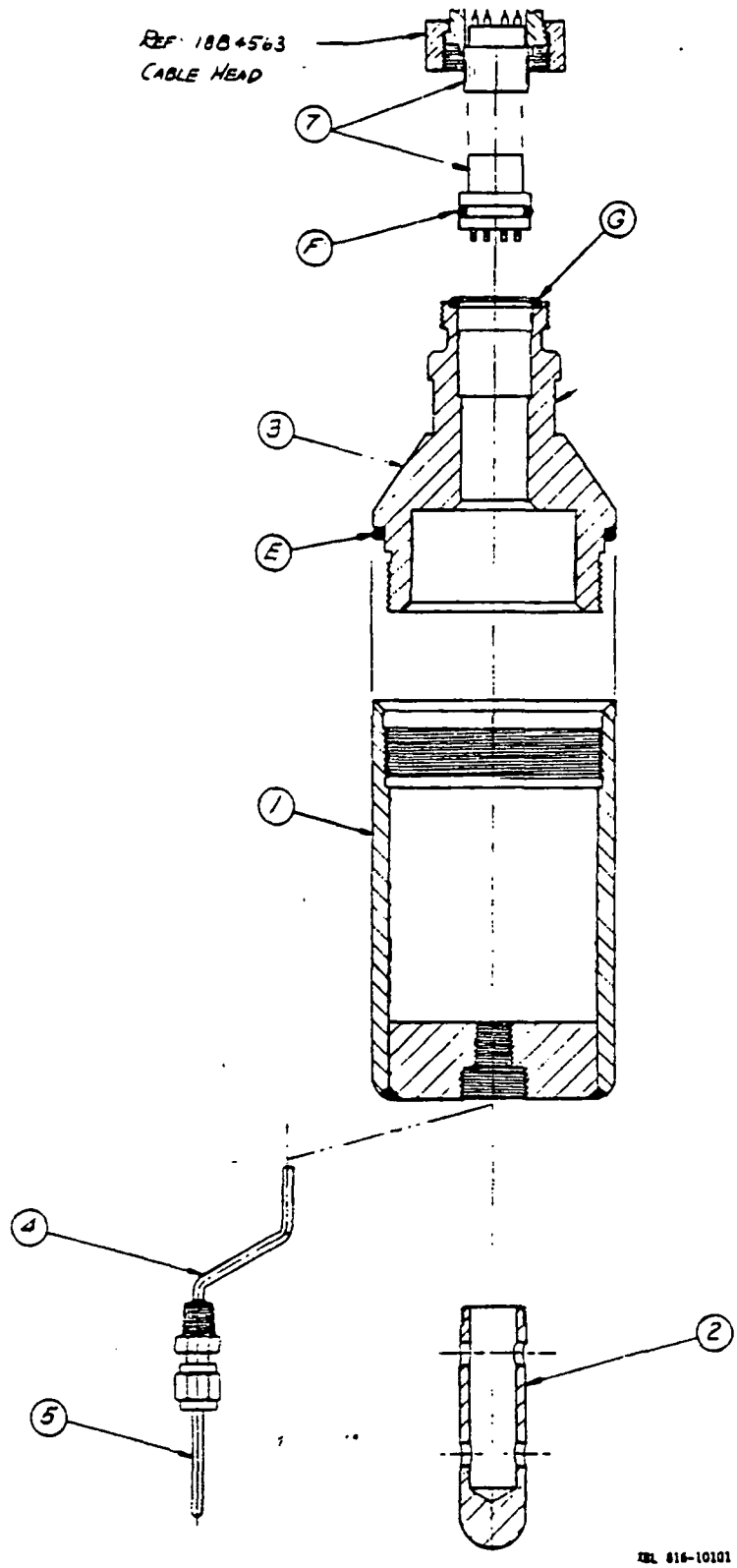

Figure D-3. Downhole pressure and temperature instrument continued.

The combination pressure-temperature chambers are lowered into the well on armored four-conductor cable. The cable is connected to the tool by a designed cablehead, but can also be run with a conventional multiconductor cablehead. The temperature sensing element is a YSI 44011 100,000 ohm at 25°C thermistor, isolated from the well fluid by 1/8 in. outside diameter stainless steel tubing with a 0.010 in. wall thickness. The thermistor has a resolution of ±.2°C (including thermistor interchangeability) and a response time of approximately 1 second in liquids. The resistance of the thermistor, which is temperature dependent, is read at the surface and converted to temperature.

The system has been field tested at Klamath Falls, Oregon; Susanville, California; and Cerro Prieto, Mexico.

Geothermal Multiconductor Cablehead

A cablehead is a connector used to mechanically and electrically attach the armored logging cable to a downhole instrumentation package. Commercially available cableheads perform properly in noncorrosive environments, but when subjected to the corrosive brines and the elevated temperatures found in geothermal wells, the corrosive brine will eventually enter the cablehead. This will short the electrical connectors and cause the armored steel strands to corrode. Loss of data and eventual loss of instrument package downhole can result.

The geothermal group at the Lawrence Berkeley Laboratory has designed an inexpensive multiconductor cablehead (Figure D-4). The body is machined from stainless steel with a length of 9 in. and a 1.5 in. diameter. It has an overshoot provision for retrieval should the instrument package be lost downhole. The cable is mechanically attached within the cablehead by letting a brass cone force the unbraided cable strands against the walls of an internally tapered sleeve. The cablehead incorporates an epoxy pressure seal. The high temperature epoxy used has excellent corrosion, chemical and solvent resistant properties. The epoxy is rated for continuous operation at temperatures up to 600°F. The epoxy seal is formed by pouring the epoxy mix around the electrical conductors inside the specially machined

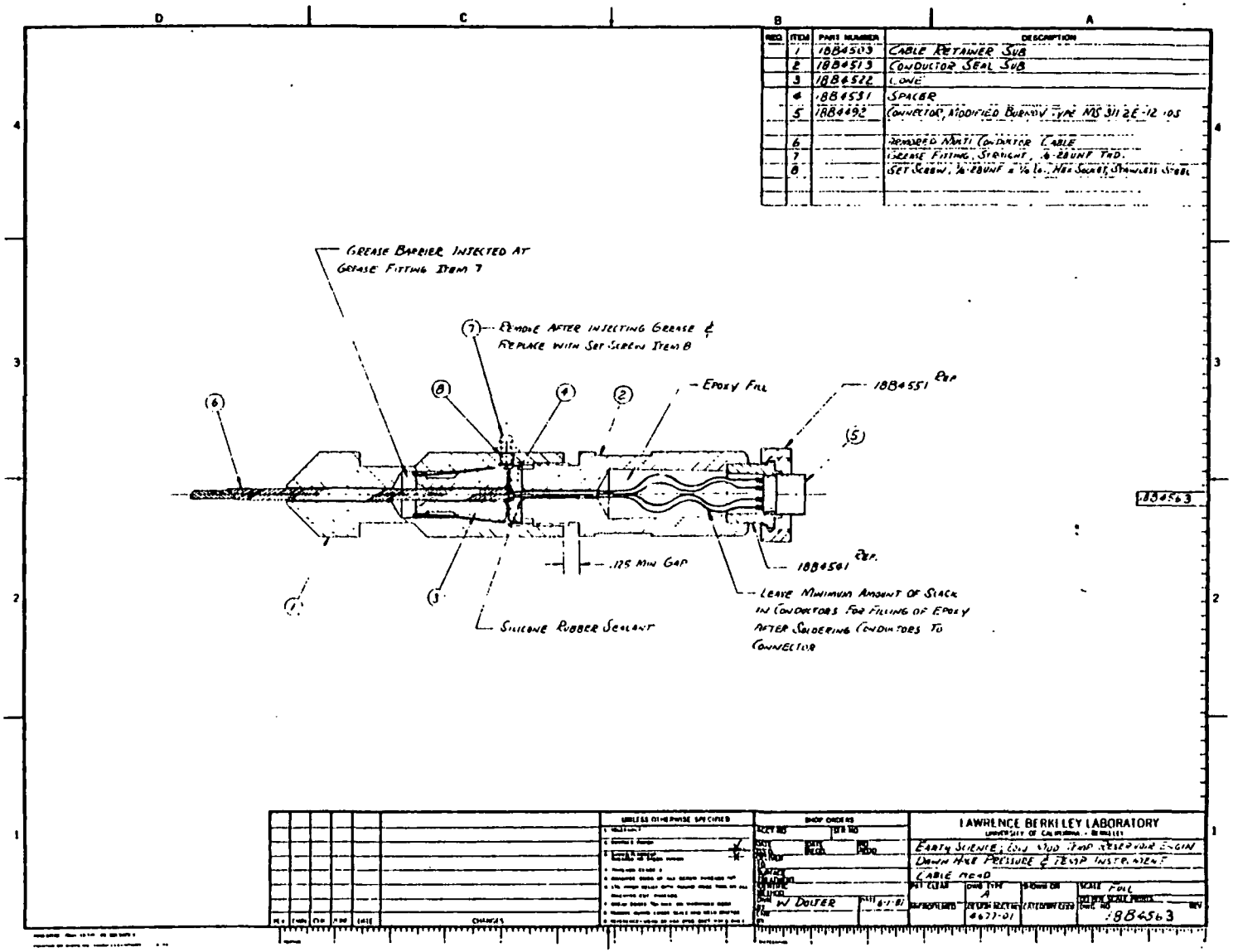

XBL 816-10097

Figure D-4. Multiconductor cablehead.

tapered cablehead cavity. The insulation on the conductors has been previously etched to ensure maximum adhesion of the epoxy. Should it become necessary, the epoxy seal can be easily removed with the aid of an electric drill. The cable can then be reheaded and a new seal poured in place. This can be carried out even under field conditions.

The cablehead also incorporates a grease barrier. A high temperature grease is pumped through a removable zerk fitting and fills void spaces within the cablehead assembly. This procedure keeps the often very corrosive, well bore fluid from entering the cablehead assembly. This eliminates the frequent reheading of the cable due to strand corrosion. The connection of cablehead to instrument package is made with a threaded fastener incorporating an "O" ring seal, and multi-conductor electrical connector.

Line Drivers

When using a Paroscientific pressure transducer it is often desirable to transmit the signal from the measurement location to a central data acquisition location. This allows for accurate clock synchronization and continuous observation of the instrument function. Because the transducer has a limited range in transmitting its frequency output, it is necessary to amplify the signal before it is relayed to the central data acquisition location.

The Field Systems Group at Lawrence Berkeley Laboratory designed an inexpensive line driver that detects, amplifies, and transmits the frequency signal from the transducer. The line driver provides power to the transducer from a 12 V automatic battery and transmits the output signal to a central location on an inexpensive twisted two-conductor wire.

The line driver is housed in a small instrument enclosure. The electronic circuit uses inexpensive commercially available components. A schematic of how the line driver is used in conjunction with the pressure tool is shown in Figure D-5.

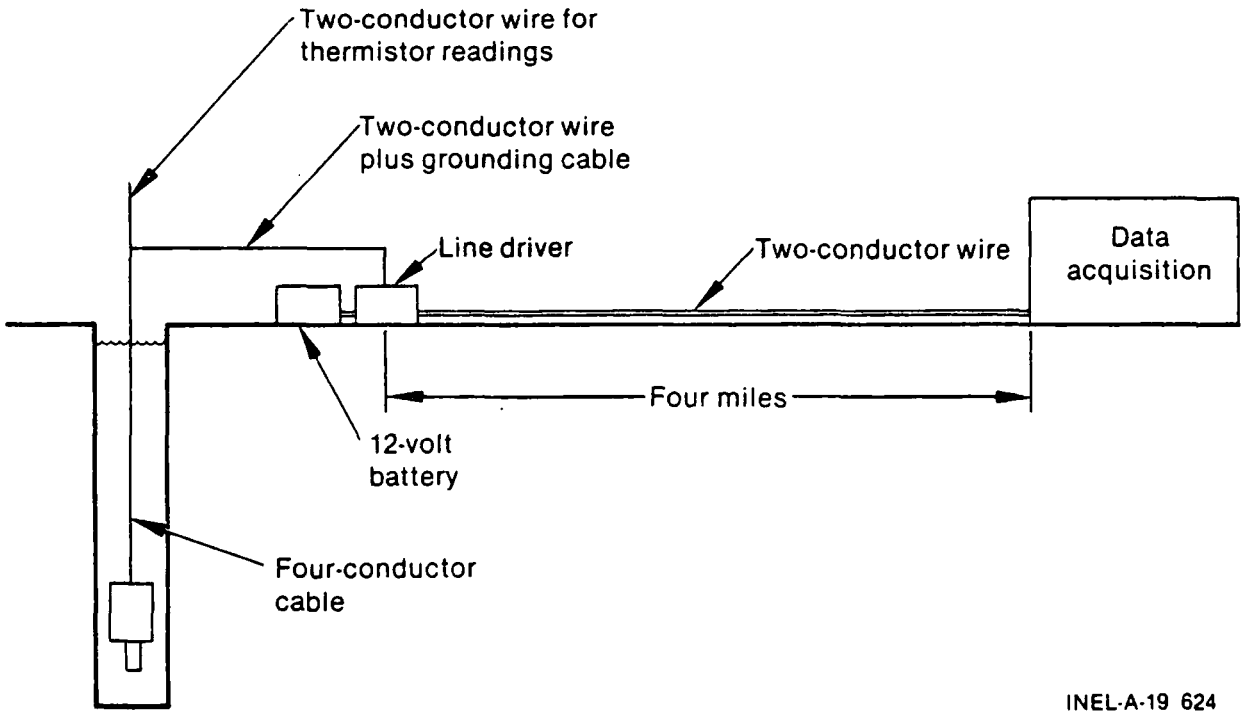

Figure D-5. Schematic of a line driver used in conjunction with the pressure tool.

Water Level Indicator

Description

Fluid level indicators, as used in well testing, are portable instruments used to detect the water level in the wellbore. The most commonly used type of probe is a conductivity-type gauge. The weighted probe attached to a two conductor cable is run down a well. When the probe contacts the water an electrical circuit is completed and the current flow is measured at the surface. When used in cold water wells, such a probe performs adequately; but for hot wells it is often unreliable. Because a conductivity-type gauge relies solely on the conductivity of the downhole fluid to complete the electrical circuit, erroneous readings may result due to heavy steam layers, spill over from pumps, and casing leaks. Nonconductive fluids floating on the water surface, such as liquid paraffin or oil, can also cause erroneous readings.

By replacing a conventional conductivity-type probe with a GEMS model LS-1700 liquid-level switch, these problems can be avoided. In the GEMS unit a magnet-equipped float rises with the fluid level and closes a reed switch encased in the unit's central stem. An electrical circuit is completed and the current is detected at the surface. The assembly drawing for this unit is shown in Figure D-6. It is easily fabricated and the instructions to do so follow.

Fabrication

The assembly and fabrication drawings are as shown. The GEMS liquid-level switch (model LS-1700) is inexpensive and readily available. The parts surrounding the unit, Parts 3 and 4 (see assembly drawing) should be made of a nonmagnetic material to avoid interference with the operation of the probe.

1. Insert the GEMS liquid level switch into the fabricated housing (Items 3 and 4) letting the leads and threaded portion of the GEMS unit protrude through the hole (Item 4). Slip the hose fitting (Item 2) over the leads.

2. Fill the hose fitting with silicon rubber sealant and screw it securely to the GEMS unit.

3. Insert the two-conductor cable with the conductivity type probe removed through a one-foot section of appropriately-sized heat shrink tubing.

4. Solder the leads from the GEMS Unit to the leads of the two-conductor cable approximately two inches beyond the end of the hose fitting. Cover the solder joint, the cable, and the end of the hose fitting with silicon rubber sealant.

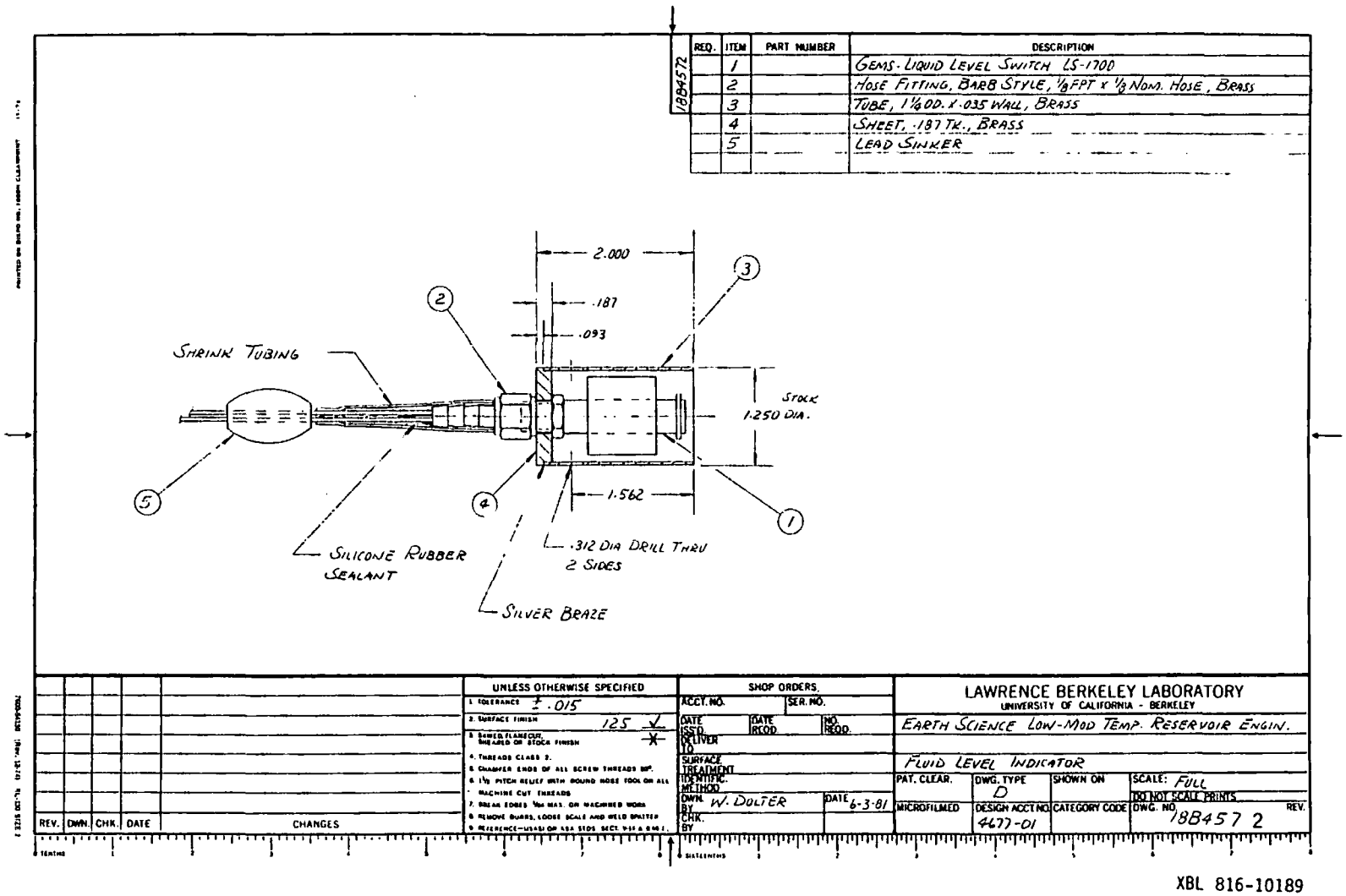

Figure D-6. Fluid level indicator.

5. Slip the shrink tubing over the cable solder joint and hose fitting. Heat the shrink tubing until it fits snugly on the cable. Do not use the probe until the silicon rubber sealant has set.

6. Add split-type lead weights to the cable to facilitate running the probe down a well.

Use

The unit described here can be substituted on the end of a conventional conductivity-type water-level indicator. When the fluid level is reached, a current will be detected on the current-detecting instrument at the surface. If an entire water level detector is to be constructed, a suitable substitute for the surface readout is an ohmmeter. When the fluid level is reached by the probe, the ohmmeter will indicate that a circuit has been closed.

REFERENCE

D-1. Recently Developed Well Test Instrumentation for Low-to-Moderate Temperature Hydrothermal Reservoirs, LBL-13260.

APPENDIX E
VARFLOW PROGRAM USER'S GUIDE

APPENDIX F

VARFLOW PROGRAM USER'S GUIDE

Before a well test is conducted, you should calculate the anicipated drawdown at each of the wells to be monitored during the test. If a single well is being flowed at a constant rate, the drawdown can easily be calculated from the equations in Section 6 of Volume I. However, if two or more wells are flowing and/or you are also reinjecting the produced brine, the calculations are more complicated. Also, if the flow rate from the well is not held at a constant rate, the calculations are more complex. The following computer program can be used to calculate the anticipated pressure response at up to 10 wells, due to the flow rate of up to 10 production and/or injection wells.

Program Description

VARFLOW calculates pressure changes in response to fluid production/injection from/into an idealized reservoir system. The program is set up to calculate pressure changes at up to ten observation wells. These observation wells may be interference monitoring wells or production wells. The reservoir description is as follows:

1. The reservoir is of infinite areal extent, or bounded on one side by a linear constant potential or barrier boundary.

2. The reservoir is completely saturated with a slightly compressible single phase fluid.

3. The reservoir is isothermal.

4. The reservoir is horizontal and has a constant thickness, H.

5. The flow of fluid in the reservoir is described by Darcy's law.

6. The reservoir is homogeneous and bounded above and below by impermeable layers.

7. The reservoir permeability can be anisotropic in a horizontal plane (x-y anisotropy) or isotropic.

The flow into or from a fully penetrating well is uniformly distributed over the length of the well. The well is modeled as a line source. However, a skin effect, indicative of wellbore condition can be included in the analysis.

Flow rates from up to ten wells can vary arbitrarily. Flow rates are modeled by superposition of consecutive "production pulses." Within any "production pulse" the flow rate may be constant or vary linearly. Figure E-1 demonstrates the construction and definition of a "production pulse." With this scheme for modeling flow rates, any variable flow rate history can be represented to the desired accuracy by a series of sequential straight-line segments, each of the appropriate duration and inclination.

Basic Equations

Variable Flow Rate

In an isotropic reservoir, which complies with the description discussed above, pressure changes caused by production/injection from a single well with a variable flow rate can be calculated from Equation (E-1).

$$\Delta P(t) = \frac{\mu}{4\pi kH} \int_{\tau_n}^{\tau_{n+1}} \frac{q(\tau)}{t - \tau} \exp\left[\frac{-r^2}{4\eta(t - \tau)}\right] d\tau \qquad \text{(E-1)}$$

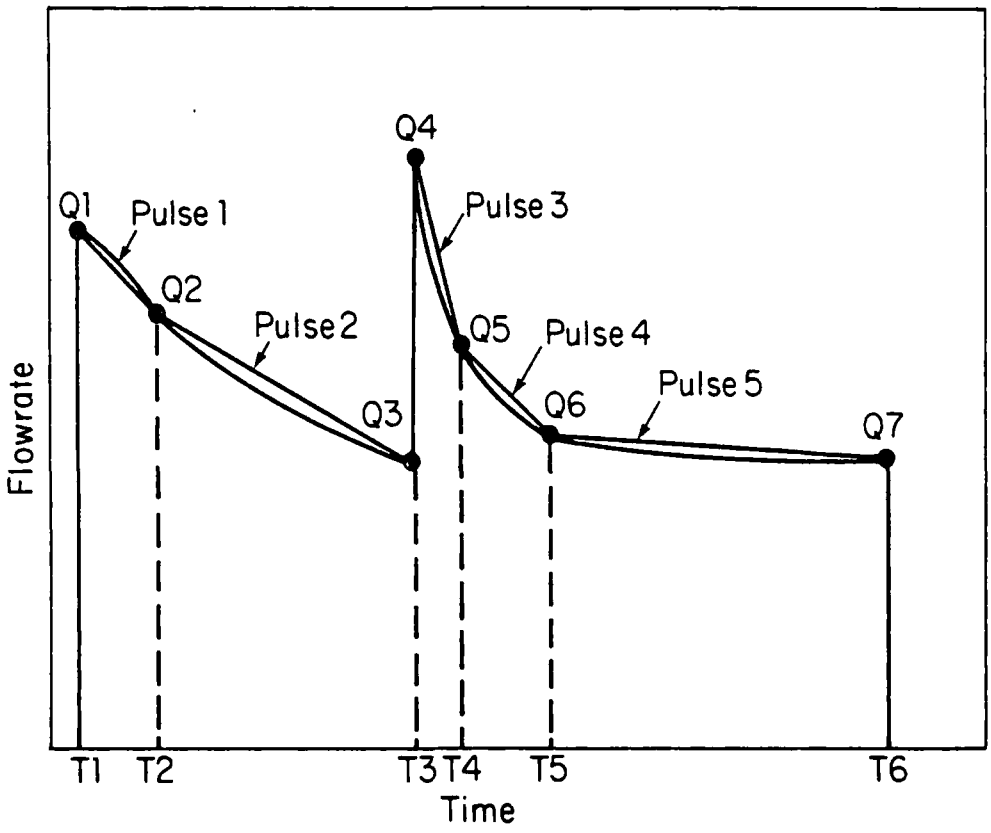

Flowrate Points
0. ,0.
T1 ,0.
T1 ,Q.1
T2 ,Q2
T3 ,Q3
T3 ,Q4
T4 ,Q5
T5 ,Q6
T6 ,Q7
T6 ,0.

XBL 815-3075

Figure E-1. Representation of a production pulse.

where

$\Delta P(t)$ = pressure change at time t due to the flow rate $q(\tau)$ for $\tau_n < t < \tau_n + 1$

μ = dynamic viscosity of the fluid

k = permeability

H = reservoir thickness

τ_n = time at which the flow starts

τ_{n+1} = time at which the flow stops

$q(\tau)$ = volumetric flow rate at time τ

r = distance between the observation well and the production/injection well

η = the hydraulic diffusivity ($k/\phi\mu c$)

ϕ = storage coefficient = $c_r (1 - \phi) + c_f \phi$.

Then, if $q(\tau)$ expressed as

$$q_n(\tau) = A_n + B (\tau - \tau_n) \qquad \text{(E-2)}$$

where

$q_n(\tau)$ = the flow rate at time τ which is within production pulse n

A_n = the flow rate at the beginning of production pulse k

B = the slope of the production pulse

$= (A_{n+1} - A_n) / (\tau_{n+1} - \tau_n)$

τ_n = the time at which production pulse n begins

and it:

$$u_n = \frac{\mu\phi c r^2}{4k(t - \tau_n)}$$

$$u_{n+1} = \frac{\mu\phi c r^2}{4k(t - \tau_{n+1})}$$

$$w(u) = \int_u^\infty \frac{\exp(-y)}{y}\, dy$$

N = the total number of production pulses which begin prior to time τ,

then, the pressure response is calculated by Equation (E-3).[E-2, E-3]

$$\Delta P(t) = \frac{\mu}{4\pi kH} \sum_{n=1}^{N} \Big\{ [A_n + B_n (t - \tau_n)(1 + u_n)] [w(u_n) - w(u_{n+1})] - B_n [(t - \tau_n) \exp(-u_n) - (t - \tau_{n+1}) \exp(-u_{n+1})] \Big\} . \quad \text{(F-3)}$$

The pressure response, caused by production/injection from more than one well is calculated by summing the response due to each production/injection well.

Anisotropy. If the reservoir is anisotropic then the equations are modified in the following manner. If that the principal axes of anisotropy are at 90 degrees to each other and that the x and y axes are chosen to be the principal axes (see Figure E-2) the Equation (E-1) is rewritten as Equation (E-4).[E-4]

$$\Delta P(t) = \frac{1}{4\pi} \left(\frac{\mu}{kH}\right)_e \int_{\tau_n}^{\tau_{n+1}} \frac{q(\tau)}{t - \tau} \exp\left(\frac{-r^2}{4\eta_\theta (t - \tau)}\right) d\tau \quad \text{(E-4)}$$

where

$(kH/\mu)_e$ = effective transmissivity

$$= \sqrt{(kH/\mu)_x \cdot (kH/\mu)_y}$$

and

$$\eta_\theta = \frac{(kH/\mu)_\theta}{\phi cH}$$

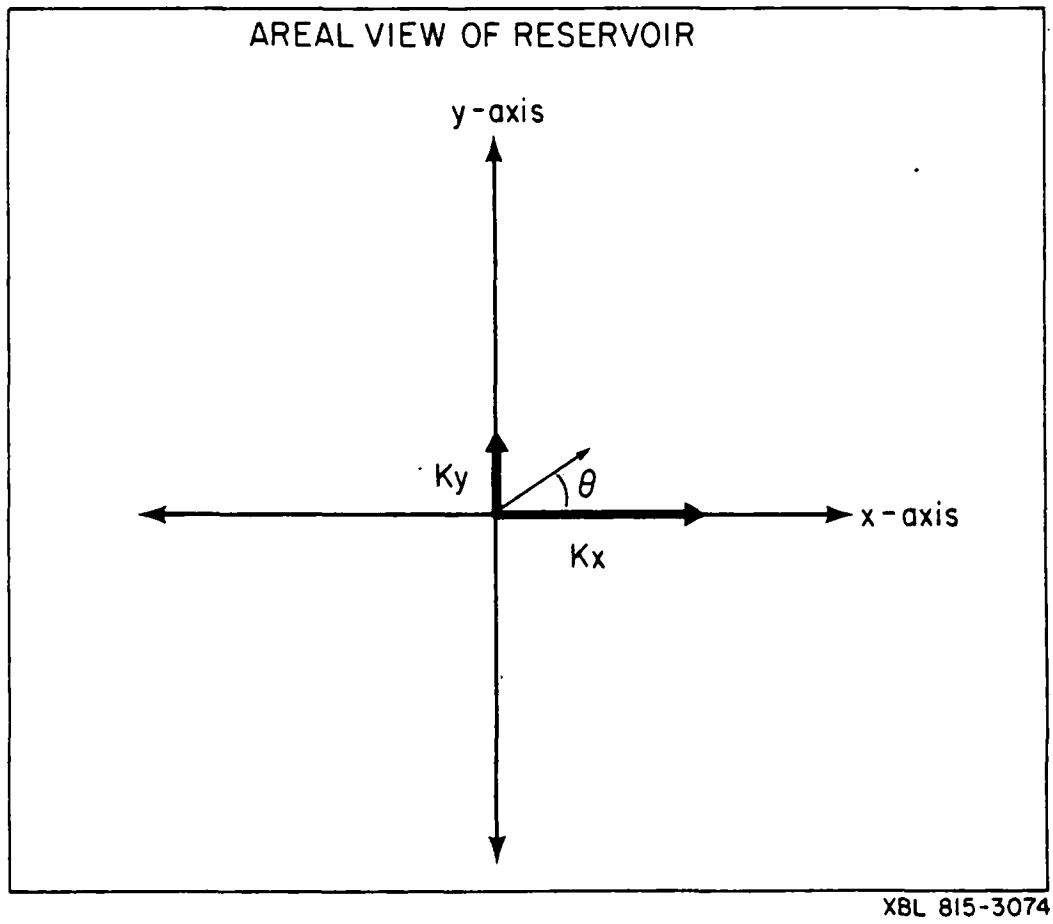

Figure E-2. Anisotropy representation.

$$(kH/\mu)_\theta = \frac{(kH/\mu)_x}{\cos^2\theta + \frac{(kH/\mu)_x}{(kH/\mu)_y}\sin^2\theta} \quad .$$

Theta is defined as the angle between the line adjoining the observation well and the production/injection well as measured counter-clockwise from a line parallel to the x-axis. (See Figure E-2). Since both $(kH/\mu)_e$ and η_θ are constants for any single production-observation well pair, the integral in Equation (E-4) may be evaluated analogously to the integral in Equation (E-1). In addition, because the reservoir is still homogeneous, regardless of the anisotropy, superposition of pressure responses, from each production well, is allowable.

Hydrologic Boundaries

A single fully penetrating linear hydrologic boundary can be modeled using the method of images.[E-5] Briefly stated, a boundary may be modeled as a line of bilateral symmetry about which image wells are arrayed in one-to-one symmetric correspondence with the real production/injection wells. Figure E-3 shows the image well locations for a case with two production wells and a barrier boundary. A barrier boundary is modeled by using image wells which have flow rates which are identical to the production/injection well counterparts. A constant potential boundary (leaky boundary) is modeled using image wells which have flow rates that are identical in magnitude but opposite in sign to the production/injection well counterparts. The image wells contribute an additional pressure response at each observation well.

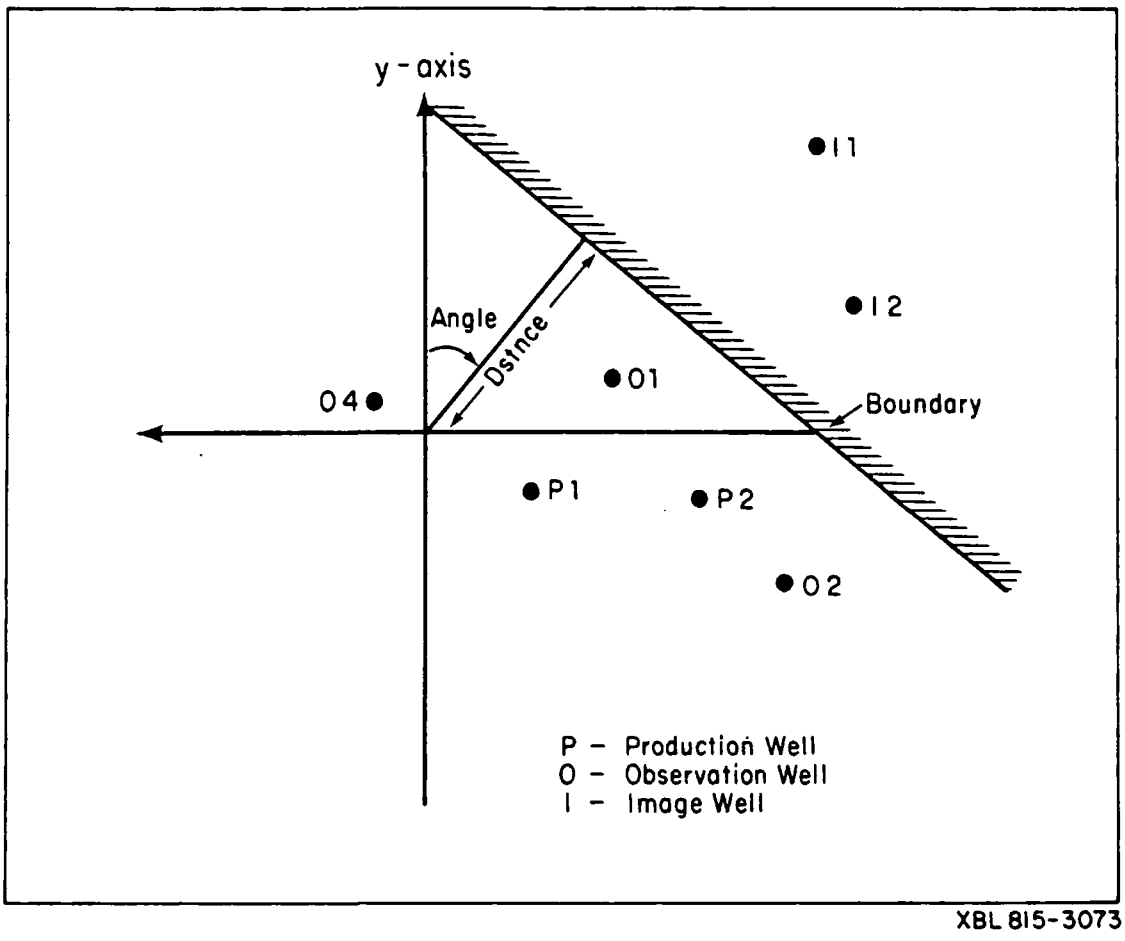

Figure E-3. Boundary location scheme.

Skin Effect

The calculated pressure response at a production well may also include the effects of a zone of enhancement or damage around a wellbore. The pressure change is calculated using the steady-state pressure change as defined below in Equation (E-5).[E-6]

$$\Delta P_{skin}(t) = s \frac{q(t)\mu}{2\pi kH} \qquad \text{(E-5)}$$

where

$q(t)$ = the instantaneous value of the flowrate at time t

s = the skin value

$\Delta P(t)_{skin}$ = the pressure change due to the skin at time t.

A damaged wellbore is indicated by a positive skin value and an enhanced wellbore is indicated by a negative skin value. When the reservoir is anisotropic, kH/μ is replaced by $(kH/\mu)_e$.

Program Input

Input Data Categories

Run Parameters and Problem Description. To run the program, the following information must be specified:

Variable name	Description
IHH	The number of observation wells in this run. (default 0) (maximum 10)

Variable name	Description
JJ	The number of production wells in this run. (default 0) (maximum 10)
IDIMEN	A flag to indicate that the data are not being input in S.I. units. (0 default--data are input in S.I. units) (1 set flag--data are not in S.I. units) See the following section for a description of the conversion factors.
NTIMES	The number of times at which pressure changes will be calculated. (default 0) (maximum 100)
RKHUX	The transmissivity $(kh/\mu)_x$ in the x-direction.
NOTE:	The x-axis is always a principal direction of anisotropy, and the second axis is at 90 degree to it, in the y direction. (default value 0.0) (default units $m^3/Pa \cdot s$)
RKHUY	The transmissivity $(kh/\mu)_y$ in the y-direction. (default value 0.0) (default units $m^3/Pa \cdot s$)
PCH	The storativity (ϕch). (default value 0.0) (default units m/Pa)

Variable name	Description
ANGLE	The azimuth to the boundary (see Figure E-3) measured clockwise from the positive y-axis.
DSTNCE	The perpendicular distance to the boundary from the origin of the coordinate system. (default value 0.0) (default units m)
BOUND	If the effects of a boundary are to be included, then the type of boundary, either barrier or constant potential, is input as an alphanumeric variable; either 10HBARRIER, or or 10HLEAKY,. which must be specified

Unit Conversion Factors. All parameter inputs are converted to S.I. units for internal calculation. At the termination of the calculation they are all converted back to the original input units. The conversion factor data required are listed below.

If IDIMEN was set to 1, the following information must be supplied. If IDIMEN is equal to 0, this data card is eliminated altogether.

Variable name	Description
PAPRESS	Number of pascals per pressure input unit.
CMSFLOW	Number of m^3/s per flow rate input unit.
SECTIME	Number of seconds per time input unit.

Variable name	Description
MLENGTH	Number of meters per length unit.
PASVISC	Number of pascal*seconds (Pa*s) per viscosity input unit.
SMPERM	Number of m^2 per permeability input unit.

Observation Well Locations and Specifications. The observation wells may be located at any position as specified by a set of x-y coordinates in a cartesian coordinate system. The following is a list of the specifications required for each observation well(I):

Variable	Description
NAME(I)	An alphanumeric name for the well. (default--blank)
OX(I)	The x-coordinate of the well. (default 0.) (default units m)
OY(I)	The y-coordinate of the well. (default 0.) (default units m)
YSTART(I)	The initial pressure at the well prior to any production or injection. (default units Pa)
LOBS(I)	A number (as read) that indicates that this observation well(I) is also production well LOBS(I). (Default 0 indicates the well is an interference monitoring well.)

Variable	Description
SKIN(I)	If the well(I) is also production well LOBS(I) the well may be assigned a non-zero skin value. (default 0. no skin)

Production Well Specifications and Flow Rate. To input a flow rate schedule, the data must be put in the format of pairs of flow rate points such that the flow rate is specified at the beginning and the end of a production pulse. Then, the flow rate, at all times, between the beginning and end of a production pulse, is known from Equation (E-3). The flow rate record will then consist of consecutive production pulses arranged in chronological order. If there is a step change from one flow rate to another, this is represented by two sequential production pulses, and must be input as such (see Sample Problem 1).

The following is a list of the specifications for each production well(J):

Variable	Description
PNAME(J)	An alphanumeric name for production well (J). (default value--BLANK)
PX(J)	The x-coordinate, in cartesian coordinates of production well(J). (default value 0.0) (default units m)
PY(J)	The y-coordinate, in cartesian coordinates, of production well(J). (default value 0.0) (default units m)

Variable	Description
KKJ(J)	The number of flow rate points for production well (J). (default value 0)
[TQ(K,J), AQ(K,J)]	The flow rate data points for well(J) which are of the form (time, flow rate). Up to 100 points per well are allowed. (default [0.0, 0.0]) (default units [s, m^3/s]) (K = 1, KKJ(J))

Times at Which Pressures Are To Be Calculated. Up to 100 different times can be specified at which pressure changes will be calculated:

Variable	Description
TIMES (L)	The times at which pressure calculations will be made up to 100 points. (default value 0.0) (default units, s)

INPUT DATA FORMAT

PROBLEM DESCRIPTION AND UNIT CONVERSION FACTORS

---

1 CARD	-	Title card alphanumeric to 80 characters	(8A10)
1 CARD	-	IHH, II, IDIMEN, NTIMES	(4I10)

If IDIMEN Is set equal to 1 on CARD 2

THEN INCLUDE

1 CARD - PAPRESS, CMSFLOW, SECTIME, RLENGTH, PASVISC, SMPERM (6E10.4)

OTHERWISE

1 CARD - RKHUX, RKHUY, PCH, ANGLE, DSTNCE, BOUND (5E10.4, A10)

OBSERVATION WELL DATA

IIH CARDS - NAME(I), OX(I), OY(I), YSTART(I),
LOBS(I), SKIN(I), etc.
(I = 1, IIH) (A10, 2F10.2, E10.4, I10, F10.2)

Repeat for each observation well.

PRODUCTION WELL DATA

JJ SETS OF CARDS - PNAME(J), PX(J), PY(J), KKJ(J) (A10, 2F10.2, I10)

TQ (1, J)	, AQ (1, J)	(2E10.4)
•	•	
•	•	
•	•	
•	•	
TQ (KKJ(J),J)	AQ (KKJ(J), J)	

Repeat this set of cards for each production well.

TIMES FOR CALCULATIONS OF PRESSURE CHANGES

TIMES(1), TIMES(2), TIMES(3),.....TIMES(8) (8E10.4)

Put eight per card - repeat until amount specified by NTIMES on CARD 2.

Sample Problems

Four sample problems are discussed in which the various capabilities of the program are demonstrated. Data decks and outputs are provided for each problem.

Sample Problem

No Anisotropy--Variable Flow Rate (Step-Wise)

In this problem a single production well is produced at a step wise variable flow rate and four observation wells monitor the pressure response. The observation wells are located symmetrically around the observation well (Figure E-4). Since there is no x-y reservoir anisotropy, the pressure drop at each of the observation wells should be identical. The flow rate from the production well is shown in Figure E-5. As is shown, there are three consecutive "production" pulses, the first two lasting 1000 minutes each, and the third lasting 2000 minutes.

The data deck for Sample 1 is shown in Figure E-6. The first card (card 1) gives the title information for the problem. The second card indicates that there are four observation wells (column 10, 1 production well (column 20), the IDIMEN flag is set (column 30) and the pressure changes will be calculated at 56 times (columns 30-40). On card three, the unit conversion factors are shown. The following table shows the units used for each quantity and the conversion factor to S.I. units.

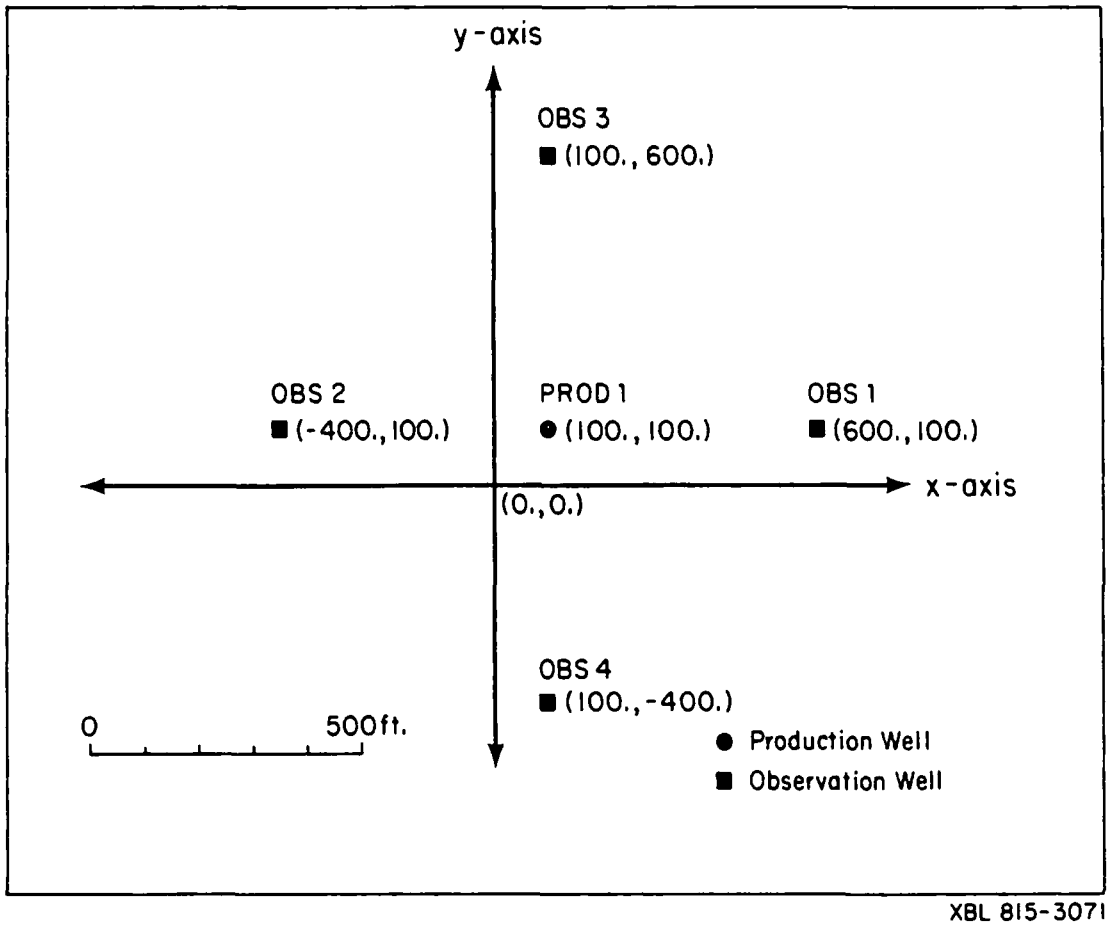

Figure E-4. Location scheme, in cartesian coordinates, for the production well and observation wells for Sample Problem 1.

Quantity	Unit	Conversion factor
Pressure	Psia	6895
Flow rate	Gal/min	6.31×10^{-5}
Time	Hours	3600
Length	Feet	0.3048
Viscosity	Centipoise	1×10^{-3}
Permeability	Millidarcies	9.862 x 10-16

It is important to note that once a time or distance unit is chosen, it must be used consistently throughout the input deck. For instance, when the flow rate is input, the time units must be the same as the time units used for the specification of times at which pressure calculations will be made.

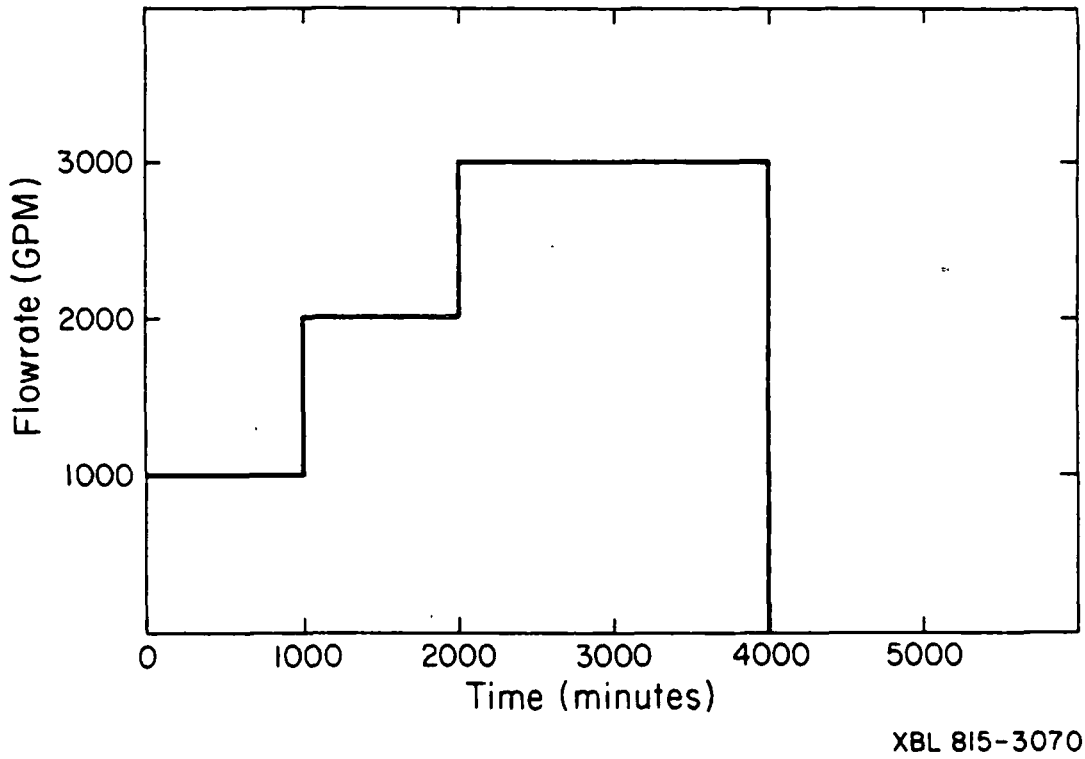

Figure E-5. Variable flow rate schedule for the production well in Sample Problem 1.

Card 4 lists the information about the x and y direction transmissivity and the reservoir storativity. For this problem, since there is no anisotropy, both the x-direction and y-direction transmissivity are equal and set to 150,000 md-ft/cp. The storativity for this problem is set equal to 2×10^{-3} ft/psi.

Cards 5 through 8 list the alphanumeric names for each observation well (columns 1-10), the (x,y) coordinates of each well (columns 11-20 and 21-30 respectively) and the initial reservoir pressure for each well (columns 31-40). The coordinates of each well are shown in Figure E-4.

Cards 9 through 15 contain all of the relevant information about the production well. On card 9, the alphanumeric name of the production well (column 1-10), the coordinates of the production well (columns 11-20, 21-30) and the number of flow rate points (columns 31-40, format I10) are input. For this problem six flow rate points are used to model the stepwise variable flow rate shown in Figure E-5. Note the construction of three "production pulses" to represent the flow rate.

CODED BY YOU GROUP GEOTHERMAL PROGRAM VARFLOW DATE NOW

PROBLEM SAMPLE PROBLEM 1

DATA ENTRY FORMS

PAGE 1

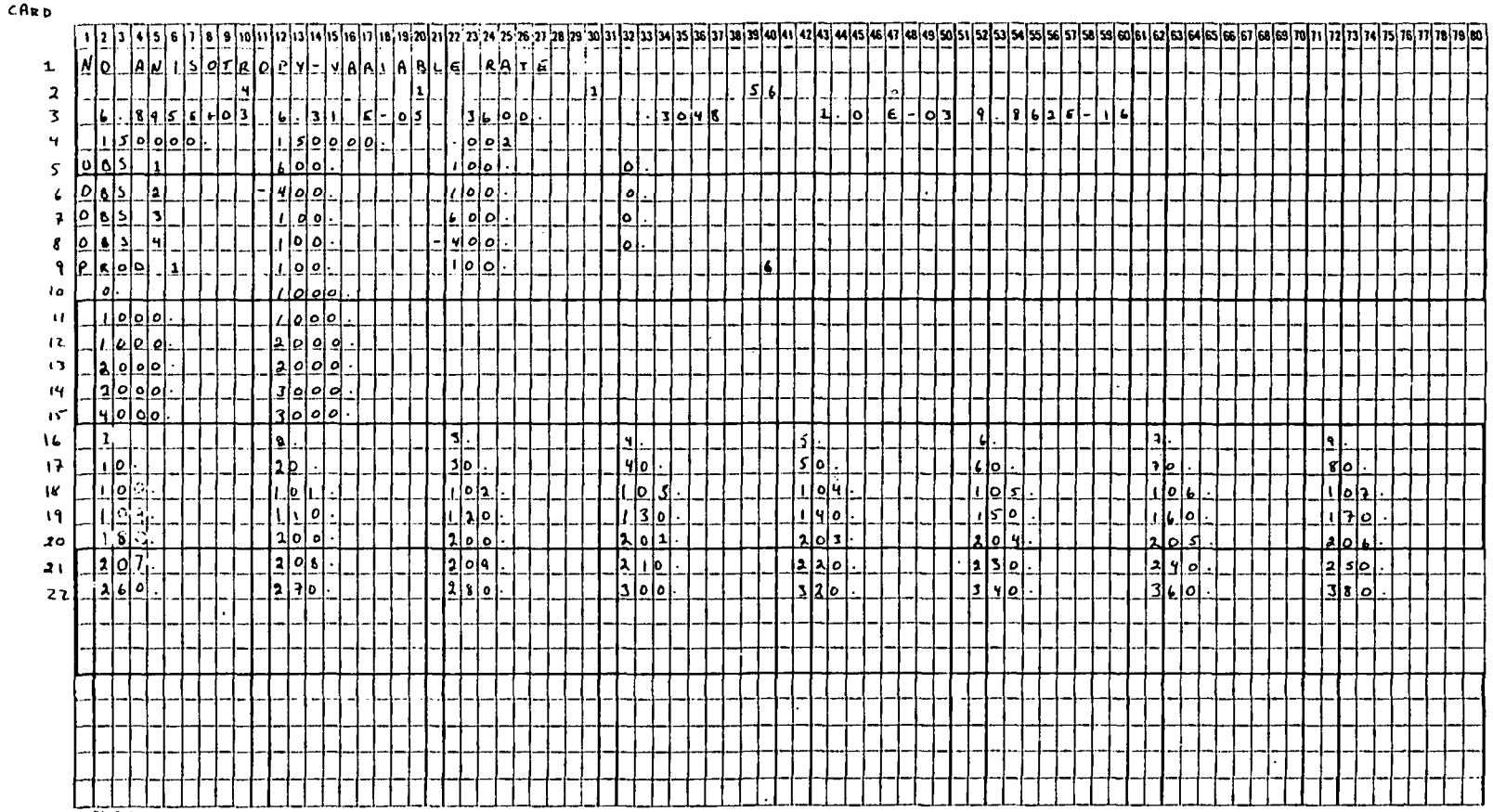

Figure E-6. Input deck for Sample Problem 1.

Cards 16 through 22 specify times at which pressure calculations, at each of the four observation wells, will be calculated. For this problem, pressures will be calculated at 1 hour, 2 hours, 3 hours, etc. to 380 hours. The units for the times specified here are input on card 3. If 3.6×10^3s had not been specified, the default units would have been used, implying that pressures would be calculated at 1 s, 2 s, 3 s, etc., to 380 s.

The output for this problem is shown in Figure E-7. As can be seen, the pressure drop at each well is identical, because each well is equidistant from the production well (500 ft). The next sample problem will show a similar problem but one in which there is extreme x-y anisotropy.

```
 NO ANISOTROPY-VARIABLE FLOWRATE

NUMBER OF OBSERVATION WELLS          4
NUMBER OF PRODUCTION WELLS           1
NUMBER OF TIMES AT WHICH PRESSURES WILL BE CALCULATED        56

                  CONVERSION FACTORS
                  ==================

        PRESSURE UNIT PER PASCAL                          .6895E+04
        FLOWRATE UNIT PER CUBIC METER PER SECOND          .6310E-04
        TIME UNIT PER SECOND                               3600.00
        LENGTH PER METER                                       .30
        VISCOSITY PER PASCAL-SECOND                       .100E-02
        PERMEABILITY PER SQUARE METER                     .9862E-15

   PARAMETER VALUES
   ================
   X-AXIS TRANSIMISSIVITY = .1500E+06
   Y-AXIS TRANSMISSIVITY = .1500E+06
   STORATIVITY = .2000E-02


OBSERVATION WELL NUMBER      1
   WELL OBS   1     COORDINATES (     600.00,     100.00)
   INITIAL PRESSURE=0.


OBSERVATION WELL NUMBER      2
   WELL OBS 2       COORDINATES (    -400.00,     100.00)
   INITIAL PRESSURE=0.
```

Figure E-7. Output for Sample Problem 1.

```
OBSERVATION WELL NUMBER      3
   WELL OBS 3       COORDINATES (     100.00,     600.00)
   INITIAL PRESSURE=-.0

OBSERVATION WELL NUMBER      4
   WELL OBS 4       COORDINATES (     100.00,    -400.00)
   INITIAL PRESSURE=-.0

PRODUCTION WELL NUMBER           1
   PROD 1        COORDINATES (     100.00,     100.00)
   NUMBER OF FLOWRATE POINTS=     6

                     TIME          FLOWRATE

                    0.             .1000E+04
                     .1000E+03     .1000E+04
                     .1000E+03     .2000E+04
                     .2000E+03     .2000E+04
                     .2000E+03     .3000E+04
                     .4000E+03     .3000E+04

DISTANCES BETWEEN OBSERVATION WELLS AND PRODUCTION WELLS

          OBS   1      OBS 2        OBS 3        OBS 4
PROD 1         500.00       500.00       500.00       500.00

         TIME   OBS   1      OBS 2        OBS 3        OBS 4
          1.00  -.1715E+00  -.1715E+00  -.1715E+00  -.1715E+00
          2.00  -.1433E+01  -.1433E+01  -.1433E+01  -.1433E+01
          3.00  -.3238E+01  -.3238E+01  -.3238E+01  -.3238E+01
          4.00  -.5102E+01  -.5102E+01  -.5102E+01  -.5102E+01
          5.00  -.6878E+01  -.6878E+01  -.6878E+01  -.6878E+01

          6.00  -.8531E+01  -.8531E+01  -.8531E+01  -.8531E+01
          7.00  -.1006E+02  -.1006E+02  -.1006E+02  -.1006E+02
          9.00  -.1278E+02  -.1278E+02  -.1278E+02  -.1278E+02
         10.00  -.1400E+02  -.1400E+02  -.1400E+02  -.1400E+02
         20.00  -.2292E+02  -.2292E+02  -.2292E+02  -.2292E+02

         30.00  -.2867E+02  -.2867E+02  -.2867E+02  -.2867E+02
         40.00  -.3291E+02  -.3291E+02  -.3291E+02  -.3291E+02
         50.00  -.3627E+02  -.3627E+02  -.3627E+02  -.3627E+02
         60.00  -.3905E+02  -.3905E+02  -.3905E+02  -.3905E+02
         70.00  -.4142E+02  -.4142E+02  -.4142E+02  -.4142E+02
```

Figure E-7. (continued).

TIME	OBS 1	OBS 2	OBS 3	OBS 4
80.00	-.4349E+02	-.4349E+02	-.4349E+02	-.4349E+02
100.00	-.4697E+02	-.4697E+02	-.4697E+02	-.4697E+02
101.00	-.4729E+02	-.4729E+02	-.4729E+02	-.4729E+02
102.00	-.4871E+02	-.4871E+02	-.4871E+02	-.4871E+02
103.00	-.5067E+02	-.5067E+02	-.5067E+02	-.5067E+02
104.00	-.5268E+02	-.5268E+02	-.5268E+02	-.5268E+02
105.00	-.5461E+02	-.5461E+02	-.5461E+02	-.5461E+02
106.00	-.5641E+02	-.5641E+02	-.5641E+02	-.5641E+02
107.00	-.5809E+02	-.5809E+02	-.5809E+02	-.5809E+02
109.00	-.6110E+02	-.6110E+02	-.6110E+02	-.6110E+02
110.00	-.6246E+02	-.6246E+02	-.6246E+02	-.6246E+02
120.00	-.7275E+02	-.7275E+02	-.7275E+02	-.7275E+02
130.00	-.7976E+02	-.7976E+02	-.7976E+02	-.7976E+02
140.00	-.8517E+02	-.8517E+02	-.8517E+02	-.8517E+02
150.00	-.8962E+02	-.8962E+02	-.8962E+02	-.8962E+02
160.00	-.9342E+02	-.9342E+02	-.9342E+02	-.9342E+02
170.00	-.9675E+02	-.9675E+02	-.9675E+02	-.9675E+02
180.00	-.9973E+02	-.9973E+02	-.9973E+02	-.9973E+02
200.00	-.1049E+03	-.1049E+03	-.1049E+03	-.1049E+03
201.00	-.1053E+03	-.1053E+03	-.1053E+03	-.1053E+03
202.00	-.1068E+03	-.1068E+03	-.1068E+03	-.1068E+03
203.00	-.1088E+03	-.1088E+03	-.1088E+03	-.1088E+03
204.00	-.1109E+03	-.1109E+03	-.1109E+03	-.1109E+03
205.00	-.1129E+03	-.1129E+03	-.1129E+03	-.1129E+03
206.00	-.1148E+03	-.1148E+03	-.1148E+03	-.1148E+03
207.00	-.1165E+03	-.1165E+03	-.1165E+03	-.1165E+03
208.00	-.1182E+03	-.1182E+03	-.1182E+03	-.1182E+03
209.00	-.1197E+03	-.1197E+03	-.1197E+03	-.1197E+03
210.00	-.1211E+03	-.1211E+03	-.1211E+03	-.1211E+03
220.00	-.1322E+03	-.1322E+03	-.1322E+03	-.1322E+03
230.00	-.1399E+03	-.1399E+03	-.1399E+03	-.1399E+03
240.00	-.1460E+03	-.1460E+03	-.1460E+03	-.1460E+03
250.00	-.1511E+03	-.1511E+03	-.1511E+03	-.1511E+03
260.00	-.1555E+03	-.1555E+03	-.1555E+03	-.1555E+03
270.00	-.1594E+03	-.1594E+03	-.1594E+03	-.1594E+03
280.00	-.1630E+03	-.1630E+03	-.1630E+03	-.1630E+03
300.00	-.1693E+03	-.1693E+03	-.1693E+03	-.1693E+03
320.00	-.1747E+03	-.1747E+03	-.1747E+03	-.1747E+03
340.00	-.1794E+03	-.1794E+03	-.1794E+03	-.1794E+03
360.00	-.1838E+03	-.1838E+03	-.1838E+03	-.1838E+03
380.00	-.1877E+03	-.1877E+03	-.1877E+03	-.1877E+03

Figure E-7. (continued).

Sample Problem 2

Verification of Anisotropy. In Sample Problem 2 a well in an anisotropic reservoir is produced at a constant flow rate of 1000 GPM for a period of 5000 hours. Four observation wells, located symmetrically about the production well, along the major axes of anisotropy, are used to observe the pressure changes. For this problem, the x-axis permeability was chosen to be 150 times larger than the permeability in the y-direction. Thus, transmissivity values of 150,000 md*ft/cp and 1000 md*ft/cp were used. Figure E-8 shows the well location scheme and the representation of the reservoir anisotropy.

The data deck for Sample Problem 2 is shown in Figure E-9. The first three cards are the same as they are in Sample Problem 1. On card 4 the x-direction transmissivity (column 1-10) is set to 150,000 md*ft/cp, and

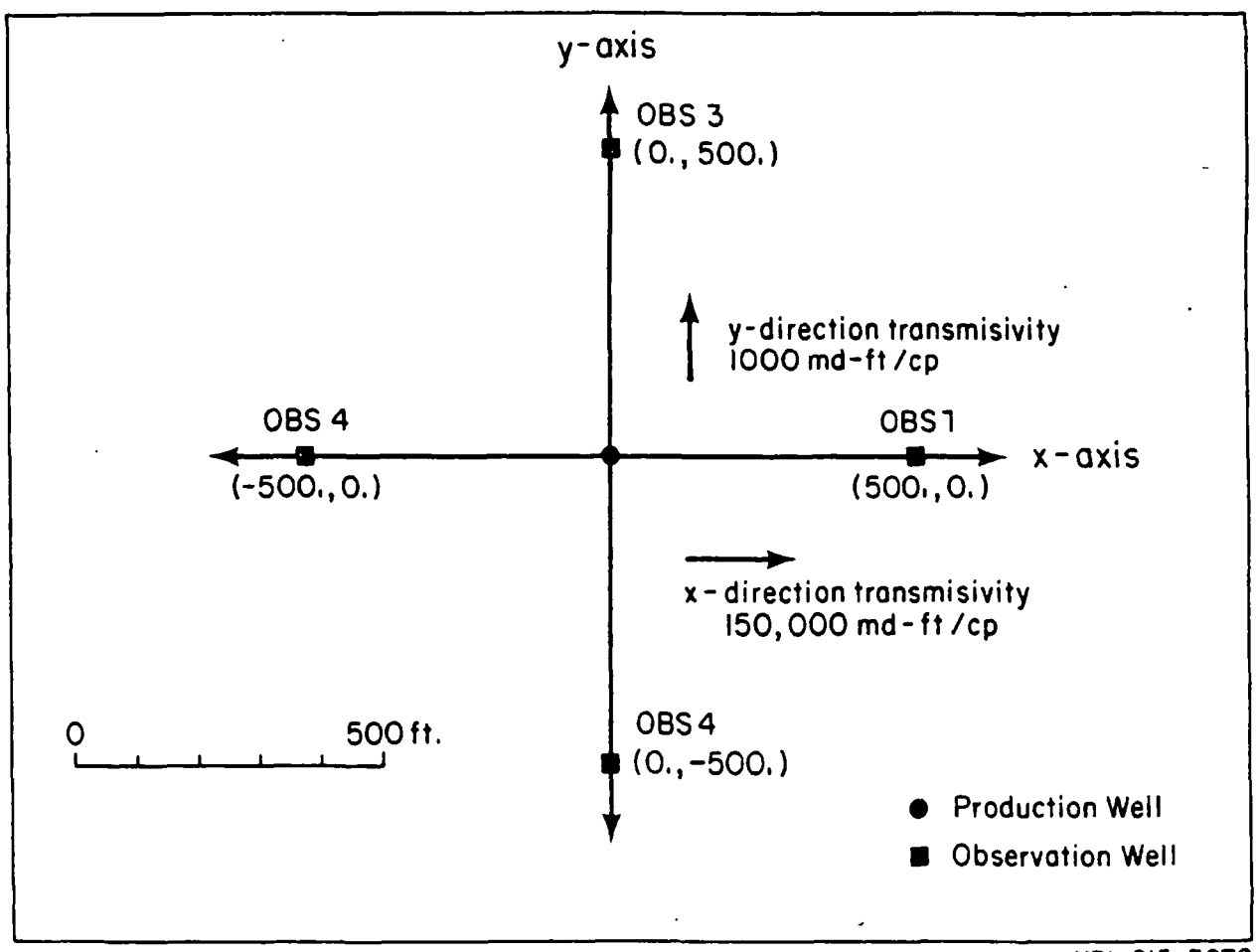

Figure E-8. Well location scheme for Sample Problems 2 and 3.

```
VERIFICATION OF ANISOTROPY
      04          1          1          56
6.895 E+03 6.310E-05   3.5E+03  .3048     1.0  E-03 9.862E-16
150000.   1000.      .002       00.        0000.
OBS   1     500.      0.          0.                0        0.
OBS 2      -500.      0.          0.
OBS 3       000.        500.
OBS 4       000.        -500.
PROD 1        0.         0.                2
0.          1000.
5000.       1000.
1.          2.         3.         4.         5.         6.         7.         9.
10.         20.        30.        40.        50.        60.        70.        80.
100.        101.       102.       103.       104.       105.       106.       107.
109.        110.       120.       130.       140.       150.       160.       170.
180.        200.       201.       202.       203.       204.       205.       206.
207.        208.       209.       210.       220.       230.       240.       250.
260.        270.       280.       300.       320.       340.       360.       380.
```

Figure E-9. Input deck for Sample Problem 2.

the y-direction transmissivity is set to 1000 md*ft/cp. As in Problem 1, the storativity, ϕch, is set to 0.002 ft/psi. The remaining part of the data deck is similar to that in Problem 1, except that only one production pulse or two flow rate points are required to model the flow rate.

The output for Sample Problem 2 is shown in Figure E-10. Note the effect of the extreme anisotropy on the reservoir pressure response.

Sample Problem 3

Verification of Anisotropy--Boundary Problem. Sample Problem 3 is identical to Problem 2 except that there is a barrier boundary in the reservoir 1000 ft from the production well, in a direction perpendicular to the x-axis. Figure E-11 shows the well locations and the boundary location scheme. Note that the alpha is measured clockwise from the positive y-axis.

The data deck (Figure E-12) for this problem is identical to the data deck in Problem 2 except for card 4. Columns 1-10 and 11-20 contain the reservoir transmissivity information and columns 21-30 contain the storativity data. Alpha, the angle seen in Figure E-11, is input in columns 31-40 and DSTNCE, the distance from the origin to the perpendicular of the boundary, is input in columns 41-50. The type of boundary is indicated alphanumerically in columns 51-60. Note that the type, either BARRIER or LEAKY must begin in column 51.

```
VERIFICATION OF ANISOTROPY

NUMBER OF OBSERVATION WELLS          4
NUMBER OF PRODUCTION WELLS           1
NUMBER OF TIMES AT WHICH PRESSURES WILL BE CALCULATED        56

                  CONVERSION FACTORS
                  ==================

        PRESSURE UNIT PER PASCAL                          .6895E+04
        FLOWRATE UNIT PER CUBIC METER PER SECOND          .6310E-04
        TIME UNIT PER SECOND                               3600.00
        LENGTH PER METER                                       .30
        VISCOSITY PER PASCAL-SECOND                       .100E-02
        PERMEABILITY PER SQUARE METER                     .9862E-15

    PARAMETER VALUES
    ================
    X-AXIS TRANSIMISSIVITY = .1500E+06
    Y-AXIS TRANSMISSIVITY = .1000E+04
    STORATIVITY = .2000E-02

OBSERVATION WELL NUMBER     1
    WELL OBS   1     COORDINATES (     500.00,       0.   )
    INITIAL PRESSURE=0.

OBSERVATION WELL NUMBER     2
    WELL OBS 2       COORDINATES (    -500.00,       0.   )
    INITIAL PRESSURE=0.

OBSERVATION WELL NUMBER     3
    WELL OBS 3       COORDINATES (       0.   ,     500.00)
    INITIAL PRESSURE=-.0

OBSERVATION WELL NUMBER     4
    WELL OBS 4       COORDINATES (       0.   ,    -500.00)
    INITIAL PRESSURE=-.0

  PRODUCTION WELL NUMBER           1
     PROD 1       COORDINATES (       0.   ,       0.   )
    NUMBER OF FLOWRATE POINTS=     2

                      TIME              FLOWRATE

                       0.               .1000E+04
                    .5000E+04           .1000E+04

   DISTANCES BETWEEN OBSERVATION WELLS AND PRODUCTION WELLS

             OBS   1      OBS 2        OBS 3        OBS 4
PROD I        500.00       500.00       500.00       500.00
```

Figure E-10. Output for Sample Problem 2.

TIME	OBS 1	OBS 2	OBS 3	OBS 4
1.00	-.2101E+01	-.2101E+01	-.3917-206	-.3917-206
2.00	-.1755E+02	-.1755E+02	-.8058-103	-.8058-103
3.00	-.3966E+02	-.3966E+02	-.2625E-68	-.2625E-68
4.00	-.6251E+02	-.6249E+02	-.5152E-51	-.5152E-51
5.00	-.8435E+02	-.8424E+02	-.1286E-40	-.1286E-40
6.00	-.1048E+03	-.1045E+03	-.1136E-33	-.1136E-33
7.00	-.1239E+03	-.1232E+03	-.1064E-28	-.1064E-28
9.00	-.1587E+03	-.1566E+03	-.4742E-22	-.4742E-22
10.00	-.1746E+03	-.1715E+03	-.1026E-19	-.1026E-19
20.00	-.3029E+03	-.2915E+03	-.4294E-09	-.4294E-09
30.00	-.3935E+03	-.3553E+03	-.1870E-05	-.1870E-05
40.00	-.4754E+03	-.4131E+03	-.1373E-03	-.1373E-03
50.00	-.5399E+03	-.4618E+03	-.1916E-02	-.1916E-02
60.00	-.5954E+03	-.5043E+03	-.1151E-01	-.1151E-01
70.00	-.6441E+03	-.5424E+03	-.4241E-01	-.4241E-01
80.00	-.6875E+03	-.5769E+03	-.1147E+00	-.1147E+00
100.00	-.7522E+03	-.6377E+03	-.4767E+00	-.4767E+00
101.00	-.7555E+03	-.6406E+03	-.5048E+00	-.5048E+00
102.00	-.7589E+03	-.6432E+03	-.5341E+00	-.5341E+00
103.00	-.7622E+03	-.6461E+03	-.5644E+00	-.5644E+00
104.00	-.7655E+03	-.6488E+03	-.5959E+00	-.5959E+00
105.00	-.7688E+03	-.6515E+03	-.6286E+00	-.6286E+00
106.00	-.7721E+03	-.6542E+03	-.6624E+00	-.6624E+00
107.00	-.7753E+03	-.6569E+03	-.6975E+00	-.6975E+00
109.00	-.7917E+03	-.6623E+03	-.7712E+00	-.7712E+00
110.00	-.7943E+03	-.6649E+03	-.8098E+00	-.8098E+00
120.00	-.8250E+03	-.6903E+03	-.1267E+01	-.1267E+01
130.00	-.8530E+03	-.7141E+03	-.1861E+01	-.1861E+01
140.00	-.8792E+03	-.7365E+03	-.2597E+01	-.2597E+01
150.00	-.9038E+03	-.7579E+03	-.3480E+01	-.3480E+01
160.00	-.9269E+03	-.7780E+03	-.4509E+01	-.4509E+01
170.00	-.9488E+03	-.7972E+03	-.5683E+01	-.5683E+01
180.00	-.9695E+03	-.8155E+03	-.6997E+01	-.6997E+01
200.00	-.1008E+04	-.8496E+03	-.1002E+02	-.1002E+02
201.00	-.1010E+04	-.8514E+03	-.1019E+02	-.1019E+02
202.00	-.1012E+04	-.8530E+03	-.1035E+02	-.1035E+02
203.00	-.1013E+04	-.8546E+03	-.1052E+02	-.1052E+02
204.00	-.1015E+04	-.8563E+03	-.1069E+02	-.1069E+02
205.00	-.1017E+04	-.8579E+03	-.1086E+02	-.1086E+02
206.00	-.1019E+04	-.8595E+03	-.1103E+02	-.1103E+02

Figure E-10. (continued)..

TIME	OBS 1	OBS 2	OBS 3	OBS 4
207.00	-.7160E+03	-.7160E+03	-.6501E+01	-.6501E+01
208.00	-.7169E+03	-.7169E+03	-.6598E+01	-.6598E+01
209.00	-.7178E+03	-.7178E+03	-.6695E+01	-.6695E+01
210.00	-.7188E+03	-.7188E+03	-.6793E+01	-.6793E+01
220.00	-.7278E+03	-.7278E+03	-.7806E+01	-.7806E+01
230.00	-.7365E+03	-.7365E+03	-.8874E+01	-.8874E+01
240.00	-.7448E+03	-.7448E+03	-.9992E+01	-.9992E+01
250.00	-.7528E+03	-.7528E+03	-.1116E+02	-.1116E+02
260.00	-.7604E+03	-.7604E+03	-.1236E+02	-.1236E+02
270.00	-.7678E+03	-.7678E+03	-.1361E+02	-.1361E+02
280.00	-.7749E+03	-.7749E+03	-.1489E+02	-.1489E+02
300.00	-.7884E+03	-.7884E+03	-.1755E+02	-.1755E+02
320.00	-.8011E+03	-.8011E+03	-.2031E+02	-.2031E+02
340.00	-.8129E+03	-.8129E+03	-.2316E+02	-.2316E+02
360.00	-.8241E+03	-.8241E+03	-.2607E+02	-.2607E+02
380.00	-.8348E+03	-.8348E+03	-.2904E+02	-.2904E+02

Figure E-10. (continued).

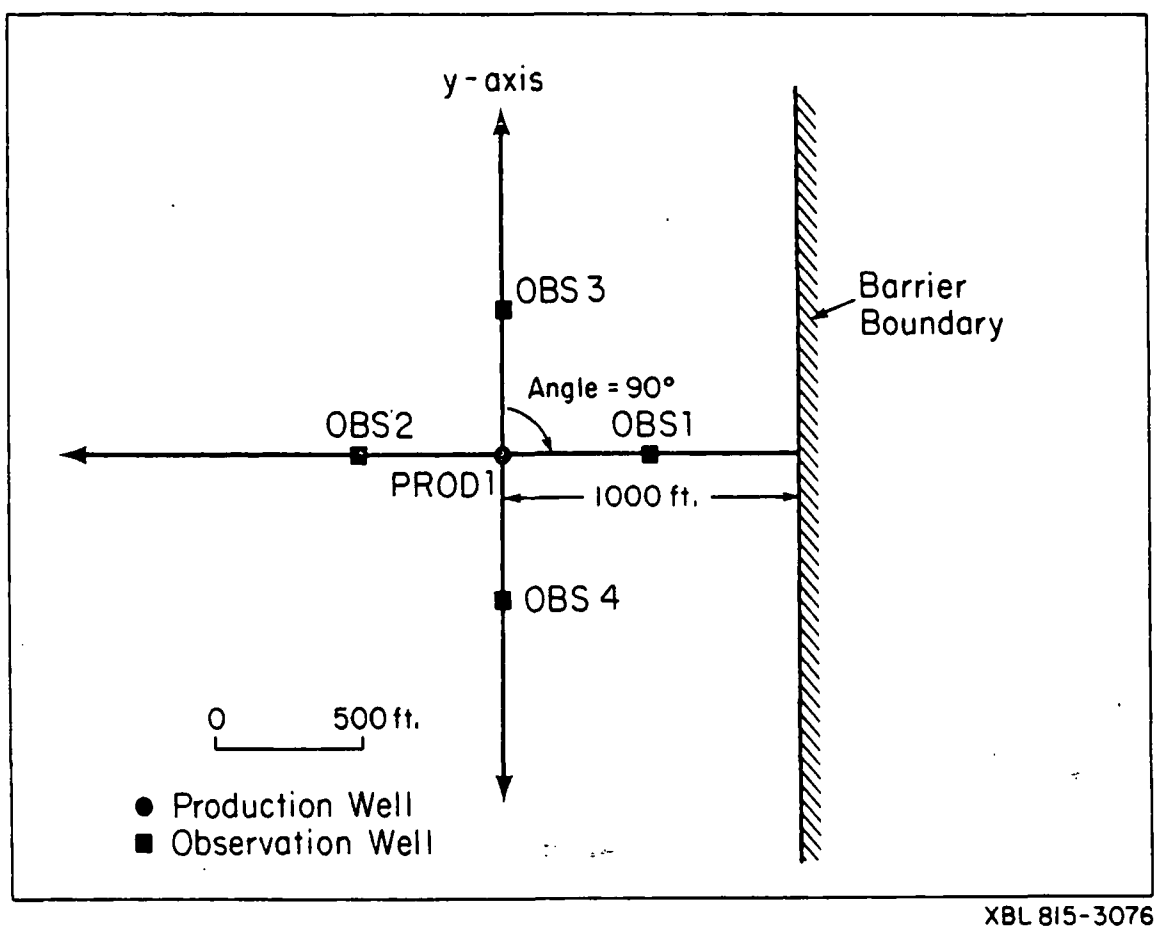

Figure E-11. Boundary location scheme for Sample Problem 3.

```
VERIFICATION OF ANISOTROPY-RUN TO COMPARE WITH BOUNDARY
        04          1          1          56
6.895 E+03 6.310E-05   3.6E+03   .3048    1.0  E-03 9.862E-16
150000.    1000.      .002       90.      1000.      BARRIER
OBS   1     500.       0.         0.                  0          0.
OBS 2      -500.      0.         0.
OBS 3       000.       500.
OBS 4       000.      -500.
PROD 1        0.        0.                  2
0.         1000.
5000.      1000.
1.         2.         3.         4.         5.         6.         7.         9.
10.        20.        30.        40.        50.        60.        70.        80.
100.       101.       102.       103.       104.       105.       106.       107.
109.       110.       120.       130.       140.       150.       160.       170.
180.       200.       201.       202.       203.       204.       205.       206.
207.       208.       209.       210.       220.       230.       240.       250.
260.       270.       280.       300.       320.       340.       360.       380.
```

Figure E-12. Input deck for Sample Problem 3.

The output for the Sample Problem 3 is shown in Figure E-13.

Sample Problem 4

Verification of Anisotropy--Run to Compare with Boundary. Sample Problem 4 demonstrates how the algorithm in VARFLOW accounts for the effects of a barrier or constant potential boundary in the pressure calculations. In this calculation the existence of a boundary is not specified, however, a well which would be the image well for the calculation in Sample Problem 3 is explicitly included in the calculation. The well locations for the observation wells, the production well and the "image" production well are shown in Figure E-14.

The input deck (Figure E-15) for the problem is similar to the data decks in problems 2 and 3. Note that on Card 2, Column 20, it is specified that there are two production wells for this problem. The production data and production well specifications for the second production well, PROD2, are on Cards 12-14. Note that the production rate for PROD2 is identical to that of PROD1.

The output for this problem is shown in Figure E-16. Note that the pressure response is identical to the pressure response in Problem 3.

```
VERIFICATION OF ANISOTROPY-RUN TO COMPARE WITH BOUNDARY

 NUMBER OF OBSERVATION WELLS          4
 NUMBER OF PRODUCTION WELLS           1
 NUMBER OF TIMES AT WHICH PRESSURES WILL BE CALCULATED        56

                  CONVERSION FACTORS
                  ==================

        PRESSURE UNIT PER PASCAL                          .6895E+04
        FLOWRATE UNIT PER CUBIC METER PER SECOND          .631OE-04
        TIME UNIT PER SECOND                               3600.00
        LENGTH PER METER                                       .30
        VISCOSITY PER PASCAL-SECOND                       .100E-02
        PERMEABILITY PER SQUARE METER                     .9862E-15

     PARAMETER VALUES
     ================
     X-AXIS TRANSMISSIVITY = .1500E+06
     Y-AXIS TRANSMISSIVITY = .1000E+04
     STORATIVITY = .2000E-02

 THERE IS A BARRIER   BOUNDARY AT AN ANGLE OF      90.00 DEGREES AND A DISTANCE OF    1000.00

 OBSERVATION WELL NUMBER     1
    WELL OBS   1    COORDINATES (    500.00,       0.  )
    INITIAL PRESSURE=0.

 OBSERVATION WELL NUMBER     2
    WELL OBS 2      COORDINATES (   -500.00,       0.  )
    INITIAL PRESSURE=0.

 OBSERVATION WELL NUMBER     3
    WELL OBS 3      COORDINATES (      0.  ,    500.00)
    INITIAL PRESSURE=-.0

 OBSERVATION WELL NUMBER     4
    WELL OBS 4      COORDINATES (      0.  ,   -500.00)
    INITIAL PRESSURE=-.0

 PRODUCTION WELL NUMBER          1
    PROD 1      COORDINATES (      0.  ,      0.  )
    NUMBER OF FLOWRATE POINTS=    2

                    TIME          FLOWRATE

                   0.             .1000E+04
                    .5000E+04     .1000E+04

 DISTANCES BETWEEN OBSERVATION WELLS AND PRODUCTION WELLS

           OBS   1     OBS 2       OBS 3       OBS 4
 PROD 1       500.00      500.00      500.00      500.00
```

Figure E-13. Output for Sample Problem 3.

TIME	OBS 1	OBS 2	OBS 3	OBS 4
1.00	-.2101E+01	-.2101E+01	-.3917-206	-.3917-206
2.00	-.1755E+02	-.1755E+02	-.8058-103	-.8058-103
3.00	-.3966E+02	-.3966E+02	-.2625E-68	-.2625E-68
4.00	-.6251E+02	-.6249E+02	-.5152E-51	-.5152E-51
5.00	-.8435E+02	-.8424E+02	-.1286E-40	-.1286E-40
6.00	-.1048E+03	-.1045E+03	-.1136E-33	-.1136E-33
7.00	-.1239E+03	-.1232E+03	-.1064E-28	-.1064E-28
9.00	-.1587E+03	-.1566E+03	-.4742E-22	-.4742E-22
10.00	-.1746E+03	-.1715E+03	-.1025E-19	-.1025E-19
20.00	-.3029E+03	-.2815E+03	-.4294E-09	-.4294E-09
30.00	-.3935E+03	-.3553E+03	-.1870E-05	-.1870E-05
40.00	-.4754E+03	-.4131E+03	-.1373E-03	-.1373E-03
50.00	-.5399E+03	-.4612E+03	-.1916E-02	-.1916E-02
60.00	-.5954E+03	-.5043E+03	-.1151E-01	-.1151E-01
70.00	-.6441E+03	-.5424E+03	-.4241E-01	-.4241E-01
80.00	-.6875E+03	-.5769E+03	-.1147E+00	-.1147E+00
100.00	-.7522E+03	-.6377E+03	-.4767E+00	-.4767E+00
101.00	-.7555E+03	-.6405E+03	-.5048E+00	-.5048E+00
102.00	-.7589E+03	-.6433E+03	-.5341E+00	-.5341E+00
103.00	-.7622E+03	-.6461E+03	-.5644E+00	-.5644E+00
104.00	-.7655E+03	-.6488E+03	-.5959E+00	-.5959E+00
105.00	-.7688E+03	-.6515E+03	-.6286E+00	-.6286E+00
106.00	-.7721E+03	-.6542E+03	-.6624E+00	-.6624E+00
107.00	-.7753E+03	-.6569E+03	-.6975E+00	-.6975E+00
109.00	-.7917E+03	-.6623E+03	-.7712E+00	-.7712E+00
110.00	-.7943E+03	-.6649E+03	-.8098E+00	-.8098E+00
120.00	-.8250E+03	-.6902E+03	-.1267E+01	-.1267E+01
130.00	-.8530E+03	-.7141E+03	-.1861E+01	-.1861E+01
140.00	-.8792E+03	-.7366E+03	-.2597E+01	-.2597E+01
150.00	-.9038E+03	-.7579E+03	-.3480E+01	-.3480E+01
160.00	-.9269E+03	-.7780E+03	-.4509E+01	-.4509E+01
170.00	-.9488E+03	-.7972E+03	-.5683E+01	-.5683E+01
180.00	-.9695E+03	-.8155E+03	-.6997E+01	-.6997E+01
200.00	-.1008E+04	-.8496E+03	-.1002E+02	-.1002E+02
201.00	-.1010E+04	-.8514E+03	-.1014E+02	-.1014E+02
202.00	-.1012E+04	-.8530E+03	-.1035E+02	-.1035E+02
203.00	-.1013E+04	-.8546E+03	-.1052E+02	-.1052E+02
204.00	-.1015E+04	-.8563E+03	-.1069E+02	-.1069E+02
205.00	-.1017E+04	-.8579E+03	-.1086E+02	-.1086E+02
206.00	-.1019E+04	-.8595E+03	-.1103E+02	-.1103E+02

Figure E-13. (continued).

TIME	OBS 1	OBS 2	OBS 3	OBS 4
207.00	-.1021E+04	-.8611E+03	-.1120E+02	-.1120E+02
208.00	-.1022E+04	-.8627E+03	-.1137E+02	-.1137E+02
209.00	-.1024E+04	-.8642E+03	-.1155E+02	-.1155E+02
210.00	-.1026E+04	-.8658E+03	-.1172E+02	-.1172E+02
220.00	-.1043E+04	-.8813E+03	-.1354E+02	-.1354E+02
230.00	-.1059E+04	-.8961E+03	-.1546E+02	-.1546E+02
240.00	-.1075E+04	-.9104E+03	-.1747E+02	-.1747E+02
250.00	-.1090E+04	-.9243E+03	-.1959E+02	-.1959E+02
260.00	-.1105E+04	-.9376E+03	-.2178E+02	-.2178E+02
270.00	-.1119E+04	-.9505E+03	-.2406E+02	-.2406E+02
280.00	-.1133E+04	-.9630E+03	-.2641E+02	-.2641E+02
300.00	-.1158E+04	-.9869E+03	-.3129E+02	-.3129E+02
320.00	-.1183E+04	-.1009E+04	-.3640E+02	-.3640E+02
340.00	-.1206E+04	-.1031E+04	-.4169E+02	-.4169E+02
360.00	-.1227E+04	-.1051E+04	-.4712E+02	-.4712E+02
390.00	-.1243E+04	-.1070E+04	-.5268E+02	-.5268E+02

Figure E-13. (continued).

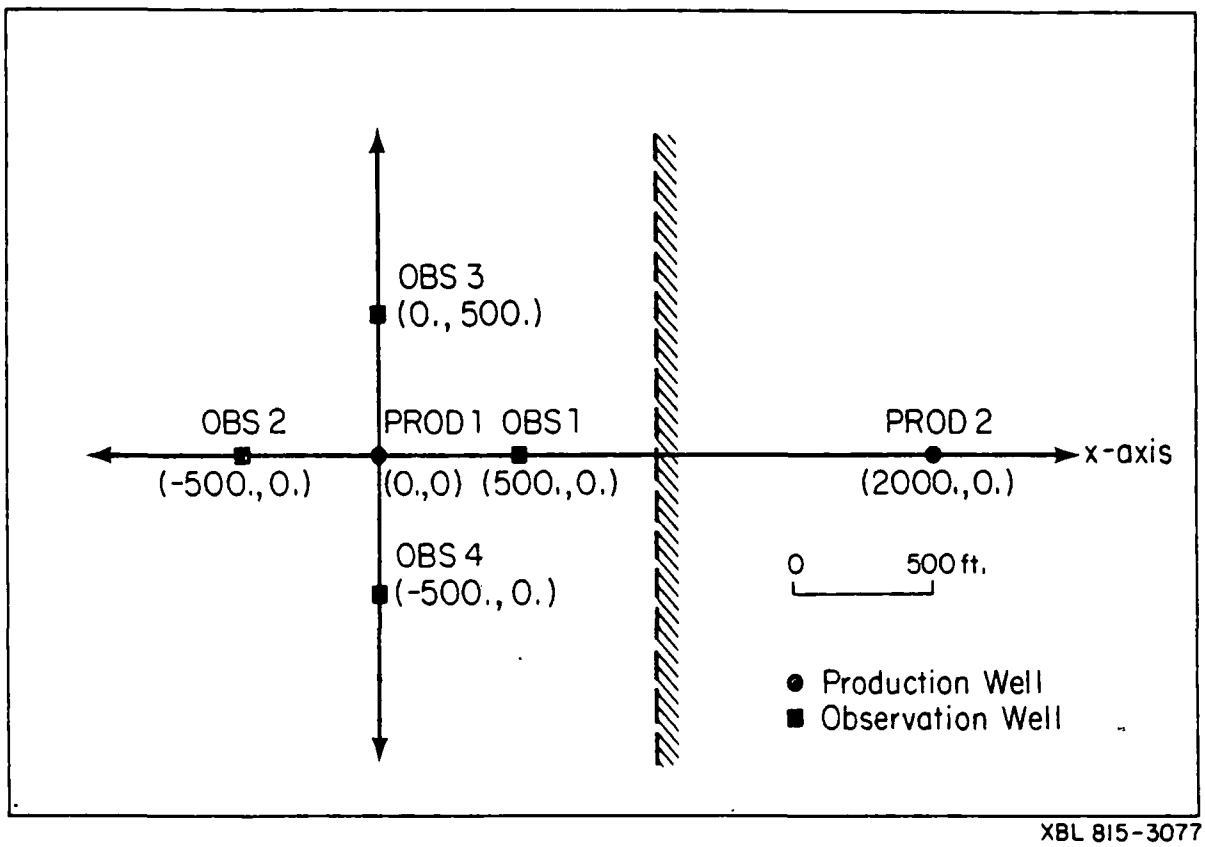

Figure E-14. Observation well locations, production well location, and "image" well location for Sample Problem 4.

```
VERIFICATION OF ANISOTROPY-RUN TO COMPARE WITH BOUNDARY
      04          2          1         56
6.895 E+03 6.310E-05   3.6E+03  .3048    1.0  E-03 9.862E-16
150000.    1000.      .002        0.          0.
OBS   1      500.      0.          0.              0        0.
OBS 2       -500.      0.          0.
OBS 3        000.      500.
OBS 4        000.     -500.
PROD 1         0.       0.              2
0.           1000.
5000.        1000.
PROD 2       2000.      0.              2
0.           1000.
5000.        1000.
1.           2.        3.        4.        5.        6.        7.        9.
10.          20.       30.       40.       50.       60.       70.       80.
100.         101.      102.      103.      104.      105.      106.      107.
109.         110.      120.      130.      140.      150.      160.      170.
180.         200.      201.      202.      203.      204.      205.      206.
207.         208.      209.      210.      220.      230.      240.      250.
260.         270.      280.      300.      320.      340.      360.      380.
```

Figure E-15. Input deck for Sample Problem 4.

```
VERIFICATION OF ANISOTROPY-RUN TO COMPARE WITH BOUNDARY

NUMBER OF OBSERVATION WELLS                                    4
NUMBER OF PRODUCTION WELLS                                     2
NUMBER OF TIMES AT WHICH PRESSURES WILL BE CALCULATED         56

                    CONVERSION FACTORS
                    ==================

          PRESSURE UNIT PER PASCAL                          .6895E+04
          FLOWRATE UNIT PER CUBIC METER PER SECOND          .6310E-04
          TIME UNIT PER SECOND                               3600.00
          LENGTH PER METER                                       .30
          VISCOSITY PER PASCAL-SECOND                        .100E-02
          PERMEABILITY PER SQUARE METER                      .9862E-15


     PARAMETER VALUES
     ================
     X-AXIS TRANSIMISSIVITY = .1500E+06
     Y-AXIS TRANSMISSIVITY = .1000E+04
     STORATIVITY = .2000E-02


OBSERVATION WELL NUMBER      1
     WELL OBS   1     COORDINATES (     500.00,       0.  )
     INITIAL PRESSURE=0.
```

Figure E-16. Output for Sample Problem 4.

```
OBSERVATION WELL NUMBER      2
   WELL OBS 2       COORDINATES (    -500.00,       0.   )
   INITIAL PRESSURE=0.


OBSERVATION WELL NUMBER      3
   WELL OBS 3       COORDINATES (       0.   ,     500.00)
   INITIAL PRESSURE=-.0


OBSERVATION WELL NUMBER      4
   WELL OBS 4       COORDINATES (       0.   ,    -500.00)
   INITIAL PRESSURE=-.0

  PRODUCTION WELL NUMBER           1
     PROD 1        COORDINATES (       0.   ,       0.   )
     NUMBER OF FLOWRATE POINTS=     2

                       TIME          FLOWRATE


                     0.                .1000E+04
                      .5000E+04        .1000E+04

  PRODUCTION WELL NUMBER           2
     PROD 2        COORDINATES (    2000.00,       0.   )
     NUMBER OF FLOWRATE POINTS=     2

                       TIME          FLOWRATE

                     0.                .1000E+04
                      .5000E+04        .1000E+04

  DISTANCES BETWEEN OBSERVATION WELLS AND PRODUCTION WELLS

             OBS   1      OBS 2        OBS 3        OBS 4
  PROD 1        500.00       500.00       500.00       500.00
  PROD 2       1500.00      2500.00      2061.55      2061.55
```

Figure E-16. (continued).

TIME	OBS 1	OBS 2	OBS 3	OBS 4
1.00	-.2101E+01	-.2101E+01	-.3917-206	-.3917-206
2.00	-.1755E+02	-.1755E+02	-.8058-103	-.8058-103
3.00	-.3966E+02	-.3966E+02	-.2625E-68	-.2625E-68
4.00	-.6249E+02	-.6249E+02	-.5152E-51	-.5152E-51
5.00	-.8424E+02	-.8424E+02	-.1286E-40	-.1286E-40
6.00	-.1045E+03	-.1045E+03	-.1135E-33	-.1135E-33
7.00	-.1232E+03	-.1232E+03	-.1063E-28	-.1063E-28
9.00	-.1566E+03	-.1566E+03	-.4727E-22	-.4727E-22
10.00	-.1715E+03	-.1715E+03	-.1020E-19	-.1020E-19
20.00	-.2807E+03	-.2807E+03	-.4004E-09	-.4004E-09
30.00	-.3512E+03	-.3512E+03	-.1601E-05	-.1601E-05
40.00	-.4031E+03	-.4031E+03	-.1092E-03	-.1092E-03
50.00	-.4442E+03	-.4442E+03	-.1440E-02	-.1440E-02
60.00	-.4783E+03	-.4783E+03	-.8266E-02	-.8266E-02
70.00	-.5073E+03	-.5073E+03	-.2939E-01	-.2939E-01
80.00	-.5326E+03	-.5326E+03	-.7720E-01	-.7720E-01
100.00	-.5752E+03	-.5752E+03	-.3071E+00	-.3071E+00
101.00	-.5771E+03	-.5771E+03	-.3246E+00	-.3246E+00
102.00	-.5790E+03	-.5790E+03	-.3428E+00	-.3428E+00
103.00	-.5809E+03	-.5809E+03	-.3617E+00	-.3617E+00
104.00	-.5828E+03	-.5828E+03	-.3812E+00	-.3812E+00
105.00	-.5846E+03	-.5846E+03	-.4014E+00	-.4014E+00
106.00	-.5864E+03	-.5864E+03	-.4223E+00	-.4223E+00
107.00	-.5882E+03	-.5882E+03	-.4439E+00	-.4439E+00
109.00	-.5918E+03	-.5918E+03	-.4893E+00	-.4893E+00
110.00	-.5935E+03	-.5935E+03	-.5130E+00	-.5130E+00
120.00	-.6103E+03	-.6103E+03	-.7912E+00	-.7912E+00
130.00	-.6257E+03	-.6257E+03	-.1147E+01	-.1147E+01
140.00	-.6400E+03	-.6400E+03	-.1583E+01	-.1583E+01
150.00	-.6534E+03	-.6534E+03	-.2101E+01	-.2101E+01
160.00	-.6659E+03	-.6659E+03	-.2699E+01	-.2699E+01
170.00	-.6777E+03	-.6777E+03	-.3375E+01	-.3375E+01
180.00	-.6888E+03	-.6888E+03	-.4126E+01	-.4126E+01
200.00	-.7093E+03	-.7093E+03	-.5840E+01	-.5840E+01
201.00	-.7102E+03	-.7102E+03	-.5932E+01	-.5932E+01
202.00	-.7112E+03	-.7112E+03	-.6026E+01	-.6026E+01
203.00	-.7122E+03	-.7122E+03	-.6119E+01	-.6119E+01
204.00	-.7131E+03	-.7131E+03	-.6214E+01	-.6214E+01
205.00	-.7141E+03	-.7141E+03	-.6309E+01	-.6309E+01
206.00	-.7150E+03	-.7150E+03	-.6405E+01	-.6405E+01

Figure E-16. (continued).

TIME	OBS 1	OBS 2	OBS 3	OBS 4
207.00	-.1021E+04	-.8611E+03	-.1120E+02	-.1120E+02
208.00	-.1022E+04	-.8627E+03	-.1137E+02	-.1137E+02
209.00	-.1024E+04	-.8642E+03	-.1155E+02	-.1155E+02
210.00	-.1026E+04	-.8658E+03	-.1172E+02	-.1172E+02
220.00	-.1043E+04	-.8813E+03	-.1354E+02	-.1354E+02
230.00	-.1059E+04	-.8961E+03	-.1546E+02	-.1546E+02
240.00	-.1075E+04	-.9104E+03	-.1747E+02	-.1747E+02
250.00	-.1090E+04	-.9243E+03	-.1959E+02	-.1959E+02
260.00	-.1105E+04	-.9376E+03	-.2178E+02	-.2178E+02
270.00	-.1119E+04	-.9505E+03	-.2406E+02	-.2406E+02
280.00	-.1133E+04	-.9630E+03	-.2641E+02	-.2641E+02
300.00	-.1158E+04	-.9869E+03	-.3129E+02	-.3129E+02
320.00	-.1183E+04	-.1009E+04	-.3640E+02	-.3640E+02
340.00	-.1206E+04	-.1031E+04	-.4169E+02	-.4169E+02
360.00	-.1227E+04	-.1051E+04	-.4712E+02	-.4712E+02
380.00	-.1248E+04	-.1070E+04	-.5268E+02	-.5268E+02

Figure E-16. (continued).

```
                        **PROGRAM VARFLOW(INPUT,OUTPUT,TAPE1,TAPE2)**
 1.    0000008          PROGRAM VARFLOW(INPUT,OUTPUT,TAPE1,TAPE2)
                   C
                   CCCCCCCCCCCCCCCCCCCCCCCCCCCCCCCCCCCCCCCCCCCCCCCCCCCCCCCCCCCCCCC
                   C
                   C    THIS PROGRAM CALCULTES DRAWDOWN IN AN ANISOTROPIC,HOMOGENEOUS,
                   C    CONSTANT THICKNESS POROUS MEDIUM. THERE CAN BE UP TO 10
                   C    PRODUCTION WELLS AND TEN OBSERVATION WELLS. FLOWRATES
                   C    CAN BE VARIABLE. THE PROGRAM CAN ALSO INCLUDE DRAWDOWN DUE TO
                   C    SKIN EFFECTS AND A SINGLE LINEAR RESERVOIR BOUNDARY (BARRIER
                   C    OR CONSTANT POTENTIAL).
                   C
 2.    0022058          DIMENSION X(3),TITLE(8),YSTART(10),LOBS(10),KKJ(10),ROY(10),
                       $SKIN(10),R(10,10),TIMES(100),RI2(10,10),UX(10),UY(10),ROX(10),
                       $PX(10),PY(10),AQ(100,10),TQ(100,10),BQ(100,10),YCALC(100,10)
                       $,NAME(10),PNAME(10),RPX(10),RPY(10),RIPX(10),RIPY(10)
 3.    0022058          COMMON /SUB/ PI
 4.    0022058          DATA ((KKJ(J),J=1,10),L)/11*0/
 5.    0022058          DATA (PI,PAPRESS,CMSFLOW,SECTIME,RLENGTH,SMPERM,PASVISC)
                       &/3.141592654,6*1.0/
                   CCCCCCCCCCCCCCCCCCCCCCCCCCCCCCCCCCCCCCCCCCCCCCCCCCCCCCCCCCCCCCCC
                   C        READ IN ALL OF THE PROBLEM PARAMETERS AND FLOW RATE DATA
                   C        PRINT OUT ALL OF THE ABOVE
 6.    0022058
 7.    0022058          READ 100,(TITLE(I),I=1,8)
 8.    0130128   100    FORMAT(8A10)
 9.    0130128          PRINT 200, (TITLE(I),I=1,8)
10.    0130218   200    FORMAT(1H1,2X,8A10)
11.    0130218          READ 101,IHH,JJ,IDIMEN,NTIMES
12.    0130308   101    FORMAT(4I10)
13.    0130308          PRINT 201,IHH,JJ,NTIMES
14.    0130368   201    FORMAT(//,*  NUMBER OF OBSERVATION WELLS*,I10,
                       $/,*  NUMBER OF PRODUCTION WELLS *,I10,
                       $/,*  NUMBER OF TIMES AT WHICH PRESSURES WILL BE CALCULATED*,I10)
15.    0130368          IF(IDIMEN  .EQ.   0)GO TO 10
16.    0130378          READ 102,PAPRESS,CMSFLOW,SECTIME,RLENGTH,PASVISC,SMPERM
17.    0130508   102    FORMAT(6E10.4)
18.    0130508   10     PRINT 202,PAPRESS,CMSFLOW,SECTIME,RLENGTH,PASVISC,SMPERM
19.    0130618   202    FORMAT(//,20X,*CONVERSION FACTORS*,/,20X,18(1H=),/,
                       $/,10X,*PRESSURE UNIT PER PASCAL*,21X,E10.4,/,10X,
                       $*FLOWRATE UNIT PER CUBIC METER PER SECOND*,5XE10.4,/,10X,
                       $*TIME UNIT PER SECOND*,25XF10.2,/,10X,*LENGTH PER METER*,29XF10.2,
                       $/,10X,*VISCOSITY PER PASCAL-SECOND*,18XE10.3,/,10X,
                       $*PERMEABILITY PER SQUARE METER*,16XE10.4)
```

Figure E-17. VARFLOW Program sample.

```
0130618         READ 103,RKHUX,RKHUY,PCH,ANGLE,DSTNCE,BOUND
013072B   103   FORMAT(5E10.4,A10)
013072B         PRINT 203,RKHUX,RKHUY,PCH
013100B   203   FORMAT(//,5X,*PARAMETER VALUES*,/,5X,16(1H=),/,
               $5X,*X-AXIS TRANSIMISSIVITY =*,E10.4,/,5X,
               $*Y-AXIS TRANSMISSIVITY =*,E10.4,/,5X,*STORATIVITY =*,E10.4)
013100B         IF(BOUND  .NE.   10H              )PRINT 204,BOUND,ANGLE,DSTNCE
013110B   204   FORMAT(/,2X,*THERE IS A *,A10,*BOUNDARY AT AN ANGLE OF *,F10.2,
               $* DEGREES AND A DISTANCE OF *,F10.2)
013110B         DO 1000 I=1,IHH
013112B         READ 105, NAME(I),OX(I),OY(I),YSTART(I),LOBS(I),SKIN(I)
013132B         PRINT 205,I,NAME(I),OX(I),OY(I),YSTART(I)
013146B   1000  IF(LOBS(I)  .GT.  0)PRINT 206,LOBS(I),SKIN(I)
013161B   205   FORMAT(//,*  OBSERVATION WELL NUMBER *,I5,/,5X,*WELL *,A10,
               $* COORDINATES (*F10.2,*,*F10.2,*)*,/,5X,*INITIAL PRESSURE=*,E10.4)
013161B   206   FORMAT(5X,*THIS OBSERVATION WELL IS ALSO PRODUCTION WELL NUMBER*
               $,I10,/,5X,*IT HAS A SKIN VALUE OF*,F10.2)
013161B   105   FORMAT(A10,2F10.2,E10.4,I10,F10.2)
013161B         DO 1020 J=1,JJ
013163B         READ 106, PNAME(J),PX(J),PY(J),KKJ(J)
013177B         PRINT 207,J,PNAME(J),PX(J),PY(J),KKJ(J)
013213B         DO 1020 IJ=1,KKJ(J)
013216B         READ 107, TQ(IJ,J),AQ(IJ,J)
013231B   1020  PRINT 208,TQ(IJ,J),AQ(IJ,J)
013245B   207   FORMAT(//,*  PRODUCTION WELL NUMBER *,I10,/,5X,A10,
               $2X,*COORDINATES (*,F10.2,*,*,F10.2,*)*,2X,/,5X,
               $*NUMBER OF FLOWRATE POINTS=*,I5,//,23X,*TIME*,9X,*FLOWRATE*,//)
013245B   106   FORMAT(A10,2F10.2,I10)
013245B   107   FORMAT(2E10.4)
013245B   208   FORMAT(20X,E10.4,5X,E10.4)
013245B   108   FORMAT(8E10.4)
013245B         DO 1030 I=1,NTIMES,8
013247B   1030  READ 108, (TIMES(K),K=I,I+7)
                C
                CCCCCCCCCCCCCCCCCCCCCCCCCCCCCCCCCCCCCCCCCCCCCCCCCCCCCCCCCCCCCCCCCCCCCC
                C      SET UP THE PROBLEM
                C
                C      CALCULATE THE GRADIENTS FOR THE FLOW RATE DATA
013262B         DO 1050 I=1,JJ
013264B         DO 1050 IJ=1,KKJ(I)-1
013270B         IF( ABS(TQ(IJ+1,I)-TQ(IJ,I)) .EQ. 0. ) GO TO 1050
013277B         BQ(IJ,I)=(AQ(IJ+1,I)-AQ(IJ,I))/(TQ(IJ+1,I)-TQ(IJ,I))
013307B   1050  CONTINUE
                C
                C      CALCULATE RADIAL DISTANCES BETWEEN THE OBSERVATION WELLS
                C      AND THE PRODUCTION WELLS
013314B         DO 1070 IH=1,IHH
013316B         DO 1070 J=1,JJ
013321B   1070  R(IH,J)=SQRT((PX(J)-OX(IH))**2. + (PY(J)-OY(IH))**2.)
013343B         PRINT 211,(NAME(I),I=1,IHH)
013353B   211   FORMAT(//,*  DISTANCES BETWEEN OBSERVATION WELLS AND PRODUCTION*
               $,* WELLS*,//,12X,10(A10,2X),//)
013353B         DO 1080 I=1,JJ
013355B   1080  PRINT 210, PNAME(I),(R(IH,I),IH=1,IHH)
013374B   210   FORMAT(2X,A10,10(F10.2,2X))
                C
                CCCCCCCCCCCCCCCCCCCCCCCCCCCCCCCCCCCCCCCCCCCCCCCCCCCCCCCCCCCCCCCCCCCCC
                C       CALCULATE THE PARAMETERS
013374B          RKHUE=SQRT(RKHUX*RKHUY)
013400B         X(1)=CMSFLOW*PASVISC/4./PI/RKHUE/SMPERM/RLENGTH/PAPRESS
013406B         ALPHA=ANGLE*PI/180.
013410B         IF(BOUND    .EQ. 10H                 )GO TO 40
                CCCCCCCCCCCCCCCCCCCCCCCCCCCCCCCCCCCCCCCCCCCCCCCCCCCCCCCCCCCCCCCCCCCCC
                C      CALCULATE THE COORDINATES OF THE IMAGE WELLS
013412B         DO 1090 IH=1,IHH
013414B         ROX(IH)=OX(IH)*SIN(ALPHA)+OY(IH)*COS(ALPHA)
013424B         ROY(IH)=OY(IH)*SIN(ALPHA)-OX(IH)*COS(ALPHA)
013434B   1090  IF(BOUND  .EQ.10HLEAKY          )L=1
013443B   40    DO 2001 IH=1,IHH
013446B         DO 2002 N=1,NTIMES
013451B         YCAL(N,IH)=YSTART(IH)
013454B         DO 2000 J=1,JJ
```

Figure E-17. (continued).

```
VARFLOW                       **PROGRAM VARFLOW(INPUT,OUTPUT,TAPE1,TAPE2)**

0134608         CALL RKHUNF(RKHUX,RKHUY,OX(IH),OY(IH),PX(J),PY(J),RKHUN)
0134678         RKHUN=X(1)*RKHUE/RKHUN
0134718         X(2)=R(IH,J)*R(IH,J)*(RLENGTH**3.)*PI*PCH*RKHUN/CMSFLOW/SECTIME
0135028         IF(  BOUND  .EQ. 10H                    )GO TO 50
0135058         RPX(J)=PX(J)*SIN(ALPHA)+PY(J)*COS(ALPHA)
0135158         RPY(J)=PY(J)*SIN(ALPHA)-PX(J)*COS(ALPHA)
0135258         RIPY(J)=RPY(J)
0135268         RIPX(J)=2.*DSTNCE-RPX(J)
          CCCCCCCCCCCCCCCCCCCCCCCCCCCCCCCCCCCCCCCCCCCCCCCCCCCCCCCCCCCCCCCCCCCCCCCC
          C     CALCULATE THE DISTANCE BETWEEN THE IMAGE WELLS AND THE OBSERVATION
          C     WELLS
0135308         RI2(IH,J)=(ROX(IH)-RIPX(J))**2.  + (ROY(IH)-RIPY(J))**2.
0135368         CALL COOR(RIPX(J),RIPY(J),XI,YI,ANGLE)
0135448         CALL RKHUNF(RKHUX,RKHUY,OX(IH),OY(IH),XI,YI,RKHUN)
0135508         RKHUN=X(1)*RKHUE/RKHUN
0135528         X(3)=RI2(IH,J)*(RLENGTH**3.)*PI*PCH*RKHUN/CMSFLOW/SECTIME
0135618         NNW=3
0135628   50    IF(BOUND  .EQ. 10H                    )NNW=2
          C
          CCCCCCCCCCCCCCCCCCCCCCCCCCCCCCCCCCCCCCCCCCCCCCCCCCCCCCCCCCCCCCCCCCCCCCCC
          C     MAIN CALCULATION LOOP
0135668         TR=TIMES(N)
0135678         FII=0.
0135708         DO 1100 I=2,NNW
0135728         FI=0.0
0135728         DO 1110 KJ=1,KKJ(J)-1
0135778         IF(ABS(TQ(KJ+1,J)-TQ(KJ,J)).LT.1.E-5) GO TO 1110
0136068         TN=TR-TQ(KJ,J)
0136138         TN1=TR-TQ(KJ+1,J)
0136168         IF(TN.LE.0.) GO TO 1100
0136218         IF(TN1.LE.0.0) GO TO 80
0136238         FI=(AQ(KJ,J)+BQ(KJ,J)*(TN+X(I)))*(EI(-X(I),TN1)-EI(-X(I),TN))
                S=BQ(KJ,J)*(TN*EXP(-X(I)/TN)-TN1*EXP(-X(I)/TN1))+FI
0136648   1110  CONTINUE
0136678         GO TO 90
0136708   80    FI=-(AQ(KJ,J)+BQ(KJ,J)*(TN+X(I)))*EI(-X(I),TN)
                A-BQ(KJ,J)*TN*EXP(-X(I)/TN)+FI
0137148   90    IF(L.EQ.1.AND.I.GT.2)FI=-FI
0137238   1100  FII=FII+FI
0137278         IF(LOBS(IH).NE.J) GO TO 70
0137318         FII=(FII+2.*SKIN(IH)*(AQ(KJ,J)+BQ(KJ,J)*TN))
0137428   70    F=FII*X(1)
0137448   2000  YCALC(N,IH)=YCALC(N,IH)-F
0137528   2002  CONTINUE
0137548   2001  CONTINUE
          C
          CCCCCCCCCCCCCCCCCCCCCCCCCCCCCCCCCCCCCCCCCCCCCCCCCCCCCCCCCCCCCCCCCCCCCCCC
          C
          C     PRINT OUT RESULTS OF THE CALCULATION
0137578         PRINT 118,(NAME(I),I=1,IHH)
0137708         N=0
0137708         IN=0
0137708         DO 1120 I=1,NTIMES
0137738         PRINT 119,TIMES(I),(YCALC(I,IH),IH=1,IHH)
0140128         N=N+1
0140138         IF(N   .NE.   5)GO TO 1120
0140148         PRINT 120
0140208         IN=IN+1
0140218         N=0
0140218         IF(IN   .NE.   8)GO TO 1120
0140238         PRINT 118,(NAME(M),M=1,IHH)
0140348         IN=0
0140348   1120  CONTINUE
0140378   118   FORMAT(1H1,//,5X,*    TIME    *,10(A10,2X),/,5X,130(1H=),//)
0140378   119   FORMAT(3X,F10.2,2X,10(E10.4,2X))
0140378   120   FORMAT(/)
0140378         STOP
0140408         END

EI                            **FUNCTION EI(X,T)**

0000008         FUNCTION EI(X,T)
0000008         A=-X/T
```

Figure E-17. (continued).

```
VARFLOW          **PROGRAM VARFLOW(INPUT,OUTPUT,TAPE1,TAPE2)**

    3.  0000028          IF(A.GT.10.0) GO TO 20
    4.  0000058          ET=-ALOG(A)-.5772156649
    5.  0000108          TERM=1.0
    6.  0000118          DO 10 J=1,100
    7.  0000148          TERM=-TERM*A/J
    8.  0000168          ET=ET-TERM/J
    9.  0000218          IF(ABS(TERM/J/ET).LT.1.E-8) GO TO 12
   10.  0000218       10 CONTINUE
   11.  0000308       12 ET=-ET
   12.  0000328          RETURN
   13.  0000348       20 ET=EXP(-A)/A*(1.0-1.0/A+2.0/A**2-6.0/A**3)
   14.  0000468          RETURN
   15.  0000518          END


RKHUNF           **SUBROUTINE RKHUNF(RKHUX,RKHUY,DXD,DYD,PXD,PYD,RKHUN)**

    1.  0000008          SUBROUTINE RKHUNF(RKHUX,RKHUY,DXD,DYD,PXD,PYD,RKHUN)
    2.  0000008          COMMON /SUB/ PI
    3.  0000008          YD=DYD-PYD
    4.  0000018          XD=DXD-PXD
    5.  0000038          THETA=ATAN2(YD,XD)
    6.  0000068          PRINT 99,THETA
    7.  0000138       99 FORMAT(5X,*THETA=*,F10.2)
    8.  0000138          RKHUN=RKHUX/((COS(THETA)**2.) + RKHUX*(SIN(THETA)**2.)/RKHUY)
    9.  0000248          PRINT 100,RKHUN
   10.  0000318      100 FORMAT(5X,*RKHUN=*,F10.2)
   11.  0000318          RETURN
   12.  0000338          END


COOR             **SUBROUTINE COOR(RIPXD,RIPYD,XI,YI,ANGLE)**

    1.  0000008          SUBROUTINE COOR(RIPXD,RIPYD,XI,YI,ANGLE)
    2.  0000008          COMMON /SUB/ PI
    3.  0000008          ANG=90.-ANGLE
    4.  0000018          ANG=ANG*PI/180.
    5.  0000038          XI=RIPXD*COS(ANG)+RIPYD*SIN(ANG)
    6.  0000128          YI=RIPYD*COS(ANG)-RIPXD*SIN(ANG)
    7.  0000218          RETURN
    8.  0000248          END
```

Figure E-17. (continued).

Acknowledgments

S. M. Benson acknowledges Dr. Chin Fu Tsang and Dr. Donald McEdwards for their contribution to this work, insofar as the original variable flow rate algorithm was developed by them.

REFERENCES

E-1. H. S. Carslaw, and J. C. Jaeger, Conduction of Heat in Solids, Oxford: Clarendon Press, pp. 258-262, 1959.

E-2. D. G. McEdwards, Variable Rate Well Test Analysis (Ph.D Dissertation) Berkeley: University of California, 1979.

E-3. D. G. McEdwards, and C. F. Tsang, "Variable Rate Well Testing Analysis," in Proceedings of the Invitational Well-Testing Symposium, LBL-7027, 1977.

E-4. G. P. Kruseman and N. A. De Ridder, Analysis and Evaluation of Pumping Test Data, Ulageningen, The Netherlands: International Institute for Land Reclamation and Improvement, 1976.

E-5. M. S. Hantush, "Drawdown Around Wells of Variable Discharge" Journal of Geophysical Research, 6º, 29, 1964, pp. 4221-4235.

E-6. R. C. Earlougher, Advances in Well Test Analysis, Society of Petroleum Engineers Monographs, 1977.

APPENDIX F
REFERENCE BIBLIOGRAPHY

APPENDIX F

REFERENCE BIBLIOGRAPHY

D. W. Allman, D. Goldman, and W. L. Niemi, "Evaluation of Testing and Reservoir Parameters in Geothermal Wells at Raft River and Boise, Idaho," Geothermal Resources Council Annual Meeting, Reno, NV, September 24, 1979, p. 4.

C. B. Ammann, "Case Histories of Analysis of Characteristics of Reservoir Rock from Drill-Stem Tests," Journal of Petroleum Technology, 12, 5, 1960, p. 27.

K. E. Anderson, Water Well Handbook, St. Louis: Scholin Brothers Printing Corp., 1967.

J. K. Applegate, P. R. Donaldson, D. L. Hinkley, and T. L. Wallace, "Borehole Geophysics Evaluation of the Raft River Geothermal Reservoir, Idaho," Geophysics, 42, 1, 1977, pp. 138-139.

S. Arnorsson, "Application of the Silica Geothermometer in Low Temperature Hydrothermal Areas in Iceland," American Journal of Science 275, 1975, pp. 763-784.

S. R. Aydelotte, Transient Well Testing in Two-Phase Geothermal Reservoirs, LBL NTIS PCA07/MFA01, March 1980, p. 148.

R. Bentall, "Methods of Collecting and Interpreting Ground-Water Data," U.S. Geologic Survey Water Supply Paper, 1544-H, 1963, pp. 1-97.

R. Bentall, "Shortcuts and Special Problems in Aquifer Tests," U.S. Geological Survey Water-Supply Paper 1545-C, 1963, p. C1-C117.

H. C. Bixel, B. K. Larkin, and H. K. Van Poollen, "Effect of Linear Discontinuities, or Pressure Build-up and Drawdown Behavior," Journal of Petroleum Technolgoy, August 1963, pp. 885-895.

G. Bodvarsson, "Capacitative Perturbations in Well Interference Testing," Proceedings of the Fifth Workshop on Geothermal Reservoir Engineering, Stanford, California, December 12, 1979, pp. 85-90.

G. Bodvarsson, "Mechanism of Reservoir Testing," Proceedings Fourth Workshop Geothermal Reservoir Engineering, Stanford, California, December 13, 1978, pp. 146-152.

N. S. Boulton, "Analysis Data from Non-Equilibrium Pumping Tests Allowing for Delayed Yield from Storage," Proceedings of the Institution of Civil Engineers, London, Paper No. 6693, 26, 1963, pp. 469-178.

C. A. Brook et al., "Hydrothermal Convection Systems with Reservoir Temperatures 90°C," U.S. Geological Survey Circular 790, 1978, pp. 18-85.

D. H. Brownell et al., "Governing Equation for Geothermal Reservoirs," Water Resources, 13, 6, 1977, pp. 929-934.

D. A. Campbell, "Hot Water vs. Dry Steam Reservoir Assessment," Geothermal Environment Seminar, 1978, Sacramento, California, May 9, 1978, pp. 118-138.

H. S. Carslaw and J. C. Jaeger, Conduction of Heat in Solids, Oxford: Oxford at the Claredon Press, 1959.

B. Chen, Geothermal Reservoir and Well Test Analysis: A Literature Survey, University of Hawaii, NTIS PCA031 MFA01, 1974, p. 38.

P. Cheng and K. H. Lau, The Effects of Steady State Withdrawal of Fluid in Geothermal Reservoirs, University of Hawaii, NTIS PCA03/MFA01, 1975, p. 31.

C. Y. Chiang and C. R. Y. Chang, "Application of the Horner Method to the Estimation of Static Reservoir Temperature During Drilling Operations," Proceedings of Fifth Workshop on Geothermal Reservoir Engineering, Stanford, CA, December 12, 1979, pp. 367-372.

R. N. Clayton and A. Steiner, "Oxygen Isotope Studies of the Geothermal System at Wairakei, New Zealand," Geochemica Cosmochimica Acta, 39, 1975, pp. 1179-1186.

G. Cortecci, "Oxygen Isotropic Ratios of Sulfate Ions-Water Pairs as a Possible Geothermometer," Geothermics 3, 1974, pp. 60-64.

A. Desplan, J. Deschamps and M. Leleu, "Chemical Reactions Occurring During the Exploitation of Geothermal Well Doublet: Thermodynamic and Experimental Approach for the Case of the Dogger Reservoir in the Pairs Basin," First Seminar on Geothermal Energy, Brussels, Belgium, December 6, 1977, pp. 529-547.

R. J. M. De Wiest, "On the Storage Coefficient and the Equations of Ground-Water Flow," Journal of Geophysical Research, 71, 4, 1966.

A. Domenico, Concepts and Models in Groundwater Hydrology, New York: McGraw-Hill Book Company, Inc., 1972, p. 405.

I. G. Donaldson, "Geothermal Reservoir Engineering Research in New Zealand," Proceedings Fourth Workshop Geothermal Reservoir Engineering, Stanford, California, December 13, 1978, pp. 36-41.

M. H. Dorfman and R. W. Deller, "Well Design and Reservoir Research and Technology," Proceedings of Second Geopressured Geothermal Energy Conference, Volume I, Austin, Texas, February 23, 1976, pp. 19-23.

R. C. Earlougher, Jr., K. M. Kersch, and H. J. Ramey, "Wellbore Effects in Injection Well Testing," Journal of Petroleum Technology, November 1973, pp. 1244-1250.

R. C. Earlougher, Jr. and K. M. Kersch, "Analysis of Short-time Transient Test Data by Type Curve Matching," Journal of Petroleum Technology, July 1974, pp. 793-800, Transactions, AIME, p. 257.

R. C. Earlougher, "Advances in Well Test Analysis," SPE Monograph Series, 5, 1977.

C. Economides, "Recent Development in Well Test Analysis in the Stanford Geothermal Program," Proceedings Fourth Workshop Geothermal Reservoir Engineering, Standford, California, December 18, 1978, pp. 188-200.

M. J. Economides, "Shut-in and Flowing Button Hole Pressure Calculation for Geothermal Steam Wells," Proceedings of the Fifth Workshop on Geothermal Reservoir Engineering, Stanford, California, December 12, 1979, pp. 139-151.

R. O. Elemo, "Estimation of Stress-Sensitive Reservoirs' Initial Parameters by Use of the Conventional Well Test Methods," Fourth United States Gulf Coast Geopressured-Geothermal Energy Conference: Research and Development, Austin, Texas, October 29, 1979, pp. 960-971.

A. J. Ellis and N. A. J. Mahon, "National Hydrothermal Systems and Experimental Hot-Water/Rock Interactions," Geochemica et Cosmochimica Acta, 28, 1964, pp. 1323-1357.

G. Endo, "Numerical Model for Steam-Dominated Type Geothermal Reservoir," Third Meeting of the Japan Geothermal Energy Association, Tokyo, Japan, December 9, 1976, p. 2

Energy Research and Development Administration, "Geothermal Resource Assessment and Reservoir Engineering," DOE Workshop on Geothermal Resources Assessment and Reservoir Engineering, Larderello, Italy, September 12, 1977, p. 442.

J. G. Ferris, D. B. Knowles, R. H. Brown, and R. H. Stallman, "Theory of Aquifer Tests," U.S. Geological Survey Water-Supply Paper 1536-E, 1962, pp. 69-174.

R. O. Fournier, D. E. White, and A. H. Truesdell, "Geochemical Indicators of Subsurface Temperature-1, Basic Assumptions," U.S. Geological Survey Journal of Research, 2, 1974, pp. 259-262.

R. O. Fournier and A. H. Truesdell, "Geochemical Indicators of Subsurface Temperature-2. Estimation of Temperature and Fraction of Hot Water Mixed with Cold Water," U.S. Geological Survey Journal of Research, 2, 1974, pp. 263-269.

R. O. Fournier and A. H. Truesdell, Geochemical Indicators of Subsurface Temperature Applied to Hot Spring Waters of Yellowstone National Park, Wyoming, U.S.A.," Geothermics 2, 1970, pp. 529-535.

R. O. Fournier and R. W. Potter II, "Magnesium Correction to the Na-K-Ca Chemical Geothermometer," Geochemica Cosmochimica Acta, 43, pp. 1543-1550.

R. O. Fournier and J. J. Rowe, "Estimation of Underground Temperatures from the Silica Content of Water from Hot Springs and Wet-Steam Wells," American Journal of Science, 264, 1966, pp. 685-697.

R. O. Fournier and A. H. Truesdell, "An Empirical Na-K-Ca Geothermometer for Natural Waters," Geochemica et Cosmochimica Acta, 37, 1973, pp. 1255-1275.

R. O. Fournier, "Chemical Geothermometers and Mixing Models for Geothermal Systems," Geothermics, 5, 1977, pp. 41-50.

S. K. Garg, "Pressure Transient Analysis for Two-Phase Geothermal Reservoirs," Geothermal Resources Council Meeting, Hilo, Hawaii, July 25, 1978, pp. 203-206.

R. E. Glover, "Studies of Ground Water Movement," Bureau of Reclamation Technical Memorandum 657, Bureau of Reclamation, Denver, 1960.

C. B. Goranson and R. C. Schroeder, "Site-Specific Geothermal Reservoir Engineering Activities," LBL Earth Sciences Division Annual Report 1978, NTIS PCAS12/MFA01, pp. 97-106.

K. P. Goyal and D. R. Kassdy, "Fault Zone Controlled Charging of a Liquid-Dominated Geothermal Reservoir," Journal of Geophysics, 85, 84, pp. 1867-1875.

"Geophysics and Ground Water, An Introduction--Part I; Applied Use of Geophysics--Part II," Water Well Journal, 25, 7,; 25, 8, 1971.

K. E. Gray, "Approximating Well to Fault Distance From Pressure Build-up Tests," Journal of Petroleum Technology, July 1965, pp. 761-767.

B. D. Gunter and B. C. Musgrave, "New Evidence on the Origin of Methane in Hydrothermal Gases," Geochemica Cosmochimica Acta, 35, 1971, pp. 113-118.

M. S. Hantush, "Analysis of Data from Pumping Tests in Anisotropic Aquifers," Journal of Geophysical Research, 71, 2, January 15, 1966, pp. 421-425.

M. S. Hantush, "Analysis of Data from Pumping Tests in Leaky Aquifers," Transactions of the American Geophysical Union, 37, December 1956, pp. 702-714.

M. S. Hantush, "Hydraulics of Wells," Advances in Hydroscience, 1, 1964.

S. Hirakawa, Y. Mizuishi, Y. Fujinaga, and K. Hida, "Geothermal Reservoir Modeling," Meeting of the Mining and Metallurgical Institute, Tokyo, Japan, March 30, 1976, p. 2.

S. Hirakawa, "System Approach to Geothermal Field Development," Proceedings Fourth Workshop Geothermal Reservoir Engineering, Stanford, California, December 13, 1978, pp. 234-238.

J. R. Hoagland, "Applications of Solute Equilibrium Models to the Study of Geothermal Reservoirs," Geothermal Resources Council, San Diego, California, May 9, 1977, pp. 143-145.

W. A. Hobba, D. W. Fisher, F. J. Pearson Jr. and J. C. Chemerys, "Hydrology and Geochemistry of Thermal Springs of the Appalachians, II. Geochemistry," U.S. Geological Survey Paper, 1044-E, 1978.

R. N. Horne, D. O. Ogbe, K. Temeng and H. J. Ramey Jr., Geothermal Reservoir Engineering Computer Code Comparison and Validation Using the GEONZ Simulator Program, NTIS PCA04/MF A01, November 1980, p. 67.

D. R. Horner, "Pressure Build-up in Wells," Proceedings of the Third World Petroleum Congress, Leiden: E. J. Brill, 1951.

J. H. Howard, Geothermal Reservoir Engineering Management Program: Developmental in Fiscal 1979, NTIS PCA07/MFA01, August 1980, pp. 66-69.

M. K. Hubbert, The Theory of Ground-Water Motion and Related Papers, Hafner Publishing Co., 1969.

A. Hunsbedt, et al., "Laboratory Studies of Non-Isothermal Fluid Production from Fractured Geothermal Reservoirs," American Society Mechanical Engineering Paper No. 77-HT-53, 1977, pp. 1-8.

C. E. Jacob, "Drawdown Test to Determine the Effective Radius of an Artesian Well," Transactions of the ASCE, 112, 1947, pp. 1047-1070.

C. E. Jacob, "Flow of Groundwater: Engineering Hydraulics, New York: John Wiley and Sons, 1950, pp. 321-386.

C. E. Jacob, "Full Utilization of Groundwater Reservoirs," Transactions of the American Geophysical Union, 38, June 1957, p. 417.

C. E. Jacob and S. W. Lohman, "Nonsteady Flow to a Well of Constant Drawdown in an Extensive Aquifer," Transactions of the American Geophysical Union, 33, 4, August 1952, pp. 559-569.

C. E. Jacob, "On the Flow of Water in an Elastic Artesian Aquifer," Transactions of the American Geophysical Union, 21, part II, pp. 574-596.

W. C. Kettenacker, Two-Dimensional Simulation of the Raft River Geothermal Reservoir and Wells, INEL, NTIS PCA06/MFA01, 1977, p. 107.

W. S. Keys and L. M. MacCary, "Application of Borehole Geophysics to Water-Resources Investigations," U.S. Geological Survey Technical Water Resources Investigations, Book 2, Chapt. E1, 1971.

L. E. Klyen, "A Vessel for Collecting Subsurface Water Samples from Geothermal Drillholes," Geothermics, 2, 1973, pp. 57-60.

P. Kruger and H. J. Ramey, Jr., Geothermal Reservoir Engineering, Second Workshop Summaries, December 1-3, 1976, Stanford University, NTIS PCA16/MFA01, 1976, p. 352.

P. Kruger and H. J. Ramey, Jr. (eds), Proceedings Fourth Workshop Geothermal Reservoir Engineering, NTIS PCA15/MFA01, December 1978, p. 336.

P. Kruger and H. J. Ramey, Jr., Stimulation and Reservoir Engineering of Geothermal Resources First Annual Report, June 1, 1977-March 31, 1978, Stanford University, NTIS PCA04/MFA01, April 1978, p. 68.

J. F. Kunze and P. A. Witherspoon, "Energy Extraction and Reservoir Management of a Moderate Temperature Hydrothermal System," American Nuclear Society Topical Meeting on Energy and Mineral Recovery Research, Golden, CO, April 12, 1977, pp. 68-76.

R. B. Leonard, T. M. Brosten, and N. A. Midtlyng, "Selected Data from Thermal Springs Areas, Southwestern Montana," U.S. Geological Survey Open-File Report 78-438, 1978.

W. H. Li, "Interaction Between Well and Aquifer," Proceedings of the ASCE, 80, Separate No. 578, December 1954.

T. M. C. Li, J. W. Mercer, C. R. Faust, and R. J. Greenfield, "Simulation of Geothermal Reservoirs Including Changes in Porosity and Permeability Due to Silica-Water Reactions," Proceedings Fourth Workshop Geothermal Reservoir Engineering, Stanford, December 13, 1978, pp. 275-279.

M. J. Lippmann, C. F. Tsang, and P. A. Witherspoon, "Analysis of the Response of Geothermal Reservoirs Under Injection and Production Procedures," 47 Annual California Regional Meeting of the Society of Petroleum Engineers of AIME, Bakersfield, CA, April 13, 1977, p. 15.

R. M. Lloyd, "Oxygen Isotope Behavior in the Sulfate-Water System," Journal of Geophysical Research, 73, 1968, pp. 6099-6110.

R. Marconcini et al, "Modeling Vapor Dominated Geothermal Reservoirs," DOE Workshop on Geothermal Resources Assessment and Reservoir Engineering, Larderello, Italy, September 12, 1977, pp. 256-298.

R. H. Mariner, T. S. Presser, and W. C. Evans, "Chemical Characteristics of the Major Thermal Springs of Montana," U.S. Geological Survey Open-File Report 76-480, 1976, 31 pp.

R. H. Mariner and L. M. Willey, "Geochemistry of Thermal Waters in Long Valley, Mono County, California," Journal of Geophysical Research, 81, 1976, pp. 792-800.

R. H. Mariner, C. A. Brook, J. R. Swanson, and D. R. Mabey, "Selected Data for Hydrothermal Convection Systems in the United States with Estimated Temperatures 90°C," U.S. Geological Survey Open File Report 78-858, 1978.

C. S. Matthews and D. G. Russell, "Pressure Buildup and Flow Test in Wells," SPE Monograph Series, 1, 1967.

W. F. McKenzie and A. H. Truesdell, "Geothermal Reservoir Temperatures Estimated from the Oxygen Isotope Compositions of Dissolved Sulfate and Water from Hot Springs and Shallow Drillholes," Geothermics, 5, 1977, pp. 51-62.

T. Meider, "Geophysical Methods in Reservoir Engineering and Reservoir Management," Proceedings of the Third Annual Geothermal Conference and Workshop, Monterey, California, June 26, 1979, pp. 2.31-2.37.

D. E. Meinzer, "Large Springs in the United States," U.S. Geological Survey Water Supply Paper 557, 1927.

D. E. Meinzer, "Outline of Groundwater Hydrology," U.S. Geological Survey Water Supply Paper 494, 1923.

S. Mercado, "High Activity Hydrothermal Zones Detected by Nalk, Cerro Prieto, Mexico, Geothermics 2, 1970, pp. 1367-1376.

J. W. Mercer and C. R. Faust, Reservoir Engineering and Evaluation, USGS, NTIS PCA06/MFA01, April 1979, pp. 37-42.

"Methods and Techniques of Ground Water Investigations and Developments," UNESCO Water Resources Series, 33, 1967.

C. C. Miller, A. B. Dyes, and C. A. Hutchison, "The Estimation of Permeability and Reservoir Pressure from Bottomhole Pressure Build-up Characteristics," Transactions, AIME, 1950 pp. 91-105, 189.

F. G. Miller, H. Cinco, H. J. Ramey, Jr., F. Kucuk, "Reservoir Engineering Aspects of Fluid Recharge and Heat Transfer in Geothermal Reservoirs," Geothermal Resources Council Meeting, Hilo, Hawaii, July 25, 1978, pp. 449-452.

A. F. Moench, "Effect of Thermal Conduction Upon Pressure Drawdown and Buildup in Fissured, Vapor Dominated Geothermal Reservoirs," Proceedings Fourth Workshop Geothermal Reservoir Engineering, Stanford, December 13, 1978, pp. 112-117.

A. F. Moench and P. G. Atkinson, "Transient-Pressure Analysis in Geothermal Steam Reservoirs with an Immobile Vaporizing Liquid Phase," Geothermics, 7, 2-4, pp. 253-264.

W. G. Mook, J. C. Bommerson, and W. H. Staverman, "Carbon Isotope Fractionation Between Dissolved Bicarbonate and Gaseous Carbon Dioxide," Earth Planetary Science Letter, 22, 1974, pp. 169-176.

J. G. Morse, "Reservoir Engineering Study of a Portion of the Salton Sea Geothermal Field," Geothermal Resources Council Meeting, Hilo, Hawaii, July 25, 1978, pp. 471-474.

T. D. Mueller and P. A. Witherspoon, "Pressure Interference Effects Within Reservoirs and Aquifers," Journal of Petroleum Technology, April 1975, pp. 471-474, AIME p. 234.

M. Muskat, The Flow of Homogeneous Fluids Through Porous Media, New York: McGraw-Hill Book Company, 1937.

M. Muskat, "Use of Data on the Build-up of Bottomhole Pressures," Transactions of AIME, 1937, pp. 123, 44-88.

T. N. Narasimhan and P. A. Witherspoon, Reservoir Evaluation Tests on RRGE1 and RRGE2, Raft River Geothermal Project, Idaho, LBL NTIS PCA04/MFA01, 1977, p. 53.

M. Nathenson, T. C. Urban, and W. H. Diment, "Approximate Solution for the Temperature Distribution Caused by Flow up a Fault and its Application to Temperatures Measured in a Drillhole at Raft River Geothermal Area, Cassia County, Idaho," Geothermal Resources Council Transactions, V. 3, 1979, pp. 477-480.

M. Nathenson, " Summary of Section VII: Production Technology, Reservoir Engineering, and Field Management," Proceedings of the Second United Nations Symposium the Development and Use of Geothermal Resources, San Francisco, May 20, 1975, pp. XCVII-CI.

A. S. Odeh and L. G. Jones, "Pressure Drawdown Analysis Variable Rate Case," Journal of Petroleum Technology, August 1965, pp. 960-964.

T. Paces, "A Systematic Deviation from Na-K-Ca Geothermometer Below 75°C and above 10^{-4} ATM Pco_2," Geochemica et Cosmchimica Acta 39, 1975.

F. J. Pearson Jr. and A. H. Truesdell, "Tritium in the Waters of Yellowstone National Park (Wyoming)," Short Papers of the Fourth International Conference of Geochronology, Cosmochronology, and Isotope Geology, Open-File Report 78-701, 1978, pp. 327-329.

J. D. Pendergrass and V. J. Berry, Jr., "Pressure Transient Performance in a Multi-layered Reservoir with Cross-flow," Society of Petroleum Engineers Journal, December 1962, pp. 347-354.

G. F. Pinder, State-of-the-Art Review of Geothermal Reservoir Modelling, LBL, NTIS, PCA08/MFA01, March 1979, p. 151.

P. Polubarinova-Kochina, Theory of Groundwater Movement, Princeton: Princeton University Press, 1972.

T. A. Prickett and C. G. Lonnquist, "Selected Digital Computer Techniques for Groundwater Resource Evaluation," Illinois State Water Survey, Urbana, Bulletin 55, 1971, p. 62.

K. Pruess and R. C. Schroeder, "Basic Theory and Equations Used in the Two Phase Multi-Dimensional Geothermal Reservoir Simulator, Geothermal Resources Council Annual Meeting, Reno, Nevada, September 24, 1979, p. 5.

R. Raghavan, G. V. Cady, and H. J. Ramey, Jr., "Well Test Analysis for Vertically Fractured Wells," Journal of Petroleum Technology, August 1972, pp. 1014-1020; Transactions, AIME, p. 253.

H. J. Ramey, Jr., Interference Analysis for Anisotopic Formations--A Case History" Journal of Petroleum Technology, October 1975, pp. 1290-1298, Transactions AIME, p. 259.

H. J. Ramey, Jr., "Short-Time Well Test Data Interpretation in Presence of Skin Effect and Wellbore Storage" Journal of Petroleum Technology, January 1970, Transactions AIME, p. 249.

H. J. Ramey, Jr., "Commercialization of Geothermal Resources," Conference on Commercialization of Geothermal Resources, San Diego, California; November 28, 1978, pp. 15-17.

H. J. Ramey Jr. and P. Kruger (eds), Proceedings of Fifth Workshop on Geothermal Reservoir Engineering, December 12-14, 1979, NTIS PCA17/MFA01, December 1979, pp. 261-267.

H. J. Ramey Jr., and A. L. London, Stimulation and Reservoir Engineering of Geothermal Resources, Stanford University Geothermal Program Report No. 4, NTIS PCA05/MFA01, August 1975, p. 78.

G. S. Randall and R. F. Harrison, "Annotated Research Bibliography for Geothermal Reservoir Engineering," Proceedings Fourth Workshop Geothermal Reservoir Engineering, Stanford, California, December 13, 1978, pp. 272-274.

R. C. Reda, "Influence of Steam/Water Relative Permeability Models on Predicted Geothermal Reservoir Performance: A Sensitivity Study," Sixth Annual Workshop on Geothermal Reservoir Engineering, Stanford, California December 16, 1980, p. 7.

Republic Geothermal et al., Raft River Well Stimulation Experiments: Geothermal Reservoir Well Stimulation Program, NTIS PCA08/MFA01, August 1980, p. 158.

L. F. Rice, Pressure Drawdown and Buildup Analyses in Geothermal Reservoirs, Science and Software Systems, 1976, p. 24.

C. T. Rightmire, H. W. Young, and R. L. Whitehead, "Geothermal Investigations in Idaho, IV. Isotropic and Geochemical Analyses of Water from the Bruneau-Grand View and Weiser Areas, Southwest Idaho," Idaho Dep. Water Admin., Water Information Bulletin, 30, 1976.

R. J. Rivera, "Decline Curve Analysis--A Useful Reservoir Engineering Tool for Predicting the Performance of Geothermal Wells," Geothermal Resources Council, San Diego, California, May 9, 1977, pp. 257-259.

M. I. Rorabaugh, "Graphic and Theoretical Analysis of Step-Drawdown Tests of Artesian Wells," Proceedings of the ASCE, 79, 362, September 1953.

D. G. Russell and N. E. Truitt, "Transient Pressure Behavior in Vertically Fractured Reservoirs," Journal of Petroleum Technology, October 1964, pp. 1159-1170.

H. Sakai, "Sulfate-Water Isotope Thermometry Applied to Geothermal Systems," Geothermics, 5, 1977, pp. 67-74.

M. Saltuklaroglu, "Interference Effect of Producting Wells on Observation Wells in a Geothermal Field," Proceedings of the Fifth Workshop on Geothermal Reservoir Engineering Stanford, California, December 12, 1979, pp. 49-59.

G. Sandquist, S. Swanson, R. Stoker, and J. Kunze, "Evaluating the Energy Capacity and Lifetime of Fracture Dominated Geothermal Reservoirs," 12th Intersociety Energy Conversion Engineering Conference, Washington, D.C., August 28, 1977, pp. 804-809.

S. K. Sanyal, H. J. Ramey Jr., and H. T. Meidav, "Geothermal Reservoir Assessment Techniques Manual," EPRI Annual Geothermal Program, January 1978, pp. 2.85-2.90.

C. R. Scherer, Geothermal Reservoir Management, University of California, Berkeley, NTIS PCA10/MFA01, 1978, p. 203.

R. Schneider, "An Application of Thermometry to the Study of Ground Water," U.S. Geological Survey Water Supply Paper 1544-B, 1962.

R. J. Schicht, "Selected Methods of Aquifer Test Analysis," Water Resources Bulletin, 8, 1, February 1972, pp. 175-187.

C. S. Slichter, "Field Measurements of Rate of Movement of Underground Water," U.S. Geological Survey Water Supply Paper 140, 1905.

C. S. Slichter, "Theoretical Investigation of the Motion of Ground Waters: Washington, D.C.," U.S. Geological Survey Nineteenth Annual Report, Part 2, 1899, pp. 295-384.

G. A. Sudol, R. F. Harrison, and H. J. Ramey Jr., "Annotated Research Bibliography for Geothermal Reservoir Engineering," NTIS PCA08/MFA01, August 1979, p. 155.

W. K. Summers, The Annotated Indexed Bibliography of Geothermal Phenomena, Socorro: New Mexico Institute of Mining and Technology, 1971.

P. K. Takahashi, B. H. Chen, K. I. Mashima, and A. S. Seki, "State-of-the-Art of Geothermal Reservoir Engineering," Proceedings of American Society of Civil Engineers, 101, 1, July 1975, pp. 11-126.

C. V. Theis, "Relation Between the Lowering of the Piezometer Surface on the Rate and Duration of Discharge of a Well Using Ground Water Storage," Transactions of the American Geophysical Union, 16, 1935, pp. 519-524.

D. K. Todd, Ground Water Hydrology, New York: John Wiley and Sons, 1960.

C. F. Tolman, Ground Water, New York: McGraw-Hill Book Company, Inc., 1957 pp. 341-346.

C. F. Tsang, M. J. Lippman and P. A. Witherspoon, "Production and Reinjection in Geothermal Reservoirs," Geothermal: State of the Art, 1977, pp. 301-303.

F. VanderLeeden, Ground Water, A Selected Bibliography, New York: Water Information Center, 1971.

A. F. van Everdingen, "The Skin Effect and its Influence on the Productive Capacity of a Well," Transactions of AIME, 1953.

A. F. van Everdingen and W. Hurst, "The Application of the Laplace Transformation to Flow Problems in Reservoirs," Transactions of AIME, 1949, pp. 186, 305-324.

D. J. Vetter, "Tritium Tracer as a Means for Reservoir Verification in Geothermal Reservoirs," EPRI Annual Geothermal Program, California, January 1978, pp. 4.17-4.23.

W. C. Walton, Groundwater Resource Evaluation, New York: McGraw-Hill Book Company, Inc., 1970, p. 194.

W. C. Walton, "Selected Analytical Methods for Well and Aquifer Evaluation," Illinois State Water Survey, Department of Regulation and Education Bulletin No. 49, Urbana, 1962.

S. H. Ward, Program Review: Resource Evaluation, Reservoir Confirmation, and Exploration Technology, NTIS PCA09/MFA01, May 1978, p. 182.

J. E. Warren and P. J. Root, "The Behavior of Naturally Fractured Reservoirs" Society of Petroleum Engineers Journal, September 1963, pp. 245-255.

"Well Logging in Ground Water Hydrology," Ground Water, 6, 1, 1968, pp. 10-18.

D. Weres, "Dynamics of Steam Producing Geothermal Reservoirs," Geothermal Environmental Seminar, 1978, Sacramento, California, May 9, 1978, pp. 189-195.

P. W. Werner, "Notes on Flow-Time Effects in the Great Artesian Aquifers of the Earth; Transactions of the American Geophysical Union, 27, October 1946.

N. D. White, "Annual Report on Ground Water in Arizona," Water Resources Report, 24, 1964-1965.

P. A. Witherspoon, T. N. Narasimhan, and D. G. McEdwards, "Results of Interference Tests from Two Geothermal Reservoirs," Journal of Petroleum Engineering, 30, January 1978, pp. 10-16.